



**Adsorption, Ion Exchange
and Catalysis
Design of Operations and
Environmental Applications**

V.J. Inglezakis and S.G. Pouloupoulos



Preface

In this book, three important processes, namely, adsorption, ion exchange, and heterogeneous catalysis, are presented along with environmental issues. Specifically, this book is essentially a mixture of environmental science (Chapters 1 and 2) and chemical reactor engineering (Chapters 3 to 6).

The question is why environmental issues are being presented in a chemical engineering book containing heterogeneous processes. First of all, the processes discussed (adsorption, ion exchange, and catalysis) are largely employed in our effort to minimize the emissions of various pollutants into the environment. The use of catalytic converters in the after-treatment of automobile exhaust gases (catalysis), a subject known to almost everyone, the treatment of VOC-containing gases (catalysis, adsorption), and the removal of toxic metals from industrial wastewater (ion exchange, adsorption) are some important examples of the environmental applications of the presented heterogeneous processes. Moreover, the environment is a field of continuous research since its protection is essential in the context of sustainable development, and generally for a planet worth living on. Consequently, the environmentally oriented presentation of adsorption, ion exchange, and catalysis is of substantial importance. Engineers are often provided with a lot of information regarding heterogeneous processes, chemical phenomena, and waste treatment techniques, but lack knowledge of the very basics of environmental problems. The first two chapters of the book do not attempt to cover all environmental subjects; they are an effort of the authors to provide the reader with a basic knowledge of the major environmental problems and connect them to chemical engineering.

Why adsorption, ion exchange and heterogeneous catalysis in one book? The basic similarity between these phenomena is that they all are heterogeneous fluid–solid operations. Second, they are all driven by diffusion in the solid phase. Thus, mass transfer and solid-phase diffusion, rate-limiting steps, and other related phenomena are common. Third, the many aspects of the operations design of some reactors are essentially the same or at least similar, for example, the hydraulic analysis and scale-up. Furthermore, they all have important environmental applications, and more specifically they are all applied in gas and/or water treatment.

In connection with the engineering content of the book, a large number of reactors is analyzed: two- and three-phase (slurry) agitated reactors (batch and continuous flow), two- and three-phase fixed beds (fixed beds, trickle beds, and packed bubble beds), three-phase (slurry) bubble columns, and two-phase fluidized beds. All these reactors are applicable to catalysis; two-phase fixed and fluidized beds and agitated tank reactors concern adsorption and ion exchange as well.

Apart from the analysis of kinetics, mass transfer, and equilibrium of the processes at a fundamental level, the analysis of material, and in fixed beds energy balances in the reactors, as well as a number of analytical solutions of the reactors models are presented. Furthermore, the hydraulic behavior of the reactors is presented in detail. Hydraulic analysis is basically

flow analysis of the reactors or conducting patterns without taking into consideration the physicochemical phenomena involved, i.e. adsorption, ion exchange, or catalysis. Hydraulic analysis follows different routes for each reactor type. On the basis of the reactor characteristics, the most important aspects are analyzed: nonideal flow and liquid holdup for fixed beds, bubble analysis and phases holdup for slurry bubble columns and agitated tanks, fluidizing regimes and analysis for fluidized beds, and agitation analysis for tank reactors. Furthermore, scale-up analysis is included for all the reactors.

Special reference should be made for the last section of Chapter 3: Particle analysis. Everything in connection with particle properties and basic calculations, irrespective of its specific use, is presented: from particle surface area to calculations regarding its terminal velocity and diffusion coefficients. Furthermore, concerning materials used in adsorption, ion exchange, and catalysis, special paragraphs are included in Chapters 4 and 5 as well as the management of spent materials.

Nearly all the examples contained are based on real experimental data found in the literature with environmental interest. Most of the examples consider all aspects of operation design—kinetics, hydraulics, and mass transfer. All parameters in the examples are calculated using correlations, figures, and tables provided in the book—thus no parameters just “appear” in the text. Moreover, some text in the examples is also devoted to provide information about the pollutants removed or treated.

Special issues are found in “Look into” paragraphs. These sections could be viewed as highlights. Here, special subjects are discussed in detail. Special cases, where significant applications are presented, can also be found in the book.

Finally, Appendices I and II are structured so that the reader can easily find some basic properties of environment-related compounds and unit conversions, or smartly estimate some parameters found in relationships in the rest of the book. The Appendix does not cover all cases and compounds; however, it is a first and separate guide provided to the reader for the basic calculations and properties found in this book.

Table of Contents

1. Air and Water Pollution
2. Adsorption, Ion Exchange and Catalysis
3. Heterogeneous Processes and Reactor Analysis
4. Adsorption and Ion Exchange
5. Catalysis
6. Reactors Scale up
7. Appendices
8. References

Air and Water Pollution

1.1 INTRODUCTION

The reason for the presence of this chapter in this book is more than apparent to its authors. In the last century, human activities in combination with a lack of respect for nature, expressed by the view that raw material resources are inexhaustible and the tolerance of ecosystems to pollutant release is unlimited, led to the pollution and degradation of the environment. Chemical engineering is the field of science that combines chemistry with technology and is able to give solutions to most environmental problems. The environment is going to set the pace in chemical engineering evolution, since we have reached the point where if we do not stop destroying and polluting the environment, life on Earth will be in danger—at least life as we know it today. Sustainability is the proposal for a better future, where economic development can coexist with social cohesion and environmental protection.

Human activities harmfully influence the environment and nature in many ways. The production of undesirable wastewater, waste gas, and liquid plus solid residues seems to be inevitable during chemical processes. The public is more sensitive to pollution of the aquatic environment and the depletion of clean water resources, because they have an immediate impact on daily routine and recreational activities. However, air pollution has an adverse impact on our health in the short and long term, and the problems of the greenhouse effect and the destruction of stratospheric ozone could extinguish life from the face of the Earth. These problems are enhanced by overpopulation and urbanization. Today, urban areas can be seen as “monsters” that consume large amounts of energy, matter, and freshwater and release all kinds of waste into the environment.

The first chapter of this book is devoted to air and water pollution. Although much attention will be given to releases from chemical processes, environmental problems arising from other activities will also be dealt with. Issues concerning pollutants, emission sources, and treatment methods are going to be presented. Moreover, before focusing on the processes of adsorption, ion exchange, catalysis, and the design principles of the relevant operations in the following chapters, it is useful to show their connection with environmental protection. Emphasis is given on the current environmental situation in Europe.

1.1.1 Air pollution

Clean air is an important prerequisite for sustainable development and is a basic requirement for human health and welfare. In addition, air pollutants contribute to atmospheric problems such as acidification and global climate change, which have impacts on crop productivity, forest growth, biodiversity, buildings, and cultural monuments. The benefits from the progress made in the areas of waste gas treatment and environmental legislation are partially offset by industrialization, an increase in the number of private cars in use, and overpopulation.

Air pollutants are divided into two broad categories: *primary* and *secondary*. Primary pollutants are those emitted directly into the air, in contrast to secondary pollutants, which are created in the atmosphere by the reactions among the primary pollutants, usually in the presence of sunlight. Specifically, a variety of chemical or photochemical reactions (catalyzed by light) produce a wide range of secondary pollutants, especially in urban air. A prime example is the formation of ozone in smog.

There is a variety of problems associated with air pollution, starting from photochemical smog, ozone formation, and acid rain at a regional level, to the greenhouse effect and ozone-layer depletion at a global level. These problems have an adverse impact on both environment and public health (Table 1.1); the last two problems are a threat to life on Earth generally.

Agriculture, energy plants, road transport, and industry are the most important sources of pollutants of the atmosphere. Agriculture, for example, charges air with acidifying gases that may lead to acid rain formation with a dramatic impact on lakes, rivers, and marine life.

Air pollution is a problem at a local as well as a global level. For purposes of studying, it is useful to categorize air pollution according to the levels at which it appears:

Table 1.1

The main health effects of the most important air pollutants (Source: Parliamentary Office of Science and Technology, 2002; UNEP, 1992)

Pollutant	Main Health Effects
Sulfur dioxide	Irritation of lungs, shortness of breath, increased susceptibility to infection
Nitrogen dioxide	Irritation or damage of lungs
Particulate matter	Eye and nasal irritation, long-term exposure associated with coronary heart disease and lung cancer
Carbon monoxide	Interferes with oxygen transport by blood, resulting in the reduction of oxygen supply to the heart (chronic anoxia), heart and brain damage, impaired perception
Ozone and other photochemical oxidants	Pain on deep breathing, irritation and inflammation of lungs, heart stress or failure
Benzene	Cause of cancer
1,3-Butadiene	Cause of cancer
Lead	Kidney disease and neurological impairments, primarily affecting children

- local
- urban
- regional
- transboundary
- global.

Local level

At the local level, air pollution concerns a region within a 5-km radius. It is characterized by high concentrations of specific pollutants that may come from automobiles or industrial activities in that region. For example, emissions from vehicles can lead to high concentrations of carbon monoxide near traffic-jammed roads. High buildings and the terrain can also contribute to high local concentrations of pollutants.

Urban areas

In urban areas, there are three major types of air pollution found (EEA, 2003):

- High annual average concentration levels of various pollutants, e.g. benzene, lead, sulfur dioxide (SO₂), and particulate matter (PM). As in the case of air pollution at the local level, this type of pollution is linked to specific pollutants resulting from either large industrial and power plants or automotive vehicles.
- Winter-type smog, characterized by high concentrations of SO₂ and PM that arise mainly from the combustion of coal and fuels with a high content of sulfur. This kind of pollution occurs in urban areas with many power plants or industrial units clustered together, where low temperatures and mist are observed in the year. It has been also termed “industrial pollution.”
- Summer-type smog, characterized by high concentrations of carbon monoxide, volatile organic compounds (VOCs), and nitrogen oxides (NO_x). It is also called “photochemical smog” or “LA smog”, since it first appeared in Los Angeles. This type of pollution is closely connected to automotive vehicles, and its formation is favored by sunlight and high temperatures.

The first two types are associated with primary pollutants, namely, compounds such as nitrogen oxide (NO), carbon monoxide (CO), and sulfur dioxide (SO₂) that are emitted directly into the atmosphere from various sources, whereas the third type of urban air pollution is a more complex phenomenon associated with secondary pollutants, which are formed from reactions between primary pollutants in the atmosphere, usually in the presence of sunlight and heat. Specifically, various volatile organic compounds react in the atmosphere with nitrogen oxides by means of the ultraviolet radiation of sunlight, producing the so-called photochemical smog consisting of nitrogen dioxide, various oxidized forms of organic compounds, and ozone. The pollution of primary pollutants is easier to treat than the one associated with secondary pollutants, because the latter are produced by various organic compounds participating in numerous photochemical reactions.

Approximately half of the world’s population now lives in urban areas, and half of these people suffer an atmosphere containing harmful amounts of substances such as sulfur dioxide, ozone, and particulate matter. Approximately 4000 people died from lung and heart conditions during a London smog episode in December 1952. Globally, around 50% of cases of chronic respiratory illness are now connected with air pollution. The most

recent information on the health effects of air pollution have been summarized in a report released by the World Health Organization (WHO, 2004).

Regional

Regional air pollution (50–1000 km) can be attributed to two mechanisms:

- transport and dispersion of urban pollutants in large areas,
- transport and transformation of primary pollutants into secondary ones at the regional level.

Two types of air pollution are connected to these mechanisms. The first problem is the formation of tropospheric ozone due to the action of sunlight on mixtures of NO_x and VOCs. Tropospheric ozone is either formed in urban areas and transferred by the wind to rural areas or formed during the transfer of NO_x and VOCs from cities to rural areas by the wind and has adverse effects on crop yields and human health as well as forest ecosystems (ApSimon and Warren, 1996). About 90% of the adverse impact of air pollution on agriculture is attributed to ozone. The second problem is associated with acidifying substances, such as SO_2 , NO , and NO_2 , which are photooxidized in the atmosphere and taken up by cloud droplets, being thus transformed into the corresponding acids, causing acidification through acid rain formation or dry deposition (direct contact of acids with land and aquatic surfaces by means of wind), which constitutes an immediate danger for land and aquatic biota (Figure 1.1).

Transboundary

Transboundary air pollution is related to the transfer of air pollution from one country to another. Generally, the problems that appear on a regional level may also be exchanged

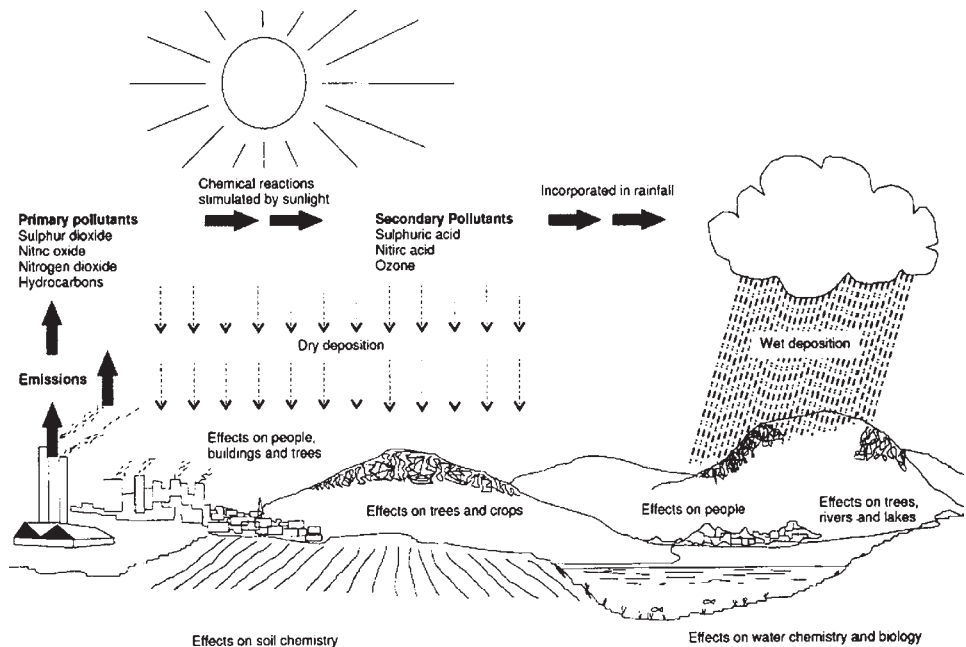


Figure 1.1 The mechanism of acid deposition (ApSimon and Warren, 1996).

between adjacent countries. For example, Greece exchanges ozone with Italy, whereas Japan and Canada “import” various types of air pollution from China and the United States, respectively. Moreover, the transboundary transport of acidifying pollutants has led to a marked change in the acidity of lakes and streams in Scandinavia, as observed in the 1960s (ApSimon and Warren, 1996). These problems have also been observed to appear on an intercontinental scale. For example, based on observations of atmospheric carbon monoxide, ozone, peroxyacetyl nitrate, radon, aerosols, and nonmethane hydrocarbons (NMVOCs), Jaffe *et al.* (1999) showed that emissions from East Asia significantly impact the air arriving to North America. North America has also been reported to “export” air pollutants to Europe (Holloway *et al.*, 2003). A number of toxic substances are capable of intercontinental atmospheric transport, including mercury, toxaphene, hexachlorobenzene, and poly-chlorinated biphenyls (PCBs) (International Air Quality Advisory Board, 2004). This type of air pollution is another proof of the fact that pollution is a problem that needs intergovernmental cooperation to be properly addressed.

Global

Global air pollution is related to two famous problems that are responsible to a great extent for the increased public awareness about environmental issues. The greenhouse effect and stratospheric ozone depletion changed our view and attitude about the environment. For the first time, it was realized that our activities could lead to a drastic global change in the climate or atmosphere. The extensive use of chlorofluorocarbons (CFCs) till 1985 resulted in a decrease in the ozone concentration in the stratosphere, which led to an increase in the amount of UV-B radiation reaching the Earth’s surface. Ozone depletion has many adverse effects on both ecosystems and humans, independent of geographical position or economic status. As a result, nonmelanoma skin cancers have increased, leading to concerns about human health, and the photosynthesis process, vital for life support on the Earth, has been put in danger (UNEP, 1992). Although Molina and Rowland reported the possibility of ozone destruction by the action of CFCs in 1974, it was the discovery of the ozone “hole” in the Antarctic stratosphere in 1984 that led to urgent and intergovernmental action (Farman *et al.*, 1985). The rapid evolution of ozone depletion and its obvious tremendous potential effects led to the decision to ban and replace all CFCs. At the same time, the emissions of some compounds into the atmosphere, mainly carbon dioxide (CO₂), seem to cause global warming. The word “seem” is used because the effect of increased levels of CO₂ in the atmosphere has not been fully understood. In contrast to the issue of ozone depletion, the greenhouse effect is still under consideration and its potential impact on the Earth has not been fully concluded.

In Table 1.2, air pollution problems are connected to the most important pollutants.

At this point, it would be interesting to examine the situation in terms of air quality around the world.

European Union

The evolution of the emissions of some atmospheric pollutants in Europe (EU-15) in the period 1990–1999 has been presented in the report of Goodwin and Mareckova (2002). The report includes acidifying pollutants (ammonia, sulfur dioxide, and nitrogen oxides), tropospheric ozone precursors, NMVOCs, carbon monoxide, and particulate matter

Table 1.2

Air pollution problems in association with the most important pollutants

Pollutant	Smog	Urban air quality	Acid deposition	Global warming	Ozone depletion	Health
Ozone	✓	✓		✓		✓
Sulfur dioxide	✓	✓	✓	✓		
Carbon monoxide	✓	✓		✓		
Carbon dioxide			✓	✓		
CFCs				✓	✓	
Nitrogen oxides	✓	✓	✓	✓	✓	
Volatile organic compounds	✓	✓		✓		
Toxics ^a	✓	✓				✓
Particles	✓	✓	✓	✓		✓
Total reduced sulfur compounds		✓				✓

^aToxic metals and organic compounds.**Table 1.3**

The most significant sources of atmospheric pollutants in Europe in 1999

Pollutant	Emission Sources
CO	Road transport (57%), industry (16%), other transport (7%)
NMVOC	Road transport (31%), solvent and other product use (32%), industry (10%), agriculture (7%), energy (6%)
NO _x	Transport (64%), energy sector (16%), industry (13%)
NH ₃	Agriculture (94%)
SO ₂	Energy sector (61%), industry (24%), commercial and domestic combustion (7%), transport (7%)
PM	Road transport (28%), energy industries (24%), industry (16%), agriculture (13%)

emissions. Between 1990 and 1999, the emissions of these pollutants have been significantly reduced (SO₂ by 70%, NO_x by 25%, NMVOCs by 28%, and CO by 32%), mainly due to the introduction of automobile catalytic converters with the exception of ammonia, whose emissions due to agriculture are very difficult to control. The energy sector, and specifically its combustion processes, plus road transport are the main sources of air pollutants except ammonia (NH₃). The most significant sources of some pollutants in EU-15, in 1999, are shown in Table 1.3.

Despite the benefits from stringent legislation and advances in environmental technology, the increase in the fleet of automotive vehicles and overpopulation in urban areas results in bad air quality. It is estimated that up to 45% of Europe's urban population remains exposed to particulate concentrations above limit values, and up to 30% to ozone concentrations above target levels that assure human health protection. The concentrations of various pollutants in the atmosphere in various cities across Europe are shown in Table 1.4. The data in the table are from WHO's Healthy Cities Air Management Information System and the World Resources Institute, which relies on various national

Table 1.4

The concentrations of various pollutants in the atmosphere in various cities in Europe, in 1995

Country	City	City population ($\times 1000$)	Total suspended particulates ($\mu\text{g}/\text{m}^3$)	Sulfur dioxide ($\mu\text{g}/\text{m}^3$)	Nitrogen dioxide ($\mu\text{g}/\text{m}^3$)
Austria	Vienna	2060	47	14	42
Belgium	Brussels	1122	78	20	48
Bulgaria	Sofia	1188	195	39	122
Croatia	Zagreb	981	71	31	–
Czech Republic	Prague	1225	59	32	23
Denmark	Copenhagen	1326	61	7	54
Finland	Helsinki	1059	40	4	35
France	Paris	9523	14	14	57
Germany	Frankfurt	3606	36	11	45
	Berlin	3317	50	18	26
	Munich	2238	45	8	53
Greece	Athens	3093	178	34	64
Hungary	Budapest	2017	63	39	51
Iceland	Reykjavik	100	24	5	42
Ireland	Dublin	911	–	20	–
Italy	Milan	4251	77	31	248
	Rome	2931	73	–	–
	Turin	1294	151	–	–
Netherlands	Amsterdam	1108	40	10	58
Norway	Oslo	477	15	8	43
Poland	Katowice	3552	..	83	79
	Warsaw	2219	..	16	32
	Lodz	1063	..	21	43
Portugal	Lisbon	1863	61	8	52
Romania	Bucharest	2100	82	10	71
Slovak Republic	Bratislava	651	62	21	27
Spain	Madrid	4072	42	11	25
	Barcelona	2819	117	11	43
Sweden	Stockholm	1545	9	5	29
Switzerland	Zurich	897	31	11	39
United Kingdom	London	7640	–	25	77
	Manchester	2434	–	26	49
	Birmingham	2271	–	9	45

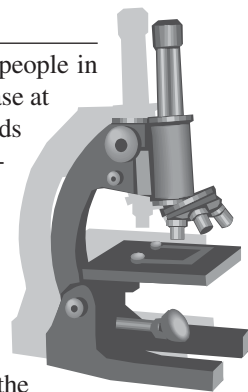
sources. For reasons of comparison, the population of each city is also presented. Total suspended particulates refer to smoke, soot, dust, and liquid droplets from combustion that are in the air. It has to be noted that particulate levels are an indicator of the quality of the air and the state of a country's technology and pollution controls. Although pollutant concentrations are sensitive to local conditions, and therefore, the data presented should be considered as a general indication of air quality in each city, some comparisons can be conducted. WHO annual mean guidelines for air quality standards are $90 \mu\text{g}/\text{m}^3$ for total suspended particulates, $50 \mu\text{g}/\text{m}^3$ for sulfur dioxide, and $50 \mu\text{g}/\text{m}^3$ for nitrogen dioxide.

Sofia, Athens, Turin, and Barcelona, all in south Europe, exhibit the highest concentrations of total suspended particulates, above the WHO standard value. Concerning sulfur dioxide, all the cities presented exhibit concentration values below the standard set by WHO. In contrast, nitrogen dioxide is a cause for concern in many European cities, since values close to or above WHO standards are common. For this compound, cities in northern Europe also have to be on alert.

The combination of Tables 1.2 and 1.3 reveals the responsibility for each kind of air pollution. Specifically, road transport is the main source of nitrogen dioxide, whereas the increased sulfur dioxide levels should be attributed to the energy sector. Both sources contribute to increased levels of total suspended particulates in the atmosphere. It is obvious that this type of information is a valuable asset for environmental policy makers. Measurements in relation to air quality and exhaust emissions from automotive vehicles have been conducted for many years, and as a result, the evolution of air quality and the contribution of vehicles are known to authorities. However, this is not the case for industry. Even if the contribution of industry to air pollution could be roughly estimated, it was very difficult to connect each kind of industrial process to each pollutant. This lack of information led to the idea of establishing a Pollutant Release and Transfer Register (PRTR), which first emerged in the United States following the tragic accident in Bhopal, India, in 1984. Shortly thereafter, the United States Congress approved the Emergency Planning and Community Right-to-Know Act, establishing a register called the Toxic Release Inventory (TRI), which tracks releases to all media (air, water, and land) and off-site transfers of more than 600 chemicals.

A look into the origins of U.S. TRI

In 1984, a deadly cloud of methyl isocyanate killed thousands of people in Bhopal, India. Shortly thereafter, there was a serious chemical release at a sister plant in West Virginia. These incidents underscored demands by industrial workers and communities in several states for information on hazardous materials. Public interest and environmental organizations around the country accelerated demands for information on toxic chemicals being released. Against this background, the Emergency Planning and Community Right-to-Know Act (EPCRA) was enacted in 1986. EPCRA's primary purpose is to inform communities and citizens of chemical hazards in their areas. Sections 311 and 312 of EPCRA require businesses to report the locations and quantities of chemicals stored on-site to state and local governments in order to help communities prepare to respond to chemical spills and similar emergencies. EPCRA



Section 313 requires the EPA and the states to annually collect data on releases and transfers of certain toxic chemicals from industrial facilities, and make the data available to the public in the Toxics Release Inventory (TRI).

Other countries, including Australia (NPI in 1998), Canada (NPRI in 1999), and the European Union (EPER in 2000), followed in developing national PRTR systems. Focusing on Europe, it is important to clarify what EPER is about, exactly.

The European Pollutant Emission Register (EPER) is the establishment of a European register with comparable data on the emissions from individual activities covered by the Council Directive 96/61/EC, known as the IPPC Directive. It is a useful monitoring tool and a suitable instrument for public dissemination of emission data and its effectiveness could be seen in the European effort to achieve the goals set in Agenda 21 of the UNECE Conference in Rio de Janeiro (1992), in the IPPC Directive (1996), and in the UNECE Aarhus Convention (1998).

The IPPC Directive was brought into effect at the end of 1999. Since then, member states have gradually adopted national regulations to comply with the IPPC Directive, including a national inventory of emission data to be reported to the commission. An inventory of principal emissions and sources responsible has to be published by the commission every three years based on data supplied by the member states.

On January 25, 2000, the committee referred to in Article 19 of IPPC Directive gave a favorable opinion of a draft Commission Decision on the implementation of a European Pollutant Emission Register. The Commission Decision (2000/479/EC), to be referred to as the EPER Decision, was adopted on July 17, 2000. According to the EPER Decision, member states shall report to the Commission on emissions into air and water from all individual facilities with one or more activities as mentioned in Annex I to the IPPC Directive. The provided data will be made publicly accessible and disseminated on the Internet. Specifically, “EPER is a publicly accessible register with emission data that enables the Commission and national governments to monitor the trends in annual emissions of large industrial activities covered by Annex I of the IPPC Directive” (Commission Decision, 2000).

EPER covers the releases into the environment from industrial facilities above a minimum production capacity. It excludes emissions from the transport sector and from most agricultural sources. The comparison with the EU-15’s total emissions of some important greenhouse gases and air pollutants (as reported under the UN Framework Convention on Climate Change and the UNECE Convention on Long-Range Transboundary Air Pollution) shows that EPER covers around—

- 42% of EU-15’s total—carbon dioxide (CO₂) emissions
- 15% of EU-15’s total—methane (CH₄) emissions
- 13% of EU-15’s total—dinitrogen oxide (N₂O) emissions
- 6% of EU-15’s total—nonmethane volatile organic carbon (NMVOC) emissions
- 26% of EU-15’s total—nitrogen oxides (NO_x) emissions, and
- 70% of EU-15’s total—sulfur oxides (SO_x) emissions.

There are still some problems about the enforcement of the relevant directives and guidelines, and at present, data are available for 2001 only. However, it should be seen as a huge

step in environmental policy, since the knowledge of the connection between facilities and pollutants combined with the data about other sources of pollution (transport and agriculture) allow authorities for the first time to take the right course of action for each type of pollution. It has to be mentioned again that all releases into the environment are included in EPER.

Suppose that the authorities have to deal with the problem of photochemical smog. This type of pollution is connected to increased NO_x levels in the atmosphere. It is well known that road transport is the main source of these compounds. But the contribution of industry is still missing. The existence of the EPER and the corresponding National Pollutant Release and Transfer Register has enabled the collection of the data in Table 1.5. Consequently, the

Table 1.5

NO_x releases to air for each activity in Europe (2001)

Activity	Total emission to air (t/yr)	Percentage
Combustion installations >50 MW	1.5×10^6	58.3
Installations for the production of cement klinker (>500 t/d), lime (>50 t/d), glass (>20 t/d), mineral substances (>20 t/d), or ceramic products (>75 t/d)	427×10^3	16.9
Metal industry	186×10^3	7.3
Mineral oil and gas refineries	177×10^3	7.0
Basic organic chemicals	72×10^3	2.8
Industrial plants for pulp from timber or other fibrous materials and paper or board production (>20 t/d)	67×10^3	2.7
Installations for the disposal or recovery of hazardous waste (>10 t/d) or municipal waste (>3 t/h)	43×10^3	1.7
Basic inorganic chemicals or fertilizers	42×10^3	1.7
Slaughterhouses (>50 t/d), plants for the production of milk (>200 t/d), other animal raw materials (>75 t/d), or vegetable raw materials (>300 t/d)	14×10^3	0.6
Installations for the disposal of nonhazardous waste (>50 t/d) and landfills (>10 t/d)	6.8×10^3	0.3
Coke ovens	5.9×10^3	0.2
Pharmaceutical products	5.2×10^3	0.2
Installations for surface treatment or products using organic solvents (>200 t/yr)	3.5×10^3	0.1
Coal gasification and liquefaction plants	1.9×10^3	0.1
Biocides and explosives	1.1×10^3	0.0
Plants for the pretreatment of fibers or textiles (>10 t/d)	941	0.0
Installations for the disposal or recycling of animal carcasses and animal waste (>10 t/d)	663	0.0
Installations for the production of carbon or graphite	441	0.0
Total	2.5×10^6	100.0

measures that will be taken have to be focused not only on road transport but also on combustion installations.

A special case: Suppose that your country has occasions of acid rain due to sulfuric acid. The main source of SO_x , which leads to sulfuric acid formation, is combustion installations. However, there are not large combustion installations in your land. Can you find the source of air pollution and the possible position of your country in Europe, using Table 1.6?

The answer is simple. You have been the victim of air pollution “traveling”. Acid rain is among the problems connected to air pollution that may appear at a transboundary level. So, your country has suffered the results of the combination of the elevated SO_x emissions from a neighboring country with favoring climatic conditions.

Air pollution is not a problem only in Europe but constitutes a reason to worry all over the world. The concentrations of total suspended particulates, sulfur dioxide, and nitrogen dioxide in the atmosphere in various cities in 1995, in America, Asia, Africa, and Australia are presented in Tables 1.7, 1.8, 1.9, and 1.10, respectively.

It is useful to recollect the limits set by WHO: $90 \mu\text{g}/\text{m}^3$ for total suspended particulates, $50 \mu\text{g}/\text{m}^3$ for sulfur dioxide, and $50 \mu\text{g}/\text{m}^3$ for nitrogen dioxide. It is apparent that the world has a long way to go till compliance with these numbers is achieved. Mexico City is notorious for bad air quality. Pollution levels exceed WHO standards 350 days per year. More than half of all children in the city have lead levels in their blood sufficient to lower intelligence and retard development. The 130,000 industries and 2.5 million motor vehicles spew out more than 5500 metric tons of air pollutants every day, which are trapped by the mountains ringing the city.

Table 1.6

SO_x releases (annual) to air for each country in Europe (2001)

Country	Total emission (t)	Percentage of European total
Austria	12,321	0.3
Belgium	105,539	2.5
Denmark	12,433	0.3
Finland	59,436	1.4
France	369,051	8.6
Germany	370,590	8.6
Greece	408,222	9.5
Ireland	91,498	2.1
Italy	509,126	11.8
Luxembourg	604	0.0
Netherlands	51,777	1.2
Portugal	166,147	3.9
Spain	1,169,999	27.2
Sweden	23,403	0.5
United Kingdom	948,488	22.1
Total	4,298,634	100.0

Table 1.7

The concentrations of various pollutants in the atmosphere in various cities in America, in 1995

Country	City	City population ($\times 1000$)	Total suspended particulates ($\mu\text{g}/\text{m}^3$)	Sulfur dioxide ($\mu\text{g}/\text{m}^3$)	Nitrogen dioxide ($\mu\text{g}/\text{m}^3$)
Argentina	Córdoba City	1294	97	–	97
Brazil	São Paulo	16,533	86	43	83
	Rio de Janeiro	10,181	139	129	–
Canada	Toronto	4319	36	17	43
	Montreal	3320	34	10	42
	Vancouver	1823	29	14	37
Chile	Santiago	4891	–	29	81
Colombia	Bogotá	6079	120	–	–
Cuba	Havana	2,241	–	1	5
Ecuador	Guayaquil	1831	127	15	–
	Quito	1298	175	31	–
Mexico	Mexico City	16,562	279	74	130
United States	New York	16,332	–	26	79
	Los Angeles	12,410	–	9	74
	Chicago	6844	–	14	57
Venezuela	Caracas	3007	53	33	57

Most of the Third World megacities (those with populations greater than 10 million people) experience similar problems. Air quality in Cairo, Bangkok, Jakarta, Bombay, Calcutta, New Delhi, Shanghai, Beijing, São Paulo, and many lesser known urban areas regularly reach dangerous levels. In the following sections, the most important problems of the atmospheric environment across the Earth are presented briefly.

North America

Electric power plants are the major source of toxic air pollutants in North America, accounting for almost half of all industrial air emissions in 2001 (CEC, 2004). According to the data provided by industrial facilities, 46 of the top 50 air polluters in North America were power plants. The sector is responsible for the 45% of the 755,502 t of toxic air releases in 2001, with hydrochloric and sulfuric acids being most commonly released from the burning of coal and oil. Power plants also accounted for 64% of all mercury emissions to the air. However, air quality in Canada and the United States shows the clearest trend of improvement among all environmental categories during the last two decades. The reports predicting that there would be a sharp decline in air quality after the signing of the North America Free Trade Agreement (NAFTA) were incorrect. For example, The Environmental Implications of Trade Agreements, released by the Ontario Ministry of Environment and Energy in 1993, predicted that pollutants such as sulfur dioxide would increase by more than 4.5% annually in North America as a direct result of NAFTA. However, data from Environment Canada, the United States, and the Organization for Economic Cooperation and Development (OECD) show that sulfur dioxide levels in North

Table 1.8

The concentrations of various pollutants in the atmosphere in various cities in Asia, in 1995

Country	City	City population ($\times 1000$)	Total suspended particulates ($\mu\text{g}/\text{m}^3$)	Sulfur dioxide ($\mu\text{g}/\text{m}^3$)	Nitrogen dioxide ($\mu\text{g}/\text{m}^3$)
China	Shanghai	13,584	246	53	73
	Beijing	11,299	377	90	122
	Tianjin	9415	306	82	50
India	Bombay	15,138	240	33	39
	Calcutta	11,923	375	49	34
	Delhi	9948	415	24	41
Indonesia	Jakarta	8621	271	–	–
Iran, Islamic Rep.	Tehran	6836	248	209	–
Japan	Tokyo	26,959	49	18	68
	Osaka	10,609	43	19	63
	Yokohama	3178	–	100	13
Korea, Rep.	Seoul	11,609	84	44	60
	Pusan	4082	94	60	51
	Taegu	2432	72	81	62
Malaysia	Kuala Lumpur	1238	85	24	–
Philippines	Manila	9286	200	33	–
Russian Federation	Moscow	9269	100	109	–
	Omsk	1199	100	9	30
	Singapore	Singapore	2848	–	20
Thailand	Bangkok	6547	223	11	23
Turkey	Istanbul	7911	–	120	–
	Ankara	2826	57	55	46
	Izmir	2031	–	–	–
Ukraine	Kiev	2809	100	14	51

Table 1.9

The concentrations of various pollutants in the atmosphere in various cities in Africa, in 1995

Country	City	City population ($\times 1000$)	Total suspended particulates ($\mu\text{g}/\text{m}^3$)	Sulfur dioxide ($\mu\text{g}/\text{m}^3$)	Nitrogen dioxide ($\mu\text{g}/\text{m}^3$)
Egypt, Arab Rep.	Cairo	9690	–	69	–
Ghana	Accra	1673	137	–	–
Kenya	Nairobi	1810	69	–	–
South Africa	Capetown	2671	–	21	72
	Johannesburg	1849	–	19	31
	Durban	1149	–	31	–

Table 1.10

The concentrations of various pollutants in the atmosphere in various cities in Australia and New Zealand, in 1995

Country	City	City population ($\times 1000$)	Total suspended particulates ($\mu\text{g}/\text{m}^3$)	Sulfur dioxide ($\mu\text{g}/\text{m}^3$)	Nitrogen dioxide ($\mu\text{g}/\text{m}^3$)
Australia	Sydney	3590	54	28	–
	Melbourne	3094	35	0	30
	Perth	1220	45	5	19
New Zealand	Auckland	945	26	3	20

America are continuing to fall. These countries are an excellent proof of the fact that economic growth can keep up with environmental protection through appropriate legislation and application of clean technologies.

Latin America

Air pollution in Latin America is a great problem in the major cities of this region, i.e. Mexico City (Mexico), Rio de Janeiro (Brazil), São Paulo (Brazil), and Buenos Aires (Argentina). Mexico City and Santiago (Chile) are among the most polluted cities in the world. Almost 70% of the population lives in urban areas and suffers high concentration levels of various pollutants. The major causes of air pollution are population growth, industrialization, and increased vehicle use. The situation is so severe that the health effects associated with air pollution are evident. In 1992, it was estimated that over 27 million people in Latin America were constantly exposed to high levels of particulate air pollution, which led to approximately 4000 cases of premature mortality each year. Indeed, the air is so polluted in these cities that they are slowly becoming uninhabitable. Despite the measures taken (introduction of unleaded gasoline, limitation of private car use), urban air pollution continues to have a severe effect on the people. If drastic measures are not taken, the day will not be too long before we see the first environmental migrants.

Asia

Half the world's population lives in urban areas in Asia. Although several attempts have been made to address air pollution in Asia, much progress needs to be made to deal with the issue of urban air quality in Asian megacities (cities with population over 10 millions). Urban air pollution in Beijing, Delhi, and Jakarta has worsened because of population growth, increased industrialization, and automobiles. The impact on public health is considerable; approximately 20–30% of all respiratory diseases are associated with air pollution.

Specifically, rapid urbanization, with the associated growth in industry and transportation systems, has increased regional concerns with regard to emissions of sulfur dioxide and nitrogen oxides. According to estimations for the year 2000, sulfur dioxide emissions in Asia surpassed the emissions of North America and Europe combined. The primary man-made source of sulfur and nitrogen in the Asia-Pacific region is fossil fuel combustion in

the energy, industry, and transportation sectors. The quality of air has deteriorated in virtually every Asian city, except for those in the Republic of Korea. The pollutant levels in these cities exceed WHO guidelines. Acid rain is another important problem in Asia. An example is the damage caused to the historic Taj Mahal in India by the local foundries, which used to burn fuel. Similarly, in China, acid rain has damaged metal structures and concrete works in cities of Chongqing and Guiyan, where SO₂ emissions are high. Weather patterns in Asia facilitate transboundary pollution. The potential was evident in the recent Indonesian forest fires. The area affected by the air pollutants from the fire spread for more than 3200 km, east to west, covering six Asian countries and affecting around 70 million people. In the Malaysian state of Sarawak, the air pollution index hit record levels of 839 (levels of 300 are equivalent to smoking 80 cigarettes a day and are officially designated as “hazardous”).

Africa

The African continent is climatically diverse. Humid tropical conditions prevail in Western and Central Africa and in the Western Indian Ocean islands; most Southern African countries experience arid and semiarid conditions, while semideserts and deserts are features of Northern Africa. The region experiences a high degree of variability and uncertainty in climatic conditions. This continent is believed to be the most vulnerable region to the impacts of climate change. In comparison to other regions, African countries emit negligible amounts of air pollutants and anthropogenic greenhouse gases. For example, Africa contributes less than 3.5% of global emissions of CO₂. Nevertheless, anthropogenic atmospheric pollution is a problem in Northern and Southern Africa, and in some large cities, mainly due to the lack of up-to-date technology.

Currently, 38% of Africa’s population lives in urban areas, but this percentage rises continuously, with a projection to reach 54% by 2030. The increasing overpopulation leads to a rise in vehicle emissions and greater industrialization, which in turn result in air quality deterioration in the continent. In many countries, the use of leaded gasoline is still widespread and vehicle emission controls are simply nonexistent. Dust from the Sahara carrying pollutants has been detected in south Europe and even in the eastern part of the United States. South Africa, Nigeria, and Egypt are the largest emitters of greenhouse gases in Africa.

Australia

Air pollution problems in Australia are insignificant compared to cities such as Mexico City and Athens. Australia is not densely inhabited and, being surrounded by oceans, does not import pollution from other countries. Moreover, various initiatives have been taken for controlling the sources of air pollution. Specifically, the use of incinerators has been considerably reduced, backyard burning has been banned, and power stations have been located far from large cities. Regarding motor vehicles, the most significant air pollution threat in Australia, new cars have been equipped with catalytic converters in their exhaust systems since 1986. However, in many cities in Australia, the combination of typical coastal conditions (the major urban airsheds are located on coastal strips with mountain ranges nearby), a high sunlight flux, and a large fleet of motor vehicles along with traffic congestion will continue to give a finite number of occasions each year when photochemical smog or particulate matter will be formed. These conditions can be considerably exacerbated by the

occurrence of bushfires or hazard reduction burning in the vicinity of the cities. Hopefully, even then, the current standards are not actually expected to be exceeded (Australian Academy of Technological Sciences and Engineering, 1997).

1.1.2 Water pollution

Water covers 71% of the planet’s surface, mainly in the form of salty water in the oceans. It is a vital substance for supporting life on Earth. For example, a tree contains 60% water, most animals are composed of about 65% water, while our bodies contain around 55% water (Tyler Miller, 1999). Everyone needs fresh water everyday to cover the daily demand in food, domestic use, etc. Fresh water is used in agriculture, construction, transport, the chemical industry, and numerous other activities of human beings. The use of abstracted water in Europe is presented in Figure 1.2. It has to be noted that in many regions on Earth, where the struggle for existence of population is continuous, it is the lack of fresh and clean water that limits the production of food. According to the United Nations, the first priority of poor countries, especially in Africa, should be not financial support or technological knowledge but clean water supply to the population.

Unfortunately, despite the fact that most of the planet is covered by water, only a small amount of this water is available as fresh water. Almost 97.5% of the total is in oceans in the form of salty water and is not suitable for drinking, watering, or industrial use as is. The remaining 2.5% is fresh water. However, not even that small amount is easily accessible or exploited, because it is stored as ice on the poles and on mountaintops. Furthermore, a significant amount of the rest lies so deep in the ground that it is very difficult to extract. In Figure 1.3, the distribution of water on Earth is presented. According

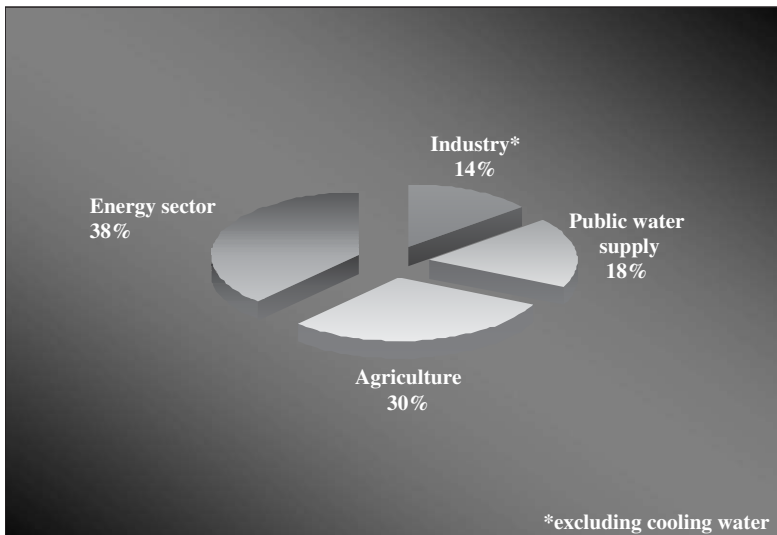


Figure 1.2 The use of abstracted water in Europe (Nixon *et al.*, 2004).

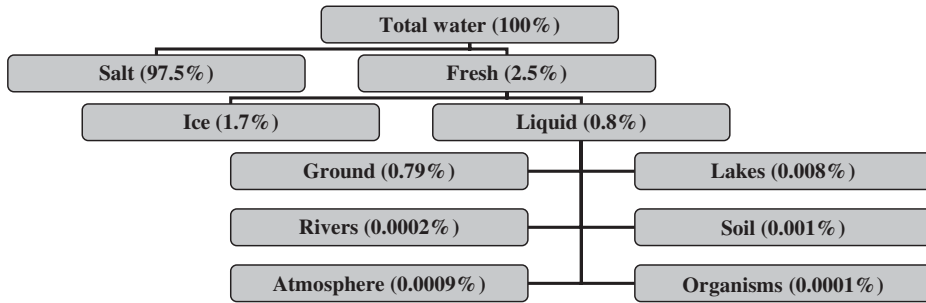


Figure 1.3 Water on Earth (Nixon *et al.*, 2004).

to the EC, less than 1% of the planet's water is available for human consumption and more than 1.2 billion people in the world have no access to safe drinking water.

Fresh water is purified and reallocated through the hydrological cycle in nature. Nowadays, this natural process is inadequate due to human activities, and specifically because of the thoughtless wasting of water and discharge of various pollutants into the aquatic environment.

These activities of human beings threaten not only the fresh water supply but also marine life. Moreover, with an ever-increasing world population, the situation is expected to worsen in the near future, especially in densely populated or industrial areas. These areas consume large amounts of fresh water, and at the same time produce and release large amounts of wastewater into the environment.

Water-quality deterioration can be attributed to water pollution or contamination. Water pollution is generally defined as any physical, chemical, or biological alteration in water quality that has a negative impact on living organisms. In the stricter sense, pollution can be defined as the transfer of any substance to the environment. However, there is a tolerance limit for each pollutant, since zero-level pollution is economically and technically unpractical. The most important kinds of water quality deterioration are the following.

Thermal Pollution

The discharge of warm wastewaters into a surface receiver may have many adverse effects on aquatic life. The increase in temperature results in a decrease in the oxygen concentration in water and the elimination of the most sensitive species. Temperature changes may also cause changes in the reproductive periods of fishes, growth of parasites and diseases, or even thermal shock to the animals found in the thermal plume.

Biological Pollution by Oxygen-Demanding Wastes

The release of oxygen-demanding wastes into water (mainly biodegradable organic compounds) results in the decrease in oxygen dissolved in water due to its consumption by the aquatic microorganisms that decay the organic pollutants. A minimum of 6 mg of oxygen per liter of water is essential to support aquatic life. A few species, like carp, can survive in low-oxygen waters. Each biodegradable waste is characterized by the

biological oxygen demand (BOD), which is a measure of the amount of dissolved oxygen needed by aquatic microorganisms for the degradation of waste.

Pollution by Persistent Organic Chemicals (POPs)

Besides biodegradable organic compounds, there are also organic substances that show great resistance and high lifespan in the environment, thus constituting a long-term danger to life. Dioxins, polychlorinated biphenyls (PCBs), and pesticides (DDT and others) are man-made compounds that remain intact for months in the environment. Consequently, people and animals at the top of the food chain eventually consume food containing these compounds. DDT, a popular compound that helped in the elimination of malaria, was proved to have many adverse effects on natural life. Paul Muller, who discovered the effectiveness of DDT as an insecticide in 1939 was awarded the Nobel Prize in medicine and physiology in 1948 for this discovery. Today, DDT is banned in most developed countries.

Eutrophication by Nitrates and Phosphorus

Eutrophication is the rapid depletion of dissolved oxygen in a body of water because of an increase in biological productivity. It is connected to the excess presence of plant nutrients in the environment, mainly nitrates and phosphorus. These compounds are connected to the excessive use or production of fertilizers.

Inorganic Pollutants

Metals, nonmetals, and acids/bases released by human activities severely deteriorate water quality, since they are toxic even at concentrations of parts per million. It has to be noted that heavy metals are extremely dangerous to human health and aquatic life. But what is worse is that there is no cycle of natural treatment of these substances. Inevitably, heavy metals remain intact in the environment and finally, they are accumulated in the food chain (bioaccumulation).

Unless we take the right course of action, problems associated with both quality and quantity of water are going to be encountered, even in regions that seem to have sufficient amounts of clean water today. After the disputes and wars over the possession of oil in the past, water may be the next conflict territory between adjacent countries, even in Europe. According to the EC, 20% of all surface water in the European Union is seriously threatened with pollution. Furthermore, water is far from being evenly distributed in Europe and this is one major reason for resource problems. For example, whereas freshwater availability is more than 100,000 m³ per capita per year in Iceland, it is less than 10,000 m³ per capita per year in Switzerland, Portugal, and Spain.

The available water in a country or region depends on the rainfall and on the net result of flows from and to its neighbors, mainly through rivers. For example, in Iceland, Norway, Sweden, Denmark, the United Kingdom, Italy, Spain, France, and Finland, more than 98% of freshwater is generated within the country, whereas in Hungary and the Netherlands more than 50% of freshwater is due to river flows from other countries (Nixon *et al.*, 2004).

So, most European countries rely more on surface water than groundwater. For example, Finland and Lithuania take more than 90% of their total supply from surface waters

and Hungary, Poland, Germany, and Ireland, more than 80%. However, in many European countries, groundwater is the main source for public water supply. In Belgium, less than 40% of the total supply is from surface waters and in Denmark, less than 5%.

We will look into the second leg of the water issue, namely the problems, sources, and pollutants associated with the pollution and contamination of the aquatic environment. Before moving on, it would be useful to examine the current situation in various regions of the world as concerns fresh water pollution (Kraemer *et al.*, 2001).

Europe

In Europe, eutrophication is one of the main water pollution problems, which originates partially from the past European common agricultural policy. The intensive cultivation of land demanded the use of large amounts of fertilizers in a relatively small total land area. Although the situation has improved in the last few years with the phosphorus levels in water being decreased, the presence of nitrates in the aquatic environment is still a problem.

Despite the fact that organic pollution still remains a problem, the steps taken to improve the situation cannot be overlooked. Specifically, the improvement in both wastewater treatment and emission controls has led to a significant decrease in the percentage of heavily polluted rivers, from 24% in the late 1970s to 6% in the 1990s in Western Europe. In contrast, the situation is not exactly the same in the southern member states, since 50% of the population is not yet connected to sewage treatment operations.

Another problem in relation to aquatic receivers in northern and eastern Europe is acidification, whereas elevated concentrations of POPs are found near large European cities and industrialized areas.

Eastern European countries involved in the accession process during the last few years have a lot to achieve in meeting the established water quality criteria set in EU legislation. In the Czech Republic and Slovakia, 57% of the drinking water in 1990 did not meet the quality criteria, whereas 70% of all water may be unacceptable for drinking in Poland. In the Russian Federation, industry, agriculture, and municipal landfills have contributed to the pollution of groundwater in 1400 areas. Moreover, high PCB concentrations have been detected in rivers and the levels of POPs draining into the Arctic may be higher than those found in urban America or Western Europe, in some cases.

North America

Agrochemical run-off is the main source of water pollution in the agricultural regions and has deteriorated the quality of groundwater in many areas. Over the past decade, however, there has been an improvement in the drinking water quality, especially in the United States, due to stricter water protection regulations in force. Nevertheless, industrialization and economic growth have resulted in new pollutants being introduced into water supplies. The case of the pollution of groundwater with MTBE (methyl *tert*-butyl ether) in many areas across the United States is characteristic. MTBE was used extensively in the 1990s as a gasoline additive instead of lead. Its properties (e.g. mobility in the water, low biodegradability) combined with its unsafe storage resulted in serious problems in the quality of drinking water, especially in the State of California.

Latin America

In Latin America, 75% of the population lives in large cities, producing sewage volumes far higher than industrial ones. This high urbanization level combined with the fact that only 2% of domestic sewage is treated causes major problems to water supply and proliferation of pathogenic diseases. The gold mining industry is also a major polluter and is responsible for the presence of mercury in water. The extensive use of pesticides and fertilizers in agriculture poses another threat to water resources in Brazil, Colombia, and Ecuador.

Japan

Despite the strengthening of environmental policies, problems in relation to cadmium and cyanide, dioxin, organic pollution, lake eutrophication, residential sewage, pesticide runoff, industrial discharges, and groundwater contamination by toxics and nitrates also need to be tackled.

Australia and New Zealand

Nitrates and particularly phosphorus remain unacceptably high in Australia. Sedimentation constitutes a problem in both Australia and New Zealand, with the situation improving due to the removal of sheep from steep pastures. Sewage pollution has also been reduced because of the construction of sewage treatment plants.

Asia

The situation is more complex in the region of Asia and the Pacific. Water quality has many enemies there. First, sedimentation constitutes a major cause of pollution in Asian rivers, since sediment loads are four times the world average. Secondly, hazardous and toxic waste deteriorates the water quality. It is noteworthy that lead levels in Asia's surface water are about 20 times higher than those in OECD countries. Thirdly, eutrophication is faced due to the extensive use of fertilizers in the last 30 years. But the list of problems does not end here. Asian rivers contain three times as many bacteria from human waste as the world average. Finally, urbanization and the release of untreated sewage and industrial waste to the environment are expected to cause severe water pollution problems.

Water pollution trends have particularly worsened in China in recent years. The industrial development (as certified from oil demand) and the intensive agriculture (China is the world's largest consumer of synthetic nitrogen fertilizers) pose a threat to water bodies.

Severe water problems are also faced in southeast Asia. For example, Bangladesh and adjacent parts of India suffer from arsenic contamination of groundwater. Specifically, arsenic poisoning of groundwater has affected more than 50% of the total area of Bangladesh. The gradual introduction of arsenic into the food chain is more than a possibility. Nitrate pollution is also a problem in these areas.

The discharge of raw and partially treated wastewater into the environment in the Mashriq subregion (Iraq, Jordan, Lebanon, Syrian Arab Republic, the West Bank, and Gaza) has deteriorated water quality and is a threat to public health.

In the West Bank and Gaza, the list of problems in connection to groundwater includes high pesticide levels, and nitrate concentrations four times the WHO limit. In some central

areas, 5 million m³ of drinking water is transported into the area every year, because groundwater is no longer potable.

1.2 POLLUTANTS AND EMISSION SOURCES

Considerable information about pollutants, emission sources, and treatment techniques has been given in the reference document on best available techniques (BATs) in common wastewater and waste gas treatment released by the European Commission in 2003 (EC, 2003).

1.2.1 Air

The sources of air emissions can be divided into two categories:

- mobile sources, such as vehicles and ships
- stationary sources, such as chemical industries.

The exhaust air emissions are classified as

- ducted emissions—process emissions released through a pipe
- diffuse emissions—emissions that are not released via specific emission points (e.g. emissions during filling storage equipment, emissions from agriculture)
- fugitive emissions—emissions due to leaks

It is easily understood that whereas ducted emissions can be rather easily treated, the other two kinds of emissions can only be prevented or minimized. For example, agricultural emissions are very difficult to control. The main air pollutants are the following.

- ***Carbon Dioxide***

Description: It is a nontoxic gas and the final product of complete combustion. Actually, it is the desirable and inevitable product of combustion. However, it is recognized as the main greenhouse gas, whose increased levels in the atmosphere play a large role in global warming.

Source: Any combustion of fossil fuels. Combustion installations are responsible for 955×10^6 t/yr released into the air and 64.9% of the total emissions from industry in Europe.

Impact: Global warming, climate change.

- ***Sulfur Oxides and other sulfur compounds (H₂S, CS₂, COS)***

Description: Sulfur dioxide (SO₂) is a gas resulting from the combustion of coal, mainly in power plants, and certain types of liquid fuels that contain sulfur. In addition, it is produced during the manufacture of paper and smelting of metals. It may cause respiratory problems and permanent damage to the lungs when inhaled at high levels. It plays a major role in the production of acid rain (EPA site). Carbon disulfide (CS₂) has many industrial

applications. It is released into the air from industries producing, using, or handling CS_2 , sanitary landfills, and natural-gas production and distribution.

Source: Any combustion of sulfur-containing fuels. Combustion installations are responsible for 2.9×10^6 t/yr released into the air and 68.3% of the total emissions from industry in Europe.

Impact: Winter-type smog, acidification.

- ***Nitrogen Oxides (NO_x , N_2O) and other nitrogen compounds (NH_3 , HCN)***

Description: Nitrogen oxides (NO_x) are produced when fuel is burned at high temperatures. The main anthropogenic sources of NO_x are motor vehicles, electric utilities, and other industrial, commercial, and residential sources that burn fuels. Nitrogen oxide (NO) is easily oxidized in the atmosphere to nitrogen dioxide, which reacts with volatile organic compounds in the atmosphere, thus contributing to photochemical smog. Nitrogen dioxide (NO_2) can also react with hydroxyl radicals in the atmosphere forming nitric acid, a major component of acid rain. It can cause lung damage and illnesses of the respiratory system. Nitrous oxide (N_2O) is one of the most drastic compounds in greenhouse effect. Moreover, it is stable for almost 120 years and can reach the stratosphere, where it participates in a reaction cycle catastrophic for ozone. Generally, nitrogen oxides may contribute to the greenhouse effect, acid rain, photochemical smog, and ground-level ozone formation.

Source: Combustion of nitrogen-containing fuels (fuel NO_x) or oxidation of atmospheric nitrogen during combustions at high temperatures. Transport is the main contributor, whereas in the industry sector, combustion installations are responsible for 1.5×10^6 t/yr released to air and 58.3% of the total emissions from industry in Europe.

Impact: Global warming, acidification, photochemical smog, ozone layer depletion.

- ***Incomplete combustion compounds, such as CO and C_xH_y***

Description: Carbon monoxide (CO) is a colorless, odorless, and poisonous gas. It is the product of any incomplete combustion of fossil fuels and many natural and synthetic products. After it is inhaled, it enters the blood through the lungs and reacts with hemoglobin, reducing the capacity of blood to carry oxygen to cells, tissues and organs. The body's parts need oxygen for energy, so high-level exposures to carbon monoxide can cause serious health effects, with death possible from massive exposures. Symptoms of exposure to carbon monoxide can include vision problems, reduced alertness, and general reduction in mental and physical functions. Carbon monoxide exposures are especially harmful to people with heart, lung, and circulatory system diseases. It may cause chest pain, vision problems, difficulties in the learning ability of young children, and generally reduction in mental and physical functions. It also has a significant role in ozone production in the troposphere. Compounds in of the form C_xH_y are hydrocarbons, which may be unburned fuel compounds or produced by incomplete combustion. Their impact on environment and public health depends on the exact structure of the compound.

Source: Road transport is the main source of carbon monoxide and unburned hydrocarbons in the atmosphere. Among industrial processes, the metal industry is responsible for 2.8×10^6 t/yr released into the air and 71.2% of the total emissions from industry in Europe.

Impact: Health problems like chest pain and vision problems, photochemical smog.

- ***Volatile Organic Compounds (VOCs) and organosilicon compounds***

Description: Volatile organic compounds are released from burning fuels (gasoline, oil, wood coal, natural gas) and volatile liquid chemicals, such as solvents, paints, and glues. Automotive vehicles are also an important source of VOCs. The list of VOCs is lengthy and includes chemicals such as benzene, toluene, and methylene chloride. Depending on the specific compound, they can take part in ozone formation or may cause serious health problems such as cancer and other undesirable effects.

Source: Road transport is the main source, whereas mineral oil and gas refineries are responsible for 0.2×10^6 t/yr released into the air, reaching 39.2% of the total industrial emissions.

Impact: Depends on the exact compound; from health effects (cancer) to photochemical smog formation.

- ***Particulate Matter (such as dust, soot, alkali, and heavy metals)***

Description: The sources of particulate matter are many: burning of wood, diesel, and other fuels, industrial plants, and agriculture. It leads to decrease in visibility in urban areas and poses a threat to health, since it enters the organism through the respiratory system. It has to be noted that compounds of low volatility that are formed secondarily in the atmosphere may be condensed on particulates, and as a result, the inhaled particles constitute a complex mixture of hazardous chemical compounds. The highest concentrations of airborne metal particles occur near mines, smelters, and metal processing/heavy engineering works. These particles are so small that they can be carried enormous distances by the wind. Mercury in particular, which largely occurs in gaseous form in the atmosphere, can be dispersed a very long way indeed.

Source: Road transport and the energy sector. Combustion installations are responsible for 77×10^3 t/yr in the atmosphere, this being 47.9% of the total emissions from industry in Europe.

Impact: Respiratory diseases, winter-type smog.

It is easily concluded from the above that road transport and combustion installations are the main sources of air pollutants. In Table 1.11, the releases of the main air pollutants in connection to the main activities as covered in EPER are presented (transport is not covered).

1.2.2 Water

The sources of water pollution are divided into

- point sources, such as chemical industries and human communities
- nonpoint sources, such as agricultural activities and landfill leachates.

Point sources are mainly responsible for the pollution of surface waters (rivers, lakes, seas), whereas nonpoint sources mainly contribute to the pollution of groundwater resources. Moreover, releases from point sources can be treated by wastewater treatment plants, whereas nonpoint source releases can only be minimized.

Table 1.11

The releases of the main air pollutants from the industrial sector in Europe (2001)

Compound	t/yr	Main source (% contribution)
Carbon dioxide	955×10^6	Combustion installations (64.9%)
Sulfur oxides	2.9×10^6	Combustion installations (68.3%)
Carbon monoxide	2.8×10^6	Metal industry (71.2%)
Nitrogen oxides	1.5×10^6	Combustion installations (58.3%)
Methane	1.4×10^6	Installations for the disposal of nonhazardous waste and landfills (89.8%)
Volatile organic compounds	0.2×10^6	Mineral oil and gas refineries (39.2%)
Ammonia	85×10^3	Installations for poultry, pigs, or sows (76.6%)
Particulate matter	77×10^3	Combustion installations (47.9%)
Nitrous oxide	54×10^3	Basic inorganic chemicals or fertilizers (39.5%)
Fluorine	6.4×10^3	Combustion installations (53.3%)
Benzene	2×10^3	Mineral oil and gas refineries (52.1%)
Polyaromatic hydrocarbons	85.2	Installations for surface treatment or products using organic solvents (32.9%)
Mercury	7.4	Combustion installations (31%)

The major amount of wastewater in the chemical industry does not come from chemical reaction steps, but from the subsequent physicochemical processing of the final reaction mixture. The most important pollutants of water are the following.

- **NH_4^+ , NO_3^- , NO_2^- , PO_4^{3-} ions**

Description: These ions enter the environment in the form of salts. Their presence is due to the extensive use of fertilizers as a result of the intensification of agriculture. As they are plant nutrients, they can lead to eutrophication—the enrichment of water by nutrients, causing an accelerated growth of algae and higher forms of plant life, leading to an undesirable disturbance in the balance of organisms present in the water and in the quality of the water.

Source: Agriculture is the main source, whereas the basic inorganic chemicals and fertilizer production activities are responsible for 29 and 25% of the total direct industrial releases of nitrogen and phosphorus, respectively, into water.

Impact: Eutrophication, drinking water quality deterioration.

- **Heavy metals**

Description: Heavy metals are generally considered to be those whose density exceeds 5 g/cm^3 . Characteristic examples of heavy metals are cadmium (Cd), mercury (Hg), and lead (Pb) (Green *et al.*, 2003). Cadmium is found in the environment due to general waste-disposal and industrial activities, including the mining industry, metal industry, coating/electroplating industry, production and deposition of batteries, burning of fossil fuels, the use of phosphate fertilizers, waste incineration, leaching from waste deposits, etc. Mercury is found in the environment due to its use in various products, e.g. batteries and

electronics. It can be found in four forms in the environment: methyl mercury, di- and monovalent ionic mercury, and metallic mercury. The main anthropogenic sources of lead in the environment are from general waste-disposal and industrial activities. Heavy metals can also be found naturally in the environment.

Source: Industrial activities, waste disposal. The metal industry is responsible for 41.68 t Pb, 8.13 t Cd, 864.25 t Cr, 45.77 t Cu, 71.55 t Ni, and 5.09 t As releases directly into water, annually.

Impact: Immediate threat to aquatic life and human population.

- ***Inorganic salts and acids***

Description: Inorganic salts come from acid mine drainage, industrial processes, and drainage flow from irrigated areas. Salt accumulation on irrigated soils causes the most damage and loss in this category. A high proportion of sodium in irrigation water supply affects plant life adversely. Acids may come from industrial activities or from acid rain and cause lakes and streams to become acidic and unsuitable for many fish.

Source: Mining industry, drain-off water.

Impact: Acidification.

- ***Oil compounds***

Description: Petroleum resulting from oil spills often pollutes water bodies. Large-scale accidents are also an important cause of pollution along shore lines. The most well-known example is the *Exxon Valdez* oil spill.

Source: Oil spills. The basic organic chemicals industry is responsible for 82.53 t/yr of benzene, toluene, ethyl benzene, and xylene (BTEX) direct releases into water.

Impact: Water quality deterioration, blocking sunlight from entering water bodies.

- ***Organic compounds***

Description: Numerous compounds are included in this category. Research is focused on persistent organic compounds such as dioxins and polychlorinated biphenyls. PCBs are a group of theoretically 209 different compounds that are man-made, but now found all over the Earth due to their persistence and relative volatility. Due to their stability, they have been extensively used in many industrial applications (as hydraulic fluids or cooling liquids) and in open systems (as lubricants or paints). Another significant type of compounds included in this category is phenols. Phenols and similar compounds are primarily present in refinery and petrochemical wastewaters and are known to have a significant negative impact on marine life and human health, as they are well-known carcinogens (IRIS, 1998). Furthermore, phenols cause an increase in oxygen demand in water, and they also impart a taste to drinking water at very low concentrations of their chlorinated derivatives. Primary sources of phenols are in wastewaters from benzene-refining plants, oil refineries, coke plants, chemical operations, and plastics production. Another example is aniline (C₆H₇N), which is a colorless oily liquid and is highly toxic. It is used in the manufacture of antioxidants and vulcanization accelerators for the rubber industry, and the manufacture of dyes and pharmaceuticals (Sharp, 1990; IRIS, 1998). Another common contaminant type found in wastewater is dyes (Forgacs *et al.*, 2004). Synthetic dyes are extensively used in industry, e.g. textile manufacturing, leather tanning, paper production, and food technology.

Source: Agriculture, industrial processes. Specifically, industrial plants for the production of pulp from timber or other fibrous materials, and paper or board production are responsible of 70% of the total organic carbon released directly into water from industry per year.

Impact: Depends on the exact type of the pollutants; from adverse long-term effects to immediate danger to human and biotic life.

- ***Pathogenic Microorganisms***

Description: Pathogenic microorganisms include bacteria, viruses, and protozoans.

Source: Untreated sewage, storm drains, run-off from farms, and particularly, boats that dump sewage.

Impact: Many adverse effects on health. Typhoid, dysentery, and skin diseases are among the possible health effects.

Commonly, wastewater contains numerous compounds and its exact composition is very difficult to determine or is even unknown, and therefore, its impact on the environment is characterized by

- the concentration of specific substances, such as NH_4^+ , NO_3^- , NO_2^- , and PO_4^{3-} ions, and heavy metals
- sum parameters, such as TSS (total solids suspended), BOD (biological oxygen demand), COD (chemical oxygen demand), pH, conductivity and temperature.
- its toxicity to organisms in the receiver
- its hydraulic load.

In Table 1.12, the direct releases of the most important pollutants into water are presented in association with the corresponding main industrial source. For purposes of comparison, it is useful here to recall that road transport and combustion installations, mainly of the

Table 1.12

The releases of the main pollutants released directly into water from the industrial sector in Europe (2001)

Compound	t/yr	Main source
Phenols	1,419,344	Basic inorganic chemicals or fertilizers (47%)
Total organic carbon	246,524	Industrial plants for pulp from timber or other fibrous materials, and paper or board production (70%)
Nitrogen	22,317	Basic inorganic chemicals or fertilizers (29%)
Phosphorus	1662	Basic inorganic chemicals or fertilizers (25%)
Chromium	864	Metal industry (87%)
BTEX	82.5	Basic organic chemicals (56.1%)
Nickel	71.5	Metal industry (45%)
Copper	45.8	Metal industry (23%)
Lead	41.7	Metal industry (40%)
Polycyclic aromatic hydrocarbons	10.3	Metal industry (74%)
Cadmium	8.1	Metal industry (66%)
Arsenic	5.1	Metal industry (22%)
Mercury	0.5	Metal industry (23%)

energy sector, are the most important sources of air pollutants. In the case of water bodies, it is obvious that agriculture and the metal industry, plus the activities in the production of inorganic chemicals and fertilizers, constitute the major polluters.

1.3 TREATMENT METHODS

The minimization of the releases into the environment can be largely achieved by

- pollution prevention measures
- waste treatment (end-of-pipe techniques).

The first approach may involve cleaner synthesis processes, improved technology, recycling of residues, improved use of catalysts, and generally, every technique integrated into the process that leads to less waste; whereas the second one is an end-of-pipe treatment of the waste that is inevitably produced by a chemical process. Both approaches have to be combined so that our releases into the environment are as minimal and harmless as possible.

Waste-treatment techniques are classified by the type of contaminant. The main techniques concerning waste gas treatment are the following.

VOCs and inorganic compounds: membrane separation, condensation, adsorption, wet scrubbing, biofiltration, bioscrubbing, biotrickling, thermal oxidation, catalytic oxidation, and flaring.

Particulate matter: separator, cyclone, electrostatic precipitator, wet dust scrubber, fabric filter, catalytic filtration, two-stage dust filter, absolute filter, high-efficiency air filter, and mist filter.

Gaseous pollutants in combustion exhaust gases: dry sorbent injection, semidry sorbent injection, wet sorbent injection, selective noncatalytic reduction of NO_x (SNCR), selective catalytic reduction of NO_x (SCR).

In Table 1.13, the conditions for the application of some treatment processes are shown.

Table 1.13

Evaluation of alternative treatment processes used to control industrial vapor-phase pollutants

Case	Activated carbons	Thermal oxidation	Scrubbers	Particulate filters	Catalytic oxidation
Low VOC levels	✓		✓		
High VOC levels		✓	✓		✓
Continuous load	✓	✓	✓	✓	✓
Intermittent loads	✓			✓	
Halogenated organics	✓				
$T > 150$ °F		✓	✓		✓
$T < 150$ °F	✓		✓	✓	
High flows	✓		✓		
Low flows	✓	✓	✓		✓
High humidity		✓		✓	✓
Inorganic particles				✓	

The main wastewater treatment techniques are

Separation or clarification techniques: grit separation, sedimentation, air flotation, filtration, microfiltration and ultrafiltration, and oil–water separation.

Physico-chemical treatment techniques: precipitation, sedimentation, air flotation, filtration, crystallization, chemical oxidation, wet air oxidation, super-critical water oxidation, chemical reduction, hydrolysis, nanofiltration, reverse osmosis, adsorption, ion exchange, extraction, distillation, rectification, evaporation, stripping, and incineration.

Biological treatment techniques: anaerobic digestion processes, aerobic digestion processes, nitrification, denitrification, and central biological wastewater treatment.

Adsorption, ion exchange, and catalysis share a great portion of environmental applications, as shown in the next section, and more extensively, in Chapter 2. Specifically, adsorption and catalysis are extensively used for the removal or destruction of air pollutants in gas streams as well as for purifying wastewaters or fresh water. Ion exchange has a special position among other techniques in the removal of heavy metals from wastewater.

1.4 ENVIRONMENTAL APPLICATIONS OF ADSORPTION, ION EXCHANGE, AND CATALYSIS

Adsorption, ion exchange, and catalysis are discussed in this book. The first two are among the end-of-pipe techniques, whereas catalysis has a role to play in either preventing pollution during the process or as an end-of-pipe technique of waste treatment. Moreover, ion exchange is mainly used in wastewater treatment, whereas adsorption and catalysis can be found in both wastewater and gas management. Specifically, ion exchange is one of the best available techniques (BAT) suggested by EC for heavy metal and inorganic salts removal from wastewaters. As shown in Table 1.12, metal industry is the major source of metal releases into the environment and ion exchange can be employed as the main pollution abatement technology. We should again mention that nature does not have any efficient way of coping with these substances, and as a result, their discharge into the environment should be minimized. Adsorption is suggested as the BAT for both the minimization of contaminants in water that are unsuitable for biological treatment and the removal of VOCs and inorganic compounds from normal waste gas streams. Catalysis is also considered as the BAT for the destruction of water pollutants that are resistant to biological treatment (as catalytic wet-air oxidation) and for the oxidation of VOCs and inorganic compounds in gas streams (as catalytic oxidation). Generally, VOCs, sulfur oxides, nitrogen oxides, and various forms of hydrocarbons can be effectively treated by means of these processes.

MULTIPLE CHOICE QUESTIONS

1. *CFCs are involved in*
 - (a) photochemical smog
 - (b) ozone depletion
 - (c) greenhouse effect
 - (d) both ozone depletion and greenhouse effect

2. *Nitrogen Oxides are involved in*
 - (a) photochemical smog
 - (b) acid rain formation
 - (c) greenhouse effect
 - (d) all of the above
3. *N₂O participates in*
 - (a) greenhouse effect and ozone depletion
 - (b) greenhouse effect
 - (c) ozone depletion
 - (d) photochemical smog
4. *Comparing pollution from primary pollutants and secondary pollutants,*
 - (a) primary pollutants are generally easier to treat
 - (b) secondary pollutants are generally easier to treat
 - (c) it depends on the case
 - (d) both kinds of pollution are equally difficult to treat
5. *During combustion NO_x may come from*
 - (a) nitrogen in fuels
 - (b) nitrogen in the atmosphere
 - (c) both of the above
 - (d) none of the above
6. *Generally, you would connect Athens and London, respectively, to which of the following types of air pollution:*
 - (a) photochemical smog and winter-type smog
 - (b) winter-type smog and photochemical smog
 - (c) winter-type smog and winter-type smog
 - (d) photochemical smog and photochemical smog
7. *The main consumer of fresh water in Europe is*
 - (a) the public
 - (b) agriculture
 - (c) industry
 - (d) energy sector
8. *Nitrates and phosphorus*
 - (a) are among inorganic pollutants
 - (b) cause eutrophication
 - (c) are persistent pollutants
 - (d) are accumulated in the food chain
9. *Eutrophication is mainly attributed to*
 - (a) agriculture
 - (b) organic industry
 - (c) refineries
 - (d) metal industry

10. *Water pollution sources are divided into*
 - (a) diffuse and ducted sources
 - (b) point and nonpoint sources
 - (c) mobile and stationary sources
 - (d) point and diffuse sources
11. *The main source of air pollution is*
 - (a) road transport
 - (b) metal industry
 - (c) refineries
 - (d) road transport and combustion installations
12. *Among industries, the metal industry is the main source of*
 - (a) carbon monoxide
 - (b) carbon dioxide
 - (c) CFCs
 - (d) NO_x
13. *The main sources of water pollutants are*
 - (a) combustion installations and metal industry
 - (b) agriculture and combustion installations
 - (c) agriculture, metal industry, and basic inorganic chemicals industry
 - (d) metal industry and combustion installations
14. *Acidification is a problem*
 - (a) that affects regions up to 100 km
 - (b) that may appear on both regional and transboundary levels
 - (c) faced all over the world
 - (d) of specific areas

ANSWERS TO MULTIPLE CHOICE QUESTIONS

1. (d) both ozone depletion and greenhouse effect
2. (d) all of the above
3. (a) greenhouse effect and ozone depletion
4. (a) primary pollutants are generally easier to treat
5. (c) both of the above
6. (a) photochemical smog and winter-type smog
7. (d) energy sector
8. (b) cause eutrophication
9. (a) agriculture
10. (b) point and nonpoint sources
11. (d) road transport and combustion installations
12. (a) carbon monoxide
13. (c) agriculture, metal industry, and basic inorganic chemicals industry
14. (b) that may appear on both regional and transboundary levels

Adsorption, Ion Exchange, and Catalysis

2.1 DEFINITIONS

2.1.1 Adsorption

The term “sorption” is used to describe every type of capture of a substance from the external surface of solids, liquids, or mesomorphs as well as from the internal surface of porous solids or liquids (Skoulikides, 1989). Depending on the type of bonding involved, sorption can be classified as follows.

(a) *Physical sorption*. In physical sorption (or physisorption), no exchange of electrons is observed; rather, intermolecular attractions between favorable energy sites take place and are therefore independent of the electronic properties of the molecules involved. Physisorption is characterized by interaction energies comparable to heats of vaporization (condensation). The adsorbate is held to the surface by relatively weak van der Waals forces and multiple layers may be formed with approximately the same heat of adsorption. The heat of adsorption for physisorption is at most a few kcal/mole and therefore this type of adsorption is stable only at temperatures below 150 °C.

(b) *Chemical sorption*. Chemical sorption (or chemisorption) involves an exchange of electrons between specific surface sites and solute molecules, and as a result a chemical bond is formed. Chemisorption is characterized by interaction energies between the surface and adsorbate comparable to the strength of chemical bonds (tens of kcal/mol), and is consequently much stronger and more stable at high temperatures than physisorption. Generally, only a single molecular layer can be adsorbed.

(c) *Electrostatic sorption (ion exchange)*. This is a term reserved for Coulomb attractive forces between ions and charged functional groups and is commonly classified as ion exchange.

The most important characteristics of physical and chemical sorption are presented in Table 2.1.

The term “adsorption” includes the uptake of gaseous or liquid components of mixtures from the external and/or internal surface of porous solids. In chemical engineering, adsorption is called the separation process during which specific components of one phase of a fluid are transferred onto the surface of a solid adsorbent (McCabe *et al.*, 1993).

Table 2.1

Physical versus chemical sorption		
	Chemisorption	Physisorption
Temperature range over which adsorption occurs	Virtually unlimited; however, a given molecule may be effectively adsorbed only over a small range	Near or below the condensation point of the gas (e.g. $\text{CO}_2 < 200 \text{ K}$)
Adsorption enthalpy	Wide range, related to the chemical bond strength—typically 40–800 kJ/mol	Related to factors like molecular mass and polarity but typically 5–40 kJ/mol (i.e. \sim heat of liquefaction)
Nature of adsorption	Often dissociative and may be irreversible	Nondissociative and reversible
Saturation uptake	Limited to one monolayer	Multilayer uptake is possible
Kinetics of adsorption	Very variable; often is an activated process	Fast, because it is a nonactivated process

When the species of the adsorbate travel between the atoms, ions, or the molecules of the adsorbent, the phenomenon of “absorption” takes place and this discriminates absorption from the main phenomenon of adsorption that takes place on the interface.

The adsorption of various substances from solids is due to the increased free surface energy of the solids due to their extensive surface. According to the second law of thermodynamics, this energy has to be reduced. This is achieved by reducing the surface tension via the capture of extrinsic substances.

Consider a molecule above a surface with the distance from the surface being normal to the surface. There are two competitive types of influence occurring: (a) repulsion between the cloud of electrons in the atoms that form the surface and those of the molecule and (b) van der Waals nuclear attraction force. The nuclear attraction has a much shorter radius of influence and as a result of the balance of these two forces, there is a “well” in the potential energy curve at a short distance from the surface, as shown in Figure 2.1. Molecules or atoms that reach this “well” are trapped or “adsorbed” by this potential energy “well” and cannot escape, unless they obtain enough kinetic energy to be desorbed.

The surface can be characterized either as external when it involves bulges or cavities with width greater than the depth, or as internal when it involves pores and cavities that have depth greater than the width (Gregg and Sing, 1967). All surfaces are not really smooth and they exhibit valleys and peaks at a microscopic level. These areas are sensitive to force fields. In these areas, the atoms of the solid can attract atoms or molecules from a fluid nearby.

The most important property of adsorbent materials, the property that is decisive for the adsorbent’s usage, is the pore structure. The total number of pores, their shape, and size determine the adsorption capacity and even the dynamic adsorption rate of the material. Generally, pores are divided into macro-, meso- and micropores. According to IUPAC, pores are classified as shown in Table 2.2.

Porosity is a property of solids that is attributed to their structure and is evident by the presence of pores between internal supermolecular structures (Tager, 1978). It is not considered

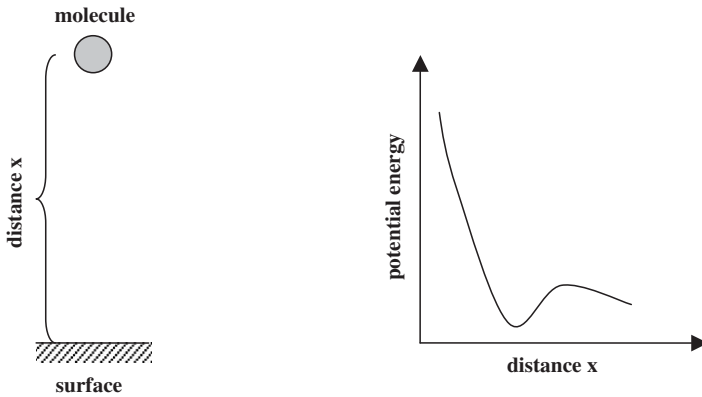


Figure 2.1 The potential energy versus distance.

Table 2.2

The classification of pores according to their size
(Rodríguez-Reinoso and Linares-Solano, 1989)

Type	Pore diameter d (nm)
Macropores	$d > 50$
Mesopores	$2 \leq d \leq 50$
Micropores	$d < 2$
Ultramicropores	$d < 0.7$
Supermicropores	$0.7 < d_0^a < 2$

^a d_0 is the pore width for slit-type pores or the pore diameter for cylindrical pores.

to be an intrinsic property of the solids, but depends on the treatment of the materials. The porosity can be developed by the aggregation of particles as well as by the detachment of a part of the mass of the solid. The pores shaped during the second process are comparable in shape and size with the particles detached.

Adsorptive molecules transport through macropores to the mesopores and finally enter the micropores. The micropores usually constitute the largest portion of the internal surface and contribute the most to the total pore volume. The attractive forces are stronger and the pores are filled at low relative pressures in the microporosity, and therefore, most of the adsorption of gaseous adsorptives occurs within that region. Thus, the total pore volume and the pore size distribution determine the adsorption capacity.

2.1.2 Ion exchange

Ion exchangers are solid materials that are able to take up charged ions from a solution and release an equivalent amount of other ions into the solution. The ability to exchange

ions is due to the properties of the structure of the materials. The exchanger consists of a so-called matrix, with positive or negative excess charge. This excess charge is localized in specific locations in the solid structure or in functional groups. The charge of the matrix is compensated by the so-called counterions, which can move within the free space of the matrix and can be replaced by other ions of equal charge sign (Helfferich, 1995).

The pores sometimes contain not only counterions but also solvent. When the exchanger is in contact with the liquid phase, the solvent can travel through the exchanger and cause “swelling” to an extent that depends on the kind of counterions. Some electrolytes can also penetrate into the exchanger along with the solvent. As a result, there are additional counterions, the so-called coions, which have the same charge sign as the fixed ions.

Normally, an exchanger has many open areas of variable size and shape that are altogether called “pores.” Only a few inorganic exchangers contain pores of uniform cross section. So, the exchangers exhibit a three-dimensional network of channels with irregular size.

Although ion exchange is similar to sorption since a substance is captured by a solid in both processes, there is a characteristic difference between them: ion exchange is a stoichiometric process in contrast to sorption (Helfferich, 1995). It means that in the ion-exchange process, for every ion that is removed, another ion of the same sign is released into the solution. In contrast, in sorption, no replacement of the solute takes place.

Ion exchange can be seen as a reversible reaction involving chemically equivalent quantities (Treybal, 1980; Perry and Green, 1999). The water-softening reaction $\text{Ca}^{2+}(\text{aq}) + 2\text{Na}^+(\text{s}) \rightarrow \text{Ca}^{2+}(\text{s})_2 + 2\text{Na}^+(\text{aq})$ constitutes a characteristic example of cation exchange. However, the characterization of an ion exchange as a “chemical process” is rather misleading. Ion exchange is in principle a redistribution of ions between two phases by *diffusion*, and chemical factors are less significant or even absent. The absence of any actual chemical reaction explains why the heat evolved in the course of an ion exchange is usually very small to negligible, often less than 2 kcal/mol (Helfferich, 1995). Only when an ion exchange is accompanied or followed by a reaction such as neutralization can the whole phenomenon be characterized as “chemical.” A characteristic example is in chelating resins where the ion exchange is followed by a chemical reaction and bond formation between the incoming ion and the solid matrix.

Ion removal by solids could involve more phenomena, as for example in inorganic natural materials where ion uptake is attributed to ion exchange and adsorption processes or even to internal precipitation mechanisms (Inglezakis *et al.*, 2004).

2.1.3 Catalysis

Catalysis is one of the most important technologies in our world. It is used extensively in industries for production and in waste treatment for the removal of pollutants. Even our body constantly uses catalysis in biological processes. Enzymatic catalysis is necessary for all living matter. Most essential of all catalytic processes is photosynthesis, which is seen in most of the simplest and earliest evolved life forms.

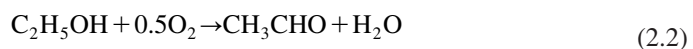
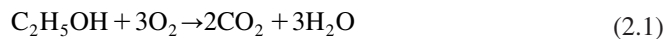
Catalysis can be generally described as the action of a catalyst, which is a substance that accelerates the rate of a chemical reaction, while itself remaining unchanged by the reaction. There are two main categories of catalysis:

- homogeneous catalysis, where the catalyst is in the same phase with the reactants,
- heterogeneous catalysis, where the catalyst is present in a different phase from the reactants in the reaction.

Heterogeneous catalysis is often called surface catalysis as it mainly occurs between a solid surface and a gas. There are basically three stages in this process:

- adsorption (physisorption or chemisorption as described previously) of reactants on the catalyst surface,
- chemical reaction on the surface,
- desorption of products from the catalyst surface.

The following points have to be noted about the action of catalysts. First, catalysts do not alter the thermodynamics of the reactions. No catalyst favors a thermodynamically unfeasible reaction. Consequently, the reaction would proceed even without the catalyst, though perhaps too slowly to be observed or be of use in a given context. Furthermore, the use of a catalyst does not change the equilibrium composition because it increases the rates of the forward and reverse reactions by the same extent. Here arises the question: since a catalyst cannot change the position of equilibrium, why is it said that from the practical point of view, the most important characteristic of a catalyst is its selectivity? We should keep in mind that in the event of a complex reaction network, which is often the case, the catalyst might affect each reaction to a different extent, thus changing the overall reaction selectivity. For example, the reaction between gaseous ethanol and oxygen in nitrogen, at 150–300 °C under atmospheric pressure, is not just a simple oxidation reaction but a network consisting of the following reactions (Poulopoulos *et al.*, 2002):

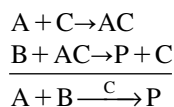


Consequently, under these conditions, ethanol may be totally oxidized to carbon dioxide via the first reaction, partially oxidized to acetaldehyde via the second reaction, dehydrogenized

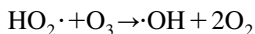
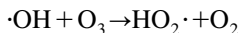
to acetaldehyde via the third reaction, dehydrated to ethylene via the fourth reaction, dehydrated to diethylether via the fifth reaction, and finally decomposed to methane via the last reaction. It is obvious that what could be misunderstood as a simple oxidation is really a complex scheme of reactions. The presence of a catalyst may enhance one or more of these reactions or even all of them by various degrees, leading to a different overall selectivity. Its selection would be made on the basis of the desired products, and catalyst selectivity is the key characteristic to practical applications.

So, catalysts enable reactions to occur much faster and allow the use of milder conditions of temperature for achieving reaction rates of practical use. They achieve this by providing an alternative pathway of lower activation energy for the reaction to proceed. As shown in Figure 2.2, a catalyst lowers the energy of the transition state without changing the energy of the reactants and products. For example, the uncatalyzed value of the activation energy of the decomposition of nitrogen oxide to nitrogen and oxygen is 1240 kJ/mol, whereas with a gold catalyst this becomes +120 kJ/mol.

Since the catalyzed path requires lower activation energy, more molecules will have sufficient energy to react effectively than in the case of the uncatalyzed path. In homogeneous catalysis, this is generally achieved by the reaction between the catalyst and one or more reactants to form an unstable chemical intermediate, which subsequently reacts to produce the final product. The catalyst is regenerated in the final step. For example, if reactant A reacts with B to form the product (P) in the presence of a catalyst (C), a possible reaction scheme is



An example of great environmental interest is the catalytic mechanism for ozone destruction by the hydroxyl radical, which is believed to be



The hydroxyl radical is regenerated in the second reaction and may continue its action.

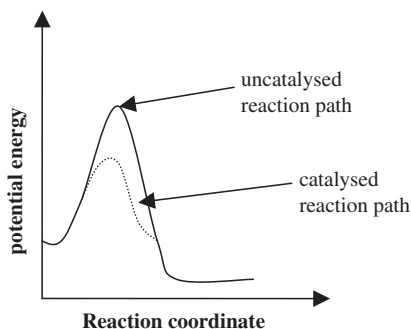
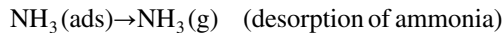
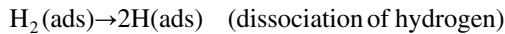
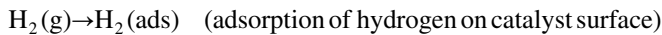
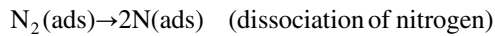
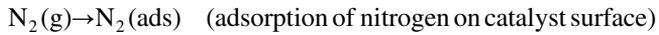


Figure 2.2 The catalyzed and the uncatalyzed reaction path.

In heterogeneous catalysis, the catalyst provides a surface on which the reactants are adsorbed. The chemical bonds of the reactants become weakened on the catalytic surface and new compounds are formed. These compounds (products) have weaker bonds with the catalyst and consequently are released. An example of heterogeneous catalysis is the industrial synthesis of ammonia, which requires solid catalysts to obtain significant rates of reaction between nitrogen and hydrogen:



It has to be noted that the adsorption of reactants is generally not uniform across the catalyst surface. Adsorption, and therefore catalysis, takes place mainly at certain favorable locations on a surface called active sites. In environmental chemistry, catalysts are essential for breaking down pollutants such as automobile and industrial exhausts.

2.2 HISTORICAL ASPECTS

2.2.1 Adsorption

The first known use of adsorption was made in 3750 B.C. by Egyptians and Sumerians who used charcoal for the reduction of copper, zinc, and tin ores for the manufacture of bronze. Around 1550 B.C., Egyptians applied charcoal for medicinal purposes, whereas around 460 B.C., Hippocrates and Pliny introduced the use of charcoal to treat a wide range of infections. Around the same age, Phoenicians used charcoal filters to treat drinking water. So, this must have been the first use of adsorption for environmental purposes. In 157 B.C., Claudius Galen introduced the use of carbons of vegetable and animal origin to treat a wide range of complaints.

These early applications of adsorption were based on intuition and not on a systematic study. It was in 1773 that Scheele made the first quantitative observations in connection with adsorption, whereas F. Fontana in 1777 reported his experiments on the uptake of gases from charcoal and clays. However, the modern application of adsorption is attributed to Lowitz. Lowitz used charcoal for the decolorization of tartaric acid solutions in 1788. The next systematic studies were published by Saussure in 1814. He concluded that all types of gases can be taken up by a number of porous substances and this process is accompanied by the evolution of heat (Dabrowski, 2001).

The term “adsorption” was first used by H. Kayser in 1881. J. W. McBain introduced a similar term in 1909, i.e. “absorption”, to determine an uptake of hydrogen by carbon much slower than adsorption. He proposed the term “sorption” for adsorption and absorption (Dabrowski, 2001).

In 1903, Tswett was the first to study selective adsorption. He investigated the separation of chlorophyll and other plant pigments using silica materials. This technique proposed by Tswett has been called “column solid–liquid adsorption chromatography.” However, there was no sound theory that enabled the interpretation of adsorption isotherm data until 1914. Despite the fact that the Freundlich equation was used, there was no theoretical justification for it. It was an empirical equation, proposed actually by van Bemmelen in 1888. However, it is today known as the Freundlich equation because Freundlich assigned great importance to it and popularized its use. Langmuir was the first to have introduced a clear concept of the monomolecular adsorption on energetically homogeneous surfaces in 1918 and derived the homonymous equation based on kinetic studies (Dabrowski, 2001).

The first practical applications of adsorption were based on the selective removal of individual components from their mixtures using other substances. The first filters for water treatment were installed in Europe and the United States in 1929 and 1930, respectively. Activated carbon was recognized as an efficient purification and separation material for the synthetic chemical industry in the 1940s. By the late 1960s and early 1970s, activated carbon was used in many applications for removing a broad spectrum of synthetic chemicals from water and gases.

In Table 2.3, the history of adsorption is presented briefly.

2.2.2 Ion exchange

The first citation of an application of ion exchange can be found in Aristotle’s *Problematica*, where it is mentioned that sand filters were used for the purification of sea and impure drinking waters. That is also the first environmental application. In the same book, Aristotle suggested that desalination resulted from density effects. It seems that practical applications of ion exchange were well recognized before the 19th century. However, the underlying physical phenomenon was not known. Credit for the identification of the ion-exchange phenomenon is attributed to two agriculture chemists, Thomson and Way. In 1848, Thomson reported to Way that he had found that urine was decolorized and deodorized during the filtration of liquid manure through a bed of an ordinary loamy soil. It was Way, who illustrated the basic characteristics of ion exchange after conducting several experiments (Lucy, 2003).

After soil and clays, natural and synthetic aluminum silicates and synthetic zeolites were tested as ion-exchange materials by other scientists. However, the first practical applications of ion exchange took place in the early 20th century.

The first synthetic organic resins were synthesized in 1935. This spectacular evolution began with the finding of two English chemists, Adams and Holmes, who found that crushed phonograph records exhibited ion-exchange properties (Helfferich, 1962). Much progress was made during World War II in the field of ion exchange, but the results

Table 2.3

Brief history of adsorption (Dabrowski, 2001)

Scientist(s) Name(s)	Breakthrough	Year
C. W. Scheele, F. Fontana	Experiments on the uptake of gases by charcoal and clays	1773–1777
T. Lowitz	Decolorization of tartaric acid utilizing charcoal	1776–1778
D. M. Kehl	Application of carbons of animal origin for the removal of colors from sugar. The English sugar industry used charcoal as a decolorization agent in 1794	1793
T. de Saussure	Systematic studies on adsorption. He discovered the exothermic character of adsorption	1814
H. Kayser	Introduced the term “adsorption”	1881
Van Bemmelen H. Freundlich	The Freundlich equation was first proposed by van Bemmelen and popularized by Freundlich	1888
R. Von Ostreyko	Set the basis for the commercial development of activated carbons	1901
M. S. Tswett	Discovered selective adsorption. He used the term and technology of “column solid–liquid adsorption chromatography”	1903
J. Dewar	Found selective adsorption of oxygen from a mixture with nitrogen, during the uptake of air by charcoal	1904
W. A. Zelinsky	Applied the use of active carbons as an adsorption medium in a gas mask for the needs of World War I	1915
I. Langmuir	Derived the concept of monolayer adsorption, formed on energetically homogeneous solid surfaces. Was awarded the Nobel Prize in chemistry in 1932	1918
S. Brunauer P. H. Emmet, E. Teller	The milestone in the development of adsorption science was the multilayer isotherm equation, known as BET	1938
A. J. P. Martin B. L. M. Syngé	Introduced to laboratory practice the solid–liquid partition chromatography, both in column and planar form	1941
R. M. Barrer D. W. Breck	Invented the method of zeolite synthesis. In the same year, the North-American Linde Company started the production of synthetic zeolites on a commercial scale	1956

obtained were not published for some years due to reasons of confidentiality. Afterwards, there was a rapid development of ion-exchange materials and methods (Lucy, 2003). A brief history of ion exchange is presented in Table 2.4.

2.2.3 Catalysis

Catalysis is not a new phenomenon, but its intentional utilization by humans has begun only in this century. One of the first catalytic processes was probably the fermentation of fruits to obtain alcoholic beverages. Enzymes found in yeast were used as catalysts for the conversion of sugar into alcohol. In fact, ancient Sumerians described beer preparation on

Table 2.4

Brief history of ion exchange (Lucy, 2003; Helfferich, 1962)

Scientist(s) name(s)	Breakthrough	Year
H. S. Thompson	Thompson passed a solution of manure through a filter made of ordinary garden soil and found that the ammonia was removed from solution.	1845
H. S. Thompson J. T. Way J. Spence	Recognition of the phenomenon of ion exchange and a description of its basic characteristics. The ion exchange property of soils was found to be based on their containing small amounts of zeolites.	1848–1852
H. Eichorn	Proved that the adsorption of ions by clays and zeolites constitutes a reversible reaction.	1858
J. Lemberg	Zeolites recognized as carriers of base exchange in soils; equivalence of exchange of bases proved.	1876
F. Harm A. Rumpler S. Mayert K. Halse	Artificial zeolites used for removal of potassium from sugar juices. First synthetic industrial ion exchanger. Manufacture of sulfonated coals and suggestion for the removal of potassium from sugar juices.	1901–1902
R. Gans	Discovered that zeolites could be used to soften hard water. He also invented processes for synthesizing zeolites and designed the equipment—the zeolite water softener—used for the recovery of gold from sea water.	1905
O. Folin, R. Bell	The first analytical application of ion exchange.	1917
J. Whitehorn	The first use of ion exchange in column chromatography.	1923
A. Bahrtdt	The first use of an ion-exchange column for anion analysis.	1927
O. Liebknecht P. Smit	Entirely new types of cation exchangers were developed. Not only could they be used in the sodium cycle when regenerated with salt, but also in the hydrogen cycle when regenerated with an acid. One group of these cation exchangers was the carbonaceous type, which was made by the sulfonation of coal.	1934–1939
B. A. Adams E. L. Holmes	Synthesis of the first organic ion exchanger.	1934–1935
G. F. D'Allelio	Invention of sulfonated polystyrene polymerization cation exchangers.	1942
G. E. Boyd J. Schubert A.W. Adamson	Demonstration of the applicability of ion exchange for adsorption of fission products in trace amounts (lanthanides).	1942
C. H. McBurney	Invention of aminated polystyrene polymerization anion exchangers.	1947
A. Skogseid	Preparation of a potassium-specific polystyrene cation-exchanger chelating resin.	1947
J. A. Marinsky L. E. Glendenin C. D. Coryell	The discovery of promethium (element 61), an element not found in nature, is attributed to ion exchange	1947
D. K. Hale D. Reichenberg N. E. Topp C. G. Thomas	Development of carboxylic addition polymers as weak acid cation exchangers.	1949–1956
R. M. Barrer D. W. Breck	New zeolites as molecular sieves with ion-exchange properties.	1951–1956

(Continued)

Table 2.4 (*Continued*)

Scientist(s) name(s)	Breakthrough	Year
H. P. Gregor K. W. Pepper L. R. Morris	Invention and development of chelating polymers.	1952–1971
M. A. Peterson, H. A. Sober	Development of cellulose ion exchangers.	1956
1956–58	Preparation and studies of nonsiliceous inorganic ion exchangers—insoluble salts, heteropolyacids	1956
F. Helfferich	Foundations laid for the new theoretical treatment of ion exchange.	1959
T. R. E. Kressmann J. R. Millar	Invention and development of isoporous ion-exchange resins.	1960
J. Weiss	Thermally regenerable ion-exchange resins and water desalination based on them.	1964

clay plates many millennia ago. A few examples of the utilization of catalysis in ancient civilizations are the following:

- 6000 B.C.—beer brewing by malting procedure (malt enzymes)
- 3000 B.C.—wine making by fermentative conversion of grape juice sugars
- 2000 B.C.—making alcohol by fermentation of various carbohydrate sources
- 800 B.C.—cheese making by casein hydrolysis with calf stomach extract (calf rennet)

The phenomenon under consideration was studied systematically in the beginning of the 19th century. In 1815, Davy performed experiments that dealt with catalytic combustion on platinum gauzes. The term “catalysis”, however, was introduced by Berzelius in 1836. He first defined a catalyst (Berzelius, 1836) as “a compound, which increases the rate of a chemical reaction, but which is not consumed during the reaction.” This definition was later amended by Ostwald (1853–1932) in 1895 to involve the possibility that small amounts of the catalyst are lost in the reaction or that the catalytic activity is slowly decreased: “A catalyst is a substance that increases the rate of approach to equilibrium of a chemical reaction without being substantially consumed in the reaction.” It was more than a century after Berzelius’ first definition that Marcel Prettre’s introduced the notion of yield: “The catalyst is a substance that increases the rate of a chemical transformation without modifying the yield, and that is found intact among the final products of the reaction.”

It is fascinating that even today, heterogeneous catalysis still remains an empirical science. Although the application of catalysts in the chemical industry is a fact for at least 150 years, the experimental techniques for investigation of catalysis at the atomic level did not become routine until less than 25 years ago; the computational techniques are even younger and have hardly become routine yet. For this reason, a vast amount of empirical knowledge exists and awaits systematic investigation. A short history of heterogeneous catalysis is presented in Table 2.5.

Table 2.5

Brief history of heterogeneous catalysis

Scientist(s) name(s)	Breakthrough	Year
von Marum	Studies the dehydrogenation of alcohols using metals.	1796
J. Dalton	Suggests that chemical compounds consist of molecules and molecules consist of atoms.	1808
H. Davy	Studies the oxidation of methane on platinum wires.	1817
W. Henry	Studies oxidations catalyzed by platinum adsorbed on clay pellets.	1824
M. Faraday	Studies the ignition of hydrogen in air at platinum surfaces.	1825
J. Berzelius	Formulates the definition of catalysis.	1836
E. Frankland	Formulates the concept of valency.	1852
C. W. Guldberg P. Wage	Formulation of the law of mass action.	1867
von Hoffmann	Develops Ag as a catalyst for the oxidation of CH ₃ OH to HCHO.	1869
R. Messel	Develops the industrial oxidation of SO ₂ catalyzed by Pt	1875
J. W. Gibbs	Publishes "On the equilibrium of heterogeneous substances", which contains Gibbs' phase law	1876
C. Winkler	Invention of the contact process for the synthesis of sulfuric acid.	1879
Badische Anilin and Soda Fabrik Germany	Industrial synthesis of sulfuric acid using a platinum catalyst	1889
W. Ostwald	Discovers that the reaction $2\text{NH}_3 + 5/2\text{O}_2 = 2\text{NO} + 3\text{H}_2\text{O}$ is catalyzed by Pt.	1901
S. Sabatier	Studies hydrogenation of alkenes catalyzed by Ni (1902–1905).	1902
F. Haber	Reports the production of small amounts of NH ₃ from N ₂ + 3H ₂ using an iron catalyst	1905
W. Ostwald	Receives the Nobel prize in chemistry for his work on catalysis, chemical equilibrium, and the rate of chemical reactions.	1909
P. Sabatier	Receives the Nobel prize in chemistry for the development of the hydrogenation of organic compounds catalyzed by small metal particles.	1912
I. Langmuir	Formulates a theory of adsorption.	1915
Chemical Construction Co.	Builds an industrial nitric acid plant based on the Ostwald process.	1917
J. Frenkel	Publishes a theory of adsorption.	1924
H. S. Taylor	Theory of catalysis.	1925
I. Langmuir	Formulate the principles of Langmuir–	1927
W. Hinselwood	Hinselwood kinetics.	
I. Langmuir	Receives the Nobel prize in chemistry for his work on surface chemistry	1932
G. Damköhler	Introduces the Damköhler group.	1937
E. W. Thiele	Introduces the effectiveness factor and the Thiele modulus.	1939
H. Kramers	Publishes the definitive treatment of kinetics.	1940

(Continued)

Table 2.5 (Continued)

Scientist(s) name(s)	Breakthrough	Year
G. Natta	Continues the study initiated by Karl Ziegler on metal-organic catalysts for polymerization of alkenes	1953
P. Kisluk	Publishes a theory of precursor kinetics for chemisorption.	1957
	Catalytic converters are introduced in new cars in the United States.	1975
R. Kelley, D. Goodman	Measure the rate of a reaction catalyzed by a single crystal (methanation, Ni single crystals)	1982

2.3 ADSORPTION, ION EXCHANGE, AND CATALYSIS: THREE RELATED PHENOMENA

At a first glance, adsorption, ion exchange, and catalysis are three different phenomena with diverse characteristics. However, despite these differences, there are many common features among these processes. In the following sections, a relationship between them will be attempted.

2.3.1 Adsorption and ion exchange

Ion exchange is similar to adsorption, since mass transfer from a fluid to a solid phase is common in both processes, i.e. they are basically diffusion processes. Ion exchange is also a sorption process, but ions are the sorbed species in contrast to adsorption, where electrically neutral species are sorbed (Noble and Terry, 2004; Perry and Green, 1999). It is generally accepted that adsorption and ion exchange can be grouped together as sorption for a unified treatment in practical applications.

Most of the mathematical theories and approaches have been developed originally for sorption rather than ion exchange. However, they are sufficiently general to be applicable with minor, if any, modifications to a number of similar phenomena such as ion exclusion and ligand exchange. According to Helfferich (1995), the applicability of a simplified theory depends more on the mode of operation than on the particular mechanism of solute uptake.

A significant feature of physical adsorption is that the rate of the phenomenon is generally too high and consequently, the overall rate is controlled by mass (or heat transfer) resistance, rather than by the intrinsic sorption kinetics (Ruthven, 1984). Thus, sorption is viewed and termed in this book as a “diffusion-controlled” process. The same holds for ion exchange.

2.3.2 Catalysis and adsorption

As discussed earlier, the first step in heterogeneous catalysis is the adsorption of the molecules of the reactants on the surface of the adsorbent or of the catalyst (inner and outer surfaces). Then, molecular dissociation of at least one or two reacting components takes place, usually preceded by surface diffusion. The next step is a surface reaction, which is

often the rate-determining step in a catalytic reaction. Then, desorption of the product occurs because the surface bond is broken, and the final product enters the bulk phase, diffusing through and out of the catalyst pores. This very simple picture highlights the basic idea of heterogeneous catalysis. Consequently, the development of catalysis is closely related to the evolution of adsorption.

Most of the adsorbents used in the adsorption process are also useful to catalysis, because they can act as solid catalysts or their supports. The basic function of catalyst supports, usually porous adsorbents, is to keep the catalytically active phase in a highly dispersed state. It is obvious that the methods of preparation and characterization of adsorbents and catalysts are very similar or identical. The physical structure of catalysts is investigated by means of both adsorption methods and various instrumental techniques derived for estimating their porosity and surface area. Factors such as surface area, distribution of pore volumes, pore sizes, stability, and mechanical properties of materials used are also very important in both processes—adsorption and catalysis. Activated carbons, silica, and alumina species as well as natural amorphous aluminosilicates and zeolites are widely used as either catalyst supports or heterogeneous catalysts. From the above, the following conclusions can be easily drawn (Dabrowski, 2001):

- adsorption and catalysis are closely related to each other,
- the action of solid catalysts results from their capacity to adsorb reacting substances,
- the same porous solids can be used as adsorbents, catalyst supports, and catalysts,
- the chemical character and size of solid surface areas, their porous structure, mechanical properties, and thermal stability play an essential role in both adsorption and catalysis,
- the development of theoretical studies on adsorption, design, and manufacture of new adsorbents affects heterogeneous catalysis development.

2.3.3 Catalysis and ion exchange

Catalysis of reactions by ion exchangers can be explained in terms of the catalytic activity of the exchanging ions and is analogous to homogeneous-phase catalysis by dissolved electrolytes (Hellferich, 1995). Ion-exchange resins can act as insoluble acids and bases for the catalysis of chemical reactions. Heterogeneous catalysis with resins can be carried out in aqueous or nonaqueous solvent solutions (Guzzo, 1997). It is interesting that ion exchangers can be used for catalyzing reactions in the gas phase. However, its relation to the ion-exchange properties of the catalyst is less distinct.

Despite the presence of two phases, solid and liquid, catalysis by ion exchangers is not a true case of heterogeneous catalysis and may be described more adequately as homogeneous catalysis in the pore phase. This is because the ions of the exchangers that are involved in the catalytic reaction are dissolved in the pores of the solid, where they act as in a homogeneous solution (Hellferich and Hwang, 1988). A good example is the acid-catalyzed hydrolysis of cane sugar, which is carried out in solution using a strong acid cation-exchange resin in its hydrogen form. The “inversion” of sucrose is a commercial process in which ion-exchange catalysis has been widely used (Purolite Co.).

Despite the fact that it is not clear whether the catalytic activity is related to the ability of the solid to act under different conditions as an ion exchanger, there is a variety of

materials used in both catalysis and ion exchange, such as zeolites and clays. Some catalytic applications of zeolites and clays, materials used as ion exchangers, are presented in Table 2.6.

Furthermore, in the manufacture of zeolite catalysts, ion exchange plays an outstanding role. Brönsted acid sites can be readily generated by introducing ammonium ions followed by a heat treatment or by introducing multivalent metal cations, again followed by heat treatment (Weitkamp, 2000). However, not all these applications incorporate the ion exchange and catalysis phenomena at the same time, i.e. simultaneous action of these two mechanisms.

Catalysis by ion exchangers exhibits some advantages over homogeneous catalysis by dissolved electrolytes, such as

- the catalyst can be easily separated from the liquid phase by filtration or other suitable means,
- continuous operation in fixed beds is possible,
- in some cases, it is possible to isolate reaction intermediates that cannot be obtained by homogeneous catalysis,
- the ion exchanger is generally more selective, i.e. it distinguishes more sharply between the various reactant molecules than the dissolved catalyst.

Table 2.6

Catalytic reactions for which zeolites and clays are used (Tsitsishvili *et al.*, 1992; Mumpton, 1999; Armbruster, 2001; Chitnis and Sharma, 1997)

Material	Application
Natural erionite-clinoptilolite	Selective-forming catalyst
Hydrogen-exchanged natural mordenite	Hydrocarbon conversion catalyst for the deprotonization of toluene to benzene and xylene
Cation-exchanged clinoptilolite	Hydromethylation of toluene
Clinoptilolite	Isomerization of <i>n</i> -butene, the dehydration of methanol to dimethyl ether, and the hydration of acetylene to acetaldehyde
Acid-treated clays	Alkylation reactions (e.g. of benzene with benzyl chloride) Dimerization reactions (e.g. of <i>a</i> -methylstyrene) Etherification reactions (e.g. of <i>tert</i> -butanol with methanol) Condensation reactions (e.g. of cyclohexanone) Separation of close boiling aromatic amines Separation of isomers of xylene
Thermally pillared clays	Dimerization of unsaturated fatty acids to dimer acids Removal of olefins from "BTX", ethylbenzene, cumene, etc. streams Decolorization of industrial oil derivatives Purification of kerosene and other mineral oil derivatives

Catalysis with ion-exchange resins provides effective and efficient answers to a number of catalytic problems:

- the resins do not introduce counterions (which would have to be removed from the final product made under homogeneous catalysis conditions),
- they may be regenerated and reused over relatively long periods,
- corrosion arising from the presence of strong acids in the bulk phase is eliminated,
- resins may be tailored in particle size, pore volume, surface area, swelling in solvents, etc.

However, it should be noted that the maximum operating temperature recommended for ion-exchange resin catalysts is in the range 137–145°C. Thus, the use of resins as catalysts is limited to systems that operate at relatively low temperatures. In the case of elevated temperatures, zeolites could be used instead, because they exhibit higher stability for temperatures as high as 800°C (e.g. clinoptilolite). In many applications, acid-treated clays could be used as an alternative. Clays, being naturally occurring aluminosilicates, are readily available and inexpensive compared to other types of heterogeneous acid catalysts, e.g. ion-exchange resins (Chitnis and Sharma, 1997). Clays, in general, are thermally stable up to 200 °C and they can be greatly improved by the pillaring process. Furthermore, in many cases, they exhibit higher selectivity than resins. The disadvantage of clays is that their activity is lower than resins, their use is restricted to nonaqueous reactions systems only, and their mechanical strength is low.

2.4 ENVIRONMENTAL APPLICATIONS OF ADSORPTION, ION EXCHANGE, AND CATALYSIS

2.4.1 Adsorption

There are many environmental applications of adsorption in practice and many others are being developed (Noble and Terry, 2004). Activated carbons and clays are frequently used for the removal of organic contaminants, such as phenol and aniline, both of which are prevalent in industry wastewaters and are known to have a significant negative impact on marine life and human health (IRIS, 1998; Dabrowski *et al.*, 2005). Moreover, the adsorption on inexpensive and efficient solid supports has been considered a simple and economical viable method for the removal of dyes from water and wastewater (Forgacs *et al.*, 2004). Activated carbon, clays, coal, vermiculite, and other adsorbents have been used for this purpose. Specifically, adsorption can be employed in (Noble and Terry, 2004; Dabrowski, 2001):

- the removal of water from organic solvents
- the removal of organics from water
- taste and odor regulation in wastewater treatment
- the removal of radon, hydrogen sulfide, and other sulfur compounds from gas streams
- mercury removal from chlor-alkali-cell gas effluent

- heavy-metal removal in clay barriers
- nitrogen and phosphorus removal from wastewater, i.e. removal and recovery of nutrients
- solvent recovery and solvent vapor fractionation
- volatile organic compounds recovery from gas streams and groundwater
- water removal from gas streams containing acid gases

Other important applications of adsorption are the control of “greenhouse” gases (CO, CH₄, N₂O), the utilization of CH₄, the flue gas treatment (SO_x, NO_x, Hg removal), and the recovery of the ozone-depleting CFCs (Dabrowski, 2001). Activated carbons and hydrophobic zeolites are used for the adsorption of HCFCs (Tsai, 2002).

The most commonly used adsorbents are shown in Table 2.7. The adsorption process can be used for substance recovery as well as for the abatement of undesirable emissions in wastewaters (Table 2.8) and gas streams (Table 2.9).

Table 2.7

The most common adsorbents

Wastewater treatment	VOC removal
Activated carbon (mainly as granulates)	Granular activated carbon
Lignite coke	Zeolites
Activated aluminum oxide	Macroporous polymer particles
Adsorber resins	Silica gel
Zeolites	Sodium–aluminum silicates

Table 2.8

Representative commercial liquid-phase adsorption separations

Liquid bulk separations (adsorbate concentration in the feed >10% wt.)	Adsorbent
Fructose/glucose	Zeolites
<i>p</i> -Xylene/ <i>o</i> -xylene, <i>m</i> -xylene	Zeolites
Detergent-range olefins/paraffins	Zeolites
Normal paraffins/isoparaffins, aromatics	Zeolites
<i>p</i> -Diethyl benzene/isomer mixture	Zeolites
Liquid Purifications (adsorbate concentration in the feed <3% wt.)	Adsorbent
Sulfur compounds/organics	Zeolites
Organics/H ₂ O	Activated carbon
Odor, taste/drinking H ₂ O	Activated carbon
H ₂ O/organics	Silica, alumina, zeolite
Decolorizing petroleum fractions, sugar syrups, vegetable oils, etc.	Activated carbon

Table 2.9

Representative commercial gas-phase adsorption separations

Gas bulk separations (adsorbate concentration in the feed >10% wt.)	Adsorbent
N ₂ /O ₂	Zeolite
O ₂ /N ₂	Carbon molecular sieve
H ₂ O/ethanol	Zeolite
CO, CH ₄ , CO ₂ , N ₂ , NH ₃ /H ₂	Zeolite, activated carbon
Acetone/vent streams	Activated carbon
C ₂ H ₄ /vent streams	Activated carbon
Gas purifications (adsorbate concentration in the feed <3% wt.)	Adsorbent
H ₂ O/olefin-containing cracked gas, natural gas, air, synthesis gas	Silica, alumina, zeolite
SO ₂ /vent streams	Zeolite
CO ₂ /C ₂ H ₄ , natural gas	Zeolite
Organics/vent streams	Activated carbon and others
Sulfur compounds/natural gas, hydrogen, liquefied petroleum gas (LPG)	Zeolite
Solvents/air	Activated carbon
Odors/air	Activated carbon
NO _x /N ₂	Zeolite

As any process, adsorption has both some advantages and disadvantages:

Advantages

- high removal efficiency
- enables removal of refractory and/or toxic organic compounds
- possibility of compounds recovery (preferably with zeolites)
- simple installation and maintenance
- capability of systems for fully automatic operation
- a large variety of adsorbents available

Disadvantages

- adsorbents deteriorate in capacity gradually
- particulates in the feed can cause problems
- high content of macromolecular compounds decreases efficiency and may cause irreversible blockage of active sites
- risk of bed fires in the VOC abatement
- spent adsorbent has to be regenerated (high energy consumption) or disposed (causing waste)
- relatively high capital cost

Special applications: The environmental control and life support system on a spacecraft maintains a safe and comfortable environment, in which the crew can live and work, by supplying oxygen and water and by removing carbon dioxide, water vapor, and trace contaminants from cabin air. It is apparent that the processes aimed at the recycling of air and water are vital for supporting life in the cabin. These recycling processes include separation and reduction of carbon dioxide, removal of trace gas-phase contaminants, recovery and purification of humidity condensate, purification and polishing of wastewater streams, and are performed totally or in part by adsorption equipment (Dabrowski, 2001).

Another special application of adsorption in space is presented by Grover *et al.* (1998). The University of Washington has designed an *in situ* resource utilization system to provide water to the life-support system in the laboratory module of the NASA Mars Reference Mission, a piloted mission to Mars. In this system, the Water Vapor Adsorption Reactor (WAVAR) extracts water vapor from the Martian atmosphere by adsorption in a bed of type 3A zeolite molecular sieve. Using ambient winds and fan power to move atmosphere, the WAVAR adsorbs the water vapor until the zeolite 3A bed is nearly saturated, and then heats the bed within a sealed chamber by microwave radiation to drive off water for collection. The water vapor flows to a condenser where it freezes and is later liquefied for use in the life-support system.

2.4.2 Ion exchange

Although there are some applications in gas emissions reduction, for example, hydrogen sulfide and ammonia removal by utilizing carboxylic acid resins and ammonium anion-exchange resins, ion exchange is mainly used in wastewater treatment. Some characteristic environmental applications are the following (Noble and Terry, 2004):

- treatment of mine drainage water: removal of metal cations and anions using silico-titanates and layered titanates
- removal of nitrates and ammonia from groundwater
- treatment of nuclear waste solutions:
 - (1) strontium removal by clinoptilolite and heulandite (Chernjatskaja, 1988), (2) cesium removal using hexacyanoferrate exchanger and phenolic resins (Harjula *et al.*, 1994; Samanta *et al.*, 1992), (3) treatment of liquid nuclear wastes using titanate ion exchangers (Dosch *et al.*, 1993), and (4) thorium ions removal using zeolites (Sinha *et al.*, 1994)
- plating industry:
 - (1) treatment of raw water to produce high-quality rinse water, (2) chemical recovery from rinse water, (3) treatment of plating baths to remove contaminants, and (4) as a primary end-of-pipe treatment process

Some of the cons and pros of ion exchange are

Advantages

- in principle, all ions or ionizable species can be removed from aqueous liquids
- recovery of valuable species is possible
- high efficiency
- a large variety of specific resins is available

Disadvantages

- prefiltration is required (suspended particles in the feed should be less than about 50 mg/L to prevent plugging)
- interference of competing cations in the wastewater
- low-temperature resistance of organic (resin) ion exchangers

Special application: Ion exchange was in the foreground in World War II during the Manhattan Project. The need for separation of reactor fission products for analysis purposes led Boyd and coworkers to suggest the use of resins for the uptake of several fission products. This study paved the way for the development of several ion-exchange methods. However, the results of the Manhattan Project in connection with ion exchange were not published until 1947 on grounds of confidentiality.

2.4.3 Catalysis

Catalysis has been widely used in numerous industrial processes for at least 150 years. Catalysts are selected to increase the reaction rate and the yield of the desired products. Heterogeneous catalysis is largely an empirical science, more of an art than a science, and a large amount of knowledge in this field is empirical. The great range of catalyst applications led to the development of various practical rules concerning their selection and use, much earlier than the advance in the experimental techniques for the investigation of catalysis.

The emphasis on environmental protection in the last three decades, as industrial and economic growth gave birth to many forms of pollution threatening human health and Earth ecosystems, resulted in the growth of environmental catalysis. So, catalysts are not only used to promote processes in the production field, but also to reduce the emissions of undesirable or hazardous compounds to the environment. For example, catalytic combustion has been proposed and developed as an effective method for controlling the emissions of hydrocarbons and carbon monoxide.

In fact, most of us benefit from the use of catalysis. Automotive catalytic converters have represented the most massive application of environmental catalysis and one of the most challenging and successful cases in catalysis, generally. Automobile catalysts deserve a few more comments. The engine exhaust emission is a complex mixture, whose composition and flow rate change continuously depending on a variety of factors such as driving conditions, acceleration, and speed. Despite the variability of the conditions, three-way catalysts have achieved the reduction of exhaust carbon monoxide, hydrocarbons, and

nitrogen oxides by over 70%. Today, about one-third of the world market for catalysts involves environmental catalysis.

Generally, catalysts are called into action to eliminate emissions from mobile (cars) and stationary (industry) sources, to take part in liquid and solid waste treatment, and contribute to the effort to reduce volatile organic compounds and gases that pose major environmental problems such as photochemical smog and (at a global level) the greenhouse effect.

The use of catalysts for exploiting renewable energy sources, producing clean fuels in refineries, and minimizing the by-product formation in industry also fall within the definition of environmental catalysis. In the future, the continuous effort to control transport emissions, improve indoor air quality, and decontaminate polluted water and soil will further boost catalytic technology. All in all, catalysts will continue to be a valuable asset in the effort to protect human health, the natural environment, and the existence of life on Earth.

There are, however, some distinctive differences between the environmental and the other aspects of catalysis. First, the feed and operation conditions of environmental catalysts cannot be changed in order to increase conversion or selectivity, as commonly done for chemical production catalysts. Second, environmental catalysis has a role to play not only in industrial processes, but also in emission control (auto, ship, and flight emissions), and even in our daily life (water purifiers). Consequently, the concept of environmental catalysis is vital for a sustainable future. Last but not least, environmental catalysts often operate in more extreme conditions than catalysts in chemical production. There are also cases, such as automotive vehicles, where they have to operate efficiently for a continuously varying feed flow rate and composition.

The most important catalytic production processes are the following:

- the Haber process for ammonia synthesis
- steam reforming of hydrocarbons to produce synthesis gas
- methanol synthesis
- Fischer–Tropsch synthesis
- hydrogenation/dehydrogenation of organic compounds,
- sulfuric acid production
- nitric acid production
- maleic anhydride production
- petroleum refining and processing

In the area of environmental application of catalysis, the most important processes are

- catalytic reduction of NO_x
- catalytic oxidation of SO_2
- catalytic oxidation of CO, VOC, and hydrocarbons
- catalytic denitrification of drinking water
- catalytic oxidation of persistent organic pollutants in wastewater

The main advantages and disadvantages of catalysts are

Advantages

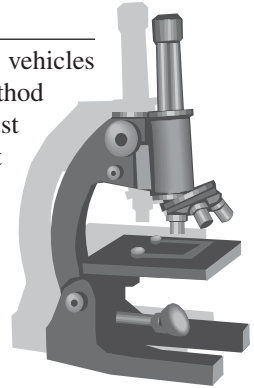
- high efficiency in the treatment of gas emissions
- large variety of catalysts
- simple installation

Disadvantages

- deactivation phenomena (mainly in the wastewater treatment)
- spent catalysts have to be appropriately disposed
- a specific temperature is required for their operation
- for low concentrations of VOCs, the heating of large volumes of emissions to the temperature required for catalytic activity is expensive

A look into three-way catalysis

The need for controlling the exhaust emissions from automotive vehicles has been recognized since 1975. The most effective and tested method proved to be the installation of three-way catalysts at the exhaust emission system of cars. The development and the improvement of such catalysts was and will be a complicated effort, since a catalyst placed in a vehicle should simultaneously accelerate oxidation and reduction reactions, under continuously changing conditions of temperature and space velocity, in contrast to industrial applications where catalysts operate under fixed and controlled conditions. Generally, the catalytic converter of a vehicle has to satisfy the following requirements:



- facilitate the oxidation reactions of carbon monoxide and unburned hydrocarbons and the reduction of nitrogen oxides (three reactions to perform; hence they are named “three-way catalysts”)
- start its operation at the lowest possible temperature, since the emissions are high during the first minutes of engine operation, where the temperature is still low
- show resistance for a short time at temperatures up to 1000 °C
- exhibit a satisfactory operation for at least 150,000 km
- be highly active in order to achieve the desired conversions for high volumetric feed of emissions that take place at the engine exhaust
- all the above have to take place at continuously changing air-to-fuel ratios.

The presence of a three-way catalyst is mandatory for every car produced in the United States and Europe since 1981 and 1993, respectively. It is the most massive and one of the most successful stories in the history of catalysis.

The demand for occupying less space, operation at high volumetric feed, and low loss of power led to the adoption of monoliths for the automobile catalyst. A monolith

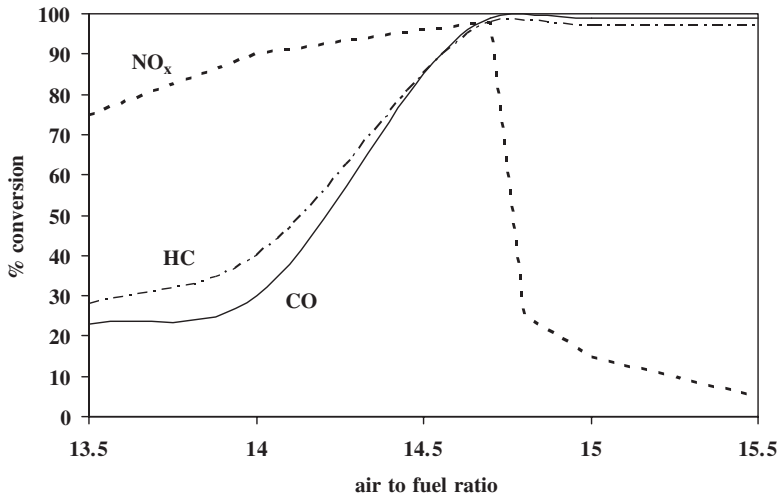


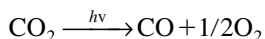
Figure 2.3 The activity of catalytic converter in relation with air to fuel ratio (Shelef and McCabe, 2000).

is a ceramic support structured in many channels and shapes that achieve large catalytic surface at small volume. The search for the appropriate active catalytic components ended with the use of Pt, Pd, and Rh. These metals proved to have the required activity, durability at high temperatures, and sufficient resistance to poisoning from the lead traces present in fuels. However, it was the development of electronics and the installation of the so-called “lambda” sensor that allowed the sound operation of catalytic converters by adjusting the air-to-fuel ratio at a specific range of values (Figure 2.3).

As mentioned earlier, the oxidation of carbon monoxide and hydrocarbons should be achieved simultaneously with the reduction of nitrogen oxides. However, the first reaction needs oxygen in excess, whereas the second one needs a mixture (fuel-oxygen) rich in fuel. The solution was found with the development of an oxygen sensor placed at exhaust emissions, which would set the air-to-fuel ratio at the desired value in real time. So, the combination of electronics and catalysis and the progress in these fields led to better control of the exhaust emissions from automotive vehicles.

A special application: The Earth itself takes advantage of catalytic processes. It seems that catalysis plays a very important role in the global chemistry of Earth atmosphere. Photocatalytic processes may occur in the troposphere on aerosol particles containing Fe_2O_3 , TiO_2 , and ZnO under the action of the near-ultraviolet, visible, and near-infrared solar light. Photocatalysis is anticipated to affect the intensity of acid rains, the concentration of some greenhouse gases, and free the atmosphere from harmful compounds. Thus, desert areas where continental dust is generated may, perhaps, serve as “kidneys” for the Earth (Zamaraev, 1997).

Catalysis may be of interest even on Mars. The Martian atmosphere consists of 95% carbon dioxide and Breedlove *et al.* (2001) have presented that nickel cluster catalysts could be used in a photoelectrochemical process to split carbon dioxide, according to the reaction



to provide both oxygen to support life systems and carbon monoxide, which can be used as a substitute for hydrogen fuel, in a manned mission to Mars.

MULTIPLE CHOICE QUESTIONS

- A value of 3 kcal/mol refers to*
 - physical sorption
 - chemical sorption
 - electrostatic sorption
- Adsorption of a molecule is the result of*
 - the competitiveness between repulsion and the van der Waals force
 - the attraction of the molecule to the adsorbent's surface
 - the repulsion between the cloud of electrons in atoms that form the surface and those of the molecule
- The most important property of an adsorbent is*
 - its shape
 - the shape of its pores
 - the number of its pores
 - its pore structure
- A pore with a diameter of 15 nm is characterized as a*
 - macropore
 - mesopore
 - micropore
 - ultramicropore
- Ion exchangers are able to*
 - remove organic compounds from a solution
 - release ions when heated
 - take up charged ions from a solution and release an equivalent amount of other ions to the solution
- Catalysts can*
 - accelerate chemical reactions
 - favor reactions that would not take place otherwise
 - increase the yield of a reaction by changing the equilibrium composition
 - alter both the rate and the thermodynamics of a reaction

7. *A catalyst changes the selectivity of a chemical process by*
 - (a) altering the thermodynamics
 - (b) affecting each reaction to a different extent
 - (c) changing the equilibrium position
8. *In heterogeneous catalysis, the catalyst provides an alternative pathway of lower activation energy generally through*
 - (a) weakening the chemical bonds of the reactants on its surface
 - (b) forming an unstable intermediate with the reactants
 - (c) none of the above
9. *The terms of “catalyst” and “adsorption” were used for the first time respectively, by*
 - (a) Keyser and Berzelius
 - (b) Lowitz and Berzelius
 - (c) McBain and Ostwald
10. *Adsorption and ion exchange can be*
 - (a) considered as two totally different processes
 - (b) described in a mathematically exact manner
 - (c) grouped together as sorption for a unified treatment in practical applications
11. *Catalysis by clays is*
 - (a) possible for temperatures up to 200°C
 - (b) possible in the hydromethylation of toluene
 - (c) preferable to catalysis by resins in aqueous systems
12. *For decolorizing petroleum fractions by adsorption, you would suggest the use of*
 - (a) zeolites
 - (b) alumina
 - (c) activated carbons
13. *In the adsorption process, there is generally*
 - (a) a risk of bed fires in the VOC abatement
 - (b) low capital cost
 - (c) complex installation and maintenance procedure
14. *Carbon adsorption is preferably used in water treatment*
 - (a) in the case of removing organics with concentrations around 15,000 mg/L
 - (b) if materials being removed are mostly metals
 - (c) for removing ketones
15. *If we wanted to remove VOCs from a gas stream containing moisture using the adsorption process, we would suggest the use of*
 - (a) zeolites
 - (b) activated carbon
 - (c) a polar adsorbent
16. *Ion exchange can be used*
 - (a) at high temperatures
 - (b) without prefiltration of the feed to be treated
 - (c) for the treatment of nuclear waste solutions

17. *Catalysts are appropriate*
 - (a) for industrial processes
 - (b) for VOC abatement from stationary sources
 - (c) for both industrial production and environmental applications
18. *For the efficient operation of a catalytic converter placed in a car, it is important to adjust the air-to-fuel ratio*
 - (a) according to the current engine operating conditions
 - (b) around a specific value
 - (c) so that oxygen excess is achieved
19. *Monoliths are used in catalytic converters of automobiles mainly because*
 - (a) they provide large surface at small volume and low loss of power
 - (b) of their low cost
 - (c) of their activity
20. *Catalytic oxidation is preferable to adsorption, in VOC abatement, if*
 - (a) the temperature is below 150°F
 - (b) intermittent loads are involved
 - (c) high concentrations of gaseous pollutants have to be dealt with

ANSWERS TO MULTIPLE CHOICE QUESTIONS

1. (a) physical sorption
2. (a) the competitiveness between repulsion and the van der Waals force
3. (d) its pore structure
4. (b) mesopore
5. (c) take up charged ions from a solution and release an equivalent amount of other ions to the solution
6. (a) accelerate chemical reactions
7. (b) affecting each reaction to a different extent
8. (a) weakening the chemical bonds of the reactants on its surface
9. (a) Keyser and Berzelius
10. (c) grouped together as sorption for a unified treatment in practical applications
11. (a) possible for temperatures up to 200 °C
12. (c) activated carbons
13. (a) a risk of bed fires in the VOC abatement
14. (b) if materials being removed are mostly metals
15. (b) activated carbon
16. (c) for the treatment of nuclear waste solutions
17. (c) for both industrial production and environmental applications
18. (b) around a specific value
19. (a) they provide large surface at small volume and low loss of power
20. (c) high concentrations of gaseous pollutants have to be dealt with

– 3 –

Heterogeneous Processes and Reactor Analysis

3.1 INTRODUCTION TO HETEROGENEOUS PROCESSES

In the relevant literature, many definitions of reaction rates can be found, especially in the case of catalytic systems. Depending on the approach followed, a catalytic reaction rate can be based on catalyst volume, surface, or mass. Moreover, in practical applications, rates are often expressed per volume of reactor. Each definition leads to different manipulations and special attention is required when switching from one expression to another. In the following, the various forms of catalytic reaction rates and their connection is going to be presented. Starting from the fundamental rate defined per active site, the reader is taken step –by step to the rate based on the volume of the reactor and the concept of the overall rate in two- and three-phase systems.

The analysis in this chapter mainly concerns catalytic reactions. However, the basic principles are applicable to any heterogeneous process, though with different terminology and levels of importance. Concerning adsorption and ion exchange, only the reaction rate per unit mass of solid phase (r_m) and per unit volume of reactor (R) are used in practice, whereas the concepts analyzed in the overall rate and rate-controlling sections are equally applicable to ion exchange and adsorption.

3.1.1 Reaction rate in heterogeneous catalysis: from active sites to reactor level

Fundamental—Active site level

As mentioned in Chapter 2, a catalytic reaction is not catalyzed over the entire surface of the catalyst but only at certain active sites (Fogler, 1999). Then, the reaction rate of *any reaction component* i at a fundamental level for catalytic reactions can be defined with respect to active sites as follows:

$$r_i = \frac{1}{n} \frac{dN}{dt} \quad (3.1)$$

where:

- N = the moles of reactant that appear in the reaction
- t = time
- n = the number of active sites on the catalyst surface.

This rate is usually referred to as the *turnover frequency* and it is the number of molecules reacting per active site per unit time at the conditions of the experiment (Boudart, 1985; McNaught and Wilkinson, 1997; Fogler, 1999). Boudart (1995) used the term “turnover frequency” to define the number of revolutions of the catalytic cycle per unit time and active site. In each revolution, one mole of reactant is consumed. For example, the revolution of a catalytic cycle for SO_2 oxidation is shown in Figure 3.1.

Frequently, the number of active sites is expressed in mole units (the number of active sites divided by the Avogadro number) and thus, turnover frequency is found in s^{-1} units. For a specific reaction, the turnover frequency depends on the nature of the catalytic active site, the temperature, and the reactants’ concentration. The above-defined catalytic rate could be described as an “active-site level” rate.

Following the reaction rate definition of the form given in eq. (3.1), if component i is a reaction product the rate is positive; if it is a reactant that is being consumed, the rate is negative; thus, the rate of disappearance of the reactant is $-r_i$. In environmental applications, as we are interested in the disappearance of a pollutant, the rate is expressed as $-r$, which is positive. The rate of disappearance is used in Chapters 3 and 5, where for simplicity it is referred to as the reaction rate.

Catalyst level—active site plus support

The rate of a catalytic reaction as defined above exhibits a great disadvantage: the number of the active sites is unknown and cannot be easily determined from common experiments. The difficulties associated to the measurement of active sites leads, for the time being, to the use of “catalyst level rates,” in most practical applications.

Specifically, the most common reaction rate types used are expressed per unit volume of the solid phase (r_{vs}), per unit surface of the solid surface (r_s) or per unit mass of the solid

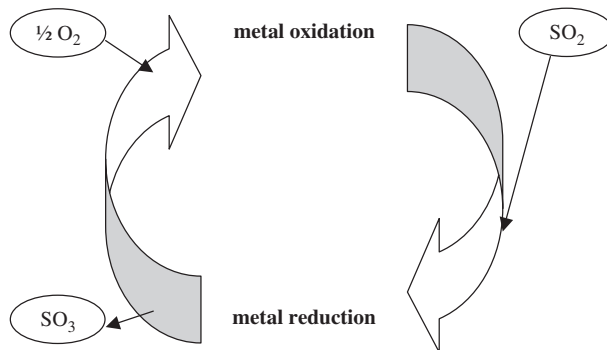


Figure 3.1 Revolution of a catalytic cycle for SO_2 oxidation.

phase (r_m), defined as follows (Levenspiel, 1972):

$$r_{vs} = \frac{1}{V_s} \frac{dN}{dt} \quad (3.2)$$

$$r_s = \frac{1}{S} \frac{dN}{dt} \quad (3.3)$$

$$r_m = \frac{1}{M_s} \frac{dN}{dt} \quad (3.4)$$

where:

- V_s = the volume of solid phase
- S = the surface of the solid phase
- M_s = the mass of the solid phase.

For a specific reaction, the reaction rates, as defined in eqs. (3.2)–(3.4), depend on the nature of the catalytic active site, the surface arrangement of the catalyst, the temperature, and the reactants concentration. *Surface arrangement* here denotes the macroscopic and measurable catalyst basic properties:

- the specific area of the catalyst ($S_s = S/M_s$)
- the number of catalytic active sites per unit area (n/S)

These two basic properties of the catalyst (n/M_s) can be related as follows:

$$\frac{n}{M_s} = \frac{S}{M_s} \frac{n}{S} = S_s \frac{n}{S} \quad (3.5)$$

The number of active sites per unit mass of catalyst (n/M_s) can be referred to as “active sites concentration.”

The principal difference between these “catalyst level” reaction rates and the turnover frequency is that the latter does not depend on the surface arrangement of the catalyst, or in more practical terms, does not depend on the specific physicochemical characteristics of the catalyst as a composite of the active catalytic reagent plus the support.

The turnover frequency and the catalyst level reaction rates can be related through the following equalities:

$$\frac{1}{n} \frac{dN}{dt} = r_t = \frac{V_s}{n} r_{vs} = \frac{S}{n} r_s = \frac{M_s}{n} r_m \quad (3.6)$$

It is noteworthy that the form of the rate ($r_i = f(\text{state of the system})$) does not actually depend on our choice of reaction rate definition. Only the rate coefficients and their dimensions change with each rate definition (Levenspiel, 1972).

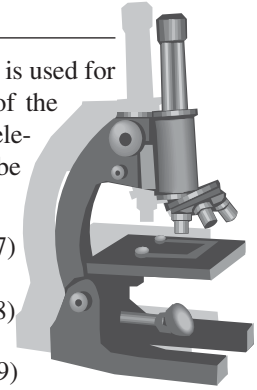
A look into the rate coefficient

Following Carberry (1976), in this book the term “rate coefficient” is used for the proportionality coefficients k_i in the typical rate expression of the form: $r_i = k_i f(C)$. To simplify the following analysis, a first-order elementary reaction is considered. Then the intrinsic reaction rate can be expressed as

$$r_m = k_m C_s \quad (3.7)$$

$$r_{vs} = k_{vs} C_s \quad (3.8)$$

$$r_s = k_s C_s \quad (3.9)$$



where: C_s = the surface concentration of the reactant, (moles/m³) of fluid.

The several rate coefficients have the following units:

$$k_m \rightarrow \frac{1 \text{ m}^3 \text{ fluid}}{\text{s kg solid}}$$

$$k_{vs} \rightarrow \frac{1 \text{ m}^3 \text{ fluid}}{\text{s m}^3 \text{ solid}} = \frac{1}{\text{s}}$$

$$k_s \rightarrow \frac{1 \text{ m}^3 \text{ fluid}}{\text{s m}^2 \text{ solid surface}} = \frac{\text{m}}{\text{s}}$$

Then, after some rearrangements:

$$\frac{1}{n} \frac{dN}{dt} = r_t = \underbrace{\frac{1}{\rho_p} \left(\frac{M_s}{n} \right)}_{k_t} k_{vs} C_s = \underbrace{\frac{S}{n}}_{k_t} k_s C_s = \underbrace{\frac{M_s}{n}}_{k_t} k_m C_s \quad (3.10)$$

where, ρ_p is the particle density. The parameter k_t has the following units:

$$k_t \rightarrow \frac{1 \text{ m}^3 \text{ fluid}}{\text{s } n}$$

This rate coefficient corresponds to the reaction rate r_t , namely, to the reaction rate defined per active site. This rate coefficient for a specific reaction and a fixed catalytic agent and temperature can be considered constant.

In the case of a porous catalyst, where the internal area contributes the most to the total area, S_s can be considered to be independent from the catalyst shape and size. Furthermore, the number of catalytic active sites per unit area (n/S_s) can be considered a fixed property for a given catalyst. Consequently, the active sites concentration can (n/M_s) be also be

considered a given property for a specific catalyst. Then, if the rate coefficient k_i is constant, the rate coefficients k_m , k_{vs} and k_s are constants too.

The previously reported relationship (eq. (3.10)) manifests one more important characteristic of the catalyst level rate coefficients—for the same reaction, temperature, catalytic agent, and support but for different surface arrangement, i.e. active site concentration, these coefficients will be different; and this is an advantage of the usage of k_p , and in general, of turnover frequency (active site level reaction description).

In the case of non-porous spherical particles,

$$S = S_{\text{ex}} = \pi d_p^2 \quad (3.11)$$

$$M_s = \rho_p V_s = \rho_p \frac{\pi d_p^3}{6} \quad (3.12)$$

where S_{ex} denotes the external surface area. Thus,

$$S_s = \frac{S_{\text{ex}}}{M_s} = \frac{6}{\rho_p d_p} \quad (3.13)$$

Then

$$\frac{n}{M_s} = \frac{S_{\text{ex}}}{M_s} \frac{n}{S_{\text{ex}}} = \frac{6}{\rho_p d_p} \frac{n}{S_{\text{ex}}} \quad (3.14)$$

This result means that the number of active sites per unit mass of catalyst is *not constant* since it depends on the particle size. Again, the term n/S_{ex} can be considered to be a constant property for a given catalyst, prepared by the same technique, for all catalyst sizes. Then

$$\frac{1}{n} \frac{dN}{dt} = r_i = \frac{1}{\rho_p} \underbrace{\left(\frac{M_s}{n} \right)}_{k_t} k_{vs} C_s = \frac{S_{\text{ex}}}{n} \underbrace{k_s}_{k_t} C_s = \frac{M_s}{n} \underbrace{k_m}_{k_t} C_s \quad (3.15)$$

Then, if the rate coefficient k_i is constant, k_s is constant too, whereas k_m and k_{vs} are not constants and are dependent on the particle size of the catalyst (eq. 3.14).

The anatomy of rate coefficient

In reactions where the rate is expressed as $r_i = k_i f(C)$, the rate coefficient will often depend on the concentrations, because the latter expression does not take into account the interactions between molecules in a reaction mixture that is thermodynamically nonideal (Froment and Bishoff, 1990). In such a case, if the concentrations are substituted by activities, the rate coefficient is merely independent of the concentration of the reacting species, but one should keep in mind that it is still not truly a constant (Fogler, 1999).

The rate coefficient is almost always dependent on temperature. However, it can be influenced by total pressure, in both gas and liquid systems, plus ionic strength and solvent in liquid systems. Following Fogler (1999), in the present book, the rate coefficient is considered to be a function of only temperature, assuming that the effect of other variables is much less.

Reactor level—Catalyst plus reactor arrangement

The principal difference between homogeneous and heterogeneous reaction rates is that the latter is based on mass, volume, or more rarely, on the area of the solid and not on the fluid-phase volume or reactor volume. The reactor volume or liquid-phase volume is of secondary significance in heterogeneous reactions since the reaction takes place on the solid rather than throughout the reactor volume. Moreover, the mass of the solid is usually used instead of the solid volume or surface, because it is the most easily measured property.

However, for purposes of mass balance in reactors, the following rates have to be also considered: the rate of reaction per unit volume of the fluid phase (r_u) and per unit volume of reactor (R), defined as follows (Levenspiel, 1972):

$$r_u = \frac{1}{V_L} \frac{dN}{dt} \quad (3.16)$$

$$R = \frac{1}{V_R} \frac{dN}{dt} \quad (3.17)$$

where:

$$\begin{aligned} V_L &= \text{the fluid volume} \\ V_R &= \text{the reactor volume.} \end{aligned}$$

So, r_m , r_{vs} , r_s , and r_i are the appropriate rates for expressing the intrinsic catalytic reaction rate, whereas r_u and R are phenomenological rates, used for reactor design. More specifically, r_u is also called the “pseudo-homogeneous rate” (Schmidt, 2005).

For these rates, the following is valid:

$$r_u = \frac{1}{V_L} \frac{dN}{dt} = \frac{V_S}{V_L} r_{vs} = \frac{S}{V_L} r_s = \frac{M_S}{V_L} r_m \quad (3.18)$$

The overall rate of reaction (R) per unit volume of the reactor is (Levenspiel, 1972)

$$R = \frac{1}{V_R} \frac{dN}{dt} = \frac{V_S}{V_R} r_{vs} = \frac{S}{V_R} r_s = \frac{V_L}{V_R} r_u = \frac{M_S}{V_R} r_m \quad (3.19)$$

The design of a reactor is connected to certain preferred parameters and it is useful to know how they are related to each other. For instance, it is very important to use the appropriate terms in order to correlate the reactor volume to the fluid and solid volumes. In Table 3.1, the most important ratios per reactor are presented. V_R denotes the total volume of the reactor, V_S denotes the volume of the solid, and V_L is the fluid volume in two-phase systems and the liquid-volume in three phase systems.

Table 3.1The most important ratios per reactor^a

Reactor	Subtype	Reaction rate ^b	$\frac{V_s}{V_L}$	$\frac{V_s}{V_R}$	$\frac{V_L}{V_R}$	Other
Fixed bed	Two-phase and Trickle bed	R	$\frac{1-\varepsilon}{\varepsilon}$	$1-\varepsilon$	ε	$\frac{M_s}{V_R} = \rho_b$
Slurry	Bubble Columns and Agitated Vessels ^c	r_u	$\frac{m_s}{\rho_p}$	h_s	h_L	$\frac{M_S}{V_L} = m_s$
Fluidized beds	Bubble phase	R	γ_b	$\varepsilon_{\text{bub}}\gamma_b$	ε_{bub}	—
(Two-phase model)	Emulsion phase	R	$\frac{1-\varepsilon_{\text{fm}}}{\varepsilon_{\text{fm}}}$	$(1-\varepsilon_{\text{bub}})(1-\varepsilon_{\text{fm}})$	$(1-\varepsilon_{\text{bub}})\varepsilon_{\text{fm}}$	—
Fluidized beds (L-K model)	All phases	r_u	γ_i	—	—	—
For all Reactors	—	—	—	—	—	$\frac{M_S}{V_S} = \rho_p$

^a ε is the fixed-bed porosity (voidage), ρ_b is the bulk density of solids, ρ_p is the particle density, m_s is the mass of solid per unit volume of bubble-free liquid in slurry reactors, h_s and h_L are the fractional solid and liquid hold-up in slurry reactors, γ_i is the volume of a specific phase per unit volume of the fluid bubbles phase in fluidized beds, ε_{bub} and ε_{fm} are the fraction of the bed occupied by fluid bubbles and the bed voidage at minimum fluidization state in fluidized beds, respectively.

^bThe reaction rate that is most commonly used in the analysis of the corresponding reactor type or model.

^cThree- (slurry) and two-phase systems.

Another critical issue that definitely needs to be clarified is the *surface* of the catalyst per unit volume of reactor or fluid, which is used in reactor analysis. The total surface area of a catalyst includes the internal and the external surface areas. Thus

For fixed-beds:

- for porous particles,

$$\frac{S}{V_R} = \frac{S_s M_s}{V_R} = S_s \rho_b \quad (3.20)$$

- for nonporous particles,

$$\frac{S_{\text{ex}}}{V_R} = \alpha_u \quad (3.21)$$

For slurries:

- for porous particles,

$$\frac{S}{V_L} = \frac{S_s M_s}{V_L} = S_s m_s \quad (3.22)$$

- for nonporous particles,

$$\frac{S_{\text{ex}}}{V_L} = \alpha_c \quad (3.23)$$

For particles:

- for porous particles,

$$\frac{S}{V_s} = \frac{S_s M_s}{V_s} = S_s \rho_p \quad (3.24)$$

- for nonporous particles,

$$\frac{S_{\text{ex}}}{V_s} = \frac{6}{d_p} \quad (3.25)$$

where:

S_s = the surface area per unit mass of catalyst

S_{ex} = the external surface area of catalyst.

By using these ratios and the relationships (3.18) and (3.19), we can alter the material balance expressions and the corresponding solutions of the reactor models if we use other rate expressions. It should be noted that in practice, in fixed-beds and slurries of porous particles, the external area of the particle and thus the parameters a_u and a_c are used, respectively.

It should be noted that when referring to the reaction rate per unit surface of a porous particle or to the corresponding rate coefficient, it should be clarified whether the rate or the rate coefficient is based on the external or the total surface area. Then, for example, in a slurry reactor where the reaction rate is expressed per unit volume of liquid, the rate could be

$$r_u = S_s m_s k_s f(C) \quad (3.26)$$

or

$$r_u = a_c k_s f(C) \quad (3.27)$$

These two expressions are equivalent only for nonporous particles. For porous particles, $S_s \cdot m_s$ is very different from a_c as well as the corresponding k_s values.

A look into turnover frequency

Beyond the difficulties met in the determination of the number of active sites in order to estimate the turnover frequency, there are more problems to be solved. The turnover frequency, even in the case that it is measured by employing an ideal experiment, might be only an average one. This is partly because the active sites could exhibit different reactivities, i.e. they are not identical in respect to the catalytic reaction.

An interesting question, expressed by Boudart (1985), is the following: As particle size grows from that of a small cluster to infinite value for a single macroscopic crystal, how does the value of turnover frequency change for a given reaction on a given metal?

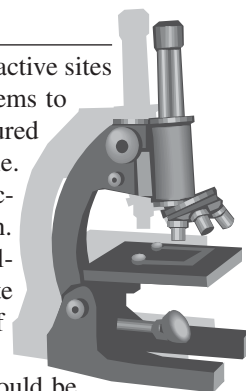
Several experimental results revealed that turnover frequency could be different for a class of reactions called “structure-sensitive” (Boudart, 1981; Yates, 1981). An operational definition of structure sensitivity (Boudart, 1995) is that “the turnover frequency depends on surface crystalline anisotropy revealed by working on different faces of a single crystal or on clusters of varying size between 1 and 10 nm.” The surface crystalline anisotropy is directly related to the crystallographic orientation (planes) of the supported catalytically active atoms, which in turn, is affected by the particle size (Boudart, 1981). It should be noted that the term “particle” here has the meaning of a pure active agent structure. Thus, by increasing particle size, the number of active sites is increased too.

In contrast, structure-insensitive reactions are those for which turnover frequency under fixed conditions does not depend or depends slightly on the surface crystalline anisotropy of clusters of varying size or of single crystals exposing different faces. For these kinds of reactions, all accessible surface atoms can be considered as equally active sites (Boudart, 1981 and 1995).

In order to avoid any confusion, the “surface structure” used in sensitive and insensitive reaction analysis has nothing to do with the “surface arrangement” used in the catalyst level rates analysis—the first refers to the microscopic level of the active site, whereas the latter to the catalyst level.

The usage of turnover frequency exhibits various advantages (Boudart, 1995):

- The value of the turnover frequency can be reproduced in different laboratories, if the method of measurement of the rate and the counting of sites are kept the same. Moreover, the use of turnover frequency allows the comparison between two catalysts that differ in metal or size for a specific reaction. The great advantage of such a comparison is that the activity of different catalysts is compared at active site level without the considerations of catalyst arrangement. To be more specific, using turnover frequency, we can compare the activity of the pure active site, ignoring the specific area of the catalyst.
- By definition, the turnover frequency is expressed per number of active sites. So, catalytic samples that differ only in the amount active sites must exhibit the same values of turnover frequency. If not, heat and mass transfer phenomena are present. Specifically, the correct measurement of intrinsic kinetic data in heterogeneous catalysis is difficult due to the effect of heat and mass transfer, especially inside the pores of high specific-area materials. The turnover frequency reveals these phenomena. In other words, in the case of supported



metals, if the same value of turnover frequency is obtained for a specific reaction at fixed conditions on two catalytic samples containing different amounts of metal on the porous support, the kinetic data are not obscured by heat or mass transfer phenomena.

3.1.2 The concept of the overall reaction rate in heterogeneous reactions

General

In heterogeneous reactions, phase boundaries exist between phases and transport processes; the intrinsic rate of reaction should be taken into account simultaneously in reactor design. The combination of mass transfer rates and reaction rates leads to the so-called overall rate. The goal is to express the global rate in terms of the bulk properties of the phases, eliminating the interphase properties.

If the overall phenomenon requires that a number of steps take place in *series*, then, at steady state, all these steps will proceed at the same rate, which is equal to the overall rate (Levenspiel, 1972):

$$r_{\text{overall}} = r_1 = r_2 = \dots = r_n \quad (3.28)$$

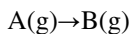
There are cases, as in catalysis, where some steps are *in parallel*. In these systems, the overall rate is greater than the rate of each individual step. If these steps are independent of each other, the overall rate is the sum of all individual rates (Levenspiel, 1972).

$$r_{\text{overall}} = \sum_{n=1}^n r_i \quad (3.29)$$

The elimination of the interphase concentrations could be done easily if the rate expressions of all steps are linear in concentration. However, for nonlinear expressions, it is difficult to evaluate and handle the overall rate. We will examine some simple cases in two- and three-phase systems.

Two-phase systems

In the case of two fluids, two films are developed, one for each fluid, and the corresponding mass-transfer coefficients are determined (Figure 3.2). In a fluid–solid system, there is only one film; whereas the resistance within the solid phase is expressed by the solid-phase diffusion coefficient, however, in many cases an “effective” mass-transfer coefficient is used in the case of solids as well. Consider the irreversible catalytic reaction of the form



Here, we consider the general case of a porous catalyst, where the internal diffusion effect is included in the effectiveness factor (η_s).

The intrinsic rate of reaction per unit mass of catalyst is (in mol/m²s)

$$(-r_s) = -\frac{1}{S} \frac{dN}{dt} = \eta_s k_s C_s \quad (3.30)$$

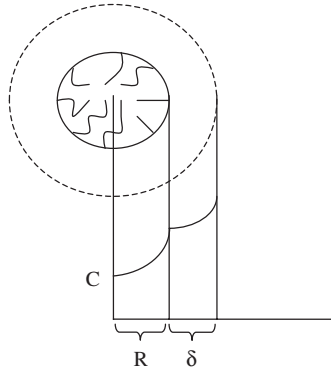


Figure 3.2 Two-phase system.

This is the rate of disappearance of the reactant A and

S = the total surface of the catalyst, m^2

k_s = the rate coefficient, m^3/m^2s

C_s = the concentration of reactant at the outer surface of the catalyst particle, mol/m^3 .

The rate of mass transfer from the bulk of the gas to the catalyst surface is:

$$r_g = k_g(C_G - C_s) \quad (3.31)$$

where:

k_g = the mass transfer coefficient in the gas film, m/s

C_G = the concentration of reactant in the bulk gas phase, mol/m^3 .

At steady state,

$$(-r_s) = r_g = -\frac{1}{S} \frac{dN}{dt} = \eta_s k_s C_s = k_g(C_G - C_s) \quad (3.32)$$

From the equality of the rates, the concentration of reactant at the outer surface of the catalyst particle can be expressed in terms of bulk concentration:

$$C_s = \frac{k_g}{k_g + \eta_s k_s} C_G \quad (3.33)$$

Then, the overall reaction rate (r_{ov}) can be also expressed in terms of the bulk concentration of the reactant:

$$r_{ov} = (-r_s) = r_g = \eta_s k_s \frac{k_g}{k_g + \eta_s k_s} C_G = k_{ov} C_G \quad (3.34)$$

where k_{ov} is the overall coefficient in m/s .

The reciprocal of this coefficient is referred to as total resistance:

$$\frac{1}{k_{ov}} = \frac{1}{k_g} + \frac{1}{\eta_s k_s} \quad (3.35)$$

It should be noted that the overall coefficient (k_{ov}) has been derived under the assumption that the reaction is taking place mainly in the internal surface of the catalyst. See Chapter 5 for a more rigorous analysis on the subject.

The concept of the rate-controlling step

When a process consists of several individual steps in series, the concept of the rate-controlling step simply states that one of the several steps involved provides the major resistance to the overall process. In such a case, this slow step is termed the “rate-controlling step” and can be considered as acting alone (Levenspiel, 1972).

Instead of molecules flowing, consider water flowing through a pipe with a number of partially opened valves. The flow of the water in the pipe will be determined by the valve that offers the largest resistance to the flow. Actually, we could come up with a fairly accurate estimate of the flow by calculating the resistance to the flow in this valve, neglecting all the others.

Consider the first-order reaction analyzed in the previous paragraph. In the limiting case where $k_s \rightarrow \infty$ or $k_s \gg k_g$, the resistance to the overall rate is due to the gas film around the catalyst and $C_s \rightarrow 0$. The rate-controlling step is the diffusion in the gas film and the overall rate is

$$(-r_s) = k_g C_G \quad (3.36)$$

On the other hand, if $k_g \rightarrow \infty$ or $k_g \gg k_s$, the resistance to the overall rate is owing to the intrinsic reaction rate and $C_G \rightarrow C_s$. The rate-controlling step is the reaction rate and the overall rate is

$$(-r_s) = \eta_s k_s C_G \quad (3.37)$$

Note that due to the equality of the individual rates, if $k_s \rightarrow \infty$ then $C_s \rightarrow 0$, and if $k_g \rightarrow \infty$ then $(C_G - C_s) \rightarrow 0$ or $C_G \rightarrow C_s$; and so, the individual rates are finite and equal to the overall rate. It is the resistance of the individual step and not the corresponding rate that could be zero under certain operating conditions.

The concept of the rate-controlling step is much more useful in complex kinetic expressions, where the overall rate is nonlinear and cannot be obtained by following a simple procedure as presented above for the case of a first-order reaction.

For example, consider a second order reaction. In this case, the intrinsic reaction rate is

$$(-r_s) = k_s C_s^2 \quad (3.38)$$

while the rate of mass transfer from the bulk of the gas to the catalyst surface is

$$r_g = k_g (C_G - C_s) \quad (3.39)$$

Then

$$(-r_s) = r_g = k_s C_s^2 = k_g (C_G - C_s) \quad (3.40)$$

Working as in the first-order reaction case, it can be proved that after the elimination of the surface concentration we have

$$C_s = \frac{-k_g + \sqrt{k_g^2 + 4k_g k_s C_G}}{2k_s} \quad (3.41)$$

It is obvious that the reaction rate becomes a complicated expression with the introduction of the surface concentration.

$$r_{ov} = (-r_s) = r_g = -\frac{k_g}{2k_s} (2k_s C_G + k_g - \sqrt{k_g^2 + 4k_g k_s C_G}) \quad (3.42)$$

In this case, we cannot work as in the case of the first-order reaction to derive more simple expressions. However, the principle of the rate-controlling step is still applicable. If the rate-controlling step is the diffusion in the gas film, the overall rate (r_{ov}), is

$$r_{ov} = k_g C_G \quad (3.43)$$

If the rate-controlling step is the reaction rate, the overall rate (r_{ov}), including the effectiveness factor, is

$$r_{ov} = \eta_s k_s C_G^2 \quad (3.44)$$

Three-phase systems

In three-phase systems, two interfaces exist, i.e. the gas bubble–liquid interface and the liquid–solid interface and thus, four mass-transfer steps and the corresponding films are involved in the process (Figure 3.3)

- mass transfer from the bulk gas to the gas bubble–liquid interface (gas-bubble film)
- mass transfer from the bubble interface to the bulk liquid (liquid film around the bubble)
- mass transfer to the solid surface (liquid film around the particle)
- mass transfer within the solid phase

All these mechanisms along with any reaction in the solid phase are considered to be processes in series (Smith, 1981). In three-phase systems, three interface concentrations, two in the gas–liquid interface $C_{G,i}$ and $C_{L,i}$, and one in the liquid–solid interface C_s , have to be eliminated. If equilibrium exists at the bubble–liquid interface, $C_{G,i}$ and $C_{L,i}$ are related by Henry's law:

$$C_{G,i} = H C_{L,i} \quad (3.45)$$

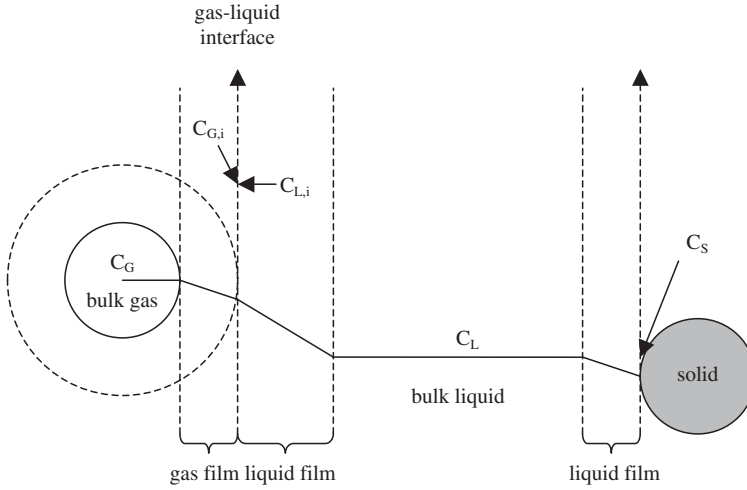


Figure 3.3 Mass transfer in three-phase systems.

where H is the dimensionless Henry's constant.

Similar to the two-phase case, for a first-order reaction (in mol/m²s),

$$(-r_s) = k_s \eta_s C_S \quad (\text{reaction on the solid surface}) \quad (3.46)$$

$$r_f = k_f (C_L - C_S) \quad (\text{bulk liquid to catalyst surface}) \quad (3.47)$$

where:

k_f = the liquid–solid mass transfer coefficient, m/s

C_L = the liquid-phase bulk concentration.

In three-phase systems, two more films exist and the corresponding mass transfer rates are

$$r_g = k_g (C_G - C_{G,i}) \quad (\text{bulk gas to bubble interface}) \quad (3.48)$$

$$r_{fg} = k_{fg} (C_{L,i} - C_L) \quad (\text{bubble interface to bulk liquid}) \quad (3.49)$$

where k_{fg} is the gas–liquid interface liquid mass transfer coefficient, m/s.

At steady state,

$$r_{ov} = (-r_s) = r_f = r_g = r_{fg} \quad (3.50)$$

Then, the above equations can be combined appropriately to eliminate the unknown concentrations and the rate can be expressed solely in terms of the concentration of the reactant in the bulk of the gas:

$$r_{ov} = K_{ov} C_G \quad (3.51)$$

where K_{ov} is an overall coefficient (in m/s):

$$\frac{1}{K_{\text{ov}}} = \frac{1}{k_g} + \frac{H}{k_{\text{fg}}} + H \left(\frac{1}{k_f} + \frac{1}{\eta_s k_s} \right) \quad (3.52)$$

It is noteworthy that not all the resistances are significant in every case. If only a pure gas constitutes the gas phase and for slightly soluble gases, the resistance to the mass transfer on the liquid side of the interface is predominant. Under these conditions, $C_G = C_{G,i}$ and the above equation reduces to

$$\frac{1}{K_{\text{ov}}} \cong H \left(\frac{1}{k_{\text{fg}}} + \frac{1}{k_f} + \frac{1}{\eta_s k_s} \right) \quad (3.53)$$

Even when the gaseous reactant is in a mixture with other components in the bubbles, k_g appears to be much larger than k_{fg}/H and thus, the last equation is applicable.

Derivation of an overall gas transfer rate

In many three-phase systems, the two resistances in the gas–liquid interface are combined in one overall gas mass transfer coefficient K_L . To do this, we combine the following rates:

$$r_g = k_g(C_G - C_{G,i}) \quad (\text{bulk gas to bubble interface}) \quad (3.54)$$

$$r_{\text{fg}} = k_{\text{fg}}(C_{L,i} - C_L) \quad (\text{bubble interface to bulk liquid}) \quad (3.55)$$

If equilibrium exists at the bubble–liquid interface, $C_{G,i}$ and $C_{L,i}$ are related by Henry's law:

$$C_{G,i} = HC_{L,i} \quad (3.56)$$

Then

$$C_{L,i} = \frac{k_g C_G + k_{\text{fg}} C_L}{k_{\text{fg}} + \frac{k_g}{H}} \quad (3.57)$$

The rate becomes

$$r_{\text{fg}} = k_{\text{fg}}(C_{L,i} - C_L) = \frac{Hk_g k_{\text{fg}}}{k_{\text{fg}} + Hk_g} \left(\frac{C_G}{H} - C_L \right) \quad (3.58)$$

Defining an overall gas-phase mass transfer coefficient K_L (in m/s),

$$K_L = \frac{Hk_g k_{\text{fg}}}{k_{\text{fg}} + Hk_g} \Leftrightarrow \frac{1}{K_L} = \frac{1}{Hk_g} + \frac{1}{k_{\text{fg}}} \quad (3.59)$$

we have

$$r_{fg} = r_g = K_L (C_{L,eq} - C_L) \quad (3.60)$$

where $C_{L,eq}$ is the equilibrium concentration in the liquid:

$$C_{L,eq} = \frac{C_G}{H} \quad (3.61)$$

This is the concentration in equilibrium with the bulk gas concentration C_G . It is important to note that in the general case,

$$C_{L,eq} \neq C_{L,i} \quad (3.62)$$

$$C_G \neq C_{G,i} \quad (3.63)$$

Note that

$$C_{L,i} = \frac{C_G + (k_{fg}/k_g)C_L}{\frac{k_{fg}}{k_g} + H} \quad (3.64)$$

$$C_{G,i} = C_{L,i}H \quad (3.65)$$

In the case of $k_g \rightarrow \infty$, or in other words, when there is no resistance in the gas phase (gas phase consists of a pure gas),

$$C_{L,i} = \frac{C_G}{H} = C_{L,eq} \quad (3.66)$$

$$C_{G,i} = C_G \quad (3.67)$$

$$K_L = k_{fg} \quad (3.68)$$

Finally, if the liquid is saturated with gas,

$$C_{L,eq} = C_L \quad (3.69)$$

3.2 HETEROGENEOUS REACTORS

3.2.1 Introduction

Chemical reactors vary widely in shape and in the mode of operation. Consequently, there are various ways of classifying them. The first classification is based on the number of the

involved reacting phases—

- homogeneous reactors, where one phase such as liquid or gas exists in the reactor
- heterogeneous reactors, where two or three distinct phases coexist in the reactor.

A further classification of homogeneous and heterogeneous reactors is based on the nature of the involved reacting phases—

- homogeneous reactors
 - liquid-phase reactors
 - gas-phase reactors
- heterogeneous reactors
 - liquid–solid (L–S) reactors
 - gas–solid (G–S) reactors
 - liquid–gas (L–G) reactors
 - liquid–gas–solid (L–G–S) reactors

Finally, classification could be based on the contacting pattern of the involved reacting phases, as it is described in the following sections.

3.2.2 Homogeneous reactors

Plug-flow tubular reactor (PFTR): This reactor is operated under steady-state condition. The reactor is of tubular shape, the reactants enter at the inlet and the composition is a function of the distance from the inlet. However, the composition is not a function of time. The ideal plug-flow reactor is characterized by the absence of mixing in the direction of flow and complete mixing in the transverse direction.

Continuous-stirred tank reactor (CSTR): This reactor is operated under steady-state condition. The reactants flow continuously in and out of the vessel at a constant flow rate and are perfectly mixed by mechanical means, and thus the composition is the same throughout the reactor. The result is that the exit concentration is the same as the one in the reactor. The concentration is constant, i.e. is not time-dependent.

Batch-stirred tank reactor (BSTR): In this type of reactor, the reactants are fed into the container, they are well mixed by means of mechanical agitation, and left to react for a certain period of time. This is an unsteady-state operation, where composition changes with time. However, the composition at any instant is uniform throughout the reactor.

3.2.3 Heterogeneous reactors

Gas–liquid heterogeneous reactors

Gas–liquid continuous-stirred tank reactor: This is a CSTR, where the liquid and gas phases are mechanically agitated (Figure 3.4).

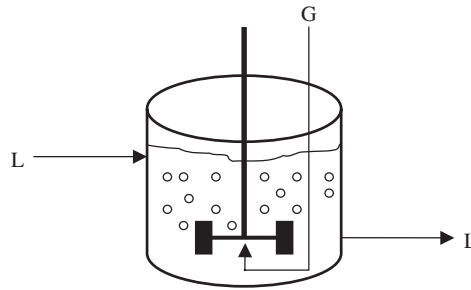


Figure 3.4 A gas–liquid continuous-stirred tank reactor.

Gas–liquid bubble column: This reactor is of tubular shape (Figure 3.5). The liquid phase is agitated by the bubble rise of the gas phase. The gas phase flows through the reactor upward at a constant rate. The liquid phase is continuous. This reactor could be of continuous type, if the liquid is flowing through the reactor continuously; or semibatch, if the liquid is stationary in the reactor.

Two-phase fluid–solid heterogeneous reactors

Agitated tank reactors *Batch agitated reactor:* This is a batch stirred tank reactor. For liquid–solid systems, the liquid is agitated by a mechanical apparatus (impeller) and the reactor is of tank shape. For gas–solid systems, the gas is agitated and rapidly circulated through a fixed-bed of solids. This reactor is basically an experimental one used for adsorption, ion exchange, and catalysis studies.

Carberry reactor: The gas flows continuously through the tank-type reactor, whereas the catalyst is placed in rotating baskets in the reactor. This reactor is also experimental and suitable for catalysis as well as for adsorption studies (Figure 3.6).

Fixed-bed reactors *Fixed-bed reactor (FBR):* Gas or liquid reactants flow at a constant rate over a fixed-bed of solids placed in a tubular vessel (Figure 3.7). The fixed-bed reactor can be viewed as a semibatch reactor, where the solid phase is fixed and the fluid is flowing continuously through the reactor. The operation is steady state for catalysis and unsteady state for adsorption and ion exchange. Some applications of FBR are the following: HDS of naphtha, catalytic reforming, steam reforming, water-gas shift, methanation, ammonia synthesis, and methanol synthesis. This contacting pattern is by far the most common in adsorption and ion-exchange processes.

Monolith reactor: This type of reactor is used extensively for the abatement of automobiles exhaust emissions. The gas flows continuously through the reactor, whereas the catalyst is a continuous phase consisting of a ceramic support and the active phase, which is dispersed onto the support. The support is structured in many channels and shapes that achieve large catalytic surface at small volume. A typical application of monolith reactors is the exhaust gas cleaning.

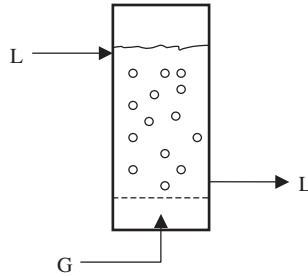


Figure 3.5 A bubble column reactor.

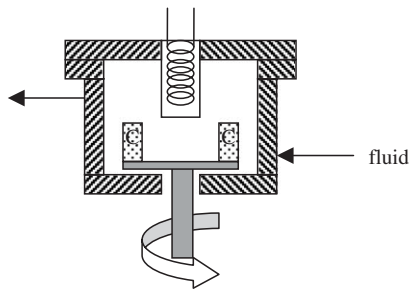


Figure 3.6 A Carberry reactor (C is the catalyst).

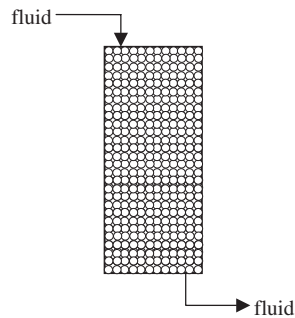


Figure 3.7 The fixed-bed reactor.

Reactors with moving solid phase *Moving-bed reactor:* There are various installations of moving-bed reactors. In the combustion of large coal, the solid phase is in cross-flow to the air supply by means of a moving strip. In another type of moving-bed reactor, the solid particles are fed at the top and continuously move downward to be discharged at the bottom. Catalytic reforming and coal combustion are typical applications of this type of reactor.

Fluidized-bed reactor (FLBR): The up-flow gas or liquid phase suspends the fine solid particles, which remain in the reactor (Figure 3.8). This reactor is of tubular shape with a relatively low aspect ratio of length to diameter. The most common application of FLBR is the classical FCC process.

Entrained flow reactor (riser): This is a fluidized-bed reactor in which the solid is entrained by the fluid phase and is recycled throughout the operation (Figure 3.9). Some applications of this reactor type are the modern FCC process and the calcination of alumina hydrate.

Three-phase heterogeneous reactors

Three-phase reactors are generally needed in cases where there are both volatile and non-volatile reactants, or when a liquid solvent is necessary with all reactants in the gas-phase (Smith, 1981). Some examples are

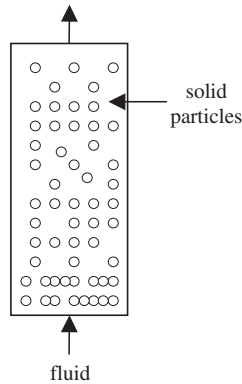


Figure 3.8 The fluidized-bed reactor.

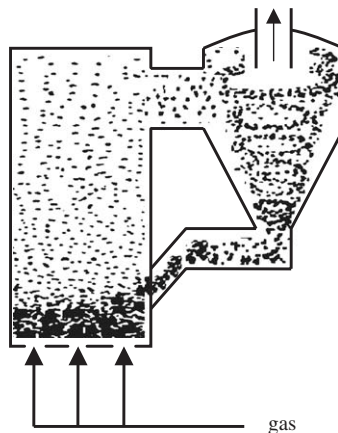


Figure 3.9 The entrained flow reactor.

- hydrogenation of oils
- oxidation of liquids
- oxidation of pollutants dissolved in liquids
- polymerization reactions.

Fixed-bed reactors *Trickle-flow reactor (TFR)*: This is a tubular flow reactor with a concurrent down-flow of gas and liquid over a fixed-bed of catalyst (Figure 3.10). Liquid trickles down whereas the gas phase is continuous. This reactor is mainly used in catalytic applications. Typical application examples of this reactor type are the following: HDS of heavy oil fractions and catalytic hydrogenation of aqueous nitrate solutions.

Packed Bubble Bed Reactor (BBR): This is a tubular flow reactor with concurrent up-flow of gas and liquid (Figure 3.11). The catalyst bed is completely immersed in a continuous liquid flow while gas rises as bubbles. Some applications of BBR are the catalytic denitrification of aqueous nitrate solutions and the hydrogenation processes.

Reactors with moving solid phase *Three-phase fluidized-bed (ebullated-bed) reactor*: Catalyst particles are fluidized by an upward liquid flow, whereas the gas phase rises in a dispersed bubble regime. A typical application of this reactor is the hydrogenation of residues.

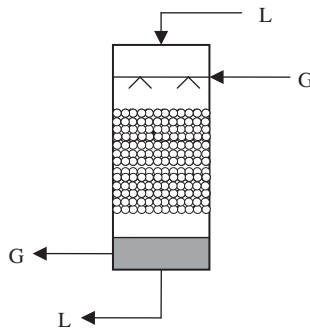


Figure 3.10 The trickle-bed reactor.

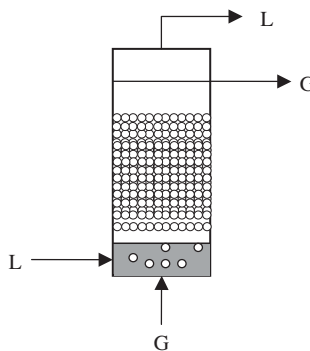


Figure 3.11 The packed bubble bed reactor.

Slurry Bubble Column Reactors (SBCR): This reactor is tubular (Figure 3.12). The liquid is agitated by means of dispersed gas bubbles. Gas bubbles provide the momentum to suspend the catalyst particles. The gas phase flows upward through the reactor at a constant rate. This reactor could be of continuous type or of semibatch type. This type is used only in catalysis.

Agitated slurry reactor (ASR): This is a mechanically agitated gas–liquid–solid reactor (Figure 3.13). The liquid is agitated by a mechanical apparatus (impeller). The fine solid particles are suspended in the liquid phase by means of agitation. Gas is sparged into the liquid phase, entering at the bottom of the tank, normally just under the impeller. This reactor can also be of continuous type or of semibatch type. This type is used only in catalysis.

3.3 TWO-PHASE AGITATED REACTORS

The analysis of this type of reactor requires a uniform composition of fluid phase throughout the volume. While this is easily achieved by standard agitation devices for liquid–solid systems, i.e. impellers, it requires special design to be achieved for gas–solid systems. This type of reactor is basically used for laboratory experimentation.

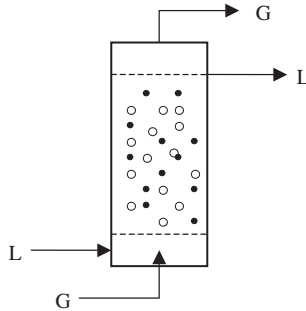


Figure 3.12 The slurry bubble column reactor.

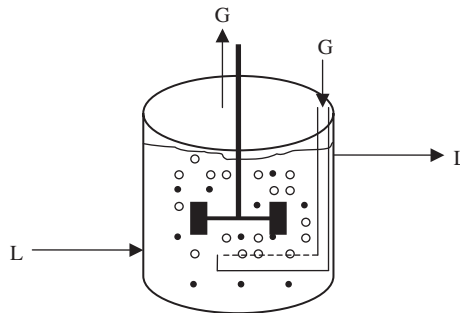


Figure 3.13 The agitated slurry reactor.

3.3.1 Mixing in liquid–solid reactors

An agitator is a device consisting of at least a power package, a shaft, and an impeller to agitate the contents of a vessel. Mechanical agitation of a liquid by a rotating device such as an impeller is especially suitable for dispersing solids, liquids, or gases into liquids; and is used for a variety of applications where mass transfer is of principal importance. In general, agitators are able to produce highly turbulent flows, which at the same time produce good mass transfer coefficients and effective dispersion of solids, liquids, and gases.

The impeller is the part of the agitator that impacts force to the material being mixed. Propellers, turbines, gates, anchors, and paddles are all types of impellers. Typically, the impeller is a single propeller or turbine blade connected to a shaft that is driven by an electric motor at a fixed speed. There are two classes of impeller agitators: axial-flow and radial-flow, and the mixing characteristics are shown in Figure 3.14.

Axial-flow impellers generate currents parallel to the axis of the impeller shaft. Radial-flow impellers generate currents in a direction tangential or radial to the axis of the impeller shaft. Within the two classes of impellers, there are three main types of impeller design. These are propeller, turbine, and paddle. The three main types are utilized in about 95% of most batch liquid agitation systems. Standard propellers have three blades, but two-bladed, four-bladed, or impellers encased by a circular guard can also be used.

Axial-flow and mixed-flow impellers

Propeller A propeller is a three- or four-bladed flow impeller, having helically shaped blades. The flow is primarily axial (discharge flow parallel to the agitator shaft) and is most effective in low-viscosity fluids. The marine-type propeller (Figure 3.15) is characteristically operated at relatively high speed, particularly in low-viscosity liquids (Treybal, 1980).

A revolving propeller traces out a helix in the fluid. One full revolution moves the liquid a fixed distance. The ratio of this distance to the propeller diameter is known as the pitch. In the case of turbines, “pitch” is the angle the blades make with the horizontal plane. Propellers are members of the axial class of impeller agitators. The propeller is turned so that it produces a flow toward the bottom of the vessel. Propellers are more frequently used for liquid blending operations than for mass transfer purposes (Treybal, 1980).

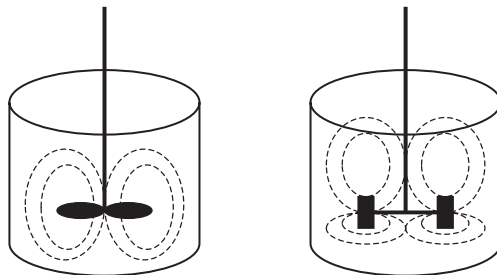


Figure 3.14 *Left:* Axial-flow pattern (marine impeller). *Right:* Radial-flow pattern (flat blade turbine impeller).

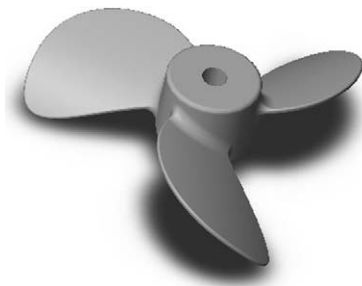


Figure 3.15 Marine-type (propeller) impeller.

Pitched blade turbine The pitched blade turbine is essentially a modified open flat-blade turbine with the blades angled (Figure 3.16). It is available with different blade angles and the 4-blade, 45° pitch turbine is the most common and popular type. The flow is discharged both axially and radially, depending on the angle. For the typical case of a 45° axial-flow turbine, one half of the total flow is discharged axially and one half radially (mixed-flow).

The 45° axial-flow turbine is more efficient at all Reynold's numbers than the flat-blade radial turbine. However, as the pitch angle decreases below 45° , the impeller becomes increasingly sensitive to high viscosity.

The pitched-blade turbine is a reasonably cost-effective impeller in both turbulent and laminar flow. It is also a suitable impeller for applications where the viscosity changes over a wide range causing the flow regime to vary between turbulent and laminar flow. Moreover, it is a cost-effective impeller for solid suspensions.

Radial-flow impellers and turbines

Flat-blade radial-flow impellers The flat-blade radial turbine has vertical blades, parallel to the mixer shaft. Four blades are most commonly used although radials are available with as few as two blades to as many as eight. The flow is discharged radially and splits into two equal flows after leaving the blade tips. Two types of radial turbines are generally in use. They are the open type with blades fastened to the impeller hub (open-type turbines), or the disc type with blades fastened to a disk, which is attached to the hub (Rushton turbines). The turbine diameter is typically 30 – 50% of the vessel diameter. Radial-flow impellers have blades that are parallel to the axis of the drive shaft. The smaller multiblade ones are known as turbines; larger, slower speed impellers with two or four blades are often called paddles. Paddles are two or four blades mounted on the end of the agitator shaft. They are a subset of the radial class of impeller agitators. Typically, the impeller diameter of paddles is 50 – 80% of the tank diameter. Turbines, particularly the flat-blade designs, are frequently used for mass transfer operations (Treybal, 1980).

Open-type turbines This kind of turbines is also called “full-blade turbines” (Figure 3.17). The blades are vertical (parallel to the axis of the drive shaft) and could be straight or curved. They are cost-effective impellers for operations very near the floor of a tank for agitating the

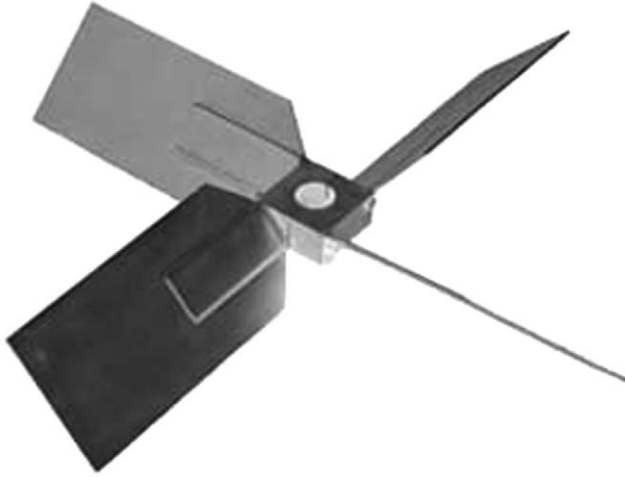


Figure 3.16 Pitched-blade turbine.

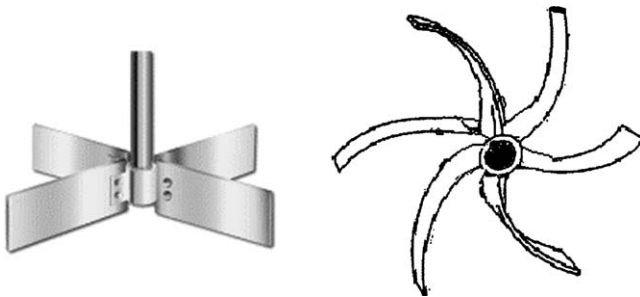


Figure 3.17 *Left:* Straight-blade open turbine. *Right:* Curved-blade open turbine.

heel in solid suspension applications. Moreover, they are effective in laminar flow applications, especially when impeller Reynolds numbers drop below 50.

Disc-type turbines In this type of turbines, blades can be straight or curved. In the related literature, the term “straight” is some times replaced by the term “flat.” The most popular turbine of this type is the straight-blade disc turbine, which is better known as the “Rushton turbine” (Figure 3.18). The same turbine is also called “flat-blade turbine, vaned disc” or simply “flat-blade turbine.”

This type is a good cost-effective impeller for low concentrations of immiscible liquid or gas. Two very strong trailing vortices are shed from each blade. These areas of high shear are responsible for breaking the larger droplets to smaller droplets. Maximum aeration numbers should be limited to 0.1. Like all radial-flow impellers, the Rushton turbine is designed to provide the high shear conditions required for breaking bubbles and thus increasing the oxygen transfer rate.

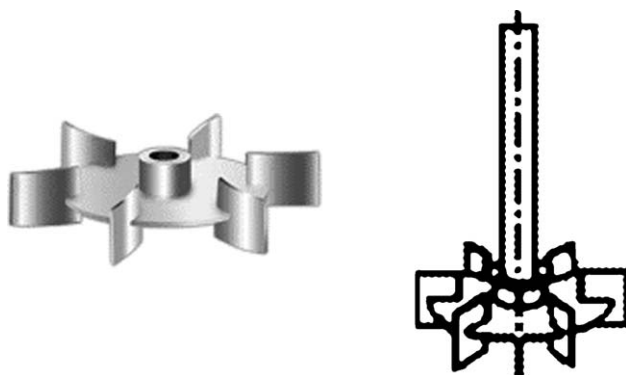


Figure 3.18 Rushton impellers.

Vertical blade disc turbines can have “curved” blades, and in this case they are called “Smith” turbines.

Flow patterns in agitated vessels

Unbaffled tanks If a low-viscosity liquid is stirred in an unbaffled tank by an axially mounted agitator, there is a tendency for a swirling flow pattern to develop regardless of the type of impeller (Perry and Green, 1999). Figure 3.19 shows a typical flow pattern. A vortex is produced owing to the centrifugal force acting on the rotating liquid. In spite of the presence of a vortex, satisfactory process results often can be obtained in an unbaffled vessel. However, there is a limit to the rotational speed that may be used, since once the vortex reaches the impeller, severe air entrainment may occur. The so-called surface aeration is undesirable due to its negative effect on the mass transfer coefficients (see Section 3.5.3).

In addition, the swirling mass of liquid often generates an oscillating surge in the tank, which coupled with the deep vortex, may create a large fluctuating force acting on the mixer shaft. The drawing of gas into liquid is frequently undesirable, in addition, vortex formation leads to difficulties in scaling up, so that steps are usually taken to prevent vortices (Treybal, 1980) (Figure 3.20).

Baffled tanks In this case, the tank is supplied with baffles that are flat vertical strips placed radially along the tank wall so that adequate agitation of thin suspensions can be achieved, as shown in Figure 3.21. Usually, four baffles are enough. A common baffle width is one-tenth to one-twelfth of the tank diameter (radial dimension). In the agitation of slurries, the accumulation of solids near the walls or baffles has to be avoided. It can be prevented by placing the baffles at a distance that is half their width, from the vessel wall. For Reynolds numbers greater than 2000, baffles are commonly used with turbine impellers and with on-centerline axial-flow impellers. The use of baffles results in a large top-to-bottom circulation without vortexing or severely unbalanced fluid forces on the impeller shaft. In the transition region ($10 < N_{Re} < 10,000$), the width of the baffle may be reduced to one-half the standard width. In the case that the circulation pattern is satisfactory in an

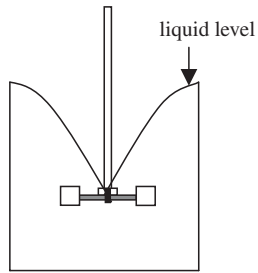


Figure 3.19 Typical flow pattern in an un baffled tank.

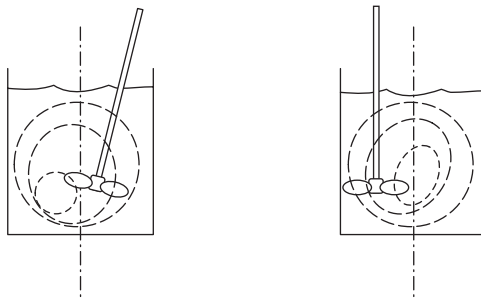


Figure 3.20 Typical flow pattern for a noncentered impeller.

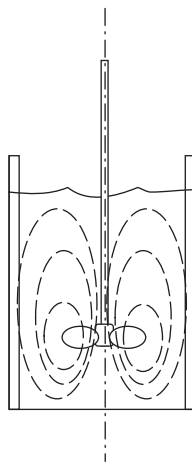


Figure 3.21 Typical flow pattern in a baffled tank.

unbaffled tank but a vortex creates problems, partial-length baffles may be used. These are of standard width and extend downward from the surface into about one-third the liquid volume. In the region of laminar flow ($N_{Re} < 10$), the same power is consumed by the impeller whether baffles are used or not, and they are not usually required. The flow pattern may be affected by the baffles, but not always advantageously. When they are needed, the baffles are usually placed one or two widths radially off the tank wall, to allow fluid to circulate behind them and at the same time produce some axial deflection of flow.

3.3.2 Mixing in gas–solid systems

Batch reactors

To ensure complete and uniform mixing conditions of the fluid throughout the reactor, in such systems, a special design is required. Such a design has been presented by Levenspiel (1972) and it is shown in Figure 3.22.

In this type of reactor, an agitator is used for mixing the fluid in the main body of the vessel, whereas the gas is rapidly circulated throughout the reactor and forced to flow through the catalyst bed. A low conversion per pass through the catalyst is required so that uniform composition in the reactor is achieved.

Continuous flow reactors

A mixed-flow reactor requires uniform composition of the fluid phase throughout the volume while the fluid is constantly flowing through it. This requires a special design in order to be achieved in the case of gas–solid systems. These reactors are basically experimental devices, which closely approach the ideal flow conditions and have been devised by Carberry (Levenspiel, 1972). This device is called a “basket-type mixed reactor” (Figure 3.6). The catalyst is contained in four rapidly spinning wire baskets.

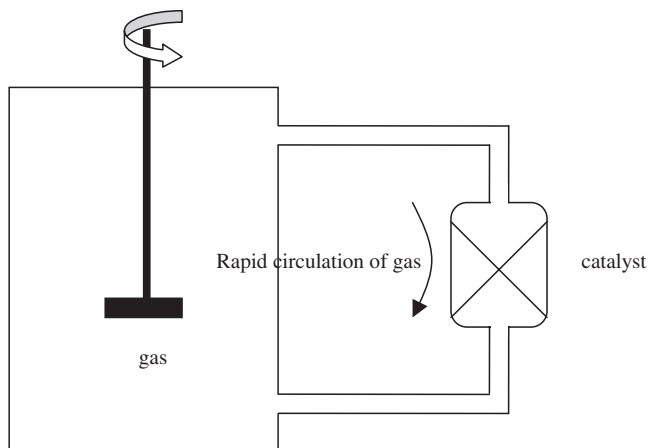


Figure 3.22 Mixing in gas–solid batch reactors.

This kind of reactor is very useful in experimental studies when the goal is the elimination of the external fluid film resistance. It is used for catalytic as well as adsorption systems (Ruthven, 1984).

3.3.3 Material balances in two-phase agitated reactors

Batch reactors

For any reactor, the conservation principle can be represented by the following relationship:

$$\left\{ \begin{array}{c} \text{rate of flow} \\ \text{of } i \text{ into} \\ \text{volume element} \end{array} \right\} - \left\{ \begin{array}{c} \text{rate of flow} \\ \text{of } i \text{ out of} \\ \text{volume element} \end{array} \right\} \pm \left\{ \begin{array}{c} \text{rate of consumption } (-) \\ \text{or production } (+) \text{ of } i \\ \text{within volume element} \end{array} \right\} = \left\{ \begin{array}{c} \text{rate of accumulation} \\ \text{of } i \text{ within} \\ \text{volume element} \end{array} \right\} \quad (3.70)$$

In the ideal batch stirred-tank reactor (BSTR), the fluid concentration is uniform and there are no feed or exit streams. Thus, only the last two terms in the previous equation exist. For a volume element of fluid (V_L), the mass balance for the limiting reactant becomes (Smith, 1981; Levenspiel, 1972)

$$\begin{aligned} (-r_u) &= -\frac{1}{V_L} \frac{dN}{dt} = -\frac{1}{V_L} \frac{d(CV_L)}{dt} \\ &= -\frac{1}{V_L} \left(V_L \frac{dC}{dt} + C \frac{dV_L}{dt} \right) \end{aligned} \quad (3.71)$$

where C is the concentration of a species at any time t , r_u is the overall rate of disappearance per unit volume of the fluid phase, and the fractional conversion of the limiting reactant x is defined as (Levenspiel, 1972)

$$x = \frac{N_i - N_t}{N_i} \quad (3.72)$$

where N_i and N_t are the initial moles and moles at time t , respectively.

The limiting reactant is what will run out first during the reaction, i.e. the reactant whose quantity is less than that defined by the stoichiometry of the reaction. Note that the fluid volume (V_L) is generally a variable, i.e. a function of time. If the volume of the reaction mixture is constant, eq.(3.71) becomes

$$(-r_u) = -\frac{dC}{dt} = C_i \frac{dx}{dt} \quad (3.73)$$

where:

$$x = \frac{C_i - C_t}{C_i} \quad (3.74)$$

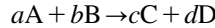
and r_u is the overall rate of reaction (disappearance) per unit volume of the fluid phase. Note that this is identical to the definition of the (homogeneous) reaction rate. This is because the restrictions of uniform concentration and temperature are satisfied in an ideal BSTR and the volume has been assumed to be constant. Since BSTR is used mainly for liquid-phase reactions, the latter assumption usually holds.

It should be noted here that while in catalytic systems the rate is based on the moles disappearing from the fluid phase $-dC/dt$, and the rate has the form $(-r_u) = f(k, C)$, in adsorption and ion exchange the rate is normally based on the moles accumulated in the solid phase and the rate is expressed per unit mass of the solid phase dq/dt where q is in moles per unit mass of the solid phase (solid loading). Then, the rate is expressed in the form of a partial differential diffusion equation. For spherical particles, mass transport can be described by a diffusion equation, written in spherical coordinates r :

$$r_m = \frac{dq}{dt} = D_s \left(\frac{\partial^2 q}{\partial t^2} + \frac{2}{r} \frac{\partial q}{\partial r} \right) \quad (3.75)$$

where D_s is the solid diffusion coefficient and q is the solid-phase concentration of the solute.

Finally, the rate of change of a species is related to the stoichiometry. For the general reaction of the form



the rates are (Fogler, 1999)

$$-\frac{1}{a}r_A = -\frac{1}{b}r_B = \frac{1}{c}r_C = \frac{1}{d}r_D \quad (3.76)$$

Continuous flow reactors

In the ideal CSTR, the fluid concentration is uniform and the fluid flows in and out of the reactor. Under the steady state condition, the accumulation term in the general material balance, eq. (3.70), is zero. Furthermore, the exit concentration is equal to the concentration in the reactor. For a volume element of fluid (V_L), the mass balance for the limiting reactant becomes (Levenspiel, 1972)

$$F_i - F_o - (-r_u)V_L = 0 \quad (3.77)$$

where F is the molar feed rate of the limiting reactant. Subscripts i and o denote the inlet and outlet parameters, respectively. In analogy to the batch reactor,

$$x = \frac{F_i - F_o}{F_i} \quad (3.78)$$

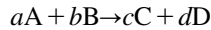
then

$$F_i x_A = (-r_u) V_L \quad (3.79)$$

Variable-volume systems

A variable-volume batch reactor is a constant-pressure (piston-like) closed tank. On the other hand, a variable-pressure tank is a constant-volume batch reactor (Fogler, 1999). Thus, in batch reactors, the expansion factor is used only in the case of a constant-pressure tank whereas and not in a constant-volume tank, even if the reaction is realized with a change in the total moles. However, in continuous-flow reactors, the expansion factor should be always considered. In the following section and for the continuous-flow reactors, the volume V can be replaced by the volumetric flow rate Q , and the moles N by the molar flow rate F in all equations.

Change in the total moles in gas–solid reactions Consider a reaction of the form



where all the reactants and products are gases and A is the limiting reactant. Then, based on the conversion level of A, initial moles,

$$N_{\text{tot},i} = N_{A,i} + N_{B,i} + N_{C,i} + N_{D,i} \quad (3.80)$$

final moles after a conversion level x of A,

$$N_A = N_{A,i} - x_A N_{A,i} \quad (3.81)$$

$$N_B = N_{B,i} - \frac{b}{a} x_A N_{A,i} \quad (3.82)$$

$$N_C = N_{C,i} + \frac{c}{a} x_A N_{A,i} \quad (3.83)$$

$$N_D = N_{D,i} + \frac{d}{a} x_A N_{A,i} \quad (3.84)$$

and thus,

$$N_{\text{tot}} = N_{\text{tot},i} + x_A N_{A,i} \delta \quad (3.85)$$

where x_A is the conversion of the limiting reactant A,

$$x_A = \frac{N_{A,i} - N_{A,o}}{N_{A,i}} \quad (3.86)$$

and δ is defined as

$$\delta = \frac{c + d - a - b}{a} \quad (3.87)$$

This parameter can be termed as “fractional mole change.” Note that in the calculation of δ , inerts that are involved in the gas phase are not taken into account. They are taken into account only in the determination of the total moles of the reacting system.

The expansion factor ε_R is defined as (Fogler, 1999)

$$\varepsilon_R = \frac{N_{\text{tot},(x=1)} - N_{\text{tot},i}}{N_{\text{tot},i}} = \frac{N_{A,i}}{N_{\text{tot},i}} \delta \quad (3.88)$$

Then

$$\frac{N_{\text{tot}}}{N_{\text{tot},i}} = 1 + \varepsilon_R x_A \quad (3.89)$$

Since

$$N = \frac{PV}{ZRT} \quad (3.90)$$

where Z is the compressibility factor. In practice, the compressibility factor does not change significantly during the course of reaction, and thus $Z \approx Z_i$. Then, the volume change in the case of nonisothermal and nonisobaric operation is (Fogler, 1999)

$$\frac{V}{V_i} = (1 + \varepsilon_R x_A) \frac{P_i}{P} \frac{T}{T_i} \quad (3.91)$$

For a constant volume container (batch reactor), $V = V_i$ and thus, eq. (3.91) can be used to calculate the pressure inside the reactor as a function of temperature and conversion.

Under constant P and T , eq. (3.91) becomes

$$\frac{V}{V_i} = 1 + \varepsilon_R x_A \quad (3.92)$$

In this relationship, V_i is the initial (feed) volume of the gas. This is the case of Levenspiel’s simplification where the volume of the reacting system varies linearly with conversion (Levenspiel, 1972). The last equation shows that even if we have a change in moles ($\varepsilon_R \neq 0$), if the conversion of the limiting reactant is very low, the volume of the reaction mixture could be taken as constant and ε_R is not involved in the solutions of the models (since $\varepsilon_R x_A$ can be taken as approximately zero).

In the general case, the concentration of a gas reactant A is

$$\begin{aligned} C_A &= \frac{N_A}{V} = \frac{N_{A,i}(1-x_A)}{V_i(1+\varepsilon_R x_A)(P_i/P)(T/T_i)} \\ &= C_{A,i} \left(\frac{1-x_A}{1+\varepsilon_R x_A} \right) \left(\frac{P}{P_i} \right) \left(\frac{T_i}{T} \right) \end{aligned} \quad (3.93)$$

where N_A are the moles of the reactant and V the total volume of gas phase. Then, for constant P and T (isobaric and isothermal operation, respectively),

$$C_A = \frac{N_A}{V_i(1+\varepsilon_R x_A)} = C_{A,i} \frac{1-x_A}{1+\varepsilon_R x_A} \quad (3.94)$$

and the concentration of B is

$$C_B = \frac{N_B}{V_i(1+\varepsilon_R x_A)} = \frac{C_{B,i}}{1+\varepsilon_R x_A} - \frac{b}{a} \left(\frac{C_{A,i} x_A}{1+\varepsilon_R x_A} \right) \quad (3.95)$$

In the case of $\varepsilon_R = 0$ and constant P and T ,

$$C_A = C_{A,i}(1-x_A) \quad (3.96)$$

$$C_B = C_{B,i} - \frac{b}{a} C_{A,i} x \quad (3.97)$$

where $C_{A,i}$ is the initial (feed) concentration of A.

Note that the volume change in a system involving a gas component could be a result of

- a change in the total number of moles due to the reaction ($\varepsilon_R \neq 0$),
- a change in temperature ($T \neq T_i$),
- a change in pressure ($P \neq P_i$), or
- a combination of the above cases.

In reactions involving only liquid components without phase change, the pressure and temperature variation do not have any significant effect on the volume of the reaction mixture, and at the same time, the expansion factor is always zero. Thus, $V=V_i$ in batch or $Q = Q_i$ in continuous-flow systems and eqs. (3.96) and (3.97) are applicable.

Example 1

If P and T are constant, use the following Levenspiel's relationship for the fractional change in the volume of the system between no conversion and complete conversion of the reactant, where x is the conversion of reactant:

$$\varepsilon_R = \frac{V_{(x=1)} - V_{(x=0)}}{V_{(x=0)}}$$

to derive the definition of the expansion factor (eq.(3.88)).

Solution

Under constant P and T ,

$$\varepsilon_R = \frac{V_{(x=1)} - V_{(x=0)}}{V_{(x=0)}} = \frac{N_{(x=1)} - N_{(x=0)}}{N_{(x=0)}}$$

Since

$$N_{(x=0)} = N_{\text{tot},i}$$

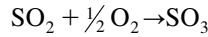
$$N_{(x=1)} = N_{\text{tot},i} + N_{A,i} \delta$$

and this gives the definition equation (3.88)

$$\varepsilon_R = \frac{N_{A,i}}{N_{\text{tot},i}} \delta$$

Example 2

Suppose a gas mixture consisting of 18% O_2 , 3% SO_2 and 79% nitrogen is fed into a reactor so that the following reaction takes place:



Express the concentration of SO_2 and O_2 as a function of conversion.

Solution

The limiting reactant is SO_2 and thus, by using the stoichiometry of the reaction, we have

$$N_{\text{tot},i} = 18 + 3 + 79 = 100$$

$$N_{\text{SO}_2} = 3(1 - x_{\text{SO}_2})$$

$$N_{\text{O}_2} = 18 - 1.5x_{\text{SO}_2}$$

$$N_{\text{SO}_3} = 3x_{\text{SO}_2}$$

Then

$$\delta = \frac{1 + 0 - 1 - 0.5}{1} = -0.5$$

$$\varepsilon_R = \frac{3}{100}(-0.5) = -0.015$$

Then

$$C_{\text{SO}_2} = C_{\text{SO}_2,i} \frac{1 - x_{\text{SO}_2}}{1 - 0.015x_{\text{SO}_2}}$$

$$C_{\text{O}_2} = \frac{C_{\text{O}_2,i}}{1 - 0.015x_{\text{SO}_2}} - 0.5 \frac{C_{\text{SO}_2,i}x_{\text{SO}_2}}{1 - 0.015x_{\text{SO}_2}}$$

Example 3

Consider the gas-phase reaction



which is carried out isothermally and isobarically. The reaction rate is first order in A and first order in B. The feed concentration of A and B is 0.5 mol/L. Express the rate of reaction $-r_A$ solely as a function of conversion, evaluating all possible parameters involved.

Solution

First of all, we have to determine which the limiting reactant is. The way to determine which reactant is limiting is to divide the moles of each reactant by the coefficient from the balanced equation associated with that reactant. The smallest number that comes out indicates which reactant is the limiting one. This reactant limits how much of every other species made or needed for the reaction. For A, this calculation gives 0.25 and for B, 0.5. Thus, A is the limiting reactant and the calculation of δ , ε_R , and x should be based on it. The parameter δ is

$$\delta = \frac{c + d - a - b}{a} = \frac{2 + 0 - 2 - 1}{2} = -\frac{1}{2}$$

The expansion factor ε_R is

$$\varepsilon_R = \frac{N_{A,i}}{N_{\text{tot},i}} \delta = \frac{0.5}{1} \left(-\frac{1}{2} \right) = -0.25$$

The moles of A and B after a conversion level of A equal to x are

$$N_A = N_{A,i}(1 - x)$$

$$N_B = N_{B,i} - N_{A,i} \frac{x}{2}$$

The concentrations of A and B are

$$C_A = \frac{N_A}{V_i(1 + \varepsilon_R x_A)} = C_{A,i} \frac{1 - x_A}{1 + \varepsilon_R x_A} = 0.5 \frac{1 - x_A}{1 - 0.25x_A}$$

$$C_B = \frac{N_B}{V_i(1 + \varepsilon_R x_A)} = \frac{C_{B,i}}{1 + \varepsilon_R x_A} - \frac{C_{A,i}x_A}{2(1 + \varepsilon_R x_A)} = 0.5 \frac{1 - 0.5x_A}{1 - 0.25x_A}$$

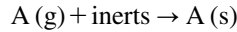
where x_A the conversion of A

$$x_A = \frac{N_{A,i} - N_{A,o}}{N_{A,i}}$$

Then

$$\begin{aligned} (-r_A) &= kC_A C_B = k \left[0.5 \frac{1-x_A}{1-0.25x_A} \right] \left[0.5 \frac{1-0.5x_A}{1-0.25x_A} \right] \\ &= 0.25k \frac{(1-x_A)(1-0.5x_A)}{(1-0.25x_A)^2} \end{aligned}$$

Expansion factor in gas–solid adsorption systems The meaning of the expansion factor is the same in gas adsorption. Consider the adsorption of a species (A) from the gas phase.



where A(s) denotes that the solute (A) is in the solid phase. Although this is not a reaction, it has the same result; the removal of the solute from the gas phase is equivalent to the consumption of a species in a reaction.

For such a case, A(s) is not taken into account for the volume change in the gas, and thus $\delta_R = -1$, and in the absence of inerts, $\varepsilon_R = -1$; whereas if the inerts are in great excess, $\varepsilon_R \cong 0$. This result is similar to the one in three-phase systems, as presented in Section 3.4.5.

3.3.4 Space-time and space velocity in flow reactors

Space-time in flow reactors

The time required to process one reactor volume of feed at specified conditions is called “space-time” and is defined normally at actual entering conditions (Levenspiel, 1972).

$$\tau = \frac{V_R}{Q_i} \quad (3.98)$$

where:

$$\begin{aligned} Q_i &= \text{the volumetric flow rate in the entrance of the reactor} \\ V_R &= \text{the reactor volume.} \end{aligned}$$

Space-time is commonly referred to as “mean residence time,” “holding time,” or simply “residence time.” However, for a system with expansion (variable density system), these quantities are not equal and the residence time is a variable (Levenspiel, 1972):

$$t_{m,z} = \frac{V_R}{Q_z} = \frac{V_R}{Q_i(1 + \varepsilon_R x)} \quad (3.99)$$

where:

- Q_z = the volumetric flow rate in the reactor at length z
- x = the conversion of the limiting reactant at the same length
- ε_R = the expansion factor.

In fixed-beds, the space-time as defined above is the superficial space time, as it is based on the total volume of the bed. The real space-time for a bed of bed voidage ε is

$$\tau = \frac{\varepsilon V_R}{Q_i} \quad (3.100)$$

Another important feature related to mean residence time in fixed-beds is the fluid holdup based on the empty bed volume $h_{e,t}$. If the fluid occupies the whole empty bed volume, then $h_{e,t} = \varepsilon$. However, this is not the case when $h_{e,t} < \varepsilon$, i.e. when there is a bypass of the fluid from some regions in the bed, most commonly in the upper section of the bed in a downflow operation, and the fluid is a liquid. In this case, the real residence time is

$$t_m = \frac{h_{e,t} V_R}{Q_i} \quad (3.101)$$

The actual residence time of a reactor is measured by employing residence time distribution (RTD) experiments utilizing tracing techniques. Furthermore, several correlation forms estimating the fluid holdup can be found in the related literature.

Space velocity in flow reactors

The number of reactor volumes of feed at specified conditions, which can be treated in a unit time is called “space velocity” and is (Levenspiel, 1972)

$$s = \frac{1}{\tau} = \frac{Q_i}{V_R} \quad (3.102)$$

This parameter is frequently used in ion-exchange and adsorption operations in fixed-beds and it is frequently called “relative volumetric flow rate”:

$$s = \frac{Q_i}{V_R} = \frac{Q_{rel} V_R}{V_R} = Q_{rel} \quad (3.103)$$

The most common unit of Q_{rel} is bed volumes per hour (BV/h). Space velocity is also used in catalytic reactors, especially in three-phase fixed-beds, and is referred to as liquid hourly space velocity (LHSV) for the liquid phase, and gas hourly space velocity (GHSV) for gas phase. As mentioned above, space-time and space velocity are measured under the *entrance conditions*. However, for space velocity, other conditions are frequently used (Fogler, 1999). For example, the LHSV is measured at 60 to 75 °F, and GHSV at standard temperature and pressure.

3.3.5 Hydraulics

Hydrodynamic analysis of agitated vessels

The impeller Reynolds number is defined as follows:

$$N_{Re} = \frac{D_a^2 N \rho_L}{\mu_L} \quad (3.104)$$

where:

- N = the impeller rotational speed, r/s
- D_a = the impeller diameter, m
- ρ_L = the liquid density, kg/m³
- μ_L = the dynamic liquid viscosity, Pa s.

The flow is called turbulent in the case $N_{Re} > 10,000$, whereas the flow is laminar in the case $N_{Re} < 10$. In the case $10 < N_{Re} < 1000$, the flow is characterized as transient (Perry and Green, 1999).

The following equations relate velocity head, pumping rate, and power under turbulent-flow conditions:

$$Q = N_Q N D_a^3 \quad (3.105)$$

$$H = \frac{N_p N^2 D_a^2}{N_Q g} \quad (3.106)$$

$$P = N_p \rho_L N^3 \left(\frac{D_a^5}{g_c} \right) = \rho_L H Q \frac{g}{g_c} \quad (3.107)$$

where:

- Q = the impeller discharge rate, m³/s
- N_Q = the discharge coefficient, dimensionless
- N_p = power number, dimensionless,
- H = the velocity head, m
- P = the power, Nm/s = J/s = W
- g_c = 1 when using SI units
- g = the gravitational acceleration, m/s².

It should be noted that for relatively dilute solid–liquid mixtures, except for fibrous solids, the power to agitate at a given speed is essentially the same as for the clear liquid (Treybal, 1980). Concentrated slurries and suspensions of fibrous solids are likely to be non-Newtonian in character.

Given the delivered power P and the friction losses, the required motor power P_m can be calculated as

$$P_m = \frac{P}{100 - \% \text{ losses}} \quad (3.108)$$

These losses are from the loss of usable energy in the form of work through the motor, shaft gearing, and bearings, and could be as high as 20–30%. The agitation intensity could be characterized as mild, vigorous, and intensive, depending on the power delivered per unit volume of liquid. For water, the approximate values are presented in Table 3.2.

The discharge rate has been measured for several types of impellers, and discharge coefficients have been calculated (Perry and Green, 1999). For turbines, N_Q ranges from 0.7 to 2.9, depending on the impeller geometrical characteristics. For a standard flat blade turbine (Ruhston) in a baffled vessel, this value is 1.3. For a four-blade 45° turbine and a baffled vessel, this value is 0.87, and for marine propellers and a baffled vessel, it is 0.5 (McCabe *et al.*, 1993). More specifically, for the typical case of six-bladed turbines (Ruhston), the following approximation can be used (Perry and Green, 1999):

$$N_Q = 0.93 \frac{D_T}{D_a} \quad (3.109)$$

where D_T is the tank diameter in m. Power number N_p ranges from 0.35 to 7, depending on the impeller type, its geometrical characteristics, and vessel design. This number is very important since it is needed for the evaluation of power consumption, which in turn, is used for the determination of mass transfer coefficients. The geometry of the agitation system plays a critical role. The typical geometrical ratios are presented in Table 3.3.

In Figure 3.23, the various dimensions are presented.

Baffles are frequently arranged with a *clearance*, which may be half the baffle width, between the baffle and the tank wall to prevent accumulation of solids behind the baffles (Treybal, 1980).

The height of the impeller above vessel floor is frequently called “clearance,” and is the distance between the vessel bottom and the impeller *centerline*. On the other hand, C_b is the distance from the bottom to the bottom of the impeller. The relationship between these two parameters is

$$Z_a = C_b + \frac{W}{2} \quad (3.110)$$

In Table 3.4, the power number is presented for several cases.

The values of N_p are approximate. At low Reynolds numbers, about 300, the power number curves for baffled and unbaffled tanks are identical (McCabe *et al.*, 1993). For higher N_{Re} , the power number for unbaffled tanks is lower than the values for baffled tanks.

Table 3.2

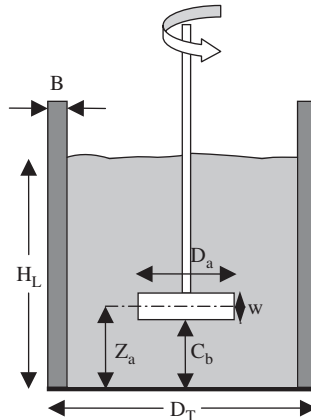
Agitation intensity versus power/volume for water

Agitation	Power/volume (kW/m ³)
Mild	0.09–0.17
Vigorous	0.34–0.51
Intensive	0.68–1.69

Table 3.3

Geometrical ratios (Perry and Green, 1999; Treybal, 1980; McCabe *et al.*, 1993; Nouri and R.M.Hockey, 1998; Armenante and Nagamine, 1998; Pavlov *et al.*, 1979; Fishwick *et al.*, 2003; Kato *et al.*, 2001; Rewatkar *et al.*, 1991)

Ratio	Description	Range
D_T/D_a	Tank diameter/impeller diameter	2.64–3.7 (typically 3)
Z_a/D_T	Height of impeller above vessel floor /tank diameter	1/3
D_a/W	Impeller diameter/width of blade	3–8
D_T/B	Tank diameter/affle width	6–25 (typically 10–12)
H_L/D_T	Liquid depth in vessel/tank diameter	0.67–1.5 (typically 1)
–	Number of impeller blades	3 (Propellers) 6 (Turbines) 2 (Paddles)
length/degrees	Pitch/angle	0–45–60° (angle) 1–2 D_a (pitch)
–	Number of baffles	4

**Figure 3.23** Dimensions of agitated vessels.

Typical values for the rest of the geometrical ratios and other characteristics are given in Table 3.3. Generally, the higher values of N_p in Table 3.4 correspond to the higher Reynolds numbers, where N_p becomes practically constant (Figure 3.24).

For Rushton turbines (flat-blade disc turbines), the following equation can be used (Nouri and Hockey, 1998):

$$N_p = 1.98 Re^{0.082} \quad (3.111)$$

Table 3.4

Power number for several types of impellers and vessel characteristics (Perry and Green, 1984, 1999; McCabe *et al.* 1993; Nouri and Hockey, 1998)

Impeller type	D_a/W	D_T/B	No. of blades	Pitch/angle	N_p	N_{Re} (approximate values)
Propeller ^a	–	10	3	Pitch = $2D_a$	0.9–1	$>10^3$
Propeller ^a	–	10	3	Pitch = D_a	0.32–0.35	$>10^4$
Pitched-blade turbine	4	10	6	60°	2.2–2.5	$>3 \times 10^2$
Pitched-blade turbine	8	12	6	45°	1.5	$>10^4$
Pitched-blade turbine (6) ^b	8	12	6	45°	1.3–1.5	$>10^3$
Straight-blade open Turbine (4)	8	12	6	–	2.7–3	$>10^4$
Straight-blade open turbine (2)	5	10–12	6	–	4	$>2 \times 10^3$
Curved-blade open turbine (5)	8	10–12	6	–	2.7–2.8	$>10^4$
Curved-blade open turbine	5	10–12	6	–	4.8–5	$>10^4$
Flat-blade disc turbine (3)	8	10–12	6	–	3	$>10^4$
Flat-blade disc turbine	5	6	6	–	7	$>10^4$
Flat-blade disc turbine (1)	5	10–12	6	–	5–5.75	$>10^4$
Flat-blade disc turbine	–	10	4	–	5.31	$>10^4$
Flat-blade disc turbine	5	25	6	–	4	$>10^4$
Flat paddle	4	10	2	–	1.8–2.25	$>10^4$
Flat paddle	6	10	2	–	1.7	$>10^4$
Flat paddle	8	10	2	–	1.15	$>10^4$
Flat paddle	6	10	4	–	2.75	$>10^4$
Flat paddle	6	10	6	–	3.82	$>10^4$

^aThe same value holds for the angular off-center position of the impeller in an un baffled vessel.

^bThe number in parenthesis corresponds to the curves in Figure 3.24.

For $N_{Re} > 8 \times 10^4$ and $N_p \cong 5$, Nouri and Hockey used a typical Rushton impeller and the following vessel characteristics: $D_T = H_L$, 4 baffles with $B = D_T/10$, $D_a = D_T/3$, $D_a/W = 5.4$, and $Z_a/D_T = 1/3$.

The minimum volume of the vessel is equal to the volume of the liquid to be treated, and thus for a cylindrical vessel we have

$$V_L = \frac{\pi D_T^2}{4} H_T \quad (3.112)$$

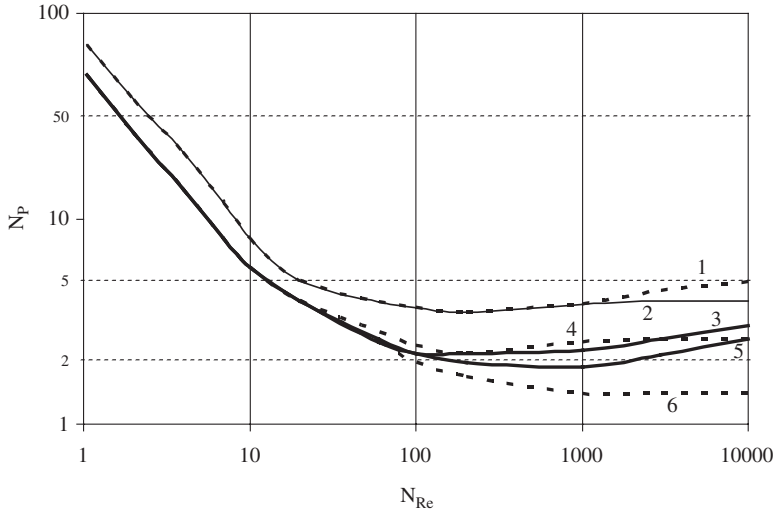


Figure 3.24 Dimensionless power number in stirred tanks for a typical configuration (Perry and Green, 1999). A typical configuration consists of a baffled tank with D_T/B values of 10 – 12 and a six-blade impeller.

Since in design practice $H_L = D_T$, we have

$$D_T = \left(\frac{4}{\pi} V_L \right)^{1/3} \quad (3.113)$$

Using this relationship and the ratios as presented in Table 3.3, the appropriate impeller diameter D_a , Reynolds number, and the other geometrical characteristics of the agitated tank can be calculated.

Minimum rotational speed for complete solid suspension in solid-liquid systems

The following equation of Zwietering is used for liquid–solid systems and agitated vessels (McCabe *et al.* 1993; Zwietering, 1958; Dohi *et al.*, 2002):

$$N_{js} = SX_{\%}^{0.13} \nu^{0.1} \frac{d_p^{0.2}}{D_a^{0.85}} \left(\frac{g \Delta \rho}{\rho_L} \right)^{0.45} \quad (3.114)$$

where:

- N_{js} = the minimum (critical) rotational speed, r/s
- $X_{\%}$ = the solid loading, wt.%
- ν = the kinematic viscosity of the liquid, m^2/s
- $\Delta \rho$ = the density difference between solid and liquid, kg/m^3 .

For the rest of the parameters, SI units are used. For the evaluation of density difference, the hydraulic density for the solid phase is used:

$$\Delta\rho = \rho_h - \rho_L = (1 - \varepsilon_p)(\rho_s - \rho_L) \quad (3.115)$$

where:

- ε_p = the particle porosity
- ρ_s = the skeletal density of the solid.

The parameter S is called the proportionality constant or shape factor, and depends on the impeller and vessel geometry (Armenante and Nagamine, 1998):

$$S = s_1 \left(\frac{D_T}{D_a} \right)^{s_2} \exp \left(s_3 \frac{C_b}{D_T} \right) \quad (3.116)$$

where C_b is the impeller clearance measured from the bottom of the impeller to the bottom of the tank, in m. The constants s_i depend upon the type of the impeller, and for cylindrical baffled vessels, are presented in Table 3.5 (Armenante and Nagamine, 1998).

These values were obtained for $1/48 < C_b/D_T < 1/2.5$. The values of S given by McCabe directly for several types of impellers (McCabe *et al.*, 1993) are shown in Table 3.6.

Table 3.5

Constants of parameter S .

Impeller type	s_1	s_2	s_3
Flat blade disc turbine with six blades	0.99	1.4	2.18
Straight blade open turbine with six blades	1.43	1.2	1.95
Pitched-blade (45°) turbine with six blades	2.28	0.83	0.65
Fluidfoil Chemineer HE-3 impeller	3.49	0.79	0.66

Table 3.6

Value of the shape factor S .

Impeller type	D_T/D_a	D_T/Z_a	S
Flat-blade disc turbine with six blades ($D_a/W = 5$, $N_p = 6.2$)	2	4	4.1
	3	4	7.5
Paddle with two blades ($D_a/W = 4$, $N_p = 2.5$)	2	4	4.8
	3	4	8
	4	4	12.5
Propeller with three blades ($N_p = 0.5$)	3	4	6.5
	4	4	8.5
	4	2.5	9.5

3.3.6 External mass transfer in liquid–solid systems

The slip-velocity theories are based on the correlations of steady state transfer to particles fixed in space, with the average slip velocity used to calculate the Reynolds number. When natural convection effects are absent and when the Reynolds number is greater than 1, the transfer rate for single spheres is given by the semitheoretical equation (Harriot, 1962)

$$Sh = 2 + 0.6Re_p^{0.5}Sc^{0.33} \quad (3.117)$$

Here, the particle Reynolds number is based on the slip velocity. If terminal velocity is used, then the above correlation gives the minimum value for the mass transfer coefficient. Minimum mass transfer coefficients further depend on the density difference between solid particles and solvent. For the typical case of water, the approximate values presented in Table 3.7 can be used (Harriot, 1962).

These values hold for particle diameters of 100 – 10,000 μm or 0.1 – 10 mm, covering all practical applications. Furthermore, the typical density difference is about 1, since particle densities are around 2 g/cm^3 .

Harriot (1962) measured the mass transfer coefficients in baffled tanks, using six-blade turbines and several liquids such as water and glycerine. According to that study,

- Mass transfer coefficients are probably the same for any stirrer location if the particles are completely suspended.
- For small ion-exchange particles in water, the mass transfer coefficient decreases with increasing particle size, but is almost independent of size for particles larger than about 200 μm .
- Viscosity has only a small effect on the mass transfer coefficient.
- The effect of particle shape was not determined, but is expected to be of minor importance.
- The coefficients in unbaffled tanks increased with only the 0.3 power of the stirrer speed. At the speed needed for complete suspension in a baffled tank, the coefficients are about the same with or without baffles. At higher speeds, the more uniform dispersion of the particles and the greater velocity fluctuations make the coefficients larger with baffles present.

Table 3.7

Mass transfer coefficient range (approximate values).

Density difference (g/cm^3)	Minimum mass transfer coefficient range (cm/s)
3	0.008–0.01
1	0.005–0.007
0.3	0.003–0.005
0.1	0.0025–0.003

Then, the actual mass transfer coefficients, which cover a hundred-fold range, are about 1.5–8 times that predicted from the correlations for fixed particles if the terminal velocity is used to calculate the particle Reynolds number. McCabe gives the narrower range of 1.5–5, for a wide range of particle sizes and agitation conditions (McCabe *et al.*, 1993). Using these values and Table 3.7, we can calculate the ranges of the actual mass transfer coefficients.

The solid–liquid mass transfer coefficient without aeration is a function of power consumption per unit volume of the liquid. One typical case is the Levins and Glastonbury correlation for small particles (<2 mm), fully suspended and moderate density differences (Treybal, 1980):

$$\frac{k_f d_p}{D_f} = 2 + 0.47 \left[d_p^{4/3} (P_s g_c)^{1/3} \frac{\rho_L^{2/3}}{\mu_L} \right]^{0.62} \left(\frac{D_a}{D_T} \right)^{0.17} Sc^{0.36} \quad (3.118)$$

where P_s is the power consumption per unit volume of liquid (W/m^3) and D_f the diffusion coefficient of the solute in the fluid phase. For the rest of the parameters, SI units should be used. In practice, for baffled tanks, the value of P_s is 33–82 W/m^3 for blending, 82–247 W/m^3 for homogeneous reactions, around 824 W/m^3 for liquid–liquid mixtures, 824–1647 W/m^3 for gas–liquid mixtures, and around 1647 W/m^3 for slurries.

For large particles (>2 mm), fully suspended,

$$\frac{k_f d_p}{D_f} = 0.222 \left[d_p^{4/3} (P_s g_c)^{1/3} \frac{\rho_L^{2/3}}{\mu_L} \right]^{3/4} Sc^{1/3} \quad (3.119)$$

One more correlation is that of Calderbank–Moo–Young for the solid–liquid mass transfer coefficient in stirred tanks without aeration (Kato *et al.*, 2001)

$$k_f = 0.13 \left(\frac{P_s v_L}{\rho_L} \right)^{0.25} Sc^{-2/3} \quad (3.120)$$

where v_L is the kinematic viscosity of the liquid.

The high shear stress around an agitation impeller is not acceptable for cell cultures or other sensitive materials in stirred (bio) reactors (Kato *et al.*, 2003; Michell *et al.*, 1999). In these cases in which the solid phase is sensitive to high shear stress, shaking vessels can be used. The main types are the reciprocally and rotational shaking vessels. For these cases, see Kato *et al.* (2003).

3.4 SLURRY REACTORS

3.4.1 General

Slurry reactors are similar to fluidized-bed reactors in that a gas is passed through a reactor containing solid catalyst particles suspended in a fluid. In slurries, the catalyst is suspended in a liquid, whereas in fluidized beds, the suspending fluid is the reacting gas itself.

These reactors employ small particles in the range 0.05 – 1.0 mm (0.0020 – 0.039 in) with the minimum size being limited by filterability. Small diameters are used to provide as large an interface as possible, since the internal surface of porous pellets is poorly accessible to the liquid phase (Perry and Green, 1999). The catalyst concentration in slurry reactors is limited by the agitation power of the mechanical stirrer or by the gas flow.

The advantages of slurry reactors over trickle bed reactors, which are the principal alternative to slurry reactors, are the following (Satterfield, 1975; Smith, 1981; Perry and Green, 1999):

- A high heat capacity to provide good temperature control, especially in the case of highly exothermic reactions, and thus good temperature stability. Temperature control is relatively simple due to the large amount of liquid present and the possibility to install coolers inside the reactor.
- Heat recovery and transfer can readily be achieved. Uniform temperature conditions prevail approximately throughout the reactor.
- Operation in batch or flow mode.
- Easy replacement of catalyst in case of its deactivation.
- The employment of small particles results in effectiveness factors near unity. In other words, the intraparticle diffusion resistance is low.

Due to the use of small particles in slurry reactors, which leads to low resistance from intraparticle diffusion, much higher values of global rates are observed in these reactors than in fixed-bed ones, especially when very active catalysts are used. This is because diffusivities in liquid-filled pores are relatively low, of the order 10^{-5} cm²/s compared to values around 10^{-2} cm²/s, typical for gases. In case of partial degradation of catalytic activity, the catalyst can be partially removed and replenished during operation (Perry and Green, 1999). Especially in case of rapid catalyst deactivation, where continuous catalyst removal and regeneration is crucial, slurry reactors are most likely to be applied. Furthermore, the high heat-transfer rates that are observed in slurry reactors, lead to low temperature differences between the particle and the liquid. As a consequence, external temperature gradients can be normally neglected in slurry reactors (Smith, 1981).

However, there are some serious disadvantages in using slurry reactors. The most important one is the difficulty in retaining the catalyst in the vessel. In addition, it is difficult to separate the catalyst from the product, if entrainment takes place. Screens and other devices placed in the outlet lines tend to clog and could be unreliable. Another disadvantage is the low conversion for a given size because of essentially complete backmixing. Finally, high power consumption for agitation to keep the catalyst in suspension and to enhance heat transfer, and the possibility of homogeneous side reactions taking place due to the high ratio of liquid-to-solid volume, are among the disadvantages of slurry reactors (Satterfield, 1975; Perry and Green, 1999).

3.4.2 Basic types of slurry reactors

There are two types of slurry reactors: slurry bubble column reactor (SBCR, Figure 3.25) and agitated slurry reactor (ASR, Figure 3.26). These reactors differ in that the solid

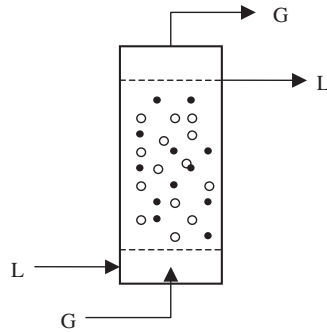


Figure 3.25 Slurry bubble column reactor (SBCR)

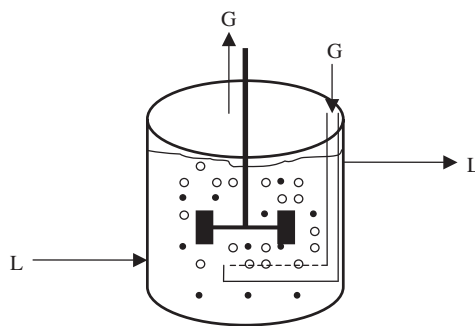


Figure 3.26 Agitated slurry reactor (ASR).

particles are kept suspended in the liquid by means of the gaseous reactants that enter the reactor from the bottom, usually through a sparger in SBCRs, whereas in ASRs, mechanical agitation is employed for retaining the suspension of the solids.

In general, much higher amounts of solids can be loaded in a bubble column than in an agitated slurry reactor. Actual loadings of over 30% (v/v) are known, whereas the respective values for ASR rarely exceed 5% (v/v) (Stitt, 2002). In general, bubble columns seem more attractive than ASRs. Besides the high solid loadings that can be achieved, the operation of bubble columns is relatively flexible, exhibiting good heat and mass transfer behavior. Another advantage of bubble columns over ASRs is the ease of cleaning. Although bubble columns are superior to ASRs in terms of performance, they have more problems associated with scale-up (Stitt, 2002).

Slurry reactors could be of continuous type if the slurry (liquid and solids) flows through the reactor or of batch type if the slurry is stationary in the reactor. In the following analysis, we basically consider the batch type of slurry reactors (ASR and SBCR).

3.4.3 Slurry bubble column reactors

Slurry bubble column reactors have many applications in both industrial and environmental processes. For example, they are used in the Fischer–Tropsch synthesis in industry, or in wastewater treatment. The most important applications of these reactors are presented in Table 3.8 (Shah *et al.*, 1982).

Typical operating conditions of these reactors are

- Length-to-diameter column in the range 2–30
- Diameter of solid particles below 50 μm
- Operation temperatures in the range 20 $^{\circ}\text{C}$ –300 $^{\circ}\text{C}$
- Operation pressures in the range 1–200 atm
- Gas velocities lower than 50 cm/s and much higher than the liquid velocity.

3.4.4 Modelling of slurry bubble column reactors

In the common case, in slurry bubble column reactors, the catalyst phase remains in the reactor while the liquid phase could remain in the reactor with a continuous flow of gas (semibatch operation). Both gas and liquid could be in plug flow or could be well mixed.

Regardless of the arrangement, the modeling procedure is to write mass balance equations for all reactants, for all reactions. If reactants exist in both gas and liquid phase, separate conservation equations are necessary for each phase. By using the global rate, model equations will be expressed in terms of bulk concentrations, and thus the solution gives the relation between the conversion of reactants and reactor volume, analogous to the results for single-phase reaction systems (Smith, 1981).

Before analyzing the several forms of the material balances, the concept of *limiting reactant* will be presented first as the sizing of the reactor is normally based on this reactant.

Limiting reactant in three-phase reacting systems

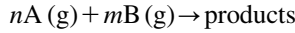
As it has been already mentioned, the limiting reactant is the reactant that will run out first during the reaction, i.e. the reactant whose quantity is less than the one defined by the

Table 3.8

The most important applications of slurry bubble column reactors

Industrial applications	Environmental applications
Coal liquefaction	Adsorption of SO_2 in an aqueous slurry of magnesium oxide and calcium carbonate
Fischer–Tropsch synthesis	SO_2 or removal from tail gas
Synthesis of methanol	Wet oxidation of waste sludge
Hydrogenation of oils	Catalytic desulfurization of petroleum fractions
Alkylation of methanol and benzene	Wastewater treatment
Polymerization of olefins	
Hydrogenation of coal oils, heavy oil fractions, and unsaturated fatty acids	

stoichiometry of the reaction. When applying mass balances in reactors, it is reasonable to base the analysis on the limiting reactant. Consider the catalytic reaction of the form



Suppose that A is in great excess in the gas phase and that its solubility is much lower than that of B. Under this condition, although A is in excess in the gas phase, it could control the reaction rate in the liquid phase where the reaction takes place. However, considering the whole reaction system, i.e. the gas and liquid phase, B will run out *first* and is the *real* limiting reactant, as defined earlier. Now consider the reaction rate

$$r = k C_A^n C_B^m \quad (3.121)$$

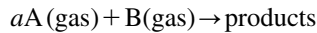
The reaction takes place solely in the liquid phase, where B could be in excess. In such cases, it is frequently found that the reaction becomes of zero order with respect to (B), i.e. with respect to the component that is in excess in the reaction space or, in general, depending on the nature of the reaction with respect to the component whose concentration is relatively high. In these cases, the reaction rate becomes a function of only the liquid-phase concentration of A.

Thus, in three-phase systems, the term “limiting reactant” has two different meanings:

- Considering the material balances, the limiting reactant is the component that runs out first from the whole reacting system, i.e. both the gas and liquid phase (the reactant B in our case).
- Considering the reaction rate, the limiting reactant is the one that is in shortage in the phase where the reaction takes place (the liquid phase and the reactant A in our case).

Gas-phase reaction in continuous and semi-batch operations

For the common case of continuous operation for both phases, where gas flows under plug-flow condition and liquid under complete mixed-flow condition, and for a reaction of the form (nonreacting liquid phase)



The gas-phase mass balance is

$$\frac{\tau}{C_{G,i}} = \frac{V_L}{F_i} = \int_{x_i}^{x_o} \frac{dx}{(-r_u)} \quad (3.122)$$

$$\tau = \frac{V_L}{Q_{G,i}} \quad (3.123)$$

$$(-r_u)_B = \frac{(-r_u)_A}{a} \quad (3.124)$$

where the subscripts (o) and (i) denote the outlet and the inlet conditions, respectively.

The above equations are the same as those of the plug-flow tubular reactor for homogeneous reactions (Smith, 1981; Levenspiel, 1972). The differential form of equation (3.122) can be written in several equivalent forms (Levenspiel, 1972):

$$\begin{aligned} F_i dx &= (-r_u) dV_L = (-r_{vs}) dV_S \\ &= (-r_s) dS = (-r_m) dM_S = (-R) dV_R \end{aligned} \quad (3.125)$$

The gas-reactant liquid-phase mass balance is

$$\frac{Q_L}{V_L} (C_{L,i} - C_{L,o}) + (K_L a_{GL}) \left(\frac{C_{G,z}}{H} - C_{L,o} \right) - (k_f a_c) (C_{L,o} - C_S) = 0 \quad (3.126)$$

where:

- K_L = the overall gas-phase mass transfer coefficient as defined in equation (3.59)
- k_f = the liquid-solid mass transfer coefficient
- a_c = the external surface area of the particles per unit volume of the liquid phase as defined in equation (3.218)
- a_{GL} = the gas-liquid interfacial area as defined in equation (3.228)

Note that the gas-phase concentration $C_{G,z}$ varies with the distance from the entrance z due to the plug-flow condition. If the gas phase is in complete mixed flow, then $C_{G,z} = C_{G,o}$. Finally, the component mass balance around the catalyst is

$$(k_f a_c) [C_{L,o} - C_S] = (-r_u) \quad (3.127)$$

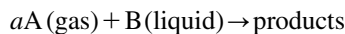
These material balances could be written for both reactants.

In a typical slurry bubble column operation, the liquid velocity is one order of magnitude lower than the one of gas, and in general, is very low. This mode of operation can be approximated by a semibatch operation. The semibatch operation is frequently used and is the case where the liquid and the catalyst comprise a stationary phase (slurry) in the reactor. In this case, the material balance, eq. (3.122) is used along with the overall rate based on the bulk gas-phase concentration (see Section 3.4.6). In the following, the semibatch operation is presented.

Gas-Liquid reaction and batch liquid (semibatch operation)

If the liquid phase is reacting and batch, the system becomes dynamic as the liquid phase concentrations change with time. To simplify the reactor model, we consider the common case of constant gas-phase concentration. Furthermore, the liquid phase is considered to be under complete mixing condition.

The reaction can be represented as follows:



The conservation equation for B in the liquid phase is a batch-reactor model:

$$(-r_u)_B = C_{BL,i} \frac{dx_B}{dt} = -\frac{dC_{BL}}{dt} \quad (3.128)$$

Here, the subscript i denotes the initial concentration of component B in the liquid at $t = 0$. Then, the material balance is used along with the overall rate based on the bulk gas-phase concentration (see Section 3.4.6).

The gas-phase mass balance for A is not needed as the concentration in this phase is constant. In Chapter 5, a solution is given for the case of variable gas-phase concentration.

Gas–liquid reactions and continuous flow of both phases under plug flow

If the process is continuous and under plug flow, for both the gas and slurry phases, the equations derived for trickle bed reactors are applicable (see Section 3.7.2) (Hopper *et al.*, 2001) by using the appropriate mass transfer coefficients. Note that in trickle beds, the material balances are based on the reactor volume.

Gas–liquid reactions and continuous flow of both phases in complete mixed flow

If the process is continuous and in the complete mixed-flow mode, for both the gas and slurry phases, the equations derived for agitated slurry reactors are valid (see Section 3.5.1) (Ramachandran and Chaudhari, 1980) by simply applying the appropriate mass transfer coefficients. Note that in slurry-agitated reactors, the material balances are based on the volume of the bubble-free liquid. Furthermore, in reactions of the form $aA(g) + B(l) \rightarrow$ products, if gas phase concentration of A is constant, the same treatment holds for the plug flow of the gas phase.

Finally, the relationship between the several rate expressions for slurry bubble column reactors is (see Section 3.1.1 for derivation)

$$\begin{aligned} (-r_u) &= -\frac{1}{V_L} \frac{dN}{dt} = \frac{V_S}{V_L} (-r_{vs}) \\ &= \frac{S}{V_L} (-r_s) = \frac{M_S}{V_L} (-r_m) = \frac{V_R}{V_L} (-R) \end{aligned} \quad (3.129)$$

For slurries,

$$\frac{V_S}{V_L} = \frac{(M_S/\rho_p)}{V_L} = \frac{m_s}{\rho_p} \quad (3.130)$$

$$\frac{M_S}{V_L} = m_s \quad (3.131)$$

$$\frac{V_R}{V_L} = \frac{1}{h_L} \quad (3.132)$$

Then, the overall rate of the reaction ($-r_u$) per unit volume of liquid is

$$(-r_u) = -\frac{1}{V_L} \frac{dN}{dt} = \frac{m_s}{\rho_p} (-r_{vs}) = m_s (-r_m) = \frac{1}{h_L} (-R) \quad (3.133)$$

These relationships can be used along with the material balances and rate expressions, and the solutions can be expressed in various forms of the rate coefficient in conjunction with different variables.

3.4.5 Expansion of gas phase in three-phase systems

To follow the same analysis as in two-phase systems, the stoichiometry of the reaction should be used for the determination of the final moles in the gas phase after the reaction. However, in slurry reactors, a liquid phase is involved and the reactants are dissolved and react in the liquid phase. In this case, the moles remaining in the gas phase after the reaction are not only determined from the reaction stoichiometry. This is why a part of the moles that disappear from the gas phase is unreacted and dissolved in the liquid. This situation introduces some complications in the determination of the expansion factor.

At this point, there is an opportunity to analyze the effect of dissolution of reacting species in a second fluid in the overall material balance in a reactor. The overall material balance is convenient in the case where the conversion of one species is known and we want to estimate the conversion of the other species without solving the reactor models.

However, as will be analyzed, this approach should be followed with great attention as it can lead to erroneous results and conclusions.

The case of the overall material balance

Consider the reaction



where A is the limiting reactant. The final concentration of reactants is

$$C_{B,G} = C_{B,i} - bC_{A,i}x_A \quad (3.134)$$

$$C_{A,G} = C_{A,i}(1 - x_A) \quad (3.135)$$

Then the concentration difference is

$$C_{B,i} - C_{B,G} = bC_{A,i}x_A \quad (3.136)$$

$$C_{A,i} - C_{A,G} = C_{A,i}x_A \quad (3.137)$$

and thus the overall material balance in the reactor is

$$(C_{B,i} - C_{B,G}) = b(C_{A,i} - C_{A,G}) \quad (3.138)$$

This overall material balance is valid only if the reaction is very fast, i.e. the unreacted A and B in the liquid phase are in negligible amounts.

If the above condition is not met, the calculations based solely on overall material balance do not take into account the dissolved unreacted A and B that remain in the liquid phase after the reaction in a batch reactor, or which may flow out of the reactor with the liquid in a continuous-flow system. This way, it is assumed that the removal of a reactant is purely a result of the reaction.

The case of the expansion factor

The calculations for the expansion factor in systems involving a gas and a liquid phase are based solely on the gaseous species. The following cases can be found in practice:

1. The gas phase is dilute, i.e. it contains the reactant A and inerts in great excess. The other reactants and products are nonvolatile and are present only in liquid phase. In this case, the expansion could be taken as zero.
2. The reaction is very fast in the liquid phase and thus the concentration of A in this phase is essentially zero. In this case, the expansion can be evaluated as described in two-phase systems.
3. All reactants and products are gases. If the limiting reactant, on which the expansion factor is based, is in very low concentration, i.e. the nonlimiting reactants are in great excess, then the gas volume cannot be changed considerably. This case is equivalent to the existence of a great excess of inerts, and the expansion could be taken as zero.
4. The gaseous limiting reactant has a very low solubility. This means that the moles lost by the dissolution of gas in the liquid are very small, and thus the moles that disappear are mainly due to reaction. In this case, the expansion can be evaluated as described in two-phase systems.

The first two assumptions as well as the fourth are used by Levenspiel for gas-liquid absorption operations.

Example 4

Consider the gas-phase reaction



which is carried out isothermally and isobarically. The gas feed is pure A. The limiting reactant is A. Express the concentration of A as a function of conversion.

Solution

The parameter δ takes into account only the gas-phase species A:

$$\delta = \frac{0 - 0 - a}{a} = -1$$

The expansion factor ε_R is

$$\varepsilon_R = \frac{N_{A,i}}{N_{\text{tot},i}} \delta = -1$$

Then

$$\frac{V}{V_i} = 1 - x_A$$

and thus

$$C_A = C_{A,i} \frac{1 - x_A}{1 - x_A} = C_{A,i}$$

Example 5

Consider the gas-phase reaction



which is carried out isothermally and isobarically. The limiting reactant is B while the gas feed is pure A. Express the concentration of A as a function of conversion.

Solution

For the expansion factor, we cannot use the expression (3.88) in the form

$$\varepsilon_R = \frac{N_{B,i}}{N_{\text{tot},i}} \delta$$

This is why the limiting reactant is B and expansion factor should be based on B, but this is not a gaseous species, and thus does not contribute to the volume of the gas-phase. However, we can use the same equation in the following form:

$$\varepsilon_R = \frac{N_{\text{tot},(x=1)} - N_{\text{tot},i}}{N_{\text{tot},i}}$$

In this expression, we should take into account only the gas species, i.e. reactant A. We have

$$N_{\text{tot},i} = N_{A,i}$$

$$N_{\text{tot}} = N_{A,i} - \frac{a}{b} N_{B,i} x_B$$

where, for $x_B = 1$,

$$N_{\text{tot},(x=1)} = N_{A,i} - \frac{a}{b} N_{B,i}$$

Then

$$\varepsilon_R = \frac{N_{\text{tot},(x=1)} - N_{\text{tot},i}}{N_{\text{tot},i}} = \frac{\left(N_{A,i} - \frac{a}{b}N_{B,i}\right) - N_{A,i}}{N_{A,i}} = -\frac{a}{b} \frac{N_{B,i}}{N_{A,i}}$$

Also

$$\frac{V}{V_i} = 1 - \frac{a}{b} \frac{N_{B,i}}{N_{A,i}} x_B$$

and thus,

$$C_A = \frac{N_{A,i} - N_{B,i} \frac{a}{b} x_B}{V_i \left(1 - \frac{N_{B,i}}{N_{A,i}} \frac{a}{b} x_B\right)} = \frac{N_{A,i}}{V_i} \left(\frac{1 - \frac{N_{B,i}}{N_{A,i}} \frac{a}{b} x_B}{1 - \frac{N_{B,i}}{N_{A,i}} \frac{a}{b} x_B} \right) = C_{A,i}$$

Note that in examples 4 and 5, which represent common cases in three-phase systems, the concentration of a pure A gas-phase is unchanged throughout the reactor volume and is equal to the inlet one. However, moles and reaction volume (or the gas volumetric flow rate) are changing during the reaction.

3.4.6 On the overall rates

“Overall rate” means the expression of the rate of the process in terms of the bulk liquid or gas-phase concentration. The overall rate can be expressed in terms of the bulk liquid concentration for continuous and semibatch operation. However, the overall rate can be expressed in terms of bulk gas-phase concentration only in the case of a semibatch operation, i.e. continuous flow of gas and batch liquid. Both cases are analyzed in detail in the following sections.

The overall rate of reaction in semibatch systems (batch liquid)

Nonreacting liquid Under the assumption of complete mixing for the liquid phase and at steady-state conditions, mass transfer from gas to the liquid phase is equal to the mass transfer at the liquid–solid interface:

$$(K_L a_{GL}) \left(\frac{C_{G,z}}{H} - C_{L,o} \right) - (k_f a_c) (C_{L,o} - C_S) = 0 \quad (3.139)$$

The component mass balance around the catalyst is

$$(k_f a_c) [C_{L,o} - C_S] = (-r_u) \quad (3.140)$$

For a first-order reaction, in either reactant, the combination of these equations and the elimination of the surface and liquid-phase concentrations lead to the formulation of an overall rate, expressed as a function of the bulk gas-phase concentration. This procedure is essentially the same as the one presented analytically in Section 3.1.2 for the derivation of an overall rate in three-phase systems.

Note that the gas-phase is flowing under plug-flow condition, and thus its concentration will change with position $C_{G,z}$. Thus, the procedure of the formulation of the overall rate is made for a certain axial position (z) in the reactor where at steady state, the gas-phase concentration is constant.

Following the procedure described in Section 3.1.2, the rate per unit volume of bubble-free liquid in terms of the concentration of the reactant in the gas phase is

$$(-r_u) = K^\circ C_{G,z} \quad (3.141)$$

where K° is an overall coefficient (in s^{-1}):

$$\frac{1}{K^\circ} = \frac{1}{k_g a_{GL}} + \frac{H}{k_{fg} a_{GL}} + H \left(\frac{1}{a_c k_f} + \frac{1}{\eta_s m_s k_m} \right) \quad (3.142)$$

with a_{GL} and a_c being the gas-liquid and liquid-solid interfacial area per unit volume of bubble-free liquid (in m^2/m^3), respectively. The parameter m_s is the catalyst loading per unit volume of bubble-free liquid (in kg/m^3).

The overall mass transfer coefficient K_L is

$$\frac{1}{K_L} = \frac{1}{Hk_g} + \frac{1}{k_{fg}} \quad (3.143)$$

If the gas-phase resistance is negligible (Section 3.1.2), then

$$\frac{1}{K^\circ} \cong H \left(\frac{1}{k_{fg} a_{GL}} + \frac{1}{k_f a_c} + \frac{1}{\eta_s m_s k_m} \right) \quad (3.144)$$

Here, it is important to note that the value of K° is different if it is based on different reactants due to the different values of Henry's constant.

Reacting liquid-phase *First-order in gas reactant and constant gas-phase concentration:*
The overall rate is exactly the same as in the nonreacting liquid:

$$(-r_u) = K^\circ C_{G,i} \quad (3.145)$$

Note that here the gas-phase concentration is constant and thus its inlet concentration is present in the overall rate expression.

First-order in gas reactant, saturated liquid-phase, and constant gas-phase concentration: If the liquid phase is saturated with the gas reactant, the overall rate can be derived in terms of the bulk liquid concentration of the gas reactant by using the balance around the catalyst:

$$(k_f a_c)[C_L - C_S] = (-r_u) \quad (3.146)$$

where

$$(-r_u) = m_s \eta_s k_m C_S \quad (3.147)$$

Following the procedure described in Section 3.1.2, the rate per unit volume of bubble-free liquid in terms of the concentration of the reactant in the liquid phase is

$$(-r_u) = k^\circ C_L = k^\circ \frac{C_G}{H} \quad (3.148)$$

where

$$\frac{1}{k^\circ} = \frac{1}{k_f a_c} + \frac{1}{m_s \eta_s k_m} \quad (3.149)$$

Note that since the liquid is saturated with the gas reactant, the liquid-phase concentration is in equilibrium with the bulk gas concentration.

First order in liquid reactant: In this case, the overall reaction rate can be expressed only in terms of the bulk liquid concentration of the liquid reactant by using the mass balance of the reactant around the catalyst:

$$(k_f a_c)[C_{L,t} - C_{S,t}] = (-r_u) \quad (3.150)$$

where

$$(-r_u) = m_s \eta_s k_m C_{S,t} \quad (3.151)$$

Following the procedure described in Section 3.1.2, the rate per unit volume of bubble-free liquid in terms of the concentration of the reactant in the liquid phase is

$$(-r_u) = k^\circ C_{L,t} \quad (3.152)$$

where

$$\frac{1}{k^\circ} = \frac{1}{k_f a_c} + \frac{1}{m_s \eta_s k_m} \quad (3.153)$$

In the above equations, the liquid and solid concentrations of liquid reactant are time-dependent (note subscript t).

The overall rate of reaction in continuous-flow systems

The concept of an overall rate based on the gas-phase bulk concentration and K° is not particularly helpful in the reactor design procedure when liquid and gas phases are in continuous flow (Smith, 1981). Instead, the overall rate should be expressed in terms of the bulk liquid concentration. The same analysis is followed for agitated slurry for continuous flow of both phases and for trickle-bed reactors. For a first-order reaction, using eq. (3.127) for the catalyst,

$$(-r_u) = k_f a_c (C_L - C_S) = m_s \eta_s k_m C_S \quad (3.154)$$

or

$$C_S = \frac{k_f a_c}{k_f a_c + m_s \eta_s k_m} C_L \quad (3.155)$$

and thus

$$(-r_u) = k^\circ C_L \quad (3.156)$$

where

$$k^\circ = \frac{k_f a_c m_s \eta_s k_m}{k_f a_c + m_s \eta_s k_m} \Leftrightarrow \frac{1}{k^\circ} = \frac{1}{k_f a_c} + \frac{1}{m_s \eta_s k_m} \quad (3.157)$$

3.4.7 Hydraulics

Since the superficial velocity of a liquid in the continuous-type operation is an order of magnitude lower than that of a gas, it is the gas superficial velocity that is the dominant parameter that affects the fluid dynamics of the reactor (Dudukovic *et al.*, 1999). Thus, whether the type of operation is continuous (concurrent or countercurrent to the flow of the gas) or batch (in respect to liquid flow) is immaterial from the fluid dynamics point of view. The gas, which is sparged at the bottom of the column, results in a buoyancy-driven flow that creates a strong liquid recirculation. In addition, as long as they are small (typically less than 60 μm), slurry particles follow liquid motion, with perhaps the exception of very high slurry loadings exceeding 20–30% (Dudukovic *et al.*, 1999). In contrast, in fluidized beds, a relative movement between the particles and fluid exists (Smith, 1981). Thus, in practice, the liquid and solids can be viewed as one flowing phase, frequently called “slurry” in the continuous-type operation, whereas in the batch-type operation, the slurry is considered to be a well-mixed phase. In agitated slurry reactors, under sufficient agitation, the whole reactor volume can be considered to be well-mixed, and is essentially equivalent to the CSTR.

Flow regimes in slurry bubble column reactors

The hydrodynamics of bubble columns and slurry bubble column reactors depend strongly on the flow regime (Figure 3.27). There are three flow patterns that prevail in these reactors (Wallis, 1969; Shah *et al.*, 1982):

- homogeneous regime or bubbly flow or quiescent bubbling
- heterogeneous regime or churn-turbulent flow
- slug-flow regime.

In the bubbly flow regime, there is a homogeneous distribution of small and almost identical gas bubbles, generally in the range 1–7 mm (Krishna, 2000). The gas velocity is usually less than 0.05 m/s and the interaction among gas bubbles is weak. Under these conditions, the gas bubbles do not affect the liquid motion and almost no liquid mixing is observed. The gas bubble formation in this regime depends strongly on the injection point (Magaud *et al.*, 2001; Sarafi *et al.*, 1999).

As the gas velocity is increased, there is more interaction among gas bubbles and both coalescence and breakup of bubbles are observed. This is the churn-turbulent flow or the heterogeneous regime, where the larger gas bubbles (generally in the range 20–150 mm) move in plug flow, creating liquid recirculation as well as backmixing (Shah *et al.*, 1982). The large

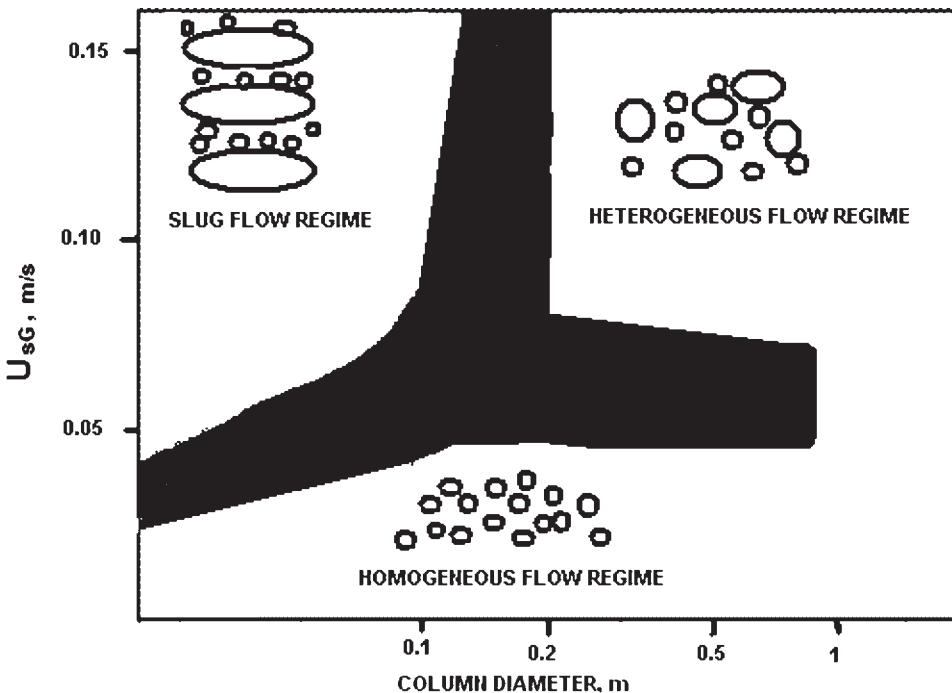


Figure 3.27 Flow regimes in slurry bubble reactors

bubbles travel through and up the column at high velocities, in the range 1–2 m/s, in near plug-flow motion. The smaller gas bubbles, on the other hand, are entrained within the liquid recirculation (Krishna *et al.*, 2000; Krishna, 2000). In general, the transition between the homogeneous and heterogeneous regime is difficult to be characterized. Furthermore, in small diameter columns, as the gas velocity increases, gas bubbles tend to coalesce to form slugs, whose diameters can be as large as the column diameter. This regime is called as slug-flow regime. Bubble slugs can be observed in columns of diameters lower than 0.15 m (Shah *et al.*, 1982). While bubble flow (homogeneous flow regime) is used in some applications (gas velocities smaller than 2–3 cm/s), churn-turbulent flow (gas velocities between 10 and 50 cm/s) is of current industrial interest (Dudukovic *et al.*, 1999).

Koide (1996) recommended that for air–water systems, if $D \delta \geq 2 \times 10^{-4} \text{ m}^2$, the flow can be considered to be in the heterogeneous regime. In this relationship, D is the column diameter and δ the nozzle or hole diameter of the gas distributor. The transition region can be defined in terms of gas holdup by using Marrucci's and Akita–Yoshida equations as presented in Figure 3.28 (Koide, 1996).

Gas distribution

Gas distributors are an integral part of the design and scale-up of bubble columns and SBCRs. There are numerous types of gas distributors, which differ significantly in their size and number of orifices. Porous plates, perforated plates (sieve plate/sieve tray), multiple/single-orifice nozzles, bubble caps, perforated rings, annular shears, spider-type, injectors, and hollow fibers among others, account for the most commonly used spargers in bubble and slurry bubble column reactors. Figure 3.29 illustrates some of these gas distributors. Opening size, number of openings, sparger positioning, and nozzles position/orientation are the most important characteristics of a gas distributor. Figure 3.30 shows a sparger-type gas distributor.

The porous plate usually consists of microsize pores with mean diameters ranging between 1.7 and 300 μm (Smith *et al.*, 1996; Vial *et al.*, 2001; Bouaifi *et al.*, 2001). The perforated plate design, however, takes into account the number, pitch, and diameter of the

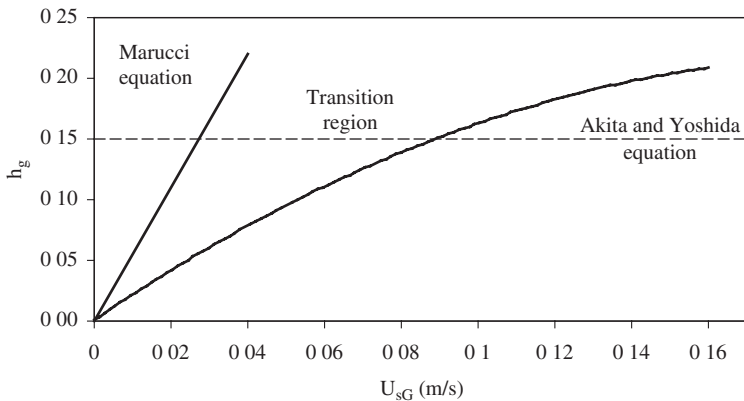


Figure 3.28 Transition region in two-phase water–air bubble columns (Koide, 1996).

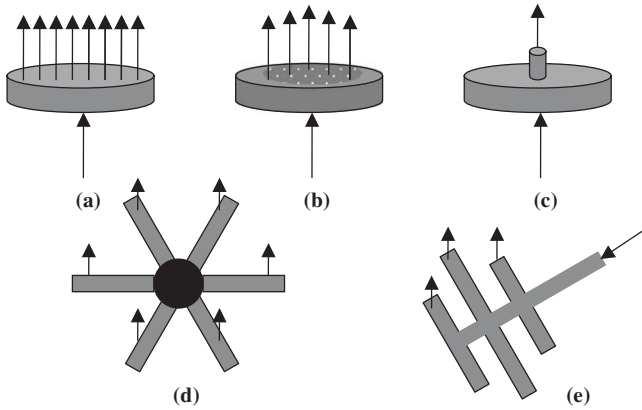


Figure 3.29 Gas-phase distributors: (a) porous plate, (b) perforated plate, (c) single-orifice nozzle, (d) spider-type sparger, and (e) multiple-orifice nozzle

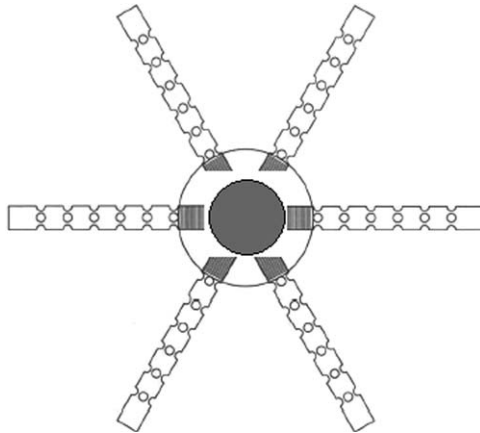


Figure 3.30 Sparger-type gas distributor.

holes. Each hole has the same diameter, usually in the millimeter range. For example, sieve plates of 0.5–2.5 mm hole diameter, 4 holes/cm², and square or triangular pitch of 5–7 mm sides have been used (Vandu and Krishna, 2004; Bouaifi *et al.*, 2001). Similarly, the diameter of the single-orifice nozzle is also in the millimeter range and is often reported to maintain a heterogeneous flow regime in the bubble column for a superficial gas velocity as low as 0.04 m/s. Finally, an example of the spider-shaped sparger, which has been used for 63-cm-diameter bubble columns, has a hole diameter of 2.5 mm and 64 holes, while the diameter of the tubes are 25 mm (Vandu and Krishna, 2004).

Generally, it can be stated that at a low superficial gas velocity (<0.04 m/s), only a single-orifice nozzle can provide a heterogeneous flow regime, in contrast to other types of spargers, i.e. perforated plates, porous plates, and multiple-orifice nozzles, which would maintain a homogeneous flow regime. In that case, the effect of gas spargers is negligible.

Criteria for suspension of solid particles in the slurry phase

For maximum utilization of the solid phase in a bubble column, it is essential that all particles be suspended in the reactor (Ramachandran and Chaudhari, 1984). This means that the gas velocity should be sufficiently high to enable suspension of all solids in the liquid. In slurry bubble column reactors, two suspension states exist:

- complete suspension, in which all particles are suspended in the liquid, and
- homogeneous suspension, in which the solids concentration is uniform throughout the reactor.

The gas velocities that are required for homogeneous suspension are far greater than those required for complete suspension. The gas velocity required to achieve complete suspension can be obtained from the correlation of Roy *et al.* (Ramachandran and Chaudhari, 1984):

$$\frac{m_{s,\max}}{\rho_L} = \frac{6.8}{10000} \frac{\mu_{L,m} D u_{sG} \rho_G}{\mu_G} \left(\frac{\sigma_L h_G}{u_{sG} \mu_L} \right)^{-0.23} \left(\frac{h_G u_{\text{ter}}}{u_{sG}} \right)^{-0.18} \gamma^{-3} \quad (3.158)$$

where

$$\mu_{L,m} = 0.232 - 0.1788 \log(\mu_L) + 0.1026 [\log(\mu_L)]^2 \quad (3.159)$$

with:

- $m_{s,\max}$ = the maximum solid loading at a given gas velocity, g/cm³
- σ_L = the surface tension of the liquid, dyne/cm
- D = the reactor diameter
- u_{ter} = the terminal velocity of the particles
- γ = the wettability factor, which can be considered equal to unity for most of the catalyst particles.

CGS units should be used with this equation.

Gas holdup

Before analyzing the subject of gas holdup, it has to pointed out that while u_b is the bubble rising velocity and Z/u_b is the bubble residence time, the superficial gas velocity present in the following equation is equivalent to the superficial gas velocity in fixed beds:

$$u_{sG} = \frac{Q_G}{A} \quad (3.160)$$

where A is the cross-sectional area of the vessel and Q_G the gas volumetric flow rate. The superficial velocity in a slurry, as in the case of a fixed bed, is not equal to the real velocity of the fluid. In fixed beds, the real velocity is the interstitial velocity u_i/ϵ , while in slurries the real velocity of the gas phase is the bubble rising velocity. In case of a fixed bed, the bed porosity decreases the fluid velocity, while in a slurry the decrease of gas velocity is due to its interaction with the liquid phase, e.g. for the same superficial velocity, the real

velocity of the gas phase will be much lower in a fluid of low viscosity than in a liquid of much higher viscosity.

For the heterogeneous flow regime, the Akita–Yoshida correlation derived for bubble column reactors is proposed (Akita and Yoshida, 1973; Ramachandran and Chaudhari, 1984; Behkish, 2004; Koide, 1996):

$$H_{AY} = \frac{h_G}{(1-h_G)^4} = n \left(\frac{gD^2 \rho_L}{\sigma_L} \right)^{1/8} \left(\frac{gD^3 \rho_L^2}{\mu_L^2} \right)^{1/12} \frac{u_{sG}}{(gD)^{0.5}} \quad (3.161)$$

where $n = 0.2$ for pure liquids and nonelectrolytes, and 0.25 for electrolyte solutions. SI units should be used with this equation. Akita and Yoshida (1973) investigated the effect of liquid flow for liquid superficial velocities up to 0.044 m/s and found that the effect on gas holdup is negligible. Furthermore, Fox and Degen (1990) studied the Fisher–Tropsch synthesis in slurry bubble columns and reported that the effect of liquid flow is important only in systems where foam is present. To have an idea of the effect of liquid flow, the following correlation for bubble columns has been given by Hughmark (1967) (Saxena, 1991; Koide, 1996):

$$h_G = \frac{1}{2 + \left(\frac{0.35}{u_{sG,f}} \right) \left[\left(\frac{\rho_L}{\rho_w} \right) \left(\frac{\rho_L}{\rho_w} \right) \right]^{1/3}} \quad (3.162)$$

where

$$u_{sG,f} = h_G \left[\left(\frac{u_{sG}}{h_{G,f}} \right) - \left(\frac{u_{sL}}{1-h_{G,f}} \right) \right] \quad (3.163)$$

with

u_{sL} = the superficial liquid velocity

$h_{G,f}$ = the gas holdup in the case of liquid flow.

For batch liquid, $u_{sG,f} = u_{sG}$. The subscript “w” in symbols denotes water property. SI units are used in this equation. For the derivation of this correlation, air velocities up to 0.305 m/s and liquid velocities up to 0.09 m/s were used. The Hughmark correlation has been derived for the heterogeneous flow regime. In Figure 3.31, the effect of liquid flow on gas holdup for the air–water system is presented.

It has been reported that for diameters less than 7.62 cm, the gas holdup depends on the column diameter, whereas it is independent of it for diameters greater than 10.2 cm (Hughmark, 1967; Saxena, 1991). The same has been found in studies of the Fisher–Tropsch synthesis in slurry bubble columns, where it has been reported that the effect of the column diameter is negligible when foam is not present in the system (Fox and Degen, 1990).

Reilly *et al.* (1986) proposed the following correlation for turbulent bubble columns at ambient conditions (Reilly *et al.*, 1986; Behkish, 2004; Saxena, 1991):

$$h_G = 0.009 + 296 u_{sG}^{0.44} \rho_L^{-0.98} \sigma_L^{-0.16} \rho_G^{0.19} \quad (3.164)$$

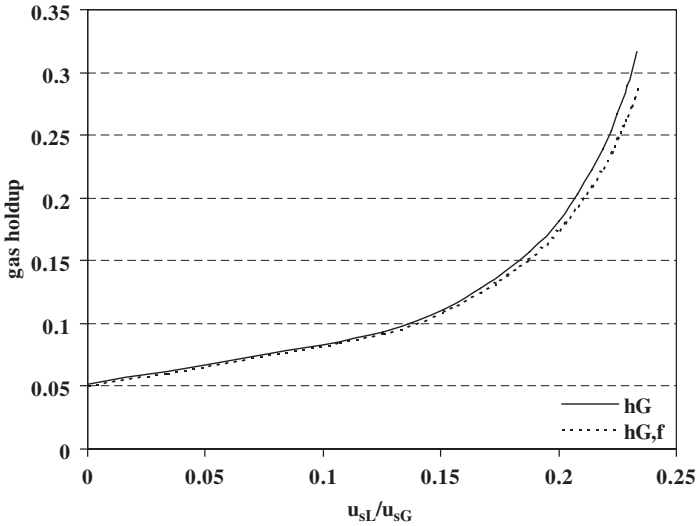


Figure 3.31 The effect of liquid flow on gas holdup for air–water bubble columns.

This correlation has been proposed for slurry bubble columns as well, as the authors found that the effect of solids addition has a negligible effect on gas holdup. SI units should be used in this correlation.

The addition of solids has been found to increase or even decrease the gas holdup, depending on the experimental conditions. When the solids addition promotes bubble break up, the average bubble size is smaller, the bubble rising velocity is reduced, and the gas holdup increases (DOE, 1985). The following correlation of Koide *et al.* (1963) is used in slurry bubble columns and for the heterogeneous and transition regimes (Koide *et al.*, 1984; Koide, 1996):

$$H_K = \frac{h_G}{(1-h_G)^4} = n \left(\frac{u_{sG} \mu_L}{\sigma_L} \right)^{0.918} \left(\frac{g \mu_L^4}{\rho_L \sigma_L^3} \right)^{-0.252} K_O \quad (3.165)$$

$$K_O = \frac{1}{1 + 4.35 \varphi_S^{0.748} \left(\frac{\rho_s - \rho_L}{\rho_L} \right)^{0.881} Re_D^{-0.168}} \quad (3.166)$$

$$Re_D = \frac{u_{sG} D \rho_L}{\mu_L} \quad (3.167)$$

where $n = 0.277$ for water and aqueous solutions of glycerol and glycol, and $n = 0.364$ for aqueous solutions of inorganic electrolytes. SI units are used in this correlation. Note that

in this correlation, the solid density is used. For nonporous particles, it is equal to the particle density. However, for porous solids, it is more appropriate to use the hydraulic density as defined in Section 3.9.6.

It is evident from Figure 3.32 that fractional gas holdup is decreased by the addition of solids and this decrease is higher for higher gas velocity, solid concentration, and solid density.

The three types of fractional holdup are related as follows (Behkish, 2004):

$$h_G + h_S + h_L = 1 \tag{3.168}$$

where:

- h_G = the fractional holdup of the gas phase
- h_L = the fractional holdup of the liquid phase
- h_S = the fractional holdup of solids.

The fractional holdup of each phase is defined as

$$h_i = \frac{V_i}{V_{tot}} = \frac{V_i}{V_L + V_G + V_S} \tag{3.169}$$

where V_{tot} is the total volume of the slurry and V_S is the total volume of solids:

$$\rho_p = \frac{M_{particle}}{V_{particle}} \Rightarrow V_{particle} = \frac{M_{particle}}{\rho_p} \tag{3.170}$$

$$V_S = \frac{M_{particle} n_{particles}}{\rho_p} = \frac{M_S}{\rho_p} \tag{3.171}$$

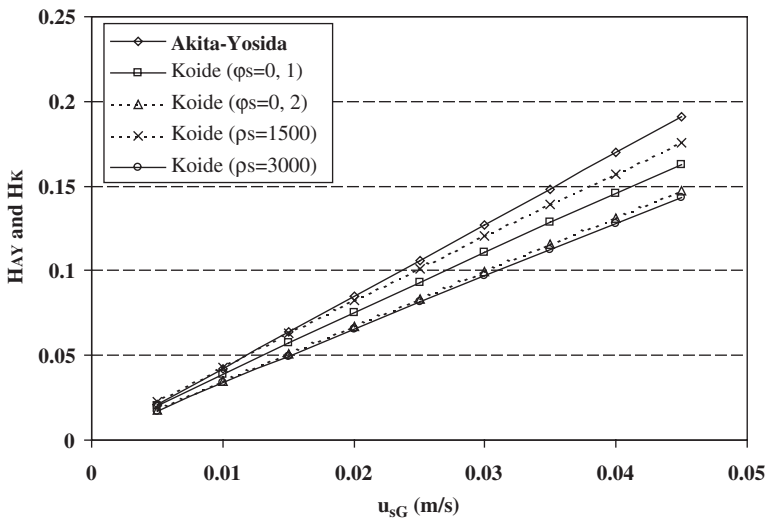


Figure 3.32 Comparison of Akida–Yoshida and Koide correlations for aqueous electrolyte solutions, $D = 0.1$ m; $\phi_S = 0.1$; $\rho_S = 1500, 2000,$ and 3000 kg/m³; $\phi_S = 0.1$ and 0.2 ; and $\rho_S = 2000$ kg/m³.

Another parameter, similar to fractional holdup but different in value, is the volume fraction of solid and liquid in the slurry (Koide, 1996; Kantarci *et al.*, 2005).

$$\varphi_S = \frac{V_S}{V_S + V_L} \quad (3.172)$$

$$\varphi_L = \frac{V_S}{V_S + V_L} \quad (3.173)$$

In this definition, the term “slurry” is used to denote the phase consisting of the liquid and the solid, and thus the term “bubble-free slurry” would be a more appropriate term to be used for this phase.

Smith (1981) uses the parameter V_B , referred to in his book as “gas holdup,” which is defined as “the volume of bubbles per unit volume of liquid,” which is different from the fractional holdup value:

$$V_B = \frac{V_G}{V_L} = \frac{V_G}{V_L} \frac{V_{\text{tot}}}{V_{\text{tot}}} = \frac{V_G}{V_{\text{tot}}} \frac{V_{\text{tot}}}{V_L} = \frac{h_G}{h_L} \quad (3.174)$$

Then, following Smith’s terminology, the “total gas holdup” is

$$V_B V_L = V_G \quad (3.175)$$

which is simply the total volume of gas in the reactor.

The fractional gas holdup can be easily measured from the height of the expanded column height Z_f and the settled slurry height Z_s , i.e. the height of the column before aeration (liquid volume plus solids volume) (DOE, 1985; NTIS, 1983):

$$h_G = \frac{Z_f - Z_s}{Z_f} \quad (3.176)$$

Define the mass concentration of solids in a slurry as

$$m_s = \frac{M_S}{V_L} \quad (3.177)$$

where V_L is the volume of liquid then

$$V_L = \frac{M_S}{m_s} \quad (3.178)$$

and finally

$$\frac{V_S}{V_L} = \frac{m_s}{\rho_p} \quad (3.179)$$

Consider a bubble-free slurry. It is known that solid concentrations up to 10% can be handled in slurry reactors (Perry and Green, 1999). Thus, for particle densities of 1–3 g/cm³ and water as liquid phase, the maximum values of V_S/V_L are 0.1–0.03, which means that h_S is 3.2–9.1%. However, for low m_s , e.g. 2% (w/v) (g/100 cm³), these values drop to 0.6–1.9%, which is fairly low. Considering that on introducing the gas-phase, the total volume of the reactor will be even higher, the solid-phase holdup is decreased even more and becomes minimal in many practical applications.

Bubble velocity and diameter

Gogoi and Dutta (1996) proposed the Cliff–Grace–Webber correlation for the terminal bubble rising velocity for turbulent slurry bubble columns (Cliff *et al.*, 1978; Shah *et al.*, 1982):

$$u_{\text{bub,ter}} = \frac{\mu_L}{\rho_L d_{\text{bub}}} M^{-0.149} (J - 0.867) \quad (3.180)$$

where d_{bub} is the bubble diameter, and

$$M = \frac{g\mu_L^4(\rho_L - \rho_G)}{\rho_L^2 \sigma_L^3} \quad (3.181)$$

$$Re_{\text{bub}} = \frac{d_{\text{bub}} u_{\text{bub,ter}} \rho_L}{\mu_L} \quad (3.182)$$

$$Eo = \frac{g(\rho_L - \rho_G) d_{\text{bub}}^2}{\sigma_L} \quad (3.183)$$

$$H = \frac{4}{3} Eo M^{-0.149} \left(\frac{\mu_L}{\mu_W} \right)^{-0.14} \quad (3.184)$$

and

$$J = 0.94H^{0.747} \text{ for } 2 \leq H \leq 59.3 \quad (3.185)$$

$$J = 3.42H^{0.441} \text{ for } H > 59.3 \quad (3.186)$$

The above equations are valid for $M < 10^{-3}$, $Eo < 40$, and $Re_{\text{bub}} > 0.1$.

For bubble columns, the Akita–Yoshida equation can be used for determining of bubble diameter (Shah *et al.*, 1982; Koide, 1996):

$$\frac{d_{\text{bub}}}{D} = 26 \left(\frac{D^2 g \rho_L}{\sigma_L} \right)^{-0.5} \left(\frac{D^3 g \rho_L^2}{\mu_L^2} \right)^{-0.12} \left(\frac{u_{sG}}{\sqrt{Dg}} \right)^{-0.12} \quad (3.187)$$

where D is the column diameter. This correlation has been derived for columns of 0.3 m maximum diameter and 0.07 m/s maximum gas superficial velocity. Furthermore, the bubbles size and formation is affected by the orifice type and diameter (Figure 3.33).

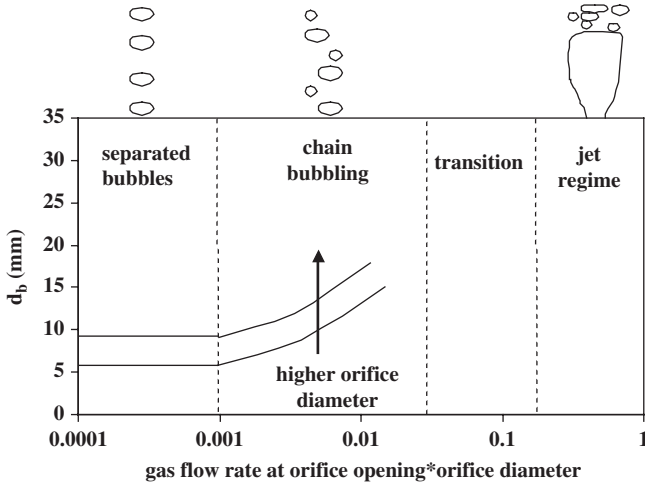


Figure 3.33 Air-bubble formations at the orifice in water (Heijnen and Van't Riet, 1984).

Addition of solids in the liquid increases the bubble coalescences, and in turn, the bubble size (Koide, 1996). Fukuyama et al. (1987) proposed the following correlation for slurry bubble columns:

$$d_{\text{bub}} = \frac{0.59}{g} \left(\frac{\gamma}{h_G} \right)^2 \quad (3.188)$$

$$\gamma = u_{sG}(1 - h_G) - u_{sL}h_G \left(\frac{1 - h_G}{h_L} \right) \quad (3.189)$$

Bubble diameter d_{bub} is also referred to as “volume-surface mean diameter of bubbles” or “Sauter mean bubble diameter.” SI units are used with this correlation.

The Rayleigh–Taylor instability is the balance of surface tension and gravity acting on a gas bubble. If the latter is greater than the former, the bubble will eventually break up. According to Bellman and Pennington (1953), if the diameter of a certain spherical cap bubble exceeds a critical diameter, it will break up. This critical diameter is referred to as the maximum stable bubble size and is generally expressed as (Bellman and Pennington, 1953; Behkish, 2004)

$$d_{\text{bub,max}} = 2\pi \left[\frac{\sigma_L}{g(\rho_L - \rho_G)} \right]^{0.5} \quad (3.190)$$

Krishna *et al.* (2001) used a different and simpler approach for determining the bubble rising velocity and bubble diameter. They employed a two-phase model, analogous to the one

used for gas–solid bubbling fluidized beds. The single bubble rising velocity is a relationship originating from the equation of Mendelson (Mendelson, 1967; Krishna, 2000):

$$u_{bs} = \left(\frac{2\sigma_L}{\rho_L d_{bub}} + \frac{gd_{bub}}{2} \right)^{0.5} \quad (3.191)$$

For values of the Eotvos number higher than 40 (for the air–water system, this corresponds to $d_{bub} > 17$ mm), the above equation simplifies to the well-known Davies–Taylor equation:

$$u_{bs} = 0.71(gd_{bub})^{0.5} \quad (3.192)$$

Eotvos number is defined as (Krishna, 2000)

$$Eo = \frac{g(\rho_L - \rho_G)d_{bub}^2}{\sigma_L} \quad (3.193)$$

The scaling factor accounts for the influence of the column diameter:

$$S_f = 1 \quad \text{for } \frac{d_{bub}}{D} < 0.125 \quad (3.194)$$

$$S_f = 1.13 \exp\left(-\frac{d_{bub}}{D}\right) \quad \text{for } 0.125 < \frac{d_{bub}}{D} < 0.6 \quad (3.195)$$

$$S_f = 0.496 \left(\frac{D}{d_{bub}}\right)^{0.5} \quad \text{for } \frac{d_{bub}}{D} > 0.6 \quad (3.196)$$

and the single-bubble rising velocity is

$$u_{bs} = 0.71(gd_{bub})^{0.5} S_f \quad (3.197)$$

The rise velocity of the bubbles population is

$$u_{bub} = u_{bs} A_f \quad (3.198)$$

where A_f is the acceleration factor. For low-viscosity liquids ($\mu < 0.0029$ Pa s) (Krishna, 2000):

$$A_f = 2.73 + 4.505(u_s - u_{trans}) \quad (3.199)$$

where u_s is the superficial gas velocity and u_{trans} , the transition velocity from homogeneous to heterogeneous flow regime. The latter is practically equal to zero for slurries

with solids concentration higher than 36% v/v (Krishna et al., 2001). Finally, the average bubble diameter is

$$\begin{aligned} d_{\text{bub}} &= 0.069(u_s - u_{\text{trans}})^{0.376} \\ \Rightarrow (u_s - u_{\text{trans}}) &= \left(\frac{d_{\text{bub}}}{0.069} \right)^{1/0.376} \end{aligned} \quad (3.200)$$

Since the velocity of a given phase in the bubble column usually differs from the other phases, the volumetric flow rate fraction of that phase is not equal to its corresponding holdup, and hence the slip velocity is introduced to account for this difference:

$$U_s = \frac{u_{\text{sG}}}{h_G} - \frac{u_{\text{sL}}}{1 - h_G} \quad (3.201)$$

If the operations run in the semibatch mode and the linear superficial slurry velocity u_{sL} is zero, the above equation would become the mean bubble rise velocity in the swarm (Shah et al., 1982).

Dispersion in liquid and gas phase

Liquid phase Liquid dispersion is related to how well the gas flowing through the reactor can mix the slurry phase. Ideal mixing is a theoretical limit whereby any liquid molecule can move to any other part of the reactor from one instant to the next. In practice, when D_{LL} is greater than 0.01 m²/s, a well-mixed behavior exists (NTIS, 1985).

The liquid-phase dispersion coefficient can be estimated using the Deckwer et al. (1974) correlation (Ramachandran and Chaudhari, 1980):

$$D_{\text{LL}} = 2.7D^{1.4}u_{\text{sG}}^{0.3} \quad (3.202)$$

where D is the reactor diameter. CGS units are used with this equation.

Koide provides correlations derived for three-phase systems and one of them is the Kato and Nishiwaki correlation (Koide, 1995):

$$D_{\text{LL}} = u_{\text{sG}}D \frac{1 + Fr^{0.85}}{13Fr} \quad (3.203)$$

where the Froude number is

$$Fr = \frac{u_{\text{sG}}}{(gD)^{0.5}} \quad (3.203)$$

SI units are used with this correlation. In general, the addition of solids reduces the liquid mixing.

In the case of continuous flow of both phases, the liquid phase can be considered well mixed if (Ramachandran and Chaudhari, 1980)

$$\left(\frac{u_{sL}d_p}{D_{LL}}\right)\left(\frac{Z}{d_p}\right) \leq 4 \quad (3.205)$$

Gas phase For the gas-phase dispersion coefficient, the Field and Davidson equation is proposed (Koide, 1995):

$$D_{LG} = 19.7D^2u_{sG} \quad (3.206)$$

SI units are used with this correlation.

3.4.8 External mass transfer

Mass transfer coefficients: liquid to particle (k_f)

Gogoi and Dutta (1996) studied the solid-liquid mass transfer in a three-phase sparged reactor. They derived the following correlation:

$$\frac{k_f d_p}{D_f} = 2 + 0.21 \left(\frac{u_T d_p \rho_L}{\mu_L}\right)^{0.1094} \left(\frac{\mu_L}{\rho_L D_f}\right)^{0.45} \quad (3.207)$$

The liquid-phase turbulence, which enhances the particle-liquid drag force thereby increasing the value of the mass transfer coefficient, is characterized by the turbulence intensity (u_T), as defined by the following relation:

$$u_T = 0.49 \left\{ gD \left[u_{sG} - h_G u_b - h_S u_{sh} \left(\frac{\rho_s - \rho_L}{\rho_L} \right) \right] \right\}^{1/3} \quad (3.208)$$

$$u_{sh} = 1.1 u_{sG}^{0.026} u_{ter}^{0.8} \left(\frac{h_L}{1 - h_G} \right)^{3.5} \quad (3.209)$$

$$u_{ter} = \frac{g(\rho_s - \rho_L)d_p^2}{18\mu_L} \quad (3.210)$$

where:

u_T = the turbulence intensity (in m/s)

u_b = the bubble rising velocity

- h_L = the fractional holdup of the liquid phase
 D = the column diameter
 h_G = the fractional holdup of the gas phase
 h_S = the fractional holdup of solids
 u_{sh} = the hindered settling velocity of spherical particles
 u_{ter} = the terminal settling velocity of spherical particles.

SI units should be used with this correlation.

Another simpler equation is that of Sano et al. (1974; Ramachandran and Chaudhari, 1984; Koide, 1996):

$$\frac{k_f d_p}{D_f F_s} = 2 + 0.4 \left(\frac{g u_{sG} d_p^4 \rho_L^3}{\mu_L^3} \right)^{0.25} \left(\frac{\mu_L}{\rho_L D_f} \right)^{1/3} \quad (3.211)$$

where D_f is the liquid-phase diffusion coefficient and F_s is a shape factor and can be taken as unity for spherical particles.

Liquid–solid interfacial area in slurry reactors

By definition, the liquid–solid interfacial area is the total external particle area per unit volume of bubble-free liquid a_c , and is given by

$$a_c = \frac{A_{\text{particles,total}}}{V_L} \quad (3.212)$$

For spherical particles,

$$A_{\text{particles,total}} = \pi d_p^2 n \quad (3.213)$$

$$V_{\text{particle}} = \frac{\pi d_p^3}{6} \quad (3.214)$$

$$M_{\text{particles,total}} = V_{\text{particle}} \rho_p n \quad (3.215)$$

$$m_s = \frac{M_{\text{particles,total}}}{V_L} \Rightarrow V_L = \frac{M_{\text{particles,total}}}{m_s} \quad (3.216)$$

$$V_L = \frac{V_{\text{particle}} \rho_p n}{m_s} = \frac{\pi d_p^3 \rho_p n}{6 m_s} \quad (3.217)$$

$$a_c = \frac{A_{\text{particle,total}}}{V_L} = \frac{\pi d_p^2 n}{\left[\frac{\pi d_p^3 \rho_p n}{6 m_s} \right]} = \frac{6 m_s}{d_p \rho_p} \quad (3.218)$$

where

- ρ_p = the particle density,
- n = the number of solid particles,
- m_s = the concentration of catalyst in the slurry, g catalyst/cm³ liquid.

Note that α_c is equivalent to α_u for fixed-beds. The liquid–solid interfacial area per unit volume of reactor is

$$a_{c,\text{tot}} = a_c h_L \quad (3.219)$$

Mass transfer coefficients: gas bubble to liquid (k_{fg})

Normally, even when the bubble phase is a gas mixture, the major mass transfer resistance for slightly soluble gases is in the gas–liquid interface. Thus, the mass transfer coefficient in the liquid film around the bubble is the important one in gas bubble-to-liquid mass transfer (Smith, 1981; Treybal, 1980).

In the absence of mechanical agitation and for bubbles with diameter less than 2.5 mm (the usual size range for slurry reactors), the following correlation of Calderbank is available (Smith, 1981):

$$k_{fg} \left(\frac{\mu_L}{\rho_L D_{fg}} \right)^{2/3} = 0.31 \left(\frac{\Delta\rho_{fg} \mu_L g}{\rho_L^2} \right)^{1/3} \quad (3.220)$$

where

- $\Delta\rho_{fg}$ = the difference in density between liquid-phase and gas bubbles, g/cm³
- μ_L = the viscosity of liquid-phase, g/cm s
- ρ_L = the density of liquid-phase, g/cm³
- g = the acceleration of gravity, cm/s²
- k_{fg} = the mass transfer coefficient, cm/s.
- D_{fg} = the liquid-phase diffusion coefficient of the gas solute, cm²/s

Although the above correlation was developed for a column with no solids present, it has been applied with some success to slurry bubble columns. Another correlation, presented by Hikita et al. (1981), which was developed under ambient conditions in the absence of solid particles and for $0.042 < u_{sG} < 0.38$ m/s (bubble column), is the following (Hikita et al., 1981; Behkish, 2004):

$$\frac{k_{fg} a_{GL,\text{tot}} u_{sG}}{g} = 14.9 \left(\frac{u_{sG} \mu_L}{\sigma_L} \right)^{1.76} \left(\frac{\mu_L^4 g}{\rho_L \sigma_L^3} \right)^{-0.248} \left(\frac{\mu_G}{\mu_L} \right)^{0.243} \left(\frac{\mu_L}{\rho_L D_{fg}} \right)^{-0.604} \quad (3.221)$$

where u_{sG} is the superficial gas velocity and $\alpha_{GL,\text{tot}}$ the gas-liquid interfacial area per unit volume of reactor, as defined in eq. (3.230).

Another equation is the Akita–Yoshida correlation derived for bubble column reactors (Shah et al., 1982; Ramachandran and Chaudhari, 1984):

$$k_{fg} \alpha_{GL,\text{tot}} = 0.6 \frac{D_{fg}}{D^2} \left(\frac{\mu_L}{D_{fg} \rho_L} \right)^{0.5} \left(\frac{g D \rho_L}{\sigma_L} \right)^{0.62} \left(\frac{g D^3 \rho_L^2}{\mu_L^2} \right) h_G^{1.1} \quad (3.222)$$

This equation has been also proposed for slurry bubble column reactors and has been derived for water–air and glycol–air systems; $0.003 < u_{sG} < 0.4$, $0 < u_{sL} < 0.44$ m/s. SI units should be used in this equation.

The following correlation by Yasunishi et al. has been used for slurry bubble bed columns (Yasunishi et al., 1986; Koide, 1996):

$$k_{fg}\alpha_{GL,tot} = 3.09 \times 10^{-7} u_{sG} \left\{ \left[1 - \frac{\varphi_s}{0.6(1-h_G)} \right] \mu_L^{-1} \right\}^{1.5} \quad (3.223)$$

where φ_s is the volume fraction of solid in the bubble-free slurry (liquid and solid phase). SI units are used for all parameters except u_{sG} which is in cm/s.

Gas–Liquid interfacial area in slurry reactors

The total external bubble area per unit volume of bubble-free liquid (a_{GL}) by definition is

$$a_{GL} = \frac{A_{\text{bubbles,total}}}{V_L} \quad (3.224)$$

For spherical bubbles,

$$A_{\text{bubbles,total}} = \pi d_{\text{bub}}^2 n \quad (3.225)$$

where n is the number of bubbles. The volume of liquid V_L can be determined as follows:

$$V_L = \frac{V_L}{\left(\frac{V_G}{V_R}\right)} \left(\frac{V_G}{V_R}\right) = \frac{\left(\frac{V_L}{V_R}\right)}{h_G} V_G = \frac{h_L}{h_G} V_G \quad (3.226)$$

where V_R is the total volume of the reactor, i.e. the volume of slurry (volume of liquid, gas, and solids) and

$$V_G = V_{\text{bubble}} n = \frac{\pi d_{\text{bub}}^3}{6} n \quad (3.227)$$

Then

$$a_{GL} = \frac{A_{\text{bubbles,total}}}{V_L} = \frac{\pi d_{\text{bub}}^2 n}{\frac{h_L}{h_G} \left(\frac{\pi d_{\text{bub}}^3}{6} n\right)} = \frac{6}{d_{\text{bub}}} \frac{h_G}{h_L} \quad (3.228)$$

In mass-transfer correlations, the volumetric mass-transfer coefficient is expressed using the gas–liquid interfacial area per unit volume of slurry (or expanded column or reactor, V_R) (Koide, 1996; Kantarci *et al.*, 2005; NTIS, 1983):

$$a_{GL,tot} = \frac{A_{bubbles,total}}{V_R} = \frac{\pi d_{bub}^2 n}{\left(\frac{V_G}{h_G}\right)} = \frac{\pi d_{bub}^2 n}{\left(\frac{\pi d_{bub}^3 n}{6}\right)} h_G = \frac{6}{d_{bub}} h_G \quad (3.229)$$

$$a_{GL,tot} = a_{GL} h_L \quad (3.230)$$

Note that from the correlation of Hikita *et al.* (1981),

$$\begin{aligned} \frac{k_{fg} a_{GL,tot} u_{sG}}{g} = f &\Leftrightarrow k_{fg} a_{GL,tot} \\ &= \frac{fg}{u_{sG}} \Leftrightarrow k_{fg} a_{GL,tot} \frac{a_{GL}}{a_{GL,tot}} = \frac{fg}{u_{sG}} \frac{a_{GL}}{a_{GL,tot}} \end{aligned} \quad (3.231)$$

or

$$k_{fg} a_{GL} = \frac{fg}{u_{sG}} \frac{1}{h_L} \quad (3.232)$$

where

$$f = 14.9 \left(\frac{u_{sG} \mu_L}{\sigma_L}\right)^{1.76} \left(\frac{\mu_L g}{\rho_L \sigma_L^3}\right)^{-0.248} \left(\frac{\mu_G}{\mu_L}\right)^{0.243} \left(\frac{\mu_L}{\rho_L D_{fg}}\right)^{-0.604} \quad (3.233)$$

3.5 AGITATED SLURRY REACTORS

3.5.1 Agitated slurry reactor models

In CSTR reactors, both phases are considered to be in complete mixed and continuous-flow condition. In the general case where reactants can be gases and liquids, the following material balances can be applied (for simplicity we consider constant-density systems) (Hopper *et al.*, 2001)

Liquid reactant (nonvolatile component) liquid-phase mass balance:

$$\frac{Q_L}{V_L} (C_{L,i} - C_{L,o}) - (k_f a_c) (C_{L,o} - C_S) = 0 \quad (3.234)$$

Gas reactant (volatile component) liquid-phase mass balance:

$$\frac{Q_L}{V_L}(C_{L,i} - C_{L,o}) + (K_L a_{GL}) \left(\frac{C_{G,o}}{H} - C_{L,o} \right) - (k_f a_c)(C_{L,o} - C_S) = 0 \quad (3.235)$$

Gas-phase mass balance:

$$\frac{Q_G}{V_L}(C_{G,i} - C_{G,o}) - (K_L a_{GL}) \left(\frac{C_{G,o}}{H} - C_{L,o} \right) = 0 \quad (3.236)$$

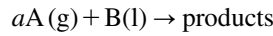
Component mass balance around the catalyst:

$$(k_f a_c)[C_{L,o} - C_S] = (-r_u) \quad (3.237)$$

where the subscripts (o) and (i) denotes outlet and inlet conditions, respectively. These material balances should be written for all reactants wherever applicable. In the following, some common cases will be examined.

Gas-liquid reactions and continuous flow of both phases

General case Consider the reaction of the form



In this case, the material balance (3.234) is applicable only for B, while material balances (3.235) and (3.236) are applicable only for A.

Nonvolatile component liquid-phase mass balance:

$$\frac{Q_L}{V_L}(C_{BL,i} - C_{BL,o}) - (k_f a_c)_B(C_{BL,o} - C_{BS}) = 0 \quad (3.238)$$

Volatile component liquid-phase mass balance:

$$\begin{aligned} \frac{Q_L}{V_L}(C_{AL,i} - C_{AL,o}) + (K_L a_{GL})_A \left(\frac{C_{AG,o}}{H_A} - C_{AL,o} \right) \\ - (k_f a_c)_A(C_{AL,o} - C_{AS}) = 0 \end{aligned} \quad (3.239)$$

Gas-phase mass balance:

$$\frac{Q_G}{V_L}(C_{AG,i} - C_{AG,o}) - (K_L a_{GL})_A \left(\frac{C_{AG,o}}{H_A} - C_{AL,o} \right) = 0 \quad (3.240)$$

Component mass balance around the catalyst:

$$(k_f a_c)_A [C_{AL,o} - C_{AS}] = (-r_u)_A = m_s (-r_m)_A \quad (3.241)$$

$$(k_f a_c)_B [C_{BL,o} - C_{BS}] = (-r_u)_B \quad (3.242)$$

where

$$(-r_u)_B = \frac{(-r_u)_A}{a} = \frac{m_s}{a} (-r_m)_A \quad (3.243)$$

and

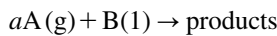
- Q = the volumetric flow rate (G for gas and L for liquid as subscripts)
- V_R = the reactor volume
- $(-r_m)_A$ = the overall rate of reaction (disappearance) per unit mass of catalyst based on component A
- $(-r_u)_A$ = the overall rate of reaction (disappearance) per unit volume of bubble-free liquid based on component A
- $(-r_u)_B$ = the overall rate of reaction (disappearance) per unit volume of bubble-free liquid based on component B.

Subscripts i and o denote the inlet and outlet concentrations of reactants, respectively.

Constant gas-phase concentration In the case of constant gas-phase concentration of A, eq. (3.236) is not needed. The rest of the model remains the same.

Gas-liquid reactions and batch liquid

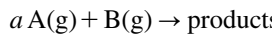
Consider the reaction of the form



In this case, the model equations derived for the slurry bubble column reactor are applicable. Note that if the gas-phase concentration is constant, the gas-phase material balance is not needed (where the two reactors have different model equations).

Gas-phase reactions and batch liquid

Consider the reaction of the form



In this case, the material balance in the liquid phase (3.238) is not applicable as both reactants are gases. Furthermore, as in slurry bubble columns, if the liquid is batch, the overall rate based on the bulk gas-phase concentration is used and the overall mass-transfer coefficient K^o is found in the solution of the model (Chapter 5).

The gas-phase material balances can be written in the classic form of CSTR reactor material balances (Levenspiel, 1972):

$$\frac{\tau}{C_{AG,i}} = \frac{V_L}{F_{A,i}} = \frac{x_A}{(-r_u)_A} \quad (3.244)$$

$$\frac{\tau}{C_{BG,i}} = \frac{V_L}{F_{B,i}} = \frac{x_B}{(-r_u)_B} \quad (3.245)$$

where

$$(-r_u)_B = \frac{(-r_u)_A}{a} \quad (3.246)$$

$$\tau = \frac{V_L}{Q_{G,i}} \quad (3.247)$$

and x is the conversion of the reactants. Note that the above equation is based on the volume of bubble-free liquid. The conversion can be expressed in terms of the gas-flow rate (Smith, 1981):

$$x = \frac{Q_{G,i}C_{G,i} - Q_{G,o}C_{G,o}}{Q_{G,i}C_{G,i}} \quad (3.248)$$

where $Q_{G,i}$ and $Q_{G,o}$ is the inlet and outlet gas-flow rate, respectively. For A as the limiting reactant and by analogy to the volume change in batch reactors (eq. (3.92)),

$$Q_{G,o} = Q_{G,i}(1 + \varepsilon_R x_A) \quad (3.249)$$

while (as for moles in batch reactors)

$$F_{A,o} = F_{A,i}(1 - x_A) \quad (3.250)$$

for the general case of $\varepsilon_R \neq 0$,

$$C_{A,o} = C_{A,i} \frac{1 - x_A}{1 + \varepsilon_R x_A} \quad (3.251)$$

or

$$x_A = \frac{1 - \frac{C_{G,o}}{C_{G,i}}}{1 + \varepsilon_R \frac{C_{G,o}}{C_{G,i}}} = \frac{C_{G,i} - C_{G,o}}{C_{G,i} + \varepsilon_R C_{G,o}} \quad (3.252)$$

for $\varepsilon_R = 0$ (Levenspiel, 1972),

$$C_{A,o} = C_{A,i}(1 - x_A) \quad (3.253)$$

$$x_A = \frac{C_{G,i} - C_{G,o}}{C_{G,i}} \quad (3.254)$$

Note that the relationship between the several rate expressions is the same as in the slurry bubble column reactors (Section 3.4.4).

3.5.2 Hydraulics

The special characteristic of three-phase systems is the demand for simultaneous and efficient gas dispersion and solid suspensions.

Down-pumping axial flow impellers are more appropriate for most particle-suspension operations (Perry and Green, 1984). Typical dimensional ratios are $D_T/D_a = 2-3.3$, and $Z_a/D_T = 0.25-0.5$. The power can be calculated as in the case of liquid agitation (see eq. (3.107)) (Perry and Green, 1984).

It is well known that the critical impeller speed for solid suspensions is higher in the presence of a gas, depending mainly on the superficial gas velocity (Rewatkar *et al.*, 1991). This is because of a decrease in the impeller power draw due to the formation of ventilated cavities behind the impeller blades on gassing. For example, for Rushton turbines, $D_T/D_a = 2-3.3$:

$$N_{jsg} = N_{js} + 0.85Q_{gv} \quad (3.255)$$

where N_{jsg} is the critical impeller speed for solid suspensions under gassing conditions, and Q_{gv} is the gassing rate in volume of gas per volume of liquid per minute (vvm). This correlation holds for vessels up to 1.8 m diameter, 20% solids, and 3.5 vvm. Under similar conditions and for other typical impellers (45° pitched blade impellers and hydrofoils), the N_{jsg}/N_{js} ratio is between 1 and 2 ($0.25 < Q_{gv} < 3.5$ vvm).

Another important function of the impeller in three-phase systems is to generate finely dispersed and homogeneously distributed bubbles throughout the vessel. At the same time, the turbulent velocities should be sufficiently high to prevent coalescence of gas bubbles. The most important variable concerning gas dispersion is the gas holdup in the vessel.

Apart from the critical impeller speed for solid suspension and efficient gas dispersion, flooding is also a very important phenomenon in three-phase systems. Flooding may take place at low impeller speed or high gassing rate. Under these conditions, the gas is dispersed just around the central shaft of the tank, whereas the solids are settled at the bottom. Flooding characteristics are not affected by particles. Furthermore, high-viscosity liquids are able to handle more gas before flooding than low-viscosity liquids.

Birch and Ahmed (1997) have shown that the location of the sparger has an important role in the flooding characteristics of impellers, and thus on efficient solids suspension.

The energy of dissipation per unit mass of liquid in a liquid–solid agitated vessel is related to the power consumption per unit volume of liquid (P_s) as follows (Kato *et al.*, 2001):

$$\varepsilon_o = \frac{P_s}{\rho_L} = \frac{P}{M_L} \quad (3.256)$$

where M_L is the mass of liquid and ε_o in cm^2/s^3 ($= \text{erg}/\text{g s}$, where $\text{erg} = \text{g cm}^2/\text{s}^2$). In case of gas injection in the liquid, the energy of dissipation per unit mass of liquid in a fully

baffled agitated system, in turbulent flow, is given by (Prasher and Wills, 1973; Smith, 1981; Ramachandran and Chaudhari, 1984)

$$\bar{\varepsilon} = \varepsilon_0 \varphi \quad (3.257)$$

where φ is a correction factor,

$$\varphi = 1 - 1.26 \frac{Q_G}{ND_a^3}, \frac{Q_G}{ND_a} < 3.5 \times 10^{-2} \quad (3.258)$$

$$\varphi = 0.62 - 1.85 \frac{Q_G}{ND_a^3}, \frac{Q_G}{ND_a} > 3.5 \times 10^{-2} \quad (3.259)$$

with Q_G being the gas flow rate in cm^3/s , D_a in cm, and N in r/s. The presence of a gas in the vessel contents results in lowering the power required to turn an impeller at a given speed, probably because of the lowered mean density of the mixture (Treybal, 1980).

The above correlations have been suggested for gas–liquid systems. In the presence of a solid, in three-phase systems, the energy of dissipation can be approximately 25–50% higher depending on the loading and density of particles (Ramachandran and Chaudhari, 1984).

Gas holdup and bubble size

Simple impeller The Calderbank correlation has been derived for stirred gas–liquid reactors (Calderbank, 1958; Laakkonen *et al.*, 2005):

$$h_G = \left(\frac{u_{sG} h_G}{0.265} \right)^{0.5} + 0.000216 \left(\frac{P_g}{V_L} \right)^{0.4} \frac{\rho_L^{0.2}}{\sigma_L^{0.6}} \left(\frac{u_{sG}}{0.265} \right)^{0.5} \quad (3.260)$$

where h_G is the fractional holdup and P_g is the power consumption in aerated liquid. Then,

$$\frac{P_g}{V_L} = \left(\frac{P\varphi}{M_L} \right) \frac{1}{\rho_L} = \bar{\varepsilon} \rho_L \quad (3.261)$$

where

M_L = the mass of the liquid

φ = a correction factor accounting for the influence in the liquid-phase of gas injection on the power consumption, as defined in eq. (3.257)

P = the power consumption in a gas-free liquid system.

Furthermore, the superficial gas velocity u_{sG} in slurry reactors is equivalent to the superficial gas velocity in a fixed bed:

$$u_{sG} = \frac{Q_G}{A} \quad (3.262)$$

where A is the cross-sectional area of the vessel.

For single-impeller systems, the correlation of Calderbank can be used (Bouaifi *et al.*, 2001; Laakkonen *et al.*, 2005):

$$d_{\text{bub}} = 4.15 \frac{\sigma_L^{3/5} h_G^{0.5}}{\rho_L^{3/5} \left(\frac{P_g}{V_L} \right)^{2/5}} + 0.0009 \quad (3.263)$$

These correlations have been derived for Rushton turbines, but they can be applied for flat-blade impellers as well (Laakkonen *et al.*, 2005). SI units should be used in these correlations.

Double-impeller combinations Bouaifi *et al.* (2001) derived the following correlations for stirred gas–liquid reactors with various combinations of double impellers. The impellers used were the lightning axial flow impeller (A-310), the four 45° pitched blade turbine pumping down (PBSD) and the Rushton disk turbine (RDT). Furthermore, the tank was a dish-bottom cylindrical tank equipped with four baffles, while the gas was introduced by a ring sprayer. The gas-flow rate ranged from 0.54 to 2.62 L/s, whereas the rotational speed was from 1.66 to 11.67 s⁻¹. The gas holdup is

$$h_G = C \left(\frac{P_g}{V_L} \right)^{0.24} u_{sG}^{0.65} \quad (3.264)$$

where h_G is in %, P_g/V_L in W/m³, $u_{sG} > 0.018$ m/s, and C is between 22.4 and 24.8. The gas holdup was found to be lower than 10% as in the case of simple impeller configurations (Panja and Phaneswara Rao, 1993). This correlation holds for operating conditions beyond the complete dispersion point, corresponding to the situation of homogeneous gas dispersion in which bubbles reach the bottom of the tank. It should be noted that in the case of agitated vessels, it is difficult to propose a general correlation to predict gas holdup, because it is dependent on the stirrer configuration and sparger type (Bouaifi *et al.*, 2001). Furthermore, gas holdup is expected to be influenced by the solids in three-phase systems. The Sauter mean diameter is affected by the specific power consumption, but not by the gas flow rate (Bouaifi *et al.*, 2001). For double-impeller combinations (Bouaifi *et al.*, 2001),

$$d_{\text{bub}} = 10.1 \times 10^{-3} \left(\frac{P_g}{V_L} \right)^{-0.20} \quad (3.265)$$

where d_{bub} is in m. SI units are used with this correlation.

The effect of solids

In general, the addition of solids influences the bubble diameter due to the greater number of bubble collisions resulting in increased coalescence, and thus, in an increase in bubble size (Panja and Phaneswara Rao, 1993).

3.5.3 External mass transfer

Mass transfer coefficients: liquid to particle (k_p)

According to Fishwick *et al.* (2003), the injection of gas in a baffled vessel leads to a decrease in the mass transfer coefficients and this effect becomes more intense at higher gas rates. The significance of gas dispersion is, however, less pronounced at higher agitation speeds. It is also observed that under high agitation speeds in baffled vessels, a considerable amount of air is dispersed inside the vessel even in the absence of an injected gas.

The proposed correlation for agitated slurry reactors is that of Sano *et al.* (1974; Ramachandran and Chaudhari, 1984; Koide, 1996):

$$\frac{k_f d_p}{D_f F_s} = 2 + 0.4 \left(\frac{\bar{\varepsilon} d_p^4 \rho_L^3}{\mu_L^3} \right)^{0.25} \left(\frac{\mu_L}{\rho_L D_f} \right)^{1/3} \quad (3.266)$$

where F_s is a shape factor and can be taken as unity for spherical particles. CGS units should be used with this equation.

The Hiraoka correlation proposed for liquid–liquid dispersion in an impeller mixing vessel (Kato *et al.*, 2001) is

$$\frac{k_f d_p}{D_f} = 0.45 \left(\frac{d_p^4 P_s}{\rho_L \nu_L^3} \right)^{0.193} Sc^{1/3} \quad (3.267)$$

The observed values of the mass transfer coefficient- in three-phase systems between solid and liquid for the conventional impellers and a typical baffled vessel (e.g. Rushton turbine, propeller) are between the values predicted by Hiraoka (liquid–liquid dispersion, eq. (3.267)) and Levins and Glastonbuty (solid–liquid dispersion, eq. (3.118)) correlations. However, as an approximation, the Levins and Glastonbuty correlation could be used for three-phase systems (Smith, 1981).

Mass transfer coefficients: gas bubble to liquid (k_{fg})

Normally, even when the bubble phase is a gas mixture, the major mass transfer resistance for slightly soluble gases is in the liquid. Thus, the mass transfer coefficient in the liquid film around the bubble is the important one in gas bubble-to-liquid mass transfer (Smith, 1981; Treybal, 1980).

The mass transfer coefficient in the liquid film around the gas bubble can be estimated as follows (Prasher and Wills, 1973; Smith, 1981):

$$k_{fg} = 0.592 D_{fg}^{0.5} \left(\frac{\bar{\varepsilon}}{\nu_L} \right)^{0.25} \quad (3.268)$$

where D_{fg} is the molecular diffusivity of solute gas in the liquid and ν_L the kinematic viscosity of the liquid. A higher gas rate results in a lower liquid side mass transfer

coefficient. This correlation has been derived for gas–liquid systems. However, it can be used for agitated slurry reactors as well (Smith, 1981). CGS units are used with this correlation.

Another equation is the Yaki–Yoshida correlation, which is proposed for agitated slurry reactors (Ramachandran and Chaudhari, 1984):

$$\frac{k_{fg} a_{GL,tot} D_a^2}{D_T} = 0.06 \left(\frac{D_a^2 N \rho_L}{\mu_L} \right)^{1.5} \left(\frac{D_a N^2}{g} \right)^{0.19} \left(\frac{\mu_L}{D_T \rho_L} \right)^{0.5} \left(\frac{\mu_L u_{sG}}{\sigma_L} \right)^{0.6} \left(\frac{N D_a}{u_{sG}} \right)^{0.32} \quad (3.269)$$

where N is the impeller rotational speed (r/s). CGS units should be used with this equation. The CGS unit of surface tension is mN/m (dyn/cm).

Finally, for double-impeller combinations and gas–liquid systems, the Bouaifi *et al.* (2001) correlation can be used:

$$k_{fg} a_{GL} = 0.0218 \left(\frac{P_g}{V_L} \right)^{0.5} u_{sG}^{0.6} \quad (3.270)$$

where a_{GL} is based on the volume of liquid and $u_{sG} \leq 0.018$ m/s. SI units are used with this correlation.

The effect of surface aeration on k_{fg}

As has been noted elsewhere, the aeration of liquid is generally not desirable. This is why the gas phase that is employed for the reaction is mixed with the air dissolved due to surface aeration, and thus the mass-transfer coefficient decreases due to the reduction of the partial pressure of the reacting gas in this gas–air mixture. Calderbank proposed an equation for the minimum stirring rate for surface aeration for gas–liquid systems (Panja and Phaneswara Rao, 1993):

$$\frac{N_a D_a^{1.98}}{D_T^{1.1}} = 1.34 \left(\frac{\sigma_L g}{\rho_L} \right)^{0.15} \quad (3.271)$$

Thus, aeration takes place for $N > N_a$ (in s^{-1}). SI units should be used with this correlation.

3.6 TWO-PHASE FIXED BEDS

3.6.1 Introduction

Adsorption and ion exchange

Fixed bed is the most frequently used operation for ion-exchange and adsorption processes. The adsorption or ion-exchange medium is contained inside a steel vessel,

which could be under pressure, with the flow distribution system allowing liquid or gas to flow with a specified rate. Retention screens on the inlet and outlet prevent the solids from escaping into the process loop. The low porosity of beds of powdered media restricts their use to thin layers, usually as a “precoat” on a filter medium. In practical applications, the particle size used is in the range 0.25–3 mm.

The fixed-bed operation is usually a semicontinuous process. When the medium gets spent, the fixed-bed operation is stopped and the material is replaced with a fresh batch. In fixed-bed operation, the determination of the medium being spent is usually based on the breakpoint, which is the point at which the exit concentration of the solutes being removed starts to increase sharply to some predetermined level (typically below 10%). If interruptions in the process to replace the adsorbent or the ion exchange media are not desirable, multiple fixed beds can be connected in parallel. While one set is in operation, the other is filled with a fresh medium or, after refilling, is on standby.

Catalysis

Fixed- or packed-bed reactors refer to two-phase systems in which the reacting fluid flows through a tube filled with stationary catalyst particles or pellets (Smith, 1981). As in the case of ion-exchange and adsorption processes, fixed bed is the most frequently used operation for catalysis (Froment and Bischoff, 1990; Schmidt, 2005). Some examples in the chemical industry are steam reforming, the synthesis of sulfuric acid, ammonia, and methanol, and petroleum refining processes such as catalytic reforming, isomerization, and hydrocracking (Froment and Bischoff, 1990).

In the case where a rapid removal or addition of heat is needed, it may not be possible to use a single fixed bed or large diameter. In this case, the reactor can be built up of a number of tubes, containing the catalyst particles and encased in a single body (Smith, 1981). Then, the heat exchange can be easily done by circulating a fluid in the space between the tubes.

If efficient contacting in the reactor is of primary importance, then the fixed-bed reactor is preferred to a fluidized-bed reactor (Levenspiel, 1962). Other advantages of fixed operations are the following:

- the flow regimes approach plug flow, so high conversion can be achieved
- pressure drop is low
- owing to the high holdup, there is better radial mixing and channeling is not encountered
- high catalyst load per unit volume of reactor is possible.

All types of catalytic reactors with the catalyst in a fixed bed have some common drawbacks, which are characteristic of stationary beds (Mukhlyonov *et al.*, 1979). First, only comparatively large-grain catalysts, not less than 4 mm in diameter, can be used in a filtering bed, since smaller particles cause increased pressure drop. Second, the area of the inner surface of large particles is utilized poorly and this results in a decrease in the utilization (capacity) of the catalyst. Moreover, the particles of a stationary bed tend to sinter and cake, which results in an increased pressure drop, uneven distribution of the gas, and lower catalyst activity. Finally, porous catalyst pellets exhibit low heat conductivity and as a result the rate of heat transfer from the bed to the heat exchanger surface is very low. Intensive heat removal and a uniform temperature distribution over the cross-section of a stationary bed cannot, therefore, be achieved. The poor conditions of heat transfer within

a filtering catalyst make the close control of temperature and the maintaining of optimum temperature conditions rather impossible.

3.6.2 Modeling of fixed beds

In the following, the one-dimensional model will be presented. The basic ideal models assume that concentration and temperature gradients occur in the axial direction (Froment and Bischoff, 1990). The model for a fixed-bed reactor consists of three equations, which will be presented in the following sections and are

- material balance equation
- energy balance equation
- pressure drop equation

Material balance equation

Consider a solution of concentration of C_W (mol/vol of fluid) entering at W in a control volume of length Δz and effective cross-sectional area A , with a volumetric flow rate Q (Figure 3.34). The reaction takes place with rate $(-R)$ in (mol disappearing/time vol of the reactor) and the exit concentration is C_E (mol/vol of fluid).

Under the assumption of complete mixing in the radial direction, the material balance is

$$\left\{ \begin{array}{l} \text{rate of change} \\ \text{in the direction} \\ \text{of flow due to} \\ \text{flow and axial} \\ \text{dispersion} \end{array} \right\} - \left\{ \begin{array}{l} \text{rate} \\ \text{of} \\ \text{consumption} \end{array} \right\} = \left\{ \begin{array}{l} \text{rate of} \\ \text{accumulation} \\ \text{of moles} \end{array} \right\} \quad (3.272)$$

The terms in this material balance are in moles per unit time.

In the following analysis, ε is the volume occupied by the fluid phase per unit volume of the control element. Then, the corresponding volume fraction for the solid phase is $(1 - \varepsilon)$. The first term in eq. (3.272) is

$$\left\{ \begin{array}{l} \text{rate of change} \\ \text{in the direction} \\ \text{of flow due to} \\ \text{flow and axial} \\ \text{dispersion} \end{array} \right\} = \left\{ \begin{array}{l} \text{axial} \\ \text{dispersion} \\ \text{term} \end{array} \right\} + \left\{ \begin{array}{l} \text{flow} \\ \text{term} \end{array} \right\} \quad (3.273)$$

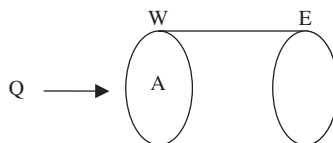


Figure 3.34 Control volume in a fixed bed.

where

$$\left. \begin{array}{l} \text{Axial} \\ \text{Dispersion} \\ \text{Term} \end{array} \right\} = [\text{outlet-inlet}] = \left(-D_L A \frac{\partial C}{\partial z} \Big|_W \right) - \left(-D_L A \frac{\partial C}{\partial z} \Big|_E \right) \quad (3.274)$$

$$\left. \begin{array}{l} \text{Flow} \\ \text{Term} \end{array} \right\} = [\text{outlet-inlet}] = (QC_W) - (QC_E)$$

The reaction is considered to take place only on or within the solid particles and thus the consumption rate per unit volume of particles is

$$\rho_p (-r_m) \quad (3.275)$$

The volume of particles in the control element is

$$(1 - \varepsilon) A \Delta z \quad (3.276)$$

Thus,

$$\left\{ \begin{array}{l} \text{rate} \\ \text{of} \\ \text{consumption} \end{array} \right\} = A(1 - \varepsilon) \Delta z [\rho_p (-r_m)] \quad (3.277)$$

The accumulation of moles in the liquid phase is

$$\frac{C_E - C_W}{\Delta t} \quad (3.278)$$

The units of this term are moles per unit time per unit volume of fluid phase. The volume of the fluid phase in the control element is

$$\varepsilon A \Delta z \quad (3.279)$$

and thus

$$\left\{ \begin{array}{l} \text{rate of} \\ \text{accumulation} \\ \text{of moles} \end{array} \right\} = \varepsilon A \Delta z \frac{C_E - C_W}{\Delta t} \quad (3.280)$$

The material balance becomes

$$\left(-D_L A \frac{\partial C}{\partial z} \Big|_W + QC_W \right) - \left(-D_L A \frac{\partial C}{\partial z} \Big|_E + QC_E \right) - (1 - \varepsilon) A \Delta z [\rho_p (-r_m)] = \varepsilon A \Delta z \frac{(C_E - C_W)}{\Delta t} \quad (3.281)$$

Dividing by the term ($A\Delta z$) we have

$$\begin{aligned} \frac{D_L}{\Delta z} \left(-\frac{\partial C}{\partial z} \Big|_W + \frac{\partial C}{\partial z} \Big|_E \right) + \frac{Q}{A\Delta z} (C_W - C_E) \\ -(1-\varepsilon)[\rho_p(-r_m)] = \varepsilon \frac{(C_E - C_W)}{\Delta t} \end{aligned} \quad (3.282)$$

Setting $\Delta z \rightarrow 0$, we can derive the differential form of equation (3.282). Taking into account that

$$\begin{aligned} \Delta z &\rightarrow \partial z \\ \Delta t &\rightarrow \partial t \\ C_W - C_E &\rightarrow -\partial C \\ \frac{\partial C}{\partial z} \Big|_E - \frac{\partial C}{\partial z} \Big|_W &\rightarrow \partial \left(\frac{\partial C}{\partial z} \right) \\ \frac{\partial \left(\frac{\partial C}{\partial z} \right)}{\partial z} &= \frac{\partial}{\partial z} \left(\frac{\partial C}{\partial z} \right) = \frac{\partial^2 C}{\partial z^2} \end{aligned} \quad (3.283)$$

eq. (3.282) becomes

$$D_L \frac{\partial}{\partial z} \left(\frac{\partial C}{\partial z} \right) - \frac{Q}{A} \frac{\partial C}{\partial z} - (1-\varepsilon)[\rho_p(-r_m)] = \varepsilon \frac{\partial C}{\partial t} \quad (3.284)$$

or

$$D_L \frac{\partial^2 C}{\partial z^2} - u_s \frac{\partial C}{\partial z} - (-R) = \varepsilon \frac{\partial C}{\partial t} \quad (3.285)$$

The material balance including the effect of incomplete mixing in the radial direction is (Perry and Green, 1999)

$$\left(-u_s \frac{\partial C}{\partial z} + D_L \frac{\partial^2 C}{\partial z^2} \right) + D_R \left(\frac{\partial^2 C}{\partial r^2} + \frac{1}{r} \frac{\partial C}{\partial r} \right) - (-R) = \varepsilon \frac{\partial C}{\partial t} \quad (3.286)$$

where:

- ε = the bed voidage
- ρ_b = the bulk density
- u_s = the superficial fluid velocity
- D_L = the axial dispersion coefficient
- D_R = the radial dispersion coefficient
- C = the solution concentration.

For an ideal plug-flow operation, the material balance (3.286) is greatly simplified:

$$-u_s \frac{\partial C}{\partial z} - (-R) = \varepsilon \frac{\partial C}{\partial t} \quad (3.287)$$

This equation holds for adsorption, ion exchange as well as for catalytic systems, which are in a transient operating condition, e.g. during severe catalyst deactivation. For a steady state catalytic fixed-bed operation, eq. (3.287) becomes

$$u_s \frac{dC}{dz} + (-R) = 0 \quad (3.288)$$

It should be noted here that while in catalytic systems the rate is based on the moles disappearing from the fluid phase $-r_m$, in adsorption and ion exchange, the rate is normally based on the moles accumulated in the solid phase r_m , and the rate is expressed per unit mass of the solid phase as

$$r_m = \frac{dq}{dt} \quad (3.289)$$

where q is the moles per unit mass of the solid phase (solid loading).

Note that the material balances for fixed beds are valid for the case of constant-density (constant volume) systems. The important term here is the one including the fluid velocity, i.e. the term $u_s \partial C / \partial z$. For a variable volume system,

$$\frac{dF}{dV} = -F \frac{dx}{dV} = \frac{d(QC)}{dV} = C \frac{dQ}{dV} + Q \frac{dC}{dV} \quad (3.290)$$

For a constant volume system,

$$\frac{dQ}{dV} = 0 \quad (3.291)$$

and only then we have

$$\frac{dF}{dV} = Q \frac{dC}{dV} = Q \frac{dC}{d(zA)} = \frac{Q}{A} \frac{dC}{dz} = u_s \frac{dC}{dz} \quad (3.292)$$

Thus, the term $u_s \partial C / \partial z$ comes from the derivative $\partial F / \partial V$, which should be used instead in eq. (3.287) for a variable-volume system. For catalytic fixed beds, in the typical case of a steady-state operation, eq. (3.288) takes the familiar form

$$\frac{dF}{dV} + (-R) = 0 \quad (3.293)$$

where F is the molar flow rate in mole per unit time:

$$F = QC = u_s AC \quad (3.294)$$

In the forms presented above, the material balance is expressed in moles per time per unit volume of reactor V_R (see Section 3.1.1 for derivation):

$$(-R) = -\frac{1}{V_R} \frac{dN}{dt} = \frac{V_S}{V_R} (-r_{vs}) = \frac{V_L}{V_R} (-r_u) = \frac{M_S}{V_R} (-r_m) \quad (3.295)$$

For fixed beds,

$$\varepsilon = \frac{V_L}{V_R} \quad (3.296)$$

$$1 - \varepsilon = 1 - \frac{V_L}{V_R} = \frac{V_R - V_L}{V_R} = \frac{V_S}{V_R} \quad (3.297)$$

$$\rho_b = \frac{M_S}{V_R} \quad (3.298)$$

Then, the overall rate of the reaction $-R$ per unit volume of reactor is

$$(-R) = -\frac{1}{V_R} \frac{dN}{dt} = (1 - \varepsilon)(-r_{vs}) = \varepsilon(-r_u) = \rho_b(-r_m) \quad (3.299)$$

or using the other definitions of rate,

$$V_R(-R) = V_S(-r_{vs}) = V_L(-r_u) = M_S(-r_m) \quad (3.300)$$

Energy balance equation

The general balance equation for an unsteady-state fixed-bed operation is (Ruthven, 1984; Froment and Bischoff, 1990)

$$\left(-u_s \rho_f c_{p,f} \frac{\partial T_f}{\partial z} + \lambda_L \frac{\partial^2 T_f}{\partial z^2} \right) + \lambda_R \left(\frac{\partial^2 T_f}{\partial r^2} + \frac{\lambda}{r} \frac{\partial T_f}{\partial r} \right) - (-R) \Delta H - \frac{4h^\circ}{D} (T_f - T_w) = \left[\varepsilon c_{p,f} \rho_f \frac{\partial T_f}{\partial t} + \rho_b c_{p,s} \frac{\partial T_s}{\partial t} \right] \quad (3.301)$$

where

T_f, T_s, T_w	= the fluid, solid, and wall temperature, respectively (K)
$c_{p,f}, c_{p,s}$	= the specific heat of the fluid and solid, respectively (J/kg K)
ρ_f	= the fluid density (kg/m ³)
ΔH	= the heat of reaction (J/mol). Heat of reaction is negative for an exothermic reaction and positive for an endothermic reaction.
λ_L	= the axial effective thermal conductivity (J/s m K)
λ_R	= the radial effective thermal conductivity (J/s m K)
h^o	= the overall heat transfer coefficient (J/s m ² K)
D	= the bed diameter (m).

Note that on the right-hand side of eq. (3.301), the accumulation term is a function of the temperature change of the fluid and solid with time. The heat generated (or consumed) during the reaction increases (or decreases) the temperature in the solid and at the same time is transferred to (or is transferred from) the fluid phase.

The last term on the left-hand side of eq. (3.301) corresponds to the heat transfer to the external fixed-bed wall. The overall heat transfer resistance is the sum of the internal, external, and wall resistances. In an adiabatic operation, the overall heat transfer coefficient is zero so the corresponding term in the energy balance expression drops out, while in an isothermal operation this coefficient is infinite, so that $T_f = T_s = T_w$.

In general, large industrial fixed beds operate under near-adiabatic conditions, whereas small laboratory-scale fixed beds may approach isothermal operation (Ruthven, 1984). Especially, for most environmental applications, for catalytic, adsorption, and ion-exchange operations, the species to be removed are in such low concentrations that the operation is nearly isothermal. Thus, the heat transfer to the external fixed-bed wall is often of minimal importance.

The energy balance (3.301) is applicable for catalysis, adsorption, and ion exchange. More specifically, in catalysis, where the steady-state condition exists, frequently the accumulation term is zero. In contrast, adsorption and ion exchange operate under unsteady-state condition. The analysis of the energy balance equation for catalytic fixed beds is presented in detail in Section 5.3.4.

Pressure drop equation

For a fixed bed, the Ergun equation for pressure drop in a differential form is

$$\frac{dP}{dz} = - \left[\frac{150\mu u_s (1-\varepsilon)^2}{\Phi_s^2 d_p^2 \varepsilon^3} + \frac{1.75\rho u_s^2 (1-\varepsilon)}{\Phi_s d_p \varepsilon^3} \right] \quad (3.302)$$

where d_p is the diameter of spherical particles or the nominal diameter of irregular-shaped particles, ρ is the density of the fluid, g is the gravity acceleration constant (9.81 m²/cm), μ is the dynamic viscosity of the fluid, ε is the fixed-bed voidage, u_s is the superficial fluid velocity, and Φ_s is the sphericity of the particle. In eq. (3.302), the pressure-dependent parameters are the superficial velocity and the gas density, which in turn are related to the

concentration of the reacting species. Then, as analyzed in detail in Section 5.3.4, the pressure drop equation is coupled with the material and energy balance equations:

$$\frac{dP}{dz} = -f(x_A, \frac{P_i}{P}, \frac{T_i}{T}) \quad (3.303)$$

and the reactor model becomes a system of three, coupled, differential equations, which should be solved simultaneously.

In liquid-phase systems, or generally, in incompressible flow, the effect of pressure drop on the concentration of solutes (on the density of the fluid) is negligible (Fogler, 1999). Thus, when designing a fixed-bed reactor, the pressure drop is excluded from the calculations. However, in the case where a gas phase is involved, or more generally in a compressible flow, the concentration of the gas species (the gas density) is proportional to the total pressure and thus, the pressure drop may play a significant role in the fixed-bed design. In general, a compressible flow is a fluid flow where the change in density is more than 5–10% (Perry and Green, 1999).

As can be proved (see Section 5.3.4), the pressure drop becomes independent of the conversion and thus from the material balance if the expansion factor is near zero, and then the two differential equations are decoupled. Furthermore, for nearly isothermal operation, the pressure drop is not a function of temperature. Under these conditions, the fixed-bed model is greatly simplified.

Considering most environmental applications, for catalytic as well as for adsorption operations, the gas species to be removed are in such low concentrations (large excess of inerts) that the expansion factor is practically zero and the temperature is nearly constant throughout the reactor volume.

The case of incomplete filling of the fixed bed with the flowing fluid

In the analysis above, the void volume of the fixed bed (εV_R) is considered to be fully filled with the fluid phase, i.e. the fluid holdup based on the total volume of the bed $h_{e,t}$ is equal to the bed voidage ε . While this is expected in the case of a gas as fluid, it is not always true in the case of a liquid, especially in the case of downflow operation. In the case of incomplete filling of the bed with the fluid phase, the active bed volume is lower, and thus a portion of the solid phase is not in contact with the fluid, or in other words, is inactive in terms of reaction.

The void bed volume is εV_R while the total volume occupied by solid is

$$V_R - \varepsilon V_R = (1 - \varepsilon)V_R \quad (3.304)$$

However, in the case of incomplete filling of the fixed bed with the flowing fluid, the volume of the bed occupied by the fluid is $h_{e,t} V_R$. Then, the fraction of the void bed volume occupied by the fluid is equal to the fluid volume/void bed volume, i.e.

$$h_{v,t} = \frac{h_{e,t} V_R}{\varepsilon V_R} = \frac{h_{e,t}}{\varepsilon} \quad (3.305)$$

where: $h_{v,t}$ = the total fluid holdup based on the void volume of the bed.

This fraction could be viewed as a “fixed-bed wetting efficiency.” If $h_{e,t} = \varepsilon$ and $h_{v,t} = 1$, the bed is completely filled with fluid (fully wetted). The term $h_{v,t}$ is analogous to the catalyst wetting efficiency f_w for trickle beds (Section 3.7.3). However, this equality is valid solely in fixed beds where a single fluid flows through. The active volume of the solid, which is occupied by the fluid, amounts to the fixed-bed volume occupied by the fluid minus the volume occupied by fluid:

$$\frac{h_{e,t}}{\varepsilon} V_R - h_{e,t} V_R = \frac{h_{e,t}}{\varepsilon} V_R - \frac{h_{e,t}}{\varepsilon} (\varepsilon V_R) = \frac{h_{e,t}}{\varepsilon} (1 - \varepsilon) V_R \quad (3.306)$$

and the mass of the solid in contact with fluid is

$$\rho_p \frac{h_{e,t}}{\varepsilon} (1 - \varepsilon) V_R = \frac{h_{e,t}}{\varepsilon} \rho_b V_R \quad (3.307)$$

Then, in the material balance, the following corrections should be made:

$$\varepsilon \rightarrow h_{e,t} \quad (3.308)$$

$$1 - \varepsilon \rightarrow \frac{h_{e,t}}{\varepsilon} (1 - \varepsilon) = \frac{h_{e,t}}{\varepsilon} - h_{e,t} = h_{v,t} - h_{e,t} \quad (3.309)$$

$$\rho_b \rightarrow h_{v,t} \rho_b \quad (3.310)$$

3.6.3 Hydraulics

Nonideal flow in fixed beds

The classic analysis of reactors involves two idealized flow patterns— plug flow and mixed flow. Though real reactors never fully follow these flow patterns, in many cases, a number of designs approximate these ideals with negligible error. However, deviation from ideality can be considerable. Typically, in a reaction vessel, we can have several immediate cases closer to plug or mixed flow. Of course, nonideal flow concerns all types of reactors used in heterogeneous processes, i.e. fixed beds, fluidized beds, continuous-flow tank reactors, and batch reactors. However, we will focus on fixed beds and batch reactors, which are the common cases.

The study of nonideal flow and liquid holdup can be done by residence time distribution (RTD) experiments (tracing techniques) or by use of correlations derived from literature. During this step, physical mechanisms that are sensitive to size are investigated separately from chemical (kinetic or equilibrium) studies (Trambouze, 1990). Here, the fixed bed is

examined with respect to its flow patterns, as a vessel, for example, irrespective of the specific chemical reaction or physical phenomenon that will take place in it. In the present book, the several methods used for RTD studies as well as the mathematical background will not be presented. This information can be found elsewhere (Levenspiel, 1962). Instead, several correlations will be presented to assess the behavior of fixed beds.

Axial mixing Packed bed is an array of voids into which fluid flows at relatively high velocity. Acceleration occurs in the ports created by particle–particle intersections, and deceleration upon entering the voids. The net result of this situation is axial mixing. In the ideal case, this mixing is perfect and the bed may be viewed as a series of perfectly mixed vessels (voids) interconnected by ports consisting of closely packed regions. Plug flow is the situation where axial mixing between the several cross-sections of the bed is minimal, whereas radial mixing in each section is maximal.

Axial and radial dispersion coefficients are equal at low Reynolds numbers because the dispersion is due to the molecular diffusion and the axial and radial structures of the bed are similar (Gunn, 1968). However, at high Reynolds numbers, the convective dispersion dominates and the values are different because the axial dispersion is primarily caused by differences in the fluid velocity in the flow channels, whereas the radial dispersion is primarily caused by deviations in the flow path caused by the particles.

Ideal flow is studied and represented using the classic dispersion or dispersed plug-flow model of Levenspiel (1962). Recall the material balance of a fixed-bed reactor with perfect radial mixing (eq. (3.285)):

$$D_L \frac{\partial^2 C}{\partial z^2} - u_s \frac{\partial C}{\partial z} - (-R) = \varepsilon \frac{\partial C}{\partial t} \quad (3.311)$$

In the case of ideal plug flow $D_L = 0$, while in ideal mixed flow $\frac{\partial^2 C}{\partial z^2} = 0$. Thus, in ideal, mixed, or plug flow, the first term is zero.

The main parameter in this model characterizing the quality of the flow is the axial dispersion coefficient. The term “axial” is used to distinguish mixing in the direction of flow from mixing in the radial direction. Then, based on this parameter, the particle Peclet number is introduced:

$$Pe_p = \frac{ud_p}{D_L} \quad (3.312)$$

where

- d_p = the particle diameter
- D_L = the axial dispersion coefficient
- u = the interstitial fluid velocity.

Multiplying this number with the term Z/d_p , where Z is the fixed-bed length, we obtain the vessel Peclet number. A high vessel Peclet number means better flow quality, thus closer to ideal flow. Typically, if this number is higher than about 100, the flow is considered to be ideal (plug flow).

Liquid–solid fixed beds: In the related literature, there are correlations for the evaluation of the particle Peclet number (Pe_p) for materials that are frequently used in adsorption and

ion-exchange systems, such as zeolites and similar particles of irregular shape (Inglezakis *et al.*, 2001; Specchia and Baldi, 1977; Colombo and Baldi, 1976). For this kind of materials, which are common in wastewater treatment applications, the following equation can be used (Inglezakis *et al.*, 2001):

$$Pe_p = LRe_p^k \tag{3.313}$$

where L is 0.523 for upflow and 0.050 for downflow, k is equal to -0.645 for upflow and 0.475 for downflow. This correlation has been derived for $0.6 < Re_p < 8.5$ where Re_p is based on superficial velocity (Figure 3.35). In all equations, the Reynolds number is based on superficial velocity, unless otherwise specified.

Generally, for spherical and other irregular-shaped particles (intalox saddles, rasching rings, berl saddles), the particle Peclet number is found to be between 0.3 and 0.8 for Reynolds number between 0.01 and 150 (Ebach and White, 1958). For a wide range of values of the Reynolds number, the Chung equation can be used (Chung and Wen, 1968):

$$Pe_p = \frac{1}{\varepsilon}(0.2 + 0.011Re_p^{0.48}) \tag{3.314}$$

This correlation has been derived using glass beads, aluminum beads, and steel beads. Furthermore, according to Chung and Wen (1968), the particle Peclet number is between 0.06 and 0.3, showing no particular trend, for $0.01 < Re_p < 10$, whereas it steadily increases for $Re_p > 10$.

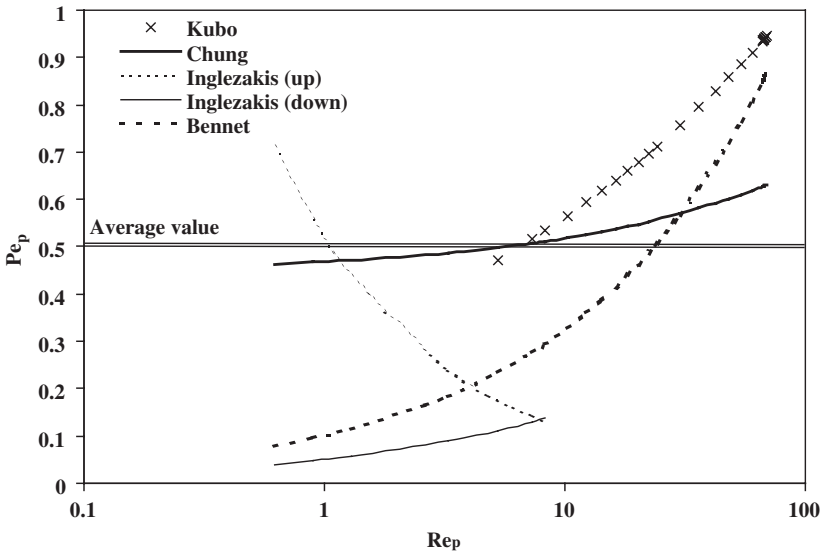


Figure 3.35 Axial dispersion in liquid–solid fixed beds (for $\varepsilon = 0.45$ and $Sc = 1000$). Average value is estimated by data given by Levenspiel (1972).

The equation proposed by Kubo *et al.* (1983) can be used for $10 < Re_p/\varepsilon < 2000$ (experiments took place in upflow mode):

$$Pe_p = 0.243\varepsilon^{-0.27} Re_p^{0.27} \quad (3.315)$$

For ceramic rasching rings of diameters between 10 and 60 mm, Bennett and Goodridge (1970) proposed the following correlation:

$$Pe_p = 0.1Re_p^{0.51} \quad (3.316)$$

It should be noted here that particles of irregular shape result in higher degrees of axial dispersion and thus lower Peclet numbers.

Gas–solid fixed beds: For axial dispersion in gas–solid fixed beds, the Edwards–Richardson correlation can be used (Wen and Fan, 1975; Andriago *et al.*, 1999).

$$\frac{1}{Pe_p} = \frac{0.5}{1 + 9.5 \frac{\varepsilon}{Re_p Sc}} + \frac{0.75\varepsilon}{Re_p Sc} \quad (3.317)$$

This correlation has been tested on many experimental data and it is valid for $0.08 < Re_p < 400$ and $0.28 < Sc < 2.2$.

For gases, Hiby proposed the following correlation for $0.04 < Re_p < 400$ and random beds of spheres (Gunn, 1968):

$$\frac{1}{Pe_p} = \frac{0.65}{1 + 7 \left(\frac{\varepsilon}{Re_p Sc} \right)^{0.5}} + \frac{0.67\varepsilon}{Re_p Sc} \quad (3.318)$$

In Figure 3.36, the Edwards–Richardson and Hiby correlations are compared for gas–solid systems, while in Figure 3.37, the Edwards–Richardson and Kubo correlations are compared for gas–solid and liquid–solid systems, respectively.

From Figure 3.37, it is clear that the Peclet number is greater in gas–solid systems, and thus the flow is closer to plug flow for the same Reynolds number.

Radial Mixing Radial dispersion can be viewed as a result of stream slitting and side-stepping. A stream of fluid at a particular radial position strikes a solid particle in its axial journey and is split into two by the collision. On average, half the stream moves laterally to the right and the other to the left. This happens repeatedly and the result is that the original single stream is laterally dispersed toward the wall.

The particle Peclet number is defined as (Carberry, 1976)

$$Pe_p = \frac{ud_p}{D_R} \quad (3.319)$$

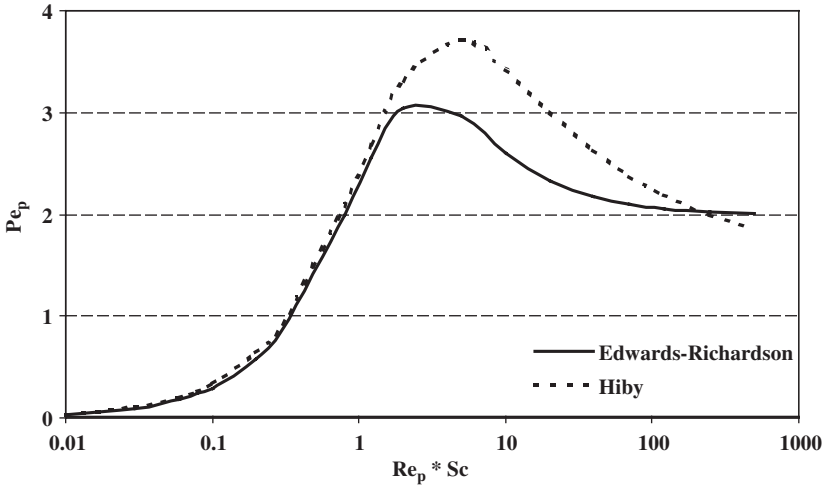


Figure 3.36 Edwards–Richardson versus Hiby’s correlation (for $\epsilon = 0.45$ and $Sc = 1$).

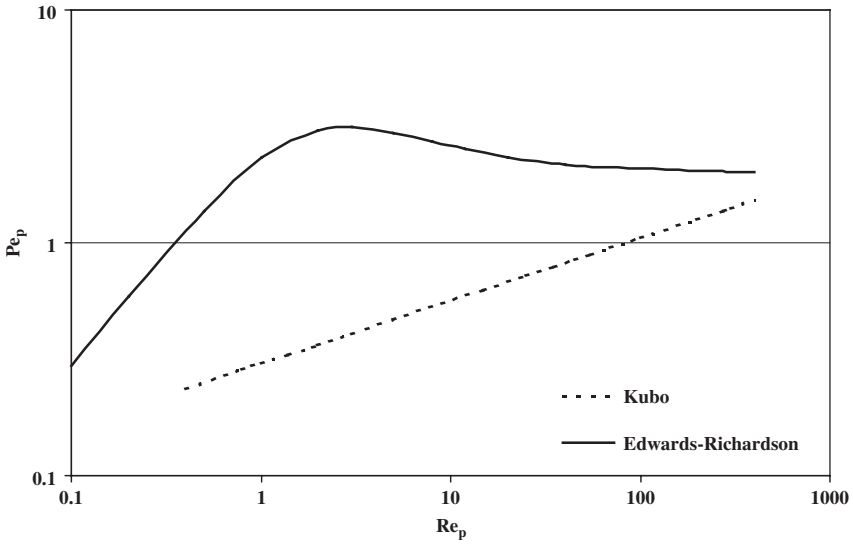


Figure 3.37 Comparison of Edwards–Richardson and Kubo correlations (for $\epsilon = 0.45$, for liquid $Sc = 1000$ and for gas $Sc = 1$).

where D_R is the axial dispersion coefficient. Multiplying this number with the term $D/2d_p$, where D is the fixed-bed diameter, we obtain the vessel radial Peclet number. A low vessel radial Peclet number means better flow quality, thus closer to ideal flow. This is because complete mixing (high D_R) in radial flow is the ideal flow condition.

Liquid–solid fixed beds. According to Gunn (1968), for random beds of spheres ($\epsilon = 0.4$), the radial Peclet numbers are from about 10 – 40 for $0.08 < Re_p < 1000$.

Gas–solid fixed beds. The following correlation is provided by Gunn for random beds of spheres (1968):

$$\frac{1}{Pe_p} = \frac{1}{11} + \frac{\epsilon}{\gamma Re_p Sc} \tag{3.320}$$

where γ is the tortuosity factor, whose typical value is around 1.5. In Figure 3.38, the axial and radial Peclet numbers for gases are compared.

From Figure 3.38, it is clear that the radial Peclet number is greater than the axial Peclet number in gas–solid systems for the same Reynolds number.

Other comments on nonideal flow Recalling the partial differential equation for a fixed bed (eq. (3.286)):

$$\begin{aligned} -\frac{Z}{u_s}(-R) &= \epsilon \frac{Z}{u_s} \frac{\partial C}{\partial t} + \frac{\partial C}{\partial(z/Z)} - \frac{D_L \epsilon}{u_s Z} \frac{\partial^2 C}{\partial(z/Z)^2} \\ -\frac{D_R \epsilon}{u_s R_o} \frac{Z}{R_o} &\left(\frac{\partial^2 C}{\partial(r/R_o)^2} + \frac{1}{r/R_o} \frac{\partial C}{\partial(r/R_o)} \right) \end{aligned} \tag{3.321}$$

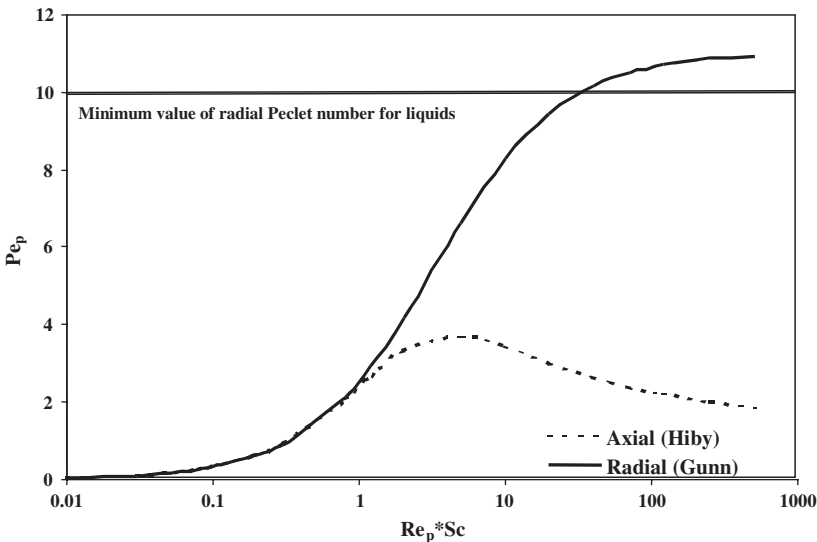


Figure 3.38 Comparison of axial (Hiby) and radial (Gunn) Peclet numbers for gases (for $\epsilon < 0.45$, $Sc = 1$). The minimum value corresponds to $0.05 < Re_p$ and $Re_p > 80$ and is given by Gunn (1968).

we have two terms for dispersion: the axial term

$$\frac{D_L \varepsilon}{u_s Z} \frac{\partial^2 C}{\partial (z/Z)^2} = \frac{1}{Pe_p} \frac{d_p}{Z} \frac{\partial^2 C}{\partial (z/Z)^2} \quad (3.322)$$

and the radial term

$$\begin{aligned} & \frac{D_R \varepsilon}{u_s R_o} \frac{Z}{R_o} \left(\frac{\partial^2 C}{\partial (r/R_o)^2} + \frac{1}{(r/R_o)} \frac{\partial C}{\partial (r/R_o)} \right) \\ &= \frac{1}{Pe_p} \frac{d_p}{R_o} \frac{Z}{R_o} \left(\frac{\partial^2 C}{\partial (r/R_o)^2} + \frac{1}{(r/R_o)} \frac{\partial C}{\partial (r/R_o)} \right) \end{aligned} \quad (3.323)$$

where R_o is the fixed-bed radius. To have ideal flow, omitting these two terms from the equation of continuity, one of the following must apply (Carberry, 1976):

- axial dispersion should be low (low D_L), thus axial Pe_p should be high, and the bed should be deep, i.e. high Z/d_p
- radial dispersion should be high (high D_R), thus radial Pe_p should be low, and the bed should be deep and of small diameter, i.e. high Z/R_o and low R_o/d_p . The increase in Z/d_p has the same effect.

Clearly, in the absence of a radial temperature or velocity gradient, no radial mass transfer can exist unless, of course, a reaction occurs at the bed wall. When a system is adiabatic, a radial temperature and concentration gradient cannot exist unless a severe radial velocity variation is encountered (Carberry, 1976). Radial variations in fluid velocity can be due to the nature of flow, e.g. in laminar flow, and in the case of radial variations in void fraction. In general, an average radial velocity independent of radial position can be assumed, except from pathological cases such as in very low Reynolds numbers (laminar flow), where a parabolic profile might be anticipated.

Finally, certain geometrical analogies should be kept within the following limits to avoid large-scale maldistribution of the flow (Treybal, 1980; Gunn, 1968, Carberry 1976; Chen *et al.*, 1968):

$$\begin{aligned} \frac{Z}{D} &\geq 5 \\ \frac{D}{d_p} &\geq 12 - 30 \\ \frac{Z}{d_p} &\geq 50 - 150 \end{aligned} \quad (3.324)$$

where D is the bed diameter, Z is the bed height, and d_p is the particle diameter. To “transfer” experimental data from the small to the large unit, maldistribution and liquid holdup should be kept at a satisfactory level and similar in both scales. Large-scale maldistribution can result from inadequate initial distribution, from structural deviations or pathologies within the fixed bed (Chapter 6).

Liquid holdup in liquid–solid fixed beds

Liquid holdup is critical in the downflow operation of fixed beds, in contrast to the upflow operation where the liquid occupies practically the whole external free void volume of the bed. Total liquid holdup h_t consists of two parts: static h_s and dynamic holdup h_d . Static holdup is related to the volume of liquid that is adherent to the particles' surface, whereas dynamic holdup is related to the flowing part of the liquid.

Liquid holdup based on the total volume of the bed (empty bed volume) occupied by the liquid h_e and liquid holdup based on the void volume of the bed (bed voidage) occupied by the liquid h_v are related as follows:

$$h_v = \frac{V_{\text{liquid}}}{\varepsilon V_{\text{totalbed}}} = \frac{1}{\varepsilon} \left(\frac{V_{\text{liquid}}}{V_{\text{totalbed}}} \right) = \frac{h_e}{\varepsilon} \quad (3.325)$$

Then, $0 \leq h_e \leq \varepsilon$ while $0 \leq h_v \leq 1$.

In the following equations, the Reynolds number is based on the superficial velocity.

Fu and Tan correlation has been derived from experiments conducted in three-phase fixed beds packed with spherical particles and for particle diameters between 0.5 and 1.9 mm. Fixed bed operated under downflow conditions and a liquid distributor was used. The correlation was derived for Re_p between 0.1 and 10 (Fu and Tan, 1996):

$$h_{v,t} = 1.505 Re_p^{0.29} Ga^{-0.32} d_h^{-0.22} \quad (3.326)$$

$$d_h = \left[\frac{16\varepsilon^3}{9\pi(1-\varepsilon)^2} \right]^{1/3} d_p \quad (3.327)$$

$$Ga = \frac{d_p^3 g \rho^2}{\mu^2} \quad (3.328)$$

where: d_h = the hydraulic diameter of the particles in (m).

Here, liquid holdup (in m^3/m^3) refers to the portion of void (available) bed volume occupied by the liquid.

More general is the equation proposed by Otake and Okada, derived for several particle shapes and for Re_p between 10 and 2000. The proposed equation has been derived in two-phase fixed beds, operating under downflow condition and utilizing a liquid distribution system at the top of the bed (Doraiswamy *et al.*, 1984; Van Swaaij *et al.*, 1969):

$$h_{v,d} = 1.29(Re_p)^{0.675} (Ga)^{-0.44} (a_u d_p) \quad (3.329)$$

$$a_u = \frac{6(1-\varepsilon)}{d_p} \quad (3.330)$$

The following equation was derived utilizing direct weighting methods, in two-phase fixed beds operating under downflow condition and utilizing a liquid distributor at the bed inlet. This equation holds for particles of several shapes, including irregular-shaped particles of activated carbon of 1 mm diameter and for $0.3 < Re_p < 3000$ (Specchia and Baldi, 1977; Colombo and Baldi, 1976):

$$h_{v,d} = 3.86 Re_p^{0.545} Ga^{-0.42} \left(\frac{a_u d_p}{\varepsilon} \right)^{0.65} \quad (3.331)$$

Here, liquid holdup (in m^3/m^3) refers to the portion of void (available) bed volume occupied by the liquid.

For zeolites and other similarly shaped materials with water as fluid, the following equation can be used (Inglezakis *et al.*, 2001):

$$\%h_{v,t} = 21 + 99.72 u_s^{0.52} \quad (3.332)$$

In this equation, $\%h_{v,t}$ corresponds to the % portion of the void (available) bed volume, which is occupied by the liquid, where u_s is in cm/s. The constant part in the liquid holdup correlation (21%) is the static liquid holdup. This correlation is derived in beds with no liquid distributors and for particle sizes in the range 1.18–1.4 mm.

For different particle sizes, the dynamic holdup can be calculated as follows. According to the related holdup equations, the dynamic liquid holdup based on the void (available) bed volume is proportional to $d_p^{-0.54}\varepsilon^{-0.66}$, $d_p^{-0.72}\varepsilon^{-0.65}(1-\varepsilon)^{0.65}$, and $d_p^{-0.65}\varepsilon^{-1}(1-\varepsilon)$. The bed voidage can be considered to be the same for different particle sizes, which is true for low d_p/D values (see the following subsection). Thus, the following analogy can be used:

$$\frac{\%h(d_{p1})}{\%h(d_{p2})} \cong \left(\frac{d_{p2}}{d_{p1}} \right)^m \quad (3.333)$$

A typical value for m is between 0.54 and 0.72. For dynamic holdup, the value of 0.72 can be used for irregular-shaped particles similar to activated carbon and zeolites.

Static holdup is a function of the Eotvos number Eo (Van Swaaij *et al.*, 1969):

$$Eo = \frac{\rho g d_p^2}{\sigma_L} \quad (3.334)$$

where σ_L is the surface tension in N/m. For water, this value is equal to 71.2×10^{-3} . For small Eo , namely below 10, the static holdup based on the total volume of the bed is constant, approaching the value of $0.05 m^3/m^3$, whereas for higher values of Eo , the static holdup decreases constantly.

However, the most rigorous analysis on static holdup is found in the work of Saez *et al.* (1991), where the maximum value of static holdup based on the total volume of the bed

for low EO , up to 0.01, is equal to $0.11 \text{ m}^3/\text{m}^3$. The following equation holds for spherical particles:

$$h_{e,s} = \frac{0.11}{1 + EO} \quad (3.335)$$

where the static holdup $h_{e,s}$ is based on the total volume of the bed. For aqueous solutions at ambient temperature and particle sizes between 0.2 and 3.5 mm, the following equation can be derived from the above equations:

$$h_{e,s} = -0.0453d_p + 0.053 \quad (3.336)$$

where d_p is in m, while $h_{e,s}$ is based on the total volume of the bed. For zeolite-packed beds and particle sizes of 1.2–1.3 mm, this equation results in a static holdup equal to 18.4%, very close to the one found for the zeolites holdup equation (3.332).

Bed voidage considerations

The above analysis on liquid holdup determination for different particle sizes (eq. (3.333)) and as will be analyzed, the procedure of scaleup (Chapter 6) is based on the grounds that the bed voidage is approximately the same for different beds of the same material.

However, bed voidage depends on d_p/D (Dixon, 1988). It can be proved that for d_p/D values lower than 0.1, the bed voidage can be considered practically constant. Indeed, it is common practice to use ratios of d_p/D lower than 0.1, and therefore, the bed voidage can be actually considered the same for common fixed beds. For instance, a bed consisting of particles with 2 mm diameter should have a diameter greater than 2 cm, which leads to a d_p/D ratio with a value of 0.1 maximum. Consequently, the bed voidage is critical only in laboratory experiments. In Figure 3.39, Dixon's correlations are presented for spheres and cylinders, in the case of $d_p/D < 0.4$ (Dixon, 1988). For cylinders, d_p is equal to the diameter of a sphere of equal volume.

It is obvious that for $d_p/D < 0.1$, the differences of bed voidage are small, whereas for $d_p/D > 0.1$, the bed voidage is greatly affected by the diameter ratio. For irregularly shaped particles, measurements should be conducted in order to evaluate bed voidage and its dependence on d_p/D . For example, for irregularly shaped particles of zeolite (clinoptilolite), the bed voidage was measured to be in the range 0.48–0.51 for d_p/D between 0.019 and 0.074 (Inglezakis, 2002). Finally, as the pressure drop is very sensitive to the bed voidage, the ratio d_p/D has a great effect on the pressure drop across the bed in the case of $d_p/D > 0.1$ (Afandizadeh and Foumeny, 2001; Fumeny *et al.*, 1996). Again, this happens because for $d_p/D > 0.1$, the bed voidage changes considerably (Figure 3.39).

Loading of particles in fixed beds

A major problem associated with loading methods could be the inconsistency in bed structure, i.e. mean and local voidage properties, from fill to fill. Taking into consideration the fact that pressure drop is greatly influenced by the bed voidage and that pressure drop is critical for gas-phase systems, the loading of particles is of great importance, especially in gas-phase reactors (Afandizadeh and Foumeny, 2001).

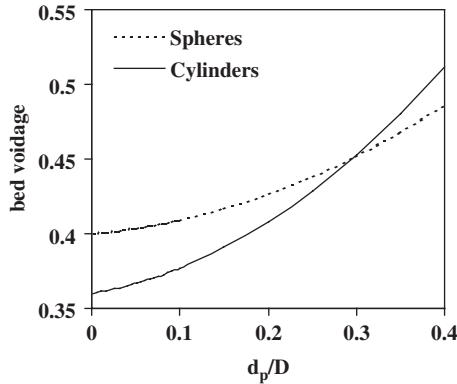


Figure 3.39 Bed voidage versus d_p/D .

A well-known method is the “snow-storm filling,” as shown in Figure 3.40 (Afandizadeh and Foumeny, 2001). This method involves passing the packing material over staggered wires or wire meshes so that the fall of the particles is interrupted before reaching the bed face. The flow interruption causes radial dispersion of particles, and as a consequence, the entire bed face is covered at a uniform rate.

Liquid flow distribution in fixed beds

General Generally, from a macroscopic point of view, maldistribution can be divided into two different phenomena (Stanek, 1994). The first one is small-scale maldistribution, which is connected mainly to the so-called preferred paths. It is the case where the liquid follows specific paths through bed and travels with velocities considerably higher than the mean. The same phenomenon is characterized as chaneling. The second case is large-scale maldistribution, which is connected to the nonhomogeneous (nonuniform) initial distribution of the liquid and is referred to as “wall effects.” The concepts of distributor quality and liquid maldistribution in fixed beds are frequently found in the related technical literature, and these concepts are connected to each other—the better the distributor quality, the better the liquid distribution and flow into bed (Klemas and Bonilla, 1995).

The distributor quality D_Q , is expressed as the portion (%) of the fixed-bed cross-sectional area (inlet surface), which is homogeneously wetted by the liquid. The initial maldistribution in the bed inlet (M_{do}) is a statistical average of the mass flow rate standard deviation divided by the free surface in the bed inlet. These parameters are related as follows (Klemas and Bonilla, 1995):

$$M_{do} = 100[(100 - D_Q)/D_Q]^{0.5} \quad (3.337)$$

For example, for a distributor quality of 90–95%, the initial maldistribution is 23–33%. This means that the distributor should have excellent quality to lead to a good initial liquid

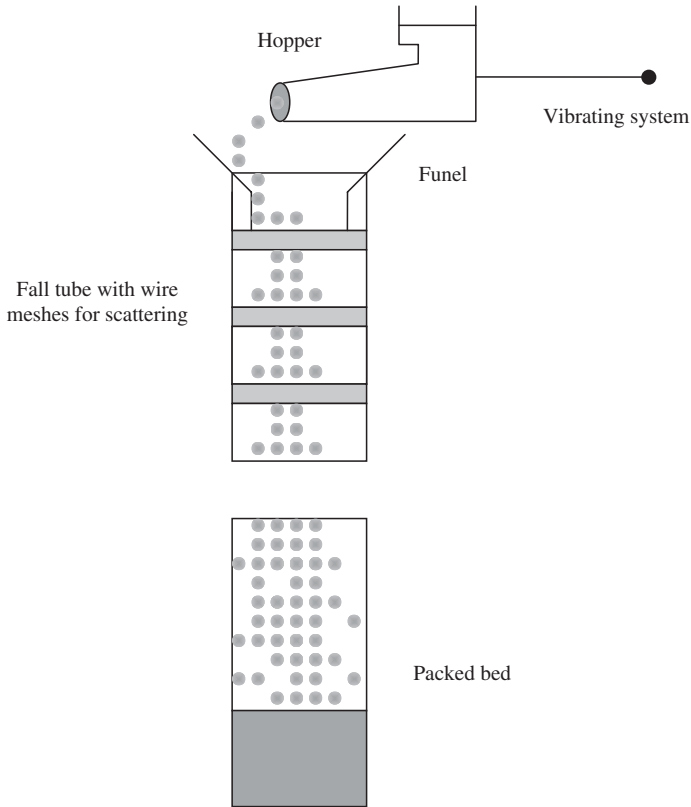


Figure 3.40 Apparatus for snow-storm filling of fixed beds

distribution in the bed. The liquid flow at the entrance of the bed (AB and BC) to the fully developed flow section (CD) is shown in Figure 3.41.

There are three basic factors that affect the liquid distribution quality (Perry *et al.*, 1990):

- (a) the number of drip points (density),
- (b) the geometrical homogeneity of drip points, and
- (c) the homogeneous flow of fluid through these points.

In the ideal case, the number of openings (pour or drip points) of the distributor should be equal to the physical density of the bed channels (Stanek, 1994). In practice, in beds of high diameter, this number should be between 35 and 251 openings/m² or alternatively, at least one opening for every 10 – 12 particles that occupy the cross-section of the bed (Klemas and Bonilla, 1995).

For fixed beds, redistribution of flow within the bed should be provided at intervals equal to 3–10 times the diameter of the bed (Treybal, 1980). It is a general rule that in fixed beds

and a single-phase flow, the flow becomes homogeneous at a distance 4–5 times the bed diameter from the bed inlet, whereas in the case of low ratios of bed-to-particle diameter (typically lower than 15), the flow becomes nonhomogeneous at a distance of 3–6 bed diameters from the bed inlet, even in the case of an adequate flow distribution (Perry and Green, 1999). The basic types of liquid-phase distributors are the following: perforated pipe distributors, slot-type distributors, perforated plates, and screens and beds of solids.

Design of perforated pipe distributors This type of distributor is perhaps the most suitable, especially for beds of small diameter and of simple design. In Figure 3.42, this type of distributor is presented.

The design of this distributor is as follows. The approach is based on turbulent flow into the distributor, and thus for $Re_D > 2100$ (based on the distributor diameter and the liquid velocity at the inlet of the distributor). Furthermore, the diameters of the distributor openings as well as the distance between them are considered to be uniform throughout its length. Under these assumptions, the pressure drop across the distributor is (Perry and Green, 1999)

$$\Delta p = \left(\frac{4fL}{3D} - 2K \right) \frac{\rho u_i^2}{2} \quad (3.338)$$

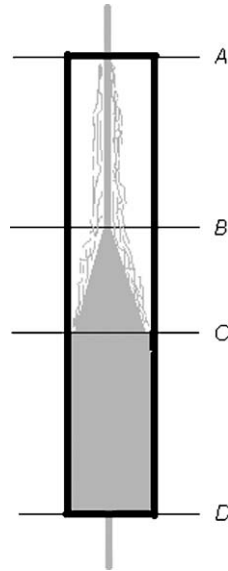


Figure 3.41 Liquid maldistribution in the entrance of the fixed bed.

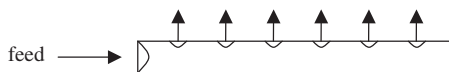


Figure 3.42 Perforated pipe distributor.

where:

- f = the Fanning friction factor, dimensionless
- L = the length of the distributor, m
- D = the diameter of the distributor, m
- u_i = the velocity of the liquid in the inlet of the distributor, m/s
- ρ = the fluid density, kg/m³
- K = the resistance coefficient, dimensionless
- Δp = the pressure drop, Pa.

The factor K is considered to be 0.5 for this type of distributors (Feintuch, 1977). The Fanning friction factor f for $Re_D > 4000$ is calculated using the Churchill equation (Perry and Green, 1999):

$$\frac{1}{\sqrt{f}} = -4 \log \left[\frac{0.27 \varepsilon_D}{D} + \left(\frac{7}{Re_D} \right)^{0.9} \right] \quad (3.339)$$

where ε_D is the roughness of the material of the distributor in (m), having a value 0.046 mm for common iron pipes. In any case, the relationship $Re_D - f - \varepsilon/D$ can be used (Perry and Green, 1999).

The mean pressure drop at the openings Δp_o (in Pa) is

$$\Delta p_o = \frac{1}{C_{K_o}^2} \frac{\rho u_o^2}{2} \quad (3.340)$$

where:

- C_{K_o} = the opening exit factor
- u_o = the average liquid velocity in the outlet of the opening.

The opening exit factor is in practice between 0.60 and 0.63 (Feintuch, 1977). If the mean pressure drop Δp_o at the openings is significantly higher than the pressure drop Δp across the distributor, the total pressure drop from opening to opening will not vary much, and consequently, the exit feed rate at each opening will be more or less the same. The relative variation of feed, expressed as % difference between the first and the last opening M_{do} is (Perry and Green, 1999)

$$M_{do} = 100 \left(1 - \sqrt{\frac{\Delta p_o - |\Delta p|}{\Delta p_o}} \right) \quad (3.341)$$

The last relation is valid for relatively small variations of the flow across the distributor. The value of M_{do} can be considered equal to 5%, in general. Δp_o can be calculated from eqs. (3.341) and (3.338), and u_o can also be determined from eq. (3.340). Subsequently, the total cross-section A_o of the openings can be calculated.

$$A_o = \frac{Q}{u_o} \quad (3.342)$$

For N openings, the diameter of each one is

$$D_o = \left(\frac{4A_o}{\pi N} \right)^{0.5} \quad (3.343)$$

Considering that the distance between the openings L_o should be the same, and keeping the same distance between the wall of the bed and the ends of the distributor, the distance L_o is

$$L_o = \frac{L - ND_o}{N + 1} \quad (3.344)$$

The total number of openings N affects the flow rate, velocity, and Re_D in the region of the last opening, which is determined to $(1/N)$ of the opening at the entrance of the distributor. So, Re_D at the first and the last opening of the distributor can be calculated, and in turn, the corresponding values of the fanning friction factors can be estimated. The mean value of these two factors should be used in the calculations in this procedure.

Finally, given the length of the distributor—which is approximately equal to the bed diameter, the feed rate and the distributor material, the diameter of the distributor's openings can be calculated on the grounds that the diameter and the number of openings has been chosen. In practice, the diameter of the distributor, which is a small percentage of the bed ($<20\%$), and the number of openings define the Re_D number at the ends of the distributor, which should be high (typically >2100). From this point of view, the design procedure is a trial-and-error process, based largely on experience.

During calculations, it has to be taken into account that the pressure drop Δp across the distributor should be always negative. Moreover, for $M_{do} = 5\%$, this pressure drop should be approximately equal to one-tenth the mean pressure drop at the openings. Finally, the number of openings should be chosen appropriately to lead to easy construction of the distributor.

Example 6

Suppose that a perforated-pipe distributor made from iron will be used for a feed rate of 428 L/h. The distributor has a length of 1.8 cm (8.5% of the diameter of the bed, $D = 21$ cm), and length shortly less than the diameter of the bed (20.9 cm). According to the calculations, for the specific feed rate, the distributor will have four round openings with a diameter of 6.6 mm each. The distance between the openings as well as the distance between the terminal openings and the ends of the distributor is 36 mm. However, these calculations can be repeated for various feed rates to choose the optimum distributor design.

Gas-phase distribution in fixed beds

The problem of gas distribution is similar and typical gas distributors are given in Figure 3.43.

3.6.4 External heat and mass transfer

Liquid–solid systems

The liquid mass transfer coefficient (or convection coefficient) is a flow-dependent parameter, which can be evaluated from several correlations found in the related literature.

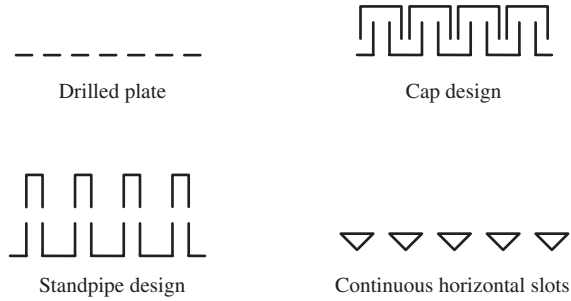


Figure 3.43 Common distributor designs for gases.

The following one gives the best prediction of the individual liquid-film mass transfer coefficient in water-treatment situations (Chern and Chien, 2002):

$$Sh = (2 + 0.644Re_p^{1/2}Sc^{1/3})[1 + 1.5(1 - \varepsilon)] \quad (3.345)$$

For $0.04 < Re_p < 52$, the Williamson correlation is proposed and used in adsorption processes for wastewater, using granular activated carbon (Ko *et al.* 2000; Crittenden *et al.*, 1987):

$$Sh = 2.4\varepsilon^{0.66}Re_p^{0.34}Sc^{0.33} \quad (3.346)$$

Also, the Kataoka correlation has been used in adsorption systems from liquid phase with $Re_p < 40$ (Perry and Green, 1999).

$$Sh = 1.85(Re_pSc)^{1/3} \left(\frac{1 - \varepsilon}{\varepsilon} \right)^{1/3} \quad (3.347)$$

For $0.0015 < Re_p < 55$, the Wilson–Geankoplis correlation has been used in adsorption from liquid phase (Perry and Green, 1999; Xiu and Li, 2000; Chen and Wang, 2004).

$$Sh = \frac{1.09}{\varepsilon} Sc^{1/3} Re_p^{1/3} \quad (3.348)$$

and for $55 < Re_p < 1050$ and liquid phase (Perry and Green, 1999),

$$Sh = \frac{0.25}{\varepsilon} Sc^{1/3} Re_p^{0.69} \quad (3.349)$$

For $2 < Re_p < 2000$, the Garner–Suckling correlation has been used in ion-exchange systems (Perry and Green, 1999; Rivero *et al.*, 2004):

$$Sh = 2 + 0.95Sc^{1/3} Re_p^{0.5} \quad (3.350)$$

Re_p is based on the superficial velocity for all equations in this section.

The double lines in Figure 3.44 represent the Sh number based on the mass transfer coefficient, in the case of a single-particle fall in water, for three different particle densities (Harriot, 1962). This value is considered to be the minimum mass-transfer coefficient in liquid–solid films in agitated vessels. Taking into account the fact that the actual Sh value in an agitated vessel is 1.5–8 times its minimum value, it is apparent that the mass transfer coefficients are much higher in the case of agitated vessels.

Gas–solid systems

For the gas and liquid phases with $3 < Re_p < 10^4$, the most general equation is the Wakao equation (Perry and Green, 1999):

$$Sh = 2 + 1.1Sc^{0.33}Re_p^{0.6} \quad (3.351)$$

and for $Re_p > 1$, the following is the most general equation (Perry and Green, 1999):

$$Sh = \left(\frac{Re_p}{\varepsilon} \right)^{0.5} Sc^{0.33} \quad (3.352)$$

Petrovic and Thodos proposed the following correlation for gases with $3 < Re_p < 2000$ (Ruthven, 1984):

$$Sh = \frac{0.357}{\varepsilon} Re_p^{0.64} Sc^{0.33} \quad (3.353)$$

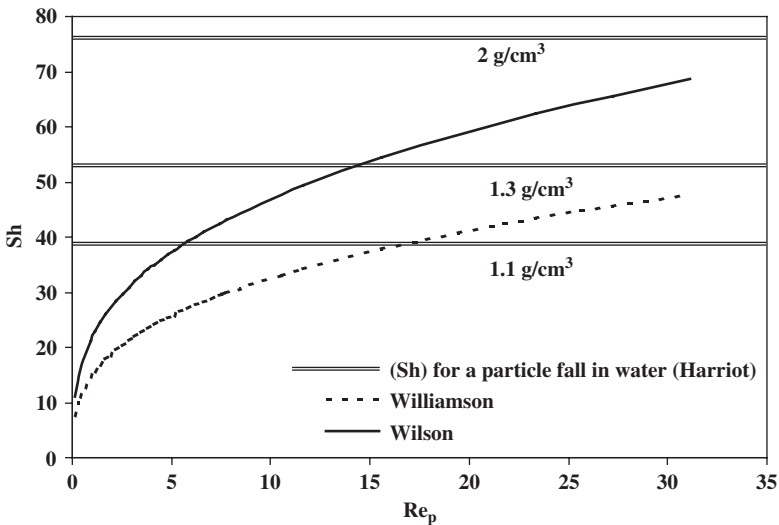


Figure 3.44 Sherwood number for fixed beds (for $d_p = 1.3$ mm, $\rho_p = 1.1, 1.3,$ and 2 g/cm³, $\varepsilon = 0.5$, $D_f = 10\text{--}5$ cm²/s and $Sc = 1000$).

A typical value of Sh is 1000 and 1 for liquids and gases, respectively. Thus, Sh numbers are considerably lower for gases, about one order of magnitude, for the same Re_p number (Perry and Green, 1999). However, k_f in gases is much higher due to the higher D_f values.

For both gas and liquid–solid systems, the Dwivedi and Upadhyay equation could be used (Smith, 1981):

$$j_D \text{ or } j_H = \frac{0.458}{\varepsilon} \left[\frac{d_p G}{\mu} \right]^{-0.407} \quad (3.354)$$

$$j_D = \frac{k_f}{u_s} Sc^{2/3} \quad (3.355)$$

$$j_H = \frac{h_f}{c_p \rho u_s} \left(\frac{c_p \mu}{\lambda_f} \right)^{2/3} \quad (3.356)$$

where:

$G = u_s \rho$, the fluid mass superficial velocity, $\text{kg/m}^2 \text{ s}$

$h_f =$ the heat transfer coefficient, $\text{W/m}^2 \text{ K}$

$c_p =$ the specific heat capacity of the fluid, J/kg K

$\lambda_f =$ the thermal conductivity of the fluid, W/m K .

The above equations hold for $Re_p > 10$. At temperatures above about 400°C and for large particles (> 0.25 in), heat transfer by radiation may be significant and should be taken into account.

For all the equations presented,

$$Sh = \frac{k_f d_p}{D_f} \quad (3.357)$$

$$Re_p = \frac{d_p u_s}{\nu} \quad (3.358)$$

$$Sc = \frac{\nu}{D_f} \quad (3.359)$$

where:

$Re_p =$ the particle Reynolds number

$Sh =$ the Sherwood number

$Sc =$ the Schmidt number

$u_s =$ the superficial velocity

$D_f =$ the diffusion coefficient of the solute in the liquid phase

$d_p =$ the particle diameter

$\nu =$ the liquid kinematic viscosity.

Table 3.9

Basic properties of air and water (at 20 °C, 1 atm)

	D_f (m ² /s)	μ (Pa s)	ν (m ² /s)	ρ (kg/m ³)	c_p (kJ/kg K)	λ_f (W/m K)
Water	$\approx 10^{-9}$	10^{-3}	10^{-6}	1000	4.181	606×10^{-3}
Air	$\approx 10^{-5}$	1.82×10^{-5}	1.52×10^{-5}	1.2	1.007	26.3×10^{-3}

In Table 3.9 the basic properties for air and water needed for the determination of Sh , Sc and Re numbers are presented.

3.7 THREE-PHASE FIXED BEDS: TRICKLE-BED AND PACKED BUBBLE-BED REACTORS

3.7.1 Hydraulic regimes in three-phase fixed beds

Trickle beds

When the liquid and gas phase flows over a fixed bed of catalytic particles in the downflow mode, the nature of the flow regime is a composite function of the gas flow rates (Smith, 1981). In Table 3.10 and Figures 3.47, 3.48, the various operating regimes are presented.

In trickle beds, the flows of gas and liquid are concurrent downward. The liquid feed is at such a low rate that it is distributed over the packing as a thin film, in rivulets from one particle to the next, and flows by gravity, helped along by the drag of the gas (Figure 3.45). The gas phase is continuous. This mode is suitable for reactions where low reaction times are required, usually in seconds, short enough to forestall undesirable side reactions such as carbon formation. One of the advantages of the concurrent operation is the possibility of using high flow rates of the phases without flooding.

The trickling regime is also called the “low interaction” regime, while the rest belong to the group “high interaction” regime. In trickle beds, typical mass velocities for gas and liquid phases are in the range 10–300 and 100–3000 g/cm²h, respectively (Figures 3.46 and 3.47). Superficial gas and liquid velocities in pilot plants are 2–45 and 0.01–0.3 cm/s, respectively. In commercial reactors, these values are 15–300 and 0.1–2 cm/s, respectively (Ramachandran and Chaudhari, 1984). Industrial trickle-beds are typically 3 – 6 m deep and up to 3 m in dia-meter, whereas pilot plants might be about 1 m deep and 4 cm in diameter. The particle size of catalysts is in the range 0.08–0.32 cm diameter. Kinetics and/or thermodynamics of reactions conducted in trickle-bed reactors often require high temperatures. Elevated pressures (up to 30 MPa) are required to improve the gas solubility and the mass transfer rates. In petroleum refining, pressures of 34 –102 atm and temperatures of 345 –425 °C are used (Satterfield, 1975).

Trickle-bed reactors are often employed in highly exothermic reactions such as the hydrogenation of unsaturated hydrocarbons. However, they exhibit poor capability of removing the excess heat of the reaction. Since the gas has low heat capacity, the liquid is responsible for removing this heat. If the generated heat is not adequately removed, hot spots may be created. These hot spots may lead to sintering of catalyst particles, with an

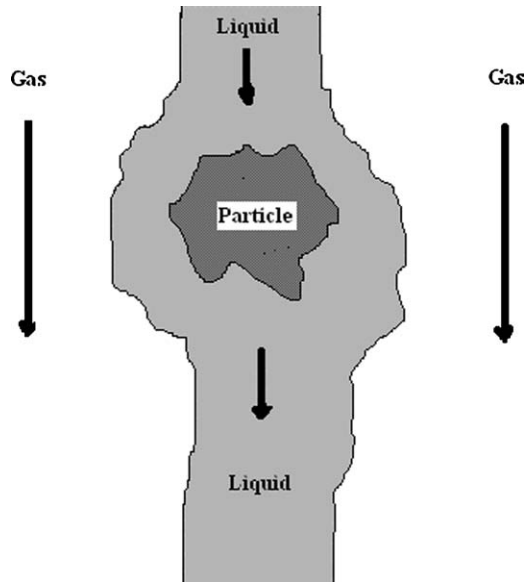


Figure 3.45 Trickle-flow regime with liquid rivulets (complete wetting of the outer surface of the particle).

Table 3.10

Flow regimes in three-phase fixed beds

Gas flow rate	Liquid flow rate	Regime	Gas phase	Liquid phase
Low	Low	Trickle flow	Continuous	Rivulets
Low	High	Dispersed bubble	Bubbles	Continuous
Very high	Low	Spray	Continuous	Droplets
High	High	Pulsed flow	Slugs	Slugs

undesirable impact on catalyst activity and surface area. Consequently, the life span of the catalyst decreases and the operation cost increases. In the worst scenario, safety issues and reactor failure may come up because of these hot spots. Moreover, undesirable reactions and varying residence time of reactants may take place as a result of nonuniformity of the temperature in the reactor. So, it is obvious that these hot spots must be avoided, especially for safety reasons. This can be achieved in various ways:

- smaller catalyst particles can improve wetting and internal mass transfer,
- cycling the liquid feed concentration can control temperature,
- by decreasing reactant concentration if a maximum bed temperature is reached,
- by periodical flooding of the tricklebed, and
- the operation of a trickle-bed reactor in the pulsing flow regime.

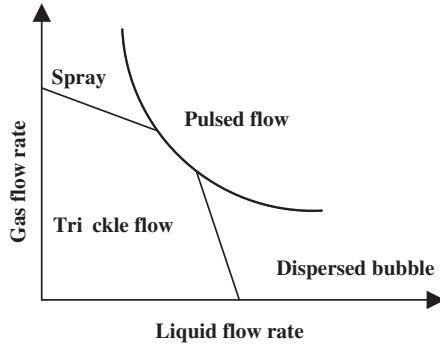


Figure 3.46 Flow regimes in three-phase fixed-beds.

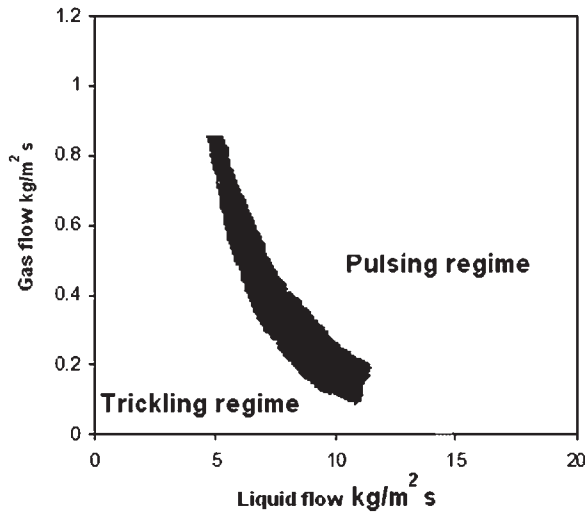


Figure 3.47 Trickling and pulsing regimes.

Trickle-bed reactors are found in many industries such as the petroleum, petrochemical, and chemical industry, and in various applications, i.e. wastewater treatment and biochemical and electrochemical processing.

Packed bubble bed reactor

The analysis in this section is primarily dedicated to trickle-bed reactors. However, some basic aspects of packed bubble bed reactors will be presented as well. A bubble fixed-bed reactor is actually a tubular-flow reactor with concurrent upflow of gas and liquid. The catalyst bed is completely immersed in a continuous liquid flow, while gas rises as bubbles.

The packed-bed reactor is particularly useful in two cases:

- (a) if a relatively small amount of gas is to be treated with a large amount of liquid, and
- (b) if a large residence time is desired (Ramachandran and Chaudhari, 1984).

In packed-bed reactors, the catalyst is fully wetted, whereas the heat and mass transfer efficiency is higher than that observed in trickle-bed reactors. However, low operation efficiency may appear due to backmixing of the liquid phase. Moreover, high liquid-phase residence times can result in the occurrence of homogeneous side reactions.

Some examples of bubble fixed-bed reactors application are the hydrogenation of nitro compounds, amination of alcohols, and ethylnylation of formaldehyde to butynediol (Ramachandran and Chaudhari, 1984).

3.7.2 Modeling of trickle-bed reactors

The employment of three-phase reactors is mostly desirable when there are some reactants that are too volatile to liquefy, whereas some others are too nonvolatile to vaporize. Hence, the situation where a gaseous component reacts with another reactant in the liquid-phase is of great interest. The following reaction represents this case (Smith, 1981):



Characteristic examples of this form are the hydrogenation reactions, e.g. hydrodesulfurization of petroleum fractions, hydrogenation of oils, and oxidation reactions, e.g. oxidation of pollutants dissolved in liquids. In a few cases such as the Fischer–Tropsch synthesis, the liquid is inert and acts as a heat-transfer medium.

Here, issues in relation to the trickle flow regime—*isothermal operation and plug flow for the gas phase*—will be dealt with. Also, it is assumed that the flowing liquid completely covers the outer surface particles ($f_w = 1$ or $a_{LS} = a_u$) so that the reaction can take place solely by the mass transfer of the reactant through the liquid–particle interface. Generally, the assumption of isothermal conditions and complete liquid coverage in trickle-bed processes is fully justified with the exception of very low liquid rates. Capillary forces normally draw the liquid into the pores of the particles. Therefore, the use of liquid-phase diffusivities is adequate in the evaluation of intraparticle mass transfer effects (effectiveness factors) (Smith, 1981).

In most applications, the axial dispersion in both phases can be considered to be negligible (Smith, 1981). Moreover, no radial gradients of concentration and velocity exist for the gas or liquid.

Conservation equations for each flowing phase—Smith's approach

For reactant A in the gas phase, at steady state, and for a volume element that extends across the reactor,

$$\frac{dF_{AG}}{dV} + (K_L a_{GL})_A \left[\frac{C_{AG}}{H_A} - C_{AL} \right] = 0 \quad (3.360)$$

where:

V = the reactor volume

F_{AG} = the molar flow rate of A in the gas phase, mol/s.

and

$$F_{AG} = Q_G C_{AG} = u_{sG} A C_{AG} \quad (3.361)$$

For a variable volume system, $\varepsilon_R \neq 0$ by analogy to batch reactor.

$$\frac{dF_{AG}}{dV} = \frac{d(Q_G C_{AG})}{dV} = C_{AG} \frac{dQ_G}{dV} + Q_G \frac{dC_{AG}}{dV} = -F_{A,i} \frac{dx_A}{dV} \quad (3.362)$$

For a constant-volume system, $\varepsilon_R = 0$,

$$\frac{dQ_G}{dV} = 0 \quad (3.363)$$

and thus,

$$\frac{dF_{AG}}{dV} = Q_G \frac{dC_{AG}}{dV} = Q_G \frac{dC_{AG}}{d(zA)} = \frac{Q_G}{A} \frac{dC_{AG}}{dz} = u_{sG} \frac{dC_{AG}}{dz} \quad (3.364)$$

In this case, by substituting in eq. (3.360), we have the well-known equation (Smith, 1981; Singh, 2004; Hopper *et al.*, 2001)

$$u_{sG} \frac{dC_{AG}}{dz} + (K_L a_{GL})_A \left[\frac{C_{AG}}{H_A} - C_{AL} \right] = 0 \quad (3.365)$$

where:

K_L = an overall mass transfer coefficient between gas and liquid,

u_{sG} = the superficial gas velocity

(C_{AG}/H_A) = the bulk liquid-phase concentration in equilibrium with the bulk gas concentration.

Since Henry's law has been applied to A, K_L is related to the individual film coefficients in the gas film (k_g) and liquid film (k_{fg}) (for the derivation, see Section 3.1.2):

$$\frac{1}{K_L} = \frac{1}{Hk_g} + \frac{1}{k_{fg}} \quad (3.366)$$

As noted elsewhere, if A is slightly soluble in the liquid (H is large) then $K_L \cong k_{fg}$. The same holds in the case of pure A in the gas phase (no resistance in the gas film).

For reactant A in the liquid phase, at steady state, and for a volume element that extends across the reactor,

$$D_L \frac{d^2 C_{AL}}{dz^2} - u_{sL} \frac{dC_{AL}}{dz} + (K_L a_{GL})_A \left[\frac{C_{AG}}{H_A} - C_{AL} \right] - (k_f a_u)_A [C_{AL} - C_{AS}] = 0 \quad (3.367)$$

where C_{AS} is the concentration of A in the liquid–solid interface u_{sL} the superficial liquid velocity.

The third mass conservation equation needed is that for reactant B in the liquid phase.

$$D_L \frac{d^2 C_{BL}}{dz^2} - u_{sL} \frac{dC_{BL}}{dz} - (k_f a_u)_B [C_{BL} - C_{BS}] = 0 \quad (3.368)$$

Here, it has been assumed that B is nonvolatile. The velocity u_{sL} is the superficial liquid velocity.

The reaction rate expressed in terms of surface concentrations provides the relationship between C_S and C_L . From the definition of the effectiveness factor, we may express the required equality of mass transfer and reaction rates as

$$(k_f a_u)_A [C_{AL} - C_{AS}] = (-R_A) = \rho_b (-r_m)_A \quad (3.369)$$

$$(k_f a_u)_A [C_{BL} - C_{BS}] = (-R_B) = \frac{(-R_A)}{a} = \frac{\rho_b}{a} (-r_m)_A \quad (3.370)$$

where ρ_b is the bulk density of the bed, a the stoichiometric coefficient, $(-r_m)_A$ represents the rate of reaction per unit mass of catalyst, and $-R_A$ and $-R_B$ represent the rate of reaction per unit volume of reactor. Note that subscripts A and B denote that the mass transfer coefficient could be different for different species due to the difference in the diffusion coefficients.

As in the case of two-phase fixed beds, the material balances of trickle beds are expressed in terms of the reactor volume V_R (see Section 3.1.1 for the derivation) and the following relationship holds:

$$(-R) = -\frac{1}{V_R} \frac{dN}{dt} = (1 - \varepsilon)(-r_{vs}) = S_s \rho_b (-r_s) = \rho_b (-r_m) \quad (3.371)$$

Example 7

An interesting case is a reaction with $\varepsilon_R = -1$. A typical example is the catalytic reaction of the form



where the gas feed is pure A and it is the limiting reactant. Analogous to batch systems,

$$\frac{Q_G}{Q_{G,i}} = 1 + \varepsilon_R x_A = 1 - x_A$$

and thus,

$$C_A = \frac{F_A}{Q_G} = \frac{F_{A,i}(1-x_A)}{Q_{G,i}(1-x_A)} = \frac{F_{A,i}}{Q_{G,i}} = C_{A,i}$$

Since the system is a variable volume one $\varepsilon_R \neq 0$,

$$\frac{dF_{AG}}{dV} = C_{AG} \frac{dQ_G}{dV} + Q_G \frac{dC_{AG}}{dV}$$

for $\varepsilon_R = -1$, C_A is constant and thus

$$\frac{dC_{AG}}{dV} = 0$$

Then

$$\frac{dF_{AG}}{dV} = C_{AG} \frac{dQ_G}{dV}$$

and eq. (3.360) becomes

$$C_{AG} \frac{dQ_G}{dV} + (K_L a_{GL})_A \left[\frac{C_{AG}}{H_A} - C_{AL} \right] = 0$$

Comparing it with eq. (3.365),

$$u_{sG} \frac{dC_{AG}}{dz} + (K_L a_{GL})_A \left[\frac{C_{AG}}{H_A} - C_{AL} \right] = 0$$

It is obvious that if the gas-phase constitutes only one pure compound A, the use of eq. (3.365) is not sound, because it leads to zero values of the derivative and it seems that the equation is not needed. The latter is true only when the conversion of A is too low and so Q_G can be considered practically constant. For systems of variable volume, eq. (3.360) or the equation derived in the previous example can be applied instead. The equation derived in the previous example specifically shows that it is the change of volume (flow rate) of the gas phase that affects the reactor operation and not the concentration change, since the concentration of A is constant throughout the reactor. Of course, the change of flow rate is due to the change in moles (x_A is variable).

The following cases are usually found in many practical applications.

(a) *The gas feed comprises of only one compound A:* Since the feed is a pure gas, the phase concentration is constant, and thus the mass balance (3.365) applied to the gas phase is not

required. Smith (1981) states that the concentration is constant when pure A is used in reactions of the form aA (gas) + B (liquid) \rightarrow products. In this case, there is no resistance in the gas film, and thus $K_L \cong k_{fg}$, and in turn $C_{G,i} = C_G$ and $C_L = C_{G,i}/H = C_G/H$. However, if the expansion factor is not zero, eq. (3.365) is not applicable, since it does not include this effect. Smith's approach of constant gas concentration is valid in the following situations:

- The expansion factor is zero. This means that there are gas products and the stoichiometric coefficients can result in $\delta = 0$. In this case, we can work with eq. (3.365), the underlying fact being that the concentration of A in the gas phase cannot be constant since the gas phase is a mixture due to gas products (the feed is pure A, not the reaction mixture). However, the gas-phase concentration of A could be practically constant if it is in great excess and/or the concentration of B is so low that the consumption of A is in turn low enough and the concentration of the gas products is also very low. In this case, the derivative in eq. (3.365) is practically zero and the equation is not needed.
- If all products are liquids and the gas phase constitutes only one compound A, irrespective of whether it is the limiting reactant or not, its gas-phase concentration is constant (see Examples 4 and 5). However, in this case, the expansion factor is -1 , and thus we cannot use eq. (3.365) to draw conclusions unless the conversion of A is very low.
- If $\delta \neq 0$ and thus $\epsilon_R \neq 0$, and if A is the limiting reactant,

$$C_A = \frac{F_A}{Q_G} = \frac{F_{A,i}(1-x_A)}{Q_{G,i}(1+\epsilon_R x_A)} = C_{A,i} \frac{(1-x_A)}{(1+\epsilon_R x_A)} \quad (3.372)$$

Then, if $x_A \rightarrow 0$, or in other words, if the conversion of A is extremely low, the concentration of A remains practically unchanged. So, eq. (3.359) is not applicable since

$$\frac{dF_{AG}}{dV} = -F_{A,i} \frac{dx_A}{dV} \rightarrow 0 \quad (3.373)$$

(b) *The liquid feed is saturated in A throughout the reactor:* The liquid phase mass balance (3.367) is eliminated. In this case, $C_{L,i} = C_L = C_{G,i}/H = \text{constant}$, whereas for a pure compound A in the gas phase, $C_L = C_{G,i}/H = C_G/H$.

Furthermore, the trickle-bed model eqs. (3.365), (3.367), and (3.368) hold for the general case, where more than one reactant is present in the gas and liquid phase. Specifically,

- The gas-phase mass balance (3.365) is used for reactants that are present in both the gas and the liquid phase.
- The liquid-phase mass balance (3.367) is used for volatile reactants being originally in the liquid phase and for reactants that are in the gas phase and are dissolved in the liquid phase. This mass balance is also called "volatile liquid-phase mass balance" (Hopper *et al.*, 2001).
- The liquid-phase mass balance (3.368) is used for non-volatile reactants that are present in the liquid-phase. This mass balance is called "non-volatile liquid-phase mass balance" (Hopper *et al.*, 2001).

Finally, the same equations can be used after the appropriate modifications for (Hopper *et al.*, 2001)

- three-phase fluidized beds
- concurrent upflow three-phase fixed bed (packed bubble bed reactor)
- slurry bubble column reactors for the continuous flow of gas and slurry

Material balances using an overall rate—Fogler's approach

The above analysis, using the material balances for both phases for the gas-phase reactant A, has been derived by Smith (1981). From eq. (3.367), it is obvious that the individual rates of mass transfer are not equal, and thus it is not possible to derive an overall rate based on the gas-phase concentration of A. However, Fogler (1999) followed the overall rate approach and proposed the use of a single material balance for the gas reactant A. Obviously, this can be applied if in the material balance for A in the liquid phase (eq. (3.367)),

$$u_{sL} \frac{dC_{AL}}{dz} \rightarrow 0 \quad (3.374)$$

and axial dispersion is negligible. Condition (3.374) means that the concentration of A remains practically constant along the reactor length due to very low liquid flow rates or because of very low solubility of A. The last relation is also valid if the liquid phase is saturated with A, thus resulting in a constant concentration of A in the liquid phase throughout the reactor.

As in the fluidized beds analysis (Section 3.8.3), a similar simplification has been made in Kunii–Levenspiel model for the material balances in the emulsion phase, where again the corresponding derivatives have been omitted (eqs. (3.529) and (3.530)). As in the case of liquid flow in trickle beds, the flow of the gas in the emulsion phase is considered too small and so the superficial velocities can be neglected. Thus, in trickle beds, from eq. (3.367),

$$(K_L a_{GL})_A \left[\frac{C_{AG}}{H_A} - C_{AL} \right] - (k_f a_u)_A [C_{AL} - C_{AS}] = 0 \quad (3.375)$$

or

$$(K_L a_{GL})_A \left[\frac{C_{AG}}{H_A} - C_{AL} \right] = (k_f a_u)_A [C_{AL} - C_{AS}] \quad (3.376)$$

From the definition of the effectiveness factor and for a first-order reaction with respect to A

$$(k_f a_u)_A [C_{AL} - C_{AS}] = \rho_b \eta k_m C_{AS} \quad (3.377)$$

Now, working these equations and following the method used for slurry bubble columns (see Section 3.4.6), C_{AS} can be eliminated and an overall reaction rate can be written in terms of the gas-phase concentration:

$$(-R_A) = K^\circ C_{AG} \quad (3.378)$$

where

$$K^{\circ} = \frac{1/H}{\frac{1}{(K_L a_{GL})_A} + \frac{1}{(k_f a_u)_A} + \frac{1}{\rho_b \eta k_m}} \quad (3.379)$$

and

$$(-R_A) = (K_L a_{GL})_A \left[\frac{C_{AG}}{H_A} - C_{AL} \right] = (k_f a_u)_A [C_{AL} - C_{AS}] = \rho_b \eta k_m C_{AS} \quad (3.380)$$

Using the general material balances presented in the previous paragraph and the above approach: for reactant A, at steady state, and for a volume element that extends across the reactor,

$$\frac{dF_{AG}}{dV} + (-R_A) = 0 \quad (3.381)$$

for reactant B (for plug flow of liquid),

$$-u_{sL} \frac{dC_{BL}}{dz} - (k_f a_u)_B [C_{BL} - C_{BS}] = 0 \quad (3.382)$$

or

$$-u_{sL} \frac{dC_{BL}}{dz} - (-R_B) = 0 \quad (3.383)$$

where

$$(k_f a_u)_B [C_{BL} - C_{BS}] = (-R_B) = \frac{(-R_A)}{a} \quad (3.384)$$

For the case of $\alpha = 1$ and first-order reaction rate with respect to A and B

$$(k_f a_u)_B [C_{BL} - C_{BS}] = (-R_B) = (-R_A) = \rho_b \eta k_m C_{AS} C_{BS} \quad (3.385)$$

and using the above approach, we can derive the equations used by Fogler (1999):

$$(-R_A) = K_A^{\circ} C_{AG} \quad (3.386)$$

where

$$K_A^o = \frac{1/H}{\frac{1}{(K_L a_{GL})_A} + \frac{1}{(k_r a_u)_A} + \frac{1}{\rho_b \eta k_m C_{BS}}} \quad (3.387)$$

and

$$(-R_B) = K_B^o C_{BL} \quad (3.388)$$

where:

$$K_B^o = \frac{1}{\frac{1}{(k_r a_u)_B} + \frac{1}{\rho_b \eta k_m C_{AS}}} \quad (3.389)$$

Material balances for packed bubble bed reactors

In general, the material balances and the corresponding solutions for trickle and bubble bed reactors are the same, under the assumption that the plug-flow condition holds for both phases. Of course, the appropriate correlations should be used for the estimation of mass transfer coefficients. However, in packed bubble bed reactors, the liquid-phase is frequently found in a complete mixed state, and thus some adjustments have to be made to the aforementioned models. Two special cases will be presented here.

Continuous flow of both phases in upflow and complete mixing of phases For packed bubble columns (upflow of both gas and liquid phases), under the assumption of complete mixed flow, the backmixing model of Ramachandran and Chaudhari (1980) is applicable. The relevant equations are presented in Section 3.5.1 for the continuous flow of gas and slurry phases in complete mixed-flow conditions (slurry CSTR reactor).

Continuous flow of both phases in upflow with recycling of liquid-phase For packed bubble columns and trickle beds, under the assumption of complete recycling of the liquid-phase, the solutions are the same as in slurry bubble columns and slurry CSTR with batch and reacting liquid-phase (see Section 3.5.1) (Ramachandran and Chaudhari, 1980). In this operation, V_L/V_R is greater than unity. Recycling is useful when the per-pass conversion of the liquid phase is very small.

3.7.3 Hydraulics

Pressure drop in trickle-bed reactors

The two-phase pressure drop ($\Delta P_{GL}/Z$) can be related to the pressure drops of each phase ($\Delta P_G/Z$) and ($\Delta P_L/Z$). According to Larkins *et al.* (Larkins *et al.*, 1961; Perry and Green, 1999),

$$\ln \left[\frac{(\Delta P_{GL}/Z)}{(\Delta P_L/Z) + (\Delta P_G/Z)} \right] = \frac{5.0784}{3.531 + (\ln X)^2} \quad (3.390)$$

$$X = \left[\frac{(\Delta P_L/Z)}{(\Delta P_G/Z)} \right]^{0.5} \quad (3.391)$$

where $(\Delta P_{GL}/Z)$ is the pressure drop in the trickle bed in Pa/m or N/m³ (Pa = N/m²). This equation holds for $0.05 < X < 30$. Souandia and Latifi (2001) presented two similar equations based on X (Midoux *et al.*, 1976; Tosun, 1984):

$$\varphi = 1 + \frac{1}{X} + \frac{1.424}{X^{0.576}} \quad \text{for } 0.4 \leq X \leq 60 \quad (3.392)$$

$$\varphi = 1 + \frac{1}{X} + \frac{1.14}{X^{0.54}} \quad \text{for } 0.1 \leq X \leq 80 \quad (3.393)$$

where

$$\varphi = \left[\frac{(\Delta P_{GL}/Z)}{(\Delta P_L/Z)} \right]^{0.5} \quad (3.394)$$

Pressure drop in packed bubble bed reactors

The two-phase pressure drop term $(\Delta P_{GL}/Z)$ can be calculated using the correlation of Huntington (Ramachandran and Chaudhari, 1984):

$$\frac{\Delta P_{GL}}{Z} = \frac{2u_{sG}^2 \rho_G \zeta}{d_{pe}} \quad (3.395)$$

where

$$d_{pe} = \frac{2}{3} d_p \frac{\varepsilon}{1 - \varepsilon} \quad (3.396)$$

$$\ln(\zeta) = 8 - 1.12 \ln(\psi) - 0.0769[\ln(\psi)]^2 + 0.0152[\ln(\psi)]^3 \quad (3.397)$$

$$\psi = \left[\frac{\left(\frac{u_{sG} \rho_G d_{pc}}{\mu_G} \right)^{1.167}}{\left(\frac{u_{sL} \rho_L d_{pc}}{\mu_L} \right)^{0.767}} \right] \left(\frac{\mu_w}{\mu_L} \right)^{0.9} \quad (3.398)$$

with μ_w being the dynamic viscosity of water and $\Delta P/Z$ is in dyn/cm^3 . To convert to N/m , multiply by 10 ($1 \text{ dyn} = 1 \text{ g cm/s}^2 = 10^{-5} \text{ N}$). In these equations, CGS units should be used.

Liquid holdup in trickle bed reactors

Although liquid holdup is mainly affected by the liquid flow rate, the shape, size, and wetting characteristics of the particles, the gas flow rate, and the initial distribution of the liquid are also factored. One of the simpler correlations is that of Midoux *et al.* (Perry and Green, 1999):

$$\frac{h_{e,t}}{\varepsilon} = \frac{0.66X^{0.81}}{1 + 0.66X^{0.81}} \quad (3.399)$$

where $h_{e,t}$ is the total liquid holdup based on the *total* volume of the empty bed (m^3/m^3). This relationship is valid for $0.1 < X < 80$.

The correlation of Sato takes into account the wall effects (Ramachandran and Chaudhari, 1984):

$$\frac{h_{e,t}}{\varepsilon} = 0.185 a_{u,m}^{1/3} X^{0.22} \quad (3.400)$$

$$a_{u,m} = \frac{6(1-\varepsilon)}{d_{p,m}} \quad (3.401)$$

$$d_{p,m} = \frac{d_p}{1 + \frac{4d_p}{6D(1-\varepsilon)}} \quad (3.402)$$

where D is the bed diameter in cm. In this equation CGS units should be used. Pironti *et al.* (1999) derived the following correlation for high Re numbers:

$$h_{e,d} = 0.048 Re_{L,m}^{0.403} Re_{G,m}^{-0.077} \quad (3.403)$$

where

$$\begin{aligned} 11 &\leq Re_{L,m} \leq 90.4 \\ 9 &\leq Re_{G,m} \leq 110 \end{aligned}$$

$$Re_{i,m} = \frac{u_s \rho d_p}{\mu} \frac{1}{1 - \varepsilon} \quad (3.404)$$

and $h_{e,d}$ is the dynamic liquid holdup based on the total volume of the empty bed (m^3/m^3).

The following equation of Specchia and Baldi, derived for particles of several shapes, can be applied to trickle beds for $0.3 < Re_L < 300$ (Specchia and Baldi, 1977; Ramachandran and Chaudhari, 1984):

$$h_{v,d} = 3.86 Re_L^{0.545} Ga_{L,m}^{-0.42} \left(\frac{a_u d_p}{\varepsilon} \right)^{0.65} \quad (3.405)$$

where

$$Ga_{L,m} = \frac{d_p^3 \rho_L (\rho_L g + \Delta P_{GL}/Z)}{\mu_L^2} \quad (3.406)$$

Here, the dynamic liquid holdup (in m^3/m^3) refers to the portion of the void (available) bed volume that has been occupied by the liquid. There are also correlations for the static holdup, that is, when the flow rate is zero after wetting. Dynamic liquid holdup is normally between 0.03 and 0.25, whereas the static liquid holdup is between 0.01 and 0.05, and for nonporous catalysts, usually $h_{e,s} < 0.05$ (see Section 3.6.3; Perry and Green, 1999).

Liquid holdup in packed bubble bed reactors

The Achwal–Stepanek correlation can be used in a bubble flow regime (Ramachandran and Chaudhari, 1984):

$$\frac{h_{g,e}}{\varepsilon} = \frac{2}{1 + (1 + 72.3 u_{sL}^{-0.229} \omega^{0.423})^{0.5}} \quad (3.407)$$

where

$$\omega = \frac{u_{sL}}{u_{sG}^2} \quad (3.408)$$

and $h_{g,e}$ is the total gas holdup based in the total volume of the empty bed (cm^3/cm^3). Then, the liquid holdup is given by

$$h_{e,t} = \varepsilon - h_{g,e} \quad (3.409)$$

In these equations, CGS units should be used.

Wetting efficiency in trickle bed reactors

Two kinds of wetting must be defined for porous catalysts— *internal wetting*, which is the amount of internal area wetted by the liquid, and *external wetting*, which is the amount of the

external area that is wetted by the flowing liquid (Gianetto *et al.*, 1978). Here, the external wetting efficiency, defined as the fraction of the external catalyst area that is covered by the flowing liquid film, is to be used (Burghardt *et al.*, 1995; Wu, 1996; Al-Dahhan *et al.* 1997).

$$f_w = \frac{a_{LS}}{a_u} \quad (3.410)$$

where a_{LS} is the effective mass transfer surface (liquid–solid interfacial area) per unit volume of reactor and a_u the total surface area of the particles per unit volume of reactor. The part that is not covered by the flowing liquid is covered with a thin film of liquid, frequently called the gas-covered part (Leung *et al.*, 1987). Thus, this part is not completely “dry”. Furthermore, capillary forces also hold liquid in the pores of the pellet surface exposed directly to the gas phase (Valerius *et al.*, 1996). This way, the reaction also takes place in pore openings, or in the liquid thin film of the “dry” part of the catalyst, where gas and liquid reactants can be found simultaneously. Finally, the internal volume of the particles has been shown to be completely filled with liquid (Leung *et al.*, 1987).

In a reactor completely filled with liquid, the wetting efficiency is 100% or, in other words, the external wetting of the catalyst is complete (Burghardt *et al.*, 1995). While it is true that when a fixed bed is completely filled with liquid wetting is complete (wetting efficiency is unity), the opposite is not true; in a trickle bed, a portion of the bed voids will be always occupied by the gas phase. Thus, while in a well-operated trickle bed the wetting efficiency could be unity, its total liquid holdup based on the void volume is always lower than the bed voidage, i.e. the bed is never completely filled with liquid.

The analysis of partial wetting involves two scales—the bed and the particle size. At the bed scale, deficiencies in the liquid distributor design are responsible for partial wetting, whereas at the particle scale, the partial wetting is due to the liquid mass velocity being insufficient to cover the catalyst particles with a continuous liquid film (Dudukovic *et al.*, 2002). During trickle flow, there are regions of nonirrigated, partially irrigated, and completely irrigated catalyst particles. Almost complete wetting is established at high liquid flow rates.

The catalyst wetting efficiency of the external catalyst surface can be calculated at atmospheric pressure using the correlation of El-Hisnawi *et al.* (1981; Wu, 1996):

$$f_w = 1.617 Re_L^{0.146} Ga_L^{-0.071} \quad (3.411)$$

where

$$Ga_L = \frac{d_p^3 \rho_L^2 g}{\mu_L^2} \quad (3.412)$$

The Reynolds number is based on superficial velocity and SI units are used.

In Figure 3.48, the effect of particle size, liquid density, and liquid dynamic viscosity on wetting efficiency is presented. It is evident that by increasing particle size and liquid density, and decreasing liquid dynamic viscosity, the wetting efficiency is decreased.

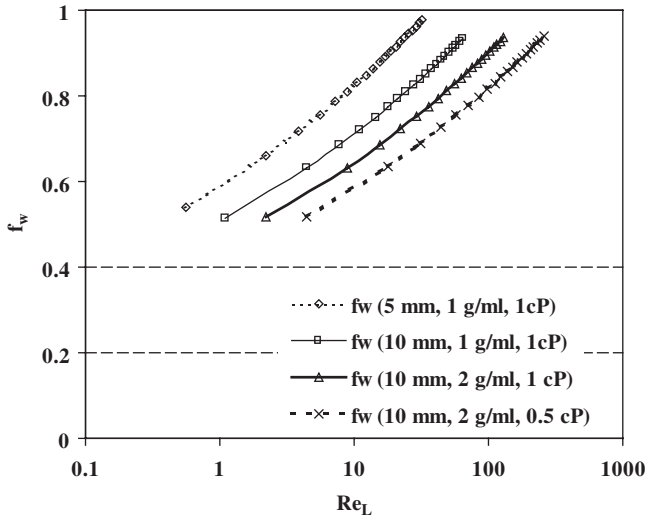


Figure 3.48 The effect of particle size, liquid density, and liquid dynamic viscosity on wetting efficiency.

In Figure 3.49, the minimum liquid superficial velocity versus particle size in order to have a wetting efficiency higher than 90% for water as liquid phase at 25 °C is presented.

For the typical case of water systems used in environmental applications, e.g. removal of SO₂ from gas streams, the minimum superficial velocity of water for a wetting efficiency higher than 90% v.s. can be correlated to particle size as follows:

$$u_s = 0.141d_p^{0.486} \quad (3.413)$$

where u_s is in cm/s and d_p is in mm. At high pressure, the correlation reported by Al-Dahhan *et al.* (1995) can be used (Wu, 1996):

$$f_w = 1.104Re_L^{1/3} \left\{ \frac{1 + [(\Delta P/Z)/(\rho_L g)]}{Ga_L} \right\}^{1/9} \quad (3.414)$$

The Reynolds number is based on superficial velocity and SI units are used. Another correlation is that of Burghardt *et al.* (1995):

$$f_w = 3.38Re_L^{0.222} Re_G^{-0.083} (Ga_L^*)^{-0.512} \quad (3.415)$$

where

$$Ga_L^* = \frac{d_p}{[\mu_L^2/(\rho_L^2 g)]^{1/3}} = Ga^{1/3} \quad (3.416)$$

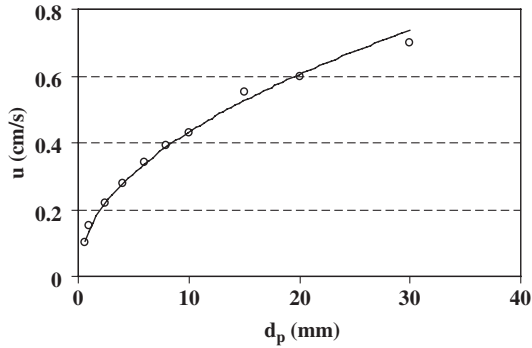


Figure 3.49 Minimum liquid superficial velocity versus particle size in order to have a wetting efficiency higher than 90% (liquid-phase: water at 25 °C).

The Reynolds number is based on superficial velocity. This equation is proposed for applications with organic liquids such as *n*-hexane, light petroleum fractions, and similar species. In the trickle flow regime, the increase in the gas flow rate leads to a decrease in the wetting efficiency (Burghardt *et al.*, 1995).

The importance of the wetting efficiency results mainly from the fact that it is closely related to the reaction yield, and more specifically to the catalyst effectiveness factor (Burghardt *et al.*, 1995). The reaction rate over incompletely covered catalytic particles can be smaller or greater than the rate observed on completely wetted packing, depending on whether the limiting reactant is present only in the liquid-phase or in both gas and liquid-phases.

If the reaction is liquid-limited and the liquid reactant is nonvolatile, then a decrease in the catalyst–liquid contacting reduces the surface for mass transfer between the liquid and the catalyst, causing a decrease in the reaction rate. But if reactants are volatile and significant heat effects exist, then a gas-phase reaction can occur on the dry solid area and consequently, a higher reaction rate is observed. A higher rate is achieved in this case where the gas reactant can access the catalyst pores from the externally dry area (Saroha and Nigam, 1996). Since for a completely wetted particle, the gaseous reactant must overcome both the gas–liquid and liquid–solid mass transfer resistances, partial wetting facilitates a much more effective transport of the gaseous reactant at the dry surface. It could be of some advantage to design a trickle-bed reactor for partial wetting in the case of gas-limited reactions. It is possible that some existing beds in industry owe their performance to this type of mechanism, whether by design or not. The main problem is to attain partial wetting without gross maldistribution, which usually leads to unpredictable and uncontrollable reactor performance. If large sections of the bed are completely dry, the reaction becomes severely limited by the liquid-phase reactant transfer. On the other hand, on dry areas well fed by volatile reactants, hot spots may occur.

Axial dispersion in trickle-bed reactors

The values of the axial dispersion coefficients in trickle beds are 1/3 – 1/6th those of the liquid flow alone at the same Reynolds numbers. A correlation by Michell and Furzer is available (Satterfield, 1975; Perry and Green, 1999):

$$Pe_L = \left(\frac{Re_L}{\lambda} \right)^{0.7} \left(\frac{\mu_L^2}{d_p^3 g \rho_L^2} \right)^{0.32} \quad (3.417)$$

where

$$\lambda = 0.68 Re_L^{0.8} \left(\frac{\mu_L^2}{d_p^3 g \rho_L^2} \right)^{0.44} a_u d_p \quad (3.418)$$

The Reynolds and Peclet numbers are based on the superficial liquid velocity, whereas d_p and a_u are expressed in cm and cm^2/cm^3 , respectively. For gas-phase dispersions, the Hochman–Effron correlation is available (Satterfield, 1975):

$$Pe_G = 1.8 Re_G^{-0.7} 10^{-\psi} \quad (3.419)$$

where

$$\psi = 0.005 Re_L \quad (3.420)$$

Here, the Reynolds and Peclet numbers are based on the superficial liquid velocity. This equation holds for $11 < Re_G < 22$ and $5 < Re_L < 80$.

Gas-phase dispersions have also been found to be one or two orders of magnitude less than in single-phase gas flows. Normally, in trickle beds, both phases are substantially in plug flow (Perry and Green, 1999). According to Satterfield (1975), the gas-phase dispersion is not ordinarily of concern in trickle-bed processing.

In trickle beds, the criterion of Mears can be used (Satterfield, 1975):

$$\frac{Z}{d_p} > \frac{20n}{Pe_L} \ln \left(\frac{C_i}{C_o} \right) \quad (3.421)$$

where C_i and C_o are the feed and outlet concentrations, respectively, and n , the reaction order. This criterion gives the minimum Z/d_p ratio required to hold the reactor length within 5% of that needed for plug flow.

Axial dispersion in packed bubble bed reactors

The Peclet number of the liquid is given by the Stiegel–Shah correlation (Ramachandran and Chaudhari, 1984):

$$Pe_L = 0.128\varepsilon Re_L^{0.245} Re_G^{-0.16} (a_u d_p)^{0.53} \quad (3.422)$$

In these equations, CGS units should be used. The Reynolds numbers are based on the superficial velocity.

Concerning packed bubble bed reactors, the evaluation of the Peclet number of the liquid-phase is important in order to decide if we have to use a plug- or backmixed-flow model. The liquid-phase can be considered well mixed if (Ramachandran and Chaudhari, 1980)

$$Pe_L \frac{Z}{d_p} \leq 4 \quad (3.423)$$

Note that in eqs (3.417) to (3.423) the Reynolds and Peclet numbers are based on the particle size, i.e. they are *particle* numbers.

Liquid maldistribution in trickle-bed reactors

Liquid-phase maldistribution has to be definitely taken into account during the design, scale-up, and operation of trickle-bed reactors (McManus *et al.*, 1993). Large parts of the bed can be bypassed by the liquid, being thus unexploited, due to a variety of reasons: ineffective liquid inlet distribution, packing anisotropy, and catalyst fines (Moller *et al.*, 1996). Specifically, the reactor is not fully utilized if some regions of the bed remain unwetted, since no reaction takes place there. However, if a sufficient amount of liquid is vaporized, the reaction still proceeds in these unwetted regions, but hot spots may be formed due to inefficient reaction-heat removal as a result of the absence of the liquid-phase. Proper design of liquid distributors and the installation of devices for redistribution of the liquid can deal with this problem.

In the trickle-flow regime, the liquid appears in the form of films, rivulets, pendular structures, and liquid pockets, the latter two being highly stagnant in nature. Even for an “ideal” liquid distribution at the top of the column, rivulets can follow a nonideal flow due to nonuniform porosity and the capillary pressure effect. Rivulets formed at low liquid flow rates gradually expand with increasing liquid flow rate. Large catalyst particles, uneven catalyst loading, and a nonuniform liquid inlet distribution enhance channeling. Prewetting of the bed is an important factor for improving the liquid distribution during operating conditions (Moller *et al.*, 1996). The knowledge of the distribution of wetting at bed-scale and particle-scale is essential for the sound prediction of the reactor performance.

Liquid and gas distribution in trickle-bed reactors

The simplest choice of a liquid distributor is a perforated plate with 10 openings/dm² (10 openings/15.5 in²), where the gas enters through several risers about 15 cm (5.9 in) high. More sophisticated distributors like caps are also used. The thickness of the liquid film developed in trickle-bed reactors has been estimated to vary between 0.01 and 0.2 mm (Perry and Green, 1999).

Burghardt *et al.* (1995) studied, among others, the liquid distribution using needle-type distributors in trickle beds and found that the density of the liquid feed points does have an important effect on the value of the liquid holdup, and thus on the performance of the reactor. They concluded that for a density of more than 5000 feeding points per square meter, the liquid holdup was stabilized.

Another typical liquid distributor, which is shown in Figure 3.50, essentially consists of a single parting box and weir troughs. Liquid loading, gas loading, and the column diameter determine the number of parting boxes and weir troughs.

3.7.4 External Mass transfer

In trickle beds, the gas-to-liquid, $k_{fg}a_{GL}$, and liquid-to-particle, $k_{fL}a_{LS}$, coefficients are used to represent the effect of the external mass transfer resistances. The interfacial areas a_{GL} and a_{LS} refer to the effective mass transfer surface per unit volume of empty reactor. Due to the fact that the coefficients k_{fg} and k_{fL} cannot be easily estimated independently from the corresponding interfacial areas a_{GL} and a_{LS} respectively, by simple experimental techniques, correlations are normally reported for the products $k_{fg}a_{GL}$ and $k_{fL}a_{LS}$ (Smith, 1981).

Gas-liquid mass transfer in trickle-bed reactors

The mass transfer coefficient in the gas-to-liquid interface $k_g a_{GL}$ is evaluated using the following correlation (Fogler, 1999):

$$k_g a_{GL} = 2 + 0.91\gamma^{2/3} \quad (3.424)$$

$$\gamma = 20.96 \left(\frac{\Delta P_G}{Z} \right) u_{sG} \quad (3.425)$$

where the pressure drop of the gas phase is in kPa/m, the superficial gas velocity in m/s, and the mass transfer coefficient in s^{-1} . As in the agitated three-phase mass transfer, the liquid-side mass transfer coefficient is the most significant coefficient in trickle beds, because the gas phase is often either a nearly pure component, e.g. hydrogenations, or a slightly soluble gas, e.g. oxidations, in these reactors (Smith, 1981).



Figure 3.50 Liquid distributors with single parting box and weir troughs.

In the trickle flow regime and in aqueous solutions, the Goto and Smith equation could be used (Smith, 1981; Fogler, 1999; Singh *et al.*, 2004):

$$\frac{k_{fg}a_{GL}}{D_g} = 7.8 \left(\frac{G_L}{\mu_L} \right)^{0.4} \left(\frac{\mu_L}{\rho_L D_g} \right)^{0.5} \quad (3.426)$$

CSG units are used in this equation.

In the trickle-flow regime and in organic solutions, the following equation can be used (Fogler, 1999):

$$\frac{k_{fg}a_{GL}}{D_g} = 16.8 \frac{Re_L^{0.25}}{Ga_L^{0.22}} \left(\frac{\mu_L}{\rho_L D_g} \right)^{0.5} \quad (3.427)$$

where:

$$k_{fg}a_{GL} = \text{in } s^{-1}$$

D_g = the molecular diffusivity of the diffusing component in the liquid-phase, cm^2/s

G_L = the superficial mass velocity of the liquid, $(g/cm^2 \text{ s})$.

CSG units are used in this equation. Furthermore, Ga_L is the Galileo number and Re_L is the particle Reynolds number based on the superficial liquid velocity.

$$Re_L = \frac{d_p u_{sL} \rho_L}{\mu_L} \quad (3.428)$$

$$Ga_L = \frac{d_p^3 \rho_L^2 g}{\mu_L^2} \quad (3.429)$$

Gas–liquid interfacial area in trickle-bed reactors

A correlation has been given by Charpentier (Perry and Green, 1999):

$$\frac{a_{GL}}{a_u} = 0.05 \left(\frac{\Delta P_{GL} \varepsilon}{a_u} \right)^{1.2} \quad (3.430)$$

where

$$a_u = \frac{6}{d_p} (1 - \varepsilon) \quad (3.431)$$

SI units should be used in this equation.

Gas–liquid mass transfer in packed bubble bed reactors

The gas–liquid mass transfer coefficient is given by Reiss correlation (Ramachandran and Chaudhari, 1984):

$$k_{fg}a_{GL} = 5.48 \times 10^{-3} \left(u_{sL} \frac{\Delta P_{GL}}{Z} \right)^{0.5} \quad (3.432)$$

In this equation, CGS units should be used.

Liquid–solid mass transfer in trickle-bed reactors

A correlation of Dharwadkar and Sylvester is suitable for trickle beds in the region $0.2 < Re_L < 2400$ (Perry and Green, 1999; Smith, 1981):

$$k_f a_{LS} = 1.637 a_u u_{sL} Re_L^{-0.331} \left(\frac{\rho_L D_g}{\mu_L} \right)^{2/3} \quad (3.433)$$

where:

D_g = the diffusion coefficient of gas in the liquid-phase

k_f = the liquid–solid mass transfer coefficient in m/s

a_u = the total external area of particles per unit volume of reactor.

SI units should be used in this equation. The following correlations were proposed by Fogler (1999):

$$\text{for } Re_L < 60: \frac{d_p k_f}{D_{fg}} = 0.815 Re_L^{0.8} Sc^{1/3} \quad (3.434)$$

$$\text{for } Re_L < 20: \frac{d_p k_f}{D_{fg}} = 0.266 Re_L^{1.15} Sc^{1/3} \quad (3.435)$$

Liquid–solid mass transfer in packed bubble bed reactors

The liquid–solid mass transfer coefficient is given by the Mochizuki–Matsui correlation (Ramachandran and Chaudhari, 1984):

for $Re_L < 5$,

$$\frac{k_f d_{pe}}{D_{fg}} = 48 \left(\frac{u_{sG} \rho_G d_{pe}}{\mu_G} \right)^{0.25} \quad (3.436)$$

where

$$d_{pe} = \frac{2}{3} d_p \frac{\varepsilon}{1 - \varepsilon} \quad (3.437)$$

for $Re_L > 5$,

$$\frac{k_f d_{pe}}{D_{fg}} = 0.75 \left(\frac{u_{sL} \rho_L d_{pe}}{\mu_L} \right)^{0.5} \left(\frac{\mu_L}{\rho_L D_{fg}} \right)^{0.33} (1 + 4\theta) \quad (3.438)$$

where

$$\theta = \frac{\left(\frac{u_{sG} \rho_G d_{pe}}{\mu_G} \right)^{0.55}}{\left(\frac{u_{sL} \rho_L d_{pe}}{\mu_L} \right)^{0.7}} \quad (3.439)$$

In these equations, CGS units should be used.

Liquid–solid interfacial area in trickle and packed bubble bed reactors

By definition, the total external particle area per reactor volume is (Smith, 1981)

$$a_u = \frac{A_{\text{particles, total}}}{V_{\text{BED, total}}} \quad (3.440)$$

The external area and the volume of a single spherical particle are

$$A_{\text{particle}} = \pi d_p^2 \quad (3.441)$$

$$V_{\text{particle}} = \frac{\pi d_p^3}{6} \quad (3.442)$$

The mass of the single particle is

$$M_{\text{particle}} = V_{\text{particle}} \rho_p \quad (3.443)$$

and the total mass of particles in the bed is

$$M_{\text{particles, total}} = V_{\text{particle}} \rho_p n_{\text{particles}} \quad (3.444)$$

From the definition of the bulk density,

$$\rho_b = \frac{M_{\text{particles, total}}}{V_{\text{BED, total}}} \Rightarrow V_{\text{BED, total}} = \frac{M_{\text{particles, total}}}{\rho_b} \quad (3.445)$$

then

$$V_{\text{BED, total}} = \frac{V_{\text{particle}} \rho_p n_{\text{particles}}}{\rho_b} = \frac{V_{\text{particle}} n_{\text{particles}}}{1 - \varepsilon} = \frac{\pi d_p^3 n_{\text{particles}}}{6(1 - \varepsilon)} \quad (3.446)$$

and finally,

$$a_u = \frac{A_{\text{particles,total}}}{V_{\text{BED,total}}} = \frac{\pi d_p^2 n_{\text{particles}}}{\left[\frac{\pi d_p^3 n_{\text{particles}}}{6(1-\varepsilon)} \right]} = \frac{6(1-\varepsilon)}{d_p} \quad (3.447)$$

3.8 TWO-PHASE, FLUID–SOLID FLUIDIZED BED REACTORS

3.8.1 General

The requirement for mechanical agitation can be avoided by using a fluidized bed reactor. In this type of reactor, the agitation and mixing are achieved by means of the moving liquid that carries the solids through the reactor or mixes with the particle phase. Thus, high heat and mass transfer rates are assured.

Fluidized beds are used in both catalytic and noncatalytic systems. Typical examples of catalytic uses are hydrocarbon cracking and reforming, oxidation of naphthalene to phthalic anhydride, and ammoxidation of propylene to acrylonitrile. Examples of noncatalytic uses are roasting of sulfide ores, coking of petroleum residues, calcination of ores, incineration of sewage sludge, and drying (Perry and Green, 1999).

Fluidized beds are also extensively used in wastewater treatment (aerobic and anaerobic treatment of municipal and industrial wastewaters). In this application, they are specifically called “biological fluidized beds.” Sand or granular activated carbon is usually used as a carrier for the growth of biological organisms. Fluidized beds are also found in adsorption and ion-exchange processes, where they are used if the influent contains significant amounts of suspended matter, or the solid is of very low size, like PAC. The upward superficial velocity of the gas is usually between 0.15 and 6 m/s. Generally, bed heights are not less than 0.3 m or more than 15 m (Perry and Green, 1999).

The employment of fluidized beds has many disadvantages. First of all, uniformity of temperature is achieved, even for highly exothermic reactions, since heat transfer is conducted by convection by means of the continuous motion of the particles. As a result, the heat-transfer coefficient from the fluidized bed to the heat-exchanger surface is tens of times that for a fixed bed. Intensive heat removal from the bed does not result in extinction of the reaction in the catalyst bed, and processing of gas mixtures with high concentrations of reactants does not lead to overheating of the catalyst. The isothermal conditions within each layer of the fluidized bed allow the automatic stabilization of the temperature regime inside the reactor. In the case of exothermic reactions, higher yields of products can be achieved in fluidized beds in comparison to fixed beds, due to temperature uniformity (Mukhlyonov *et al.*, 1979; McCabe *et al.*, 1983).

Another feature in favor of fluidized beds is the increased productivity of the catalyst—due to the smaller size of the particles, which in turn leads to better utilization of the surface area of the catalyst. In addition, the removal of solids from a fluidized bed is an easy task (Mukhlyonov *et al.*, 1979).

However, there are also some drawbacks associated with the use of fluidized beds. The complete mixing of the gas phase in this type of reactor decreases the process driving force. Moreover, the formation of large bubbles makes the process less efficient and difficult to handle. However, the main disadvantages of fluidized beds are the erosion of the reactor, the attrition of the solids, and the irregular conduction between the gas and the solid phase (McCabe *et al.*, 1983).

3.8.2 Hydraulics of fluidized beds

Fluidization regimes

The operation of fluidized-bed reactors can be seen as the transition region between continuous-stirred tank and packed-bed reactors. In a fluidized bed, a bed of solid particles is fluidized by the upward flow of the gas or liquid stream, which may be inert or contain material relevant to the reaction. The several fluidization regimes are shown in Figure 3.51.

Because of greater mechanical damage catalyst particles at high fluid velocities, and because of the poor retentivity of fines produced by attrition in beds of large particles, the use of small-diameter catalyst particles in fluidized beds is more usual (Gunn, 1968). In many applications of fluidization, the particles are in the range 30 –300 μm (Smith, 1981;

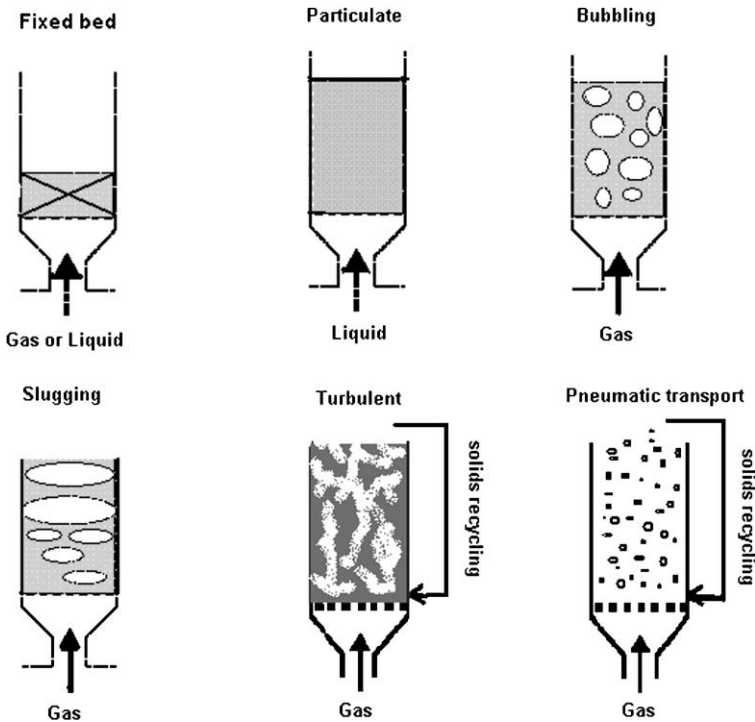


Figure 3.51 Fluidization regimes.

McCabe *et al.*, 1983). However, very small particles frequently act as if damp, even though dry, forming agglomerates or fissures in the bed, or spouting (Perry and Green, 1999). According to Gunn (1968), the grinding of solids to very small particle sizes is expensive, and as a result in many cases particles of sizes greater than 0.5 mm are used, as in the case of combustion of coal, or even as large as 6 cm in other applications (Perry and Green, 1999). However, large particles cause instability and result in slugging or massive surges.

For velocities higher than the minimum fluidization velocity, the appearance of fluidized beds is often quite different (McCabe, 1983). In most liquid systems, as the velocity is increased, the motion of the particles becomes more vigorous, whereas the bed density at a given velocity is the same in all sections of the bed. This is called “particulate fluidization” (or smooth fluidization/nonbubbling fluidization/homogeneous fluidization, Figure 3.51) and its characteristic is the large but uniform expansion of the bed at high velocities. This type of fluidization appears when the fluid and the solids have similar densities. In contrast, the density difference is very high when the fluid is a gas, which results in the so-called bubbling fluidization (or aggregative fluidization or heterogeneous fluidization)—the gas moves through the reactor either forming “bubbles” that contain relatively few solid particles, or as a continuous “dense” phase where the particle concentration is high (particulate or emulsion phase).

Although, in general, liquids are associated with particulate fluidization and gases with bubbling fluidization, it is not always the case. The density difference is the decisive parameter and thus bubbling fluidization appears in water systems of heavy solids, and particulate fluidization in high-pressure gas systems of fine particles (McCabe, 1983). However, a gas is usually the fluid in fluidized beds and the bubbling regime prevails (Smith, 1981). Industrial reactors, particularly for solid-catalyzed gas-phase reactions, often operate in that regime, with typical values of gas velocities in the range $5\text{--}30u_{\text{fm}}$ or even $250u_{\text{fm}}$, where u_{fm} is the minimum fluidization velocity (Levenspiel, 1972).

Another type of fluidization is the slugging fluidization. It represents the case where the bubbles form slugs of gas, usually when the size of the bubbles is about one-third the diameter of the bed. In general, slugging is undesirable because it is accompanied by high pressure, which may cause dangerous vibrations to the reactor.

Finally, it should be noted that in the case of multisized solids, the operating velocity should be higher than the minimum fluidization velocity of the largest particle and smaller than the elutriation velocity of the smallest particles.

Geldart (1973) classified powders into four groups according to their fluidization properties by air at ambient conditions. This classification is now used widely in all fields of powder technology.

- *Group A powders:* They give a region of nonbubbling fluidization beginning at the minimum fluidization velocity (u_{fm}), followed by bubbling fluidization as fluidizing velocity increases. This velocity limit is called minimum bubbling velocity ($u_{\text{bm}} > u_{\text{fm}}$). These materials have small mean particle size ($d_p < 30\ \mu\text{m}$) and/or low particle density ($< \sim 1.4\ \text{g/cm}^3$). Fluid-cracking catalysts are typically in this category.
- *Group B powders:* They give only bubbling fluidization. Bubbles are formed as soon as the gas velocity exceeds the minimum fluidization velocity ($u_{\text{bm}} = u_{\text{fm}}$). Most particles

of this group have sizes from 150 μm to 500 μm and densities from 1.4 to 4 g/cm^3 . Typically used group B materials are glass beads (ballotini) and coarse sand.

- *Group C powders*: Very fine, cohesive powders are classified into this category, which are incapable of fluidization in the strict sense and tend to rise as a slug of solids. Their sizes are usually less than 30 μm , and they easily give rise to channeling. Examples of group C materials are talc, flour, and starch.
- *Group D powders*: They are large particles that are distinguished by their ability to produce deep spouting beds (spurt or jet of gas through the bed). Roasted coffee beans, lead shot, and some roasted metal ores are examples of group D materials.

It is noteworthy that the group classification depends not only on the particle but also on the gas properties. Moreover, the above classification is related to the fluidization in the presence of air at ambient conditions. For a different fluid and operating conditions, a powder may appear in a different group. Thus, Figure 3.52 can be helpful in classifying a powder only for ambient conditions and with air as the fluid.

In Table 3.11, a summary of the typical properties of the different powder classes is shown.

Thus, a more general classification should be based on the fluidization regime rather than the particle and fluid characteristics. The following classification is introduced in the present book.

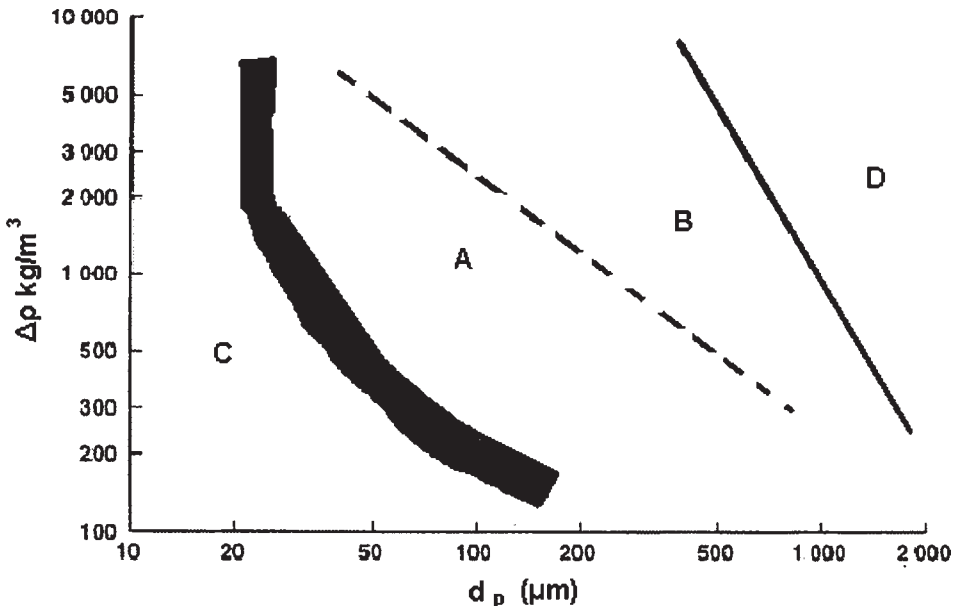


Figure 3.52 Geldart classification of particles, $\Delta\rho = \rho_p - \rho$.

Table 3.11

Geldart's (1973) classification of powders

Approximate particle size	A Aeratable 30–100 μm	B Bubbling 100–1000 μm C	C Cohesive <30 μm D	D Spoutable >1000 μm
Main characteristic	Ideal for fluidization; particulate fluidization is possible	Only bubbling fluidization	Difficult to fluidize	Coarse solids
Example	Cracking catalyst, milk powder	Building sand	Flour, cement	Gravel, coffee beans
Bed expansion	High	Moderate	Low because of channeling	Low
Bubble properties	Maximum bubble size is less than 10 cm	No limit to size, limited only by vessel size	No bubbles, formation of channels	No limit to size, limited only by vessel size
Solids mixing	High	Moderate	Very low	Low
Gas backmixing	High	Moderate	Very low	Low
Spouting	No	Only in shallow beds	No	Yes

- Type A fluidization:* This fluidization type consists of a nonbubbling region beginning at the minimum fluidization velocity (u_{fm}), and a bubbling region as fluidizing velocity increases. This velocity limit is called the minimum bubbling velocity ($u_{bm} > u_{fm}$). It is obvious that in the case of air as a fluidizing agent at ambient conditions, Group A particles will give a Type A fluidization. It should be noted that for Type A fluidization, the range of gas velocities over which nonbubbling fluidization occurs is small, and the minimum bubbling velocity is higher than the minimum fluidization velocity. Thus, the particulate phase is not under minimum fluidization condition when bubbling begins and thus its porosity is different from the porosity at minimum fluidization velocity (ϵ_{fm}). To distinguish the bubbling region in Type A fluidization from the Type B fluidization, the term “Type A bubbling fluidization” is used in the following sections. The region before bubbling will be referred to as “particulate fluidization”.
- Type B fluidization:* This fluidization type consists solely of a bubbling region. Bubbles are formed as soon as the gas velocity exceeds the minimum fluidization velocity ($u_{bm} = u_{fm}$). It is obvious that in the case of air as a fluidizing agent under ambient conditions, Group B particles will give a Type B fluidization. It should be noted that by definition, the minimum bubbling velocity in Type B fluidization is equal to the minimum fluidization velocity. Thus, the particulate phase is at minimum fluidization conditions when bubbling begins, and thus its porosity is equal to the porosity at minimum fluidization velocity (ϵ_{fm}). Type B fluidization is also referred to as “bubbling fluidization” in the following sections.

Pressure drop in fluidized beds

For a bed of particles of hydraulic density ρ_h (see Sections 3.9.6 and 3.9.8) fluidized by a fluid of density ρ to form a bed of depth Z and voidage ϵ , in a vessel of cross-sectional area A , the pressure drop is (Richardson and Zaki, 1954)

$$\frac{\Delta p}{Z} = (1 - \epsilon)(\rho_h - \rho)g \tag{3.448}$$

The fluid pressure drop across the bed versus superficial fluid velocity through the bed would appear as shown in Figure 3.53.

Figure 3.53 corresponds to an upflow operation, where the fluidized-bed pressure drop remains constant after the minimum fluidization velocity. On the contrary, if a fixed bed is operated in downflow mode, the pressure drop continues to increase by increasing the fluid velocity (dense line). This is the reason that fluidized beds may exhibit a lower pressure drop and thus the power cost is lower, for high fluid velocities.

The region BC is the fluidized-bed region where eq. (3.448) applies. The straight-line region OA is the fixed-bed region, where the particles do not move relative to one other. The pressure drop in this region is described by the Ergun equation (Perry and Green, 1999):

$$\frac{150\mu u_s}{\Phi_s^2 d_p^2} \frac{(1 - \epsilon)^2}{\epsilon^3} + \frac{1.75\rho u_s^2}{\Phi_s d_p} \frac{(1 - \epsilon)}{\epsilon^3} = \frac{-\Delta p}{Z} \tag{3.449}$$

or

$$\left[\frac{150\mu G}{\Phi_s^2 d_p^2} \frac{(1 - \epsilon)^2}{\epsilon^3} + \frac{1.75G^2}{\Phi_s d_p} \frac{(1 - \epsilon)}{\epsilon^3} \right] \frac{1}{\rho} = \frac{-\Delta p}{Z} \tag{3.450}$$

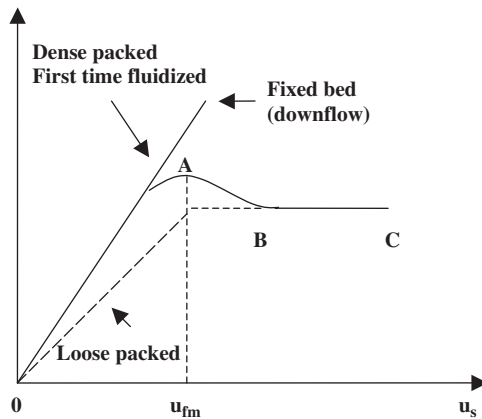


Figure 3.53 The fluid pressure drop versus its velocity for packed and fluidized beds.

where:

- d_p = the diameter for spherical particles or the nominal diameter for irregular-shaped particles
- ρ = the density of the fluid
- g = the gravity acceleration constant (=9.81 m²/cm)
- μ = the dynamic viscosity of the fluid
- ε = the fixed-bed voidage
- u_s = the superficial fluid velocity
- Φ_S = the sphericity of the particle
- G = the superficial mass velocity.

Note that while the fluid density may be a function of the pressure in the bed in a compressible flow, the superficial mass velocity is constant. The Ergun equation in the form given in eq. (3.450) is more convenient when analyzing the effects of pressure drop in the fluid density.

Minimum fluidization velocity

The minimum fluidization velocity can be calculated if the pressure drop in a fluidized bed (eq. (3.448)) is set equal to the pressure drop in a fixed bed (eqs. (3.449) and (3.450)):

$$\frac{150\mu u_{fm}}{\Phi_s^2 d_p^2} \frac{1-\varepsilon_{fm}}{\varepsilon_{fm}^3} + \frac{1.75\rho u_{fm}^2}{\Phi_s d_p} \frac{1}{\varepsilon_{fm}^3} = g(\rho_h - \rho) \quad (3.451)$$

or

$$\left[\frac{150\mu G_{fm}}{\Phi_s^2 d_p^2} \frac{1-\varepsilon_{fm}}{\varepsilon_{fm}^3} + \frac{1.75G_{fm}^2}{\Phi_s d_p} \frac{1}{\varepsilon_{fm}^3} \right] \frac{1}{\rho} = g(\rho_h - \rho) \quad (3.452)$$

where:

- ρ_h = the hydraulic density of the particles
- G_{fm} = the superficial mass velocity based on the minimum fluidization velocity
- ε_{fm} = the voidage at minimum fluidization.

This equation can be expressed as a function of the minimum Reynolds number for fluidization (Re_{fm}) and the Archimedes number (Ar):

$$Ar = 150 \frac{(1-\varepsilon_{fm})}{\Phi_s^2 \varepsilon_{fm}^3} Re_{fm} + 1.75 \frac{1}{\Phi_s \varepsilon_{fm}^3} Re_{fm}^2 \quad (3.453)$$

where

$$Ar = \frac{d_p^3 \rho (\rho_h - \rho) g}{\mu^2} \quad (3.454)$$

and

$$Re_{fm} = \frac{u_{fm} \rho d_p}{\mu} = \frac{G_{fm} d_p}{\mu} \quad (3.455)$$

Note that as in the case of G , Re_{fm} is constant when changing the fluid density.

Wen and Yu (1966) correlated the terms containing the bed voidage at incipient fluidization for $0.0508 < d_p < 50$ mm, $0.385 < \epsilon_{fm} < 0.935$, $0.136 < \Phi_S < 1$, and particle diameter to column diameter ratio ranging from 0.000807 to 0.25:

$$\frac{(1 - \epsilon_{fm})}{\Phi_S^2 \epsilon_{fm}^3} \cong 11 \quad (3.456)$$

$$\frac{1}{\Phi_S \epsilon_{fm}^3} \cong 14 \quad (3.457)$$

Then, the minimum fluidization velocity can be calculated using the equation

$$Ar = 1650 Re_{fm} + 24.5 Re_{fm}^2 \quad (3.458)$$

This equation needs iteration to be solved for the minimum fluidization velocity. Wen and Yu (1966) proposed the following correlation for the direct evaluation of the minimum fluidization velocity (Wen and Yu, 1966):

$$Re_{fm} = (1136 + 0.0408 Ar)^{0.5} - 33.7 \quad (3.459)$$

It should be noted that eqs. (3.458) and (3.459) do not give the same results. In the case of the gas fluidization equation, eq. (3.459) is considered to be more suitable for particles larger than 100 μm and $0.1 < Re_{fm} < 1000$, whereas the minimum fluidization velocity for particles less than 100 μm is better estimated using the correlation of Bayens (Rhodes, 1998; Abrahamsen and Geldart, 1980):

$$u_{fm} = \frac{[(\rho_h - \rho_G)g]^{0.934} d_p^{1.8}}{1110 \mu_G^{0.87} \rho_G^{0.066}} \quad (3.460)$$

Here, d_p is the mean sieve size of the powder (SI units).

On the fluid density variance

Eqs. (3.448) and (3.449) assume constant fluid density, in other words, they hold for incompressible flow. However, in compressible flow, the density of the fluid is a function of the pressure drop (see Section 5.3.4). Then, we have to use the differential forms of

eqs. (3.448) and (3.449), which lead to the same equation for the minimum fluidization velocity. Still, we need a representative value for the fluid density, which appears in the minimum fluidization equation (eqs. (3.451) and (3.452)). For this purpose, we can use the equations developed in Section 5.3.4 for nonisobaric fixed bed operation:

$$\frac{P}{P_i} = \left[1 + \left(\frac{dP}{dZ} \right)_i \frac{2Z}{P_i} \right]^{0.5} \quad (3.461)$$

where approximately $Z = Z_{\text{fm}}$. Then,

$$\frac{\rho}{\rho_i} = \frac{P}{P_i} \quad (3.462)$$

Further, an average value of fluid density can be used:

$$\bar{\rho} = \frac{\rho + \rho_i}{2} \quad (3.463)$$

A trial-and-error procedure is needed. Note that when using correlations for the determination of minimum fluidization velocity (or other relevant parameters) as in eqs. (3.459) and (3.460), it is reasonable to assume that the fluid-phase density involved is measured at inlet or ambient conditions, and thus no correction is needed. This is why, in analogy to the case of the hydraulic density of solids (Section 3.9.6), the minimum fluidization velocity is directly correlated to the inlet fluid density.

Minimum voidage at incipient fluidization

The bed voidage at incipient fluidization can be evaluated using the approximations of Wen and Wu (1996):

$$\varepsilon_{\text{fm}} = \left(\frac{0.071}{\Phi_s} \right)^{1/3} \quad (3.464)$$

$$\varepsilon_{\text{fm}} = \left(\frac{0.091(1 - \varepsilon_{\text{fm}})}{\Phi_s^2} \right)^{1/3} \quad (3.465)$$

In the case of spherical particles, the first equation results in the value 0.414, which is very close to the typical voidage of a fixed bed consisting of spherical particles (0.39–0.40). This is the reason that the voidage at incipient fluidization is considered to be approximately equal to the fixed-bed voidage for spherical particles. Using the Wen–Yu equations (3.456) and (3.457), the voidage at incipient fluidization is found to be between 0.41 and 0.5. For the determination of the minimum fluidization velocity, the fixed-bed porosity ε is often used instead of the corresponding voidage at minimum fluidization ε_{fm} . In this way, we can obtain a crude value of u_{fm} . However, in practice, the voidage at the onset of fluidization may be greater than ε . When the particles are large, the predicted porosity could

be too small. If a value below about 0.4 is predicted, it should be considered suspicious. Values around 0.5 are typical.

By using the experimental data of Wen and Yu (1996), it can be shown that the proposed correlation predicts the lower values of ε_{fm} well, while it fails to predict higher ε_{fm} values. Furthermore, in a number of published experimental data for gas–solid fluidized beds presented by Broadhurst and Becker (1975), ε_{fm} is considerably influenced by particle size and it is higher for lower particle sizes. The Wen–Yu equations have been tested for $0.05 < d_p < 50$ mm, resulting in an average standard deviation of 34%. However, the deviation is 21% for $d_p > 0.5$ mm and 38% for $d_p < 0.5$ mm. It seems that the effect of particle size is the reason for the higher deviation of the Wen–Yu equations. Thus, it can be stated that these equations could be used safely for particle sizes greater than 0.5 mm. Broadhurst and Becker (1975) proposed the following correlation for gas–solid fluidized beds, which takes into account the effect of particle size on ε_{fm} :

$$\varepsilon_{fm} = 0.586\Phi_S^{-0.72} \left[\frac{\mu^2}{\rho_G d_p^3 g (\rho_p - \rho_G)} \right]^{0.029} \left(\frac{\rho_G}{\rho_p} \right)^{0.021} \quad (3.466)$$

This equation has been derived for

$$0.5 < \Phi_S < 1$$

$$500 < \frac{\rho_p}{\rho_G} < 50000$$

$$1 < \left[\frac{\mu^2}{\rho_G d_p^3 g (\rho_p - \rho_G)} \right]^{-1} < 10^5$$

Eq. (3.466) has correlated several experimental data giving a maximum deviation of 0.04, for low particle sizes (< 0.4 mm diameter). This correlation is valid only in the creeping flow regime, i.e. $Re_{fm} < 10$, for relatively small particles. The minimum predicted value of porosity is 0.37. Thus, the lower values predicted by the Broadhurst–Becker equation should not be used. This is the case of large particles, where the Wen–Yu correlations should be used.

Using the above equation for air at 20 °C and hydraulic density within 1500–4000 kg/m³, the porosity at minimum fluidization is

- within the range 0.4–0.5 for particle size of 0.03–0.25 mm and $\Phi_S = 1$
- within the range 0.56–0.71 for particle size of 0.03–0.25 mm and $\Phi_S = 0.6$

An equation similar to that of Wen and Yu that has been proposed for the liquid–solid fluidization is that of Limas–Ballesteros (Lee *et al.*, 2005):

$$\varepsilon_{fm} = \frac{0.42}{\Phi_S^{0.376}} \quad (3.467)$$

If we consider a total mass balance of the solids, assuming that no solids are entrained and carried out of the bed in the case of fluidization, the total mass of the solids in the fixed bed is constant and given by

$$M_{\text{tot}} = \rho_p(1 - \varepsilon)AZ \quad (3.468)$$

where A is the cross-sectional area of the bed. Under different bed conditions, the porosity and the bed height vary but the rest of the terms in this equation are constant. This means that the porosities and the bed heights of fixed and fluidized bed are related by

$$Z_f(1 - \varepsilon_f) = Z(1 - \varepsilon) \quad (3.469)$$

At the minimum fluidization condition,

$$Z_{\text{fm}} = Z \frac{1 - \varepsilon}{1 - \varepsilon_{\text{fm}}} \quad (3.470)$$

where Z_{fm} is the bed height at incipient fluidization.

Bed voidage in particulate fluidization

In particulate fluidization, for $u_s > u_{\text{fm}}$ and $Re_p < 10$, the relationship between the fluidized bed voidage and velocity can be derived from the Ergun equation (McCabe *et al.*, 1983):

$$\frac{150\mu u_s}{\Phi_s^2 d_p^2 g(\rho_h - \rho)} = \frac{\varepsilon_f^3}{1 - \varepsilon_f} \quad (3.471)$$

The expanded bed height is

$$Z_f = Z \frac{1 - \varepsilon}{1 - \varepsilon_f} \quad (3.472)$$

where Z is the fixed bed height and ε is the fixed bed voidage.

For relatively large particles (of several millimeters) in water, the equation proposed by Lewis, Gilliland, and Bauer (LGB) can be used (McCabe *et al.*, 1983):

$$\varepsilon_f = \left(\frac{u_s}{u_{\text{fm}}} \right)^{1/m} \varepsilon \quad (3.473)$$

The exponent m is a function of particle Reynolds number based on the minimum fluidization velocity. It can be estimated by the following correlation:

$$m = 4.21 Re_{\text{fm}}^{-0.0804} \quad (3.474)$$

for $1 < Re_{fm} < 1000$. In this region, m is approximately between 2.5 and 4.2. The value of m is between 4.2 and 4.5 for $0.1 < Re_{fm} < 1$ and an average value of 4.35 can be used as a first approximation.

Pavlov (1979) gives a simpler equation based on the Archimedes number (Ar), for $u_{bm} > u_s > u_{fm}$:

$$\varepsilon_f = \left(\frac{18Re_p + 0.36Re_p^2}{Ar} \right)^{0.21} \quad (3.475)$$

It is easy to show that for the same superficial velocity, smaller particles result in higher bed porosity.

Bed voidage in type B fluidization

The following analysis holds for Type B fluidization and for Type A bubbling fluidization, when the region of particulate fluidization is so small that it can be ignored. In the framework of the two-phase model (see the subsection Hydrodynamic modeling of bubbling fluidization), the bed expansion in terms of the fraction of the bed occupied by bubbles ε_{bub} is

$$\varepsilon_{bub} = \frac{Z_f - Z_{fm}}{Z_f} = \frac{u_s - u_{fm}}{u_{bub}} \quad (3.476)$$

where:

- Z_{fm} = the bed height at incipient fluidization
- Z_f = the fluidized bed height
- u_{bub} = the mean rise velocity of a bubble in the bed.

According to Grace (1984), in practice, the bubble volume fraction ε_{bub} never exceeds 0.4. If a higher value is calculated, ε_{bub} should be taken as 0.4, or the bed may be operating in the turbulent fluidization regime, invalidating the basis of the two-phase and bubbling bed models (see the subsection Hydrodynamic modeling of bubbling fluidization).

Then,

$$Z_f = \frac{Z_{fm}}{1 - \varepsilon_{bub}} \quad (3.477)$$

The mean bed voidage is

$$(1 - \varepsilon_f) = (1 - \varepsilon_{bub})(1 - \varepsilon_{fm}) \quad (3.478)$$

where ε_{fm} is the bed voidage at the minimum fluidization value of velocity. Then, in order to evaluate the fluidized bed height and the corresponding voidage, the u_{bub} value is needed (see the subsection Hydrodynamic modeling of bubbling fluidization).

The use of internals can improve the smoothness of fluidization, when this is desirable. The use of vertical cylindrical tubes immersed in the bed is a representative example. These tubes are sufficiently long to extend from the distributor to the top of the bed. For this type of beds and for perforated plate distributors, the following correlation can be used for the estimation of fluidized-bed porosity in gas–solid fluidization (Hilal, 2000):

$$\frac{u_s - u_{fm}}{u_{ter} - u_{fm}} = \left(\frac{\varepsilon_f - \varepsilon_{fm}}{1 - \varepsilon_{fm}} \right)^w \quad (3.479)$$

where:

$$w = 1.28 + 0.00033P^3 \quad (3.480)$$

where u_{ter} is the terminal velocity of the particles and P is the hole pitch of the perforated plate. A square pitch of 7–12 mm is typical.

Criteria for distinguishing fluidization regimes

The minimum bubbling velocity for Group A particles (or more generally, for Type A fluidization) and gas–solid systems is (Abrahamsen and Geldart, 1980; Ye *et al.*, 2005)

$$u_{bm} = \frac{2.07\rho_G^{0.06}d_p\exp(0.716X_{45})}{\mu_G^{0.347}} \quad (3.481)$$

where X_{45} is the fraction of particles with size smaller than 45 μm and d_p the sieve diameter. In this equation, SI units should be used. In the region of Group B particles (for ambient conditions and air as gas phase) or in the Type B fluidization regime (for other conditions), where $u_{bm} = u_{fm}$, the above equation results in $u_{bm} < u_{fm}$, which is not acceptable. For example, for ambient conditions and air as gas, if $d_p = 0.24$ mm and $\varepsilon_h = 1500$ kg/m^3 , we are in the region of Group B particles (Figure 3.52) and the result is $u_{bm} = 0.022$ m/s, while $u_{fm} = 0.028$ m/s.

Using the Bayens equation (3.460) and eq. (3.481), the ratio of minimum bubbling velocity to minimum fluidization velocity is

$$\frac{u_{bm}}{u_{fm}} = \frac{2300\rho_G^{0.126}\mu_G^{0.523}\exp(0.716X_{45})}{d_p^{0.8}(\rho_p - \rho_G)^{0.934}g^{0.934}} \quad (3.482)$$

For type B fluidization, we obtain ($\frac{u_{bm}}{u_{fm}} = 1$), while for type A fluidization ($\frac{u_{bm}}{u_{fm}} > 1$). In the second case, the fluidization regime is

- particulate, if $u_{fm} < u_s < u_{bm}$
- type A bubbling, if $u_s > u_{bm}$

In Figure 3.54, the ratio of the minimum bubbling velocity to the minimum fluidization velocity is plotted for air at 20 °C, and ρ_p is 1000–3000 kg/m^3 . From Figure 3.52 and the

specific density difference, the particle size is kept within the appropriate region, within $0.035 < d_p < 0.1$ mm, depending on the density difference, to be in the Group A particles regime (Type A fluidization). Since the minimum bubbling velocity could not be less than the minimum fluidization velocity, the ratio is set equal to unity when $u_{bm} < u_{fm}$.

In Figure 3.54, it is clear that while approaching the limit of Group B particles (large particle density and particle size), u_{bm} approaches u_{fm} , as expected. On the other hand, the difference between the two velocities is increased constantly for smaller particles and lower particle density, while it is very high for $d_p < 0.045$ mm where $X_{0.45} = 1$. This could be useful in the case where an expanded region of particulate fluidization is desirable in gas–solid systems.

Since in the region between u_{fm} and u_{bm} the fluidization is particulate, eq. (3.475) could be used for the determination of bed voidage at minimum bubbling velocity, setting $u_s = u_{bm}$. In Figure 3.55, ε_{bm} and ε_{fm} are compared to each other for Group A particles—an air system at 20 °C ($\Phi_s = 1$, $\varepsilon = 0.4$, $\rho_p = 1000\text{--}3000$ kg/m³, $X_{45} = 0$ for $d_p > 0.045$ mm, and $X_{45} = 1$ for $d_p < 0.045$ mm). From Figure (3.52) and the specific density difference, the particle size is kept within the appropriate region, within $0.035 < d_p < 0.23$ mm, depending on the density difference, to be in the Group A particles regime.

Pavlov's equation (3.475) is used for voidage determination at minimum bubbling conditions (for $u_s = u_{bm}$), and since $d_p < 0.5$ mm, the Broadhurst–Becker equation (3.466) is used for ε_{fm} . For a wide range of particle sizes, the values of ε_{fm} and ε_{bm} are close to each other, within a ratio between 0.95 and 1.1 for all particle densities. Values of $\varepsilon_{bm}/\varepsilon_{fm}$ ratio

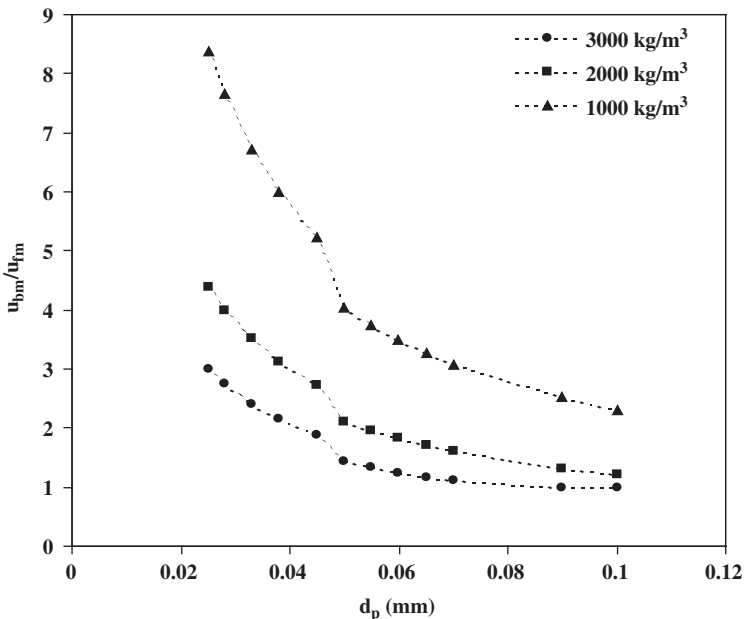


Figure 3.54 Ratio of minimum bubbling velocity to minimum fluidization velocity. For $d_p > 0.045$ mm, $X_{45} = 0$ and for $d_p < 0.045$ mm, $X_{45} = 1$ is assumed.

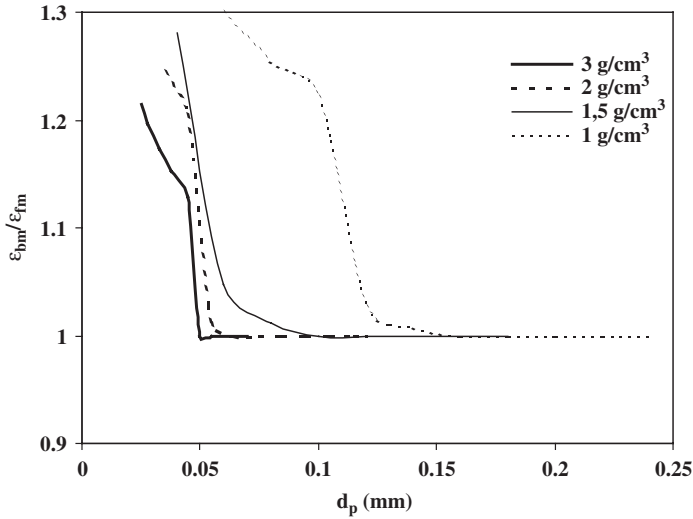


Figure 3.55 The values of ε_{bm} and ε_{fm} versus d_p .

lower than 1 are not acceptable since ε_{bm} cannot be lower than ε_{fm} . In these cases, the ratio is set equal to unity.

Foscolo and Gibilaro (1984) proposed the following criterion for both gas and liquid–solid systems:

$$\frac{(gd_p)^{0.5}}{u_{\text{ter}}}\left(\frac{\rho_h - \rho_f}{\rho_h}\right)^{0.5} = 0.56n(1 - \varepsilon_t)^{0.5}\varepsilon_t^{n-1} \quad (3.483)$$

where ε_t is the voidage at which a transition from particulate to bubbling fluidization occurs, and n is the exponent in the Richardson–Zaki equation ($2.4 \leq n \leq 4.8$). In practice, ε_t is taken equal to ε_{bm} . The terminal velocity u_{ter} can be estimated using Table 3.12.

The Foscolo–Gibilaro equation indicates multiple solutions for ε_t . However, two solutions at maximum are to be expected in the operating range between 0.4 and 1. The second solution exists because bubbling beds are known to revert to particulate behavior at high voidages (Foscolo and Gibilaro, 1984).

To demonstrate the behavior of the Foscolo–Gibilaro equation, the following form is used:

$$FC = [0.56n(1 - \varepsilon_t)^{0.5}\varepsilon_t^{n-1}] - A = 0 \quad (3.484)$$

where

$$A = \frac{(gd_p)^{0.5}}{u_{\text{ter}}}\left(\frac{\rho_h - \rho_f}{\rho_h}\right)^{0.5} \quad (3.485)$$

Table 3.12Equations to calculate n and u_{ter} for different Re_{ter}

Re_{ter}	n	u_{ter}
$Re_{\text{ter}} < 0.2$	$4.65 + 20(d_p/D) \approx 4.65$	$\frac{d_p^2(\rho_p - \rho_f)g}{18\mu}$
$0.2 < Re_{\text{ter}} < 1.0$	$[4.35 + 1.75(d_p/D)]Re^{-0.03} \approx 4.35 \cdot Re^{-0.03}$	$\frac{d_p^2(\rho_p - \rho_f)g}{18\mu}$
$1.0 < Re_{\text{ter}} < 2.0$	$[4.45 + 18(d_p/D)]Re^{-0.1} \approx 4.45Re^{-0.1}$	$\frac{d_p^2(\rho_p - \rho_f)g}{18\mu}$
$2.0 < Re_{\text{ter}} < 200$	$[4.45 + 18(d_p/D)]Re^{-0.1} \approx 4.45Re^{-0.1}$	$0.153 \frac{d_p^{1.14} [(\rho_p - \rho_f)g]^{0.71}}{\mu^{0.43} \rho_f^{0.29}}$
$200 < Re_{\text{ter}} < 500$	$4.4Re^{-0.1}$	$0.153 \frac{d_p^{1.14} [(\rho_p - \rho_f)g]^{0.71}}{\mu^{0.43} \rho_f^{0.29}}$
$Re_{\text{ter}} > 500$	2.39	$1.74 \left[\frac{d_p(\rho_p - \rho_f)g}{\rho_f} \right]^{0.5}$

In Figure 3.56, eq. (3.484) is plotted for several values of A found in the original paper of Foscolo and Giliardo (1984) (0.1–0.4) and for $n = 3$ representing an intermediate value of Re_{ter} ($0.2 < Re_{\text{ter}} < 500$).

The roots of the equation represent the values of ε_c . So,

(a) If $1 > \varepsilon_{t2} > \varepsilon_{t1} > \varepsilon_{\text{fm}}$, the fluidization is of Type A and more specifically,

- particulate, in the regions $\varepsilon_{\text{fm}} < \varepsilon_f < \varepsilon_{t1}$ and $\varepsilon_f > \varepsilon_{t2}$
- type A bubbling, in the region $\varepsilon_{t1} < \varepsilon_f < \varepsilon_{t2}$

This is the case of $A = 0.4$ and $A = 0.3$

(b) If $\varepsilon_{t1} < 0.4$ (or generally, lower than ε_{fm}), the fluidization is of Type A and more specifically,

- particulate, in the region $\varepsilon_{\text{fm}} < \varepsilon_f < \varepsilon_{t2}$
- Type A bubbling, in the region $\varepsilon_f > \varepsilon_{t2}$

This is the case of $A = 0.1$.

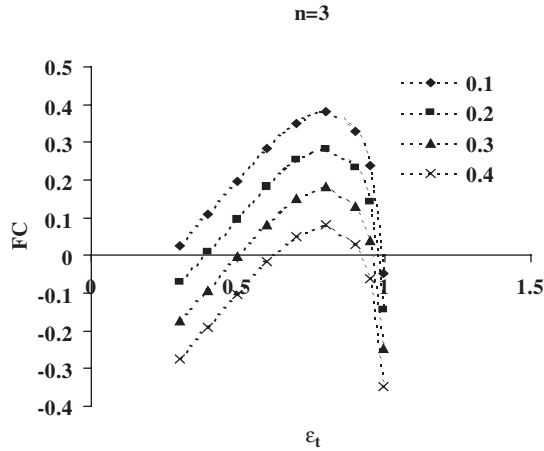


Figure 3.56 Foscolo and Gibilaro criterion ($n = 3$).

(c) If $\varepsilon_{t1} = \varepsilon_{fm}$, the fluidization regime is

- particulate, in the region $\varepsilon_f > \varepsilon_{t2}$
- Type B fluidization, in the region $\varepsilon_{fm} < \varepsilon_f < \varepsilon_{t2}$

This is the case of $A = 0.2$ (assuming $\varepsilon_{fm} = 0.4$).

As can be shown for several combinations of A and n , in the cases (b) and (c), ε_{t2} is typically very high (>0.98), and the regime is practically particulate and of Type B fluidization respectively, for the whole region following the incipient fluidization condition. The same holds for case (a), where in practice, reversion from Type A bubbling to particulate fluidization is rather rare and is expected only for high values of A , typically in the region of 0.4 and higher.

The determination of the minimum bubbling condition is rather difficult because a trial-and-error procedure is needed for the evaluation of n and u_{ter} and subsequently, the nonlinear Foscolo and Gibilaro equation has to be solved. Furthermore, in order to find the operating fluidization regime, ε_f is needed, which in turn means that the fluidization regime has to be known. To avoid this situation, the resulting characteristic voidages should be “transformed” into the corresponding characteristic velocities using, for example, Pavlov’s equation. Then, using the known operating superficial velocity u_s , the operating fluidization regime can be found.

Thus, the Foscolo–Gibilaro criterion is useful only when it is desirable to find the expected regimes for a specified fluidization system.

The following criterion could also be used to find the expected fluidization regime for a specified system. Experiments on particulate fluidization show that particle and fluid densities and fluid viscosity are the most significant factors affecting fluidization behavior. On the basis of this, a dimensionless discrimination number D_n has been suggested to

determine the fluidization pattern, for both liquid and gas–solid systems (Liu *et al.*, 1996; Li *et al.*, 2003).

$$D_n = \left(\frac{Ar}{Re_{fm}} \right) \left(\frac{\rho_p - \rho_f}{\rho_f} \right) \quad (3.486)$$

In this equation, Ar is based on the particle and not on the hydraulic density. Experiments showed that

- Particulate fluidization exists for $0 < D_n < 10^4$.
- Transitional fluidization exists for $10^4 < D_n < 10^6$. “Transitional fluidization” includes the behavior of Type A fluidization.
- Type B fluidization exists for $D_n > 10^6$.

To distinguish between particulate and bubbling fluidization, the Romero and Johnson criterion is useful (Kwauk and Liu, 2000):

particulate fluidization exists if

$$Fr_{fm} Re_{fm} \frac{\rho_h - \rho_f}{\rho_f} \frac{Z_{fm}}{D} < 100 \quad (3.487)$$

bubbling fluidization exists if

$$Fr_{fm} Re_{fm} \frac{\rho_h - \rho_f}{\rho_f} \frac{Z_{fm}}{D} > 100 \quad (3.488)$$

where Fr_{fm} is the Froude number at incipient fluidization:

$$Fr_{fm} = \frac{u_{fm}^2}{d_p g} \quad (3.489)$$

where:

- d_p = the particle diameter
- D = the bed diameter
- Z_{fm} = the fixed bed height at incipient fluidization.

Another simpler criterion is that of Wilhelm and Kwauk (Kwauk and Liu, 2000), which is based solely on the Fr_{fm} number—if it is lower than 0.13, particulate fluidization exists and if it is higher than 1.3, bubbling fluidization exists.

Finally, in gas–solid fluidization, slugging will not occur provided the following criterion is satisfied (Beyens and Geldart, 1974):

$$\frac{Z_{fm}}{D} \leq \frac{1.9}{(\rho_p d_p)^{0.3}} \quad (3.490)$$

where d_p is the mean sieve size of the particles.

If the bed is deeper than this critical height, slugging will take place for a gas velocity higher than the minimum velocity of slugging:

$$u_{sm} = u_{fm} + 0.16(1.34D^{0.175} - Z_{fm})^2 + 0.07(gD)^{0.5} \quad (3.491)$$

where Z_{fm} is the height of the bed at incipient fluidization. In these equations, SI units should be used.

Finally, in beds exhibiting low ratios of diameter to height, the bubbles can grow and become as large as the cross-section. As a result, the bubbles move through the bed separated by slugs of solids. This phenomenon is called “slugging” and has to be generally avoided because it can lead to pressure fluctuations and entrainment of solids as well (McCabe *et al.*, 1983).

Hydrodynamic modeling of bubbling fluidization (type B fluidization)

The modeling of fluidized beds begins with the analysis of the two most important hydrodynamic flow models presented by Davidson (Davidson and Harrison, 1963) and Kunii and Levenspiel (1968).

Two-Phase theory of Davidson According to the two-phase theory, two phases exist in the bubbling fluidized bed: (a) the bubbling phase consisting of gas bubbles, and (b) the particulate phase, namely the solids around the bubbles. The particulate phase is alternatively called “the emulsion phase.” Bubbles stay in the bubble phase and penetrate only a small distance into the emulsion phase. This zone of penetration is called “cloud” since it envelops the rising bubble.

If the gas flow rate is higher than that required for the onset of fluidization, the gas will move through the bed in the form of bubbles. So, in bubbling fluidization, for a gas velocity above the minimum bubbling velocity, the formation of bubbles will lead to a bed expansion. In such a case, the condition of the particulate phase is unchanged and thus, the porosity of the particulate phase is constant after this point. At gas flow rates above the point of minimum fluidization, the fluidized bed resembles with a boiling liquid—bubbles of gas rise rapidly and burst on the surface, and the emulsion phase is thoroughly agitated. Davidson and Harrison (1963) were the first to state that the fluidized bed had to be treated as a two-phase system consisting of an emulsion phase and a bubble phase (often called the dense and lean phases, respectively). This was the basis of the so-called two-phase model (Figure 3.57).

Focusing on the bubbles, it should be mentioned that they are not exactly spherical. They contain very small amounts of solids and have an approximately hemispherical top and a pushed-in bottom. Each bubble of gas has a wake that contains a significant amount of solids. These characteristics are illustrated in Figure 3.58. Consequently, during their journey in the reactor, the bubbles carry an amount of solids. The net flow of the solids in the emulsion phase must therefore be downward. The gas within a particular bubble remains largely within that bubble and only a small part of it penetrates a short distance into the surrounding emulsion phase, forming the so-called cloud.

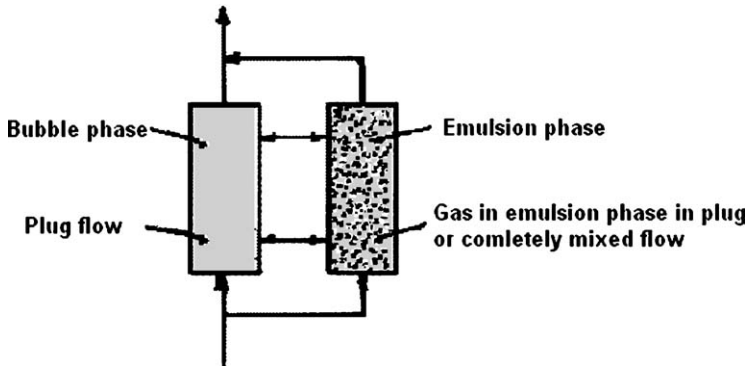


Figure 3.57 General representation of the two-phase model.

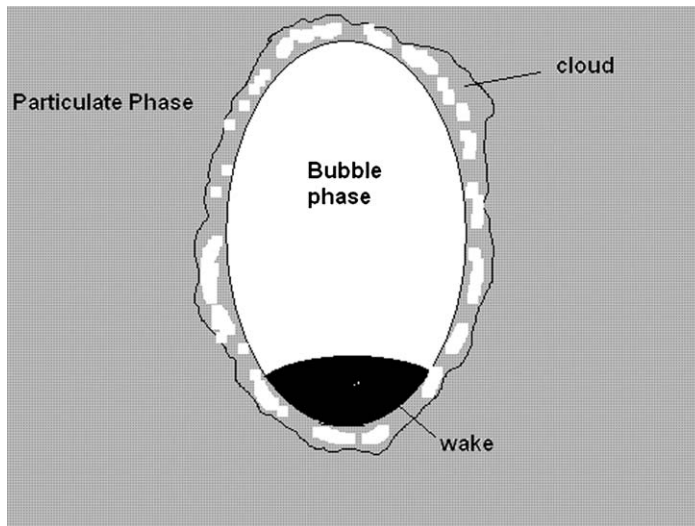


Figure 3.58 Bubble and particulate phase.

Bubbling bed model of Kunii and Levenspiel Rowe and Partidge (1962) also found out that each bubble of gas drags a substantial wake of solids up the bed. On the basis of these findings, Kunii and Levenspiel (1972) developed the bubbling bed model. The assumptions used in that model are the following:

- The emulsion phase stays at minimum fluidizing conditions. Thus, the relative velocity of the gas and solid remains unchanged.
- All bubbles have the same size.
- The solids in the emulsion phase flow smoothly downward, essentially in plug flow.

- The concentration of solids in the wake is the same as the concentration of solids in the emulsion phase, and therefore, the gaseous void fraction in the wake is also the same as in the emulsion phase. Because the emulsion phase is at the minimum fluidizing condition, the void fraction in the wake is equal to ε_{fm} . The wake, however, is quite turbulent, and the average velocities of both the solid and gas in the wake are assumed to be the same and equal to the upward velocity of the bubbles.

Applying the appropriate material balances for the solids and the gas, the fraction of the bed occupied by the bubbles and wakes can be estimated using the Kunii–Levenspiel model. The fraction of the bed occupied by that part of the bubbles which does not include the wake, is represented by the parameter δ , whereas the volume of the wake per volume of the bubble is represented by α . Consequently, the bed fraction in the wakes is $\alpha\delta$ and the bed fraction in the emulsion phase (which includes the clouds) is $1 - \delta - \alpha\delta$. Then (Fogler, 1999)

$$u_{ss} = \frac{\alpha\delta u_{bub}}{1 - \delta - \alpha\delta} \quad (3.492)$$

The velocity of the gas in the emulsion phase is

$$u_e = \frac{u_{fm}}{\varepsilon_{fm}} - u_{ss} \quad (3.493)$$

The ε_{fm} is present in this equation because u_{fm} is the superficial velocity, i.e., based on the cross section of the empty tube. The velocity of the moving solids, u_{ss} , is positive in the downward direction here as in most of the fluidization literature. The velocity of the gas in the emulsion u_e is taken as positive in the upward direction, but note that it can be negative under some conditions. The fraction of the bed occupied by bubbles is given by (Fogler, 1999)

$$\delta = \frac{u_s - u_{fm}}{u_{bub} - u_{fm}(1 + \alpha)} \quad (3.494)$$

Kunii and Levenspiel assumed that the last equation could be simplified to (Fogler, 1999)

$$\delta \cong \frac{u_s - u_{fm}}{u_{bub}} \quad (3.495)$$

which is valid if $u_{bub} \gg u_{fm}$. The total mass of solids in the bed (solids holdup) is

$$M_s = AZ_f(1 - \delta)(1 - \varepsilon_{fm})\rho_p \quad (3.496)$$

where α is the volume of wake per volume of bubble. According to Levenspiel (1972),

experiments showed that α ranges between 0.25 and 1. Then, the fraction of the bed occupied by clouds is

$$\beta_c = \frac{3\delta u_{fm}}{\varepsilon_{fm} u_{bs} - u_{fm}} \quad (3.497)$$

Furthermore, Levenspiel defined the following parameters (Levenspiel, 1972; Fogler, 1999):

$$\gamma_c = (1 - \varepsilon_{fm}) \left(\frac{3u_{fm}}{\varepsilon_{fm} u_{bs} - u_{fm}} + \alpha \right) = (1 - \varepsilon_{fm}) \left(\frac{\beta_c}{\delta} + \alpha \right) \quad (3.498)$$

$$\gamma_e = \frac{(1 - \varepsilon_{fm})(1 - \delta)}{\delta} - (\gamma_c + \gamma_b) \quad (3.499)$$

where:

- γ_b = the volume of solids dispersed in bubbles per volume of bubbles
- γ_c = the volume of solids within clouds and wakes per volume of bubbles
- γ_e = the volume of solids in emulsion per volume of bubbles.

Typical values of γ_b , γ_c , and γ_e are 0.005, 0.2, and 1.5, respectively (Levenspiel, 1972; Fogler, 1999). A weakness of this model is that there does not yet exist a reliable method or correlation for determining the value of γ_b .

In Figure 3.59, the flow pattern in a fluidized bed is shown.

Bubble velocity and diameter In the context of the bubbling bed theory, the rise velocity of a single bubble in a fluidized bed is given by (Wen, 1984)

$$u_{bs} = 0.711(gd_{bub})^{0.5} \quad (3.500)$$

whereas the rise velocity of bubble, cloud, and wake is

$$u_{bub} = u_s - u_{fm} + 0.711(gd_{bub})^{0.5} \quad (3.501)$$

The values of the rise velocity of the bubbles estimated by the equation above are generally higher than the ones predicted by the two-phase-model of Davidson. This difference can be explained as follows. The single-bubble velocity can be affected by various other factors, especially when many bubbles are present. Specifically, an increase in the number of bubbles leads to a lower drag force on each bubble. In other words, the bubbles carry each other up through the bed. The number of bubbles formed depends on the gas velocity. The greater the gas velocity, the greater the flow rate and thus, the more the number of bubbles formed. To sum up, an increase in the gas velocity results in an increase in the real bubble velocity. The bubble velocity is also affected by the viscosity of the gas and the size and density of the solids indirectly, since all these parameters affect the minimum fluidized velocity. Specifically, a low viscosity and a large size of particles with high density increases the minimum fluidization velocity, which in turn leads to a decrease in the velocity of the rising bubble.

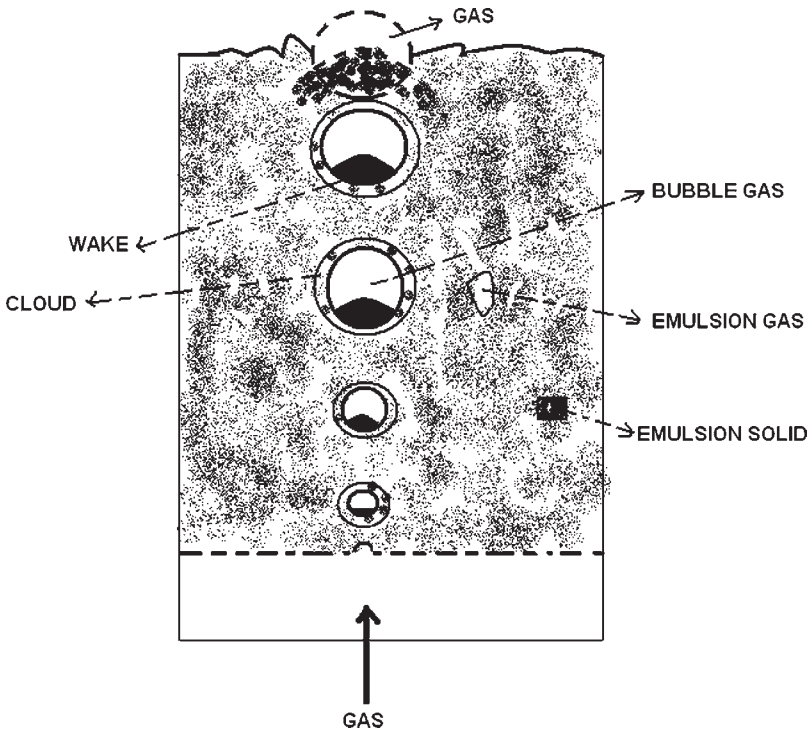


Figure 3.59 Flow pattern in a fluidized bed based on the three-phase model of Levenspiel–Kunii.

The following equation correlates the initial bubble size with the type of distributor plate. For porous plates (Mori and Wen, 1975),

$$d_{\text{bub},o} = 0.00376(u_s - u_{\text{fm}})^2 \quad (3.502)$$

whereas for perforated plates,

$$d_{\text{bub},o} = 0.347 \left[\frac{\pi D^2 (u_s - u_{\text{fm}})}{4n} \right]^{0.4} \quad (3.503)$$

where n is the number of perforations (orifices on the plate). For typical distributors, n is in the range 4–3100. In these equations, CGS units should be used.

The maximum bubble size can be evaluated as follows:

$$d_{\text{bub},\text{max}} = 0.652 \left[\frac{\pi}{4} D^2 (u_s - u_{\text{fm}}) \right]^{0.4} \quad (3.504)$$

In this equation, CGS units should be used.

So, the actual bubble diameter at height z above the bed bottom is

$$\frac{d_{\text{bub,max}} - d_{\text{bub}}}{d_{\text{bub,max}} - d_{\text{bub,o}}} = \exp\left(-\frac{0.3z}{D}\right) \quad (3.505)$$

This equation has been deduced from studies conducted with bed diameters of 7.6–130 cm, minimum fluidization velocities of 0.5–20 cm/s, solid particle sizes of 0.006–0.045 cm, and $u_s - u_{\text{fm}} < 48$ cm/s. To calculate an average value of the bubble velocity, an average bubble diameter should be used. This diameter can be taken to be equal to the bubble diameter at $z = H_f/2$. Thus, to calculate the bubble diameter and thus the bubble velocity, the fluidized bed height should be known. To solve the problem, an iteration method should be used (Figure 3.60).

In the original eq. (3.505), the height above the distributor plate h is used instead of z . However, practically, h and z are equal.

The correlation of Werther, based on a statistical coalescence model, is an alternative to estimate d_{bub} (Wen, 1984).

$$d_{\text{bub}} = 0.853[1 + 0.272(u_s - u_{\text{fm}})]^{1/3} (1 + 0.0684z)^{1.21} \quad (3.506)$$

In this equation, CGS units should be used.

Darton *et al.* (1977) and Werther (1983) presented different relationships for bubble diameter and bubble velocity for Group A and Group B particles (for bubbling fluidization). The mean rise velocity of a bubble in the bed (u_{bub}) can also be evaluated using the following equations, which include a wall effect correction (Darton *et al.*, 1977; Werther, 1983; Wen, 1984).

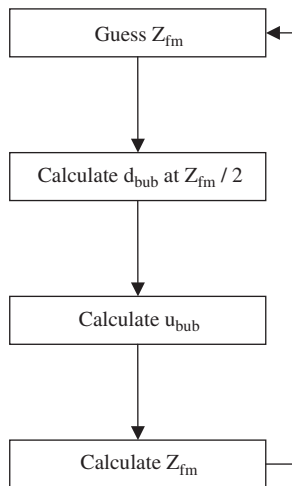


Figure 3.60 Iteration procedure.

For Group B powders (Type B fluidization)

$$d_{\text{bub}} = \frac{0.54}{g^{0.2}} (u_s - u_{\text{fm}})^{0.4} (z + 4N^{-0.5})^{0.8} \quad (3.507)$$

and

$$u_{\text{bub}} = \Phi_{\text{bub}} (gd_{\text{bub}})^{0.5} \quad (3.508)$$

where:

- d_{bub} = the equivalent volume diameter of the bubble
- z = the height above the fluid distributor (bed bottom)
- N = the number of holes per unit area in the distributor, $1/\text{m}^2$
- Φ_{bub} = a constant dependent on the bed diameter D :

$$\Phi_{\text{bub}} = \begin{cases} 0.64 & \text{for } D < 0.1 \text{ m} \\ 1.6D^{0.4} & \text{for } 0.1 < D < 1 \text{ m} \\ 1.6 & \text{for } D > 1 \text{ m} \end{cases}$$

To calculate an average value of the bubble velocity, an average bubble diameter should also be used, which can be taken to be equal to the bubble diameter at $Z = H_f/2$. An iteration method should be used (Figure 3.60). As an initial Z_f value, the fixed-bed height Z multiplied by 1.4 could be used.

For Group A powders (Type A bubbling fluidization)

For this kind of particles, bubbles reach a maximum stable size, which may be estimated from the following equations:

$$d_{\text{bub}} = 2 \frac{u_{\text{ter},2.7}^2}{g} \quad (3.509)$$

$$u_{\text{bub}} = \Phi_{\text{bub}} (gd_{\text{bub}})^{0.5} \quad (3.510)$$

where:

$$\Phi_{\text{bub}} = \begin{cases} 1 & \text{for } D < 0.1 \text{ m} \\ 2.5D^{0.4} & \text{for } 0.1 < D < 1 \text{ m} \\ 2.5 & \text{for } D > 1 \text{ m} \end{cases}$$

and $u_{\text{ter},2.7}$ is the terminal free-fall velocity for particles of diameter 2.7 times the actual mean particle diameter. In all equations, SI units should be used.

Mixing of phases in fluidized beds

For the fluidization of a bed to occur, a large amount of power is initially needed, but once achieved, further increase in the feed flow rate requires much less energy. The operation of the fluidized-bed reactor is normally in the region between the packed bed and continuous-stirred tank reactor operation, due to backmixing caused by small linear velocities of the fluid. At high flow rates and low reactor diameters, almost ideal plug-flow characteristics may be achieved. Almost ideal plug-flow behavior can be achieved if high flow rates and small reactor diameters are used. The exact mode of fluidized-bed reactor operation depends on its actual design characteristics.

Solids mixing The mixing of solids in fluidized-bed reactors is achieved by the entrainment of solids in the lower portion of bubbles, as well as by the shedding of these solids from the wake of the bubble (Rowe and Patridge, 1962). Thus, mixing will appear as the gas rate increases above its minimum value for the onset of fluidization. Especially, at high gas rates, by far higher than the minimum fluidizing rate, the intense circulation of the solids from the top to the bottom of the bed leads to rapid mixing of the solids. The particles that reach the top of the bed displace those found at the bottom of the bed. Practically, if the ratio of length to diameter of the bed ranges between 0.1 and 4, the solid phase can be considered to be completely mixed.

The complete mixing of solids in the emulsion phase is necessary for considering the various parameters, involving the mass or volume of solids constant, throughout the reactor. That is exactly the case in the two-phase model and the Levenspiel–Kunii three-phase model. This is achieved by circulation of the solids through their entrainment by bubbles, as shown in Figure 3.61. As solids fall from the upper portions of the bed, they follow

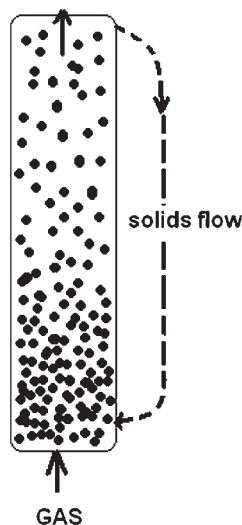


Figure 3.61 Heterogeneous solids distribution.

either a plug-flow route, as assumed in Kunii–Levenspiel model, or they are considered to be in a perfect mixing state, which means that the whole emulsion phase, and consequently the gas itself, is completely mixed throughout the reactor, as assumed in the two-phase model.

For example, in circulating fluidized beds, for a given superficial gas velocity and solid mass velocity, several studies show that the solids are distributed in two regions in the vessel—a constant solid fraction in the lower dense region of a certain height, and a solid fraction that falls exponentially with height in an upper lean region of a certain height (Kunii and Levenspiel, 2000).

Consider a first-order reaction in a fluidized bed, where we have plug-flow for the gas through the bed, while the distribution of solids across the cross-section of the bed is uniform. In general, the solution of this model, under the additional assumption of uniform solids distribution throughout the reactor, is

$$\ln \frac{C_{\text{in}}}{C_{\text{out}}} = f(k, Z_f, u_s, k_m, S_i) \quad (3.511)$$

where S_i is a parameter involving the solids fraction. For simplicity, consider this parameter to be the solid fraction itself (ε_s). If this parameter is not constant, it introduces an integral in the model:

$$\overline{\varepsilon_s} = \int_0^{Z_f} h(\varepsilon_s) dz \quad (3.512)$$

Gas mixing in bubbling fluidization In bubbling fluidization, the mixing of gases as they travel vertically through the bed is complete. In contrast, mixing in the radial direction is extremely poor and effective distributors have to be used, especially if two gases are to be mixed. In bubbling beds, for velocities less than 5–11 times that of u_{fm} , the gases will move upward in both the emulsion and the bubble phases. On the other hand, for velocities higher than about 5 to 11 times that of u_{fm} , the movement of the emulsion phase downward will carry the contained gas downward as well. The backmixing of gases increases up to a point as u_s/u_{fm} is increased. After this point, the circulating or fast regime appears and the backmixing decreases with increasing velocities.

It should be noted that since the solid phase is not stationary in a fluidized bed, the movement of the solid phase can also be described by a Peclet number. Thus, there are two Peclet numbers in fluidized beds for axial and radial mixing, i.e. one for the fluid side and one for the solid one. However, only the fluid-side Peclet numbers are presented here.

Fluid mixing in particulate fluidization In particulate fluidization, the values of Pe_p are much higher than the corresponding ones for packed beds (2–10 times) for the same value of Re_p , covering the range 0.004–0.06 for $0.4 < Re_p < 100$, and thus axial dispersion is more intense (Gunn, 1968).

The Chung–Wen correlation can be used for fixed and fluidized beds for $10^{-3} < Re_p < 10^3$ (Chung and Wen, 1968).

$$\frac{\varepsilon_f Pe_p}{\zeta} = 0.2 + 0.011 Re_p^{0.48} \quad (3.513)$$

where

$$\zeta = \frac{Re_{p, \text{fm}}}{Re_p} \quad (3.514)$$

In this equation, $Re_{p, \text{fm}}$ is the particle Reynolds number based on the minimum superficial velocity for fluidization. Moreover, for fixed-beds, we can set $\zeta = 1$ and $\varepsilon_f = \varepsilon$. The correlation is applicable for void fractions between 0.4 and 0.8 with particle density up to 480 lb/ft³. Note that by changing the Re_p number, the fluidized bed voidage ε_f is changed.

According to Gunn (1968), the radial Peclet number in particulate fluidization (liquid–solid systems) ranges between 1 and 10 for values of Re_p in the range 4–1000. Furthermore, the maximum mixing coefficient is found for $\varepsilon_f = 0.7$. Finally, the lateral (radial) mixing coefficients in gas–solid fluidized beds decrease constantly (for $Re_p > 10$) from about 10 – 0.05 by increasing the expansion ratio from 0.01 – 0.2.

Gas distribution in fluidized beds

The gas distributor has a considerable effect on the proper operation of the fluidized bed. Basically, there are two types (Perry and Green, 1999): (a) for use when the inlet gas contains solids and (b) for use when the inlet gas is free of solids. In the latter case, the distributor is designed to prevent the backflow of solids during normal operation, and in many cases, it is designed to prevent backflow during shutdown. To provide distribution, it is necessary to restrict the gas or the gas and solids flow so that the pressure drops across the restriction amount of 0.5 to 20 kPa.

To fulfill the pressure requirements, a high velocity through the grid openings may be needed. However, values of velocity have to be below 70 m/s to avoid attrition of the solids. In industrial applications, a shroud of pipe is often installed over the opening, providing velocities as high as necessary for the pressure requirements, and at the same time enabling reduced velocities for entry to the bed, thus avoiding attrition. The technique is applied to both plate and pipe spargers. Pressure drop through a pipe or a drilled plate is given by

$$\Delta P = \frac{\rho_f u_o^2}{1.28g} \quad (3.515)$$

where:

- u_o = the velocity in the hole at inlet conditions
- ρ_f = the fluid density in the hole at inlet conditions
- ΔP = the pressure drop in consistent units.

Most industrial-scale fluidized beds employ a type of jet or perforated-plate distributor (Gunn, 1968).

Fluidized beds constituent parts (internals)

These parts are used in fluidized beds for various purposes. For example, gas distributors and various types of baffles are installed to decrease the size of the bubbles. Moreover, draft tubes are used to enhance gas or solid circulation. Other devices such as horizontal baffles limit circulation and backmixing of solids and gas. Horizontal or vertical tubes are used for heat management. Devices used to control or improve fluidization behavior, to improve fluidization of cohesive particles or to achieve solids recovery are within the various internals met in fluidized bed reactors (Kelkar and Ng, 2002). Immersed tubes in small diameter beds may lead to slugging. Furthermore, attrition of particle breakage may change the size distribution and possibly change the fluidization behavior.

Generally, the use of baffles and other mechanical means is usual in fluidized-bed reactors. These devices are largely connected with the bubbles. Specifically, the size of bubbles is decreased and thus mechanical disturbances are avoided via baffles. Furthermore, this decrease in bubble size improves gas–solid conducting. The latter can be also be achieved by packing the reactor with large particles and fluidized fine solids in the interstices of the larger ones. This type of reactor is called “fluidized-packed bed” (Gunn, 1968). However, baffles increase the overall pressure drop across the reactor length, and may also make the achievement of fluidization in all stages difficult. Finally, baffles may create pockets of low solids region, which in oxidation reactors may lead to uncontrolled burning.

3.8.3 Modeling of bubbling fluidized beds with reaction (gas–solid catalysis case and Type B Fluidization)

The analysis of the following cases is based on

- isothermal operation
- non-existence of radial gradients
- negligible volume changes due to reaction ($\varepsilon_R = 0$)
- rapid internal diffusion in solid particles ($\eta_s = 1$)

Two-phase models

Gas in the emulsion phase in completely mixed state In this case, the following are also assumed: (a) two-phase model applies, (b) plug-flow of the gas in the bubble phase, (c) perfect mixing of the gas in the particulate phase (emulsion phase), and (d) throughout the reactor, the gaseous reactant is assumed to pass between the bubble and particulate phase. This model is referred to as the “two-phase model”, where the emulsion phase is well mixed (Kelkar and Ng, 2002). It is a one-dimensional model, which assumes steady state (Figure 3.62). In steady state, the concentration of the reactant in the particulate phase is constant throughout the reactor because of the assumption of perfect mixing in the particulate phase.

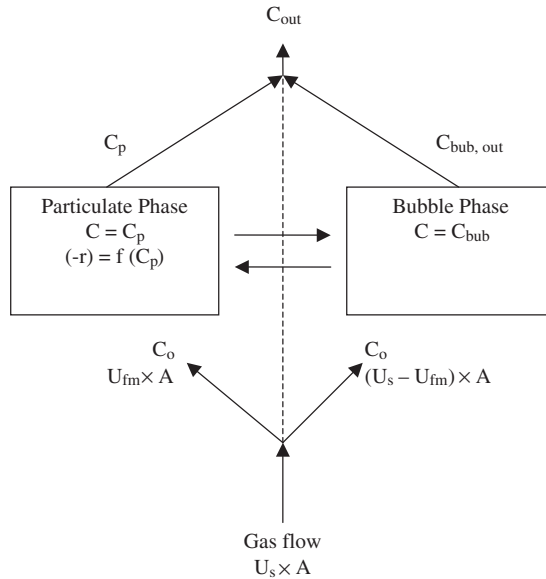


Figure 3.62 Two-phase model.

The model equations are the following:

For the bubble phase (gas phase),

$$-f_{\text{bub}}u_s \frac{dC_b}{dz} - L_{\text{be}}(C_b - C_p) - \varepsilon_{\text{bub}}\gamma_b(-r_{\text{b,vs}}) = 0 \quad (3.516)$$

where:

- L_{be} = the mass transfer coefficient between the bubble and emulsion phase (m^3 gas interchange volume/ m^3 of reactor) (1/s)
- γ_b = the volume fraction of the bubble occupied by solids
- $(-r_{\text{b,vs}})$ = the reaction rate in bubbles per unit volume of solids, based on the reactant
- f_{bub} = the fraction of the gas flow carried by the bubble phase:

$$f_{\text{bub}} = \frac{u_s - u_{\text{fm}}}{u_s} \quad (3.517)$$

The material balance is expressed per unit volume of reactor.

For the particulate phase (dense phase),

$$(1 - f_{\text{bub}})Q_G(C_o - C_p) + \int_0^{z_f} AL_{\text{be}}(C_b - C_p)dz - AZ_f(1 - \varepsilon_{\text{bub}})\varepsilon_{\text{cs}}(-r_{\text{p,vs}}) = 0 \quad (3.518)$$

where:

- ϵ_{eS} = the volume fraction of the dense phase occupied by solids ($\epsilon_{eS} = 1 - \epsilon_{fm}$)
- C_o = the feed concentration of the gas
- A = the cross-sectional area of the bed
- Z_f = the fluidized-bed height
- Q_G = the volumetric flow rate of gas through the reactor.

Gas in the emulsion phase in plug flow In this case, the following are assumed: (a) two-phase theory applies (bubble and particulate phases), (b) plug flow of gas throughout the reactor, i.e. in the bubble and emulsion phase. This model is referred to as the “two-phase model” with plug emulsion phase (Kelkar and Ng, 2002).

For the bubble phase (gas phase),

$$-f_{bub}u_s \frac{dC_b}{dz} - L_{be}(C_b - C_p) - \epsilon_{bub}\gamma_b(-r_{b,vs}) = 0 \tag{3.519}$$

where:

- L_b = in (m³ gas interchange volume/m³ of reactor) (1/s)
- γ_b = the volume fraction of bubble occupied by solids
- $(-r_{b,vs})$ = the reaction rate in bubbles per unit volume of solids, based on the reactant
- f_{bub} = the fraction of the gas flow carried by the bubble phase

The material balance is expressed per unit volume of reactor (Figure 3.63).

For the particulate phase (dense phase),

$$(1 - f_{bub})u_s \frac{dC_p}{dz} + L_{be}(C_b - C_p) - (1 - \epsilon_{bub})(1 - \epsilon_{mf})(-r_{p,vs}) = 0 \tag{3.520}$$

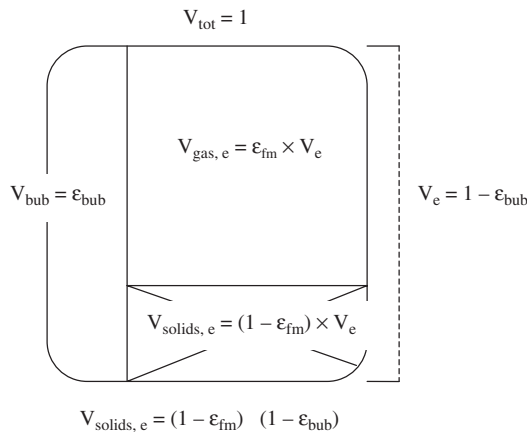


Figure 3.63 Volume fractions in a two-phase fluidized bed (where e denotes the emulsion phase).

As in the case of two-phase fixed beds and trickle beds, the material balances of fluidized beds are written in terms of reactor volume (V_R) (see Section 3.1.1 for derivation) and the following relationship holds:

$$(-R) = -\frac{1}{V_R} \frac{dN}{dt} = \frac{V_S}{V_R} (-r_{vs}) = \frac{V_L}{V_R} (-r_u) \quad (3.521)$$

For the bubble phase,

$$\frac{V_L}{V_R} = \varepsilon_{\text{bub}} \quad (3.522)$$

$$\frac{V_S}{V_R} = \frac{V_{\text{bubble}}}{V_R} \frac{V_S}{V_{\text{bubble}}} = \varepsilon_{\text{bub}} \gamma_b \quad (3.523)$$

Then, the overall rate of reaction ($-R$) per unit volume of reactor is

$$(-R) = -\frac{1}{V_R} \frac{dN}{dt} = \varepsilon_{\text{bub}} \gamma_b (-r_{vs}) = \varepsilon_{\text{bub}} (-r_u) \quad (3.524)$$

For the emulsion phase,

$$\frac{V_L}{V_R} = \frac{V_{\text{emulsion}}}{V_R} \cdot \frac{V_L}{V_{\text{emulsion}}} = (1 - \varepsilon_{\text{bub}}) \varepsilon_{\text{fm}} \quad (3.525)$$

$$\frac{V_S}{V_R} = \frac{V_{\text{emulsion}}}{V_R} \frac{V_S}{V_{\text{emulsion}}} = (1 - \varepsilon_{\text{bub}}) (1 - \varepsilon_{\text{fm}}) \quad (3.526)$$

Then, the overall rate of reaction ($-R$) per unit volume of reactor is

$$(-R) = -\frac{1}{V_R} \frac{dN}{dt} = (1 - \varepsilon_{\text{bub}}) (1 - \varepsilon_{\text{fm}}) (-r_{vs}) = (1 - \varepsilon_{\text{bub}}) \varepsilon_{\text{fm}} (-r_u) \quad (3.527)$$

Kunii-Levenspiel three-phase model (bubbling bed model)

In the following, a simplified version of the Kunii–Levenspiel model is presented (Levenspiel, 1962). This design model follows the assumptions of the bubbling bed one. According to this hydrodynamic model, the solids in the emulsion phase flow smoothly downward (plug-flow of solids). The entire emulsion phase is thoroughly agitated, whereas the emulsion exists at minimum fluidizing conditions. The gas occupies the same void fraction in this phase as it would in the entire bed at minimum fluidization. Furthermore, the reaction takes place wherever the solid exists, i.e. in the bubbles, in the wakes, and in the emulsion phase. In Figure 3.64, the model is schematically presented.

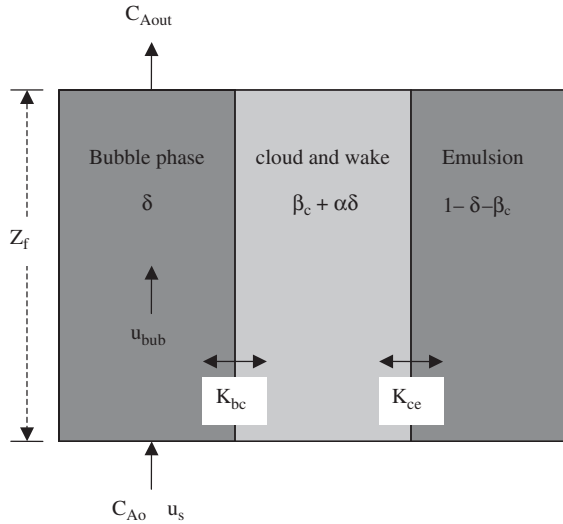


Figure 3.64 Levenspiel model (simplified Kunii–Levenspiel model).

Material balances can be written over a differential section of the bed (dz) for a reactant, in each of the three-phases (bubble, cloud, and emulsion). Then, the equations of the model are as follows:

For the bubble phase (gas phase),

$$\varepsilon_b D_{L,b} \frac{d^2 C_b}{dz^2} - u_{\text{bub}} \frac{dC_b}{dz} - K_{bc} (C_b - C_c) - \gamma_b (-r_{b,vs}) = 0 \quad (3.528)$$

where K_{bc} is the mass transfer coefficient between the bubble and cloud phase in (m^3 gas interchange volume/ m^3 of bubble) (1/s).

For the cloud phase (cloud and wake),

$$u_c \left(\frac{\beta_c + \alpha \delta}{\delta} \right) \frac{dC_c}{dz} + K_{bc} (C_b - C_c) - K_{ce} (C_c - C_e) - \gamma_c (-r_{c,vs}) = 0 \quad (3.529)$$

where K_{ce} is the mass transfer coefficient between the cloud and the emulsion phase in (m^3 gas interchange volume/ m^3 of bubble) (1/s).

For the emulsion phase (dense phase),

$$u_e \left(\frac{1 - \delta - \alpha \delta}{\delta} \right) \frac{dC_e}{dz} + K_{ce} (C_c - C_e) - \gamma_e (-r_{e,vs}) = 0 \quad (3.530)$$

where u_c and u_e are the velocities of the gas in the cloud and emulsion phases, respectively. The material balance is expressed per unit volume of bubble phase.

Note that in this case, as in the case of slurry reactors, the material balances are based on the unit volume of the fluid (bubble) phase. The relationship between the rate expressions is (see Section 3.1.1 for derivation)

$$(-r_u) = -\frac{1}{V_L} \frac{dN}{dt} = \frac{V_S}{V_L} (-r_{vs}) \quad (3.531)$$

For each one of the three-phases in the fluidized bed ($i = b, c,$ or e),

$$\frac{V_S}{V_L} = \gamma_i \quad (3.532)$$

Then, the overall rate of reaction ($-r_u$) per unit volume of liquid is

$$(-r_u) = -\frac{1}{V_L} \frac{dN}{dt} = \gamma_i (-r_{vs}) \quad (3.533)$$

Apart from the basic assumption of the corresponding hydraulic model, the following approach is valid for a fairly high gas flow rate. The gas flow in both the emulsion and the cloud volume becomes so small that the flow of gas in these regions can be neglected. Consequently, flow through the bed occurs only in the bubble phase (Levenspiel, 1972). This means that $f_{\text{bub}} = 1$ or in more practical terms, $u_s - u_{\text{fm}} \gg u_{\text{fm}}$. This is a real situation in industrial catalytic reactors, which are characterized by high gas velocities, much higher than the minimum fluidization velocity (Werther, 1980).

The Kunii-Levenspiel model can be simplified by assuming that the derivative terms of eqs. (3.529) and (3.530) are unimportant compared to the rest of the terms. Furthermore, plug flow can be assumed for gas (bubble) phase. Under these assumptions, the set of equations reduces as follows (Carberry, 1976; Fogler, 1999):

For the bubble phase (gas phase),

$$-u_{\text{bub}} \frac{dC_b}{dz} - K_{bc}(C_b - C_c) - \gamma_b(-r_{b,vs}) = 0 \quad (3.534)$$

or

$$-u_{\text{bub}} \frac{dC_b}{dz} - (-r_{b,u})_{\text{overall}} = 0 \quad (3.535)$$

The overall rate of reactant disappearance in the gas phase is

$$(-r_{b,u})_{\text{overall}} = \gamma_b(-r_{b,vs}) + K_{bc}(C_b - C_c) \quad (3.536)$$

where $-r_{b,vs}$ is the reaction rate per unit volume of solids and $(-r_{b,u})_{\text{overall}}$ the reaction rate in bubbles per unit volume of bubbles.

For the cloud phase,

$$K_{bc}(C_b - C_c) = K_{ce}(C_c - C_e) + \gamma_c(-r_{c,vs}) \quad (3.537)$$

For the gas in the emulsion phase (dense phase),

$$K_{ce}(C_c - C_e) = \gamma_e(-r_{e,vs}) \quad (3.538)$$

3.8.4 Liquid–solid particulate fluidization (liquid–solid catalysis, adsorption, and ion exchange)

Three models of the fluidized-bed process can be considered (Menoud *et al.*, 1998):

- complete backmixing of the liquid and the solid (CSTR model);
- near plug flow of the liquid and a complete backmixing of the solid, which is the plug-flow model with backmixing of the solid;
- near plug-flow of the liquid with no backmixing of the solid, which is the plug-flow model.

Since the particulate flow regime is characterized by a relatively uniform expansion of the bed without the formation of bubbles, it can be approximated as an expanded fixed bed (Wen, 1984; Hopper, 2001). Thus, the fixed bed models can be used for the particulate flow regime in fluidized beds for catalysis as well as for adsorption and ion exchange. Fluidized-bed operation in adsorption and ion exchange is rare and has been studied for heavy metals removal from the liquid phase to a chelating resin, and for the determination of mass transfer rates in a magnetically stabilized liquid fluidized bed of magnetic ion-exchange particles (Menoud *et al.*, 1998; Hausmann *et al.*, 2000).

The main mass transport resistance in liquid fluidized beds of relatively small particles lies in the liquid film. Thus, for ion exchange and adsorption on small particles, the mass transfer limitation provides a simple liquid-film diffusion-controlled mass transfer process (Hausmann *et al.*, 2000; Menoud *et al.*, 1998). The same holds for catalysis. It should be noted that in the material balances, the fluidized bed voidage should be used instead of fixed-bed voidage, and that the appropriate mass transfer correlations should be used for particulate fluidization.

3.8.5 External mass transfer

In fluidized beds, mass transfer involves two different mechanisms. The first one is the ordinary mass transport between the fluid and the solid. The treatment of this type of transport is quite similar to fluid–solid mass transfer found in other types of operations such as fixed beds and agitated tank reactors. This mechanism of mass transfer is not always significant in fluidized beds and can be totally neglected in some cases.

In contrast, the second mechanism is quite different and it is found only in fluidized-bed reactors. It concerns the mass transfer between the bubbles and the particulate phase

through an intermediate phase called “cloud” and cannot be overlooked, at least in most of the fluidized beds.

Fluid–solid mass and heat transfer in particulate fluidization

In fluidized beds, the gas bubbles in combination with the high heat-transfer area per unit mass of catalyst, lead to mixing in the emulsion phase, and in turn to temperature uniformity throughout the reactor (Smith, 1981). Considering that the same large area is also available to mass transfer, one can easily understand why the temperature and concentration gradients between the fluid and particle surface are usually negligible. It should be noted that the mass and heat transfer coefficients in fluidized beds are less than those in fixed beds, where large differences in temperature and concentration between the fluid and the solids exist. However, the area is much higher in fluidized beds as a result of the use of smaller particles, which leads to higher products of transfer coefficient and area. Note that the mass transfer is a function of the transfer coefficient and the available surface.

The mass and heat transfer coefficient between the gas or liquid phase and the solid phase can be evaluated using the Chu–Kaiil–Wetterath correlation (Smith, 1981):

$$j_D \text{ or } j_H = 1.77 \left[\frac{d_p G}{\mu(1 - \varepsilon_f)} \right]^{-0.44} \quad (3.539)$$

This equation is valid within the limits

$$30 < \frac{d_p G}{\mu(1 - \varepsilon_f)} < 5000$$

and

$$j_D = \frac{k_f \rho}{G} \left(\frac{a_m}{a_t} \right) \left(\frac{\mu}{\rho D_f} \right)^{2/3} \quad (3.540)$$

$$j_H = \frac{h_f}{c_p G} \left(\frac{a_m}{a_t} \right) \left(\frac{c_p \mu}{\lambda_f} \right)^{2/3} \quad (3.541)$$

where:

- ε_f = the void fraction of the fluidized bed
- G = $u_s \rho$, the fluid mass superficial velocity, kg/m² s
- a_t = the total mass transfer area
- a_m = the effective mass transfer area
- D_f = the solute diffusivity in the fluid phase
- h_f = the heat transfer coefficient, W/m² K
- c_p = the specific heat capacity of the fluid, J/kg K
- λ_f = the thermal conductivity of the fluid, W/m K.

At temperatures above 400 °C and for large particles, heat transfer by radiation should be also taken into account.

If a fluidized and a fixed bed are operated at the same Re_p , the mass transfer coefficient is higher in the latter. However, the fixed bed can be operated only in downflow mode, because the solids would be entrained in upflow, at high Reynolds numbers. Re_p should be lower than the value of 1.8 times the minimum Re_p for fluidization to avoid excessive attrition of the particles in the fluidized bed. For the system shown in Figure 3.65, the minimum Re_p for fluidization is about 8, and thus, the upper limit for the fixed-bed operation in downflow mode is lower than 13. Furthermore, high residence times and thus low superficial velocities and low Re_p are met in fixed beds. For example, Re_p values lower than 8 are typical in ion exchange and adsorption from liquid phase in fixed beds. For the system shown in Figure 3.65, if the Re_p in the fixed bed is lower than 8 but is higher than this value in the fluidized bed, the fluidized-bed mass transfer coefficient is higher than that in the fixed bed.

For $5 < Re_p < 100$, the following correlation, obtained by Rahman and Streat for mass transfer, is valid for conventional liquid fluidized beds (Rahman and Streat, 1981; Hausmann *et al.*, 2000):

$$Sh = \frac{0.86}{\varepsilon_f} Re_p^{0.5} Sc^{1/3} \quad (3.542)$$

For lower Reynolds numbers ($0.22 < Re_p < 1$), the Koloini–Sospic–Zumer correlation is more accurate (Koloini *et al.*, 1977; Hausmann *et al.*, 2000).

$$Sh = \frac{0.7}{\varepsilon_f} Re_p Sc^{1/3} \quad (3.543)$$

Here, the Re_p is based on superficial velocity.

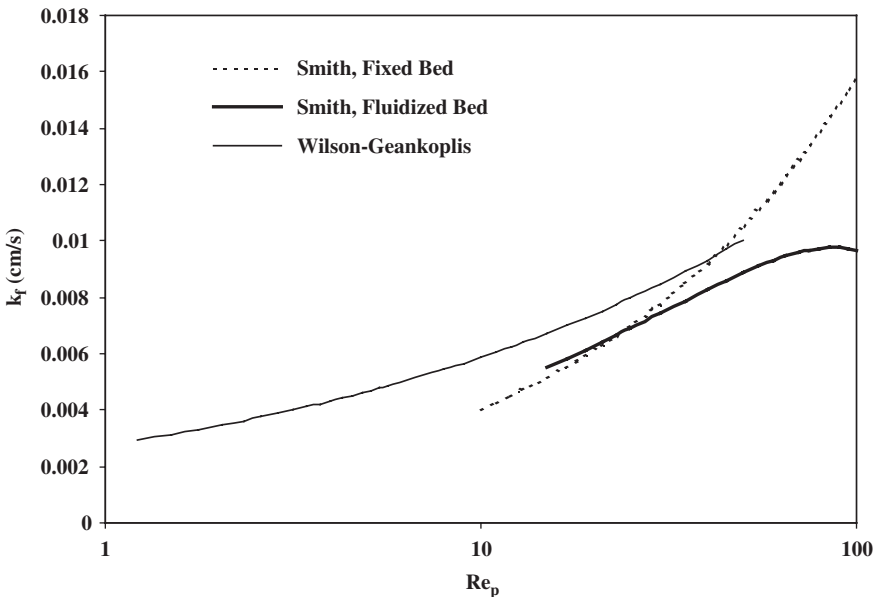


Figure 3.65 Comparison of mass transfer coefficients for fixed and fluidized beds (system: water at 20 °C, $\Phi_s = 1$, $\rho_h = 2.08 \text{ g/cm}^3$, $\varepsilon = 0.4$, $D_f = 10^{-5} \text{ cm}^2/\text{s}$, and $d_p = 1 \text{ mm}$).

Bubble–particulate phase mass transfer (bubbling fluidization)

Following the bubbling bed model of Kunii–Levenspiel, the mass transfer coefficient of gas between the bubble and the cloud is (Levenspiel, 1972; Fogler, 1999)

$$K_{bc} = 4.5 \frac{u_{fm}}{d_{bub}} + 5.85 \frac{D_g^{1/2} g^{1/4}}{d_{bub}^{5/4}} \quad (3.544)$$

where the units of K_{bc} is (m^3 gas interchange volume/ m^3 bubble)(1/s) and D_g is the diffusion coefficient of the solute in the gas phase. Here, CGS units are used. A typical value of K_{bc} is 2 s^{-1} .

The mass transfer coefficient of gas between the cloud and the emulsion is

$$K_{ce} \cong 6.78 \left(\frac{\varepsilon_{fm} D_g u_{bub}}{d_{bub}^3} \right)^{1/2} \quad (3.545)$$

where the units of K_{ce} is (m^3 gas interchange volume/ m^3 bubble)(1/s). CGS units are also used in this relation. A typical value of K_{ce} is 1 s^{-1} . Here, both mass transfer coefficients are based on bubble volume. Another useful expression in reactor modeling is that of a mass transfer coefficient based on reactor volume:

$$L = K \varepsilon_{bub} \quad (3.546)$$

where:

- ε_{bub} = the volume fraction of the bubble phase, m^3 bubbles/ m^3 reactor
- L = the mass-transfer coefficient based on the reactor volume, (m^3 gas interchange volume/ m^3 of reactor) (1/s)
- K = the mass-transfer coefficient based on the bubble volume, (m^3 gas interchange volume/ m^3 of bubble) (1/s)

Mass transfer coefficients are also expressed in m/s. These units are related to the other ones as follows (Kelkar and Ng, 2002):

$$k_m = \frac{L}{\alpha_{bub}} \Rightarrow L = k_m \alpha_{bub} \quad (3.547)$$

and

$$k_m = \frac{K}{a_{bub}^o} \Rightarrow K = k_m \alpha_{bub}^o \quad (3.548)$$

where:

- k_m = the mass transfer coefficient, m/s or in the equivalent unit of (m^3 gas interchange volume/ m^2 of bubble interfacial area) (1/s)
- L = the mass transfer coefficient, (m^3 gas interchange volume/ m^3 of reactor) (1/s)
- α_{bub}^o = the interfacial area of the bubble phase per bubble volume (m^2 bubble/ m^3 bubble)

a_{bub} = the interfacial area of the bubble phase per reactor volume, m^2 bubbles/ m^3 reactor, estimated by (Kelkar and Ng, 2002)

$$a_{\text{bub}} = \frac{6\varepsilon_{\text{bub}}}{d_{\text{bub}}} \quad (3.549)$$

and

$$a_{\text{bub}}^{\circ} = \frac{6}{d_{\text{bub}}} \quad (3.550)$$

On the basis of these relationships, Kelkar and Ng (2002) presented the following relationships for k_m :

Bubbling bed model

Mass transfer between bubble and cloud:

$$k_{\text{bc}} = \frac{3}{4}u_{\text{fm}} + 0.975 \frac{D_g^{1/2}g^{1/4}}{d_{\text{bub}}^{1/4}} \quad (3.551)$$

where the unit of k_{bc} is in m/s .

Mass transfer between cloud and emulsion:

$$k_{\text{ce}} = \left(\frac{4\varepsilon_{\text{fm}}D_g u_{\text{bub}}}{\pi d_{\text{bub}}} \right)^{1/2} \quad (3.552)$$

where the unit of k_{bc} is in m/s .

Two-phase model

Mass transfer between bubble and emulsion:

$$k_{\text{be}} = \frac{u_{\text{fm}}}{3} + \left(\frac{4\varepsilon_{\text{fm}}D_g u_{\text{bub}}}{\pi d_{\text{bub}}} \right)^{1/2} \quad (3.553)$$

where the unit of k_{bc} is in m/s .

3.9 PARTICLE ANALYSIS

In this section, various issues concerning solid particles are presented. The analysis covers the most important particle properties (surface area, particle shape and size distribution, mechanical strength, and density) as well as the behavior of a single particle in suspension (terminal velocity) and of a number of particles in fluidization state. Finally, the diffusion of molecules in a porous particle (diffusion coefficients) is also discussed.

This “particle analysis” is of paramount importance when dealing with heterogeneous operations like adsorption, ion exchange, and catalysis.

3.9.1 Surface area

The solid provides an extended surface to the reaction or adsorption to take place. The area provided by the solid is the sum of the exterior and interior ones. Consequently, the solid surface includes not only the geometrical one as determined from the solid's shape but also the interior surface that is the result of its porous structure. The surface area is expressed as specific surface area in units of m^2/g . Its value may be from a few m^2/g up to hundreds of m^2/g . In the case of a porous solid, the interior surface constitutes the greatest percentage of the total surface, and high values of specific surface area may be achieved. Specifically, the specific area of an activated carbon can reach the value of $1500 \text{ m}^2/\text{g}$. So, the available area for a hydrocarbon to react on 4 g of activated carbon is equal to that of a football field.

3.9.2 Particle shape

Sphericity is a measure of how close a particle is to being a sphere and is defined as

$$\Phi_s = \frac{\text{surface area of a sphere with same volume as the particle}}{\text{actual surface area of the particle}} \quad (4.554)$$

For granular particles, typical values of sphericity range between 0.6 and 0.95. In Table 3.13, the sphericity of selected materials is presented.

3.9.3 Particle size

The size (diameter) and the shape of the solid particles affect the mass transfer phenomena within the particle, and thus the effectiveness in the case of a catalyst. The following shapes and sizes are frequently used in applications:

- 20–100 μm diameter spheres for fluidized-bed reactors
- 0.3–0.7 cm diameter spheres for fixed-bed reactors
- 0.3–1.3 cm diameter cylinders with a length-to-diameter ratio of 3–4
- up to 2.5 cm diameter hollow cylinders or rings

When particles of irregular shape are involved, the particle diameter corresponding to a sphere of the same volume d_{sph} is used in many equations. For instance, a cubic particle with a side of 5 mm has a volume of 5^3 , and thus the d_{sph} is

$$V_{\text{sphere}} = 125 = \frac{4}{3} \pi \left(\frac{d_{\text{sph}}}{2} \right)^3 \Rightarrow d_{\text{sph}} = 6.20 \text{ mm}$$

However, in the typical case of an irregular-shaped particle, it is not easy to calculate its volume and thus d_{sph} is taken equal to the mean nominal diameter measured by sieve analysis d_p . In the present book, d_p is considered to be equal to the average sieve diameter.

Table 3.13

Sphericity of selected materials (McCabe et al., 1983; Perry and Green, 1984 and 1999; Broadhurst and Becker, 1975)

Material	Sphericity
Spheres	1
Iron shot	0.95
Clover seed	0.95
Cracking catalyst	0.95
Ottawa sand	0.95
Tungsten powder	0.89
Short cylinder (length = diameter)	0.87
Rounded sand	0.83
Cube	0.81
Sand (average for various types)	0.75
Coal dust	0.73
Cork	0.69
Flint sand (jagged)	0.65
Coal dust (natural and up to 3/8 in)	0.65
Crushed glass	0.65
Most crushed materials	0.6–0.8
Wilcox sand (jagged)	0.6
Raschig rings	0.33–0.58
Berl saddles	0.3
Mica flakes	0.28

For polydispersed beds consisting of particles having different diameters, the equivalent diameter d_{eq} should be preferably used (Pavlov *et al.*, 1979):

$$d_{eq} = \frac{1}{\sum_1^n \frac{w_i}{d_i}} \quad (3.555)$$

where:

- n = the number of fractions
- d_i = the average screen size of the i -th fraction
- w_i = the mass content of the i -th fraction in the particle mixture.

The average screen size of a fraction is the mean arithmetical value of the average size of the screen mesh through which a fraction passes and the mesh that retains the fraction. Finally, the United States standard screen series is used (mesh size) for expressing the particle size. In Table 3.14, the conversion from mesh size to (cm) is given.

3.9.4 Pore structure

Beyond the surface area and the pore volume, the distribution of the pore radii of a catalyst has to be known, since the pore radius allows or does not allow a molecule to move

Table 3.14

Conversion from mesh to cm for particle radius	
Mesh	Particle radius (cm)
5	0.2
10	0.1
16	0.06
20	0.042
30	0.030
40	0.021
50	0.015
60	0.013
70	0.011
80	0.0089
100	0.0075
120	0.0063
140	0.0053
170	0.0044
200	0.0037
230	0.0031
270	0.0027
325	0.0022

through the pores depending on its size. Consequently, a portion of the surface area may not be available to reactants, or generally, to the diffusing species. As discussed earlier, most of the solids used in catalysis, adsorption, and ion exchange, which exhibit large surface areas, are porous. Porosity is a term used to describe the pore space of a material, defined as the fraction of the bulk volume that is occupied by pore or void space. Void is the space or interstices between particles.

The individual pores may vary greatly in both size and shape within a given solid, and between one solid and another. As presented in Chapter 2, the pores can be classified as (a) macropores, for diameters above 50 nm, (b) mesopores, for diameters in the range 2–50 nm, and (c) micropores, for diameters below 2 nm. It has to be mentioned that in a solid, a wide and continuous range of pore sizes is found, from macropores to micropores. A pore can also be an open pore, seen as a cavity or channel communicating with the surface of the particle, or a closed pore that is not connected to the surface.

The total pore volume is the total internal volume per unit mass of catalyst. Some of this pore volume may be completely enclosed and thus not available to the reaction molecules. Moreover, the accessible pore volume changes with the size of the diffusing molecules.

The pore-size distribution is the distribution of pore volume with respect to pore size (Figure 3.66). It is an important factor controlling the diffusion of reactants and products in the porous solid and thus an essential property for its characterization. The computation of pore size distribution involves a number of assumptions, and therefore reporting of the data should always be accompanied by an indication of the method used for its determination.

An interesting phenomenon about adsorption of gases on solids and ion exchange of ions on resins is swelling. Some porous solids expand on exposure to the vapors of adsorptives.

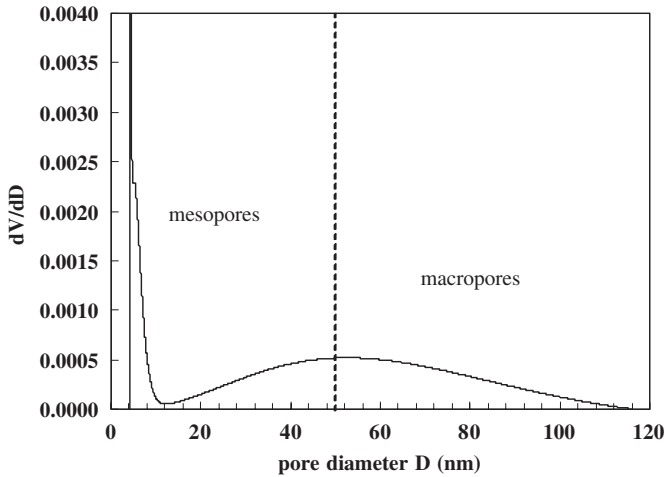


Figure 3.66 Pore size distribution of an automotive catalyst.

Rigid adsorbents, like charcoal or silica gel, swell by only a small percent, but nonrigid adsorbents, like agar-agar, may swell to several times the original size. Provided the adsorption occurs slowly, the rigid solid may accommodate the stresses, but if suddenly exposed to high vapor pressure the material may shatter.

3.9.5 Mechanical strength

The mechanical strength of a catalyst is really important in its commercial applications, since broken pieces and losses can lead to a decrease in catalytic activity and a significant expense, especially when precious metals are used as the catalytic agents. Mechanical strength is equally important in adsorption and ion exchange, especially in fixed-bed operations.

Crush strength is defined as the resistance of a formed particle to compressive forces. Measurements of crush strength provide an indication of the ability of the particle to maintain its physical integrity during handling and use. When crush strength is measured for single pieces, it is called “piece crush strength,” and when it is measured for a bulk sample it is called “bulk crush strength.” Other terms that have been used for piece crush strength but which are not recommended are static crush strength and single-pellet crush strength. The loss of solid during handling or use is called “attrition.” Abrasion, grinding, or rubbing of the particles with each other or with container walls can lead to attrition.

3.9.6 Density

In this section, definitions of terms used in relation to particle density are presented. As will be shown, these issues exhibit many alternative approaches. For instance, density is

generally defined as mass divided by volume. While mass is an easily measurable quantity, it is not the case for volume. So, referring to a porous particle, which is its volume and how can it be estimated? What should be done with the pores of the particles? Depending on the how this volume is specified, there are various types of density.

Definitions

A porous particle contains many interior voids known as open or closed pores. A pore is characterized as open when it is connected to the exterior surface of the particle, whereas a pore is closed (or blind) when it is inaccessible from the surface. So, a fluid flowing around a particle can “see” an open pore, but not a closed one. There are several densities used in the literature and therefore one has to know which density is being referred to (Table 3.15). True density may be defined as the mass of a powder or particle divided by its volume excluding all pores and voids. True density is also referred to as absolute density or crystalline density in the case of pure compounds. However, this density is very difficult to be determined and can be calculated only through X-ray or neutron diffraction analysis of single-crystal samples. Particle density is defined as the mass of a particle divided by its hydrodynamic volume. The hydrodynamic volume includes the volume of all the open and closed pores. Practically, the hydrodynamic volume is identified with the volume included by the outer surface of the particle. The particle density is also called “apparent” or “envelope” density. The term “skeletal density” is also used. The skeletal density of a porous particle is higher than the particle one, since it is the mass of the particle divided by the volume of solid material making up the particle. In this volume, the closed pores volume is included. The interrelationship between these two types of density is as follows (ASTM, 1994; BSI, 1991):

$$\rho_s = \frac{\rho_p}{1 - \varepsilon_p} \quad (3.556)$$

$$\rho_p = \frac{\rho_b}{1 - \varepsilon} \quad (3.557)$$

where:

- ε_p = the internal particle porosity
- ρ_b = the bed density
- ε = the bed porosity
- ρ_p = the particle density.

Bulk density, or packing density, includes all pores and voids (interparticle spaces) in its calculation. This value depends on the form of the particle (powder, tablets, or extrudates) and the packing procedure. It is extensively used in reactor designing since this value connects the solid volume with that of the reactor.

When a porous particle is immersed in a fluid, it has an effective density different from the skeletal and particle density. This density is termed “wet” or “effective density” (Perry and Green, 1999).

$$\rho_h = \varepsilon_p \rho_f + \rho_s (1 - \varepsilon_p) = \rho_s - \varepsilon_p (\rho_s - \rho_f) = \varepsilon_p \rho_f + \rho_p \quad (3.558)$$

Table 3.15

The density definitions

Density	Volume included in definition				
	Symbol	Solid material volume	Open pore volume	Closed pore volume	Interparticle void volume
Bulk	ρ_b	✓	✓	✓	✓
Particle	ρ_p	✓	✓	✓	
Skeletal	ρ_s	✓	✓		
True	ρ_t	✓			

where ρ_f is the fluid density. In the present book, the term “hydraulic density” is introduced in order to highlight the use of this kind of density in hydrodynamic calculations involving *suspension* of particles.

Despite the fact that this hydraulic density is essential to many calculations involving fluidization and the suspension of particles, it is characteristic that in the related literature, authors use the terms “particle density” or “solid density” without specifying if the fluid in the pores has been taken into account. However, the subject of hydraulic density has been analyzed in studies of the behavior of impermeable aggregates in fluids. As these aggregates could be seen as porous particles, the relevant analysis is interesting and will be presented here.

The case of hydraulic density

The case of impermeable spherical aggregates has been analyzed by Johnson *et al.* (Johnson *et al.*, 1996). In this work, the settling velocity of aggregates in liquids using Stoke’s law has been studied and a modified Stoke’s law has been introduced. The difference from the classical Stoke’s law is that the density difference is expressed in terms of the aggregate density.

$$\rho_a = \varepsilon_a \rho_f + \rho_s (1 - \varepsilon_a) \quad (3.559)$$

where:

- ε_a = the aggregate porosity
- ρ_a = the aggregate density
- ρ_s = the density of the particles composing the aggregate.

Thus, the aggregate–fluid density difference becomes

$$\begin{aligned} \rho_a - \rho_f &= \varepsilon_a \rho_f + \rho_s (1 - \varepsilon_a) - \rho_f \\ &= \rho_s (1 - \varepsilon_a) - \rho_f (1 - \varepsilon_a) = (1 - \varepsilon_a)(\rho_s - \rho_f) \end{aligned} \quad (3.560)$$

To highlight the difference from the classical Stoke’s equation, the density difference in the latter is $(\rho_s - \rho_f)$, where ρ_s is the skeletal density of the rigid particle. Now, it is easy to illustrate the analogy to a porous particle. A porous particle can be viewed as an aggregate,

where ρ_s is the density of the solid part (skeletal density) and ε_a is the porosity of the particle. Then, it is clear that Johnson's aggregate density is the hydraulic density defined in eq. (3.558), since the term $\rho_s(1 - \varepsilon_a)$ is equal to the particle density ρ_p .

Several forms of the modified Stoke's law have been used in a series of studies concerning aggregates in the liquid phase (Li and Yuan, 2002). In these studies, the particle–liquid density difference has been further modified and adopted for the cases of impermeable biological/microbial aggregates, permeable aggregates, and fractal aggregates.

The introduction and use of a hydraulic density, termed in a different way, in liquid–porous solid fluidization has been done by Nesbitt and Petersen (1998). They point out that for resins, which are porous in nature, it might be more correct to use an “apparent density” of fluidization (ρ_{ap}), a property relevant only when the resin is in a suspension, with the fluid phase intruding into the pores. However, the authors did not use eq. (3.558), but an experimental technique, measuring the terminal velocity of the resin particles and evaluating the “apparent density” using the Shiller and Naumann terminal velocity model:

$$Ga = 18Re_{ter} + 2.7Re_{ter}^{1.687} \quad (3.561)$$

where:

$$Ga = \frac{d_p^3 g \rho_f (\rho_{ap} - \rho_f)}{\mu_f^2} \quad (3.562)$$

$$Re_{ter} = \frac{\rho_f d_p u_{ter}}{\mu} \quad (3.563)$$

$$\text{for } 3.6 < Ga < 10$$

As in Stoke's equation, the solid–fluid density difference is also involved in the Shiller and Naumann model and so the evaluated density is equivalent in nature to the hydraulic density defined above by Johnson, which is different from skeletal and particle density. The benefit in this case is that the experimental determination of particle voidage and particle density, which could be quite complicated in some cases, is avoided and the hydraulic density is directly evaluated without using eq. (3.558). The same approach has been followed by Menoud *et al.* (1998) in a study of a fluidized bed using a chelating resin. Wet density has been used by Feng *et al.* (2003) for a fluidized-bed ion-exchange system. Finally, Griffith *et al.* (1997) used a gravimetric method for the evaluation of the so-called “effective particle density during fluidization.”

The particle and bulk densities are commonly used in mass balance equations, since the mass and the external volume of the particles are involved. On the other hand, the hydraulic density should be preferably used in hydrodynamic calculations, because buoyancy forces are involved, and so the total mass of the particle should be taken into account, including the fluid in the open pores. It is obvious that the particle density is equal to the skeletal and hydrodynamic density in the case of nonporous particles. Moreover, in the case of a porous solid in a gas–solid system, the gas density is much lower than the particle density, and thus

the latter is practically equal to the hydraulic density. This is the reason why in gas–solid fluidization, the particle density is used in all hydraulic calculations. The complication is found only in the case where porous solids are found in suspension in a liquid–solid system, e.g. fluidization and suspension/sedimentation in agitated vessels. In any case, one should be aware of the type of density used or that should be used. For example, Menoud *et al.* (1998) used two different densities for modeling the fluidized bed operation, i.e. the resin particle density for mass balances and relevant calculations, and the hydraulic density for the relevant hydraulic calculations (e.g. for the evaluation of Archimedes number).

Special reference should be made to resin–liquid systems, where the phenomenon of swelling makes the case more complex. A resin's matrix is flexible and when immersed in a liquid, its volume expands, leading to an increase in its particle diameter and in turn, to a decrease in particle density (mass of dry resin per volume of swollen particle). Furthermore, the loading of the resin with ions results in further changes in its volume (Helfferich, 1995). Thus, in these cases, the particle density and diameter as well as the hydraulic density should be referred to for the swollen and loaded resin. In practice, a mean value is frequently used.

3.9.7 Terminal velocity of a single particle

The forces that are present when an isolated porous particle is suspended in a fluid are the following.

The gravitational force F_g ,

$$F_g = M_p g \quad (3.564)$$

the buoyant force F_b ,

$$F_b = V_f g \quad (3.565)$$

and the drag force F_d .

$$F_d = F_g - F_b = \frac{\rho_f A_{pr} C_D}{2} u_{ter}^2 \quad (3.566)$$

where:

M_p = the mass of the particle

V_f = the volume of fluid displaced by the particle

A_{pr} = the area of the particle projected on a plane normal to the direction of flow (projected area perpendicular to flow)

u_{ter} = the terminal velocity

C_D = an empirical drag coefficient.

Then,

$$M_p = \rho_p V_p + \varepsilon_p \rho_f V_p \quad (3.567)$$

and

$$V_f = \rho_f V_p \quad (3.568)$$

In eq. (3.564), the gravitational force accounts for the mass of the fluid, which is included in the volume of the particle. So,

$$M_p = V_p(\rho_p + \varepsilon_p \rho_f) = \rho_h V_p \quad (3.569)$$

Using the above equations, the terminal velocity relationships can be derived. The drag force is

$$F_d = (\rho_h - \rho_f) V_p g \quad (3.570)$$

Finally, a formal definition of terminal velocity is derived from the equations above:

$$u_{\text{ter}} = \left[\frac{2g V_p (\rho_h - \rho_f)}{A_{\text{pr}} \rho_f C_D} \right]^{0.5} \quad (3.571)$$

For a spherical particle,

$$\frac{V_p}{A_{\text{pr}}} = \frac{\left(\frac{\pi d_p^3}{6} \right)}{\left(\frac{\pi d_p^2}{4} \right)} = \frac{2d_p}{3} \quad (3.572)$$

Note that the “projected area” is the area of the object projected on the perpendicular to the flow plane; for a sphere, this is equivalent to the area of a circle with the same radius.

Thus, the following well-known definition is derived (Perry and Green, 1999):

$$u_{\text{ter}} = \left[\frac{4gd_p(\rho_h - \rho_f)}{3\rho_f C_D} \right]^{0.5} \quad (3.573)$$

where C_D is the drag coefficient. This is the constant terminal velocity with which a particle falls when the accelerating effect of gravity balances the drag force.

Within the intermediate Re_{ter} region ($0.1 < Re_p < 1000$), the drag coefficient can be estimated via the relation

$$C_D = \frac{24}{Re_p} (1 + 0.14 Re_p^{0.7}) \quad (3.574)$$

Within the range of Stoke's law, $Re_{\text{ter}} < 1$ and $C_D = 24/Re_{\text{ter}}$, and thus

$$u_{\text{ter}} = \frac{gd_p^2(\rho_h - \rho_f)}{18\mu_f} \quad (3.575)$$

Within the range of Newton's law, $Re_{\text{ter}} > 1000$ and $C_D = 0.445$, and thus

$$u_{\text{ter}} = 1.73 \left[\frac{gd_p(\rho_h - \rho_f)}{\rho_f} \right]^{0.5} \quad (3.576)$$

where Re_{ter} is the Reynolds number based on the terminal particle velocity. In all the equations above, SI units should be used. For $u_s > u_{\text{ter}}$, the particle is blown out of the bed and thus it can be considered as the maximum fluidization velocity.

Haider and Levenspiel (1989) found a useful relationship for the direct evaluation of the terminal velocity of particles. They used the following equations on the grounds that $0.5 < \Phi_s < 1$:

$$U_{\text{ter}} = \left(\frac{18}{D_{\text{sph}}^2} + \frac{2.335 - 1.744\Phi_s}{D_{\text{sph}}^{0.5}} \right)^{-1} \quad (3.577)$$

where:

$$U_{\text{ter}} = u_{\text{ter}} \left[\frac{\rho_f^2}{\mu g(\rho_h - \rho_f)} \right]^{1/3} \quad (3.578)$$

and

$$D_{\text{sph}} = d_{\text{sph}} \left[\frac{\rho_f g(\rho_h - \rho_f)}{\mu^2} \right]^{1/3} \quad (3.579)$$

SI units should be used in these equations. Furthermore, the effect of particle sphericity is included. Here, d_{sph} could be taken equal to the mean nominal diameter measured by sieve analysis (d_p).

Another useful correlation is the Khan–Richardson correlation (Hilal, 2000):

$$Ar = (2.07Re_{\text{ter}}^{0.27} + 0.33Re_{\text{ter}}^{0.64})^{3.45} \quad (3.580)$$

where Re_{ter} is the Reynolds number based on the terminal particle velocity and Ar is the Archimedes number.

$$Ar = \frac{d_p^3 \rho_f (\rho_h - \rho_f) g}{\mu^2} \quad (3.581)$$

This correlation holds for both gas and liquids and for the whole region of Reynolds number. However, since it cannot be solved analytically, a trial-and-error procedure is required.

3.9.8 Particles in fluidization state

In a fluidized bed of depth Z and cross-sectional area A_b , the total number of particles (N_{tot}) can be evaluated as follows:

$$N_{\text{tot}} V_p = (1 - \varepsilon) Z A_b \Rightarrow N_{\text{tot}} = \frac{(1 - \varepsilon) Z A_b}{V_p} \quad (3.582)$$

The number of particles in a unit cross-sectional area of bed N is

$$N = \frac{N_{\text{tot}}}{A_b} = \frac{(1 - \varepsilon) Z}{V_p} \quad (3.583)$$

The total weight of the suspension is

$$B = N A_b M_p g + \varepsilon \rho_f Z A_b g \quad (3.584)$$

An overall force balance on a control volume (solids and fluid) of a fluidized bed reveals that the total weight of the suspension is supported by the net force due to the difference in the pressure intensity on the horizontal surfaces (Foscolo and Gibilaro, 1984).

$$\Delta p_1 = p_1(z) - p_1(z + Z) = \frac{B}{A_b} = N M_p g + \varepsilon \rho_f Z g \quad (3.585)$$

The effective mass of the particle is (eq. (3.569))

$$M_p = V_p (\rho_p + \varepsilon_p \rho_f) = \rho_h V_p \quad (3.586)$$

and

$$N M_p = \frac{(1 - \varepsilon) Z}{V_p} \rho_h V_p = (1 - \varepsilon) Z \rho_h \quad (3.587)$$

Then

$$\Delta p_1 = [\varepsilon \rho_f + (1 - \varepsilon) \rho_h] Z g \quad (3.588)$$

The pressure intensity is related to the piezometric pressure p , through the definition of the latter quantity:

$$p = p_1 + \rho_f g z \quad (3.589)$$

where (z) is the elevation above a datum plane. Then

$$\Delta p = p(z) - p(z + Z) = \Delta p_1 + [\rho_f g z - \rho_f g(z + Z)] = \Delta p_1 - \rho_f g Z \quad (3.590)$$

By using the above equations, the eq. (3.448) for the determination of pressure drop in a fluidised bed is derived (Section 3.8.2):

$$\Delta p = Z g [\varepsilon \rho_f - \rho_f + (1 - \varepsilon) \rho_h] \quad (3.591)$$

or

$$\Delta p = Z(1 - \varepsilon)(\rho_h - \rho_f)g \quad (3.592)$$

The same analysis could be conducted by using forces. Consider a particle of height l and of projected area perpendicular to flow A_{pr} . The net upthrust on the projected area dA_{pr} is

$$\Delta p_1 dA_{pr} = [[\varepsilon \rho_f + (1 - \varepsilon) \rho_h] g l] dA_{pr} \quad (3.593)$$

The integration of this equation over the entire projected area of the particle yields the buoyancy force:

$$F_b = [\varepsilon \rho_f + (1 - \varepsilon) \rho_h] g \int_{A_{pr}} l dA_{pr} \quad (3.594)$$

The integral in this equation is equal to the volume of particle. Thus,

$$F_b = [\varepsilon \rho_f + (1 - \varepsilon) \rho_h] g V_p \quad (3.595)$$

Comparing this equation to that of a single particle (eq. (3.565)), it is evident that in applying the Archimedes principle to a particle in a fluidized suspension, it is an average suspension density, including the particle density, rather than that of the fluid alone, that determines the buoyancy force (Foscolo and Gibilaro, 1984). The gravity force is

$$F_g = \rho_h V_p g \quad (3.596)$$

Thus, the drag force is

$$F_d = (\rho_h - \rho_f) V_p g \varepsilon \quad (3.597)$$

The pressure drop reflects the sum of single-particle drag-force contributions, which is (Foscolo and Gibilaro, 1984)

$$\varepsilon \Delta p = NF_d \quad (3.598)$$

Using this equation and the equations for F_d and N ,

$$\Delta p = Z(1 - \varepsilon)(\rho_h - \rho_f)g \quad (3.599)$$

From the analysis presented in the last two paragraphs, it is evident that the gravitational force acting upon the particle is used for the derivation of the equations for the terminal velocity and the pressure drop in the fluidized bed. Then, it is clear that the hydraulic density should be used in these equations as well as in any other equations that are derived from a similar force-balance analysis. For instance, this is the case of the Foscolo–Gibilaro criterion for determining the fluidization pattern (Section 3.8.2).

As mentioned before, the hydraulic density is not used for gases, simply because the density difference between the solid and the fluid phase is so big that this density is practically equal to the particle density. For this reason, the particle density is found in all relevant equations and correlations.

Much attention should be given to correlations for liquid–solid suspensions or fluidizing systems derived experimentally. If the experimental data have been correlated to particle density, this kind of density and not the hydraulic density should be used. For instance, this is the case of the Liu–Kwauk–Li criterion for determining the fluidization pattern (Section 3.8.2). However, for correlations that have been derived using nonporous particles, the hydraulic density should be used. This is because the correlation accounts for the whole mass included in the volume of the particle, which is the sum of the solid mass and liquid mass in the pores for porous particles.

A problem arising when using hydraulic density is the possibility of partial internal wetting of the porous particle. Using eq. (3.598), it is assumed that the pores are totally filled with liquid, which is generally, but not always, true. This is why several authors correlate data to particle density, which normally, is a given and well-defined parameter. Furthermore, for the same reason, some authors use models to indirectly determine hydraulic density.

3.9.9 Diffusion and diffusion coefficients in porous solids

General

In porous solids, it is the diffusion within the solid particles that usually controls the mass transfer in many applications, such as adsorption, ion exchange, drying, and heterogeneous catalysis. Bulk diffusion is considered to take place within the large pores, except that it is hindered by the pore walls (Perry and Green, 1999). This hindrance is expressed by the tortuosity factor τ_p , which is estimated from geometric arguments. However, this approach often results in values far from reality. Hence, a diffusion model fed with experimental measurements is generally employed for the evaluation of the effective diffusivity D_{eff} and

hence τ_p . Typical values of the tortuosity factor are in the range $2 < \tau_p < 6$ for silica gel and alumina, $5 < \tau_p < 65$ for activated carbon, and $3 < \tau_p < 4$ for catalyst particles, if no other information is available (Froment and Bischoff, 1990). Generally, the tortuosity factor should be handled as an empirical constant, which is characteristic for each material, and should be evaluated experimentally (Perry and Green, 1999).

Estimation methods

Depending on the specific pore system, the diffusion in a solid particle takes place in three ranges (Perry and Green, 1999):

- Knudsen diffusion in small pores (D_k)
- Fick's or molecular diffusion in large pores (D_F), also called "bulk diffusion"
- Transition range diffusion, which includes both mechanisms (D_t)

The Knudsen diffusion coefficient D_k corresponds to the movement of gaseous solutes in small pores and can be estimated by using the following equation (Perry and Green, 1999):

$$D_k = 9700 r_{\text{pore}} \sqrt{\frac{T}{MB}} \quad (3.600)$$

Here, D_k is in cm^2/s , r_{pore} the average pore radius (cm), MB the molecular weight of the gas (g/mol), and T the temperature in K. In the case of a narrow pore size distribution, the average pore radius can be estimated as follows (Froment and Bischoff, 1990):

$$r_{\text{pore}} = \frac{2\varepsilon_p}{S_s \rho_p} \quad (3.601)$$

where ε_p is the internal porosity of the solid, ρ_p the particle density of the solid (g/cm^3), and S_s the specific area of the solid (cm^2/g). The bulk diffusion coefficient corresponds to the movement of gaseous or liquid solutes in large pores and can be estimated as follows:

$$D_F = D_f \frac{\varepsilon_p}{\tau_p} \quad (3.602)$$

where D_f is the diffusion coefficient of the molecules in the fluid phase and τ_p the tortuosity of the solid structure, which is defined as the ratio of the actual distance a molecule travels between two points and the shortest distance between these points (Fogler, 1999). Fogler (1999) adds one more factor to the above equation:

$$D_F = D_f \frac{\varepsilon_p \sigma_p}{\tau_p} \quad (3.603)$$

where σ_p is the constriction factor that accounts for the variation in the cross-sectional area that is normal to diffusion. A typical value of the constriction factor is 0.8.

Then, the combined (transitional) diffusion coefficient is

$$D_t = \frac{1}{D_F} + \frac{1}{D_k} \quad (3.604)$$

The tortuosity could be evaluated using the Bruggemann's equation:

$$\tau_p = \frac{1}{\sqrt{\varepsilon_p}} \quad (3.605)$$

or using the Mackie and Meares equation (Perry and Green, 1999),

$$\tau_p = \frac{(2 - \varepsilon_p)}{\varepsilon_p} \quad (3.606)$$

For gel-type exchange resins and for macropore resins with a low degree of cross-linking, the following equation is proposed for the solid diffusion coefficient (Helfferich, 1962):

$$D_s = D_f \left(\frac{\varepsilon_p}{2 - \varepsilon_p} \right)^2 \quad (3.607)$$

which is Fick's or molecular diffusion in large pores, as defined before.

Although there are a lot of data in the literature regarding diffusion coefficients in liquids or their calculation from molecular properties (Appendix I, Section I.2), it is not the case for diffusion coefficients in solids, where the phenomena appearing are more complex. In solids, the molecule may be forced to follow a longer and tortuous path due to the blocking of the cross-sectional area, and thus the diffusion is somehow impaired. Several models have been developed to take into consideration this effect in the estimation of diffusion coefficients, leading, however, to a variety of results.

Adsorption and Ion Exchange

4.1 BASIC PRINCIPLES OF ADSORPTION AND ION EXCHANGE

4.1.1 Adsorption materials

Activated carbon, silica gel, and alumina are the most popular adsorbent materials in industry due to the fact that they provide large surface areas per unit weight. Activated carbon is produced from coconut shell, wood, and bone, whereas silica gel is made of hydrated silicon dioxide. Alumina can be either mined or produced by precipitated aluminum oxide and hydroxide. In the following sections, the most important adsorbents are presented in detail.

Activated carbon

Activated carbon can be manufactured from carbonaceous material, including coal such as lignite, peat, and wood, or nutshells such as coconut. The manufacturing process consists of two phases, carbonization and activation. The carbonization process includes drying and heating, the aim being the removal of several undesirable by-products from the raw material such as tar and other hydrocarbons. During the carbonization process, the material is heated at 400–600 °C in an oxygen-deficient atmosphere that cannot support combustion. Activated carbon has a very large surface area per unit weight, which makes it an ideal absorptive material. Generally, the total surface area of activated carbon ranges between 300 and 1500 m²/g, and the pore volume ranges between 0.7–1.8 cm³/g. Activated carbons made from petroleum coke can have a surface area of almost 3000 m²/g (Knaebel, 1995).

Powdered activated carbon (PAC): PAC is made up of crushed or ground carbon particles, 95–100% of which will pass through a designated sieve—0.297 mm according to the American Water Works Association Standard, or 0.177 mm according to ASTM D5158. PAC is mainly used for biological treatment.

Granular activated carbon (GAC): GAC is designated by mesh sizes such as 8 × 20, 20 × 40, or 8 × 30 for liquid-phase applications and 4 × 6, 4 × 8, or 4 × 10 for vapor-phase applications. GAC is used for the removal of toxic organic compounds from groundwater and industrial wastewater.

Bituminous GAC: Bituminous coal has a more fully developed pore distribution, including “transport pores,” and is particularly effective for water treatment. It exhibits a relatively

large surface area ($\sim 900 \text{ m}^2/\text{g}$) and an apparent density of approximately 0.50 g/cm^3 . With the exception of coconuts, this type of carbon is harder than other types, thus being more resistant to abrasion, and can be more vigorously backwashed without damage. Bituminous GAC is one of the most frequently used carbons for the treatment of low concentrations of low molecular weight organic compounds in water.

Lignite GAC: This presents a total surface area of $650 \text{ m}^2/\text{g}$ and an apparent density of 0.50 g/cm^3 , approximately. It is usually used for liquid-phase adsorption, and specifically, in decolorizing applications because it has a higher percentage of meso (transitional) and macro pores than bituminous GAC, and therefore is appropriate for larger molecules.

Coconut-shell-based GACs: These have a high portion of micropores and present surface areas generally over $1000 \text{ m}^2/\text{g}$ and apparent densities of about 0.50 g/cm^3 . Being manufactured mainly from vegetative material, they do not exhibit the fully developed pore structure of coal-based carbons. They are used in both vapor- and liquid-phase applications. Coconut shell-based carbon is slightly more expensive to produce than coal-based GAC, since about only 2% of the raw material is recoverable as GAC, versus 8–9% for coal-based carbons. In Table 4.1, the basic properties of common materials used in the manufacture of activated carbon are presented.

A look into activated carbon

Activated carbon is an adsorbent extensively used for the purification of water and gaseous waste streams. In relation to water treatment, it is generally effective in removing large organic molecules and nonpolar compounds from water, and its use is suggested for the following compounds (EPA, 2000):

- (a) *Organic compounds:* aromatic solvents (benzene, toluene, nitrobenzenes, and xylene), chlorinated aromatics (PCBs, chlorobenzenes, chloronaphthalene, endrin, and toxaphene), phenols and chlorophenols (cresol, resorcinol, and nitrophenols), polynuclear aromatics (acenaphthene, benzopyrenes, naphthalene, and biphenyl), pesticides and herbicides (DDT, aldrin, chlordane, BHCs, heptachlor, carbofuran, atrazine, simazine, alachlor, and aldicarb), chlorinated

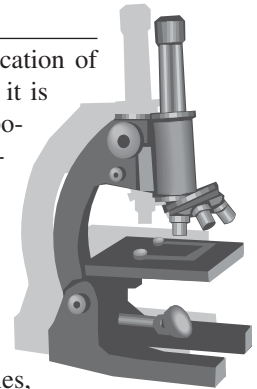


Table 4.1

Basic properties of common materials used in the manufacture of activated carbon
(Dabrowski *et al.*, 2005; Streat *et al.*, 1995)

Raw material	Carbon (%wt)	Volatiles (%wt)	Density (g/cm^3)	Ash (%wt)
Wood	40–45	55–60	1.25–2.5	0.3–1.1
Lignin	35–40	58–60	2.5–3.33	–
Nutshells	40–45	55–60	0.71	–
Lignite	55–70	25–40	0.74–1	5–6
Coal	65–95	5–30	0.55–0.8	2–15
Petroleum coke	70–85	15–20	0.74	0.5–0.7

nonaromatics (carbon tetrachloride, chloroalkyl ethers, and hexachlorobutadiene), high molecular weight hydrocarbons (dyes, gasoline, amines, humics, and kerosene, oil), and surfactants (alkyl benzene sulfonates).

- (b) *Inorganic compounds*: chlorine, bromine, iodine, fluoride, antimony, arsenic, bismuth, chromium, tin, silver, mercury, cobalt, and zirconium.

In contrast, organic compounds like alcohols, low-molecular-weight ketones, acids and aldehydes, sugars and starches, very high molecular weight or colloidal organics, low-molecular-weight aliphatics, and inorganic compounds such as nitrate, phosphate, chloride, bromide, iodide, lead, nickel, titanium, vanadium, iron, copper, cadmium, zinc, barium, selenium, molybdenum, manganese, tungsten, and radium are poorly absorbed on activated carbons.

There are a number of cases where carbon adsorption is preferably used in water treatment:

- if compounds are not compliant for biodegradation,
- if the molecule contains branched chains, has a large molecular weight, and low polarity,
- in the case of removing solids for concentrations lower than 50 ppm,
- in the case of removing oil for concentrations is lower than 10 ppm,
- generally, in the case of removing organics and inorganic species, for concentrations lower than 5000 and 1000 mg/L, respectively.

Besides the applications of water treatment, activated carbon is called into action for the removal of volatile organic compounds such as solvents, toxic gases, and odors from gaseous waste streams. Hydrogen sulfide, mercury, and radon can also be removed from gas streams by means of chemically impregnated carbons. In fact, among the adsorbents, it is the most attractive material because it is the only common nonpolar adsorbent (Noble and Terry, 2004). The polarity of the adsorbent's surface plays a major role in the type of the compounds that can be adsorbed. Polar adsorbents will preferentially adsorb moisture in gaseous waste streams, and as a result their usage in such applications is limited. In contrast, activated carbon is an appropriate material in such cases, where the goal is the control of emissions of organic solvents, odors, toxic gases, acid vapors, phenols, and hydrocarbon vapors.

Some basic rules for carbon adsorption are the following:

- Larger molecules adsorb better than smaller molecules.
- Nonpolar molecules adsorb better than polar molecules.
- Nonsoluble or slightly soluble molecules adsorb better than highly soluble molecules.
- On the basis of the polarity or solubility, or both, of the molecule being adsorbed, the pH may have an influence on the extent of adsorption.
- Temperature increases the rate of diffusion through the liquid to the adsorption sites; but since the adsorption process is exothermic, increases in temperature may reduce the degree of adsorption. This temperature effect is negligible in water-treatment applications and ambient vapor-phase applications.

The following are examples (see Table 4.2):

- Alcohols are poorly adsorbed; they are very soluble and highly polar.
- Aldehydes are highly polar, and as the molecular weight increases, the polarity decreases and adsorbability increases.
- Amines are similar in structure to ammonia (NH₃) except that the nitrogen is bonded to an organic group. Adsorption is limited by polarity and solubility.
- Chlorinated aromatics and chlorinated aliphatics are low-polarity and low-solubility compounds, which make them generally quite adsorbable.
- Glycols are water-soluble, and are not very adsorbable.
- Higher molecular weight organic compounds will generally be more adsorbable owing to adsorptive attraction relative to size.

Largely, the same principles apply for water treatment. Consequently, activated carbon is suitable for organic molecules that are nonpolar and of high molecular weight. Trichloroethylene, benzene, ethylbenzene, toluene, and xylene are easily adsorbed in the gas phase when activated carbon, for instance, is used. On the other hand, adsorption is not preferably selected in applications in relation to aldehydes, ketones, and alcohols. In a successful application, reduction in emissions from 400–2000 ppm to under 50 ppm can be achieved (EPA, 1999), especially for VOCs with boiling points between 20 –and 175 °C.

Table 4.2

From stronger adsorption to weaker adsorption on activated carbon

Compound	Molecular weight	Boiling point (°C)
Nitrobenzene	123	211
Tetrachloroethane	166	147
Tetrachloroethylene	165	121
Styrene	104	145
Xylene	106	138
Naphthalene	128	217
Toluene	92	111
Benzene	78	80
		>10% of carbon capacity
MTBE	88	55
Hexane	86	68
Ethylacrylate	100	57
Dichloroethane	99	99
Methylethylketone	72	80
Methylene chloride	84	40
Acrylonitrile	53	74
		<1% of carbon capacity
Acetone	58	56
Vinylchloride	62	–14
Chloroethane	64	12
Bromotrifluoromethane	149	–58
Methane	16	–161

For optimum efficiency, humidity levels, temperature, and pressure should be monitored and controlled during the adsorption. The adsorption process of VOCs removal is exothermic in the most cases, which should be considered as a significant design parameter, since there is a risk of fire in the removal of high loads of organic compounds that exhibit high heats of adsorption.

Activated alumina

Activated alumina is amorphous or crystalline alumina, which has been partially or completely dehydrated and has a large surface area per unit mass. Activated alumina is made from hydrated alumina, namely, $\text{Al}_2\text{O}_3 \cdot n\text{H}_2\text{O}$, where $n = 1\sim 3$, by calcining to get n closeto 0.5 (Knaebel, 1995). It is a white or tan-colored material of chalky appearance.

Stable crystalline forms are usually not thought of as adsorbents because they have very low surface areas (Knaebel, 1995). However, transitional forms, such as gamma and beta alumina (Figure 4.1), have high surface areas, typically between 200 and 400 m^2/g . They contain pores with diameters largely in the range 2–5 nm (Noble and Terry, 2004). Being extremely hydrophilic materials, they find application mainly in the removal of water from acid, gas, or organic solvent streams.

Silica gel

Silica gel is synthetic amorphous silica consisting of a compact network of spherical colloidal silica particles. Its surface area is typically between 300 and 850 m^2/g . The predominant pore diameters are in the range 22–150 Å. Silica gel is produced via the following procedure: a sodium silicate solution reacts with a mineral acid, such as sulfuric acid, producing a concentrated dispersion of finely divided particles of hydrated SiO_2 ,

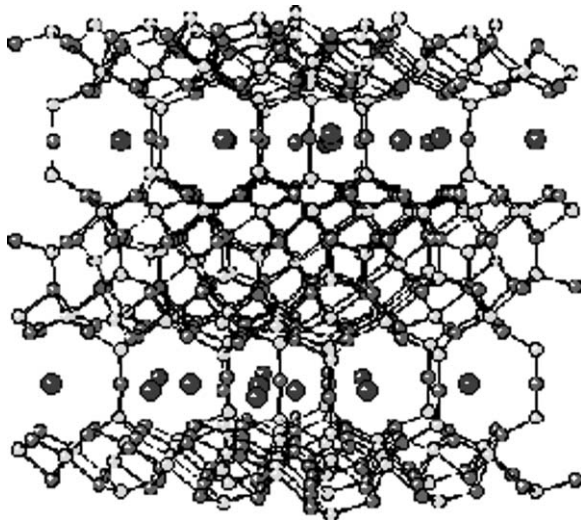


Figure 4.1 The structure of beta alumina.

which in turn polymerizes to form the silica gel. The treatment of silica gel involves also washing, drying, and activation. Silica gel is mainly used for water removal (Noble and Terry, 2004).

Organically modified clays

Organically modified clays are mixtures of anthracite and bentonite clay or bulk clay. The surface of the clay is usually activated after treating with a quaternary amine. These clays are employed only in the purification of gas streams.

Polymeric resin adsorbents

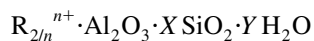
Polymeric resins found in liquid treatment can be classified into three main categories:

- (a) the carbonized ion-exchange resins,
- (b) the divinylbenzene (DB) adsorbents, and
- (c) the post-cross-linked adsorbents.

Each type is produced by following a different procedure and has its own advantages and limitations. Carbonized resins have the advantage of being structured with the desired pore distribution depending on the contaminant to be adsorbed. Divinylbenzene adsorbents can be used in environments with high relative humidity, since they are very hydrophobic materials. In general, the most important feature of polymeric resins is that they adsorb the pollutant without reacting with them. For example, the adsorption on activated carbon is generally an exothermic process that may lead to temperature elevation and bed-fire outbursts. On the other hand, safer and controlled operation can be assured using polymeric adsorbents, since they are much less reactive materials.

Zeolite molecular sieves

Zeolite molecular sieves are composed of silicon and aluminum and can be natural or man-made minerals. Molecular sieves are crystalline, hydrated aluminosilicates of (most commonly) sodium, calcium, potassium, and magnesium. The aluminosilicate portion of the structure is a three-dimensional open framework consisting of a network of AlO_4 and SiO_4 tetrahedra linked to each other by sharing all of the oxygens (Sherman, 1978). Zeolites may be represented by the empirical formula



where X is generally equal to or greater than 2, and n is the cation valence (Sherman, 1978). The zeolite framework contains pore channels and interconnected voids and cavities, which are occupied by cations and water molecules. These cations are generally mobile and can be exchanged.

A typical synthetic zeolite is the zeolite ZSM-5 shown in Figure 4.2. This zeolite is extensively used as a catalyst.

In Table 4.3, the basic characteristics of the most important zeolite molecular sieve species are presented. Zeolite micropore openings are of the same order of magnitude as

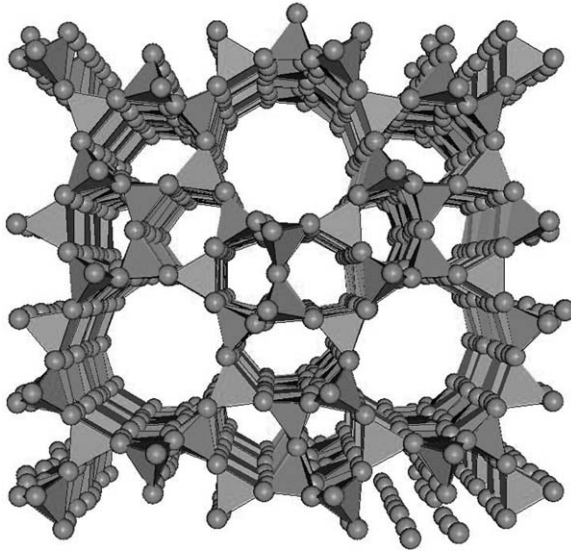


Figure 4.2 The structure of ZSM-5 zeolite.

Table 4.3

Basic characteristics of some important zeolite molecular sieve species (Sherman, 1978)

Zeolite type	Pore openings (hydrated form)	Typical SiO ₂ /Al ₂ O ₃ mole ratio
Chabazite	3.7 × 4.2 and 2.6 Å	4
Clinoptilolite	4 × 5.5, 4.4 × 7.2, and 4.1 × 4.7 Å	10
Mordenite	6.7 × 7 and 2.9 × 5.7 Å	10
Phillipsite	4.2 × 4.4, 2.8 × 4.8, and 3.3 Å	4.4
LINDE A	4.2 and 2.2 Å	2
LINDE F	3.7 Å	2
LINDE X	7.4 and 2.2 Å	2.5
LINDE Y	7.4 and 2.2 Å	2.8

the sizes of numerous molecules such as helium, water, hydrogen, nitrogen, oxygen, carbon monoxide and dioxide, and sulphur dioxide, which are between 2.2 and 4.1 Å, and methane, ethane, propane, benzene, cyclohexane, and chloroform, which are between 3.8 and 6.1 Å (Knaebel, 1995).

Zeolites are suitable for heavy-duty purifications of gas streams. Moreover, like resins, they can be manufactured with pore structures of the desired diameter in order to be used for the selective adsorption of specific contaminants based on their molecular size. They are resistant to temperature rise, being stable at temperatures up to 800 °C in dry air and up to 500 °C in humid air. Therefore, they can be treated at high temperature with air to avoid the

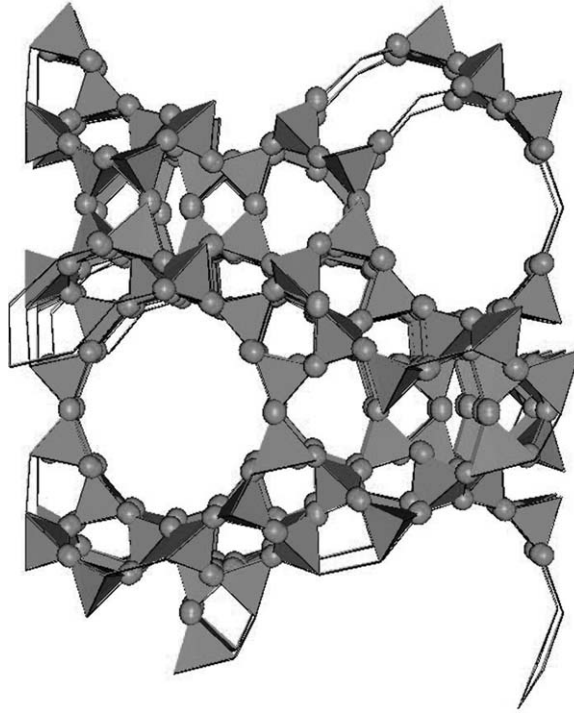


Figure 4.3 The structure of zeolite Y.

formation of contaminated condensate. They also assure safe operation since they are much less reactive than activated carbon when adsorbing reactive organic substances.

Due to the larger size of sorbates and the lower diffusion rates in liquids, larger pore sizes are needed to treat liquid effluents, normally in the range 30 Å (Noble and Terry, 2004). For gas-phase effluents, the pore sizes are in the range 10 to 25 Å. For example, zeolite Y (Figure 4.3) exhibits the FAU (faujasite) structure. It has a three-dimensional pore structure with pore diameter 7.4 Å and cavity of diameter 12 Å.

Low-cost adsorbents for wastewater treatment

Some low-cost adsorbents for the treatment of wastewater, especially for the removal of heavy metals, are the following (Babel and Kurniawan, 2003):

- *Chitosan*: Chitosan has a molecular structure similar to cellulose. This material is produced from chitin, which is widely found in the exoskeleton of shellfish and crustaceans. Chitin is the second most abundant natural biopolymer after cellulose. Chitosan is a good adsorbent for all heavy metals. It has been estimated that chitosan can be produced from shellfish and crustaceans at a market price of 15.43 \$/kg.
- *Peat moss*: Peat moss is a complex soil material containing lignin and cellulose as major constituents. It is a widely available natural substance. It has a large surface area

(>200 m²/g) and is highly porous. Peat moss is a relatively inexpensive material and is commercially sold at a price of 0.023 \$/kg in the United States.

- *Fly ash*: Fly ash is an industrial solid waste generated in thermal power plants. Fly ash can be easily solidified after the heavy metals have been adsorbed.
- *Iron (III) hydroxide waste*: Especially for heavy metals removal from wastewater, iron (III) hydroxide waste and waste slurry from the fertilizer industry, xanthate, rice husk, carbon, and coconut shell have been studied and can be considered as alternatives.

In Tables 4.4–4.7, several important adsorbents data are tabulated.

Safety considerations

Adsorption is generally an exothermic process leading to temperature rise. Although this property is useful when storage of heat is desired, it is not the case in the adsorption of VOCs. If certain hydrocarbons are involved, the carbon or metals on the carbon may catalyze the oxidation of these pollutants when the adsorbent is hot, resulting in bed fires that deteriorate the adsorbent by either altering its pore size or converting part of it to ash. Cooling of the bed or humidification of the air can be employed to avoid the outburst of

Table 4.4

Basic characteristics of common adsorbents (Perry and Green, 1999)

Adsorbent	Hydrophilic	Hydrophobic	Amorphous	Structured
Activated carbon		✓	✓	
Polymers		✓	✓	
Silica gel	✓		✓	
Activated alumina	✓		✓	
Carbon molecular sieves		✓		✓
Silicalite		✓		✓
Zeolites (3A, 4A, 5A, 13X)	✓			✓

Table 4.5

Physical properties of common adsorbents (Perry and Green, 1999; Knaebel, 1995)

Adsorbent	Micropore size (Å)	Internal porosity ϵ_p (%)	Bulk density ρ_b (kg/m ³)	Surface area S (m ² /g)	Adsorption Capacity Q_{\max} (g/g)
Carbons	> 6 ^a	35–85	250–700	100–1800	0.3–0.7
Organic polymers	Varying	40–60	420–700	80–700	0.45–0.55
Silica gel	>10	38–48	700–820	600–800	0.35–0.50
Aluminas	>6 ^b	30–57	700–930	200	0.1–0.33
Zeolites (3A, 4A, 5A, 13X)	3.9–8	30–38	580–680	600–700	0.21–0.36

^aActivated carbon.

^bActivated alumina.

Table 4.6

Alternative adsorption media (Noble and Terry, 2004)

	Typical adsorbates	Cost of adsorbent (1998) (\$/lb)
Activated carbon	Nearly all organics	1
Modified clays	Emulsified oil and grease	1.5
Polymeric resins	Chlorinated and nonchlorinated VOCs	8–35
Zeolites	Chlorinated and nonchlorinated VOCs	7–10

Table 4.7

Adsorbent types (Noble and Terry, 2004)

Adsorbent	Advantages	Disadvantages	Applications
Activated carbon	Cheapest hydrophobic adsorbent	Difficult regeneration, fire risk during regeneration	Removal of organics from aqueous and gaseous streams
Silica gel, activated alumina	Higher capacity than other materials (e.g. zeolites)	Not so effective in removing traces of water from gases	Drying of gas streams (both), hydrocarbon removal from gases (silica gel)
Zeolites	Separations can be based both on polarity and geometry	Lower capacity than many other adsorbents	Dehydration, air separation
Silicalite	Can be burned off more easily than activated carbon	More expensive than activated carbon	Removal of organics from gaseous streams
Polymer adsorbents (usually styrene)	No fouling problems compared to activated carbon	Much more expensive than activated carbon	Removal of organics from gaseous streams
Biosorbents (activated sludge on a porous support)	No regeneration needed	Lower effective capacity than other adsorbents	Removal of organics from gaseous streams

such fires. However, such effects are not only connected to the VOC to be removed but also to the type of the adsorbent. Specifically, polymers are usually used at mild temperatures, which do not allow bed fires. On the other hand, although zeolites are not flammable, they can contribute to intense heat release by promoting oxidation reactions after a minimum temperature has been provided for the start of the catalytic behavior. Normally, in case of a bed fire, the pore size of the zeolite is not altered by temperature (up to a point) since zeolites are resistant to temperature rise as mentioned above. However, the pore size of the zeolite may be decreased leading to an increase in its density, if the temperature surpasses the meta-stable range.

4.1.2 Ion-exchange materials

According to the definition given by Helfferich (1962), ion exchangers are insoluble solid materials, which carry exchangeable cations or anions. When the ion exchanger is in contact with an electrolyte solution, these ions are exchanged with an equivalent amount of other ions of the same sign. Cation and anion exchangers are the materials that carry cations and anions, respectively. Some materials have the ability of both cation and anion exchange and are called “amphoteric ion exchangers” (Helfferich, 1962). There are a number of different natural and synthetic materials that show ion-exchange properties. The most important materials are described in the following sections.

Naturally occurring ion exchangers

Natural inorganic ion exchangers Many natural minerals, such as clays (e.g. bentonite) and zeolites (e.g. clinoptilolite), are capable of exchanging ions. However, crystalline aluminosilicates are principally the common natural minerals with cation-exchange properties (Helfferich, 1995). Amongst natural inorganic ion exchangers, zeolites and clays are the most common materials. Other natural aluminosilicate materials, such as green sand, are also found in specific waste-treatment applications.

Zeolites have an open, three-dimensional framework structure with pores (channels) and interconnecting cavities in the aluminosilicate lattice. In Table 4.8, the basic characteristics of the most important zeolite species of commercial use are presented.

Clays have a loose layer structure (Figure 4.6). Characteristic minerals are montmorillonite and beidellite. Aluminosilicates such as montmorillonite, kaolinite, and feldspar can act as cation and anion exchangers.

Natural inorganic ion exchangers have the following disadvantages:

- low exchange capacity
- low mechanical durability
- low abrasion resistance
- pore size cannot be adjusted
- clay minerals tend to convert to a colloidal form
- difficult to size mechanically
- may be partially decomposed into acids or alkalis.

Table 4.8

Basic characteristics of some important zeolites (Hanson, 1995)

Species	Formula	Internal porosity (%)	Density (g/cm ³)	Ion-exchange capacity (meq/g)
Phillipsite	(K,Na) ₁₀ [(AlO ₂)(SiO ₂) ₂₂].20H ₂ O	31	2.15–2.20	3.87
Chabazite	Ca ₂ [(AlO ₂) ₄ (SiO ₂ O ₈)].13H ₂ O	47	2.05–2.10	3.81
Mordenite ^a	Na ₈ [(AlO ₂) ₈ (SiO ₂) ₄₀].24H ₂ O	28	2.12–2.15	2.29
Clinoptilolite ^b	Na ₆ [(AlO ₂) ₆ (SiO ₂) ₃₀].24H ₂ O	34	2.16	2.54

^aFigure 4.4.

^bFigure 4.5.

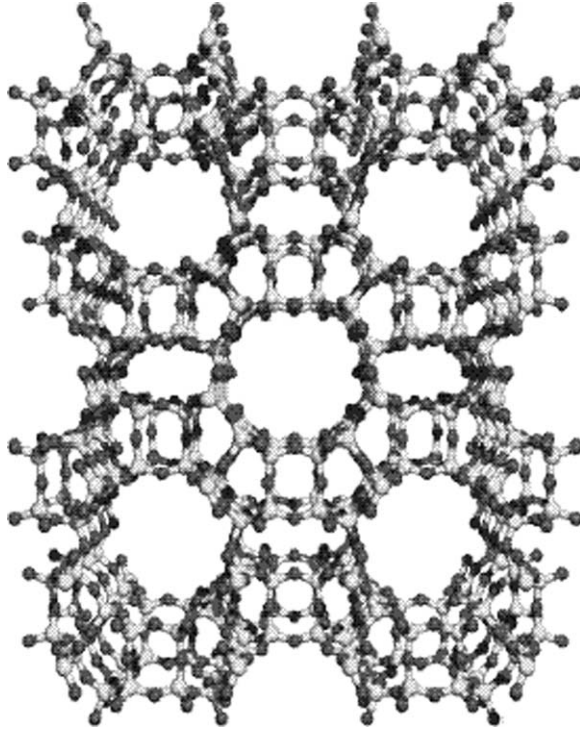


Figure 4.4 The structure of mordenite.

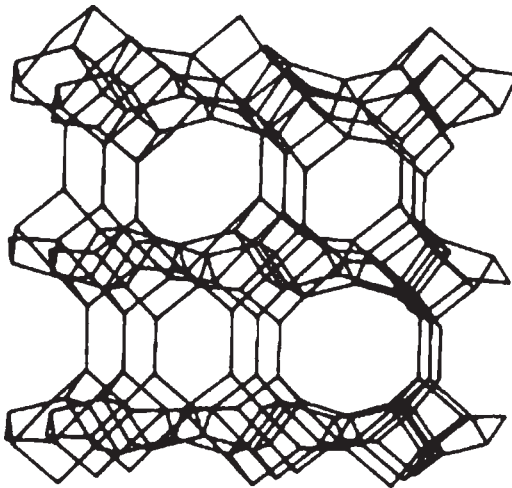


Figure 4.5 The structure of clinoptilolite.

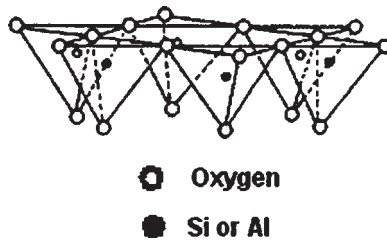


Figure 4.6 The typical structure of clays.

Natural organic ion exchangers Some common natural organic ion exchangers are

- polysaccharides, such as cellulose and peat
- proteins, such as casein, keratin, and collagen
- carbonaceous materials, such as charcoals, lignites, and coals.

However, only charcoals, coal, lignite, and peat are used in industrial applications. Although they are not as effective as synthetic organic exchangers, their low cost makes them an appealing choice. Before selecting these materials, one should keep in mind that

- they exhibit low exchange capacities
- they tend to swell or convert into a colloidal form
- they have a loose physical structure
- their physical properties are not uniform
- they are nonselective
- they are pH-sensitive

Synthetic ion exchangers

Synthetic inorganic ion exchangers *Zeolites*: Synthetic zeolites (Figure 4.7) are available as powder, pellet, or bead. The greatest advantage of synthetic zeolites against natural zeolites is that they can be manufactured with a wide variety of physicochemical properties. The main disadvantages of synthetic zeolites are

- their high cost compared to natural zeolites
- they are pH-sensitive
- their limited mechanical stability

Titanates and silico-titanates: The oxide and hydroxide of titanium are effectively used in applications of removing metal ions from water. Early studies (since 1955) have shown that hydrous titanium oxide is the most appropriate material for extracting uranium from seawater, whereas titanates and hydrous titanium oxide are suitable for removing strontium.

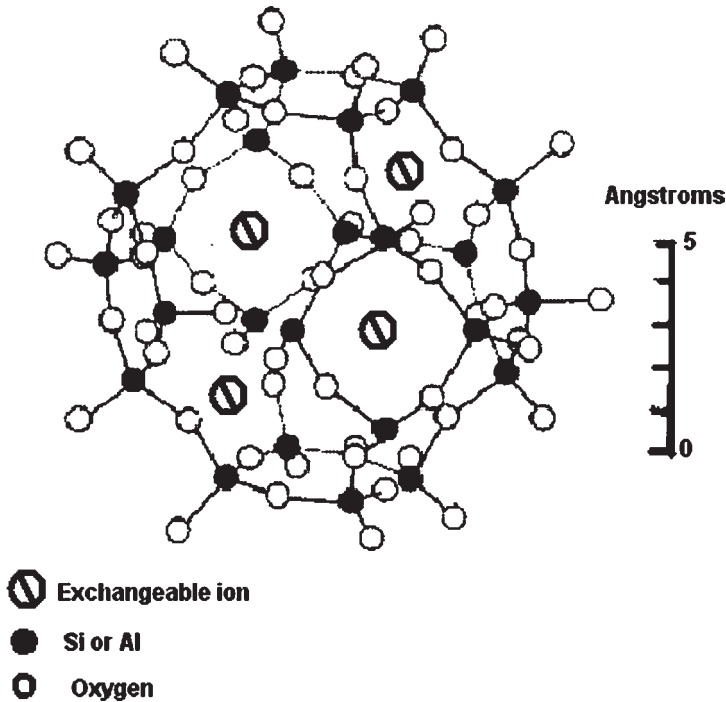


Figure 4.7 Simplified three-dimensional representation of a zeolite structure. Each Si or Al atom is surrounded by four oxygen atoms, forming tetrahedron elementary structures (primary building units).

These materials have been used for in-tank precipitation at the Savannah River Site in the United States (IAEA, 2002).

Transition metal hexacyanoferrates: These metals are very effective in extracting radioactive cesium from solutions. In India, potassium cobalt(II) hexacyanoferrate(II) has been prepared in a column-usable granular form that needs no resin support (IAEA, 2002).

Synthetic organic ion exchangers The largest group of ion exchangers available today is synthetic organic resins (Tables 4.14 and 4.15). The resin matrix is a flexible network of hydrocarbon chains, where fixed ionic charges at various fixed positions are contained. The resins are made insoluble by cross-linking the various hydrocarbon chains. The degree of cross-linking determines many of the resin properties. Specifically, if resistance to mechanical degradation is desired, a high degree of cross-linking leads to a hard resin that is not very porous and not susceptible to swelling. Here, let us recall that swelling takes place when an organic ion exchanger is placed in a solvent or solution. Besides the exchanger itself, the properties of the solution or solvent determine the extent of swelling.

The main advantages of synthetic organic ion-exchange resins are

- high capacity
- wide versatility
- low cost compared to some synthetic inorganic media.

However, there also some disadvantages. Specifically, the limited radiation and thermal stability set limits to the usage of synthetic organic ion-exchange resins. Regarding temperature, 150 °C is the maximum temperature that cation-exchange resins can withstand, whereas 70 °C is the limit for anion-exchange resins. Consequently, hot streams to be treated have to be cooled below these temperatures.

In Tables 4.9 and 4.10, a comparison of organic and inorganic ion exchangers is presented.

Classification based on matrix

Polystyrene divinylbenzene: Ion-exchange resins are commonly manufactured from a copolymer of styrene (Figure 4.8) and divinylbenzene (Figure 4.9). The divinylbenzene content in the matrix determines the degree of cross-linking. So, 5% mol divinylbenzene

Table 4.9

Qualitative comparison of organic and inorganic ion exchangers

Property	Organic exchangers	Inorganic exchangers
Chemical stability	Good	Fair to good
Thermal stability	Fair to poor	Good
Mechanical strength	Good	Variable
Exchange capacity	High	Variable
Regeneration	Good	Limited regeneration performance
Immobilization	Good; immobilized in a variety of matrixes or can be incinerated	Good; converted into equivalent mineral structures
Cost	Medium to high	Low to high

Table 4.10

Quantitative comparison of organic and inorganic cation exchangers

Exchanger	Capacity (kg/ft ³)
Natural zeolites	3–5
Synthetic zeolites	12–16
Organic	
Sulfonated coal (carbonaceous)	5–7
Organic	6–18
Synthetic	
Phenolic	
Organic	20–30
Synthetic	
Styrene base	
Organic synthetic resins	10–22

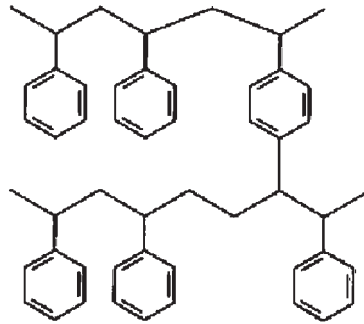


Figure 4.8 Cross-linked polystyrene.

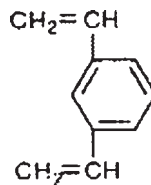


Figure 4.9 Divinylbenzene (DVB).

in the matrix corresponds to 5% cross-linking. As mentioned above, the degree of cross-linking is connected to the properties of the resin. Low divinylbenzene content means low cross-linking and the result is a soft resin prone to swelling in solvents. Then, the ion-exchange potential is created by introducing fixed ionic groups into the resin matrix. For example, in sulfonation, 8–10 $-\text{SO}_3\text{H}$ groups are introduced in the matrix for every 10 benzene rings. The H^+ ions contained in the $-\text{SO}_3\text{H}$ groups is the mobile ion or counterion that will be exchanged in a solution with different cations.

Phenolic: There are various kinds of phenolic resins. The ones that are produced from phenol–formaldehyde condensation are very weak acid exchangers, where the phenolic $-\text{OH}$ groups are the fixed-ionic groups. The formaldehyde content decides the extent of cross-linking in the resin. On the other hand, phenolsulfonic acid resins contain both strong acid $-\text{SO}_3\text{H}$ and weak acid $-\text{OH}$ groups.

Acrylic: This resin is manufactured from a copolymer of acrylic or methacrylic acid with divinylbenzene (Figure 4.10). The result is a weak acid ion-exchange resin with $-\text{COOH}$ groups that have very little salt splitting capacity, but are very effective in removing Ca^{2+} and similar ions under alkaline conditions.

Classification based on the functional groups

On the basis of the charge of the exchangeable ions, there are cation (positive mobile ions) and anion (negative mobile ions) resins. Both types are manufactured from the very same basic organic polymers. However, the ionic groups that are introduced into the matrix

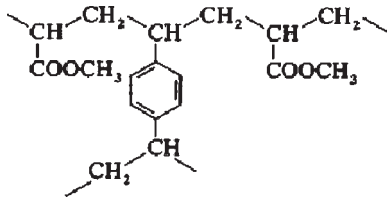


Figure 4.10 Polyacrylic matrix (cross-linked polymethacrylate).

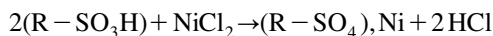
Table 4.11

Functional groups of standard ion-exchange resins (IAEA, 2002; Helfferich, 1962)

Type	Functional group
Strongly acidic (cation exchangers)	$-\text{SO}_3^-$
Weakly acidic (cation exchangers)	$-\text{COO}^-$
Other acidic (cation exchangers)	$-\text{PO}_3^{2-}$ $-\text{HPO}_2^-$ $-\text{AsO}_3^{2-}$ $-\text{SeO}_3^-$
Strongly basic (anion exchangers)	$-\text{N}(\text{CH}_3)_3^+$ $-\text{N}(\text{CH}_3)_2\text{C}_2\text{H}_4\text{OH}^+$
Weakly basic (anion exchangers)	$-\text{NH}_3^+$ $\text{R}_1-\text{NH}_2^+-\text{R}_2$

define the chemical behavior and the specific applications of the resin. Generally, resins can be typified into strong or weak acid cation exchangers and strong or weak base anion exchangers (Table 4.11).

Strong acid cation resins: These resins are highly ionized in both the acid ($\text{R}-\text{SO}_3\text{H}$) and salt ($\text{R}-\text{SO}_3\text{Na}$) form and behave like strong acids. They can convert a metal salt into the corresponding acid by the reaction



Na^+ and H^+ ions are highly exchangeable over the entire pH range. Depending on the specific usage, these resins are used either in the hydrogen or in the sodium form. For example, the sodium form is preferred if water softening (calcium and magnesium removal) is the desired action (Table 4.12). The resins can be regenerated by treatment with the appropriate solution (a strong acid for the hydrogen form or a sodium chloride solution for the sodium form). The treatment with hydrochloric acid (HCl) results in a concentrated nickel chloride (NiCl_2) solution according to the previous chemical equation.

Weak acid cation resins: Here, the ionic group is a carboxylic acid ($-\text{COOH}$) and these resins behave as if they were weak organic acids. They have a much higher affinity than strong acid resins for hydrogen ions. Therefore, fewer amounts of acids are required in

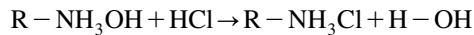
Table 4.12

Selectivity of ion-exchange resins in decreasing order of preference

Strong acid cation exchanger	Strong base anion exchanger
Barium	Iodide
Lead	Nitrate
Calcium	Bisulfite
Nickel	Cyanide
Chloride	Bicarbonate
Cadmium	Hydroxide
Copper	Fluoride
Zinc	Sulfate
Magnesium	
Potassium	
Ammonia sodium	
Hydrogen	

their regeneration compared to strong acid resins. The dissociation of a weak acid resin and thus its capacity is greatly affected by the pH of the solution.

Strong base anion resins: These resins are used in the hydroxide ($-\text{OH}$) form for water deionization and their capacity is not influenced by pH. So, they can be used over the entire pH range. They can convert an acid solution into pure water:



It is easily understood that their regeneration is achieved by treating them with concentrated sodium hydroxide (NaOH).

Weak base anion resins: Just like for weak acid resins, the operation of weak base anion resins is greatly affected by pH. They exhibit their maximum exchange capacity in the pH range up to 7.0. They hardly adsorb any strong acids: they cannot split salts.

Heavy-metal-selective chelating resins: The behavior of chelating resins resembles that of weak acid cation resins. They differ in that they are much more selective in heavy metal cations. Chelating resins tend to form stable complexes with the heavy metals and contain EDTA as the functional group. In the sodium form, they are referred to as EDTA-Na. Their groups have donor atoms such as sulfur and nitrogen and may develop bonds with metals that exhibit both covalent and ionic characteristics. Chelating resins have been extensively studied and their sorption properties are well known. Besides their selectivity in removing transition metals, another feature in favor of their use is that they can be easily regenerated with mineral acids. There are also resins that do not contain negative ionic groups but are also capable of forming complexes with metals. For example, picolylamine resins create stable complexes at low pH values. These kinds of complex-forming resins are suitable for removing trace amounts of metal cations from solutions containing high amounts of competing alkaline and alkaline-earth metal ions at acidic pH.

In Table 4.13, the relative selectivity of a commercial chelating resin for heavy metal cations is shown. The relative selectivity is based on the selectivity for calcium ions. For

Table 4.13

Chelating cation resin relative selectivities for metal ions
(relative selectivity is based on Ca^{2+})

Metal ion	Relative selectivity
Hg^{2+}	2800
Cu^{2+}	2300
Pb^{2+}	1200
Ni^{2+}	57
Zn^{2+}	17
Cd^{2+}	15
Co^{2+}	6.7
Fe^{2+}	4.7
Mn^{2+}	1.2
Ca^{2+}	1

example, the preference for mercury is 2800 times that for calcium. This means that in the treatment of a solution, which contains equal molar concentrations of mercury and calcium ions, the molar concentration of mercury ions on the resin will be 2800 times that of calcium ions.

In Figure 4.11, the formula of a chelating resin is shown with the iminodiacetic acid group as the chelating ligand, which is bonded onto a cross-linked polystyrene matrix. This type of resin shows a large affinity for alkaline-earth and transition metal ions.

In Figure 4.12, three different amines that are used as functional groups for the manufacture of chelating resins are shown.

Composite ion exchangers

If it is considered necessary for an ion exchanger to present a certain number of characteristics that cannot be found in only one adsorbent, then a composite ion exchanger can be chosen. They consist of one or more ion exchangers combined with another material, which can be inorganic or organic. For example, if it is desired that the exchanger be

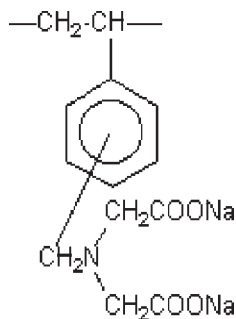


Figure 4.11 Chelating resin with the iminodiacetic acid group as the chelating ligand bonded onto a cross-linked polystyrene matrix.

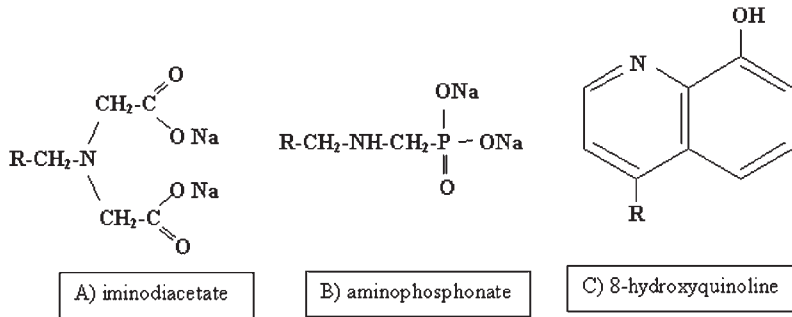


Figure 4.12 Amine groups for the manufacture of chelating resins.

removed from the liquid by means of a magnetic field, an inorganic exchanger containing magnetite can be used (IAEA, 2002). Another reason in favor of composite ion exchangers is that in this way, a granular material appropriate for column use may be formed from ion exchangers that normally do not form or only form weak granules themselves, as long as a proper inorganic binder is used.

Chemical stability of resins

The chemical stability of resins may be degraded due to chemical interactions with oxidizing agents. The latter interact with CH₂ groups and gradually lead to the destruction of the matrix. The main oxidizing substances are

- O₂ at high temperatures
- H₂O₂ leads (Fenton reaction) to the complete dissolution/destruction
- O₃ splits aromatic double bonds
- Cl₂ decomposes cation exchangers, and oxidizes amino and ammonium groups of anion exchangers
- CrO₃ (chromic acid) destroys the cross-linking of cation exchangers
- Na₂S₂O₈ separates functional groups of anion exchangers
- HNO₃ may damage polycondensation cation exchangers, easily damages functional groups of anion exchangers.

However, reductive agents may also affect resins. For example, hydrogen may damage sulfonic acid groups of strongly acidic cation exchangers.

4.1.3 Kinetics

Ion exchange shares many characteristics with adsorption, such as mass transfer from the fluid to the solid phase; there are, however, some significant differences. Specifically, although both processes can be characterized as sorption processes, the sorbed species are ions in ion exchange, whereas electrically neutral substances are sorbed in adsorption. Moreover, in ion exchange, the ions removed from the liquid phase are replaced by ions from the solid phase. So, there actually occurs an exchange of ions and not only a removal

Table 4.14

Physical properties of ion-exchange resins (Perry and Green, 1999)

Resin type	Bulk wet density ρ_b (kg/m ³)	Maximum operating temperature T_{\max} (°C)	Exchange capacity (dry resin) Q_{\max} (meq/g)
Strongly acidic cation exchangers	740–900	50–150	2–5.5
Weakly acidic cation exchangers	670–800	45–120	0.7–10
Strongly basic anion exchangers	670–700	40–100	0.57–3.8
Weakly basic anion exchangers	610–720	60–100	0.9–5.5

Table 4.15

Capacity of most common ion-exchange resins (Helfferrich, 1995)

Matrix	Ionic group	Trade name	Exchange capacity (dry resin) (meq/g)
Polystyrene resins	$-\text{SO}_3^-$	Amberlite IR-120, 122, 124 Dowex 50 Duolite C-20, 25, 27 Lewatit	4.3–5 4.9–5.2 5–5.1
S-100, 115	4.6–4.75 $-\text{N}(\text{CH}_2\text{COOH})_2$	Dowex A-1	1–1.2
C-63	$-\text{PO}_3^{2-}$ 6.6	Duolite	
IRA-400	$-\text{N}(\text{alkyl})_3^+$ 2.6	Amberlite	
IRA-401, 402, 405	3	Amberlite Dowex-1, 11 Lewatit	3.5
M-600, MP-600	3.7		
Phenolic resins	$-\text{SO}_3^-$	Duolite	
C-3, 10	2.9 $-\text{PO}_3^{2-}$	Duolite	
ES-65	3.3		
Vinyl addition polymers	$-\text{COOH}$	Amberlite	
IRC-50	9.5		
Condensation polymers	$-\text{N}(\text{alkyl})_3^+$	Zeo-Karb 226 Lewatit MN	10 2.3

in the latter process. In addition, the total charge sorbed and desorbed is exactly the same as imposed by the electroneutrality principle (Noble and Terry, 2004; Perry and Green, 1999). As Helfferrich (1962) states: “Ion exchange is inherently a stoichiometric process.” Apparent deviations from this behavior can occur because of electrolyte sorption and desorption during ion exchange (Helfferrich, 1962).

Furthermore, in ion exchange, the fluxes of at least two different ions are coupled with each other and this process cannot be described by the use of a simple diffusion equation, as in the case of adsorption and the exchange of isotopes, i.e. isotopic exchange. This electric coupling of the ionic fluxes and the stoichiometric nature of the ion-exchange process are the most important features, which distinguish ion exchange from adsorption and isotopic exchange (Helfferich, 1962). As a result, the quantitative treatment of ion exchange is much more complicated than adsorption or isotopic exchange.

It is generally accepted that adsorption and ion exchange can be grouped together as sorption for a unified treatment in practical applications. Most mathematical theories and approaches have been developed originally for adsorption rather than ion exchange. However, especially in the case of fixed beds, they are sufficiently general to be applicable with minor, if any, modifications to a number of similar phenomena such as ion exclusion and ligand exchange. According to Helfferich, the applicability of a simplified theory hinges on the mode of operation rather than on the particular mechanism of solute uptake (Helfferich, 1962). In the present book, the analysis of the ion exchange and adsorption kinetics is based on a simplified unified approach and only some solutions are given, especially for ion exchange. On the other hand, the models for adsorption and isotopic exchange are equivalent.

A significant feature of adsorption is that the rate of physical adsorption is generally too high and consequently, the overall rate is controlled by mass transfer (or heat transfer) resistance, rather than by the intrinsic sorption kinetics (Ruthven, 1984). Following this approach, adsorption is viewed and termed in the present book as a “diffusion-controlled” process. The same holds for ion exchange. As long as the rate of adsorption and ion exchange is determined by diffusion processes, the rate laws are derived by applying the well-known diffusion equations (Helfferich, 1962). In general, diffusion processes are described in terms of Fick’s first law:

$$J_i = -D \text{grad } C_i \quad (4.1)$$

where J_i is the flux of the diffusing species i , C_i its concentration, and D the diffusion coefficient. The diffusion of a species in a particle is a special case: the solid matrix occupies a substantial fraction of the particle volume and obstructs diffusion. In addition, following a more rigorous approach, the solid matrix may consist of small microporous crystals formed into a macroporous structure. In this case, two distinct diffusional resistances exist: macropore and micropore resistance (Ruthven, 1984). In the related literature, macropore diffusion is also termed “pore diffusion” while microporous diffusion is termed “solid diffusion” (Perry and Green, 1999). The term “intraparticle diffusion” includes pore and solid diffusion mechanisms. Pore diffusion is the diffusion of solutes in fluid-filled pores. These pores are so large that the solute escapes the force field of the adsorbent surface (Perry and Green, 1999). On the other hand, solid diffusion is the diffusion of solutes in the adsorbent surface. In this case, the pores are so small that the solute never escapes the force field of the adsorbent surface. The transport of solute molecules occurs by an activated process involving jumps between adsorption sites (Perry and Green, 1999). Pore and solid diffusion act in parallel, and thus the dominant transport process is the faster one.

For the needs of the present book, in the analysis of adsorption and ion-exchange kinetics, Helfferich's approach is followed—the particle, consisting of pore fluid and a solid matrix, is treated as a single quasi-homogeneous phase, regardless of its inhomogeneities in molecular or colloidal dimensions and its particular geometrical structure (Helfferich, 1962). The model solutions given by Helfferich are equivalent to the solutions of a solid diffusion-controlled process. Eq. (4.1) is valid and the corresponding diffusion coefficient is an “effective” kinetic parameter characterizing the ease of movement of the solutes in the particle in macropores and micropores. Furthermore, the diffusion coefficient is considered to be constant, or to be more realistic, an average value as it can be dependent on the solute solid-phase concentration.

Following this simplified approach, the time dependence of the concentration is related to the flux by Fick's second law (material balance or condition of continuity):

$$\frac{\partial C_i}{\partial t} = -\text{div } J_i \quad (4.2)$$

Combining eqs. (4.1) and (4.2), and for spherical particles, the following diffusion equation, written in spherical coordinates (r), describes the mass transfer process:

$$\frac{\partial C_i}{\partial t} = D \left(\frac{\partial^2 C_i}{\partial r^2} + \frac{2}{r} \frac{\partial C_i}{\partial r} \right) \quad (4.3)$$

where D is the solid diffusion coefficient and C_i the solid-phase concentration of the solute (in the following chapters, this concentration is denoted by q). Eq. (4.3) must be solved under the appropriate initial and boundary conditions. Here, it should be noted that for most nonspherical particles, their representation as an equivalent sphere is an acceptable approximation, and thus the above-mentioned equation can be used in this case as well.

Apart from the diffusion step in the particle, when the uptake process occurs from a binary or multicomponent fluid mixture, there maybe an additional resistance to mass transfer associated with the transport of solutes through the fluid layer surrounding the particle. The driving force in this case is the concentration difference across the boundary layer, and the flux at the particle surface is

$$J_i = k_f (C_{i,f} - C_{i,s}) \quad (4.4)$$

where k_f is the mass transfer coefficient and $C_{i,f}$ and $C_{i,s}$ are the concentration of solute in the bulk fluid and at the particle surface phase, respectively.

Thus, the analysis of the rate-determining step, as analyzed for heterogeneous processes in Section 3.1.2, is equally applied in adsorption and ion exchange. The only difference is that the diffusion processes in the fluid film and in the particle are followed by physical adsorption or ion exchange and not by a reaction step as in catalysis.

The analysis of adsorption and ion-exchange kinetics is presented in detail in Section 4.2.1, and is based on the diffusion processes and equations rather than on some kind of

adsorption or ion-exchange kinetics. However, the shrinking core model and some kinetic-type models are presented in brief.

4.1.4 Equilibrium

A common way to represent the equilibrium in adsorption and ion-exchange systems is the equilibrium isotherm. The equilibrium isotherm represents the distribution of the adsorbed material between the adsorbed phase and the solution phase at equilibrium. This isotherm is characteristic for a specific system at a particular temperature.

The basic difference between adsorption and ion exchange is that while there is only one isotherm at a specified temperature for adsorption, more than one isotherm can exist at a specified temperature for different normalities of the solution in the exchange of ions of different valences due to the concentration–valence effect (Helfferich, 1962). Thus, a specific ion-exchange system presents one equilibrium curve (isotherm) only under constant temperature and normality. This is why, while the term “isotherms” is used for the equilibrium curves in the case of adsorption, the term “isotherm–isonormal” should be used for ion exchange.

In the following sections, the most important isotherm types are presented.

Adsorption

Langmuir isotherm Adsorbents that exhibit the Langmuir isotherm behavior are supposed to contain fixed individual sites, each of which equally adsorbs only one molecule, forming thus a monolayer, namely, a layer with the thickness of a molecule (Perry and Green, 1999):

$$\frac{q_e}{Q_M} = \frac{KC_e}{1 + KC_e} \quad (4.5)$$

where q_e is the solid-phase concentration in equilibrium with the liquid-phase concentration C_e , Q_M is the final sorptive capacity (most commonly in mg/mg), and K is an equilibrium constant (most commonly in L/mg). The units of K are L/mol provided that C_e is expressed in (mol/L). Applying the same equation for $C_e = C_o$,

$$\frac{q_{\max}}{Q_M} = \frac{KC_o}{1 + KC_o} \quad (4.6)$$

where q_{\max} is the solid-phase concentration in equilibrium with C_o . Dividing the above equations:

$$\frac{q_e}{q_{\max}} = \frac{C_e}{C_o} \frac{1 + KC_o}{1 + KC_e} \quad (4.7)$$

Introducing the equilibrium parameter (La) as

$$La = \frac{1}{1 + KC_o} \quad (4.8)$$

the dimensionless form of Langmuir equation is

$$Y = \frac{X}{La + (1 - La)X} \quad (4.9)$$

where

$$Y = \frac{q_e}{q_{\max}} \quad (4.10)$$

and

$$X = \frac{C_e}{C_o} \quad (4.11)$$

By using the dimensionless equilibrium relationship, La can be expressed as

$$La = \frac{X(1 - Y)}{Y(1 - X)} \quad (4.12)$$

Langmuir adsorption isotherm constants for several compounds on several adsorbents/water systems at ambient temperature are presented in Table I.23, Appendix I.

Freundlich Adsorbents that follow the Freundlich isotherm equation are assumed to have a heterogeneous surface consisting of sites with different adsorption potentials, and each type of site is assumed to adsorb molecules, as in the Langmuir equation (Perry and Green, 1999):

$$\frac{q_e}{Q_M} = kC_e^{Fr} \quad (4.13)$$

where q_e is the solid-phase concentration in equilibrium with the liquid-phase concentration C_e , Q_M is the final sorptive capacity, and k and Fr are equilibrium constants. Another form of the Freundlich isotherm is the following:

$$q_e = K_F C_e^{Fr} \quad (4.14)$$

where

$$K_F = Q_M k \tag{4.15}$$

Applying eq. (4.13) for $C_e = C_o$,

$$\frac{q_{\max}}{Q_M} = k C_o^{Fr} \tag{4.16}$$

Here, q_{\max} is the solid-phase concentration in equilibrium with C_o . Dividing eqs. (4.13) and (4.16),

$$Y = X^{Fr} \tag{4.17}$$

It is important to distinguish between the values of q_{\max} and Q_M . The first is the solid-phase concentration in equilibrium with the initial fluid-phase concentration, while Q_M is higher, representing the maximum adsorption capacity, which is typically achieved in higher fluid-phase concentrations. Following the terminology of Inglezakis (2005), for ion exchange q_{\max} corresponds to the maximum exchange level (MEL), while Q_M corresponds to the real exchange capacity (REC).

The empirical constants La and Fr are related to the particular system under investigation and are obtained from laboratory experiments (Chen *et al.*, 1968; Chern and Chien, 2002). Generally, an isotherm is favorable if its shape is convex upward, and unfavorable

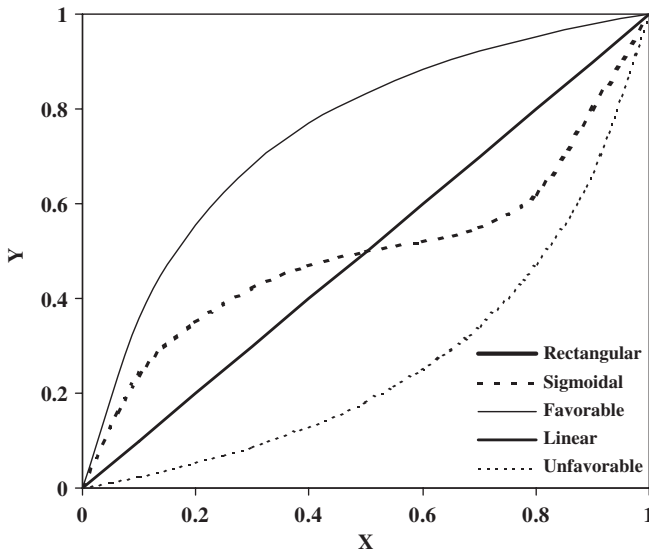


Figure 4.13 Basic isotherm types.

if its shape is concave upward in an X versus Y figure. In Figure 4.13, the characteristic isotherm shapes are presented.

The parameter La is also called the “separation factor” and provides a quantitative description of the equilibrium regions: $La = 0$ for irreversible, $La < 1$ for favorable, $La = 1$ for linear, and $La > 1$ for unfavorable adsorption. The same holds for Fr in Freundlich’s isotherm.

Freundlich adsorption isotherm constants for several compounds on several adsorbents/water systems at ambient temperature can be found in Table I.24, Appendix I.

Dubinin–Raduskevish (DR) Due to the great significance of vapor adsorption on activated carbons, the DR isotherm, which is the most widely used in such cases, will be presented. It has several advantages (Dubinin, 1966):

- predicts quite fairly the experimental data over a wide concentration range
- it includes the effect of temperature
- it is based on physical parameters
- easy application.

Dubinin assumed that the amount of vapor adsorbed (W) by an activated carbon, at a relative pressure P/P_s , is a function of the thermodynamic potential A :

$$A = RT \ln \left(\frac{P_s}{P} \right) \quad (4.18)$$

where:

R = the universal gas constant

T = the absolute temperature

P_s = the saturated vapor pressure at temperature T

P = the partial pressure of the adsorbate.

Dubinin reached the conclusion that the function was Gaussian after having studied the adsorption of simple organic compounds like benzene, and finally the classical expression of Dubinin and Radushkevich (the D–R equation) was derived (Dubinin, 1966; Cheng *et al.*, 2004):

$$q_e = q_o \exp \left[-k \left(\frac{A}{\beta} \right)^2 \right] \quad (4.19)$$

where q_o is the maximum amount that can be adsorbed and k is a parameter characterizing the adsorbent. The parameter α is called the “affinity” or “similarity” coefficient and expresses the ratio of the characteristic free energy of desorption of the test vapors to the free energy of desorption of the reference vapors. The affinity coefficients can be estimated by ratios of molar polarizabilities α (Wood, 2001):

$$\beta = \frac{\alpha}{\alpha_{\text{ref}}} \quad (4.20)$$

The ratio of molar volumes in the liquid state can also be used:

$$\beta = \frac{V}{V_{\text{ref}}} \quad (4.21)$$

By definition, benzene is standardized as the reference compound for carbonaceous materials, and thus the value of its affinity coefficient β is 1. The relevant parameters of the D–R isotherm can be found in paragraph I.4, Appendix I.

Other isotherms Some common isotherms are the following:

Langmuir–Freundlich isotherm

$$Y = \frac{X^A}{B + (1 - B)X^A} \quad (4.22)$$

Redlich–Peterson isotherm

$$Y = \frac{X}{B + (1 - B)X^A} \quad (4.23)$$

Sips isotherm

$$Y = \left(\frac{X}{B + (1 - B)X} \right)^A \quad (4.24)$$

where A and B are equilibrium constants.

However, there is no reason to use more complicated isotherm models if two-parameter models, such as Langmuir and Freundlich, can fit the data well. It should be clarified that these models are only mathematical functions and that they hardly represent the adsorption mechanisms.

Ion exchange

Let us suppose that the solid phase is initially in the B form and that the liquid-phase ion is A. The ion exchange can be represented as (Helfferich, 1962)



Then, the separation factor α_{A-B} is defined as

$$\alpha_{A-B} = \frac{q_A C_B}{q_B C_A} = \frac{Y_A X_B}{Y_B X_A} \quad (4.25)$$

with

$$Y_i = \frac{q_i}{q_{\max}} \quad (4.26)$$

$$X_i = \frac{C_i}{C_o} \quad (4.27)$$

where i is A or B. Here, q_{\max} is the MEL in equivalents per unit solid mass, which only in the case of complete exchange is equal to the REC. The REC is the “ceiling” of the solid-phase capacity. Furthermore, C_o is the initial concentration (normality) of the solution phase in equivalents per unit liquid volume, which is, in the case of ion exchange, constant throughout the exchanging process. If ion A is preferred, the separation factor is larger than unity, whereas if ion B is preferred, it is smaller than unity. The numerical value of the dimensionless separation factor is not affected by the choice of concentration units. Expressing all concentrations in equivalents,

$$\begin{aligned} X_A + X_B = 1 &\Rightarrow X_B = 1 - X_A \\ Y_A + Y_B = 1 &\Rightarrow Y_B = 1 - Y_A \end{aligned}$$

Then,

$$\alpha_{A-B} = \frac{Y_A(1 - X_A)}{X_A(1 - Y_A)} \quad (4.28)$$

Then, the relationship between α_{A-B} and the Langmuir equilibrium parameter (La) is

$$\alpha_{A-B} = \frac{1}{La} \quad (4.29)$$

That is why La is also called the “separation factor.” Furthermore, it is clear that the constant separation factor α_{A-B} in an ion-exchange system means that in practice, this system obeys a Langmuiran equilibrium isotherm, in which La is of course constant.

Another important equilibrium parameter is the distribution coefficient (λ_i) defined as

$$\lambda_i = \frac{q_i}{C_i} \quad (4.30)$$

In practice, for the specific case of the distribution coefficient, mg/g units are used for q and mg/L for C . Thus, the units of λ are L/g.

Furthermore, the selectivity coefficient K_{A-B} may be defined as follows:

$$K_{A-B} = \frac{q_A^{Z_B} C_B^{Z_A}}{q_B^{Z_A} C_A^{Z_B}} \quad (4.31)$$

where Z_i is the absolute value of the ions charge. Here, concentration units are in eq/L. If the ion A is preferred, then the selectivity coefficient is larger than unity, whereas if ion B is preferred, it is smaller than unity. It is obvious that due to the exponents, different units result in different values of the selectivity coefficient.

Ion-exchange equilibrium can be considered to be analogous to chemical equilibrium. From that point of view, the mass-action law can be used to express the state of equilibrium despite the fact that this law is defined exclusively for homogeneous systems. Derived this way, the so-called pseudo-equilibrium constant K_e is not really a constant, since it depends on the total concentration:

$$K_e = \frac{Y_A^{Z_B} X_B^{Z_A}}{Y_B^{Z_A} X_A^{Z_B}} = K_{A-B} \left(\frac{q_o}{C_o} \right)^{Z_A - Z_B} \quad (4.32)$$

However, if the valences of the exchanging cations are equal, the selectivity coefficient or pseudo-equilibrium constant is not affected by concentration. As already mentioned, one isotherm corresponds to a specific temperature in the case of adsorption or ion exchange of equal valence ions, whereas additionally, the same normality is required for the existence of only one isotherm in the case of ion exchange of different valence ions, due to the concentration–valence effect (Helfferich, 1962). The determination of the true equilibrium constant should be based on the thermodynamic activities (activity coefficients) of the species rather than concentrations. It is clear that the difficulties in the determination of activity coefficients also complicate the determination of the true equilibrium constant (Culfaz and Yagiz, 2004).

4.2 DESIGN OF ADSORPTION AND ION-EXCHANGE PROCESSES

4.2.1 Adsorption and ion-exchange kinetics in batch operations

In this section, the basic theory required for the analysis and interpretation of adsorption and ion-exchange kinetics in batch systems is presented. For this analysis, we consider the transient adsorption of a single solute from a dilute solution in a constant volume, well-mixed batch system, or equivalently, adsorption of a pure gas. Moreover, uniform spherical particles and isothermal conditions are assumed. Finally, diffusion coefficients are considered to be constant. Heat transfer has not been taken into account in the following analysis, since adsorption and ion exchange are not chemical reactions and occur principally with little evolution or uptake of heat. Furthermore, in environmental applications,

the objective is generally to remove a little amount of a pollutant from a gaseous or liquid stream, and thus, the overall heat released is very low, even if the heat per mole of adsorbed species is considerable, due to the low number of moles removed.

In the following, two general cases are considered:

- adsorption under conditions of constant or nearly constant solution concentration (infinite solution volume), and
- adsorption in batch with finite volume (finite solution volume).

In the adsorption in batch (second case), the concentration of the fluid varies from its initial to the equilibrium concentration. The partition ratio is used to discriminate between these two cases, which for the case of the solid phase initially free from the solute, is defined as (Perry and Green, 1999; Ruthven, 1984)

$$w = \frac{q_e M_s}{C_o V_o} = \frac{C_o - C_e}{C_o} \quad (4.33)$$

where:

q_e = the equilibrium concentration expressed in solid phase in mass of solute per mass of the solid

M_s = the mass of the solid

C_o = the fluid-phase initial concentration

C_e = the equilibrium fluid-phase concentration

V_o = the volume of the fluid phase.

Generally, when $w \geq 0.1$, solutions for the second case are required.

In the case of ion exchange, this ratio is somewhat differently defined (Helfferich, 1962):

$$w = \frac{Q_M M_s}{C_o V_o} \quad (4.34)$$

Then,

- for $w \ll 1$, we have the infinite solution volume condition and
- for $w \gg 1$, we have the finite solution volume condition

Here, Q_M represents the REC per unit mass of solid. Helfferich uses the total concentration of *ions in equivalents* for both phases. This difference is due to the different nature of adsorption and ion exchange. In ion exchange, the concentration in equivalents in both phases is constant throughout the process (stoichiometric phenomenon). On the other hand, in adsorption this is not the case. This is why in ion exchange, the total amount in equivalents in the solid phase Q_M is used, whereas in adsorption the equilibrium uptake q_e is used.

Adsorption and isotopic exchange

In the following analysis, adsorption models for solid diffusion control are applicable for isotopic exchange, i.e. exchange of isotopes, while in the case of liquid diffusion control and the intermediate case, only adsorption models for linear equilibrium can be used for isotopic exchange.

Furthermore, as will be analyzed in practical applications, the adsorption models can also be used as a first approximation for ion-exchange systems, i.e. in the exchange of ions of different valences.

Infinite fluid volume and solid diffusion control Practically, infinite solution volume condition ($w \ll 1$) amounts to constant liquid-phase concentration. For a constant diffusivity and an infinite fluid volume, the solution of the diffusion equations is (Helfferich, 1962; Ruthven, 1984)

$$U(t) = 1 - \frac{6}{\pi^2} \sum_{n=1}^{\infty} \frac{1}{n^2} \exp(-n^2 \pi^2 T) \quad (4.35)$$

where $U(t)$ is the fractional approach to equilibrium at time t and is defined as

$$U(t) = (q_t - q_o)/(q_{\infty} - q_o) \quad (4.36)$$

where:

q_o = solute initial concentration in the solid phase

q_{∞} = equilibrium concentration in the solid phase

q_t = the average concentration of the solute in solid phase at time t , defined as (Ruthven, 1984)

$$q_t = \frac{3}{r_o^2} \int_0^{r_o} q r^2 dr \quad (4.37)$$

where r_o is the particle radius. For a solid phase initially free from solute, q_o is zero and thus

$$U(t) = \frac{q_t}{q_{\infty}} = \frac{C_o - C_t}{C_o - C_{\infty}} \quad (4.38)$$

where C_i 's are the corresponding fluid-phase concentrations.

The dimensionless time T is defined as

$$T = \frac{D_s t}{r_o^2} \quad (4.39)$$

where D_s is the solid diffusion coefficient.

For the whole $U(t)$ range, the approximation of Vermeulen can be used (Helfferich, 1962):

$$U(t) = [1 - \exp(-\pi^2 T)]^{0.5} \quad (4.40)$$

The error of this simplified equation is less than 5% for $U(t) > 0.1$ compared to the exact solution (eq. (4.35)).

Infinite fluid volume and liquid diffusion control *General case:* For the case of the Langmuir isotherm and the solid phase initially free of solute, the solution is (Perry and Green, 1999)

$$(1 - La) \left(1 - \frac{1}{q_e} \right) U(t) - La \ln(1 - U(t)) = \frac{3k_f t}{r_o} \frac{C_o}{\rho_p q_e} \quad (4.41)$$

Linear equilibrium case: The above equation, in the case of linear equilibrium ($La = 1$), is reduced to

$$U(t) = 1 - \exp\left(-\frac{3k_f C_o t}{r_o q_e \rho_p}\right) \quad (4.42)$$

The same equation is used in the case of isotopic exchange (Helfferich, 1962):

$$U(t) = 1 - \exp\left(-\frac{3D_f C_o t}{r_o \delta Q_M \rho_p}\right) \quad (4.43)$$

where:

k_f = the fluid-film mass transfer coefficient

D_f = the diffusion coefficient in liquid phase

ρ_p = the particle density.

The only difference is that Helfferich uses D_f/δ instead of k_f , where δ is the film thickness. For a well-stirred solution, the film thickness is about 10^{-3} cm (Helfferich, 1962). Note that for ion exchange, the parameter Q_M is used in the place of q_e .

Infinite solution volume—intermediate case (between solid and liquid diffusion control) and linear equilibrium For the case of infinite solution volume and linear equilibrium, the following equation can be used (Helfferich, 1962):

$$U(t) = \frac{6\Theta^2}{r_o^2} \sum_{n=1}^{\infty} \frac{A_n \sin^2(m_n r_o)}{m_n^4} \exp(-D_s m_n t) \quad (4.44)$$

where

$$\Theta = \frac{C_o D_f}{Q_M D_s \delta \rho_p} \quad (4.45)$$

$$A_n = \frac{m_n^2 r_o^2 + (\Theta r_o - 1)^2}{m_n^2 r_o^2 + (\Theta r_o - 1) \Theta r_o} \quad (4.46)$$

Finally, the quantities m_n are the roots of the equation

$$m_n r_o = (1 - \Theta r_o) \tan(m_n r_o) \quad (4.47)$$

Note that for adsorption, the parameter q_c is used in the place of Q_M .

Finite fluid volume and solid diffusion control The solution is the following (Perry and Green, 1999):

$$U(t) = 1 - 6 \sum_{n=1}^{\infty} \frac{\exp\left(-p_n^2 D_s t / r_o^2\right)}{[9w/(1-w)] + (1-w)p_n^2} \quad (4.48)$$

where p_n are the positive roots of the equation (Figure 4.14):

$$f(p_n) = \frac{\tan(p_n)}{p_n} - \frac{3}{3 + [p_n^2/(w-1)]} = 0 \quad (4.49)$$

Halfferich (1962) gives a similar equation in a different form for isotopic exchange:

$$U(t) = 1 - \frac{2}{3w} \sum_{n=1}^{\infty} \frac{\exp(-S_n^2 T)}{1 + \frac{S_n^2}{9w(w+1)}} \quad (4.50)$$

where S_n are the roots of the equation

$$S_n \cot(S_n) = 1 + \frac{S_n^2}{3w} \quad (4.51)$$

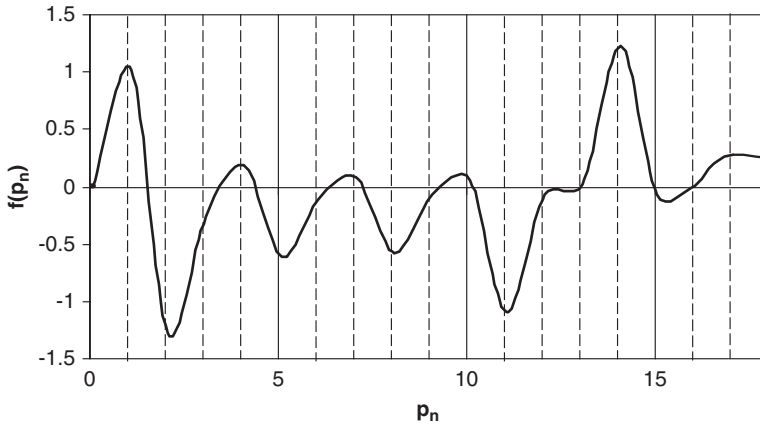


Figure 4.14 The function $f(p_n)$ for $w = 2$.

Furthermore, Helfferich (1962) gives Patterson's equation, which can be used as an approximation:

$$U(t) = \frac{w+1}{w} \{1 - f_1[f_2(1+f_3) - f_4(1+f_5)]\} \quad (4.52)$$

where (Figure 4.15)

$$f_1 = \frac{1}{a-b} \quad (4.53)$$

$$f_2 = a \exp(a^2 T) \quad (4.54)$$

$$f_3 = \operatorname{erf}(a\sqrt{T}) \quad (4.55)$$

$$f_4 = b \exp(b^2 T) \quad (4.56)$$

$$f_5 = \operatorname{erf}(b\sqrt{T}) \quad (4.57)$$

with a and b being the negative and the positive roots respectively, of the equation

$$x^2 + 3wx - 3w = 0 \quad (4.58)$$

In ion exchange, for the estimation of w , the total concentration in solid phase Q_M is taken equal to the REC. This concentration expresses the real total charge of the solid, which is

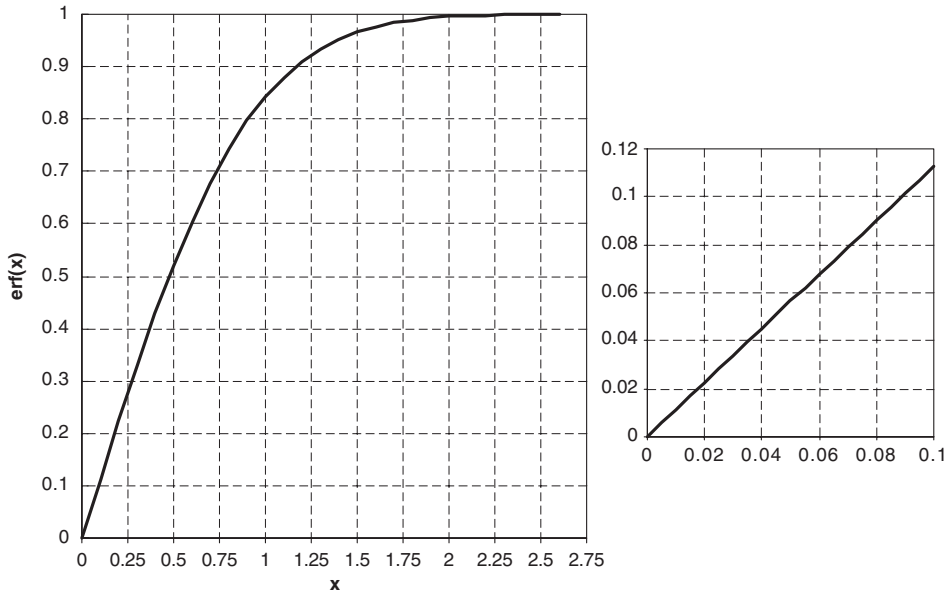


Figure 4.15 The erf(x) function. Note that erf(-x) = erf(x).

responsible for the movement of ions. The error of Patterson’s approximation is below 2% for the whole range of $U(t)$, compared to the exact solution.

Finite solution volume and liquid diffusion control *General case:* The general solution for the Langmuir isotherm is given by Perry and Green (1999):

$$\begin{aligned}
 & \left[1 - \frac{b(1 - La^\infty)}{2c} \right] \frac{1}{d} \ln \frac{(2cU(t) - b - d)(-b + d)}{(2cU(t) - b + d)(-b - d)} \\
 & - \frac{1 - La^\infty}{2c} \ln(1 - bU(t) + cU(t)^2) \\
 & = \frac{3k_f t}{r_o} \frac{C_o}{\rho_p q_e}
 \end{aligned} \tag{4.59}$$

where

$$b = \frac{1 - La^\infty}{1 - La} + w \tag{4.60}$$

$$c = w(1 - La^\infty) \tag{4.61}$$

$$d = (b^2 - 4c)^{0.5} \tag{4.62}$$

with La being the Langmuir constant and La^∞ is calculated using the same definition of La , eq. (4.8), but with the equilibrium fluid phase C_e instead of the initial fluid concentration C_o . Note that for ion exchange, the parameter Q_M is used in the place of q_e .

Linear equilibrium case: For isotopic exchange and finite solution volume, Helfferich (1962) gives the following solution:

$$U(t) = 1 - \exp\left(-\frac{3D_f(M_s q_o + V_o C_o)t}{r_o \delta Q_M V_o \rho_p}\right) \quad (4.63)$$

where ρ_p is the particle density, and as in all cases of ion and isotopic exchange, Q_M is the REC expressed per unit mass of the solid phase. Note that for adsorption, the parameter q_e is used in the place of Q_M .

Finite solution volume-intermediate case (between solid and liquid diffusion control) and linear equilibrium The solution is the following (Perry and Green, 1999):

$$U(t) = 1 - 6 \sum_{n=1}^{\infty} \frac{\exp\left(-p_n^2 D_s \frac{t}{r_o^2}\right)}{\frac{9w}{1-w} + (1-w)p_n^2 - (5w-1)\frac{p_n^2}{Bi_m} + (1-w)\frac{p_n^4}{Bi_m^2}} \quad (4.64)$$

where p_n are the positive roots of the equation

$$\frac{\tan(p_n)}{p_n} = \frac{3 - \frac{1-w}{w} \frac{p_n^2}{Bi_m}}{3 + \frac{1-w}{w} \frac{(Bi_m-1)p_n^2}{Bi_m}} \quad (4.65)$$

where Bi_m is a modified Biot number defined as

$$Bi_m = \frac{k_f r_o}{\rho_p D_s K_{\text{linear}}} \quad (4.66)$$

Finally, K_{linear} is the equilibrium parameter in the expression of the linear equilibrium:

$$q_e = K_{\text{linear}} C_e \quad (4.67)$$

Ion exchange

So far, the analysis has been restricted to adsorption and exchange of isotopes (isotopic exchange). However, in most cases, the ion-exchange process involves the exchange of

ions of different charge, size, and nature. In the following, the equations covering this more general case are presented.

Solid diffusion control and infinite solution volume In this case, the diffusion coefficient is not a constant but depends on the concentration of the ions in the solid phase. The basic diffusion equation to be solved is the following (Helfferich, 1962):

$$\frac{\partial q_B}{\partial t} = \frac{1}{r^2} \frac{\partial}{\partial r} \left(r^2 \overline{D_{AB}} \frac{\partial q_B}{\partial r} \right) \quad (4.68)$$

where

$$\overline{D_{AB}} = \frac{\overline{D_A D_B} (z_A^2 q_A + z_B^2 q_B)}{z_A^2 q_A \overline{D_A} + z_B^2 q_B \overline{D_B}} \quad (4.69)$$

is the coupled interdiffusion coefficient, q the solid-phase concentration of ion species, \overline{D}_i the self-diffusion coefficient of the ion i , and z_i its charge.

These equations, for the case of solid diffusion-controlled kinetics, are solved by arithmetic methods resulting in some analytical approximate expressions. One common and useful solution is the so-called Nernst-Plank approximation. This equation holds for the case of complete conversion of the solid phase to A-form. The complete conversion of solid phase to A-form, i.e. the complete saturation of the solid phase with the A ion, requires an excess of liquid volume, and thus $w \ll 1$. Consequently, in practice, the restriction of complete conversion is equivalent to the infinite solution volume condition. The solution of the diffusion equation is

$$U(t) = [1 - \exp(m)]^{0.5} \quad (4.70)$$

$$m = \pi^2 (c_1 T_B + c_2 T_B^2 + c_3 T_B^3) \quad (4.71)$$

where

$$\alpha = \frac{\overline{D_B}}{D_A} \quad (4.72)$$

$$T_B = \frac{\overline{D_B} t}{r_0^2} \quad (4.73)$$

The parameters c_1 , c_2 , and c_3 are functions of the parameter α , and their value is different, depending on the charge of the exchanging ions (B—initially in the solid phase, and A—initially in the liquid phase) (Helfferich, 1995):

for $z_B = z_A$ and $0.1 \leq \alpha \leq 10$,

$$c_1 = -\frac{1}{0.57 + 0.43\alpha^{0.775}} \quad (4.74)$$

$$c_2 = -\frac{1}{0.26 + 0.782\alpha} \quad (4.75)$$

$$c_3 = -\frac{1}{0.165 + 0.177\alpha} \quad (4.76)$$

for $z_B = 1$, $z_A = 2$ and $1 \leq \alpha \leq 20$,

$$c_1 = -\frac{1}{0.64 + 0.36\alpha^{0.668}} \quad (4.77)$$

$$c_2 = -\frac{1}{0.96 - 2\alpha^{0.4635}} \quad (4.78)$$

$$c_3 = -\frac{1}{0.27 + 0.09\alpha^{1.14}} \quad (4.79)$$

for $z_B = 2$, $z_A = 1$, $0.05 \leq \alpha \leq 1$, and $T_B \leq 0.04$,

$$c_1 = -\frac{1}{0.35 + 0.65\alpha^{0.86}} \quad (4.80)$$

$$c_2 = -\frac{1}{0.030 + 1.1012\alpha^{2.06}} \quad (4.81)$$

$$c_3 = -\frac{1}{0.00265 + 0.354\alpha^{1.071}} \quad (4.82)$$

for $z_B = 2$, $z_A = 1$, $0.05 \leq \alpha \leq 1$, and $T_B > 0.04$,

$$c_1 = -\frac{1}{0.438 + 0.652\alpha^{0.777}} \quad (4.83)$$

$$c_2 = -\frac{1}{0.127 + 0.915\alpha^{1.057}} \quad (4.84)$$

$$c_3 = -\frac{1}{0.008 + 0.365\alpha^{0.335}} \quad (4.85)$$

Obviously, in the case of isotopic exchange, $\alpha = 1$. Furthermore, in isotopic exchange, the diffusion coefficients are equal to the self-diffusion coefficient of each ion. For different ions (not isotopes), the self-diffusion coefficient is substituted by an empirical constant diffusion coefficient. In the general case of ion exchange, the diffusion coefficient is not constant and for practical reasons, an appropriate “average” value is used. For the case of complete conversion into A-form (infinite solution volume), this “average” diffusion coefficient is (Helfferich, 1962)

$$\overline{D}_{avr} \approx \frac{\overline{D_A D_B} (z_A + z_B)}{z_A \overline{D_A} + z_B \overline{D_B}} \tag{4.86}$$

The following equation is more general (Ruthven, 1984):

$$\overline{D}_{avr} = \frac{1}{q_2 - q_1} \int_{q_1}^{q_2} \overline{D}(q) dq \tag{4.87}$$

This diffusion coefficient is the mean diffusion coefficient for a solid phase loading ranging from q_1 to q_2 .

The use of simplified “diffusion” models in ion-exchange systems It is well-known that in practice, several simplified models for the representation and design of ion-exchange systems are used. In the following sections, such models are analyzed.

The use of isotopic models in the literature—practical limits of usage: As mentioned above, simplified solutions are employed in ion exchange for the estimation of diffusion coefficients. For example, the equations of Vermeulen and Patterson, derived from isotopic exchange systems, have been successfully used, even in processes that are not isotopic. Inglezakis and Grigoropoulou (2001) conducted an extended review of the literature on the use of isotopic models for ion-exchange systems.

The same authors (2001) studied the common case of bivalent (liquid phase)–monovalent (solid phase) exchange. In this study, two isotopic models, i.e. Vermeulen’s and Patterson’s and the Nernst–Plank model for the exchange of ions of different valence, were compared in terms of applicability (Table 4.16). Specifically, the authors studied the range

Table 4.16

Applicability range for isotopic models			
$U(t)$ limits	(w) limits	(α) limits	Model
0.3–0.8	≤ 0.1	1–20	Vermeulen
0–0.8	Any finite value	1–20	Patterson

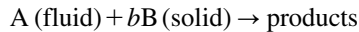
of applications of each model, examining the effect of various parameters involved. They showed that any of the tested models could be applied provided that the values of w , α , and $U(t)$ were within specific limits. Specifically, Vermeulen's approximation can be used in any case of an ion-exchange process within certain limits for $U(t)$, the lower limit depending on w and the upper limit depending on α . Patterson's approximation can be used for any value of w and up to a value of $U(t)$ depending on α . In both cases, α must however be less than 20.

Inglezakis and Grigoropoulou (2001) experimentally found that for the case of Pb^{2+} - Na^+ exchange on clinoptilolite, even for $w = 0.4$, the results using Vermeulen's approximation could be acceptable.

Exchange of trace components: The equations for adsorption (diffusion) can be equally applied in the case of isotopic exchange (exchange of isotopes) with minor changes. The same equations can be also be used in the case of the exchange of trace components of different valences (Helferich, 1962). This is the case where the uptake or release of an ion takes place in the presence of a large amount of another ion in both the solid and liquid phase. In such systems, the amounts removed are so small that the concentrations in both phases are practically constant, and thus in turn the individual diffusion coefficients also remain unaffected. Moreover, the rate-controlling step is the diffusion of the trace ion.

Shrinking core model The shrinking core model has been derived for noncatalytic solid-fluid reactions (Levenspiel, 1972). However, it has been successfully used for specific ion-exchange systems—those using synthetic ion exchangers, mainly chelating resins (Cortina *et al.*, 1998; Juang, 1999).

Consider the heterogeneous reaction between a solid and a fluid phase:



In ion exchange, A is the incoming ion and B is the ion originally found in the solid phase. The overall rate is a combination of the diffusion rate of A in the fluid film, the diffusion rate of A in the solid, and the chemical reaction rate. Note that in ion exchange, the coefficient b corresponds to the ion exchanged from the solid phase. The reaction occurs first at the outer skin of the solid particle. Then, progressively, the reaction zone moves into the solid, leaving behind completed reacted solid (ash) (Levenspiel, 1972). Consequently, at any time there exists an unreacted core of the solid, which shrinks in size during the reaction (Figure 4.16). In this model, the particle size is unchanged during the reaction. In the following, the case of elementary irreversible reactions is presented. Furthermore, a single controlling mechanism is assumed.

In all equations, the fractional conversion X_B is used:

$$1 - X_B = \frac{V_u}{V_o} = \left(\frac{r_u}{r_o} \right)^3 \quad (4.88)$$

where V_u and r_u are respectively the volume and radius of the unreacted core, and V_o and r_o are the total volume and the radius of the particle, respectively.

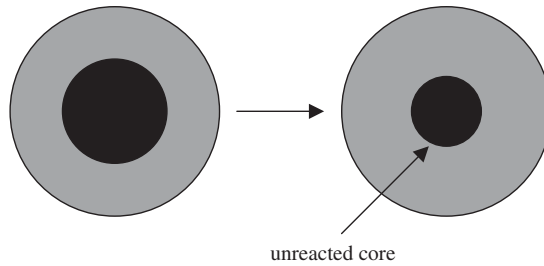


Figure 4.16 Shrinking core model: the reaction proceeds at a narrow front, which moves deeper into the solid particle as time passes.

It is well known that swelling of resins increases the particle radius. When resin beads are immersed in the solution, water uptake takes place almost immediately, resulting in a new “swollen” radius. The swollen radius is inversely proportional to the initial solution concentration (Hellferich, 1962). This effect has not been taken into account in the original model of Levenspiel (1972). However, the actual swollen radius of the resin should be used in the model equations, and so measurements should be performed in order to estimate this radius.

Furthermore, in its original form (Levenspiel, 1972), the assumption of constant and uniform bulk concentration of A in the fluid phase was made. This is similar to the infinite solution volume concept used in the analysis of adsorption and ion-exchange kinetics. In the following, the more general solutions are presented, i.e. for changing fluid concentration (finite solution volume).

Film diffusion control

$$X_B = \frac{3bk_f}{\rho_B r_0} \int_0^t C_A dt \quad (4.89)$$

where:

- k_f = the mass transfer coefficient in the fluid film surrounding the particle
- b = the stoichiometric coefficient
- C_A = the fluid phase bulk concentration of A
- ρ_B = the molar density of B in the solid phase (moles B/unit solid volume),

$$\rho_B = q_{\max} \rho_p \quad (4.90)$$

where ρ_p is the particle density and q_{\max} is the initial solid-phase concentration of B. In ion-exchange systems, this quantity is equal to the MEL under the specified experimental conditions. In most cases, if the ion exchanger is a resin, this value is equal to the REC, which is known beforehand by the producer.

Ash (solid) diffusion control

$$1 - 3(1 - X_B)^{2/3} + 2(1 - X_B) = \frac{6bD_s}{\rho_B r_o^2} \int_0^t C_A dt \quad (4.91)$$

where D_s is the effective diffusion coefficient of fluid phase reactant in the solid (ash).

Reaction kinetics control

$$1 - (1 - X_B)^{1/3} = \frac{bk}{\rho_B r_o} \int_0^t C_A dt \quad (4.92)$$

where k is the first-order rate constant for the surface reaction.

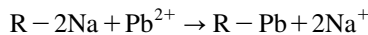
All these equations could be viewed as linear:

$$f(X_B) = S \int_0^t C_A dt \quad (4.93)$$

where the slope S and the function $f(X_B)$ are different for each controlling mechanism.

Example 1

Inglezakis *et al.* (2003) studied the removal of Pb^{2+} (500 ppm) in a batch system using the chelating resin Lewatit TP-207, under rigorous agitation (650 rpm) and ambient temperature (30 °C). The ion-exchange process is followed by an irreversible reaction in the resin phase, represented by the following scheme:



where R is the organic resin. The volume of the liquid is 350 cm³ and the mass of dry resin used is 0.6 g. The capacity of the resin is experimentally found to be 388 mg Pb/g of dry resin. The density of the resin particles is 1.18 g/cm³ and the mean particle radius is 0.55 mm. By using the kinetic data of Table 4.17, find the controlling mechanism and

Table 4.17

Experimental data (approximate values)

t (min)	C_t (ppm)
5	383
10	325
15	275
25	213
45	138
60	91

the corresponding kinetic parameter, assuming that the swelling of the resin beads is negligible.

Solution

The first step is to use the kinetic data to evaluate the conversion of the resin phase (X_B):

$$X_B = \frac{q_t}{q_{\max}}$$

where $q_{\max} = 388$ mg Pb/g of dry resin and q_t is given by

$$q_t = (C_o - C_t) \frac{V_L}{m}$$

where C is the solution concentration of Pb^{2+} , V_L the solution volume, and m the resin mass. Then, the function $f(X_B)$ for each model can be estimated. The results are shown in Table 4.18.

Model equations are in the form

$$f(X_B) = S \int_0^t C_A dt$$

where the slope S and the function $f(X_B)$ are different for each controlling mechanism. The integral on the righthand side of this equation can be easily estimated by arithmetic means, i.e. Simpson's trapezoidal rule.

The values of this integral are shown in Table 4.19.

In Figure 4.17, the function $f(X_B)$ is plotted against the integral for all models.

The next step is to find out which function is linear with zero intercept. The results are shown in Table 4.20.

Table 4.18

$f(X_B)$ versus t data

t (min)	X_B	Film diffusion	Solid diffusion	Reaction kinetics
5	0.18	0.18	0.01	0.06
10	0.26	0.26	0.03	0.10
15	0.34	0.34	0.05	0.13
25	0.43	0.43	0.08	0.17
45	0.54	0.54	0.13	0.23
60	0.61	0.61	0.18	0.27

Table 4.19

Integral values	
t (min)	$\int_0^t C_A dt$ (ppm min)
0	0
5	2207.5
10	3977.5
15	5477.5
25	7917.5
45	11427.5
60	13145

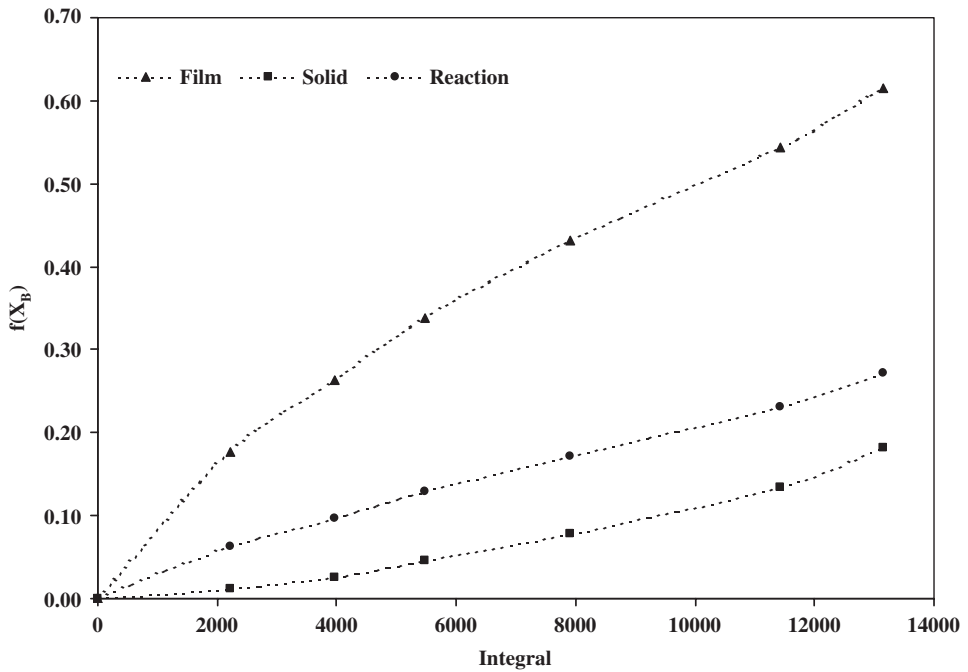


Figure 4.17 The application of the models.

Table 4.20

Regression analysis			
Model	Liquid diffusion	Solid diffusion	Reaction kinetics
R^2	0.9405	0.9284	0.9863

It is obvious that the best fit is given by the reaction kinetic control equation. The slope of the line is 2×10^{-5} L/mg min. Then,

$$\frac{bk}{\rho_B r_o} = 2 \times 10^{-5}$$

In this equation, $b = 2$ and

$$\rho_B = q_{\max} \rho_p = 457.84 \times 10^3 \text{ mg/L}$$

and

$$k = \frac{2 \times 10^{-5} \rho_B r_o}{2} = 2.52 \text{ mm/min}$$

Other simplified models for adsorption and ion exchange

The following models have been mainly used in liquid-phase adsorption and biosorption and, in some cases, for ion-exchange systems with inorganic ion exchangers (Rengaraj *et al.*, 2004; Bektas and Kara, 2004).

First-order adsorption kinetics model A simple first-order reaction model is based on a reversible reaction with equilibrium state being established between two phases (A—fluid, B—solid):



The kinetic rate in differential form and its analytical solution can be expressed as

$$\frac{dC_B}{dt} = -\frac{dC_A}{dt} = k_1 C_A - k_2 C_B \quad (4.94)$$

$$\ln(1 - U(t)) = -kt \quad (4.95)$$

where $U(t)$ is the fractional attainment of equilibrium, k the reaction constant in s^{-1} , and t the time in s.

Pseudo-first-order kinetic model (Lagergren's rate equation) In this model, the kinetic rate in differential form and its analytical solution can be expressed as

$$\frac{dq_t}{dt} = k(q_e - q_t) \quad (4.96)$$

$$\log(q_e - q_t) = \log(q_e) - \frac{k}{2.303} t \quad (4.97)$$

where q_e and q_t are the solid-phase concentration at equilibrium and at time (t), respectively. Here, k is the reaction constant in s^{-1} .

Pseudo second-order kinetic model In this model, the kinetic rate in differential form and its analytical solution can be expressed as

$$\frac{dq_t}{dt} = k(q_e - q_t)^2 \quad (4.98)$$

$$\frac{t}{q_t} = \frac{1}{kq_e^2} + \frac{1}{q_e} t \quad (4.99)$$

where q_e and q_t are the solid-phase concentration at equilibrium and at time t , respectively. Here, the units of k are $g/(mol \cdot s)$ provided that q is in mol/g .

Finding the rate-controlling mechanism

General As analyzed in Section 3.1.2, among the various steps that are part of a process, there is frequently one that is much slower than the others, thus controlling the rate of the whole mechanism. Hence, the slow step is called the “rate-limiting step” or the “rate-controlling step.” The principle of the rate-limiting step is often applied since it greatly simplifies the models used, but we should keep in mind that it is valid for processes in series. Most of the criteria that will be presented can be equally used in batch and fixed-bed operations.

Adsorption According to Fernandez and Carta (1996), who studied mass transfer in agitated reactors, the relative importance of external and intraparticle mass transfer resistances is strongly dependent on the solution composition. They used the following dimensionless number:

$$\frac{k_f d_p C_o}{10D_s q_{\max}} \quad (4.100)$$

where C_o is the initial solute concentration and q_{\max} the saturation capacity of the adsorbent. This number is dimensionless, and thus the concentration units are the same for both the liquid and solid phase (e.g. g/g). If this number is small compared to unity, the external film resistance is dominant. Conversely, if this number is large compared to unity, then intraparticle mass transfer resistance is dominant. According to this study, this criterion holds because of the rectangular shape of the isotherm (irreversible system), which means extremely favorable uptake of solute by the adsorbent. However, it is not valid for very short times when external film resistance is always predominant, and for very long times when the adsorbent is nearly saturated and intraparticle mass transfer becomes very slow. The same criterion has been used for fixed-bed operation by Fernandez *et al.* (1996).

Miura and Hashimoto (1977) used the following dimensionless number for fixed-bed operation:

$$\zeta = \frac{k_f a_u}{K(q_{\max} / C_o)} \quad (4.101)$$

$$K = \frac{15D_s \rho_b}{r_o^2} \quad (4.102)$$

$$a_u = \frac{6(1 - \varepsilon)}{d_p} \quad (4.103)$$

According to their analysis, if ζ is zero (practically much lower than 1), then the liquid-film diffusion controls the process rate, while if ζ is infinite (practically much higher than 1), then the solid diffusion controls the process rate. Essentially, the so-called mechanical parameter ζ represents the ratio of the diffusion resistances (solid and liquid film). The authors did not refer to any assumption concerning the type of isotherm for the derivation of the above-mentioned criterion: it is sufficient to be favorable (not only rectangular). They noted that for $\zeta > 7.6$, the particle diffusion is more significant, whereas if $\zeta < 0.14$, the external mass transfer controls the adsorption rate.

Other authors used the Biot (Bi) number for the same purpose in fixed-bed studies. Cooney (1993) defined the Biot number as

$$Bi = \frac{k_f d_p C_o}{2D_s q_{\max}} \quad (4.104)$$

Cooney defined q_{\max} as the solid concentration in equilibrium with C_o . This number is dimensionless, and thus the concentration units are the same for the liquid and solid phase (e.g. mg/g). Cooney pointed out that for $Bi < 0.5$, complete dominance of the liquid-film resistance exists, while for $Bi > 30$, reasonably complete dominance of intraparticle resistance exists. The only restriction is that the isotherm be favorable.

Hand *et al.* (1984) defined Biot number as

$$Bi = \frac{k_f d_p C_o}{2D_s q_{\max}} \frac{1}{\Phi_s} \quad (4.105)$$

where Φ_s is the sphericity of the particles. Obviously, this definition is broader, covering the case of nonspherical particles. This number is dimensionless; again, the concentration units are the same for the liquid and solid phase. The Biot number has been used as a criterion for the controlling mechanism for the whole favorable equilibrium region and not

only for irreversible systems. Biot numbers have been also used by Ko *et al.* (2003) for the irreversible adsorption process and by Yoshida *et al.* (1984) for irreversible adsorption and ion-exchange systems (rectangular isotherms). Concluding, Bi and similar dimensionless numbers can be used for favorable equilibrium, while the criteria based on these numbers are safer for irreversible systems.

Ion exchange The nature of the rate-determining step can be predicted by means of the simple criterion given below (Hellferich, 1962):

$$M = \frac{q_o D_s \delta}{C_o D_f r_o} \left(5 + \frac{2}{a_{A-B}} \right) \quad (4.106)$$

where:

- C_o = the total counterion concentration in the liquid-phase
- D_f = the liquid-phase diffusion coefficient
- δ = the film thickness
- r_o = the particle radius
- a_{A-B} = the separation factor.

The criterion states that

- particle diffusion controls if $M \ll 1$
- film diffusion controls if $M \gg 1$

The use of a constant separation factor is a reasonable approximation if the actual factor does not vary significantly. Film thickness for spherical particles is related to the Sh number via the relation

$$Sh = \frac{d_p}{\delta} \quad (4.107)$$

The film thickness is a fictitious quantity and cannot be measured directly. Its magnitude is usually of the order 10^{-3} – 10^{-2} cm, depending on agitation. This criterion is valid only for counterions of equal mobility and infinite solution volume. However, it is a useful approximation despite its limited precision.

Generally, control by liquid-phase mass transfer is favored by

- low liquid-phase concentration (small driving force in the liquid)
- high ion-exchange capacity (large driving force in the exchanger)
- small particle size (short mass transfer distances in the bead)
- open structure of the exchanger, e.g. low cross-linking (little obstruction to diffusion in the exchanger)
- ineffective agitation of the liquid (low contribution of convection to liquid-phase mass transfer).

In addition, selectivity also affects kinetics. When the exchanger is very selective in the entering ions, these ions are removed from the liquid as soon as they arrive at the surface, and as a result the concentration of these ions at the surface of the solid-phase remains low until substantial conversion of the bead has been achieved. Obviously, the difference between the concentrations of the bulk and bead surface, that is, the liquid-side driving force, also remains high, nearly until the end of the conversion. In contrast, if the opposite phenomenon takes place, that is, the ion that moves from the resin into the liquid is the preferred one, the concentration gradient quickly diminishes, resulting in a low driving force. So, the preference of the ion exchanger for its initially own ion leads to a rate limited by the liquid-side mass transfer.

In the case of solid diffusion control, even in the absence of agitation where the mass transfer coefficient is at its minimum value, sufficient agitation should be provided in order to avoid the negative effect of the liquid-film resistance. The effect of agitation should be taken into account in both the design and application stage.

Interruption test The best experimental technique for distinguishing between particle and film diffusion control is the so-called interruption test (Helfferich, 1962). In this test (Figure 4.18), the particles are removed from the liquid phase for a short time during which the concentration gradients within the solids are eliminated. Then, the particles are again immersed in the solution. If the diffusion within particles is rate-limiting, the rate at the time of reimmersion is expected to be higher than the one existing prior to the interruption. If such an effect is not observed, then obviously the diffusion across the film is the rate-limiting step, since the interruption does not significantly alter the concentration gradients within the film.

Another test entails the observation of the dependence of the rate on particle size. For reasons of geometry, the rate is inversely proportional to the particle radius at film diffusion control (proportional to the surface area per unit volume), and is also inversely proportional to the square of the particle radius if the rate is controlled by particle diffusion (the distance to be covered by diffusion being an additional factor). Thus, the rate-controlling step can be found by performing several experiments with particles of different radius.

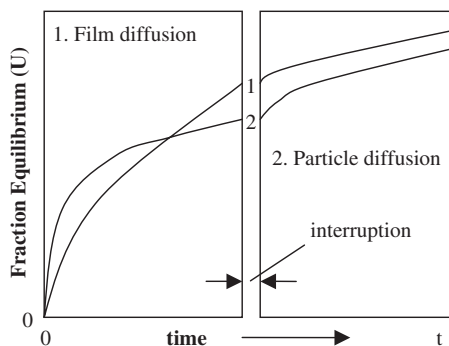


Figure 4.18 The interruption test.

Finally, the agitation rate does not affect the uptake rate if the particle diffusion controls the process. However, the latter criterion may be not safe; the agitation in solution may have attained its limiting hydrodynamic efficiency, so that a change in the agitation rate has no effect on the uptake rate even in film diffusion-controlled systems.

Shrinking core model There is a considerable difference between k_f and the other two kinetic parameters D_s and k ; the latter are independent of particle size while k_f is a function of agitation (and thus of Re_p) and is inversely proportional to particle size (Levenspiel, 1972). The time needed to achieve the same fractional conversion for particles of different but unchanging sizes is given by (Levenspiel, 1972)

$$t \propto r_o^b \quad (4.108)$$

where:

$$b = \begin{cases} 1.5 \text{ to } 2, & \text{for film diffusion control (the exponent drops as } Re_p \text{ rises)} \\ 2, & \text{for solid diffusion control} \\ 1, & \text{for chemical reaction control} \end{cases}$$

This criterion can easily distinguish between reactions in which the chemical and physical (diffusion) steps control. Furthermore, the chemical reaction step is usually more temperature sensitive than the physical (diffusion) steps. Thus, performing experiments at different temperatures could be another relatively safe way to distinguish between the controlling mechanisms.

Agitated vessels (liquid–solid systems) Below the off-bottom particle suspension state, the total solid–liquid interfacial area is not completely or efficiently utilized. Thus, the mass transfer coefficient strongly depends on the rotational speed below the critical rotational speed needed for complete suspension, and weakly depends on rotational speed above the critical value. With respect to solid–liquid reactions, the rate of the reaction increases only slowly for rotational speed above the critical value for two-phase systems where the solid–liquid mass transfer controls the whole rate. When the reaction is the rate-controlling step, the overall rate does not increase at all beyond this critical speed, i.e. when all the surface area is available to reaction. The same holds for gas–liquid–solid systems and the corresponding critical rotational speed.

It should be noted that this is not a safe criterion for the controlling mechanism. It is true that if the controlling mechanism is the reaction, then the increase of agitation above its critical value will have no effect on the overall rate. But this effect cannot be used safely as a criterion when searching for the controlling mechanism; there is a case where the liquid film diffusion could be the controlling mechanism and yet the agitation may have no effect on the overall rate. This could happen in the case where the mass transfer coefficient reaches a (practically) constant maximum value by increasing the agitation rate above a limit, and at the same time the other steps i.e. solid diffusion and/or rate are very fast. In this case, the liquid-film diffusion could be still the controlling mechanism.

Absolute rate, relative rate, and equilibrium

For any reactor, the conservation principle can be represented by the following relationship:

rate of i into volume element – rate of i out of volume element + rate of production of i within the volume element = rate of accumulation of i within the volume element

In the ideal batch-stirred tank reactor (BSTR), the fluid concentration is uniform and there are no feed or exit streams. Thus, only the last two terms in the previous equation exist. For a volume element V , the mass balance becomes (Smith, 1981)

$$(-r_i)V = -\frac{d(C_i V)}{dt} \quad (4.109)$$

where C_i is the concentration of species i at any time. If the volume of the reaction mixture is constant, the above equation becomes

$$(-r_i) = -\frac{dC_i}{dt} \quad (4.110)$$

where r_i is the intrinsic rate of the reaction. For adsorption and ion-exchange systems, it is more appropriate to call this rate the “absolute (uptake) rate.” Note that this is also the definition of a homogeneous reaction rate. The sameness is due to the fulfillment of the requirements of uniform concentration, temperature, and constant volume in an ideal BSTR.

The absolute rate, i.e. the amount adsorbed per unit time, is a function of the diffusion coefficient, i.e. the relative rate expressed by $U(t)$, as well as of equilibrium expressed by the available or active sites for adsorption or ion exchange. Since for $t_2 > t_1$

$$\begin{aligned} q(t_2) &> q(t_1) \\ C(t_2) &< C(t_1) \end{aligned} \quad (4.111)$$

then

$$q(t_2) - q(t_1) = -[C(t_2) - C(t_1)] \frac{V}{m} = [[C_o - C(t_2)] - [C_o - C(t_1)]] \frac{V}{m} \quad (4.112)$$

where

$$C_o - C(t_i) = U(t_i)(C_o - C_\infty) \quad (4.113)$$

Then

$$q(t_2) - q(t_1) = [U(t_2) - U(t_1)](C_o - C_\infty) \frac{V}{m} \quad (4.114)$$

Dividing by $\Delta t = t_2 - t_1$,

$$\frac{q(t_2) - q(t_1)}{\Delta t} = \frac{[U(t_2) - U(t_1)]}{\Delta t} (C_o - C_\infty) \frac{V}{m} \quad (4.115)$$

When $\Delta t \rightarrow 0$,

$$\frac{dq(t)}{dt} = (C_o - C_\infty) \frac{V}{m} \frac{dU(t)}{dt} \quad (4.116)$$

Finally, in terms of kinetics rate,

$$(-r_i) = -\frac{dC(t)}{dt} = \frac{m}{V} \frac{dq(t)}{dt} = (C_o - C_\infty) \frac{dU(t)}{dt} \quad (4.117)$$

In this expression, $U(t)$ is relative rate of uptake and C_∞ is relative to equilibrium, i.e. the sites available for ion exchange or adsorption for the specified ratio V/m . Thus, the absolute rate is a “coupled” result of kinetics and equilibrium. Note that in a solid diffusion–controlled process, $U(t)$ is relative to the ease of movement of the incoming species in the solid phase (through D_s).

Generally, a high diffusion coefficient means that the incoming species have the ability to make headway in any given direction relatively easily, and thus it is expected that the preference (selectivity) of the ion exchanger or adsorber for this species, and its equilibrium concentration, will be proportionally high. This general rule has some exceptions (Inglezakis *et al.*, 2004). A higher absolute rate for a species compared with another one does not necessarily mean a higher diffusion coefficient and higher preference for the incoming species, i.e. higher equilibrium concentration.

The “ease of movement” has been expressed by Inglezakis *et al.* (2004) by the term “exchange site accessibility,” while the available sites for exchange/adsorption have been expressed by the term “exchange site availability.” In the framework of the so-called exchange site accessibility concept, an exchange or an adsorption site is characterized by two factors (Inglezakis *et al.*, 2004):

- (a) *Its availability to the incoming species*: The first factor determines if a site can be occupied by the incoming species and depends on the equilibrium behavior of the system, namely, the selectivity, distribution coefficients, and equilibrium concentrations.

- (b) *Its accessibility to the incoming species:* Accessibility is used to express the ease of movement of the species within the solid phase to reach the available site. It is closely connected to the kinetic behavior (diffusion coefficients) of the system.

Here, it has to be noted that the availability and accessibility depend not only on the characteristics of the site but also on the nature of the incoming species. As shown in relevant experiments, a site can be available for the incoming species but may not be easily accessible to them and vice versa.

Design of a batch reactor system for adsorption and ion exchange

Suppose that the system obeys the following equilibrium equation:

$$Y = f(X) \quad (4.118)$$

This is a general type of adsorption isotherm. In the case of ion exchange, it is easy to correlate data in a way to have the same type of relationship for the ion that is removed from the liquid phase. When equilibrium is reached,

$$Y = \frac{q_e}{q_{\max}} \Rightarrow q_e = Yq_{\max} \quad (4.119)$$

and

$$X = \frac{C_e}{C_o} \Rightarrow C_e = XC_o \quad (4.120)$$

where C_o is in mg/L and q_{\max} is in mg/g. Here, q_{\max} is the solid-phase concentration in equilibrium with C_o for adsorption or the MEL in ion exchange. Using the equilibrium relationship (eq. (4.118)):

$$q_e = Yq_{\max} = f(X)q_{\max} \quad (4.121)$$

Applying an overall material balance in the batch reactor and using eq. (4.120),

$$q_e m = (C_o - C_e)V = (C_o - XC_o)V = (1 - X)C_o V \quad (4.122)$$

where V is the volume of the fluid in L and m the mass of the solid phase in g. Then, equating (4.121) and (4.122), we have

$$\frac{V}{m} = \frac{q_{\max}}{C_o} \frac{f(X)}{1 - X} \quad (4.123)$$

Using this equation, the ratio of the fluid volume to the solid mass needed to achieve a desired fluid-phase equilibrium concentration (X) can be calculated. We can achieve a lower liquid-phase concentration level by using a lower V/m ratio, using, for example, a higher amount of solid. Thus, equilibrium calculations result in the maximum V/m ratio that should be used to achieve the desired equilibrium (final) concentration. But, how much time do we need to achieve our goal in a batch reactor? This is a question to be answered by kinetics.

By the definition of $U(t)$, we have

$$U(t) = \frac{C_o - C(t)}{C_o - C_e} = \frac{1 - X(t)}{1 - X} \quad (4.124)$$

where $X(t)$ is given by

$$X(t) = \frac{C(t)}{C_o} \quad (4.125)$$

Then, to achieve $C(t)$ equal to the equilibrium concentration for the specified V/m ratio, $U(t)$ has to be equal to 1. Typically, this time for equilibrium is considerably high and impractical for most applications. For that reason, it is better to use V/m values lower than the maximum. By using several V/m values lower than the maximum, it is possible to calculate the corresponding equilibrium concentration X . Then, $U(t)$ could be calculated for the desired $X(t)$. Using these data, the kinetic model is applied to evaluate the time needed to achieve the desired $U(t)$.

Note that X in ion exchange and adsorption is the ratio of the species concentration to the initial concentration and is not equivalent to the conversion as defined in catalytic reactions, which is

$$x = \frac{C_o - C(t)}{C_o} \quad (4.126)$$

and thus

$$x = \frac{C_o - C(t)}{C_o} = 1 - X \quad (4.127)$$

Example 2

Meshko *et al.* (2001) studied the adsorption of a basic dye (Maxilon Goldberg GL EC 400% or MG-400) using zeolite in an agitated vessel of 0.5-L volume, under agitation (200 rpm) at ambient temperature (20 °C). The initial concentration of dye was 100 mg/L, the

volume of solution was 0.1 L, and the mass of zeolite used was 2 g. The zeolite properties were: particle size, 1–3 mm; porosity, 0.325; and solid density, 2.12 (g/cm³). The equilibrium followed the Langmuir isotherm with $Q_M = 14.91$ mg/g and $K = 0.0434$ L/mg.

Some experimental kinetic data are given in Table 4.21 (approximate values).

Meshko *et al.* (2001) used a homogeneous solid model taking into account both internal and external diffusion. They found that the adsorption of the dye had not been significantly affected by the agitation speed, which indicated that the process was solid diffusion-controlled. Furthermore, for the specified conditions, they found that $k_f = 6.66 \times 10^{-5}$ m/s and $D_s = 10^{-12}$ m²/s.

Use Patterson's equation to model the kinetic data. Furthermore, propose a design for the agitated batch reactor.

Solution

Kinetics and equilibrium analysis To use Patterson's model (eq. (4.52)), we first need the parameter w , and thus the equilibrium liquid-phase concentration C_e . The maximum loading of the zeolite particles for the specific initial concentration can be calculated by means of the equilibrium relationship (eq. (4.5)):

$$q_{\max} = Q_M \frac{KC_o}{1 + KC_o} = 12.12 \text{ mg/g}$$

Then using eq. (4.123),

$$\frac{f(X)}{1 - X} = \frac{C_o}{q_{\max}} \frac{V}{m} = 0.413$$

The function $f(X)$ is the dimensionless equilibrium relationship, which for the Langmuir isotherm is (eq. (4.9))

$$f(X) = \frac{X}{La + (1 - La)X} = 0.413(1 - X)$$

Table 4.21

Experimental data

t (min)	q_t (mg/g)
15	1
30	1.2
60	1.6
120	2.1
180	2.5

where La can be calculated by using eq. (4.8):

$$La = \frac{1}{1 + KC_o} = 0.1873$$

Then, a trial-and-error procedure is needed for estimating the equilibrium liquid-phase dimensionless concentration. In this way, we get $X = 0.1$ and thus

$$X = \frac{C_e}{C_o} \Rightarrow C_e = C_o X = 9.975 \text{ mg/L}$$

The parameter w is calculated by using eq. (4.33):

$$w = \frac{C_o - C_e}{C_o} = 0.9$$

Then, the roots of eq. (4.58) are $a = -3.477$ and $b = 0.777$. To use the model, we need to transform the solid loading q_t into $U(t)$:

$$U(t) = \frac{C_o - C(t)}{C_o - C_e}$$

where the liquid concentration $C(t)$ can be calculated from the following relationship:

$$q_t = \frac{C_o - C(t)}{m} V$$

In Table 4.22, t and the corresponding values of $U(t)$ are given.

Table 4.22

$U(t)$ versus t

t (min)	$U(t)$
15	0.22
30	0.27
60	0.36
120	0.47
180	0.56

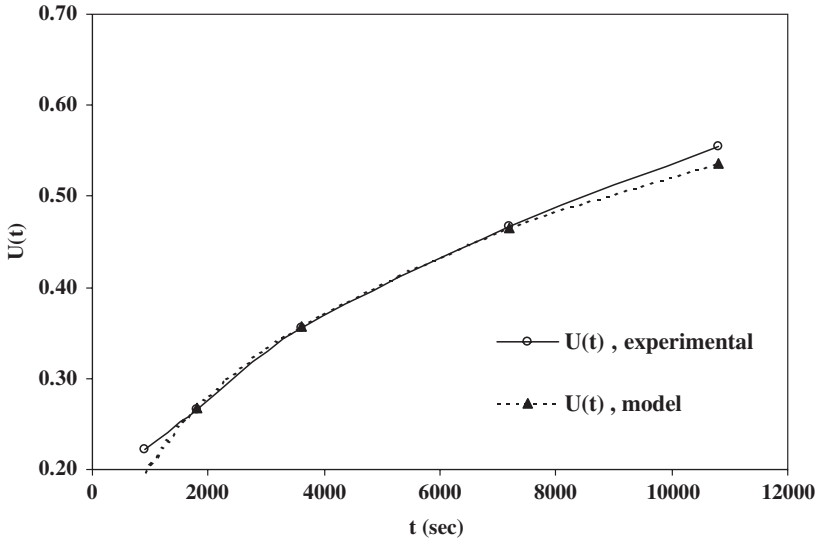


Figure 4.19 The performance of the model.

By a trial-and-error procedure, using the value of $U(t)$ and the model eqs. (4.52)–(4.58), the solid-phase diffusion coefficient is found to be 1.3×10^{-12} m²/s. This value is very close to the one given in the study of Meshko *et al.* The trial-and-error procedure can be done easily. By changing the value of D_s , the model predicts the values of $U(t)$ for each t . The best value of D_s is the one that results in the lowest mean deviation between the experimental and the model values of $U(t)$. In Figure 4.19, the performance of the model is shown. The average error is 3.1%.

Reactor design Using the typical dimension ratios of an agitated vessel (see Section 3.3.5):

$$D_T = \left(\frac{4}{\pi} V \right)^{1/3} = 5.03 \text{ cm}$$

$$D_a = \frac{D_T}{3} = 1.68 \text{ cm}$$

$$B = \frac{D_T}{10} = 5 \text{ mm}$$

Four baffles and a propeller with three blades could be used. Thus, for this specific system (eq. (3.104)),

$$N_{Re} = \frac{D_a^2 N \rho}{\mu} \cong 1000$$

For propellers, $N_p = 0.32$ (see Table 3.4) and thus (eq. (3.107))

$$P_s = \frac{P}{V} = \frac{N_p \rho N^3 D_a^5}{V} = 0.16 \text{ W/m}^3$$

Assuming that $D_f = 10^{-9} \text{ m}^2/\text{s}$ and using the Levins–Glastonburn correlation (3.118), the value of the mass transfer coefficient is found to be $k_f = 1.3 \times 10^{-5} \text{ m/s}$. The difference between this value and the value given by Meshko *et al.* is due to the approximate value of D_f used in this example.

The Biot number is (eq. (4.104))

$$Bi = \frac{k_f d_p C_o}{2D_s q_{\max}} = 82.41$$

which is much higher than the value of 30. So, it is reasonable to assume that intraparticle resistance dominates, as Meshko *et al.* (2001) found experimentally.

By means of the Zwietering equation (3.114), with $S = 6.5$ for propellers (see Table 3.6), we find that the minimum rotational speed for complete suspension is 40.58 rps, much higher than the operating value of 3.33 rps (200 rpm). This means that the solid particles are not fully suspended in the liquid phase.

Finally, using the Calderbank correlation (3.271), the minimum rotational speed for surface aeration is found to be 55.16 rps, which is fairly higher than the operation agitation speed, and thus surface aeration is avoided.

Some comments on dyes: Dyes can be a threat to both human health and environment. Focusing on the effect of dyes on human health, it should be pointed out that on exposure to an environment containing vapors of dyes, one would experience headaches and dizziness. After inhaling large portions of these vapors, limbs could get paralyzed and damage of the inner organs may take place. Nowadays, the risks associated with the use of such dyes have been widely recognized and many countries have posted many restrictions to their use. In Europe, the launch of a new standard called ISO 14000 has banned the import of all materials dyed with poisonous dyes.

Example 3

A volume of 100 L of a solution containing 1000 ppm Pb^{2+} and minor amounts of other ions has to be treated. The desired final concentration is 100 ppm. The available adsorbent is a zeolite with a particle size of 1.3 mm, density of 2 g/cm^3 , and the REC is $Q_M = 176 \text{ mg/g}$. Suppose that we have efficient agitation and solid diffusion is the controlling mechanism. Solid diffusion is about $6.4 \times 10^{-10} \text{ cm}^2/\text{s}$. Furthermore, the system obeys a favorable Langmuir isotherm with $La = 0.03$ and the maximum exchange level is $q_{\max} = 106 \text{ mg/g}$.

Estimate the time needed in an agitated batch reactor for lowering the solution concentration to the value of 100 ppm for different masses of zeolite. Furthermore, propose a design for the reactor.

Solution

The finite solution volume model for solid-diffusion control (Patterson’s model) will be used (eq. (4.52)). Following the procedure presented in the section *Design of a batch reactor system for adsorption and ion exchange* (eqs. (4.119)–(4.125)), we obtain the results shown in Table 4.23.

In Figure 4.20, the kinetic curves for different zeolite amounts are presented.

Lower V/m means a higher amount of solid. It is obvious that a faster process results in higher cost, as we have to use a larger amount of solid. The best solution is to study the system, using several combinations of time and solid mass to achieve the best operation design. Consider that 2.28 kg of solid are used.

Geometrical dimensions of the system Suppose that we use a baffled cylindrical vessel and a flat-blade turbine with six blades. Given that the volume of the liquid to be treated $V_L = 100$ L and using the analogies and equations of Section 3.3.5, we obtain impeller diameter $D_a = 16.77$ cm, vessel diameter $D_T = 50.32$ cm, impeller blade width $W = 3.35$ cm, liquid level $H_L = 50.32$ cm, impeller level above the bottom equal to 16.77 cm, and $B = 2.8$ cm. Finally, it is desirable to use a vessel height H_T somewhat higher than the

Table 4.23

Kinetic data

X	V/m (L/g)	m (kg)	$U(t)$ for $X(t) = 0.1$	t (h) for $X(t) = 0.1$
$X_{\max} = 0.1$	$(V/m)_{\max} = 0.093$	$m_{\min} = 1.08$	1	49.58
0.05	0.071	1.41	0.948	28.72
0.02	0.044	2.28	0.918	12.77

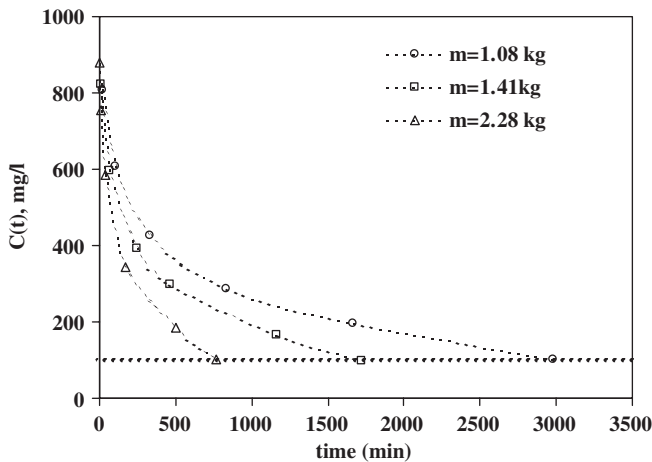


Figure 4.20 Kinetic curves.

liquid level, as a liquid vortex will result in an increase of the liquid level above the initial. So, a vessel with a 60-cm height is selected.

The critical rotational speed of the impeller for complete suspension is approximately 541 rpm (9 rps) (eq. (3.114)). This rotational speed results in a Reynolds value of about 2.54×10^5 , and thus the flow is turbulent. Here, it has to be noted that the mass transfer coefficient strongly depends on the rotational speed below the critical rotational speed needed for complete suspension, and weakly depends on the rotational speed above its critical value at which there are no particles remaining in rest for longer than 1–2 s in a fixed position.

Verification of the controlling mechanism Zeolite particles are of irregular shape and a value of $\Phi_s = 0.65$ could be used (see Table 3.13). Furthermore, as a first approach, the minimum mass transfer coefficient from Table 3.7 can be used. Thus, for density difference of 1 g/cm^3 this minimum value is $k_f = 0.005 \text{ cm/s}$. Then, using Hand's definition (eq. (4.105)), the minimum Biot number is 7.4×10^3 . This number is much higher than the limit of 30 for solid diffusion control. Thus, we conclude safely that the controlling mechanism is solid diffusion, even in the absence of agitation. However, sufficient agitation should be provided to avoid any possible negative effect of liquid-film resistance.

Using the appropriate equations and correlations of Sections 3.3.5 and 3.3.6, we can calculate the power consumption per unit volume of liquid and thus we can have an approximation of the actual mass transfer coefficient in the liquid film. $N_p = 6$ for this type of impellers and thus k_f is about 0.1 cm/s . It is obvious that k_f is about 20 times the minimum value used above for the Biot number.

A few comments on lead: The extensive use of tetraethyl lead (TEL) as a gasoline additive, for reducing engine knocking since 1922, constituted the greatest source of lead in the environment. Despite the fact that many experts were against its use and the negative effects on public health were known as early as the 1920s, the use of TEL continued till the decade of 1980 (Rosner and Markowitz, 1985).

Lead is not an exception among heavy metals. It is very harmful even in very small amounts, since once absorbed into the body, it blocks certain enzymes, causing severe physiological or neurological consequences in the long term. The list of the hazardous effects of lead on human health is quite long: anemia and other blood disorders, damage to the nervous system and brain, kidney disease, and reproductive impairments in men and women. Overexposure to lead may cause birth defects, mental retardation, behavioral disorders, and even death in fetuses and young children.

Example 4

Choy and McKay (2005) studied the removal of Cu^{2+} from aqueous phase using bone char in a batch reactor. The volume of the liquid was 1.7 L, the volume of the tank 2 L, and its diameter 0.13 m. A six-bladed flat impeller with a diameter of 0.065 m and a blade height of 0.013 m was used. Absorbent particles of 605- μm diameter were used for the adsorption experiments.

The adsorption isotherm at $20 \text{ }^\circ\text{C}$ was found to obey the Langmuir equation with $K = 69.2 \text{ L/mmol}$ and $Q_M = 0.709 \text{ mmol/g}$. For the kinetics experiments, Cu^{2+} solutions of 3.21-mM

Table 4.24

Experimental data	
t (min)	C_t (mmol/L)
25	2.3
50	2
100	1.6
150	1.3
180	1.18

concentration were mixed with 8.5 g of bone char. In Table 4.24, some experimental kinetic data are given (approximate values).

Choy and McKay used a homogeneous surface diffusion model (HSDM) taking into account both external and internal transport, and found that the mean value of the solid diffusion coefficient is 3.72×10^{-9} cm²/s while $k_f = 6.06 \times 10^{-4}$ cm/s.

Assuming a solid diffusion-controlled process, use the Patterson equation and find the corresponding solid diffusion coefficient. Furthermore, find the impeller speed in order to have the reported value for k_f .

Solution

To use Patterson's model (eq. (4.52)), we first need the parameter w and thus the equilibrium liquid-phase concentration C_e . The maximum loading of the zeolite particles for the specific initial concentration can be calculated using the equilibrium relationship (eq. (4.5)):

$$q_{\max} = Q_M \frac{KC_o}{1 + KC_o} = 0.071 \text{ mmol/g}$$

Then (eq. (4.123))

$$\frac{f(X)}{1 - X} = \frac{C_o}{q_{\max}} \frac{V}{m} = 0.910$$

The function $f(X)$ is the dimensionless equilibrium relationship, which for the Langmuir isotherm is (eq. (4.9))

$$f(X) = \frac{X}{La + (1 - La)X}$$

where La is given by (eq. (4.8))

$$La = \frac{1}{1 + KC_o} = 0.0045$$

Then, the equilibrium liquid-phase dimensionless concentration is estimated following a trial-and-error procedure, and it is easy to find that $X = 0.032$. Thus,

$$C_e = C_o X = 0.103 \text{ mmol/L}$$

The parameter w is (eq. (4.33))

$$w = \frac{C_o - C_e}{C_o} = 0.9679$$

The roots of eq. 4.58 are $a = -3.691$ and $b = 0.787$. Then

$$U(t) = \frac{C_o - C(t)}{C_o - C_e}$$

In Table 4.25, the values of $U(t)$ and the corresponding values of t are shown.

Again following a trial-and-error procedure, the solid-phase diffusion coefficient is found to be $1.82 \times 10^{-9} \text{ cm}^2/\text{s}$. This value is very close to the one given in the study of Choy and McKay. In Figure 4.21, the performance of the model is shown. The average error is 3%.

The Biot number is (eq. (4.104))

$$Bi = \frac{k_f d_p C_o}{2D_s q_{\max}} = 45.81$$

which is higher than the value of 30. So it is reasonable to assume that intraparticle resistance dominates.

Calderbank–Moo–Young equation can be used for the mass transfer coefficient (eq. (3.120)):

$$k_f = 0.13 \left(\frac{P_s v_L}{\rho_L} \right)^{0.25} Sc^{-2/3}$$

Table 4.25

$U(t)$ versus t

t (min)	$U(t)$
15	0.29
30	0.39
60	0.52
120	0.61
180	0.65

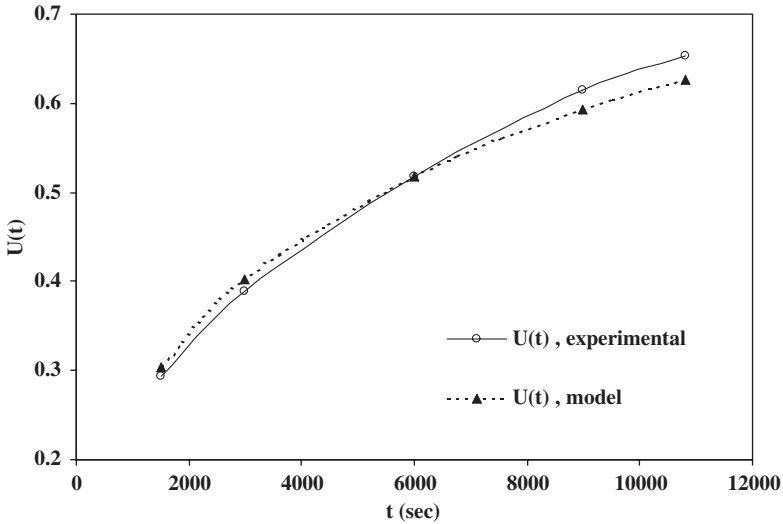


Figure 4.21 The performance of the model.

The liquid-phase diffusion coefficient can be estimated from the Nernst–Haskell eq. (I-24) (see Appendix I):

$$D_w = \frac{\lambda_i R_g T}{F^2}$$

For Cu^{2+} , $\lambda_i = 53.6 \text{ cm}^2/\Omega \text{ mol}$ (Table I-8) and thus $D_f = 1.4 \times 10^{-5} \text{ cm}^2/\text{s}$ and $Sc = 641.88$. For the given value of $k_f = 6.06 \times 10^{-4} \text{ cm/s}$, the value of P_s is

$$P_s = 0.16 \text{ W/m}^3 = \frac{P}{V} = \frac{N_p \rho N^3 D_a^5}{V}$$

Using the typical dimension ratios of an agitated vessel,

$$B = \frac{D_T}{10} = 1.3 \text{ cm}$$

Four baffles are selected. Thus, for this specific system, we can assume that $N_p = 4$ (see Table 3.4), a value which is valid for N_{Re} near or above 2×10^{-3} . Then, the agitation speed $N = 23.35 \text{ rpm}$, which results in a Reynolds number equal to

$$N_{Re} = \frac{D_a^2 N \rho}{\mu} \cong 1830$$

This justifies the use of the selected value of N_p .

A few comments on copper: Copper is an element that has found many uses in the manufacture of electrical equipment due to its high electrical and thermal conductivity. Copper salts have also been used extensively as fungicides, in ceramics and pyrotechnics, and in many other industrial applications. Obviously, the utilization of copper by man has led to the reinforcement of its presence in the environment, with mining operations, solid waste, agriculture, and sludge from sewage-treatment plants being its primary anthropogenic releases.

Gastrointestinal, hepatic, and renal effects with symptoms such as severe abdominal pain, vomiting, diarrhea, hemolysis, hepatic necrosis, hematuria, proteinuria, hypotension, tachycardia, convulsions, coma, and finally death, may result from the ingestion of grams of copper salts.

4.2.2 Fixed-bed operations for ion exchange and adsorption

Introduction

In the design of a sorption system, the knowledge of the main principles is important and many practical aspects have to be dealt with adequately. To begin with, the suitable sorbent material for our application has to be selected. It is highly desirable that its equilibrium properties such as capacity and selectivity are well known. Moreover, their dependence on temperature and component concentration has to be also understood. In addition, time and space have to be included in our design, since sorption operations are held in batch or fixed beds and exhibit a dynamic behavior. It means that steady-state operation is not the case in sorption systems in contrast to many other chemical operations that are independent of time. The fixed-bed performance has to be well related to adsorption equilibrium and rate behavior in a successful design. Many practical aspects have to be taken into account so that the process can be properly carried out. For example, dispersive phenomena at the bed scale as well as the aging mechanism have to be known and included in our design so that the behavior of the sorption system is controlled.

Fixed bed is the most frequently used operation for ion exchange and adsorption, as it is the predominant way of conducting such sorption separations. Moreover, ion exchange and adsorption are common operations used for wastewater treatment. For example, in ion-exchange processes, zeolites and resins are used for the removal of heavy metals such as Pb^{2+} , Cr^{3+} , Fe^{3+} , Cu^{2+} , and ammonia (Baycal *et al.*, 1996; Blanchard *et al.*, 1984; Inglezakis *et al.*, 2002; Cincotti *et al.*, 2001; Babel and Kurniawan, 2003), while in adsorption processes, activated carbon, peat, iron oxide, kaolin, and fly ash are used for the removal of heavy metals and several organic substances from wastewaters, such as benzene, phenolic compounds, carbon tetrachloride, nitrophenol, acid dyes, and *p*-dichlorobenzene (Weber and Pirbazari, 1982; Chern and Chien, 2002; Babel and Kurniawan, 2003; Gupta *et al.*, 1997, 2000; Ko *et al.*, 2002; Sen *et al.*, 2002). Furthermore, adsorption is frequently used for the removal of toxic compounds from gas streams, and some examples are the removal of phenanthrene (PAH) using coke (Murillo *et al.*, 2004), the removal of sulfur dioxide and hydrogen sulfide using zeolites (Gupta *et al.*, 2004; Yasyerli *et al.*, 2002), and the removal of toluene (VOC) from a gas stream using activated carbon (Cheng *et al.*, 2004).

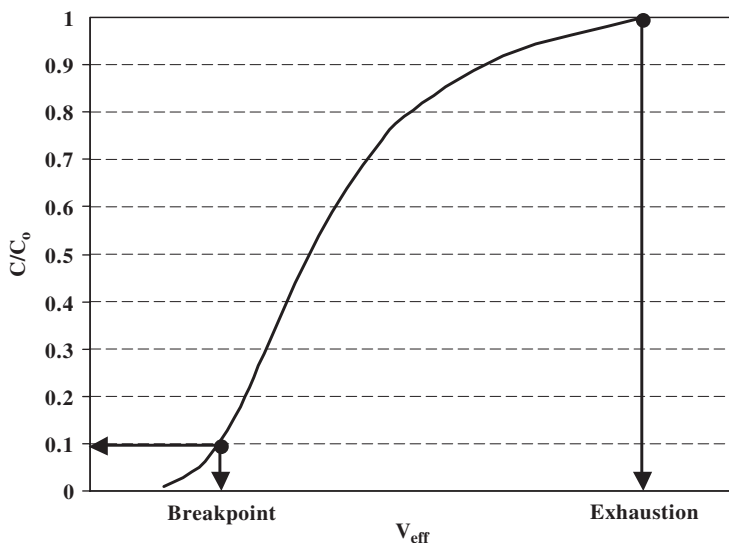


Figure 4.22 Breakthrough curve.

In Figure 4.22, a typical breakthrough curve is presented, where C/C_0 is the dimensionless exit concentration and V_{eff} is the effluent volume. The breakpoint concentration is a selected limiting value (according to the needs of the treatment) where the operation should be stopped. The main aim when sizing adsorptive columns is the ability to predict the service time (or total effluent volume) until the column effluent exceeds breakpoint concentration. Then, from the practical point of view, the breakpoint volume is the most important information—it is the fluid volume that can be treated by the column until a pre-specified breakpoint. This information could be derived from experiments conducted in laboratory columns and the scale-up goal is to “transfer” it to large unit or at least to evaluate the changes during scaling (see Chapter 6).

Although the fixed-bed mode is highly useful, its analysis is unexpectedly complex. Fixed-bed operation is influenced by equilibrium (isotherm and capacity), kinetic (diffusion and convection coefficients), and hydraulic (liquid holdup, geometric analogies, and maldistribution) factors. Thus, a predictive modeling of fixed-bed systems requires extensive experimental information (laboratory and pilot-scale experiments) and complex mathematical tools; and in many cases, for complicated multicomponent solutions, the full modeling of the process is extremely difficult. For example, even in the simple cases of Pb^{2+} , Cd^{2+} , and Cu^{2+} , and basic dyes removal from solution using clinoptilolite, peat, and activated carbon respectively, in fixed-bed operation, it is found that equilibrium parameters and/or solid diffusion coefficients seem to be unexpectedly influenced by contact time, making the modeling of the operation a complex task (Ko *et al.*, 2003; Markovska *et al.*, 2001; Inglezakis and Grigoropoulou, 2003).

The situation is even more difficult considering the scale-up procedure. Scale-up is considering the geometric similarity (referring to linear dimensions), kinematic similarity (referring to motion), and dynamic similarity (referring to forces) at the same time. Frequently, it is not possible to achieve full similarity between different scales.

The effectiveness of a fixed-bed operation depends mainly on its hydraulic performance. Even if the physicochemical phenomena are well understood and their application in practice is simple, the operation will probably fail if the hydraulic behavior of the reactor is not adequate. One must be able to recognize the competitive effects of kinetics and fluid dynamics: mixing, dead spaces, and bypasses that can completely alter the performance of the reactor when compared to the “ideal” presentation (Donati and Paludetto, 1997). The main factor of failure in liquid-phase operations is liquid maldistribution, which could be related to low liquid holdup in downflow operation, or other design problems. These effects could be critical not only in full-scale but also in pilot- or even in laboratory-scale reactors.

Basic design considerations

Material balance Ion exchange and adsorption from aqueous solutions could be considered as isothermal and isobaric operations, while gas-phase adsorption operations could be nonisothermal and nonisobaric. However, in most environmental applications, the concentration of the gas-phase solute is low, and so the heat released and the pressure drop due to adsorption are low. Thus, it can be considered that isothermal and isobaric conditions are met (Murillo *et al.*, 2004; Gupta *et al.*, 2004; Cheng *et al.*, 2004). Note that pressure drop could arise not only by the removal of a considerable amount of a species from a gaseous stream but also due to friction as gas is passed through the bed of solids. Pressure drop changes the fluid density, which in turn influences the volumetric flow rate and thus the superficial fluid velocity. The problem is analogous to the one encountered in catalytic reacting systems where the expansion factor due to the reaction and the pressured drop due to reaction *and* friction are in the picture (see Section 5.3.4). However, the pressure drop due to friction can be considered negligible in most practical applications.

The material balance for fixed beds (see eq. (3.285)) is

$$D_L \frac{\partial^2 C}{\partial z^2} - u_s \frac{\partial C}{\partial z} - (-R) = \varepsilon \frac{\partial C}{\partial t} \quad (4.128)$$

Rearranging and using eq. (3.289) for the rate expression $-R$ in ion exchange and adsorption systems, we obtain

$$\frac{D_L}{u_s Z} \frac{\partial^2 C}{\partial (z/Z)^2} - \frac{\partial C}{\partial (z/Z)} - \rho_b \frac{Z}{u_s} \frac{\partial q}{\partial t} = \varepsilon \frac{Z}{u_s} \frac{\partial C}{\partial t} \quad (4.129)$$

where the term Z/u_s is the fluid residence time (or contact time). Both C and q are dependent on time t and height Z . Hence, the expression is in the form of a partial differential equation.

Rate equations There are two basic types of kinetic rate expressions. The first and simpler is the case of linear diffusion equations or linear driving forces (LDF) and the second and more rigorous is the case of classic Fickian differential equations.

Linear diffusion equations: This is the simplest case and is used extensively in the related literature (Perry and Green, 1999; Hashimoto *et al.*, 1977; Cooney, 1990, 1993). The equations are the following:

$$\text{solid diffusion control: } \frac{\partial q}{\partial t} = K_s(q_i - q) \quad (4.130)$$

$$\text{fluid - film diffusion control: } \frac{\partial q}{\partial t} = K_f(C - C_i) \quad (4.131)$$

where K_s and K_f are constants related to the local mass transfer coefficients. The subscript “i” corresponds to the concentrations in the solid–fluid interface.

Differential diffusion equations: In this case, we have differential equations, one for each diffusion step (Perry and Green, 1999; Hall *et al.*, 1966):

$$\frac{\partial q}{\partial t} = K_f(C - C_e) \quad (4.132)$$

$$\frac{\partial q}{\partial t} = K_s \left(\frac{\partial^2 q}{\partial r^2} + \frac{2}{r} \frac{\partial q}{\partial r} \right) \quad (4.133)$$

$$\frac{\partial q}{\partial t} = K_p \frac{1}{r^2} \frac{\partial}{\partial r} \left(R^2 \frac{\partial C}{\partial r} \right) \quad (4.134)$$

where K_s , K_p , and K_f are constants related to the local mass transfer coefficients. Eq. (4.132) is for the case of fluid-film diffusion control, eq. (4.133) for solid diffusion control, and eq. (4.134) for pore diffusion control. Pore diffusion is similar to solid diffusion; it, however, represents the fluid diffusion in pores and is considered to be an intermediate diffusion step, between fluid-film and solid diffusion. For the case of fluid-film diffusion, the equation is the same as the LDF equation. However, here, the equilibrium concentration (C_e) is used in place of the interface concentration (C_i) to illustrate one significant point. These concentrations are equal only in the case of solid diffusion as the controlling mechanism; otherwise they are different. For the case of differential diffusion equations, only arithmetic solutions are possible and will not be presented in this book.

Equilibrium The physical process (reaction) of adsorption or ion exchange is considered to be so fast relative to diffusion steps that in and near the solid particles, a local equilibrium exists. Then, the so-called adsorption isotherm of the form $q = f(C_e)$ relates the stationary and mobile-phase concentrations at equilibrium. The surface equilibrium relationship between the solute in solution and on the solid surface can be described by simple analytical equations (see Section 4.1.4). The material balance, rate, and equilibrium equations should be solved simultaneously using the appropriate initial and boundary conditions. This system consists of four equations and four unknown parameters (C , \bar{q} , q , and C_e).

Predictive models

Mass transfer-controlled systems—“diffusion” models and single resistance to diffusion Predictive models can be used to model the removal process and determine the controlling step of the whole phenomenon. In most cases, particle diffusion within the solid matrix is the controlling mechanism. But the controlling step is strongly dependent on fluid linear velocity, since at low velocities the fluid-film diffusion step could be the controlling mechanism. Thus, as a first step, the lowest possible linear velocity could be used for the evaluation of the controlling step. To use simplified models, the following assumptions should be met.

1. *Plug flow*: In this case, the first term in eq. (4.128) is neglected. This assumption holds only if the axial Peclet number of the bed (Pe_L) is greater than about 100 (Levenspiel, 1972). For packing materials of irregular shape, such as zeolites and activated carbon, and 0.5 mm particle size, a bed of 50-cm height is sufficient, for superficial velocities higher than about 0.2 cm/s (Inglezakis *et al.*, 2001). However, by using upflow operation, this value could be by far lower. Generally, by using upflow mode, the quality of the flow is much better, especially at low velocities.
2. *Constant pattern condition*: This condition reduces the mass balance equation (4.128) to the simple relation: $C/C_o = \bar{q}/q_{\max}$ (see the section *A look into the “constant pattern” condition*). Practically, the constant pattern assumption holds if the equilibrium is favorable, and at high residence times (Perry and Green, 1999; Wevers, 1959; Michaels, 1952; Hashimoto *et al.*, 1977). However, the constant pattern assumption is “weak” if the system exhibits very slow kinetics (Wevers, 1959).

Various simplified models under the above assumptions have been proposed and analyzed in the related literature and are in the form of either arithmetic or analytical solutions. In the following, simplified models will be presented under the two commonly applied assumptions, namely, the constant pattern and plug-flow assumptions. The following dimensionless parameters are defined (Perry and Green, 1999):

$$\Lambda = \frac{\rho_b q_{\max}}{C_o} \quad (4.135)$$

$$T = \frac{t - \left(\frac{V_o \varepsilon}{Q} \right)}{\left(\frac{\Lambda V_o}{Q} \right)} \quad (4.136)$$

$$N_f = \frac{k_f a_u V_o}{Q} \quad (4.137)$$

$$N_p = \frac{15D_p(1-\varepsilon)V_o}{r_o^2 Q} \quad (4.138)$$

$$N_s = \frac{15D_s \Delta V_o}{r_o^2 Q} \quad (4.139)$$

where t is the time, V_o the total bed volume, ε the bed voidage, Q the volumetric flow rate, ρ_b the bulk density of the bed, and q_{\max} the operating capacity (in mass of solute per unit mass of the solid when the fluid-phase concentration is in mass of solute per unit volume of the fluid). The operating capacity is the solid-phase concentration at equilibrium with the initial fluid-phase concentration for adsorption systems and the MEL for ion-exchange systems. In general, the operating capacity is experimentally more accurately determined under dynamic conditions, i.e. in a fixed-bed system. Subscript “f” refers to the fluid, “s” to the solid, and “p” to the pore fluid-phase resistance.

The following equations constitute the approximate solutions of the fixed-bed model under the constant pattern and plug-flow assumption for the favorable Langmuir isotherm and linear driving forces (Perry and Green, 1999):

$$N_f(T-1) = \frac{\ln(X) - La \ln(1-X)}{1-La} + 1 \quad (4.140)$$

$$N_s(T-1) = \frac{1}{\Psi_s} \left[\frac{La \ln(X) - \ln(1-X)}{1-La} - 1 \right] \quad (4.141)$$

where

$$\Psi_s = \frac{0.894}{1 - 0.106La^{0.5}} \quad (4.142)$$

Eq. (4.140) is for liquid-film diffusion control and eq. (4.141) for solid diffusion control. The following equation is a solution of the fixed-bed model under the constant pattern and plug-flow assumption, for fluid-film diffusion control and the favorable Freundlich isotherm (Fleck *et al.*, 1973):

$$N_f(T-1) = 1 + \ln(X) - \frac{Fr}{1-Fr} \ln \left(1 - X^{\frac{1-Fr}{Fr}} \right) + \omega \quad (4.143)$$

$$\omega = \frac{Fr}{Fr-1} \sum_{k=1}^{\infty} \frac{Fr}{k [k(1-Fr) + Fr]} \quad (4.144)$$

In Figure 4.23, the model results for solid diffusion control (eq. (4.141)) and two different values of the Langmuir constant (La) are presented. In Figure 4.24, the model results for solid diffusion and liquid-film diffusion control (eq. (4.140)) for $La = 0.5$ are presented.

From Figure 4.23, it is clear that the more favorable the isotherm (lower value of La), the steeper the breakthrough curve, and thus, the better the performance of the operation.

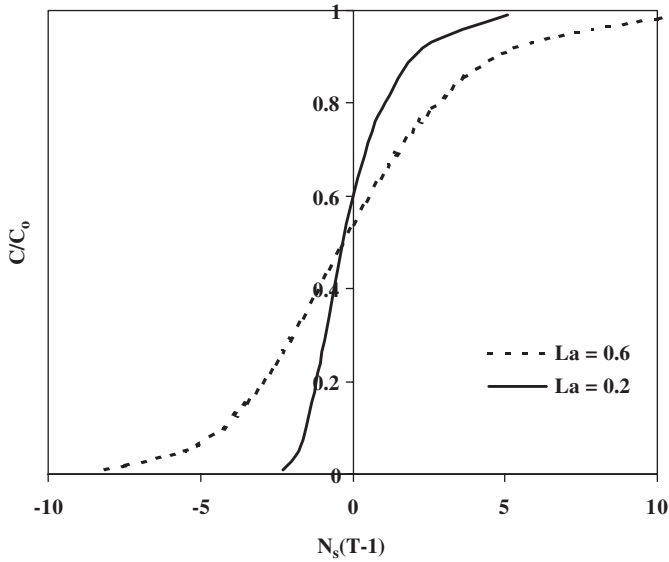


Figure 4.23 Solid diffusion control model for $La = 0.2$ and 0.6 .

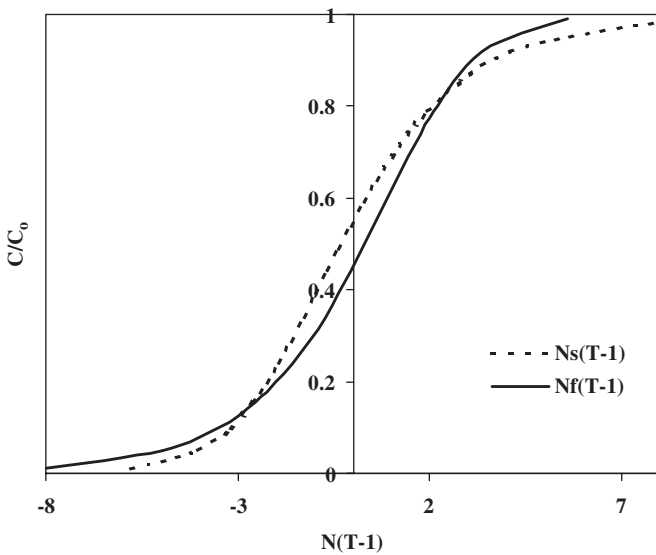


Figure 4.24 Solid and film diffusion control models for $La = 0.5$.

From Figure 4.24, it is clear that in the case of liquid-film control, the curve has a tail in the beginning, while in the case of solid diffusion control, the tail is at the end.

Finally, two models based on nonlinear driving forces will be presented. The first one covers the case of a pore diffusion control and the second one the case of solid diffusion control. Both models hold for the Langmuir-type isotherm. For the case of

pore diffusion control, the model equations are the following (Vermeulen and Quilici, 1970):

$$N_p(T-1) = \frac{1}{\psi_{\text{pore}}} \left(-2\sqrt{1-(1-La)X} - \frac{La}{1-La} \ln \rho_1 + \frac{\sqrt{La}}{1-La} \ln \rho_2 \right) + I_c \quad (4.145)$$

$$\rho_1 = \frac{1 + \sqrt{1-(1-La)X}}{1 - \sqrt{1-(1-La)X}} \quad (4.146)$$

$$\rho_2 = \frac{\sqrt{1-(1-La)X} + \sqrt{La}}{\sqrt{1-(1-La)X} - \sqrt{La}} \quad (4.147)$$

$$I_c = 2.44 - 2.15La \quad (4.148)$$

$$\psi_{\text{pore}} = \frac{1}{La^2 + 1.83(1-La)^{0.92}} \quad (4.149)$$

For solid diffusion control, the model equations are the following (Inglezakis, 2002b):

$$N_s(T-1) = \frac{1}{\psi_{\text{solid}}} \left[\frac{1}{1-La^2} (\lambda_1 + \lambda_2 + \lambda_3) \right] + I_c \quad (4.150)$$

$$\lambda_1 = \ln \left[\frac{1}{(1+La) - 2LaX - (1-La)X^2} \right] \quad (4.151)$$

$$\lambda_2 = La \ln \left(\frac{X + \frac{1+La}{1-La}}{1-X} \right) \quad (4.152)$$

$$\lambda_3 = 2La^2 \ln X \quad (4.153)$$

$$\psi_{\text{solid}} = \frac{1}{La^{1.5} + 1.688(1-La)} \quad (4.154)$$

$$I_c = -106.67La^5 + 177.82La^4 - 114.38La^3 + 31.604La^2 - 4.5323La - 0.8408 \quad (4.155)$$

Both models are good approximations, especially when we are interested in the first part of the breakthrough curve, which is of great importance in industrial applications.

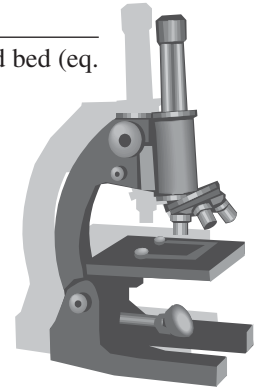
“Diffusion-type” models have been used for the adsorption of lead, copper, *p*-nitrophenol, phenol, *p*-bromophenol, *p*-toluene sulfonate and dodecyl benzene sulfonate on activated carbon (Hashimoto *et al.*, 1977; Xiu and Li, 2000; Chen and Wang, 2004; Crittenden and Weber, 1978), and ion exchange of ammonia, lead, and other heavy metals on clinoptilolite (Inglezakis and Grigoropoulou, 2003; Cincotti *et al.*, 2001; Semmens *et al.*, 1978; Cooney *et al.*, 1999).

A look into the “constant pattern” condition

Under the assumption of plug flow, the material balance in a fixed bed (eq. (4.128)) can be written as follows:

$$u_s \frac{\partial X}{\partial z} + \rho_b \frac{q_{\max}}{C_o} \frac{\partial Y}{\partial t} + \varepsilon \frac{\partial X}{\partial t} = 0 \quad (4.156)$$

In this equation, the partial derivatives with respect to time are positive, whereas the one with respect to length is negative. Furthermore, $X = C/C_o$ and $Y = q/q_{\max}$. From the above equation, we have



$$\frac{\partial z}{\partial t} = - \left(\frac{u_s}{\varepsilon + \frac{q_{\max} \rho_b}{C_o} \frac{\partial Y}{\partial X}} \right) \quad (4.157)$$

where

$$\frac{\partial z}{\partial t} < 0 \quad (4.158)$$

This partial derivative is the velocity of the concentration front in the bed. The constant pattern assumption presupposes that this velocity is constant, or in other words, is independent of the solution concentration. This means that all points on the breakthrough curve are “traveling” in the bed under the same velocity, and thus a constant shape of this curve is established (Wevers, 1959). According to the above equation, this could happen only if (Perry and Green, 1984)

$$\frac{\partial Y}{\partial X} = \text{const.} \Rightarrow Y = c_1 X + c_2 \Rightarrow Y = X \quad (4.159)$$

This relationship is the constant pattern condition. According to the literature, a criterion for the constant pattern assumption is the following (Perry and Green, 1999; Wevers, 1959):

$$\left(\frac{q_{\max}}{C_o}\right)\left(\frac{u_s}{Z}\right)^{-1}\left(\frac{\partial X}{\partial t}\right)_z \gg 1 \quad (4.160)$$

The first term is the ratio of maximum loading of solid for a specific inlet concentration to that concentration, whereas the second term is the space velocity (the reciprocal of the residence time), and the third term is the slope of the breakthrough curve. Thus, the constant pattern condition is achieved for

- dilute solutions
- materials of high capacity for the solute
- high residence time, i.e. low flow rate and deep beds
- favorable equilibrium.

Mass transfer-controlled systems—“diffusion” models and combined resistances

This model covers the case where we have combined resistances to diffusion (fluid-film and solid diffusion). In this case, the concentration in the main phase of the fluid (bulk concentration) is different from the one at the interface due to the effect of the fluid film resistance. The following equations can be used for Langmuir and Freundlich equilibrium equations (Miura and Hashimoto, 1977). The solutions of the fixed-bed model are the following:

Langmuir isotherm

$$\theta_\tau - X_\tau = \frac{1}{1+\zeta} \varphi_1 + \frac{\zeta}{1+\zeta} \frac{1}{\eta} \varphi_2 \quad (4.161)$$

$$\varphi_1 = \frac{1}{1-La} \ln X_i - \frac{La}{1-La} \ln(1-X_i) - \ln[La + (1-La)X_i] - \frac{La}{1-La} \ln La + 1 \quad (4.162)$$

$$\varphi_2 = \frac{La}{1-La} \ln X_i - \frac{1}{1-La} \ln(1-X_i) - 1 \quad (4.163)$$

$$\eta = 1 - 0.192(1-La)^3 \quad (4.164)$$

Freundlich isotherm

$$\theta_\tau - X_\tau = \frac{1}{1+\zeta} \omega_1 + \frac{\zeta}{1+\zeta} \frac{1}{\eta} \omega_2 + \frac{1}{1+\zeta} \frac{\zeta}{\zeta+\eta} \omega_3 \quad (4.165)$$

$$\omega_1 = \frac{Fr}{Fr-1} \ln(X_i^{Fr-1} - 1) + 1 + \frac{\eta}{\zeta+\eta} \frac{Fr^2}{Fr-1} I_A \quad (4.166)$$

$$\omega_2 = \frac{1}{Fr-1} \ln(1 - X_i^{1-Fr}) + \frac{\zeta}{\zeta + \eta} \frac{1}{Fr-1} I_B \quad (4.167)$$

$$\omega_3 = Fr - 1 + \frac{Fr}{Fr-1} (I_A + I_B) \quad (4.168)$$

$$\eta = 0.808 + 0.192Fr \quad (4.169)$$

$$I_A = \sum_{n=1}^{\infty} \frac{1}{n[n(1-Fr)] + Fr} \quad (4.170)$$

$$I_B = \sum_{n=1}^{\infty} \frac{1}{n[n(1-Fr)] + 1} \quad (4.171)$$

where

$$\theta_\tau = \frac{k_s a_u}{\rho_b(1+1/\zeta)} \left(t - \frac{\varepsilon Z}{u} \right) \quad (4.172)$$

$$X_\tau = \frac{k_s a_u \gamma}{1+1/\zeta} \frac{Z}{u} \quad (4.173)$$

$$k_s a_u = \frac{15D_s \rho_b}{r_o^2} \quad (4.174)$$

$$\gamma = \frac{q_{\max}}{C_o} \quad (4.175)$$

$$\zeta = \frac{k_f a_u}{k_s a_u \gamma} \quad (4.176)$$

$$a_u = \frac{3}{r_o} (1 - \varepsilon) \quad (4.177)$$

Here, q_{\max} is in mass of solute per unit mass of solid and C_o is in mass of solute per unit volume of fluid. For practical use, the infinite series I_A and I_B are shown in Figure 4.25.

The interface relative concentration X_i is related to the respective bulk relative concentration X as follows:

Langmuir

$$X = \frac{(\zeta La + \eta)X_i + \zeta(1-La)X_i^2}{(\zeta + \eta)[La + (1-La)X_i]} \quad (4.178)$$

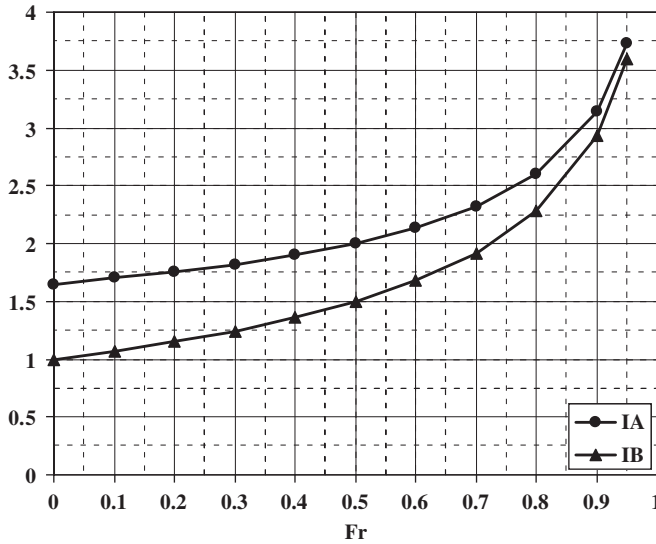


Figure 4.25 Values of I_A and I_B .

Freundlich

$$X = \frac{\zeta X_i + \eta X_i^{Fr}}{\zeta + \eta} \tag{4.179}$$

Model equations give only the relation of X_i versus $\theta_\tau - X_\tau$, and when the direct relationship between X and $\theta_\tau - X_\tau$ is required, it is desirable to represent X_i explicitly by X . For the Langmuir isotherm,

$$X_i = \frac{-b + \sqrt{b^2 - 4ac}}{2a} \tag{4.180}$$

where

$$a = \zeta(1 - La), b = (\zeta La + \eta) - (\zeta + \eta)(1 - LaX) \text{ and } c = -La(\zeta + \eta)X$$

Note that in the case of a solid diffusion control, X_i is replaced by X in the analytical solutions. The presented analytical solutions were developed primarily for solid diffusion control, also termed “surface diffusion kinetics.” However, the same equations can be used as approximations for pore diffusion as the controlling intraparticle diffusion step, if $k_s a_u$ is set equal to $15D_p(1 - \epsilon)/\gamma r_0^2$.

However, there is no explicit relationship for the Freundlich isotherm. In this case, for a desired value of X , several X_i values should be checked, and thus an extra calculation step is needed, i.e. an iteration procedure (Figure 4.26).

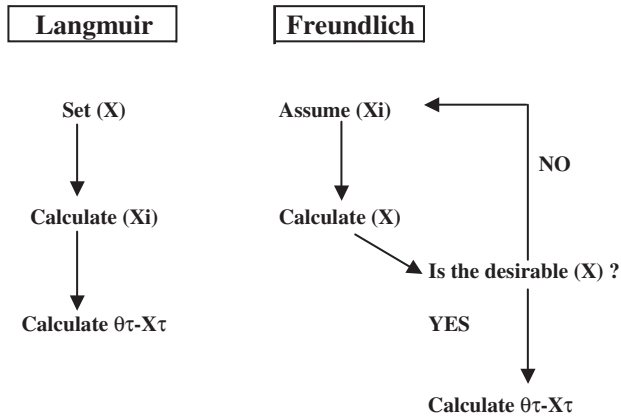


Figure 4.26 The use of Miura’s models.

The limiting cases of the analytical solutions for external fluid-film mass transfer controlling ($\zeta \rightarrow 0$) and solid diffusion controlling ($\zeta \rightarrow \infty$) are the following:

Langmuir

$$\zeta \rightarrow 0$$

$$\theta_\tau - C_\tau = \frac{1}{1-La} \ln X - \frac{La}{1-La} \ln(1-X) + 1 \tag{4.181}$$

and

$$\zeta \rightarrow \infty$$

$$\theta_\tau - X_\tau = \frac{1}{\eta} \left[\frac{La}{1-La} \ln X - \frac{1}{1-La} \ln(1-X) - 1 \right] \tag{4.182}$$

Freundlich

$$\zeta \rightarrow 0$$

$$\theta_\tau - X_\tau = 1 + \ln X - \frac{Fr}{1-Fr} \ln(1 - X^{(1-Fr)/Fr}) - \frac{Fr^2}{1-Fr} I_A \tag{4.183}$$

and

$$\zeta \rightarrow \infty$$

$$\theta_\tau - X_\tau = \frac{1}{\eta} \left[\frac{1}{Fr-1} \ln(1 - X^{1-Fr}) + \frac{1}{Fr-1} I_B \right] \tag{4.184}$$

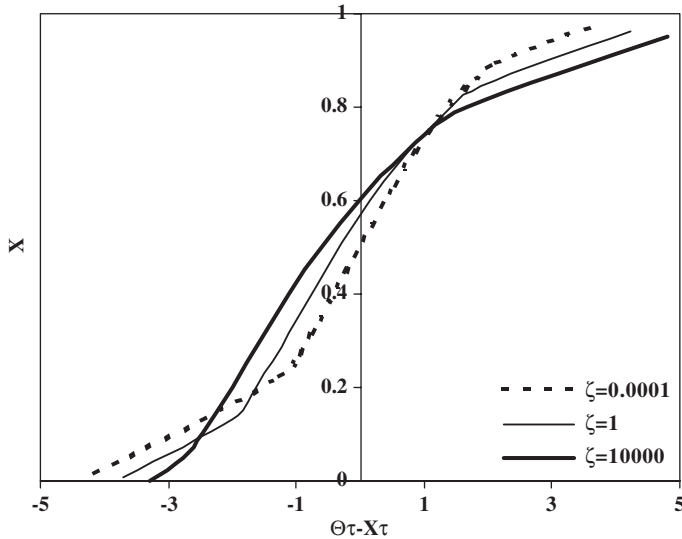


Figure 4.27 Examples of theoretical breakthrough curves calculated from the analytical solutions for the Freundlich isotherm ($Fr = 0.5$).

In Figure 4.27, some examples of theoretical breakthrough curves calculated from the analytical solutions for the Freundlich isotherm ($Fr = 0.5$) are presented. As is clear, the curve corresponds to the case of equal and combined solid and liquid-film diffusion resistances ($\zeta = 1$) which is between the two extremes, i.e. solid diffusion control ($\zeta = 10,000$) and liquid-film diffusion control ($\zeta = 0.0001$).

Example 5

Hashimoto *et al.* (1977) studied the removal of DBS from an aqueous solution in a carbon fixed-bed adsorber at 30 °C. The dimensions of the bed were $D = 20$ mm and $Z = 25.1$ cm. Carbon particles of 0.0322-cm radius were used, with 0.82 g/cm³ particle density, and 0.39 g/cm³ bulk density. The concentration of the influent stream was 99.2 mg/L and the superficial velocity was 0.0239 cm/s. The fixed bed was operated under upflow condition. Furthermore, the isotherm of the DBS–carbon system at 30 °C was found to be of Freundlich type with $Fr = 0.113$ and $K_F = 178$ (mg/g)(L/mg)^{0.113}. Finally, the average solid-phase diffusion coefficient was found to be 2.1×10^{-10} cm²/s. The approximate value of 10^{-9} m²/s could be used for DBS liquid-phase diffusion coefficient.

Using the Miura–Hashimoto model, calculate the time needed to reach a breakpoint concentration of 9.92 mg/L (10%). According to the experimental results given by Hashimoto *et al.*, the time needed for the specified breakpoint concentration is 226 hr. What is the result if the solid diffusion control approximation is used?

Solution

The dimensionless numbers needed for further calculations are

$$Re_p = \frac{d_p u_s}{\nu} = 0.154$$

$$Sc = \frac{\nu}{D_f} = 1002$$

The mass transfer coefficient in the liquid film can be calculated using the correlation of Williamson (eq. (3.346)):

$$Sh = 2.4\varepsilon^{0.66} Re_p^{0.34} Sc^{0.33} = 8.11$$

where

$$\rho_b = (1 - \varepsilon)\rho_p \Rightarrow \varepsilon = 0.524$$

and thus

$$Sh = \frac{k_f d_p}{D_f} \Rightarrow k_f = 0.00126 \text{ cm/s}$$

The solid-side mass transfer coefficient is (eq. (4.174))

$$k_s a_u = \frac{15 D_s \rho_b}{r_o^2} = 1.18 \times 10^{-6} \text{ g/s cm}^3$$

The equilibrium relationship is used for the determination of the maximum loading of the solid phase (eq. (4.14)):

$$q_o = 178 C_o^{0.113} = 229.24 \text{ mg/g}$$

Then, using eq. (4.175),

$$\gamma = \frac{q_{\max}}{C_o} = 3016.58 \text{ cm}^3/\text{g}$$

and thus, from eq. (4.176),

$$\zeta = \frac{k_t a_u}{k_s a_u \gamma} = 15.61$$

where (eq. (4.177))

$$a_u = \frac{3}{r_o} (1 - \varepsilon) = 44.31 \text{ cm}^{-1}$$

The parameter X_T is (eq. (4.173))

$$X_T = \frac{k_s a_u \gamma}{1 + 1/\zeta} \frac{Z}{u_s} = 3.528$$

For $Fr = 0.113$, $\eta = 0.8297$ (eq. (4.169)), $I_A = 1.7$ and $I_B = 1.08$ (Figure 4.25). Then, for $C/C_0 = X = 0.1$, and for eq. (4.165), we have $\theta_T - X_T = -1.217$ ($X_i = 0.066$). Finally, from eq. (4.172),

$$\theta_T = \frac{k_s a_u \gamma}{\rho_b \gamma (1 + 1/\zeta)} \left(t - \frac{\varepsilon Z}{u_s} \right) \Rightarrow t \approx 225 \text{ h}$$

This is only a difference of 0.45% from the experimental value. Constant pattern approximation does not negatively affect the final result. For solid diffusion control, $\zeta \rightarrow \infty$ and for this case, from eq. (4.184), $\theta_T - X_T = -1.277$ ($X_i = 0.1$) and $t \approx 227$ h or a difference of 0.25% from the experimental value.

It is interesting to check the Peclet number of the fixed bed. The Reynolds number is 0.154, and for this low value, the most appropriate correlation is that of Chung (eq. (3.314)). The resulting particle Peclet number is 0.39 and thus, the bed Peclet number is 151.98, which is fairly high, and we can assume that the plug-flow condition is assured.

A few comments on dibromostyrene: Known also as brominated styrene, it has been used as a flame retardant in the manufacture of thermoplastics. Although it does not seem to be toxic for the amounts present in the environment, it might have a teratogenic potential if large amounts of it are orally administered, as developmental studies in rats and rabbits have shown.

Example 6

Rivero *et al.* (2004) studied the removal of HCrO_4^- (Cr^{6+}) from polluted groundwater in a fixed bed at 24 °C. The dimensions of the bed were $D = 1.64$ cm and $Z = 13.25$ cm. An

anion exchange resin (Lewatit MP 64) of 0.59-mm particle diameter was used, with 0.654 g/cm³ bulk density. The influent stream contained 1.273 mmol/L of HCrO₄⁻ and the superficial velocity was 0.134 cm/s. Furthermore, the isotherm of the HCrO₄⁻-resin system at 24 °C was found to be of Freundlich type with $Fr = 0.194$ and $K_F = 1.815$ (mmol/g)(l/mmol)^{0.194}. Finally, the solid-phase diffusion coefficient was found to be 1.43×10^{-8} cm²/s. The approximate value of 1.19×10^{-9} m²/s could be used for the HCrO₄⁻ liquid-phase diffusion coefficient. Finally, assume the value of 0.41 for bed porosity.

Using the Miura–Hashimoto model, calculate the time needed to reach a breakpoint concentration of 0.636 mmol/L HCrO₄⁻ (50% of inlet concentration). According to the experimental results given by Rivero *et al.* (2004), the specified breakpoint concentration is reached after 1000 BV (bed volumes).

Solution

The Reynolds and Schmidt numbers are

$$Re_p = \frac{d_p u_s}{\nu} = 0.79$$

$$Sc = \frac{\nu}{D_f} = 842$$

Using the correlation of Williamson (eq. (3.346)),

$$Sh = 2.4\varepsilon^{0.66} Re_p^{0.34} Sc^{0.33} = 11.35$$

then

$$Sh = \frac{k_f d_p}{D_f} \Rightarrow k_f = 0.00229 \text{ cm/s}$$

The solid-side mass transfer coefficient is (eq. (4.174))

$$k_s a_u = \frac{15 D_s \rho_b}{r_o^2} = 0.000161 \text{ g/s cm}^3$$

where (eq. (4.177))

$$a_u = \frac{3}{r_o} (1 - \varepsilon) = 60 \text{ cm}^{-1}$$

Using the equilibrium relationship (eq. (4.14)):

$$q_o = 1.815C_o^{0.194} = 1.90 \text{ mmol/g}$$

Then, from eq. (4.175),

$$\gamma = \frac{q_{\max}}{C_o} = 1494 \text{ cm}^3/\text{g}$$

The mechanical parameter is (eq. (4.176))

$$\zeta = \frac{k_t a_u}{k_s a_u \gamma} = 0.571$$

And thus, from eq. (4.173),

$$X_T = \frac{k_s a_u \gamma}{1 + 1/\zeta} \frac{Z}{u_s} = 8.65$$

For $Fr = 0.194$, $\eta = 0.8452$ (eq. (4.169)), $I_A = 1.75$ and $I_B = 1.14$ (Figure 4.25). Then, for $C/C_o = X = 0.5$, and from eq. (4.165), we have $\theta_T - X_T = -0.0403$ ($X_i = 0.0179$). Then, from eq. (4.172),

$$\theta_T = \frac{k_s a_u}{\rho_b \gamma (1 + 1/\zeta)} \left(t - \frac{\varepsilon Z}{u_s} \right) \Rightarrow t \approx 26.71 \text{ h} \Rightarrow \text{BV} \approx 971.5$$

The Miura model predicts the experimental value found by Rivero *et al.* (2004) with a deviation of -2.85% .

A few comments on chromium (VI): As mentioned before, the contamination of water by heavy metals is a major environmental problem. Chromium is a metallic element with oxidation states ranging from chromium (–II) to chromium (+VI). In particular, there is great concern about Cr (+VI), as there is sufficient evidence for its carcinogenicity in humans. It rarely occurs naturally and its presence in the environment is anthropogenic, such as chromate production, chromate pigment production, and the chromium-plating industry. Specifically, the emissions of Cr^{6+} constituted 35% of the estimated 2.700–2.900 tn of chromium emitted into the atmosphere annually from anthropogenic sources in the United States (ATSDR, 2000). However, chromium is not dangerous only in this form. Irritation to the nose, nosebleeds, and ulcers and holes in the nasal septum may appear if high levels of chromium (VI) are inhaled. Moreover, the ingestion of large amounts of chromium (VI) may lead to stomach upsets and ulcers, convulsions, kidney and liver damage, cancer, and in the worst case, even death (ATSDR, 2000).

The Reynolds number is 0.78, and the resin particles can be assumed to be spherical. Then the most appropriate correlation is that of Chung (eq. (3.314)). The resulting particle Peclet number is 0.51, and thus, the bed Peclet number is 114.93, which is fairly high, and plug flow condition can be considered to take place.

Example 7

Murillo *et al.* (2004) studied the adsorption of phenanthrene (polycyclic aromatic hydrocarbon –PAH) from helium as carrier gas on a coke fixed-bed adsorber, at 150 °C. The isotherm of the phenanthrene–coke system at 150 °C was found to be of Freundlich type with $Fr = 0.161$ and $K_F = 1.9 \text{ (mol/kg)(m}^3\text{/mol)}^{0.161}$. The isotherm has been derived for phenanthrene concentrations between 1.71×10^{-4} and $1.35 \times 10^{-2} \text{ mol/m}^3$. Finally, the average solid-phase diffusion coefficient, calculated from several experimental runs, was found to be $6.77 \times 10^{-8} \text{ cm}^2\text{/s}$.

Suppose that coke is available with particle density of 1 g/cm^3 and particle size of 1 mm. The bed diameter is 0.2m, its height is 1 m, and the bed porosity is 0.5. The gas stream to be treated is helium containing $4.74 \times 10^{-3} \text{ mol/m}^3$ phenanthrene.

Using the Miura–Hashimoto models, calculate the time needed to reach a breakpoint of 10% of the inlet concentration under a flow rate of $31,400 \text{ cm}^3\text{/s}$.

Solution

The Reynolds and Schmidt numbers are

$$Re_p = \frac{d_p u_s}{\nu} = 4.56$$

$$Sc = \frac{\nu}{D_f} = 9.42$$

Then, using the correlation of Wakao for gases (eq. (3.351)):

$$Sh = 2 + 1.1Sc^{0.33} Re_p^{0.6} = 7.73$$

then

$$Sh = \frac{k_f d_p}{D_f} \Rightarrow k_f = 18.01 \text{ cm/s}$$

The solid side mass transfer coefficient is

$$k_s a_u = \frac{15D_s \rho_b}{r_o^2} = 0.000203 \text{ g/s cm}^3$$

where

$$a_u = \frac{3}{r_o} (1 - \varepsilon) = 30 \text{ cm}^{-1}$$

Using the equilibrium relationship:

$$q_o = 1.9C_o^{0.161} = 0.802 \text{ mol/kg}$$

then

$$\gamma = \frac{q_{\max}}{C_o} = 1.69 \times 10^5 \text{ cm}^3/\text{g}$$

The mechanical parameter is

$$\zeta = \frac{k_f a_u}{k_s a_u \gamma} = 15.73$$

And thus:

$$X_T = \frac{k_s a_u \gamma}{1 + 1/\zeta} \frac{Z}{u_s} = 32.29$$

For $Fr = 0.161$, $\eta = 0.839$, $I_A = 1.73$, and $I_B = 1.12$. Then, for $C/C_o = X = 0.1$, $\theta_T - X_T = -1.309$ ($X_i = 0.0697$). Then,

$$\theta_T = \frac{k_s a_u}{\rho_b \gamma (1 + 1/\zeta)} \left(t - \frac{\varepsilon Z}{u_s} \right) \Rightarrow t \approx 22.53 \text{ h}$$

A few comments on polycyclic aromatic hydrocarbons: A large number of polycyclic aromatic hydrocarbons (PAHs) are formed mainly during the incomplete combustion of coal, oil and gas, garbage, or other organic substances. In air, they can condense on dust particles, making them very dangerous to human health. Their presence in the aquatic environment should be attributed to the discharges from industrial and wastewater treatment plants. In water, PAHs also tend to attach to solid particles and gradually settle to the bottoms of lakes or rivers. In soil, they remain for a period of weeks to months until they are broken down by the action of microorganisms. During that period, they may move through soil to contaminate underground water (ATSDR, 1995).

The Reynolds number is 4.56 and using the Edwards–Richardson correlation (eq. (3.317)) the particle Peclet number is found equal to 2.18 and thus, the bed Peclet number is 2179, which is fairly high and the plug-flow condition is assured.

Surface reaction models—Thomas—BDST model The Thomas model is also referred to as the bed-depth-service-time (BDST) model (Low *et al.*, 1999; Lehmann *et al.*, 2001; Zulfadhly *et al.*, 2001; Walker and Wetherley, 1997; Ko *et al.*, 2000). The BDST approach is based on the irreversible isotherm model by Bohart and Adams (Ko *et al.*, 2000). However, in practice, the model is used for any equilibrium type. Furthermore, this simplified-design model ignores both the intraparticle (solid) mass transfer resistance and the external (fluid-film) resistance so that the adsorbate is adsorbed onto the solid surface directly. This means that the rate of adsorption is controlled by the surface reaction between the adsorbate and the unused capacity of the adsorbent (Zulfadhly *et al.*, 2001). This model is essentially a constant pattern model (Ko *et al.*, 2000). The expression by Thomas for an adsorption column is given as follows (Kapoor and Viraraghavan, 1998; Rao and Viraraghavan, 2002):

$$\frac{C_e}{C_o} \cong \frac{1}{1 + \exp \left[\frac{\Theta}{Q} (q_{\max} M - C_o V_{\text{tot}}) \right]} \quad (4.185)$$

where:

- C_e, C_o = the effluent and inlet solute concentrations
- q_{\max} = the maximum adsorption capacity
- M = the total mass of the adsorbent
- Q = the volumetric flow rate
- V_{tot} = the throughput volume
- Θ = the Thomas rate constant, volume/mass time.

The Thomas model is also applicable to the design of ion-exchange columns (Kapoor and Viraraghavan, 1998). The Thomas equation constants q_{\max} and Θ values can be obtained from the column data and can be used in the design of a full-scale adsorption bed. This equation is simple since it can be used in its linear form:

$$\ln \left(\frac{C_o}{C_e} - 1 \right) = \frac{\Theta q_{\max} M}{Q} - \frac{\Theta C_o}{Q} V_{\text{tot}} \quad (4.186)$$

Essentially, the above model is empirical as in real systems, both solid and fluid-film resistances play an important role in the adsorption process. An improved BDST model is found elsewhere (Ko *et al.*, 2000, 2002). Finally, q_{\max} and Θ could be flow rate–dependent parameters (Walker and Weatherley, 1997).

The Thomas model has been used for the sorption of heavy metals using fungal biomass, bone char, chitin, and goethite (Kapoor and Viraraghavan, 1998; Lehmann *et al.*,

2001; Zulfadhly *et al.*, 2001; Ko *et al.*, 2000, 2002; Sag and Actay, 2001), dyes adsorption using metal hydroxide and activated carbon (Netpradit *et al.*, 2004; Walker and Weatherley, 1997; Ko *et al.*, 2002), and phenol biosorption using biomass (Rao and Viraraghavan, 2002).

Wheeler–Jonas model for VOCs adsorption The Wheeler–Jonas equation is used for adsorption of VOCs using carbons. This equation is of the same form of the Thomas model with some modifications:

$$t_{br} = \frac{q_e M}{C_o Q} - \frac{q_e \rho_b}{k_v C_o} \ln \left(\frac{C_o - C_{br}}{C_{br}} \right) \quad (4.187)$$

where:

t_{br} = the time to reach the breakthrough concentration (C_{br})

k_v = the overall adsorption rate coefficient, time^{-1}

q_e = the equilibrium adsorption capacity of the carbon for a given vapor.

The Dubinin–Raduskevish isotherm (DR) can be used for the determination of q_{eq} .

The overall adsorption rate coefficient can be estimated using the following equations. Jonas and Rehrmann (1974) proposed a model derived for 1% breakthrough fraction:

$$k_v = 111.6 u_s^{0.5} d_p^{-1.5} \quad (4.188)$$

where u_s is the superficial velocity in cm/s and d_p is the particle diameter in cm.

Lodewyckx and Vansant (2000) proposed a model derived for 0.1% breakthrough fraction:

$$k_v = \frac{48 \beta^{0.33} u_s^{0.75}}{d_p^{1.5}} \quad (4.189)$$

Wood and Stampfer (1993) proposed the following correlation:

$$k_v = \left\{ \left(\frac{1}{u_s} + 0.027 \right) \left[0.000825 + \frac{0.063 - 0.0058 \ln \left(\frac{C_o - C_{br}}{C_{br}} \right)}{P_e} \right] \right\}^{-1} \quad (4.190)$$

where the superficial velocity is in cm/s, concentration in ppm, and P_e is the molar polarization of the adsorbate in cm^3/mol .

“Diffusion-type” models are two-parameter models, involving k_f or D_s and La , while BDST models are one-parameter models, involving only Θ , as q_{\max} is an experimentally derived parameter. The determination of La requires the whole experimental equilibrium curve, and in case of sigmoidal or other non-Langmuir or Freundlich-type isotherms, these models are unusable. From this point of view, BDST models are more easily applied in adsorption operations, at least as a first approximation.

Example 8

Cheng *et al.* (2004) studied the adsorption of toluene (VOC) in a fixed bed of activated carbon fibers at 298 °C and 1 atm. The inlet concentration of toluene was 17.36 mg/m³ and the carrier gas was air. Toluene obeys the Dubinin–Raduskevich isotherm with $k = 1.101 \times 10^{-9}$ mol²/J² and $q_o = 57.73$ kg/m³. The following data are given.

Toluene: affinity coefficient $\beta = 1$ (approximate value), molar polarizability $P_e = 3.11 \times 10^4$ cm³/mol, density = 0.8669 kg/m³, $MB = 92.14$ g/mol and saturated vapor pressure at the given temperature = 0.375×10^4 Pa.

Carbon fibers: particle radius $r = 13 \times 10^{-3}$ mm, particle density $\rho_p = 87$ kg/m³.

Bed: diameter $D = 6$ mm, height $H = 8$ mm, mass of solid phase = 15 mg and interstitial velocity $u = 17$ m/s.

According to the experimental data, the first appearance of toluene in the exit stream is at about 50 min, while after 100 min the exit concentration is 10% of the inlet one. Calculate the time needed for the same breakpoint concentration using the Wheeler–Jonas equation and Wood and Stampfer equation for the evaluation of k_v .

Moreover, examine the Wheeler–Jonas equation for the specified experimental conditions. On the basis of the results, predict the breakpoint time for lower interstitial velocities down to 1 m/s.

Solution

In the absence of more experimental data and for the purposes of the present example, we assume that the first appearance of toluene just after 50 min corresponds to an exit concentration of 0.01%, which is practically close to zero. This value will be used as the breakpoint concentration in the following calculations.

The Dubinin–Radushkevich isotherm is (eq. (4.19))

$$q_e = q_o \exp \left[-k \left(\frac{A}{\beta} \right)^2 \right]$$

where from eq. (4.18),

$$A = RT \ln \left(\frac{P_s}{P} \right)$$

These equations are applied for the determination of the equilibrium solid loading q_e for the specified inlet concentration. To do this, the partial pressure of toluene at inlet conditions is needed. This pressure is calculated by using the ideal gas law:

$$P = CRT = 0.46 \text{ Pa}$$

Then, $A = 2.23 \times 10^4$ and $q_e = 33.4 \text{ kg/m}^3$. In the Wood and Stampfer correlation (4.190), the bed voidage is needed in order to calculate the gas superficial velocity. Given the dimensions of the fixed bed, its volume is 0.226 m^3 and thus, the bulk density is

$$\rho_b = \frac{M}{V_{\text{bed}}} = 66.35 \text{ kg/m}^3$$

And thus,

$$\varepsilon = 1 - \frac{\rho_b}{\rho_p} = 0.24$$

Then, the superficial gas velocity is 403.54 cm/s and the kinetic coefficient k_v is $4.1 \times 10^4 \text{ l/s}$. Finally, using the Wheeler–Jonas equation (4.187) for $Q = 1.14 \times 10^{-4} \text{ m}^3/\text{s}$, the breakpoint time is found to be approximately equal to 43 min , which is close to the experimental value (50 min).

From Table I-15 of Appendix I, we find that the diffusion coefficient of toluene in air is $8.7 \times 10^{-6} \text{ m}^2/\text{s}$. Then, using the properties of air at $25 \text{ }^\circ\text{C}$ (Table I-6, Appendix I), we find that $Sc = 1.74$ and $Re_p = 6.92$, and using the Edwards–Richardson correlation (eq. (3.317)) the particle Peclet number is found to be 1.98 and thus, the bed Peclet number is 609.2 , which is fairly high, and plug-flow condition can be assumed.

In Figure 4.28, the model predictions are plotted for different breakpoint concentrations. Note that while the model works quite well for low C_{br} , 0.01% in our case, it fails to represent the data for higher values. For example, for $C_{br} = 1.7 \text{ mg/L}$ (10%), it predicts a breakpoint time of only 47.2 min instead of 100 min , which is the approximate experimental value. This is an expected result as normally, this kind of “breakpoint” models are designed to work at relatively low breakpoint concentrations. On the other hand, by setting the “first appearance” at lower values of exit concentration, the model gradually predicts a much lower “first appearance” time than the experimental one. Thus, it seems that a breakpoint or “first appearance” concentration in the vicinity of $0.01\text{--}1\%$ is adequate in order to have representative results (filled squares).

In Figure 4.29, the breakpoint concentration for $C_{br} = 1\%$ is presented for different values of the interstitial velocity.

It is evident that the relationship between the interstitial velocity and the breakpoint time is not linear, and thus, for values lower than about 5 m/s , the increase of the breaktime is sharp.

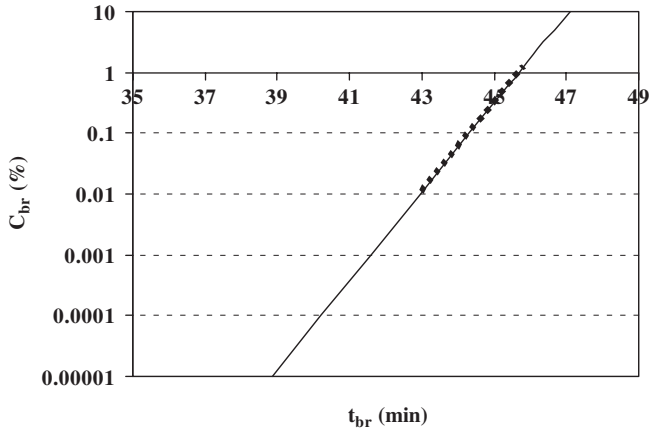


Figure 4.28 Model predictions (C_{br} versus t_{br}).

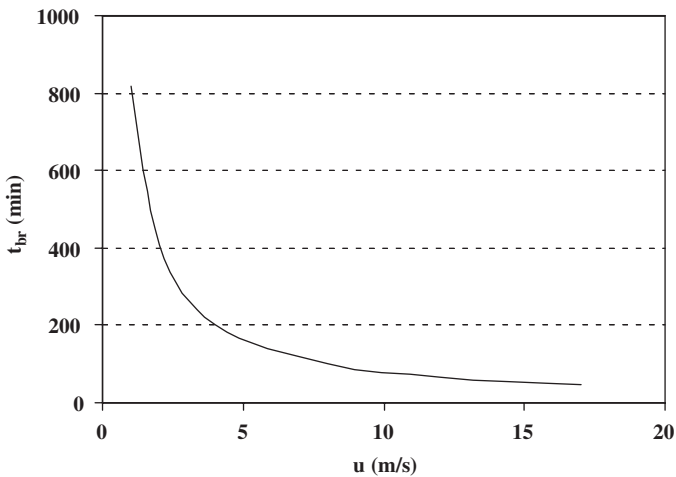


Figure 4.29 Breakpoint concentration for $C_{br} = 1\%$ for different values of interstitial velocity.

A few comments on toluene: Toluene ($C_6H_5CH_3$) is extensively used in gasoline to boost the octane number; it is also the raw material in the production of other chemicals such as benzene, benzyl chloride, phenol, cresols, vinyl toluene, and TNT. It also finds use in the production of paints, coatings, adhesives, etc.

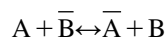
99% of the total toluene emissions are released into the atmosphere, primarily from gasoline evaporation and automobile exhaust. Industrial plants that use toluene as solvent constitute another great source of toluene (ATSDR, 1989). Due to its presence in cigarette smoke and in the releases from common household products, it is also a pollutant of indoor atmospheric environment. Being chemically and

biologically degradable in the environment, it is not expected to reach high concentrations over time in the environment (ATSDR, 1989).

Since toluene is principally released into the atmosphere, it is obvious that inhalation is the primary route of exposure to it for the general population, and for occupationally exposed individuals. CNS dysfunction and neurological impairment are the main adverse acute health effects of toluene in humans. At concentrations in the range 50–1500 ppm and for 3–8 h exposure, individuals may suffer drowsiness, impaired cognitive function, incoordination, and irritation of the eyes and throat. Increased concentrations may lead to more severe symptoms like nausea, staggering gait, confusion, extreme nervousness, and even insomnia lasting for several days (NTP, 1990). At concentrations in the range 10,000–30,000 ppm, toluene may cause narcosis and death (WHO, 1985).

Helfferich–Glueckauf model for ion exchange Although the models presented in the previous sections can be successfully applied in practice in ion-exchange systems, the Helfferich–Glueckauf approach will also be presented, which is developed especially for ion-exchange systems (Helfferich, 1962). The Helfferich–Glueckauf approach relies basically on Glueckauf’s approach. The concept of “effective plates,” originated from the theory of distillation and first applied to chromatography, is of primary importance in these models. Equilibrium theories also employ this concept and include the plate height as an empirical quantity. However, in the following approach, the plate height is calculated from fundamental data and is incorporated in a typical kinetic theory, i.e. an approach using kinetics and not only equilibrium relationships. The approach is applicable to the so-called self-harpening boundaries in columns, i.e. in the case of favorable equilibrium (Figure 4.31). Furthermore, the equations can be applied only at steady state conditions, i.e. when the boundaries attain a steady shape. In other words, here we have models that are based on the constant pattern condition.

Suppose that the solid phase is initially in say, form B and that the liquid phase ion is A. The ion exchange can be presented as (Helfferich, 1962)



The sharpness of a boundary between two counterions, A displacing B, depends on their separation factor (α_{A-B}) and on the operation conditions. At steady state conditions, the spread of the boundary is given by

$$z_A = \frac{H_p + H_o}{2} \left(\frac{1}{\alpha_{A-B} - 1} \ln \frac{1}{X_A} - \frac{\alpha_{A-B}}{\alpha_{A-B} - 1} \ln \frac{1}{1 - X_A} + 1 \right) + \frac{H_f + H_o}{2} \left(\frac{\alpha_{A-B}}{\alpha_{A-B} - 1} \ln \frac{1}{X_A} - \frac{1}{\alpha_{A-B} - 1} \ln \frac{1}{1 - X_A} - 1 \right) \quad (4.191)$$

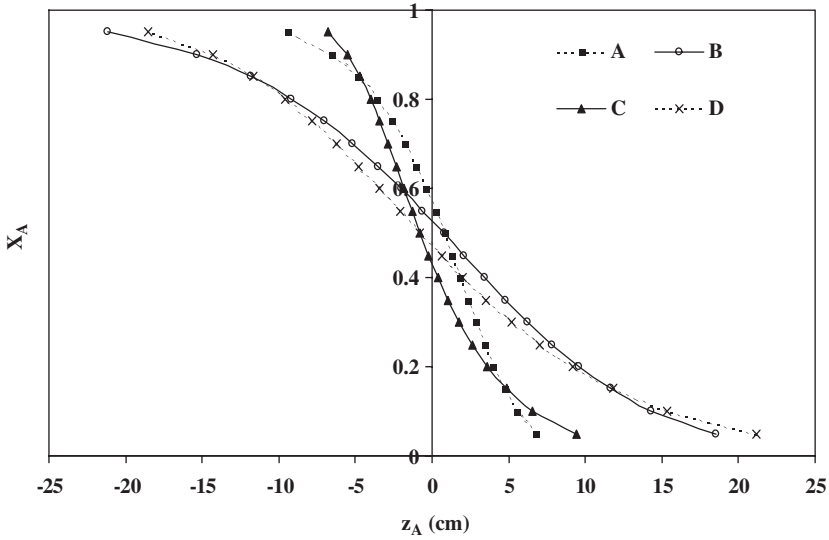


Figure 4.30 Shape of a self-sharpening boundary as calculated by Helfferich-Glueckauf model, for several combinations of diffusion resistances and separation factor. A: $\alpha_{A-B} = 10$, $H_p = 6$ cm, and $H_f = 1$ cm, B: $\alpha_{A-B} = 2$, $H_p = 6$ cm, and $H_f = 1$ cm, C: $\alpha_{A-B} = 10$, $H_p = 1$ cm, and $H_f = 6$ cm, D: $\alpha_{A-B} = 2$, $H_p = 1$ cm and $H_f = 6$ cm. For all cases, $H_o = 1$ cm.

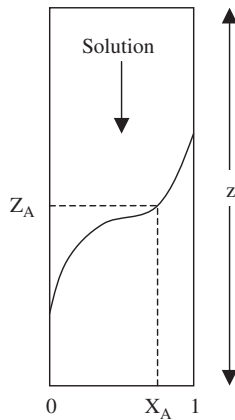


Figure 4.31 The self-sharpening boundary.

where z_A is the spread of the boundary in cm (see Figure 4.31) used for the rest of the parameters, and

$$H_o = 1.64r_o \tag{4.192}$$

$$H_p = \frac{\rho_b q_o / C_o}{(\rho_b q_o / C_o + \varepsilon)^2} \frac{0.142 r_o^2 u_s}{D_s} \quad (4.193)$$

$$H_f = \left(\frac{\rho_b q_o / C_o}{\rho_b q_o / C_o + \varepsilon} \right)^2 \frac{0.266 r_o^2 u_s}{D_f (1 + 70 r_o u_s)} \quad (4.194)$$

$$a_{A-B} = \frac{q_A C_B}{q_B C_A} = \frac{Y_A X_B}{Y_B X_A} \quad (4.195)$$

$$X_A = \frac{C_A}{C_o} \quad (4.196)$$

In the above equations, H_o , H_p , and H_f are the plate-height contributions due to the finite particle size, solid diffusion, and liquid-film diffusion, respectively. CGS units are used in these equations. Obviously, the bigger the height of the plate, the higher the resistance to the diffusion and the lower the uptake rate.

The shape of the boundary and that of the concentration profile (front), as it travels through the bed, are identical. We want a small width of boundary, i.e. the boundary to be close to $z_A = 0$. It is the case when the separation factor is high and the resistances to diffusion are weak (Figure 4.30).

For the derivation of the model, it is assumed that

- (a) the separation factor is constant (favorable Langmuir-type equilibrium isotherm),
- (b) the linear-driving-force rate laws for ion exchange are valid,
- (c) the spreads caused by solid and liquid film are additive, and
- (d) the flow in the fixed bed is ideal (plug flow)

In the original work of Helfferich, q_o is considered to be equal to the concentration of the fixed ionic groups in equivalents per unit volume of the ion exchanger, which in the course of the process will be completely used by the ion initially present in the solution phase A. However, in practice, this level is never achieved. Instead, the operating capacity, derived by employing experimental runs, can be used. Thus, q_o is the operating capacity, i.e. the maximum (A) uptake of the solid phase achieved in bed, expressed in mass (or equivalents) per unit mass of the solid phase. This value could be lower than the one measured in batch reactors and defined as the MEL and even lower than the REC. Furthermore, C_o is the initial concentration of B (normality) in the liquid phase, in equivalents per unit volume of liquid. This concentration, expressed in equivalents per unit volume of the liquid, is constant throughout the ion-exchanging process, as ion exchange is a stoichiometric process.

In the case of displacement of a single species, i.e. the exchange of a single ion from the liquid phase for a single ion in the solid phase, the effluent volume at which a given concentration X_A emerges from the column is

$$V_{\text{eff}} = A \left(\frac{\rho_b q_o}{C_o} + \varepsilon \right) [Z - z_A] \quad (4.197)$$

or in terms of time,

$$t(X_A) = \frac{A \left(\frac{\rho_b q_o}{C_o} + \varepsilon \right) [Z - z_A]}{Q} \quad (4.198)$$

where A is the cross-sectional area of the bed, Z is its height, and Q is the volumetric flow rate.

The presented model is very convenient when we want to calculate the breakthrough capacity, i.e. the solid loading obtained until breakpoint. We have (Helfferich, 1995)

$$\begin{aligned} ZAq_o &\cong ZAq_{br} + z_A Aq_o \\ q_{br} &\cong q_o - q_o \frac{z_A}{Z} \\ q_{br} &\cong q_o \left(1 - \frac{z_A}{Z} \right) \end{aligned} \quad (4.199)$$

where q_{br} is the breakthrough capacity in mass of solute per unit mass of the solid.

As the total mass of solute passed through the bed till breakpoint is $V_{br}C_o$, where V_{br} is the exit solution volume until breakpoint,

$$M_{out} = V_{br}C_o - q_{br}V_o\rho_b \quad (4.200)$$

where V_o is the bed volume and M_{out} is the mass of the solute that was not adsorbed by the bed solid and thus “escaped”, until breakpoint. That way, we can calculate the mean exit concentration:

$$C_{avr,br} = \frac{M_{out}}{V_{br}} \quad (4.201)$$

The mean exit concentration $C_{avr,br}$ is always lower than the breakpoint exit concentration.

Finally, the so-called degree of column utilization can be calculated:

$$\eta = \frac{q_{br}}{q} \quad (4.202)$$

Equilibrium-limited systems In the case of unfavorable equilibrium, the local equilibrium analysis can be applied. Essentially, assuming local equilibrium between the fluid and the solid phase, the mass transport step is neglected or is considered to have a minimal effect

on the system evolution when compared to that of unfavorable equilibrium. In this case, the equation of continuity reduces to (Perry and Green, 1999)

$$\frac{dY}{dX} = T \Leftrightarrow \frac{dF(X)}{dX} = T \quad (4.203)$$

where $Y = F(X)$ is the equilibrium relationship between Y and X . The limits of validity of this equation can be found by setting $X = 0$ (for T minimum) and $X = 1$ (for T maximum).

Using the local equilibrium analysis, the isotherm of a system can be found from breakthrough experiments using the following equation:

$$Y = \int_0^1 T dX \quad (4.204)$$

In the case of favorable equilibrium, the local equilibrium analysis predicts that at $T = 1$ the concentration X will rise instantly from 0 to 1 (ideal step change). This situation is ideal and does not correspond to real situations, as when a system exhibits favorable equilibrium, the mass transfer is always the controlling step.

In the special case of ion exchange and unfavorable equilibrium, i.e. $\alpha_{A-B} < 1$, with A originally in the solution, under the condition of sufficiently long bed, Walter's solution could be used. Walter's equation is a special case of the Thomas model for arbitrary isotherm and the kinetic law equivalent to a reversible second-order chemical reaction (Helfferich, 1962):

$$X = \frac{\bar{R} - \sqrt{\bar{R}/T}}{\bar{R} - 1} \quad (4.205)$$

for $T/\bar{R} \leq \bar{R}$. The dimensionless effluent concentration X is zero for $T < 1/\bar{R}$ and equal to 1 for $T \geq \bar{R}$. In this equation, \bar{R} is the average value of the reciprocal separation factor $1/\alpha_{A-B}$. For a Langmuir isotherm, α_{A-B} and La are related:

$$\alpha_{A-B} = \frac{1}{La} \quad (4.206)$$

In this case, $\bar{R} = 1/La$. Finally, T is the throughput ratio defined in eq. (4.136).

Experimental methods for the determination of the controlling mechanism in a fixed-bed operation

For the determination of the controlling mechanism, in the case of mass transfer-controlled systems, the following method can be used (Inglezakis, 2002b). This approximate method requires only the experimental bed data, and specifically, the set of exit concentrations and

the corresponding elapsed times. Then the $(T - 1)$ versus C/C_0 curve is constructed, where C is the exit concentration, C_0 is the inlet concentration, and T is the dimensionless time modulus.

According to Perry and Green (1999), if the experimental data are plotted in $N(T - 1)$ versus C/C_0 graph, the C/C_0 at which $N(T - 1)$ and thus $T - 1$ equals zero is called the “stoichiometric point,” and is independent of the volumetric flow rate. This is the point where the amount of solute that has “leaked” past the reference point in the bed exactly equals the residual unfilled capacity of the solid contained before that point. The characteristic C/C_0 versus $N(T - 1)$ curves are shown in Figure 4.32.

This point is always lower than about $C/C_0 = 0.7$, regardless of the controlling mechanism (fluid film, pore, or solid diffusion or a combination of them), for both Langmuir and Freundlich isotherms, which are frequently used in adsorption and ion-exchange systems (Perry and Green; Hall *et al.*, 1966; Fleck *et al.*, 1973). Furthermore, the values of $(C/C_0)_{\text{stoich}}$ (corresponding to the stoichiometric point) for solid diffusion control are between 0.51 and 0.70 and the more favorable equilibrium leads to higher values of $(C/C_0)_{\text{stoich}}$. The opposite holds for fluid-film control where the corresponding $(C/C_0)_{\text{stoich}}$ values are between 0.31 and 0.5. The above method for the determination of the controlling step is of course approximate and qualitative, and can be used only if the model cannot be applied due to experimental or other problems.

Using the approximate “diffusion” models (eqs. (4.140) and (4.141)), the X_{stoich} versus La is shown in Figure 4.33.

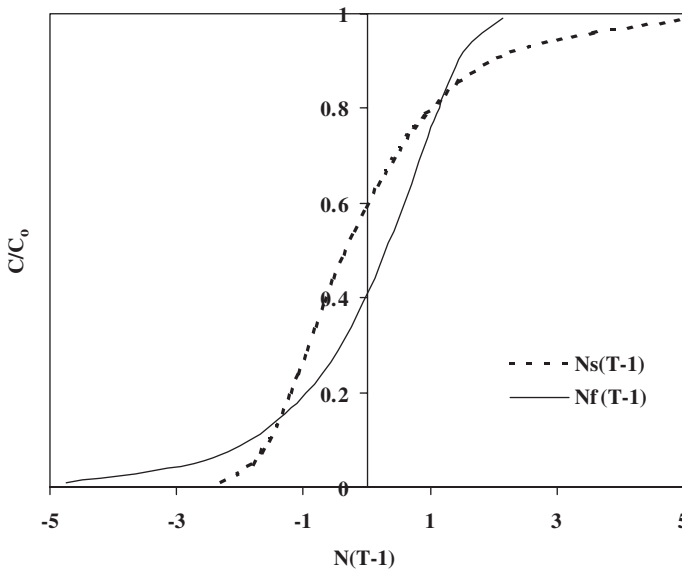


Figure 4.32 Characteristic C/C_0 versus $N(T - 1)$ curves for solid diffusion control (dotted line) and fluid-film diffusion control ($L_a = 0.2$).

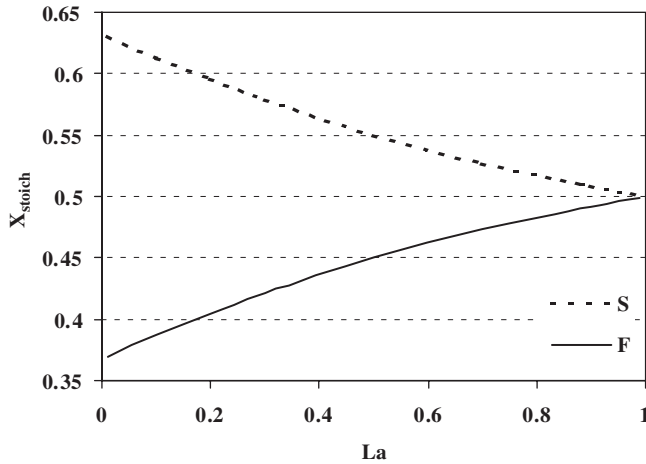


Figure 4.33 Stoichiometric point curves (S: solid diffusion control, F: fluid-film diffusion control).

For the estimation of the controlling mechanism, Miura and Hashimoto defined the mechanical parameter ζ as (Miura and Hashimoto, 1977)

$$\zeta = \frac{k_f a_u}{K(q_{\max}/C_o)} \quad (4.207)$$

$$K = \frac{15D_s \rho_b}{r_o^2} \quad (4.208)$$

$$a_u = \frac{6(1-\varepsilon)}{d_p} \quad (4.209)$$

According to their analysis, if ζ is zero (practically much lower than 1), then the fluid-film diffusion controls the process rate, while if ζ is infinite (practically much higher than 1), then the solid diffusion controls the process rate. Essentially, the mechanical parameter represents the ratio of the diffusion resistances (solid and fluid-film). This equation can be used irrespective of the constant pattern assumption and only if safe data exist for the solid diffusion and the fluid mass transfer coefficients. In multicomponent solutions, the use of models is extremely difficult as numerous data are required, one of them being the equilibrium isotherms, which is a time-consuming experimental work. The mathematical complexity and/or the need to know multiparameters from separate experiments in all the “diffusion” models makes them rather inconvenient for practical use (Juang *et al.*, 2003).

If modeling or other approximate methods are not applicable, then a number of experiments should be conducted in order to examine the effect of superficial velocity on the performance of the bed, and more specifically on the breakpoint volume. Keeping the same contact time and particle size, one can study the effect of linear velocity by changing just the length of the bed accordingly, and in this way examining the controlling step. For solid

diffusion control there is no effect of the linear velocity on the kinetics in the bed, while for film-diffusion control the kinetics will be affected. In fact, this is a scale-up procedure. From these experiments, a lower limit of the linear velocity can be found, above which the controlling mechanism is the solid diffusion control. Then, for higher linear velocities, which are expected in large-scale units, it is guaranteed that the controlling step is unaltered.

Derivation of basic experimental data

Experimentally, it is valuable to determine the following: the maximum adsorption capacity of the solid (q_{\max}), the diffusion coefficients of the solutes in the solid phase (D_s), and the equilibrium isotherm. Theoretically, the equilibrium isotherm, the maximum adsorption capacity, and the solid diffusion coefficient for a specific ion-exchange or adsorption system are independent of the experimental method used for their determination and independent of flow conditions (Helfferich, 1962; Lieu and Weber, 1981; Chen and Wang, 2004; Fernandez *et al.*, 1996). However, experimental results obtained in ion-exchange and adsorption systems showed that the maximum adsorption capacity measured in a fixed bed is different from that measured in a batch system, and it might be flow-rate dependent (Inglezakis *et al.*, 2002; Inglezakis and Grigoropoulou, 2003; Hlavay *et al.*, 1982; McKay and Bino, 1985; McLaren and Farquhar, 1973; Netpradit *et al.*, 2004; Ko *et al.*, 2003; Sen *et al.*, 2002). Furthermore, as shown in the cases of adsorption on activated carbon and the removal of Cr (III) using zeolite NaX, the equilibrium isotherm is influenced by the type of the reactor used for its measurement (fixed-bed and batch reactor) (Weber and Wang, 1987; Barros *et al.*, 2006). Finally, the diffusion coefficient may be different when measured in fixed beds or batch systems, and in some cases is found to be flow-dependent (Inglezakis and Grigoropoulou, 2003; Yoshida *et al.*, 1984; Weber and Smith, 1987; McKay and Bino, 1985; Ko *et al.*, 2003; Markovska *et al.*, 2001). All these observations seem to be a result of the limiting (low) contact time in fixed beds and of the different concentration gradients in fixed beds and batch reactors (Inglezakis and Grigoropoulou, 2003; Ko *et al.*, 2003). It must be recognized that batch reactors do not approximate the hydrodynamic and contaminant removal patterns of fixed-bed (column) reactors (Weber and Smith, 1987). Another reason responsible for such differences between batch and fixed-bed parameters is the lack of adequate mechanical strength of particles (compressed particles due to flow pressure) and the permeability of particles to fluid flow (Fernandez *et al.*, 1996). Obviously, this case is possible only when resins are used.

The maximum adsorption (or ion-exchange) and breakthrough capacity can be measured using the experimental breakthrough curve (C versus V_{eff}) by integration (Perry and Green, 1999; Helfferich, 1962):

$$q_o = \frac{\left(V_{\text{tot}} - \int_{V_f}^{V_{\text{tot}}} X(V_{\text{eff}}) dV_{\text{eff}} \right) C_o}{\rho_b V_o} \quad (4.210)$$

$$q_{\text{br}} = \frac{\left(V_{\text{br}} - \int_{V_f}^{V_{\text{br}}} X(V_{\text{eff}}) dV_{\text{eff}} \right) C_o}{\rho_b V_o} \quad (4.211)$$

where V_f is the effluent volume until the first appearance of the solute in the exit stream, V_{br} the effluent volume until breakpoint, and V_{tot} the effluent volume until the exit solute concentration is equal to its inlet concentration.

The dependence of q_o on residence time has been noticed and modeled elsewhere, in the case of zinc and acid dyes adsorption by bone char and activated carbon, respectively (Ko *et al.*, 2002). The following equations were successfully applied:

$$q_{o,bed} = q_{o,max} [1 - \exp(-\omega t_{res})] \quad (4.212)$$

$$q_{o,bed} = q_{o,max} [1 - \exp(-\omega t_{res}^{0.5})] \quad (4.213)$$

where $q_{o,bed}$ and $q_{o,max}$ are the bed maximum capacity and the real maximum capacity (measured in batch reactor systems), t_{res} the residence time, and Θ a system-specific constant. It is obvious that if the residence time is infinite, the bed maximum capacity is equal to the real maximum capacity, which is theoretically expected, as noted elsewhere (Inglezakis and Grigoropoulou, 2003). These equations have been also tested in Pb^{2+} adsorption by clinoptilolite (zeolite) and showed satisfactory results (Inglezakis, 2002b).

In conclusion, the maximum adsorption capacity should be measured in fixed-bed experiments under dynamic conditions, and if models are applicable, diffusion coefficients should be also determined in fixed-bed apparatus. Due to the fact that the equilibrium isotherms require extended data series and thus are time-consuming experiments, the latter are quite difficult to be conducted in fixed-bed reactors and from this point of view, it is more practical to evaluate equilibrium isotherms in batch reactor systems. Then, it is known that when applying fixed-bed models using an equilibrium isotherm obtained in batch-type experiments, the equilibrium discrepancy (if it exists) can be compensated by a different estimate for the solid diffusion coefficient (Inglezakis and Grigoropoulou, 2003; Weber and Wang, 1987).

Example 9

Wastewater containing 100 ppm Pb^{2+} and minor amounts of other ions has to be treated (20°C). The maximum allowable exit concentration is 10 ppm. The available adsorbent is a zeolite of particle size 2 mm ($\Phi_s = 0.8$), particle density 2 g/cm³, and bulk density 1 g/cm³. Suppose that solid diffusion is the controlling mechanism. Solid diffusion is measured and found to be about 10⁻⁹ cm²/s. Furthermore, the system obeys the favorable Langmuir isotherm with $La = 0.1$. The MEL is $q_{max} = 200$ mg/g. The available amount of the zeolite is 100 kg.

- Propose an optimum design for this operation by using an LDF model.
- Compare the LDF model with Helfferich's model for upflow operation and $Q_{rel} = 5$ BV/h.

Solution

Model analysis: The simple LDF model for solid diffusion control will be used, namely eq. (4.141). For the specified system with $La = 0.1$, the $N_s(T - 1)$ versus (C/C_0) is shown in Figure 4.34.

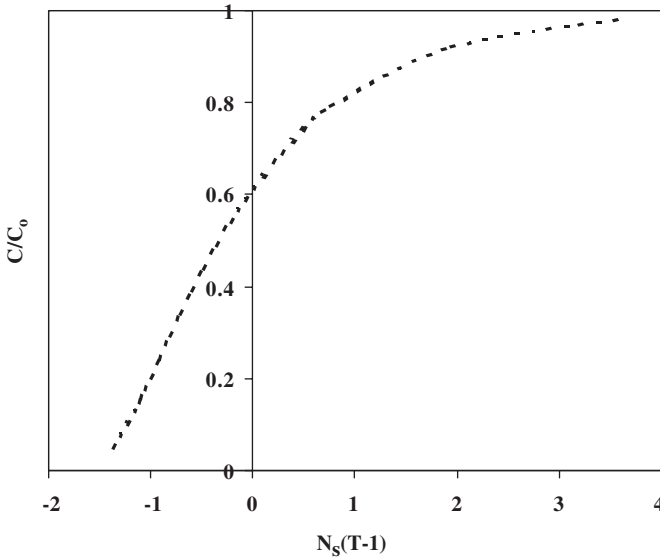


Figure 4.34 Model plot.

From the definition of T (eq. (4.136)), it is clear that since

$$t - \frac{V_0 \varepsilon}{Q} \geq 0$$

T should be positive. Using this constraint for T , it can be seen that

$$T \geq 0 \Rightarrow T - 1 \geq -1 \Rightarrow N(T - 1) \geq -N \Rightarrow N \geq -[N(T - 1)]_{\min}$$

This minimum value of $N(T - 1)$ corresponds to the lower value of X , i.e. 0. However, since the model solution, eq. (4.141), is asymptotic to the X - axis, the lower X to be used is 0.01. This dimensionless exit concentration can be viewed as the “first appearance” concentration. This restriction provides the maximum allowable relative flow rate or the minimum residence time in order to have the first appearance of the solute for $T \geq 0$. For $La = 0.1$, $[N(T - 1)]_{\min} = -1.2311$ (eq. (4.141)).

Geometrical dimensions of the fixed bed: The volume of the bed is

$$V_0 = \frac{M_s}{\rho_b} = 0.1 \text{ m}^3$$

Then

$$V_o = \frac{\pi D^2}{4} Z = \frac{\pi D^2}{4} \left(\frac{Z}{D}\right) D = \frac{\pi D^3}{4} \left(\frac{Z}{D}\right)$$

To avoid large-scale liquid maldistribution, the aspect ratio Z/D should be greater than 5 (see eq. (3.324)). If we choose the value of 10, then

$$D = \left[\frac{4V_o}{\pi} \left(\frac{D}{Z}\right) \right]^{1/3} = 0.234 \text{ m}$$

and thus $Z = 2.34 \text{ m}$. At the same time,

$$\frac{D}{d_p} = 117 > 30$$

$$\frac{Z}{d_p} = 1168 \gg 150$$

Thus, for the selected D and Z , large-scale maldistribution is prevented (see eq. (3.324)).

Relative flow rate limits: According to Ruthven (1984), a maximum linear velocity should not be exceeded in order to avoid extended friction between the packing material in both down- and upflow operations. This velocity is 0.8 times the minimum fluidization velocity for upflow operation and 1.8 times the same velocity for downflow operation (for further analysis see Chapter 6). Using eq. (3.451), the minimum fluidization velocity for the specific system is 2.36 cm/s. Thus, the maximum allowable velocities for down- and upflow operations are 4.24 and 1.89 cm/s, respectively. In terms of the relative flow rate, the corresponding values are 65.35 and 29.13 BV/h. These values are fairly high for ion-exchange systems and are rarely used in practical applications.

Apart from these “hydraulic” limits, one more limit comes from the model as analyzed before. We found that

$$N \geq -[N(T-1)]_{\min} \geq 1.2311$$

or, by using eq. (4.139),

$$\frac{15D_s \Delta V_o}{r_o^2 Q} \geq 1.2311$$

The relative volumetric flow rate is (eq. (3.103))

$$\frac{V_o}{Q} = \frac{1}{Q_{\text{rel}}}$$

we have

$$Q_{\text{rel}} \leq \frac{15D_s\Lambda}{1.2311r_0^2} \Rightarrow Q_{\text{rel}} \leq 6.66 \text{ BV/h}$$

As will be analyzed in the following section, a minimum relative flow rate arises for downflow operation.

Hydraulic analysis and controlling mechanism: For the determination of the mass transfer coefficient, and the case of wastewater treatment, the correlation proposed by Chern and Chien (eq. (3.345)) is used. As a criterion, the Biot number as defined by Hand *et al.* (eq. (4.105)) is used.

For the evaluation of the particle Peclet number and the liquid holdup, the correlations proposed by Inglezakis *et al.* are used, i.e. eqs. (3.313) and (3.332), respectively. The Biot number, liquid holdup, and bed Peclet number for downflow operation versus relative volumetric flow rate are presented in Figure 4.35.

It is obvious that for the whole flow-rate range, the rate-controlling mechanism is expected to be the solid diffusion control ($Bi > 41$). Furthermore, the flow can be characterized as ideal plug flow for flow rates above 2.15 BV/h, where Pe_L is higher than about 100. However, the liquid holdup is very low (56.83%) and this could be proved a serious problem, even with the use of a liquid distributor at the top of the bed. In order to have a satisfying liquid holdup, i.e. about 80%, the relative flow rate should be about 5.62 BV/h. Then, by means of a liquid distributor at the top of the bed, it is possible to achieve a holdup near 100%. Thus, for downflow operation the limits of the relative flow rate are (BV/h)

$$5.62 \leq Q_{\text{rel}} \leq 6.67$$

On the other hand, in upflow operation, Pe_L is higher than 140 for the whole relative flow-rate region up to the value of 6.66 BV/h. At the same time, the liquid holdup is always

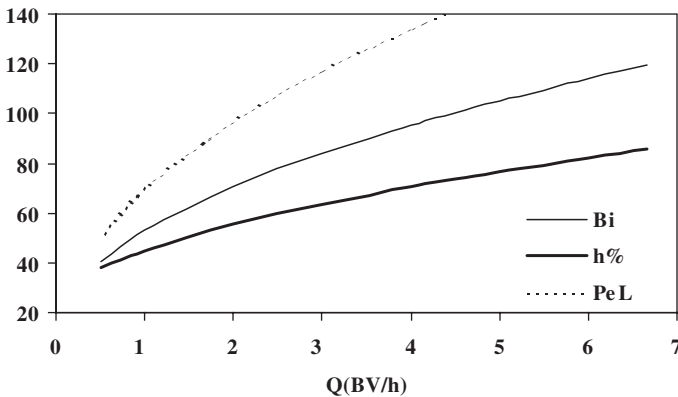


Figure 4.35 Biot number, liquid holdup, and bed Peclet number for downflow operation versus relative volumetric flow rate.

100% (in the absence of large-scale maldistribution). Thus, for upflow operation, there is only an upper limit for the relative flow rate (BV/h):

$$Q_{rel} \leq 6.67$$

Resulting performance: In Figure 4.36, the performance of the fixed bed is presented for flow rates up to 6.66 BV/h. The measure of the performance of the bed is the breakpoint time and the corresponding treated volume of the waste as calculated by utilizing the model equation (4.141).

The choice of the appropriate flow rate depends on the wastewater volume to be treated and on the desired service time, and as presented in a following section, on the degree of utilization of the fixed-bed material.

In upflow operation, a low flow rate could be used, for example, 0.5 BV/h and in this case, as much as 188 m³ of the wastewater could be treated in 157 days. On the other hand, if the bed is operated under the highest flow rate of 6.66 BV/h, the treated volume is 48 m³ and the service time 73 h. It should be noted that in downflow operation the volume that can be treated is between 48 and 72 m³, due to the limits on the relative flow rate, as analyzed in a previous section.

Comparison with Helfferich's model: The parameters of the model, for 5 BV/h relative flow rate, are the following: $H_o = 0.164$ cm, $H_f = 26.37$ cm, and $H_p = 230.19$ cm (eqs. (4.192)–(4.194)). The models are compared in Figure 4.37.

It is evident that the models are in very good agreement. However, in the region of the breakpoint they deviate. For $X = 0.1$, the LDF model results in 86.06 m³, while Helfferich's model in 70 m³, i.e. almost 23% difference. In Figure 4.38, the difference (%) of these two models versus the exit concentration is presented.

As can be seen, the difference is lower than 7% for C_{out} greater than about 20 ppm, i.e. $X > 0.20$. The differences at low X are due to the fact that Helfferich's approach

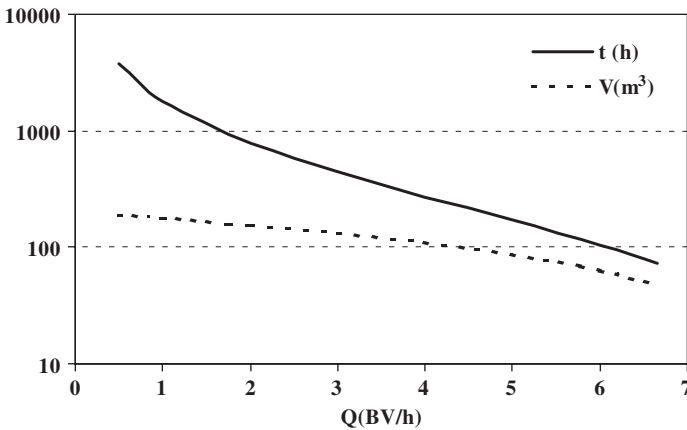


Figure 4.36 The performance of the fixed bed for flow rates up to 6.66 BV/h.

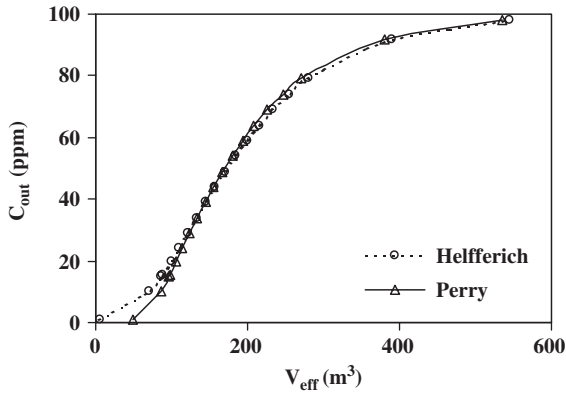


Figure 4.37 Comparison of LDF and Helfferich models for $Q_{rel} = 5$ BV/h.

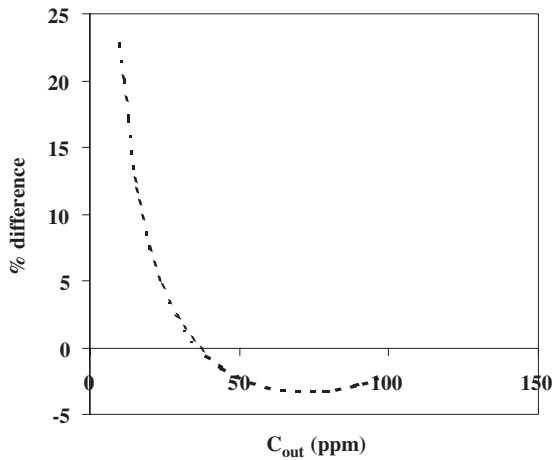


Figure 4.38 The difference (%) of LDF and Helfferich's model versus the exit concentration.

(eq. (4.191)) takes into account the resistance in the liquid film and thus the characteristic tail at the beginning of the breakthrough curve is apparent.

The utilization of the fixed bed: The value of z_A for $X = 0.1$ is 151.68 (eq. (4.191)). Then, by using eq. (4.199) and for $Q_{rel} = 5$ BV/h, the breakpoint loading of the solid phase is

$$q_{br} = q_o \left(1 - \frac{z_A}{Z} \right) = 70.11 \text{ mg/g}$$

while the degree of utilization of the bed is (eq. (4.202))

$$\eta = \frac{q_{br}}{q_o} = 0.351$$

or 35.1%. These relationships provide us with the ability to plot the utilization (%) versus Q_{rel} (BV/h) (Figure 4.39).

Low utilization means that at the breakpoint, i.e. when the operation of the bed is stopped, the portion of the solid material in the bed used during the service time is low, which is undesirable. Especially, if the material cannot be regenerated, low utilization means that the unused material is lost.

Finally, as has been noted, although the exit concentration is 10 ppm, the mean concentration of the collected waste is considerably lower. The total mass of the solute passed through the bed is $V_{br}C_o$, where V_{br} is the exit solution volume until the breakpoint. For operation under a relative flow rate of 5 BV/h (eq. (4.200)):

$$M_{out} = V_{br}C_o - q_{br}V_o\rho_b = 4598 \text{ mg}$$

Then, the mean exit concentration is (eq. (4.201))

$$C_{avr,br} = \frac{M_{out}}{V_{br}} \cong 0.03 \text{ ppm}$$

The mean exit concentration $C_{avr,br}$ is always much lower than the breakpoint exit concentration; in our example, it is almost 0.3% of the breakpoint concentration.

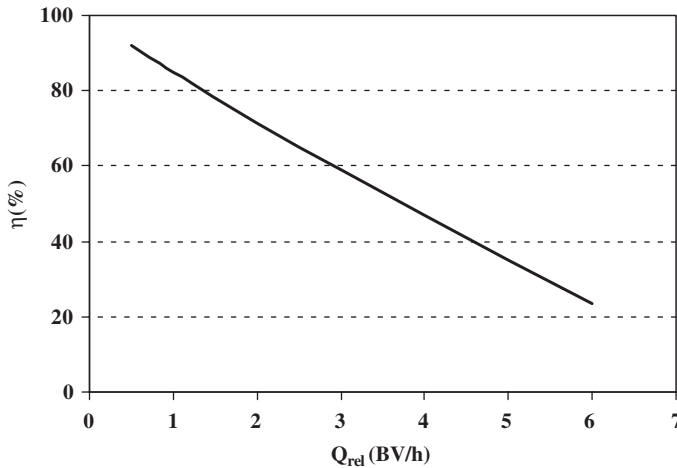


Figure 4.39 Utilization (%) versus Q_{rel} (BV/h).

4.3 MANAGEMENT OF SPENT MATERIALS

4.3.1 Activated carbon regeneration and reactivation

The adsorptive capacity of carbons is obviously finite. Consequently, it is gradually decreased and finally exhausted after the adsorption of the maximum possible amount of a substance. The exhausted carbon is then characterized as “spent” and has to be regenerated, reactivated, or properly disposed off. The regeneration of spent adsorbents is the most difficult and expensive part of adsorption technology. It accounts for about 75% of total operating and maintenance cost for a fixed-bed GAC operation.

Although the terms “regeneration” and “reactivation” are used interchangeably, “regeneration” means removing the contaminants from the carbon without destroying them while “reactivation” means destroying the contaminants and reactivating the carbon, which usually occurs at very high temperatures.

Regeneration involves the removal of the adsorbed contaminants from carbon by means of processes that destroy neither the contaminants nor the carbon. A common process is pressure swing adsorption, where low pressure is applied to remove the contaminants from the solid phase. Other common processes involve the use of steam (volatilization of adsorbed contaminants) or the use of a hot inert gas, such as nitrogen. The contaminants are recovered as liquid after a condensation step.

During the regeneration process, the contaminants are desorbed and a waste stream is produced. For instance, during steam regeneration a mixture of water and organics from the condensed desorbed vapor is produced. Thus, a regeneration process should be accompanied by a waste treatment apparatus.

In most cases, the spent carbon waste to be regenerated is treated using thermal destruction/scrubbing systems. Under these conditions, the organic contaminants are destroyed and the carbon is regenerated.

Spent carbon thermal reactivation involves the removal of the adsorbed contaminants from the spent activated carbon and their destruction at a high temperature (typically in excess of 800°C). Carbon losses during reactivation processes can be held at 3–15% (Zanitsch, 1997; Faust, 1987).

There are several cases where regeneration or reactivation of the spent carbon is either technically or economically not viable. In these cases, the common practice is the proper disposal of the spent carbon. Generally, we proceed to the disposal if

- the carbon is irreversibly contaminated by the adsorbed substance,
- the regeneration or reactivation process is too costly, mainly when dangerous substances like radioactive particles are the adsorbed species.

For example, if the carbon has been used for the removal of PCBs, dioxins, or heavy metals, and generally in the case of powdered activated carbons, the disposal of the spent material is the most appropriate method.

Starting with the presentation of the regeneration techniques, we could classify them into three categories (EPA, 1999):

- thermal swing regeneration
- vacuum regeneration
- pressure swing adsorption.

Thermal swing regeneration

The spent carbon is treated with steam so that the adsorbed VOC is volatilized and forced to leave the carbon. The vapors containing the desorbed VOCs flow through another adsorber. After the desorption is complete, the treated carbon is cooled and dried by means of cooling air. Following this procedure, the spent carbons regain their initial capacity (EPA, 1999). Besides steam, other sources of heat can be also employed in the regeneration process, such as microwaves, embedded heaters, or heated nitrogen. Thermal swing regeneration is most convenient when the adsorbed species are VOCs of low vapor pressures.

Vacuum regeneration

If the recovery of the adsorbed VOCs is highly desirable, then instead of steam, a vacuum regeneration system may be used. According to this method, the VOCs are forced to volatilize not by temperature, but by means of pressure. Specifically, a vacuum pump is employed to decrease the pressure in the carbon below the vapor pressure of the VOCs, which leads to their boiling at ambient temperature. This method is generally used with carbons, polymers, and zeolite adsorbents (EPA, 1999).

Pressure swing adsorber

This system is used for the separation of gases or vapors from air (EPA, 1999). However, the concentration of the vapors has to be of the order of tens of thousands of parts per million for this technique to be applied. So, it is not suitable for the control of emissions but for removal of vapors from vents on VOC storage tanks. On exposure to a mixture of gases, the adsorbent shows a preference for some specific gases. After admitting the gas mixture, the rest of the gases plus those that are not strongly adsorbed are vented. Then, the pressure is decreased so that the remaining gases can be desorbed. This method has been used for the separation of oxygen and carbon dioxide from flue gas (EPA, 1999).

4.3.2 Ion-exchange regeneration

Since ion exchange is a reversible process, most of the ion exchangers can be regenerated by means of the appropriate substance: strong acid for cation media or alkali for anion media. So, the operation life of the exchanger may be prolonged and thus money can be saved. However, the capacity of the exchanger is gradually exhausted and the medium has to be replaced after some time of operation, even with optimal regeneration.

Generally, regeneration has to be conducted in different vessels, a cation and an anion vessel; otherwise the application of acidic and caustic media to the combined bed (coexistence of cation and anion beads) will lead to total deactivation of the exchange media. So, the mixed

bed has to be separated into the cation and the anion beads, which is usually done using hydraulic separation *in situ* by backwashing the bed by utilizing the small differences in the densities of the cation and anion media. After the regeneration, the media are then remixed.

4.3.3 Destruction, immobilization, and encapsulation of spent materials

Spent ion-exchange and adsorption materials represent a special type of waste, and pose unique problems in the selection of their treatment options. With the evolution of environmental legislation, it is now required that spent materials meet specific quality requirements prior to disposal. In the selection of the treatment method for spent materials, their physical and chemical characteristics must be considered. Basically, there are two main treatment methods: destruction and immobilization. In several occasions, depending on the nature of the spent material, a pretreatment step is required.

Pretreatment

Available pretreatment processes include (IAEA, 2002) the following.

Dewatering: Dewatering the spent materials prior to immobilization improves the overall volume reduction and the compatibility of the waste with the immobilization process. Dewatering is generally accomplished by pressure, vacuum filtration, or centrifugation.

Drying and heating: A complete dewatering step, or drying, is sometimes required. Steam or hot air is generally used.

Crushing and grinding: Crushing and grinding techniques are used basically for size reduction of spent materials, which results in a more homogeneous waste for immobilization, allows the easier removal of nonspecific materials, and facilitates the further destruction of the material by thermal, chemical, or biological methods.

Destructive methods for spent materials

The main goal of destructive methods is to conveniently alter the physicochemical characteristics of the spent material before its final disposal. These processes can be classified as thermal and nonthermal processes.

Thermal processes *Pyrolysis:* Pyrolysis can be defined as the thermal degradation of organic species in the absence of oxygen or other reactant gases. However, practically, pyrolysis refers to any thermal degradation process in which less than the stoichiometric quantity of oxygen is used (Freeman, 1998). Furthermore, pyrolysis of inorganic materials is called “calcination.”

Pyrolysis operates under relatively low temperatures, in the range 500–700 °C. Upon heating in the absence of oxygen, thermal cracking and condensation reactions take place converting most organics into gaseous, liquid, and solid fractions (Perry and Green, 1999). The advantages of pyrolysis are

- (a) the significant reduction of the waste volume, and
- (b) the end product is biologically and geochemically stable (IAEA, 2002).

In general, pyrolysis has less environmental impact than other thermal conversion routes (Freeman, 1998).

Incineration: The incineration in an oxygen-rich atmosphere results in the oxidation of the initial feed material and produces a volume reduction factor ranging from 30 to 100. Incineration systems include, among others, rotary kiln and fluidized-bed incinerators (US DOE, 1998).

Ion-exchange resins contain significant amounts of sulfur and nitrogen, and thus their heating at high temperatures leads to the formation of SO_2 , SO_3 , and small amounts of NO_x . Therefore, an efficient scrubbing system is required for the removal of these substances from the off-gases. Additionally, the presence of radionuclides, such as cesium and ruthenium, which are volatile at temperatures above $800\text{ }^\circ\text{C}$, makes the off-gas treatment more complex. The incineration of resins loaded with radionuclides has been used in pilot and commercial scale at the Technical Research Centre in Finland, in Japan, and at the Austrian Research Centers of Seibersdorf (Valkiainen and Nykyri, 1982; Yahata and Abe, 1982; Neubauer, 1996).

Vitrification: Various molten-glass processes are commercially available for the destruction and/or immobilization of hazardous wastes (Freeman, 1998). The vitrification method destroys the combustible and some toxic portions of the waste while at the same time incorporating residuals into a glass form.

Vitrification involves a heating step under extremely high temperatures, from 1100 to $3000\text{ }^\circ\text{C}$, followed by a cooling step to form a solid mass. During the cooling step, the various contaminants are trapped into the dense glassified mass formed. Plasma torches or electric arc furnaces can be used in vitrification. It is possible that some inorganic compounds will volatilize, while some organics may be destroyed during this heating step. Consequently, a system to treat these off-gases may be needed (EPA, 1996).

The main advantage of vitrification is that the glass waste formed exhibits excellent leach resistance. Moreover, the ash coming from incineration or pyrolysis may be immobilized by this method (IAEA, 2002; Jantzen *et al.*, 1995). Vitrification can be held at similar or lower temperatures than incineration, depending on the additives that have been used during glass forming. Commercial ion-exchange resin vitrification suppliers have emerged in the United States over the last few decades (Cicero and Herman, 1998; Place, 1992).

Nonthermal processes There are a number of chemical treatment methods developed and used for the processing of hazardous chemical waste. These methods are briefly discussed in the next sections.

Acid digestion: Sulfuric and nitric acids are applied at $250\text{ }^\circ\text{C}$ to combustible waste in order to convert it into carbon dioxide and water. Although this is a very promising method for the treatment of spent ion-exchange resins, it has some serious disadvantages. The use of concentrated acids at elevated temperatures may lead to off-gases containing nitrogen and sulfur oxides that have to be treated. Moreover, very resistant materials are needed to stand the corrosion from acids, which adds to the cost of the process (Cooley and Lerch, 1974; Hawkins *et al.*, 1980).

Wet oxidation: The wet oxidation process involves the reaction of a waste with an oxidant in excess water in the presence of a catalyst (IAEA, 2002). Wet oxidation can be carried out

using oxygen or air as oxidant at a relatively low temperature (150–325 °C) and high pressure (2069—20,690 kPa gauge pressure) (Freeman, 1998). A more recent development is the wet oxidation process utilizing hydrogen peroxide as oxidant. The oxidation can be carried out at 100 °C under atmospheric pressure. The application of peroxide wet oxidation at low temperatures for the treatment organic waste and ion-exchange resins has been studied extensively in the United Kingdom (Wilks *et al.*, 1991).

Barix process: Barium is first added to the resin in the form of a liquid hydroxide. Subsequently, the resin is heated in the absence of oxygen and broken into its original components. Barium plays the role of catalyst in this depolymerization process and reacts with the sulfur in the cationic functional groups to form barium sulfate, which in turn acts as a binder for the metallic species in the waste. Moreover, the barium hydroxide adjusts the pH so that the metals contained in the resins stay in the residue after the steps of drying and destruction (IAEA, 2002).

Direct immobilization and encapsulation of spent materials

Immobilization is the process of incorporating waste into a matrix material for solidification, or directly into a storage and/or final disposal container. More specifically, solidification can be defined as encapsulation of a waste in a solid of high structural integrity (Freeman, 1998). At the same time, the goal of the solidification process is the stabilization of the waste, which means that the risk posed by the waste is reduced by converting it into a less soluble and less mobile form (Freeman, 1998).

It is possible that a pretreatment step is required for organic ion-exchange materials before immobilization, although it is not definitely the case. The immobilization matrices currently used are cement, bitumen, and some polymers.

Cement immobilization Another way to treat the spent materials is to immobilize them by adding cement or a cement-based mixture (EPA, 1996). A monolithic block of waste, which is very stable, is the result of this treatment. Moreover, the resulting waste forms exhibit high structural integrity, are noncombustible, and are resistant to radiation as well as to leaching (IAEA, 2002). Types of solidifying/stabilizing agents include the following: portland, gypsum, modified sulfur cement, and grout. With the exception of VOCs and pesticides, cement immobilization may be used for any kind of spent materials, especially for radioactive waste (EPA, 1996).

Cement has many advantages:

- high availability,
- inexpensive raw material,
- conventional well-known technology.

However, there are also some disadvantages. First of all, the final waste has a very high volume compared to the initial one. Grinding before cementation may partially solve this problem. Furthermore, when organic ion-exchange materials are stored via cementation, swelling of the resin beads may occur in contact with water, which may lead to cracking of the cement. So, the cementation of such material should be preceded by an appropriate pretreatment step.

Bitumen immobilization/asphalt blending Bitumen (asphalt) is a generic term used to cover a wide range of high molecular weight hydrocarbons, generated in crude-oil processing. Asphalt blending has many advantages for certain types of wastes. An example is the organic wastes for which asphalt is a much better solidifying material than pozzolanic binders (Freeman, 1998). Furthermore, asphaltic binders can be used in construction works.

Bitumen processes can be held either as batch or as continuous operations. In the first case, the steps of drying and mixing the dried material in molten bitumen are involved, whereas in continuous operation, the spent material is introduced as slurry to equipment that continuously mixes the bitumen at the same time. Then, the bitumen mixture flows into a suitable storage container and is solidified upon cooling. Neilson and Colombo (1982) have presented the main features of the process for ion-exchange resin wastes.

Polymer immobilization The polymers used in the immobilization of spent materials can be classified into two main categories: thermoplastic and thermosetting polymers. The first type is fed in the form of a solid, and then melts upon heating and combines with the waste. On the other hand, thermosetting polymers are supplied in a liquid form and are then polymerized to a solid form, combining with the waste upon heating or in the presence of catalysts.

Spent resins are generally compatible with the polymer matrix material. Generally, the polymer and the resin do not interact chemically. The immobilization of spent ion-exchange resins in polymers is a common application all over the world. Epoxy resins, polyesters, polyethylene, polystyrene and copolymers, polyurethane, phenol-formaldehyde, and polystyrene are among the polymers used (IAEA, 1988). Inorganic materials are generally not immobilized using polymers because they are more acceptable to other immobilization matrices such as cement.

Properties of immobilized waste forms

The properties of the immobilized waste form are decisive for the quality of disposal or storage for a long period of the spent material. Depending on the procedure followed, there is a variety of mechanical, chemical, or thermal features obtained. As mentioned earlier, cement waste forms have a very stable structure with excellent mechanical strength. However, improper formulations may lead to defects in the waste-form structure. The characteristics of bitumen waste forms are closely related to the nature of the solidifying material that has been used. The exposure of the waste form to heat or pressure may lead to its softening. Moreover, although bitumen waste forms are waterproof, rehydration of organic ion-exchange media may occur upon prolonged exposure to water and subsequent failure of the waste form due to swelling (IAEA, 2002).

In many cases, the mechanical properties of a waste form are an important part of the waste acceptance criteria for storage and/or disposal of the waste. The waste form may undergo a series of tests, such as a determination of its compressive strength, to demonstrate that it will maintain its integrity over the required period of time.

The resistance of the waste form to biodegradation in the environment during long-term storage or disposal is another feature of major importance. The action of microorganisms may lead to the release of the components of the waste form into the environment, or to the formation of gases such as hydrogen or methane that may be of concern for the design

of a repository. Since cement materials are inorganic, they are generally considered biore-sistant. However, biodegradation constitutes a threat to any organic materials contained within the matrix. Alkaline conditions and the presence of biocidal additives limit the action of microorganisms. Polymers are generally very resistant to biodegradation, and thus they are considered nonbiodegradable. However, gradual degradation of many poly-mers may take place under the long-term effect of ultraviolet radiation.

Thermal stability is another important parameter. Concerning thermal stability, there are two main considerations: the heat produced during the solidification process and the effect of exposure to heat (or cold) after the solidification of the waste form. If exothermic processes such as the polymerization of thermosetting materials are used, amounts of heat may be released high enough to deteriorate the mechanical properties of the waste. For example, at temperatures around 100 °C, the volatilization of any water contained may lead to cavities and cracks in the final waste form. After the solidification, freeze–thaw cycles may affect the properties of cement, hard bitumen, and thermoset polymer waste forms. On the other hand, the elasticity of soft bitumen and thermoplastic polymers help these materials to resist the variations of temperature. Cement waste forms are not flam-mable, in contrast to bitumen and polyethylene, both of which will melt producing a liq-uid that may maintain combustion, even after the removal of the source of the flame. Comparing thermoplastic waste forms to thermoset waste forms in terms of thermal resist-ance, the first type is less resistant to thermal damage. Thermoset polymers will char when contacted with a burning flame but do not maintain the flame if the source of the flame is removed. Thermal testing experiments have shown that polymethyl methacrylate matrices and polyester are adequately stable up to about 280 °C (Ghutta, 1997).

An issue of great importance is the resistance of any waste form to the action of water, namely to leaching. High resistance to leaching means that the exchanged ions or the adsorbed species of concern are retained within the waste form when it is subjected to wet conditions. Leaching behavior relies on two mechanisms:

- (a) in the case of most polymers and bitumens, a physical barrier between the contami-nant and the environment is developed, and
- (b) in cement-based waste forms, the contaminant often interacts with the matrix chemically.

Catalysis

5.1 TYPES OF CATALYSTS

In Chapter 2, some basic definitions about catalysis were given. In this section, subjects in relation to catalysis are discussed in depth. First of all, let us examine the various types of catalysts and properties before moving on to catalysis issues. Catalysts can be sorted in various ways depending on the criterion of classification. So, they can be classified into homogeneous or heterogeneous catalysts, depending on whether they are in the same phase as reactants and products or not. Furthermore, based on its physical state, a catalyst can be gas, liquid, or solid. Depending on the substances it has been made from, a catalyst can be organic (enzymes and organic acids) or inorganic (metals, metal oxides, etc.). Finally, based on the action, catalysts can be classified as enzymatic, acid–base, photocatalytic, etc..

Here, our attention is focused on heterogeneous catalysts, solids that accelerate reactions in gas or liquid phase. In general, a solid catalyst (the whole formulation) consists of

- *Support or carrier*: The amount of the fluid adsorbed, and thus the catalytic activity, is closely related to surface area. Consequently, large surface areas are generally desired in catalytic processes and porous solids are usually employed to provide them. Moreover, supports keep the catalytic phase highly dispersed, thus protecting it from sintering. It has to be mentioned that the support may or may not be catalytically active. Using the configuration of the support as a criterion, a catalyst can be also typed as
 - (a) porous, when the area results mainly from the porous structure of the support,
 - (b) molecular sieve, when very small pores exist in the support and it is their size that decides which molecules are going to react, and
 - (c) monolithic, when monolith structure is used, which allows high surface area to low volume, efficient heat removal, and low pressure drop across the catalyst.

When a material used for the dispersion of the active agents is bonded to a support, it is called “washcoat.” A characteristic example is the case of automotive monolithic catalysts, where the monolith is the support and a thin film of alumina attached to the monolith constitutes the washcoat, the phase where the catalytically active metals are dispersed. In contrast to these supported catalysts, there are some catalytic materials that

can be shaped to provide large surface area, the unsupported catalysts. Activated carbon, silica gel, alumina, titanium dioxide, amorphous aluminosilicates, and zeolites are widely used as catalyst supports, alumina having a particular place in environmental applications. Synthetic zeolites have been developed and used as supports since 1960, because they have open, well-controlled framework structures that create interconnected cavities. Their structure combined with the fact that the placement of the catalytic atoms at specific sites in the zeolites is possible makes them ideal for selective catalysis. Other important perspectives of huge practical importance are connected to the so-called mesoporous catalysts, exhibiting unique properties and prepared by a revolutionary synthesis method. Rationally designed, both microporous and mesoporous inorganic catalysts are already facts for many industrial and environmentally compatible technologies.

- *Catalytic agents:* Mainly metals and metal oxides are used as the catalytically active components that are dispersed onto the support. The transition group elements and subgroup I are used extensively in environmental applications. Ag, Cu, Fe, Ni, their oxides, and precious metals like Pt, Pd, and Rh are a common choice in catalysis.
- *Promoters:* Promoters are elements or compounds, such as cerium oxide or zirconia, used as additives to improve the physical or chemical properties of the catalysts. They can act in various ways:
 - maintain the dispersion of the catalytic agents
 - improve the thermal stability of the support
 - enhance the catalytic activity

The most fundamental characteristic of a catalyst is its chemical composition, which is decisive for its specific usage (Table 5.1). The properties of a catalyst, namely activity and selectivity, have been discussed in Chapter 2. The physical properties of the catalyst are also important for its successful application. They are investigated by both adsorption methods and various instrumental techniques derived for estimating their porosity and surface area.

The physical characteristics that are really important to a catalyst are surface area, particle size distribution, and particle density. These properties have been extensively discussed in Section 3.9. In Table 5.2, the surface area, pore volume, and mean pore radii are presented for some common catalysts.

5.2 BASIC PRINCIPLES OF CATALYSIS

As discussed in Chapter 2, a heterogeneous catalyst accelerates a reaction that has fluid-phase reactants and products, while itself remaining unchanged by the reaction. In general, it does this by stabilizing reactive intermediates whose formation would be energetically unfavorable in the fluid phase. The great advantage of heterogeneous catalysis over homogeneous catalysis is that since the catalyst is in a separate phase from the reacting mixture,

Table 5.1

Commercial catalysts and their uses (Gates, 1992)

Catalyst	Reaction
Metals (e.g., Ni, Pd, and Pt as powders or on supports) or metal oxides (e.g. Cr ₂ O ₃)	C=C bond hydrogenation, olefin + H ₂ → paraffin
Metals (e.g. Cu, Ni, Pt)	C=O bond hydrogenation, acetone + H ₂ → isopropanol
Metal (e.g. Pd, Pt)	Complete oxidation of hydrocarbons, oxidation of CO
Fe (supported and promoted with alkali metals)	3H ₂ + N ₂ → 2NH ₃
Ni	CO + 3H ₂ → CH ₄ + H ₂ O (methanation)
Fe or Co (supported and promoted with alkali metals)	CO + H ₂ → paraffins + olefins + H ₂ O + CO ₂ (+ other oxygen-containing organic compounds) (Fischer–Tropsch reaction)
Cu (supported on ZnO, with other components, e.g. Al ₂ O ₃)	CO + 2H ₂ → CH ₃ OH
Re + Pt (supported on <i>n</i> -Al ₂ O ₃ or γ -Al ₂ O ₃ promoted with chloride)	Paraffin dehydrogenation, isomerization, and dehydrocyclization
Solid acids (e.g., SiO ₂ -Al ₂ O ₃ , zeolites)	Paraffin cracking and isomerization
γ -Al ₂ O ₃	Alcohol → olefin + H ₂ O
Pd supported on acidic zeolite	Paraffin hydrocracking
Metal-oxide-supported complexes of Cr, Ti or Zr	Olefin polymerization, e.g. ethylene → polyethylene
Metal-oxide-supported oxides of W or Re	Olefin metathesis, e.g. 2 propylene → ethylene + butene
Ag (on inert support, promoted by alkali metals)	Ethylene + ½ O ₂ → ethylene oxide (with CO ₂ + H ₂ O)
V ₂ O ₅ or Pt	2 SO ₂ + O ₂ → 2 SO ₃
V ₂ O ₅ (on metal oxide support)	Naphthalene + 9/2 O ₂ → phthalic anhydride + 2 CO ₂ + 2 H ₂ O
Bismuth molybdate	Propylene + ½ O ₂ → acrolein
Mixed oxides of Fe and Mo	CH ₃ OH + O ₂ → formaldehyde (with CO ₂ + H ₂ O)
Fe ₃ O ₄ or metal sulfides	H ₂ O + CO → H ₂ + CO ₂

Table 5.2

Surface area, pore volume, and mean pore radii for typical solid catalysts (Wheeler, 1950)

Catalyst	Surface area (m ² /g)	Pore volume (cm ³ /g)	Mean pore radius (Å)
Activated carbons	500~1500	0.6~0.8	10~20
Silica gels	200~600	0.4	15~100
SiO ₂ -Al ₂ O ₃ cracking catalysts	200~500	0.2~0.7	33~150
Activated clays	150~225	0.4~0.52	100
Activated alumina	175	0.39	45
Celite (Kieselguhr)	4.2	1.1	11000
Synthetic ammonia catalysts, Fe	4~11	0.12	200~1000

it can stay in the reactor as the reactants and products flow through. We will not discuss the chemistry of particular catalytic systems, but will try to develop some basic approaches that can be applied to a range of systems.

The overall process of a catalytic reaction taking place in a porous catalyst particle involves the following:

1. transport of reactants from the bulk of the fluid to the exterior surface of the catalyst (external mass transfer resistance),
2. transport of reactants from the surface to the interior of the catalyst through pores (internal mass transfer resistance),
3. adsorption of reactants onto the active sites on the internal surface of the catalyst,
4. reaction of adsorbed reactants to form adsorbed products,
5. desorption of products,
6. transport of products out of the pores to the particle external surface,
7. transport of products from the external surface of the catalyst to the main body of the fluid.

This is illustrated schematically in Figure 5.1 for the generic catalytic reaction $A \rightarrow B$.

Steps 3, 4, and 5 are the chemically reactive steps, whereas steps 1, 2, 6, and 7, are related to transport phenomena.

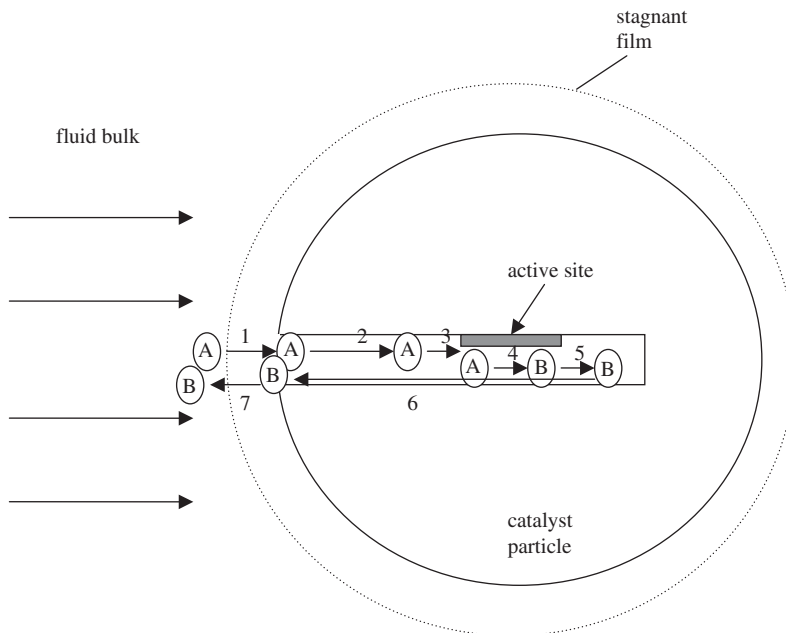


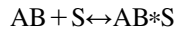
Figure 5.1 Steps involved in reactions on a solid surface.

5.2.1 Reaction rate expressions of solid–fluid catalytic reactions

The basic approach for deducing an overall rate expression of solid–fluid catalytic reactions is that each step can be considered an elementary one with its own rate law. The combination of the three rate laws (one for each step) under some assumptions leads to the derivation of the overall reaction rate expression. Before moving on, it has to be noted that catalytic reaction rate expressions can be derived in two ways: (a) the approach of Hinshelwood (1940), according to which the rates are expressed in terms of coverage θ , and (b) the approach of Hougen and Watson (1943), who derived rate equations in terms of surface concentrations of adsorbed species and free sites. Although at first glance these two approaches seem quite similar, the approach of Hougen and Watson proves to be more comprehensive. Their formulations provide for catalyst activity, activity decay, and catalyst effectiveness due to diffusion (Carberry, 1976). Here, the activity decay approach is followed.

Adsorption

The adsorption of reactants onto catalytic active sites is the first step of the “pure” catalytic process. The form of the rate law is closely connected to the mechanism adopted. Specifically, if the reactant AB is considered to be adsorbed as a molecule, it can be represented by



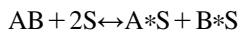
where:

AB = the reactant molecule

S = the catalytic active site

AB*S = the active site onto which a molecule of AB is adsorbed.

This type of adsorption is called “molecular adsorption” in contrast to dissociative adsorption, which takes place when the molecule dissociates into atoms during adsorption and is represented by



How a molecule is adsorbed depends strongly on the catalyst. For example, acetaldehyde is adsorbed as a molecule on Pt, whereas dissociative adsorption takes place on the Pd catalyst (Pouloupoulos *et al.*, 2001).

In the first case, the rate of attachment of AB molecules to the surface is proportional to the partial pressure of AB. Moreover, the rate is proportional to the vacant sites concentration. So, the rate of attachment is

$$\text{rate of attachment} = k_A P_{AB} C_V \quad (5.1)$$

where:

k_A = the proportionality constant for attachment, $\text{atm}^{-1} \text{s}^{-1}$

P_{AB} = the partial pressure of AB, atm

C_V = the concentration of vacant sites, $\text{mol/g}_{\text{cat}}$.

With respect to the vacant sites, the site balance can be written as

$$C_t = C_v + C_{AB^*S} \quad (5.2)$$

where:

- C_t = the total concentration of sites
- C_v = the concentration of vacant sites
- C_{AB^*S} = the concentration of the sites occupied by AB.

If other species are also adsorbed on the surface, the concentrations of the corresponding occupied sites have to be added to the site balance above. The concentration of the active sites is expressed as mole per unit mass of catalyst and is equal to the number of active sites per unit mass of catalyst divided by the Avogadro's number.

The rate of detachment of the molecules AB from the surface is directly proportional to the concentration of sites occupied by the molecules, for example, C_{AB^*S} :

$$\text{rate of detachment} = k_{-A} C_{AB^*S} \quad (5.3)$$

The net rate of adsorption is equal to the attachment rate minus the detachment one. Taking into account that the ratio $K_A = k_A/k_{-A}$ is the adsorption equilibrium constant, we obtain the following:

$$r_{AD,m} = k_A P_{AB} C_v - k_{-A} C_{AB^*S} \quad (5.4)$$

and

$$r_{AD,m} = k_A \left(P_{AB} C_v - \frac{C_{AB^*S}}{K_A} \right) \quad (5.5)$$

where $r_{AD,m}$ is the rate of adsorption per unit mass of catalyst, mol/(g_{cat} s)

In the case of dissociative adsorption, the adsorption rate takes another form. Since two adjacent vacant active sites are required for the molecule to adsorb, the rate of attachment is proportional to the square of the vacant sites concentration. The rate of detachment is now proportional to the product of the occupied sites concentration. Thus

$$r_{AD,m} = k_{AB} P_{AB} C_v^2 - k_{-AB} C_{A^*S} C_{B^*S} \quad (5.6)$$

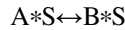
and

$$r_{AD,m} = k_{AB} \left(P_{AB} C_v^2 - \frac{C_{A^*S} C_{B^*S}}{K_{AB}} \right) \quad (5.7)$$

Surface reaction

As in the case of adsorption, a variety of surface reaction mechanisms exists (Fogler, 1999) :

- (a) The surface reaction follows a single-site mechanism:



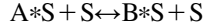
with the following rate law:

$$r_{S,m} = k_S \left(C_{A^*S} - \frac{C_{B^*S}}{K_S} \right) \quad (5.8)$$

where:

- $r_{S,m}$ = the rate of surface reaction per unit mass of catalyst, mol/(g_{cat} s)
 K_S = the surface reaction equilibrium constant
 k_S = the proportionality constant, m³/(g_{cat} s).

- (b) The adsorbed reactant interacts with another site to form the product (dual site mechanism):



with the following rate law:

$$r_{S,m} = k_S \left(C_{A^*S} C_v - \frac{C_{B^*S} C_v}{K_S} \right) \quad (5.9)$$

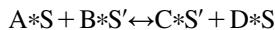
- (c) The surface reaction takes place between two adsorbed species:



and the following rate law applies:

$$r_{S,m} = k_S \left(C_{A^*S} C_{B^*S} - \frac{C_{C^*S} C_{D^*S}}{K_S} \right) \quad (5.10)$$

- (d) The surface reaction takes place between two species adsorbed on different types of sites S and S':

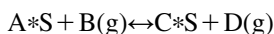


and the rate law now becomes

$$r_{S,m} = k_S \left(C_{A^*S} C_{B^*S'} - \frac{C_{C^*S'} C_{D^*S}}{K_S} \right) \quad (5.11)$$

All the above mechanisms, single or dual site, are known as Langmuir–Hinshelwood kinetics.

(e) An adsorbed molecule reacts with a molecule in the gas phase:



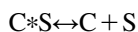
This mechanism, known as the Eley–Rideal mechanism, has the following rate law:

$$r_{S,m} = k_S \left(C_{A^*S} P_B - \frac{C_{C^*S'} P_D}{K_S} \right) \quad (5.12)$$

All these expressions were derived in the same way as those for adsorption.

Desorption

The products of the surface reaction adsorbed are subsequently desorbed into the gas phase. The rate of desorption of C is exactly the opposite in sign to the rate of adsorption of C and the desorption equilibrium constant K_{DC} is the reciprocal of the adsorption equilibrium constant K_C . For the desorption of C, according to



the desorption rate law is

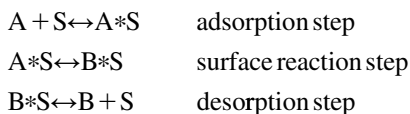
$$r_{D,m} = k_D \left(C_{C^*S} - \frac{P_C C_v}{K_{DC}} \right) = k_D (C_{C^*S} - K_C P_C C_v) \quad (5.13)$$

where:

$$\begin{aligned} r_{D,m} &= \text{the rate of desorption per unit mass of catalyst, mol}/(\text{g}_{\text{cat}} \text{ s}) \\ k_D &= \text{the proportionality constant, m}^3/(\text{g}_{\text{cat}} \text{ s}). \end{aligned}$$

Derivation of the catalytic reaction rate law

Suppose that the following three steps describe the catalytic reaction of A:



The rate law for each step is, respectively,

$$r_{AD,m} = k_A \left(P_A C_v - \frac{C_{A^*S}}{K_A} \right) \quad (5.14)$$

$$r_{S,m} = k_S \left(C_{A^*S} - \frac{C_{B^*S}}{K_S} \right) \quad (5.15)$$

$$r_{D,m} = k_D \left(C_{B^*S} - \frac{P_B C_v}{K_{DB}} \right) \quad (5.16)$$

At steady state, the rates of the three steps are equal to one another (omitting from now on the subscript “m” for reasons of simplicity):

$$r_{AD} = r_S = r_D \quad (5.17)$$

We will develop an overall rate law considering that each step is rate limiting. Our aim is to eliminate the concentrations of the adsorbed species that cannot be measured during a classical experiment.

Adsorption is rate limiting

If the adsorption limits the overall rate, then we can assume that k_S is relatively large and that

$$\frac{r_S}{k_S} \cong 0 \quad (5.18)$$

Then, the rate law of the reaction can be solved for C_{A^*S} :

$$C_{A^*S} = \frac{C_{B^*S}}{K_S} \quad (5.19)$$

The same approximation can be applied to the rate law of desorption. We set

$$\frac{r_D}{k_D} \cong 0 \quad (5.20)$$

So, we can estimate C_{B^*S} :

$$C_{B^*S} = \frac{P_B C_v}{K_{DB}} \quad (5.21)$$

Keep in mind that

$$K_{DB} = \frac{1}{K_B} \quad (5.22)$$

Consequently,

$$C_{B^*S} = K_B P_B C_v \quad (5.23)$$

Substituting C_{B^*S} into the equation of C_{A^*S} , we obtain

$$C_{A^*S} = \frac{K_B P_B C_v}{K_S} \quad (5.24)$$

The site balance is

$$C_t = C_v + C_{A^*S} + C_{B^*S} \quad (5.25)$$

Substituting C_{A^*S} and C_{B^*S} into the last equation,

$$C_t = C_v + \frac{K_B P_B C_v}{K_S} + K_A P_B C_v \quad (5.26)$$

Solving for C_v , we have

$$C_v = \frac{C_t}{1 + \frac{K_B}{K_S} P_B + K_A P_B} \quad (5.27)$$

Combining the equations for C_{A^*S} , C_{B^*S} , and C_v with the adsorption rate law, we obtain

$$-r_{ov} = r_{AD} = \frac{k_A C_t \left(P_A - \frac{K_B}{K_S K_A} P_B \right)}{1 + \frac{K_B + K_A K_S}{K_S} P_B} \quad (5.28)$$

The above expression can also be written as

$$-r_{ov} = r_{AD} = \frac{k' \left(P_A - \frac{1}{K_S} P_B \right)}{1 + K' P_B} \quad (5.29)$$

where:

$$\begin{aligned} k' &= k_A C_t \\ K' &= \frac{K_B + K_A K_S}{K_S} \\ -r_{\text{ov}} &= \text{overall reaction rate.} \end{aligned}$$

Surface reaction is rate limiting

We will follow the same approach. If surface reaction is rate limiting, we can set

$$\frac{r_{\text{AD}}}{k_A} \cong \frac{r_{\text{D}}}{k_D} \cong 0 \quad (5.30)$$

Then, one can easily obtain

$$C_{\text{A}^*\text{S}} = K_A P_A C_v \quad (5.31)$$

and

$$C_{\text{B}^*\text{S}} = K_B P_B C_v \quad (5.32)$$

The site balance is

$$C_t = C_v + C_{\text{A}^*\text{S}} + C_{\text{B}^*\text{S}} \quad (5.33)$$

Substituting $C_{\text{A}^*\text{S}}$ and $C_{\text{B}^*\text{S}}$ into the last equation,

$$C_t = C_v + K_A P_A C_v + K_B P_B C_v \quad (5.34)$$

Solving for C_v , we have

$$C_v = \frac{C_t}{1 + K_A P_A + K_B P_B} \quad (5.35)$$

Combining the equations for $C_{\text{A}^*\text{S}}$, $C_{\text{B}^*\text{S}}$, and C_v with the surface reaction rate law, we obtain

$$-r_{\text{ov}} = r_{\text{AD}} = \frac{k_S K_A C_t \left(P_A - \frac{K_B}{K_S K_A} P_B \right)}{1 + K_A P_A + K_B P_B} \quad (5.36)$$

or

$$-r_{\text{ov}} = r_{\text{AD}} = \frac{k' \left(P_A - \frac{K_B}{K_S K_A} P_B \right)}{1 + K_A P_A + K_B P_B} \quad (5.37)$$

where $k' = k_S K_A C_t$

Desorption is rate limiting

Similarly, if desorption is rate limiting, we can set

$$\frac{r_{\text{AD}}}{k_A} \cong \frac{r_S}{k_S} \cong 0 \quad (5.38)$$

Then, it is easily seen that

$$C_{\text{A}^* \text{S}} = K_A P_A C_v \quad (5.39)$$

and

$$C_{\text{B}^* \text{S}} = K_S C_{\text{A}^* \text{S}} = K_S K_A P_A C_v \quad (5.40)$$

The site balance is

$$C_t = C_v + C_{\text{A}^* \text{S}} + C_{\text{B}^* \text{S}} \quad (5.41)$$

Substituting $C_{\text{A}^* \text{S}}$ and $C_{\text{B}^* \text{S}}$ into the last equation, we obtain

$$C_t = C_v + K_A P_A C_v + K_S K_A P_A C_v \quad (5.42)$$

Solving for C_v , we have

$$C_v = \frac{C_t}{1 + K_A P_A + K_S K_A P_A} \quad (5.43)$$

Combining the equations for $C_{\text{A}^* \text{S}}$, $C_{\text{B}^* \text{S}}$, and C_v with the desorption rate law, we obtain

$$-r_{\text{ov}} = r_{\text{AD}} = \frac{k_D K_S K_A C_t \left(P_A - \frac{K_B}{K_S K_A} P_B \right)}{1 + K_A (1 + K_S) P_A} \quad (5.44)$$

or

$$-r_{\text{ov}} = r_{\text{AD}} = \frac{k' \left(P_A - \frac{K_B}{K_S K_A} P_B \right)}{1 + K' P_A} \quad (5.45)$$

where:

$$k' = k_s k_A C_t$$

$$K' = K_A (1 + K_s)$$

General comments

By plotting the initial overall rate with the initial pressure of reactant A, when B has not been yet produced, one can find which case is consistent with the experimental data and choose the appropriate rate form. Generally, the overall rate is expressed as the combination of three terms:

$$\frac{\text{rate coefficient} \times \text{driving force}}{\text{total resistance}}$$

Fromment and Bishoff (1990) presented the possible expression of each of these terms in various cases, whereas Poulopoulos *et al.* (2001) have presented various rate laws for the catalytic oxidation of volatile organic compounds, as shown in Table 5.3.

5.2.2 External mass and heat transfer phenomena

As described previously, the reactant has to first reach the external surface of the catalyst. For simplicity, we take into consideration the case of a gas reacting on a solid catalytic surface. Owing to gas film resistance, the concentration of the reactant at the catalytic surface (C_s) is lower than that in the bulk of the fluid (C_b). This difference depends on

- (a) the mass transfer coefficient from the fluid to the catalytic surface, and
- (b) the reaction rate constant.

Consequently, the overall rate is actually lower than the one estimated based on the concentration of the reactant in the main body of the fluid.

Furthermore, a temperature gradient may also be developed due to gas film resistance. This means that the temperature of the bulk of the fluid (T_b) is also different from the temperature of the exterior surface of the catalyst (T_s). As before, this difference depends on

- (a) the heat transfer coefficient between the fluid and the catalytic surface, and
- (b) the reaction rate constant.

In addition, the temperature gradient is also dependent upon whether the reaction is exothermic or endothermic. For exothermic reactions, the catalytic surface is hotter than

Table 5.3

Various reaction rate laws for the catalytic oxidation of VOCs (Poulopoulos *et al.*, 2003)

Rate-limiting step	Rate Law	Scheme
Surface reaction between adsorbed oxygen and reactant	$\frac{k_m k_{O_2} k_{React} C_{O_2} C_{React}}{(1 + k_{O_2} C_{O_2} + k_{React} C_{React})^2}$	$\begin{array}{c} R - O_2 \\ \quad \\ - S - S - \end{array}$
Surface reaction between dissociative adsorbed reactant and oxygen	$\frac{k_m (k_{O_2} k_{React} C_{O_2} C_{React})^{1/2}}{(1 + (k_{O_2} C_{O_2})^{1/2} + (k_{React} C_{React})^{1/2})^2}$	$\begin{array}{c} R - O \\ \quad \\ - S - S - \end{array}$
Surface reaction between adsorbed oxygen and reactant in the gas phase	$\frac{k_m k_{O_2} C_{O_2} C_{React}}{1 + k_{O_2} C_{O_2}}$	$\begin{array}{c} R - O_2 \\ \quad \\ - S - S - \end{array}$
Mars-van Krevelen mechanism	$\frac{k_m k_{O_2} C_{O_2} C_{React}}{k_{O_2} C_{O_2} + \gamma k_R C_{React}}$	$\begin{array}{c} R - O \\ \quad \\ - S - S - \\ A + \gamma O_2 \rightarrow CO_2 + H_2O \end{array}$
Surface reaction between adsorbed reactant and oxygen in the gas phase	$\frac{k_m k_{React} C_{O_2} C_{React}}{1 + k_{React} C_{React}}$	$\begin{array}{c} R - O_2 \\ \quad \\ - S - S - \end{array}$

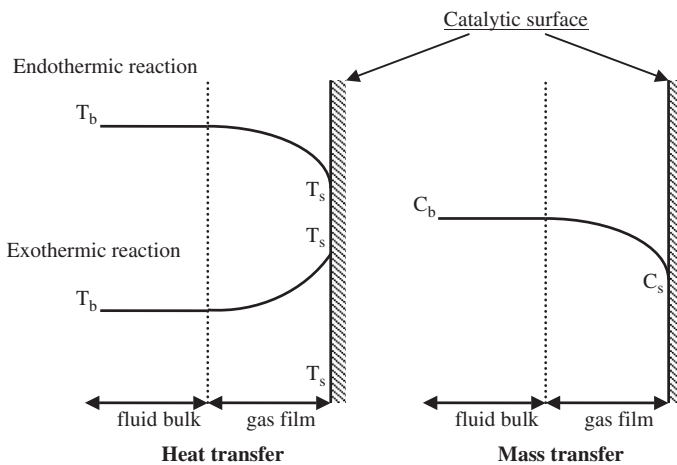


Figure 5.2 Concentration and temperature profiles for fluid–solid catalytic reactions.

the surrounding fluid, whereas the opposite is observed in the case of endothermic reactions (Figure 5.2). In the first case, the overall rate increases as a result of the higher temperature on the catalytic surface, but at the same time decreases due to the decrease in reactant concentration. The balance between these two competitive factors can result in an overall rate higher or lower than the one corresponding to the conditions of the bulk of the fluid. In the second case (endothermic reaction), the overall rate is always lower than the rate corresponding to the conditions of the bulk of the fluid.

These phenomena are called external not only because they take place outside the catalyst particle, but also because they are examined independent of the chemical reaction, in contrast to the internal mass and heat transfer phenomena.

The mass and heat transfer coefficients depend on the fluid and catalytic particle properties, flow conditions, and the reactor type. Analytical equations for estimating these coefficients according to the reactor type have been presented previously in Chapter 3.

Suppose that a gas reactant in a flowing fluid reacts on a nonporous catalyst at isothermal conditions. In steady state, the mass transfer rate of the reactant from the bulk of the fluid to the catalytic surface is equal to the reaction rate (n th order):

$$\underbrace{k_f a_s (C_b - C_s)}_{\text{mass transfer rate}} = \underbrace{k_m C_s^n}_{\text{reaction rate}} \quad (5.46)$$

where:

- k_f = mass transfer coefficient of the reactant, m/s
- k_m = reaction rate constant per unit mass of catalyst
- a_s = external surface area per unit mass of catalyst, m²/kg
- C_b = concentration of the reactant at the bulk, mol/m³
- C_s = concentration of the reactant at the catalytic surface, mol/m³
- n = reaction order.

It is desirable that the overall rate r_{ov} be expressed in terms of bulk concentration, since the concentration C_b is normally determined in an experiment. Consequently, the unknown concentration C_s has to be obtained from the equation above. The concentration C_s and the overall rate r_{ov} are presented in Table 5.4 for various reaction orders, $n = -1, 1, 1/2$, and 2. In the case of $n = 1$, the overall rate can be written as

$$r_{ov} = k_{ov} C_b \quad (5.47)$$

where

$$\frac{1}{k_{ov}} = \frac{1}{k_m} + \frac{1}{k_f a_s} \quad (5.48)$$

Table 5.4

Isothermal catalytic surface concentration and process rate for reaction order (n)

Reaction order (n)	Surface concentration (C_s)	Overall rate (r_{ov})
-1	$C_s = \left(\frac{1 + \sqrt{1 - 4 \frac{k_m}{k_f a_s} C_b^2}}{2} \right) C_b$	$r_{ov} = \frac{2k_m}{\left(1 + \sqrt{1 - 4 \frac{k_m}{k_f a_s} C_b^2} \right) C_b}$
1/2	$C_s = \left(\sqrt{\left(\frac{k_m}{2k_f a_s} \right)^2 + C_b} - \frac{k_m}{2k_f a_s} \right)^2$	$r_{ov} = k_m \left(\sqrt{\left(\frac{k_m}{2k_f a_s} \right)^2 + C_b} - \frac{k_m}{2k_f a_s} \right)$
1	$C_s = \frac{1}{1 + \frac{k_m}{k_f a_s}} C_b$	$r_{ov} = \frac{1}{\frac{1}{k_m} + \frac{1}{k_f a_s}} C_b$
2	$C_s = \frac{\sqrt{1 + 4 \frac{k_m}{k_f a_s} C_b} - 1}{2 \frac{k_m}{k_f a_s}}$	$r_{ov} = k_m \left(\frac{\sqrt{1 + 4 \frac{k_m}{k_f a_s} C_b} - 1}{2 \frac{k_m}{k_f a_s}} \right)^2$
3	$C_s = \left(\sqrt[3]{\frac{k_f a_s}{2k_m C_b^2} + \sqrt{\left(\frac{k_f a_s}{2k_m C_b^2} \right)^2 + \left(\frac{k_f a_s}{3k_m C_b^2} \right)^3}} + \sqrt[3]{\frac{k_f a_s}{2k_m C_b^2} - \sqrt{\left(\frac{k_f a_s}{2k_m C_b^2} \right)^2 + \left(\frac{k_f a_s}{3k_m C_b^2} \right)^3}} \right) C_b$	$r_{ov} = k_m \left(\sqrt[3]{\frac{k_f a_s}{2k_m C_b^2} + \sqrt{\left(\frac{k_f a_s}{2k_m C_b^2} \right)^2 + \left(\frac{k_f a_s}{3k_m C_b^2} \right)^3}} + \sqrt[3]{\frac{k_f a_s}{2k_m C_b^2} - \sqrt{\left(\frac{k_f a_s}{2k_m C_b^2} \right)^2 + \left(\frac{k_f a_s}{3k_m C_b^2} \right)^3}} \right)^3 C_b^3$

and the overall rate remains first order with a constant that is the combination of the reaction and mass transfer resistance. There are two limiting cases:

- (a) the external mass transfer is rate limiting, where $k_f \ll k_m$ and therefore $r_{ov} = k_f a_s C_b$, and
- (b) the reaction is rate limiting, where $k_f \gg k_m$ and therefore $r_{ov} = k_m C_b$ (the system behaves as if it were homogeneous).

It is useful to introduce the external effectiveness factor η_{ex} as the ratio of the observed overall rate r_{ov} to the chemical reaction rate r_o without diffusion resistance ($C_s = C_b$):

$$\eta_{ex} = \frac{r_{ov}}{r_o} = \frac{\text{the overall rate}}{\text{reaction rate without mass transfer}} \quad (5.49)$$

Moreover, the Damköhler number (Da) can be used to simplify the relations in Table 5.4:

$$Da = \frac{k_m C_b^{n-1}}{k_f a_s} \quad (5.50)$$

Since

$$\frac{k_m C_b^{n-1}}{k_f a_s} = \frac{k_m C_b^{n-1} C_b}{k_f a_s C_b} = \frac{k_m C_b^n}{k_f a_s C_b} \quad (5.51)$$

the Damköhler number can be seen as the ratio of the rate with reaction controlling to the rate with mass transfer controlling.

A high Damköhler number means that the global rate is controlled by mass transfer phenomena. So, the process rate can be rewritten in terms of the Damköhler number and the external effectiveness factor for each reaction order can be deduced, as shown in Table 5.5. In Figure 5.3, the external effectiveness factor versus the Damköhler number is depicted for various reaction orders. It is clear that the higher the reaction order, the more obvious the external mass transfer limitation. For Damköhler numbers higher than 0.10, external mass transfer phenomena control the global rate. In the case of $n = -1$, the external effectiveness factor actually increases with increasing the Damköhler number, i.e. as the mass transfer phenomenon prevails, because the negative order means that the increase in reactant concentration inhibits the reaction rate.

It is likely that at high temperatures, where k_m is greatly increased, the observed rate is controlled by mass transfer, and consequently is almost the same for both catalytic and noncatalytic reactions.

So far, the isothermal condition was examined. However, a temperature gradient can be developed in the gas film surrounding the catalyst pellet. The rate of heat transfer through the film is given by

$$Q = h_f a_s (T_s - T_b) \quad (5.52)$$

Table 5.5

The global rate expression and the external effectiveness factor for an isothermal catalytic reaction of n th order

Reaction order (n)	Overall rate (r_{ov})	External effectiveness factor (η_{ex})
-1	$\frac{2k_m}{(1 + \sqrt{1 - 4Da})C_b}$	$\frac{2}{1 + \sqrt{1 - 4Da}}$
$\frac{1}{2}$	$k_m \left(\frac{\sqrt{Da^2 + 4} - Da}{2} \right) C_b^{1/2}$	$\frac{\sqrt{Da^2 + 4} - Da}{2}$
1	$\frac{k_m C_b}{1 + Da}$	$\frac{1}{1 + Da}$
2	$k_m \left(\frac{\sqrt{1 + 4Da} - 1}{2Da} \right)^2 C_b^2$	$\left(\frac{\sqrt{1 + 4Da} - 1}{2Da} \right)^2$
3	$k_m \left(\sqrt[3]{\frac{1}{2Da} + \sqrt{\frac{1}{4Da^2} + \frac{1}{27Da^3}}} + \sqrt[3]{\frac{1}{2Da} - \sqrt{\frac{1}{4Da^2} + \frac{1}{27Da^3}}} \right)^3 C_b^3$	$\left(\sqrt[3]{\frac{1}{2Da} + \sqrt{\frac{1}{4Da^2} + \frac{1}{27Da^3}}} + \sqrt[3]{\frac{1}{2Da} - \sqrt{\frac{1}{4Da^2} + \frac{1}{27Da^3}}} \right)^3$

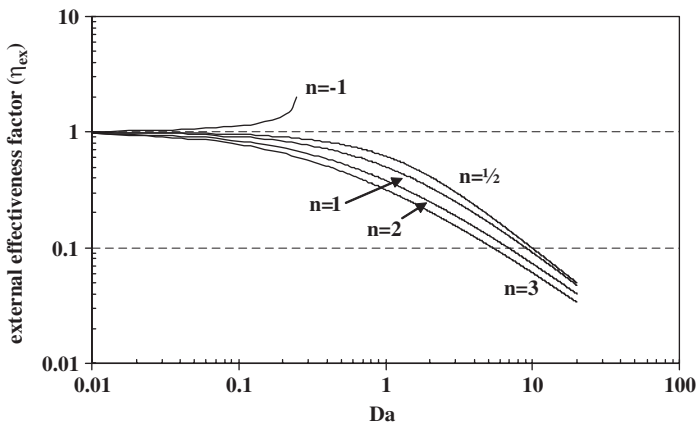


Figure 5.3 The external effectiveness factor for reaction order n .

where:

$$\begin{aligned} Q &= \text{rate of heat transfer per unit mass of catalyst} \\ h_f &= \text{heat transfer coefficient per unit of external surface area} \\ T_b &= \text{temperature at the bulk of the fluid} \\ T_s &= \text{temperature at catalytic surface.} \end{aligned}$$

The rate of heat generated by the reaction is given by

$$q = r_m(-\Delta H) = k_m C_s(-\Delta H) = k_f a_s (C_b - C_s)(-\Delta H) \quad (5.53)$$

where:

$$\begin{aligned} q &= \text{rate of heat generated per unit mass of catalyst} \\ r_m &= \text{global rate} \\ -\Delta H &= \text{heat of reaction per mole of reactant.} \end{aligned}$$

Under steady-state conditions, the following holds:

$$h_f a_s (T_s - T_b) = r_m (-\Delta H) \quad (5.54)$$

The mass transfer coefficient can be calculated using the equations presented in Chapter 3; the heat transfer coefficient can be determined by the same or analogous equations, and thus the temperature gradient can be calculated from the reaction rate data.

It has to be noted that for gas–solid catalytic reactions, the above equations can be also written in terms of pressure instead of concentration.

5.2.3 Internal mass and heat transfer phenomena

As mentioned earlier, if the rate of a catalytic reaction is proportional to the surface area, then a catalyst with the highest possible area is most desirable and that is generally achieved by its porous structure. However, the reactants have to diffuse into the pores within the catalyst particle, and as a result a concentration gradient appears between the pore mouth and the interior of the catalyst. Consequently, the concentration at the exterior surface of the catalyst particle does not apply to the whole surface area and the pore diffusion limits the overall rate of reaction. The effectiveness factor η_s is used to account for diffusion and reaction in porous catalysts and is defined as

$$\eta_s = \frac{\text{actual rate of reaction (with pore diffusion resistance)}}{\text{rate of reaction at surface conditions}}$$

Consequently, for a first-order irreversible reaction, the observed reaction rate is

$$r_m = \eta_s k_m C_s \quad (5.55)$$

Note that internal mass transfer and reaction are dealt with simultaneously, in contrast to external mass transfer, which is considered to be in series with the reaction at the catalyst external surface.

Before examining internal mass transfer and reaction, let us consider the diffusion of fluids within solid particles, which is expressed by means of the effective diffusivity.

Effective diffusivity

The details concerning the determination of D_{eff} and the relevant equations have been presented in Section 3.9.9. Here, let us just recall that the effective diffusivity D_{eff} is used to represent the diffusion of a fluid inside a catalyst particle. D_{eff} is defined on the basis that the paths inside the particle are tortuous and that the pores have various cross-sectional areas. Moreover, not all of the area normal to the direction of the flux is available for the molecules to diffuse. The diffusion can take place by one or more of three mechanisms:

- *Knudsen diffusion:* This kind of diffusion is observed if the mean free path of the molecules is significantly greater than the pore diameter. In this mode, the intermolecular collisions are much less than those between the molecules and pore walls.
- *Molecular diffusion:* If the mean free path of the molecules is much smaller than the pore radius, molecular diffusion occurs and the intermolecular collisions are much more frequent than the ones between molecules and pore walls.
- *Surface diffusion:* Here, the molecules move along the walls of the pores in the direction of decreasing surface concentration. Surface diffusion is not significant in catalysis at elevated temperatures and generally is considered to be of minor importance compared to the other types of diffusion.

In Table 5.6, the porosity and the tortuosity factor are given for some catalysts.

Now, our purpose is to find an expression for the calculation of the effectiveness factor accounting for reaction and mass transfer within various shapes of catalyst pellets.

Plate

As discussed previously, the interior surface may contribute significantly to the total one in the case of a porous catalyst. Consider the first-order irreversible reaction $A \rightarrow B$. The reaction rate is

$$r_m = k_s C_A \quad (5.56)$$

where k_s is the reaction rate constant per unit surface of catalyst.

Table 5.6

Porosity and tortuosity factors for diffusion in catalysts

Catalyst	ϵ_p	τ_p
100–110 μm powder packed into a tube	0.416	1.56
Pelletized Cr_2O_3 supported on Al_2O_3	0.22	2.5
Pelletized bohemite alumina	0.34	2.7
Girdler G-58 Pd on alumina	0.39	2.8
Haldor–Topsøe MeOH synthesis catalyst	0.43	3.3
0.5% Pd on alumina	0.59	3.9
1% Pd on alumina	0.5	7.5
Pelletized Ag/8.5% Ca alloy	0.3	6.0
Pelletized Ag	0.3	10.0

The reactant A and the product B diffuse into and out of a cylindrical catalyst pore with length L and radius r_p . The material balance for reactant A at steady state for a differential length dx of the catalyst pore is written as diffusion flux in – diffusion flux out – disappearance by reaction = 0

$$\left[-\pi r_p^2 D_{\text{eff}} \left(\frac{dC_A}{dx} \right)_x \right] - \left[-\pi r_p^2 D_{\text{eff}} \left(\frac{dC_A}{dx} \right)_{x+\Delta x} \right] - [k_s C_A (2\pi r_p \Delta x)] = 0 \quad (5.57)$$

Dividing this equation by $\pi r_p^2 D_{\text{eff}} \Delta x$, the following is obtained:

$$\frac{\left(\frac{dC_A}{dx} \right)_{x+\Delta x} - \left(\frac{dC_A}{dx} \right)_x}{\Delta x} - \frac{2k_s C_A}{D_{\text{eff}} r_p} = 0 \quad (5.58)$$

$$\lim_{\Delta x \rightarrow 0} \left[\frac{\left(\frac{dC_A}{dx} \right)_{x+\Delta x} - \left(\frac{dC_A}{dx} \right)_x}{\Delta x} - \frac{2k_s C_A}{D_{\text{eff}} r_p} \right] = 0 \quad (5.59)$$

We obtain a second-order ordinary differential equation:

$$\frac{d^2 C_A}{dx^2} - \frac{2k_s}{D_{\text{eff}} r_p} C_A = 0 \quad (5.60)$$

or

$$\frac{d^2 C_A}{dx^2} - \lambda^2 C_A = 0 \quad (5.61)$$

with

$$\lambda = \sqrt{\frac{2k_s}{D_{\text{eff}} r_p}} \quad (5.62)$$

with the following boundary conditions:

at the pore mouth: $C_A = C_{A_s}$, at $x = 0$
 at the interior end of pore: $\frac{dC_A}{dx} = 0$, at $x = L$

The general solution is

$$C_A = C_1 e^{\lambda x} + C_2 e^{-\lambda x} \quad (5.63)$$

$$\begin{aligned} \text{at } x = 0: & \quad C_{As} = C_1 + C_2 \\ \text{at } x = L: & \quad 0 = \lambda C_1 e^{\lambda L} - \lambda C_2 e^{-\lambda L} \end{aligned}$$

$$C_1 = \frac{C_{As} e^{-\lambda L}}{e^{\lambda L} + e^{-\lambda L}} \quad (5.64)$$

$$C_2 = \frac{C_{As} e^{\lambda L}}{e^{\lambda L} + e^{-\lambda L}} \quad (5.65)$$

$$C_A(x) = \frac{e^{\lambda(L-x)} + e^{-\lambda(L-x)}}{e^{\lambda L} + e^{-\lambda L}} C_{As} = \frac{\cosh[\lambda(L-x)]}{\cosh(\lambda L)} C_{As} \quad (5.66)$$

or

$$C_A(x) = \frac{\cosh\left(\phi - \phi \frac{x}{L}\right)}{\cosh\phi} \quad (5.67)$$

where

$$\phi = \lambda L = L \sqrt{\frac{2k_s}{D_{eff} r_p}} = L \sqrt{\frac{k_m \rho_p}{D_{eff}}} \quad (5.68)$$

The dimensionless quantity $\phi = \lambda L$ is called *Thiele modulus*.
Finally, we obtain

$$\eta_s = \frac{\tanh\phi}{\phi} \quad (5.69)$$

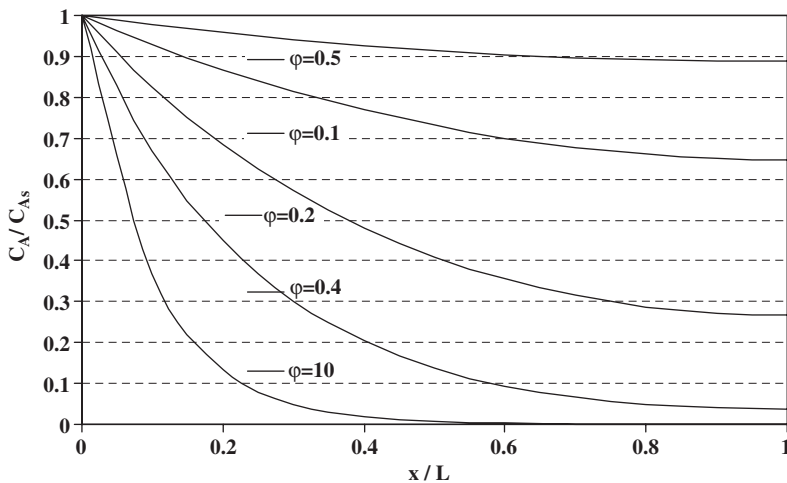


Figure 5.4 The reactant concentration within a catalyst pore as a function of the Thiele modulus.

The drop in the concentration moving into the pore is shown in Figure 5.4 for various values of the Thiele modulus.

Spherical pellet

Following the same approach as in the case of the plate:

$$\left[-4\pi r_p^2 D_{\text{eff}} \left(\frac{dC_A}{dr} \right)_r \right] - \left[-4\pi (r_p + \Delta r)^2 D_{\text{eff}} \left(\frac{dC_A}{dr} \right)_{r+\Delta r} \right] - 4\pi r_p^2 \Delta r \rho_p k_m C_A = 0 \quad (5.70)$$

$$\begin{aligned} 4\pi r_p^2 D_{\text{eff}} \left(\frac{dC_A}{dr} \right)_{r+\Delta r} - 4\pi r_p^2 D_{\text{eff}} \left(\frac{dC_A}{dr} \right)_r + 4\pi 2r_p \Delta r D_{\text{eff}} \left(\frac{dC_A}{dr} \right)_{r+\Delta r} \\ - 4\pi r_p^2 \Delta r \rho_p k_m C_A = 0 \end{aligned} \quad (5.71)$$

Dividing by $4\pi r_p^2 D_{\text{eff}} \Delta r$:

$$\left[\frac{\left(\frac{dC_A}{dr} \right)_{r+\Delta r} - \left(\frac{dC_A}{dr} \right)_r}{\Delta r} \right] + \frac{2}{r_p} \left(\frac{dC_A}{dr} \right)_{r+\Delta r} - \frac{\rho_p k_m C_A}{D_{\text{eff}}} = 0 \quad (5.72)$$

$$\lim_{\Delta r \rightarrow 0} \left(\frac{\left[\left(\frac{dC_A}{dr} \right)_{r+\Delta r} - \left(\frac{dC_A}{dr} \right)_r \right]}{\Delta r} + \frac{2}{r_p} \left(\frac{dC_A}{dr} \right)_{r+\Delta r} - \frac{\rho_p k_m C_A}{D_{\text{eff}}} \right) = 0 \quad (5.73)$$

$$\frac{d^2 C_A}{dr^2} + \frac{2}{r_p} \frac{dC_A}{dr} - \frac{\rho_p k_m}{D_{\text{eff}}} C_A = 0 \quad (5.74)$$

with the following boundary conditions:

at the center of the pellet: $\frac{dC_A}{dr} = 0$ at $r = 0$

at the outer surface: $C_A = C_{As}$ at $r = r_p$

$$C_A(r) = \frac{r_p}{r} \frac{\sinh\left(3\phi \frac{r}{r_p}\right)}{\sinh(3\phi)} C_{As} \quad (5.75)$$

where

$$\phi = \frac{r_p}{3} \sqrt{\frac{k_m \rho_p}{D_{\text{eff}}}} \quad (5.76)$$

Finally,

$$\eta_s = \frac{1}{\phi} \left(\frac{1}{\tanh(3\phi)} - \frac{1}{3\phi} \right) \quad (5.77)$$

The concentration profile inside a particle is shown in Figure 5.5 for various values of the Thiele modulus.

In Figure 5.6, the effectiveness factor for plate and spherical pellets is plotted against the Thiele modulus.

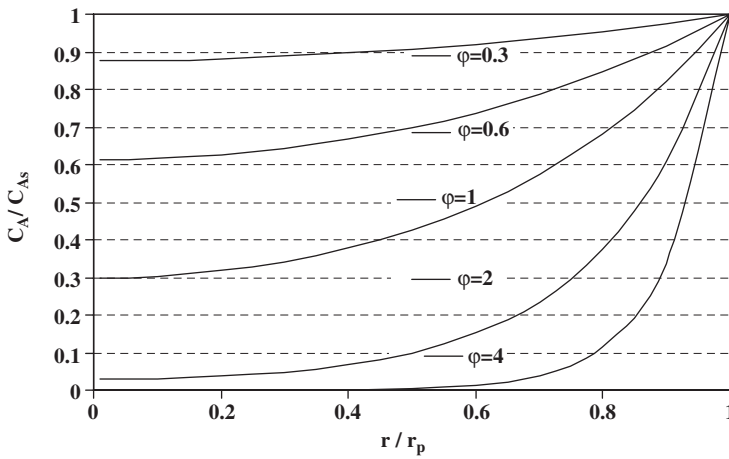


Figure 5.5 The reactant concentration within a catalyst pore as a function of the Thiele modulus.

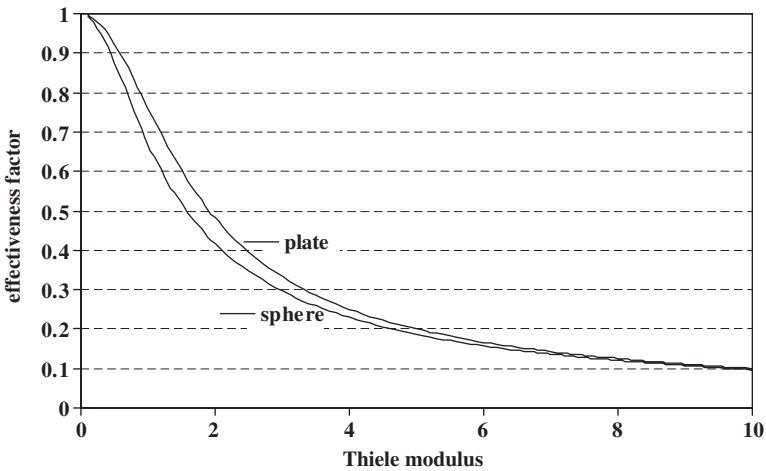


Figure 5.6 The effectiveness factor versus the Thiele modulus for plate and spherical pellets

Weisz and Prater criterion

Weisz and Prater derived a criterion of strong resistance effects inside catalyst particles depending only on the concentration of the feed, catalyst measurables, and the observed rate ($-r_{\text{obs}}$) for a first-order reaction:

No mass transfer resistance inside catalyst particles

$$\frac{(-r_{\text{obs}})L^2}{D_{\text{eff}}C_{\text{Ab}}} < 1 \quad (5.78)$$

Mass transfer resistance inside catalyst particles

$$\frac{(-r_{\text{obs}})L^2}{D_{\text{eff}}C_{\text{Ab}}} > 1 \quad (5.79)$$

Example 1

The oxidation of compound A according to the reaction $A \rightarrow B$ is to be conducted over spherical catalytic particles of radius $r_p = 0.4$ cm. The concentration distribution of A within each particle is described by the relation $C(r) = 4 \times 10^{-4} r^2$ mol/cm⁵, where r is the radial position within the particle. Given that the effective diffusivity $D_{\text{eff}} = (100\pi)^{-1}$ cm²/s, find the rate of the chemical reaction.

Solution

Since the concentration distribution of A within catalytic particles is known, the rate of the chemical reaction can be easily calculated as it is equal to the diffusion rate of A at $r = r_p$. Consequently,

$$r_{\text{obs}} = 4\pi r_p^2 D_{\text{eff}} \left(\frac{dC}{dr} \right)_{r=r_p}$$

Since

$$\left(\frac{dC}{dr} \right)_{r=r_p} = \left(\frac{d(4 \times 10^{-4} r^2)}{dr} \right)_{r=r_p} = 4 \times 10^{-4} \cdot 2 r_p = 3.2 \times 10^{-4} \text{ mol/cm}^4$$

we obtain

$$r_{\text{obs}} = 4\pi \times 0.4^2 \frac{1}{100\pi} 3.2 \times 10^{-4} = 2.048 \times 10^{-6} \text{ mol/s}$$

Example 2

The oxidation of a VOC to carbon dioxide is conducted over a catalytic bed consisting of porous particles with a diameter of 4 mm. The catalyst particles contain Pt as the active component, which is distributed evenly within each particle. It is suggested to use the same particles but with the Pt placed at the external surface of each particle and at a depth up to 1/10 of its diameter so that the activity of the catalyst is increased. If the reaction is first order with respect to the VOC, and on the grounds that the active surface of Pt remains the same in the two cases:

- (a) Estimate the change in the reaction rate.
 (b) How can Pt be saved in the second case if the desired reaction rate is the same as in the first case?

Given $D_{\text{eff}} = 10^{-8} \text{ m}^2/\text{s}$, initial observed reaction rate $r_{\text{vs}} = 10 \text{ mol}/(\text{m}_{\text{cat}}^3 \text{ s})$ for an initial VOC concentration = $10 \text{ mol}/\text{m}^3$.

Solution

- (a) *Case 1:* Pt is evenly distributed within catalytic particles.

$$\eta_s = \frac{\text{actual rate of reaction (with pore diffusion resistance)}}{\text{rate of reaction at surface conditions}}$$

or

$$\eta_s = \frac{r_{\text{observed}}}{r_{\text{intrinsic}}} = \frac{10 \text{ mol}/(\text{m}^3 \text{ s})}{k_{\text{vs}} \times 10 \text{ mol}/\text{m}^3} \Rightarrow \eta_s k_{\text{vs}} = 1 \text{ m}^3/(\text{m}_{\text{cat}}^3 \text{ s})$$

The Thiele modulus for spherical particles, and first-order reaction:

$$\phi = \frac{r_p}{3} \sqrt{\frac{k_m \rho_p}{D_{\text{eff}}}} = \frac{r_p}{3} \sqrt{\frac{k_{\text{vs}}}{D_{\text{eff}}}}$$

where:

$$r_p = 0.002 \text{ m}$$

$$D_{\text{eff}} = 10^{-8} \text{ m}^2/\text{s}$$

$$k_{\text{vs}} = \text{the reaction rate coefficient in s}^{-1}$$

Combining these two equations, we obtain

$$\phi = \frac{r_p}{3} \sqrt{\frac{1}{\eta_s D_{\text{eff}}}} \Leftrightarrow \phi^2 = \frac{r_p^2}{9} \frac{1}{\eta_s D_{\text{eff}}} \Leftrightarrow \eta_s \phi^2 = 44.4$$

If $\phi \gg 5$,

$$\eta_s = \frac{1}{\phi}$$

Substituting in the above equation, we have

$$\phi = 44.4 \quad (\text{our supposition was correct})$$

and finally,

$$\eta_{s1} = \frac{1}{44.4} = 0.022$$

and

$$k_{vs} = \frac{1}{\eta_{s1}} = \frac{1}{0.022} = 44.4 \text{ s}^{-1}$$

Case 2: Pt is evenly distributed within catalytic particles. Pt is placed at the external surface of each particle and at a depth up to 1/10 of its diameter. However, the reaction rate coefficient remains the same, because the surface of Pt is still the same. In this case, the only thing that changes is the volume of each particle available for the reaction. So

$$V_p = \frac{4}{3}\pi r_p^3 - \frac{4}{3}\pi \left(\frac{9}{10}r_p\right)^3 = 9.08 \times 10^{-9} \text{ m}^3$$

$$A_p = 4\pi r_p^2 = 50.24 \times 10^{-6} \text{ m}^2$$

Then, Thiele modulus is

$$\phi = \frac{V_p}{A_p} \sqrt{\frac{k_{vs}}{D_{\text{eff}}}} = \frac{9.08 \times 10^{-9}}{50.24 \times 10^{-6}} \sqrt{\frac{44.4}{10^{-8}}} = 12.04$$

Similar to the first case, we finally obtain

$$\eta_{s2} = 0.08$$

Since the reaction conditions are the same, the intrinsic rate does not change and thus

$$\frac{r_{\text{obs},1}}{r_{\text{obs},2}} = \frac{\eta_{s1}}{\eta_{s2}} \Rightarrow \frac{10}{r_{\text{obs},2}} = \frac{0.022}{0.08} \Rightarrow r_{\text{obs},2} = 36.36 \text{ mol}/(\text{m}^3 \text{ s})$$

or in other words,

$$r_{\text{obs},2} = 3.636 r_{\text{obs},1}$$

It is obvious that the modification of the catalyst led to an increase in the reaction rate by 364%.

- (b) Since the desired rate is the same as in the first case and the reaction conditions are kept the same, the density of Pt on each particle has to be the same for both catalysts:

$$\frac{m_{\text{Pt},1}}{V_{\text{p},1}} = \frac{m_{\text{Pt},2}}{V_{\text{p},2}} \Rightarrow \frac{m_{\text{Pt},2}}{m_{\text{Pt},1}} = \frac{V_{\text{p},2}}{V_{\text{p},1}} = \frac{\frac{4}{3}\pi r_p^3 - \frac{4}{3}\pi\left(\frac{9}{10}r_p\right)^3}{\frac{4}{3}\pi r_p^3} \Rightarrow \frac{m_{\text{Pt},2}}{m_{\text{Pt},1}} = 0.27$$

or

$$m_{\text{Pt},2} = 0.27m_{\text{Pt},1}$$

Obviously, we saved Pt by 73% with the new formulation of the catalyst.

Overall effectiveness factor

It is possible to combine the resistances of internal and external mass transfer through an overall effectiveness factor, for isothermal particles and first-order reaction. Two approaches can be applied. The general idea is that the catalyst can be divided into two parts: its exterior surface and its interior surface. Therefore, the global reaction rates used here are per unit surface area of catalyst.

The reaction takes place within the interior of the particle For a porous catalyst, it can be considered that there is a slight contribution of the exterior surface of the particle to the reaction. Then, the following analysis can be conducted. For the gas film,

$$-\frac{1}{S_{\text{ex}}}\frac{dN_{\text{A}}}{dt} = k_{\text{f}}(C_{\text{b}} - C_{\text{s}}) \quad (5.80)$$

where S_{ex} is the external surface area of catalyst.

Whereas the diffusion and the reaction (first order) inside the particle can be described by

$$-\frac{1}{V_{\text{p}}}\frac{dN_{\text{A}}}{dt} = \eta_{\text{s}}k_{\text{vs}}C_{\text{s}} \quad (5.81)$$

$$C_{\text{s}} = -\frac{1}{\eta_{\text{s}}k_{\text{vs}}V_{\text{p}}}\frac{dN_{\text{A}}}{dt} \quad (5.82)$$

Substituting for C_{s} from eq. (5.82) in eq. (5.81), we obtain

$$-\frac{1}{S_{\text{ex}}}\frac{dN_{\text{A}}}{dt} = \frac{1}{\frac{1}{k_{\text{f}}} + \frac{S_{\text{ex}}}{\eta_{\text{s}}k_{\text{vs}}V_{\text{p}}}}C_{\text{b}} \quad (5.83)$$

based on the external surface area of the particle, or

$$-\frac{1}{V_p} \frac{dN_A}{dt} = \frac{1}{\frac{V_p}{k_f S_{ex}} + \frac{1}{\eta_s k_{vs}}} C_b \quad (5.84)$$

based on the volume of the particle. Special care should be given to units while using these expressions. In the above manipulations, k_f is the mass transfer coefficient based on the exterior surface of the particle, whereas k_{vs} is the reaction rate coefficient based on the volume of the particle. If we define an overall effectiveness factor as

$$\eta_{ov} = \frac{\text{actual overall rate}}{\text{rate that would result if the entire surface were exposed to the bulk concentration } C_b} \quad (5.85)$$

So, for a first-order reaction,

$$\eta_{ov} = \frac{\text{actual overall rate}}{k_{vs} C_b} \quad (5.86)$$

which, for the specific case, results in

$$\eta_{ov} = \frac{\eta_s}{1 + \frac{\eta_s k_{vs} V_p}{k_f S_{ex}}} \quad (5.87)$$

The reaction takes place both on the exterior and within the interior of the particle

When the reaction at the exterior surface area of the catalyst cannot be overlooked, then the following manipulation has to be conducted to determine the reaction rate (Levenspiel, 1972). This is the case when the reaction is so fast that the reactant has little chance to diffuse into the particle.

For the gas film,

$$-\frac{1}{V_p} = \frac{k_f S_{ex}}{V_p} (C_b - C_s) \quad (5.88)$$

whereas the diffusion and the reaction inside the particle can be described from

$$-\frac{1}{V_p} \frac{dN_A}{dt} = \eta_s k_{vs} \frac{S_{in}}{S_{in} + S_{ex}} C_s + k_{vs} \frac{S_{ex}}{S_{in} + S_{ex}} C_s \quad (5.89)$$

where S_{in} is solely the internal surface area of the particle. Note that if $S_{in} \gg S_{ex}$ then we obtain the eq. (5.81).

Finally,

$$-\frac{1}{V_p} \frac{dN_A}{dt} = \frac{1}{\frac{V_p}{k_f S_{ex}} + \frac{1}{\eta_s k_{vs} \left(\frac{S_{in}}{S_{in} + S_{ex}} \right) + k_{vs} \left(\frac{S_{ex}}{S_{in} + S_{ex}} \right)}} C_b \quad (5.90)$$

So, the overall effectiveness factor η_{ov} is

$$\eta_{ov} = \frac{1}{\frac{k_{vs} V_p}{k_f S_{ex}} + \frac{1}{\eta_s \left(\frac{S_{in}}{S_{in} + S_{ex}} \right) + \frac{S_{ex}}{S_{in} + S_{ex}}}} \quad (5.91)$$

and the overall rate can be written as

$$r_{ov} = \eta_{ov} k_{vs} C_b \quad (5.92)$$

5.3 DESIGN OF CATALYTIC REACTORS

In Chapter 3, the reactor models have been presented along with the hydraulic and mass/heat transfer analysis. In the following sections, the solutions of the reactor models are presented along with several examples.

5.3.1 Two-phase agitated reactors

Batch reactors

The integrated form of the material balance for the case of a constant-volume system becomes (Levenspiel, 1972)

$$t = C_i \int_0^x \frac{dx}{(-r_u)} = - \int_{C_i}^{C_0} \frac{dC}{(-r_u)} \quad (5.93)$$

The integrated form of the material balance for the case of a constant-volume system can be expressed in terms of several units (Levenspiel, 1972):

$$\frac{t}{C_i} = \int_0^x \frac{dx}{(-r_u)} = \frac{V_L}{M_S} \int_0^x \frac{dx}{(-r_m)} = \frac{V_L}{S} \int_0^x \frac{dx}{(-r_s)} = \frac{V_L}{V_S} \int_0^x \frac{dx}{(-r_{vs})} = \frac{V_L}{V_R} \int_0^x \frac{dx}{(-R)} \quad (5.94)$$

Note that all rates denote the rate of disappearing of the reactant. For example, for a zero-order reaction (for $t < C_i/k$),

$$C_i x_A = kt \quad (5.95)$$

and for a first-order reaction,

$$-\ln(1 - x_A) = kt \quad (5.96)$$

The integrated form of the BCST material balance for the case of a variable-volume system becomes (Levenspiel, 1972)

$$t = N_{A,i} \int_0^{x_A} \frac{dx_A}{(-r_u)V} = C_{A,i} \int_0^{x_A} \frac{dx_A}{(-r_u)(1 + \varepsilon_R x_A)} \quad (5.97)$$

For example, for a zero-order reaction and a variable-volume system,

$$\frac{C_i}{\varepsilon_R} \ln(1 + \varepsilon_R x_A) = kt \quad (5.98)$$

and for a first-order reaction,

$$-\ln(1 - x_A) = -\ln\left(1 - \frac{\Delta V}{\varepsilon_R V_i}\right) = kt \quad (5.99)$$

Comparing this result with that of a constant-volume system, we see that the fractional conversion at any time is the same in both cases. However, the concentration of materials is not the same.

Continuous flow reactors

The material balance is

$$F_i x_A = (-r_u) V_L \quad (5.100)$$

or

$$\frac{V_L}{F_i} = \frac{\tau}{C_i} = \frac{x_A}{(-r_u)} \quad (5.101)$$

For a constant-volume system,

$$x_A = 1 - \frac{C_o}{C_i} \quad (5.102)$$

and thus

$$\frac{V_L}{F_i} = \frac{C_i - C_o}{C_i(-r_u)} \quad (5.103)$$

For example, for a first-order reaction,

$$k\tau = \frac{x_A}{1 - x_A} \quad (5.104)$$

and for a variable-volume system,

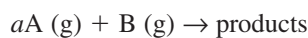
$$k\tau = \frac{x_A(1 + \epsilon_R x_A)}{1 - x_A} \quad (5.105)$$

5.3.2 Slurry bubble column reactors

In the following sections, the solutions of the models as well as various examples will be presented for the case of slurry bubble column reactors.

Gas-phase reactions and batch liquid

Consider the reaction



For a first-order reaction with respect to A, the rate form is

$$(-r_m) = k_m C_{A,s} \quad (5.106)$$

By using the appropriate equations and following the procedure illustrated in Section 3.4.6 for the derivation of the overall rate, we obtain

$$(-r_u)_A = K^\circ C_{AG,z} \quad (5.107)$$

where

$$\frac{1}{K^\circ} \cong H_A \left(\frac{1}{k_{fg} a_{GL}} + \frac{1}{k_f a_c} + \frac{1}{\eta_s m_s k_m} \right) \quad (5.108)$$

Furthermore,

$$(-r_u)_A = a(-r_u)_B \quad (5.109)$$

The equations to be solved are

$$\frac{\tau}{C_{AG,i}} = \int_{x_i}^{x_0} \frac{dx_A}{(-r_u)_A} \quad (5.110)$$

$$\frac{\tau}{C_{BG,i}} = \int_{x_i}^{x_0} \frac{dx_B}{(-r_u)_B} \quad (5.111)$$

For sizing the reactor, the equation for the limiting reactant should be used. For A as the limiting reactant, the corresponding equation becomes

$$\frac{\tau}{C_{AG,i}} = \int_{x_i}^{x_0} \frac{dx_A}{K^\circ C_{AG,z}} = \int_{x_i}^{x_0} \frac{dx_A}{K^\circ C_{AG,i} (1 - x_A)} \quad (5.112)$$

or

$$\tau K^\circ = \int_{x_i}^{x_0} \frac{dx_A}{1 - x_A} \quad (5.113)$$

and the solution for constant-density systems ($\varepsilon_R = 0$) is (Smith, 1981)

$$\tau K^\circ = -\ln \left(1 - \frac{a C_{BG,i}}{C_{AG,i}} x_A \right) \quad (5.114)$$

or

$$x_A = 1 - \exp(-\tau K^\circ) \quad (5.115)$$

Note that a_{GL} , a_c , m_s , and τ are based on the unit volume of bubble-free liquid V_L . The equation remains exactly the same, even if these parameters are expressed per unit volume of reactor V_R .

The conversion of B can be evaluated by using the stoichiometry of the reaction. It is easy to show that if A is the limiting reactant,

$$C_{BG,z} = C_{BG,i} - x_A \frac{C_{AG,i}}{a} \quad (5.116)$$

or

$$x_B = x_A \frac{C_{AG,i}}{aC_{BG,i}} \quad (5.117)$$

In the case of A as limiting reactant and a variable-density system, the solution of the model is the same as for first-order irreversible homogeneous reactions of the form $A \rightarrow \text{products}$ (Levenspiel, 1972):

$$K^\circ \tau = -(1 + \varepsilon_R) \ln(1 - x_A) - \varepsilon_R x_A \quad (5.118)$$

For B as the limiting reactant, we have

$$\frac{\tau}{C_{BG,i}} = \int_{x_i}^{x_0} \frac{dx_B}{(-r_u)_B} = \int_{x_i}^{x_0} \frac{adx_B}{(-r_u)_A} = \int_{x_i}^{x_0} \frac{adx_B}{K^\circ C_{AG,z}} \quad (5.119)$$

Note that the gas phase flows under plug-flow condition, and thus the concentrations of both reactants change with position ($C_{G,z}$). For a constant gas-phase concentration of A, the reaction rate is constant and the reaction term can be drawn out of the integration and the above equation becomes (Smith, 1981)

$$x_B = \frac{\tau K^\circ C_{AG,i}}{aC_{BG,i}} \quad (5.120)$$

This is the case when A is in great excess in the gas mixture.

For a varying gas-phase concentration of A, the exit concentration of A can be evaluated using the stoichiometry of the reaction. It is easy to show that if B is the limiting reactant at each axial position z in the reactor,

$$C_{AG,z} = C_{AG,i} - ax_B C_{BG,i} \quad (5.121)$$

Then

$$\frac{\tau K^\circ}{aC_{BG,i}} = \int_{x_i}^{x_0} \frac{dx_B}{C_{AG,i} - ax_B C_{BG,i}} = \frac{1}{C_{AG,i}} \int_{x_i}^{x_0} \frac{dx_B}{1 - ax_B \frac{C_{BG,i}}{C_{AG,i}}} \quad (5.122)$$

For $\varepsilon_R = 0$, the solution is

$$\frac{\tau K^\circ}{aC_{BG,i}} = \frac{1}{C_{AG,i}} \left[-\frac{C_{AG,i}}{aC_{BG,i}} \ln \left(1 - \frac{aC_{BG,i}}{C_{AG,i}} x_B \right) \right] \quad (5.123)$$

Thus

$$\tau K^\circ = -\ln \left(1 - \frac{aC_{BG,i}}{C_{AG,i}} x_B \right) \quad (5.124)$$

or

$$x_B = \frac{C_{AG,i}}{aC_{BG,i}} [1 - \exp(-\tau K^\circ)] \quad (5.125)$$

Here, note that

$$x_B \frac{aC_{BG,i}}{C_{AG,i}} = x_A \quad (5.126)$$

as expected. Although the solutions irrespective of the limiting reactant are the same, it has to be pointed out that the sizing of the reactor is based on the limiting reactant or, in other words, on the conversion of the limiting reactant.

Example 3

Consider the gas-phase reaction



If the feed is equimolar, derive the reactor model and express it as a function of the total pressure.

Solution

If $a = 1$, $\varepsilon_R \neq 0$ and the feed is considered to be equimolar, the number of moles of each component at a conversion level of x is the following: $A = F_A (1 - x)$, $B = F_A (1 - x)$, $C = F_A x$, and the total number of moles $= F_A (2 - x)$. At inlet conditions $x = 0$,

$$C_{G,i} = \frac{1}{2} \frac{P_{\text{total}}}{RT}$$

The parameter ε_R is

$$\varepsilon_R = \frac{F_A - 2F_A}{2F_A} = -\frac{1}{2}$$

Then

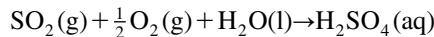
$$K^\circ \tau = \frac{1}{2} [x - \ln(1 - x)]$$

Finally,

$$\frac{\tau}{C_{G,i}} = \frac{V_L}{F_A} = \frac{1}{K^\circ} \frac{RT}{P_{\text{total}}} [x - \ln(1 - x)]$$

Example 4

The removal of sulfur dioxide from air has been studied by Komiyama and Smith (1975) in an agitated slurry reactor using activated carbon particles as catalyst at 25 °C and 1 atm. The gas stream consisted of 2.3% SO₂ and 21% oxygen, and pure water was used as liquid phase. Activated carbon catalyses the oxidation of SO₂ to SO₃, which dissolves in the water to produce H₂SO₄:



The intrinsic rate of the reaction is controlled by the rate of adsorption of oxygen on the carbon and is independent of the SO₂ concentration.

The following data have been given by Komiyama and Smith: particle size = 0.03 mm, particle density = 800 kg/m³, effectiveness factor = 0.861, and $k_{vs} = 6.6 \text{ m}^3/\text{m}^3\text{s}$.

Suppose that the reaction takes place in a slurry bubble column and that it is desirable to work in the heterogeneous flow regime. Moreover, assume that the liquid is batch and well mixed and the flow of the gas approximates the ideal plug flow.

Komiyama and Smith have studied the reaction using He as the carrier gas. However, for the purposes of the example, suppose that the intrinsic reaction constant is not affected by the carrier gas, which is the nitrogen in our case. This is reasonable as both gases are inert. Assume also zero expansion.

Design a slurry bubble column reactor and estimate its performance for catalyst loading of 20 kg/m^3 of reactor (2% catalyst loading).

Solution

The first step in the solution of the example is the design of the reactor, which will determine its hydraulic parameters and thus the mass transfer coefficients, which are an input in the model of the reactor.

Hydraulic analysis: Using Figure 3.27, the appropriate gas superficial velocity and the column diameter for the heterogeneous flow regime can be selected. An appropriate choice for the reactor diameter and the superficial gas velocity is 0.5 m and 0.1 m/s, respectively. The height to diameter ratio in columns is greater than unity and a value of 5 is reasonable. Therefore, the value of 2.5 m has been selected for the column height. As a result, the reactor volume is equal to 0.49 m^3 . This volume is occupied by the reaction mixture, which is the gas, the liquid, and the solid phase.

For the specific catalyst loading per reactor volume $m_{s,\text{tot}}$, the mass of catalyst is

$$M_s = m_{s,\text{tot}} V_R = 9.81 \text{ kg}$$

and its volume is

$$V_s = \frac{M_s}{\rho_p} = 0.012 \text{ m}^3$$

The gas volume can be determined by the gas holdup. Using the Akita–Yoshida correlation (3.161) and using a trial-and-error procedure, the gas holdup is $h_G = 0.17$ ($n = 0.2$). The gas volume is

$$V_G = h_G V_R = 0.081 \text{ m}^3$$

The use of the Akita–Yoshida correlation is justified since the catalyst loading is very low (2%), and the effect of the solids on gas holdup is expected to be minimal. The liquid volume is simply

$$V_L = V_R - V_s - V_G = 0.397 \text{ m}^3$$

and the liquid holdup is (eq. (3.169))

$$h_L = \frac{V_L}{V_R} = 0.81$$

As has been analyzed, the basic model for bubble column assumes complete mixed flow for the liquid phase and plug flow for the gas phase. The Deckwer *et al.* correlation (3.202) for the liquid phase and the Field and Davidson equation (3.206) for the gas phase can be used for the estimation of the dispersion coefficient. The resulting coefficients are $D_{LL} = 0.09 \text{ m}^2/\text{s}$ and $D_{LG} = 0.49 \text{ m}^2/\text{s}$.

Concerning the liquid phase, the dispersion coefficient is well above the value of $0.01 \text{ m}^2/\text{s}$ for liquids, which is considered to be indicative of good mixing conditions. Although the gas dispersion coefficient is much higher, this does not mean that the mixing in this phase is higher. By analogy to fixed beds, the degree of mixing depends on the dispersion coefficient as well as the velocity of the flowing phase. For plug flow, we need a low dispersion coefficient and a high fluid velocity. In our case, the liquid is batch, while the gas flows with a superficial velocity of 10 cm/s .

Here, it has to be noted that for calculating the Peclet number in fixed beds, the actual velocity has to be used, i.e. the interstitial velocity, which influences the degree of mixing. In slurry bubble column reactors, the real velocity of the fluid is the bubble velocity, which is much higher than the gas superficial velocity. The mean bubble rise velocity for a batch liquid is (eq (3.201))

$$u_{\text{bub}} = \frac{u_{\text{sG}}}{h_G} = 60 \text{ cm/s}$$

By using Fukuyama correlation (3.188), the bubble diameter is

$$d_{\text{bub}} = \frac{0.59}{g} \left(\frac{\gamma}{h_G} \right)^2 = 0.0153 \text{ m}$$

where, for a batch liquid (eq. (3.189)),

$$\gamma = u_{\text{sG}}(1 - h_G) = 0.083$$

Using the correlation of Mendelson (3.191), the single bubble rising velocity is calculated as 29 cm/s .

Mass transfer coefficients: The liquid–solid mass transfer coefficient can be evaluated by using the correlation of Sano *et al.* (eq. (3.211)): $k_f = 4.22 \times 10^{-4} \text{ m/s}$, whereas the corresponding interfacial area is (eq. (3.218))

$$a_c = \frac{6m_s}{d_p \rho_p}$$

Note that the $m_{s,\text{tot}}$ is known, i.e. the catalyst loading per unit volume of reactor. Its value per unit volume of liquid is

$$m_s = \frac{m_{s,\text{tot}}}{h_L} = \frac{20}{0.81} = 24.70 \text{ kg/m}^3$$

and thus, $a_c = 6175 \text{ m}^2/\text{m}^3 \text{ liquid}$.

The gas–liquid mass transfer coefficient is calculated using the correlation of Yasunishi (eq. (3.223)), with

$$\varphi_s = \frac{V_s}{V_L + V_s} = \frac{0.012}{0.397 + 0.012} = 0.03$$

calculated by using eq. (3.172). Then, $k_{fg}a_{GL,\text{tot}} = 0.10 \text{ s}^{-1}$. This coefficient can also be expressed per unit volume of liquid by using eq. (3.230):

$$k_{fg}a_{GL} = \frac{k_{fg}a_{GL,\text{tot}}}{h_L} = \frac{0.10}{0.81} = 0.13 \text{ s}^{-1}$$

Reactor model: The overall coefficient K° is (eq. (3.144))

$$\frac{1}{K^\circ} \cong H_A \left(\frac{1}{k_{fg}a_{GL}} + \frac{1}{k_r a_c} + \frac{1}{\eta_s m_s k_m} \right)$$

where for the specific temperature $H_A = 32.07$ (Annex I, Section I.3.2). Furthermore, from eq. (3.10),

$$k_m = \frac{k_{vs}}{\rho_p} = 8.25 \times 10^{-3} \text{ m}^3/\text{kg s}$$

then $K^\circ = 2.25 \times 10^{-3} \text{ s}^{-1}$. One more input is needed for the model, which is the inlet concentration of the reactants. By using the ideal gas law, the concentration of oxygen is found to be $8.59 \times 10^{-6} \text{ mol/cm}^3$ and that of sulfur dioxide $9.41 \times 10^{-7} \text{ mol/cm}^3$.

The limiting reactant is SO_2 and the expansion factor is zero. Then using eq. (5.125),

$$x_B = \frac{C_{AG,i}}{aC_{BG,i}} [1 - \exp(-\tau K^\circ)] = 0.81$$

or 81% (A: O_2 , B: SO_2 , and $a = 0.5$). Furthermore, from eq. (5.126),

$$x_A = x_B \frac{aC_{BG,i}}{C_{AG,i}} = 0.04$$

or 4%. Assuming constant oxygen concentration and using the simplified model (eq. (5.120)) we obtain

$$x_B = \frac{\tau K^\circ C_{AG,i}}{a C_{BG,i}} = 0.83$$

which is somewhat higher than the actual conversion, as expected.

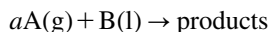
A few comments: Sulfur dioxide (SO₂) is a gas produced by volcanoes and from many industrial processes. It is sometimes used as a preservative in alcoholic drinks, or dried apricots and other fruits. Generally, the combustion of fossil fuels containing sulfur compounds such as coal and petroleum results in sulfur dioxide being emitted into the atmosphere. Beyond its irritating effect on the lungs, sulfur dioxide is also a threat to the environment, since it is well known to contribute to acid-rain formation.

Gas-liquid reactions and batch liquid

The following analysis is valid for

- slurry bubble bed column and agitated slurry reactor under the same conditions,
- packed bubble bed reactor or trickle-bed reactor under complete recycling of the liquid stream.

In the analysis given below, the following form of reaction is considered:



Constant gas-phase concentration and first-order reaction in respect to gas reactant

By using the appropriate equations and following the procedure illustrated in Section 3.4.6, for a first-order reaction with respect to A, we have

$$(-r_u)_A = K^\circ C_{AG} \quad (5.127)$$

where

$$\frac{1}{K^\circ} \cong H_A \left(\frac{1}{k_{fg} a_{GL}} + \frac{1}{k_f a_c} + \frac{1}{\eta_s m_s k_m} \right) \quad (5.128)$$

The equation to be solved is

$$(-r_u)_B = \frac{(-r_u)_A}{a} = C_{BL,i} \frac{dx_B}{dt} \quad (5.129)$$

or

$$\frac{K^\circ C_{AG}}{a} = C_{BL,i} \frac{dx_B}{dt} \quad (5.130)$$

The solution is (Ramachandran and Chaudhari, 1980)

$$t = \frac{aC_{BL,i}x_B}{K^\circ C_{AG}} = \frac{aC_{BL,i}x_B}{\left(C_{AG}/H_A\right)} \left(\frac{1}{k_{fg}a_{GL}} + \frac{1}{k_f a_c} + \frac{1}{\eta_s m_s k_m} \right) \quad (5.131)$$

or in another useful form,

$$x_B = \frac{K^\circ C_{AG}}{aC_{BL,i}} t \quad (5.132)$$

Note that a_{GL} , a_c , and m_s are based on the unit volume of bubble-free liquid V_L . If the parameters per unit volume of reactor V_R are used in this equation instead, then the right-hand side of eq. (5.131) should be multiplied with the liquid holdup h_L , or in terms of liquid and reactor volume,

$$t = \frac{V_L}{V_R} \frac{aC_{BL,i}x_B}{\left(C_{AG}/H_A\right)} \left(\frac{1}{k_{fg}a_{GL,tot}} + \frac{1}{k_f a_{c,tot}} + \frac{1}{\eta_s m_{s,tot} k_m} \right) \quad (5.133)$$

where the parameters in the parenthesis are based on the reactor volume. If the liquid phase is saturated with the gas reactant,

$$(-r_u)_B = \frac{(-r_u)_A}{a} = C_{BL,i} \frac{dx_B}{dt} \quad (5.134)$$

or

$$\frac{k^\circ C_{AG}}{aH_A} = C_{BL,i} \frac{dx_B}{dt} \quad (5.135)$$

and the solution is

$$t = \frac{aC_{BL,i}H_A x_B}{k^\circ C_{AG}} = \frac{aC_{BL,i}x_B}{\left(C_{AG}/H_A\right)} \left(\frac{1}{k_f a_c} + \frac{1}{\eta_s m_s k_m} \right) \quad (5.136)$$

Based on the reactor volume,

$$t = \frac{V_L}{V_R} \frac{aC_{BL,i}x_B}{\left(C_{AG}/H_A\right)} \left(\frac{1}{k_f a_{c,tot}} + \frac{1}{\eta_s m_s k_m} \right) \quad (5.137)$$

or in another useful form,

$$x_B = \frac{k^\circ C_{AG}}{aH_A C_{BL,i}} t \quad (5.138)$$

Note that in contrast to the Ramachandran and Chaudhari solution, the resistance of the gas–liquid interface is missing. This was expected as the liquid is saturated with the gas reactant.

For the special case of variable gas-phase concentration and zero expansion, the solution (eq. (5.131)) becomes (Ramachandran and Chaudhari, 1980)

$$t = \frac{aC_{BL,i}x_B}{K^\circ C_{AG}} = \frac{aC_{BL,i}x_B}{\left(C_{AG,i}/H_A\right)} \left(\frac{1}{\lambda} + \frac{1}{k_f a_c} + \frac{1}{\eta_s m_s k_m} \right) \quad (5.139)$$

where

$$\lambda = \frac{H_A Q_G}{V_R} \left[1 - \exp\left(-\frac{K_L a_{GL} Z}{u_{sG} H_A}\right) \right] \quad (5.140)$$

Note that the initial gas-phase concentration $C_{AG,i}$ is found in the solution. In the case of constant gas-phase concentration or if the gas is sparingly soluble even if its concentration is variable,

$$\lambda = k_{fg} a_{GL} \quad (5.141)$$

and the solution becomes identical to eq. (5.131).

Constant gas-phase concentration and first-order reaction in respect to liquid reactant

By using the appropriate equations and following the procedure illustrated in Section 3.4.6, for a first-order reaction with respect to B,

$$(-r_u)_B = (k_f a_c)_B [C_{BL} - C_{BS}] = m_s \eta_s k_m C_{BS} \quad (5.142)$$

or

$$C_{BS} = \frac{(k_f a_c)_B}{(k_f a_c)_B + m_s \eta_s k_m} C_{BL} \quad (5.143)$$

and thus

$$(-r_u)_B = m_s \eta_s k_m \frac{(k_f a_c)_B}{(k_f a_c)_B + m_s \eta_s k_m} C_{BL} = k^\circ C_{BL} \quad (5.144)$$

where

$$k^\circ = \frac{(k_f a_c)_B m_s \eta_s k_m}{(k_f a_c)_B + m_s \eta_s k_m} \Leftrightarrow \frac{1}{k^\circ} = \frac{1}{(k_f a_c)_B} + \frac{1}{m_s \eta_s k_m} \quad (5.145)$$

The equation to be solved is

$$(-r_u)_B = -\frac{dC_B}{dt} \quad (5.146)$$

or

$$k^\circ C_{BL} = -\frac{dC_B}{dt} \quad (5.147)$$

The solution is

$$\frac{C_{BL}}{C_{BL,i}} = \exp(-k^\circ t) \quad (5.148)$$

In terms of fractional removal of B:

$$x_B = \frac{C_{BL,i} - C_{BL}}{C_{BL,i}} = 1 - \exp(-k^\circ t) \quad (5.149)$$

or

$$t = \frac{1}{k^\circ} \ln \left(\frac{1}{1 - x_B} \right) = \left(\frac{1}{(k_f a_c)_B} + \frac{1}{m_s \eta_s k_m} \right) \ln \left(\frac{1}{1 - x_B} \right) \quad (5.150)$$

Based on the reactor volume:

$$t = \frac{V_L}{V_R} \frac{1}{k^\circ} \ln \left(\frac{1}{1 - x_B} \right) \quad (5.151)$$

Note that the parameter V_L/V_R in a slurry reactor is the fractional liquid holdup. In the packed bubble bed reactor and the trickle-bed reactor, under complete recycling of the liquid stream, V_L/V_R is the ratio of total volume of the liquid that is processed (recycled) to the volume of reactor, and is always greater than 1. By recycling, it is possible to process a larger volume of liquid than the reactor volume by having a surge tank in the recycle line.

Finally, note that in the solution (5.151) all the involved reactor parameters should be based on the reactor volume.

5.3.3 Agitated slurry reactors

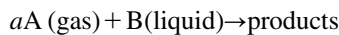
In the following sections, the solutions of the models as well as examples will be presented for the case of slurry agitated reactors.

Gas–liquid reactions and continuous flow of both phases

The following analysis is valid for

- Slurry agitated reactor for continuous flow of both phases (CSTR conditions)
- Slurry bubble bed column under complete mixing of both phases
- Packed bubble bed reactor under complete mixing of both phases.

General solution The overall catalytic reaction is



For a first-order reaction with respect to A,

$$(-r_u)_A = (k_f a_c)_A [C_{AL,o} - C_{AS}] = m_s \eta_s k_m C_{AS} \quad (5.152)$$

or

$$C_{AS} = \frac{(k_f a_c)_A}{(k_f a_c)_A + m_s \eta_s k_m} C_{AL,o} \quad (5.153)$$

and thus

$$(-r_u)_A = m_s \eta_s k_m \frac{(k_f a_c)_A}{(k_f a_c)_A + m_s \eta_s k_m} C_{AL,o} = k^\circ C_{AL,o} \quad (5.154)$$

where

$$k^\circ = \frac{(k_f a_c)_A m_s \eta_s k_m}{(k_f a_c)_A + m_s \eta_s k_m} \leftrightarrow \frac{1}{k^\circ} = \frac{1}{(k_f a_c)_A} + \frac{1}{m_s \eta_s k_m} \quad (5.155)$$

The solution of the model is

$$C_{AG,o} = C_{AG,i} \frac{\frac{Q_L}{V_L} + (K_L \alpha_{GL}) + k^\circ + \xi}{\frac{Q_L}{V_L} + (K_L \alpha_{GL}) + k^\circ + \psi} \quad (5.156)$$

$$\psi = \frac{(K_L \alpha_{GL})}{H_A} \frac{V_L}{Q_G} \left(\frac{Q_L}{V_L} + k^\circ \right) \quad (5.157)$$

$$\xi = \frac{(K_L \alpha_{GL})}{C_{AG,i}} \frac{Q_L}{V_L} C_{AL,i} \quad (5.158)$$

$$C_{AL,o} = \frac{\left(\frac{Q_L}{V_L} \right) C_{AL,i} + \frac{C_{AG,o}}{H_A} (K_L \alpha_{GL})}{\left(\frac{Q_L}{V_L} \right) + (K_L \alpha_{GL}) + k^\circ} \quad (5.159)$$

$$C_{BL,o} = \frac{\left(\frac{Q_L}{V_L} \right) C_{BL,i} - \left(\frac{k^\circ C_{AL,o}}{a} \right)}{\left(\frac{Q_L}{V_L} \right)} \quad (5.160)$$

Note that a_{GL} , a_c , m_s , and Q_i/V_i are based on the unit volume of bubble-free liquid V_L . If parameters per unit volume of reactor V_R are used instead in the above equations, then the term ξ should be divided by the liquid holdup h_L .

Constant gas-phase concentration Under the limiting condition of constant gas-phase concentration and for a first-order reaction with respect to A, the general solution is reduced to (Ramachandran and Chaudhari, 1980)

$$C_{AL,o} = \frac{\left(\frac{Q_L}{V_L} \right) C_{AL,i} + \frac{C_{AG,o}}{H_A} (K_L \alpha_{GL})}{\left(\frac{Q_L}{V_L} \right) + (K_L \alpha_{GL}) + k^\circ} \quad (5.161)$$

$$C_{\text{BL,o}} = \frac{\left(\frac{Q_L}{V_L}\right) C_{\text{BL,i}} - \left(\frac{k^\circ C_{\text{AL,o}}}{a}\right)}{\left(\frac{Q_L}{V_L}\right)} \quad (5.162)$$

where

$$k^\circ = \frac{(k_f a_c)_A m_s \eta_s k_m}{(k_f a_c)_A + m_s \eta_s k_m} \Leftrightarrow \frac{1}{k^\circ} = \frac{1}{(k_f a_c)_A} + \frac{1}{m_s \eta_s k_m} \quad (5.163)$$

For a first-order reaction with respect to B, we have

$$\frac{Q_L}{V_L} (C_{\text{BL,i}} - C_{\text{BL,o}}) - (k_f a_c)_B (C_{\text{BL,o}} - C_{\text{BS}}) = 0 \quad (5.164)$$

Component mass balance around the catalyst is

$$(k_f a_c)_B [C_{\text{BL,o}} - C_{\text{BS}}] = (-r_u)_B = m_s r_m = m_s k_m C_{\text{BS}} \quad (5.165)$$

Then

$$k^\circ = \frac{(k_f a_c)_B m_s \eta_s k_m}{(k_f a_c)_B + m_s \eta_s k_m} \Leftrightarrow \frac{1}{k^\circ} = \frac{1}{(k_f a_c)_B} + \frac{1}{m_s \eta_s k_m} \quad (5.166)$$

The solution is (Ramachandran and Chaudhari, 1984)

$$C_{\text{BL,o}} = \frac{C_{\text{BL,i}}}{k^\circ \left(\frac{V_L}{Q_L}\right) + 1} \quad (5.167)$$

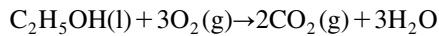
or

$$x_B = \frac{k^\circ \left(\frac{V_L}{Q_L}\right)}{k^\circ \left(\frac{V_L}{Q_L}\right) + 1} \quad (5.168)$$

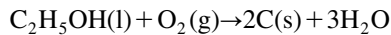
Note that a_{GL} , a_c , m_s , and Q_i/V_i are based on the unit volume of bubble-free liquid V_L . The equation remains exactly the same if parameters per unit volume of reactor V_R are used instead in the above solution.

Example 5

The catalytic oxidation of ethanol is catalyzed by Pd–Al₂O₃ at 30 °C, and is considered to be of first order with respect to oxygen (Hopper *et al.*, 2001; Ramachandran and Chaudhari, 1980). The rate constant for this reaction is $k_m = 0.0177 \text{ cm}^3/(\text{g s})$. The complete oxidation of ethanol is represented by the following reaction:



However, Hopper *et al.* (2001) as well as Ramachandran and Chaudhari (1980) considered that the stoichiometric coefficient of oxygen is unity, and thus the oxidation of ethanol can be considered to be as follows:



Estimate the conversion of ethanol in a CSTR with continuous flow of slurry and gas and rigorous agitation. The volume of the tank is 69.78 L.

Suppose that a flat-blade disk turbine with six blades is used and the agitation rate is 800 rpm. For the other characteristics of the tank assume a typical design configuration.

The following data are given: gas flow rate = 3140 cm³/s, liquid flow rate = 62.8 cm³/s, ethanol inlet concentration = $4 \times 10^{-4} \text{ mol/cm}^3$, oxygen pressure = 35.5 atm, molecular diffusivity of oxygen in water = $4.7 \times 10^{-5} \text{ cm}^2/\text{s}$, catalyst load $m_s = 0.1 \text{ g/cm}^3_{\text{liquid}}$, effectiveness factor = 0.8, catalyst particle size = 0.05 cm, and particle density = 1200 kg/m³. The inlet oxygen concentration in the liquid phase is zero. Under the specified conditions, assume that the expansion of the gas phase is zero.

Solution

The first step in the solution of the example is the design of the agitated tank, which will determine its hydraulic parameters and thus the mass transfer coefficients, which are an input in the model of the reactor.

The volume of the tank is 69.78 L. However, for safety reasons (e.g. overflow due to vortex formation), we should use a part of this volume for the reaction mixture, let's say 90%, i.e. 62.8 L. This volume is what we call “reactor volume” when analyzing slurries, i.e. it is the reaction volume, which is the sum of the liquid, gas, and solids volume.

Hydraulic analysis: Thus, we suppose a typical design for the agitated tank which means that (Table 3.3)

$$D_T = H_L$$

and

$$D_a = \frac{D_T}{3}$$

For this calculation, we use the height of the liquid in liquid–solid systems. However, in three-phase systems we should use the height of the slurry, and thus the volume of the reactor. Note that the reactor volume is the sum of the liquid, gas, and solids volume. The tank diameter can be calculated from the reactor volume (eq. (3.113)):

$$D_T = \left(\frac{4V_R}{\pi} \right)^{1/3} = 0.43 \text{ m}$$

Then, the impeller diameter is $D_a = 0.14 \text{ m}$. Having the tank dimensions and the rotational speed, we can evaluate the Reynolds number (eq. (3.104)):

$$N_{Re} = \frac{D_a^2 N \rho}{\mu} = 3.06 \times 10^5$$

and thus the power number N_p of the given impeller is 5.75 (Table 3.4). The power needed is (eq. (3.107))

$$P = N_p \rho N^3 D_a^5 = 833.09 \text{ W}$$

and the energy of dissipation per unit mass of liquid can be evaluated from eq. (3.256):

$$\varepsilon_o = \frac{P}{M_L}$$

At this point, we need the mass of liquid M_L and thus its volume V_L , which is not known. So, we have to assume a value of its volume or in other words we have to assume a value for the fractional liquid holdup h_L . Then,

$$V_L = h_L V_R$$

where V_R is the reactor volume, which is known. Because we have gas injection in the liquid, the energy of dissipation per unit mass of liquid in a fully baffled agitated system in turbulent flow is given by eq. (3.257):

$$\bar{\varepsilon} = \varepsilon_o \varphi$$

where φ is a correction factor (eq. (3.259)):

$$\frac{Q_G}{ND_a^3} = 7.95 \times 10^{-2} > 3.5 \times 10^{-2}$$

$$\varphi = 0.62 - 1.85 \frac{Q_G}{ND_a^3} = 0.47$$

This correlation has been suggested for gas–liquid systems. In the presence of solids, in three-phase systems, the energy of dissipation can be approximately 25–50% higher depending on the loading and density of particles (Ramachandran and Chaudhari, 1984). Here, we use the average value of 37.5% and thus

$$\bar{\varepsilon} = 1.375\varepsilon_0\phi$$

Having all these parameters of the system, we can evaluate the gas holdup h_G by using the Calderbank equation (3.260). At this point, we have to check if the assumed fractional liquid holdup corresponds to the real one, which is

$$h_L = \frac{V_L}{V_R}$$

where

$$V_L = V_R - V_G - V_S$$

The volume of gas is

$$V_G = h_G V_R$$

while the volume of solids is

$$V_S = \frac{m_s V_L}{\rho_p}$$

It is obvious that we need a trial-and-error procedure. A good approximation for slurry reactors is a fractional liquid holdup of 85%. This value can be used to initiate the iteration procedure. At first we assume a value of the liquid fractional holdup h_L , and thus the values of liquid volume V_L , mass volume M_L , and solids volume V_S are known. Then, we can evaluate the parameters ε_0 and $\bar{\varepsilon}$. Note that at this point, the procedure is complicated due to one more trial-and-error procedure associated with the evaluation of gas fractional holdup h_G (eq. (3.260)). After the evaluation of h_G , the gas volume V_G is known. Then we can re-evaluate the liquid volume ($V_L = V_R - V_G - V_S$) and compare it with the assumed value. The iteration continues until these two values are the same.

The trial-and-error results are given in Table 5.7.

In the above analysis, we used Calderbank's equation for the determination of gas holdup. This correlation has been derived for gas–liquid systems. However, as in the case of slurry bubble columns, the presence of solids is not expected to alter the gas holdup significantly,

Table 5.7

Trial-and-error procedure results	
Parameter	Value
$\bar{\varepsilon}$ (m ² /s ³)	11.21
h_G (m ³ /m ³)	0.17
V_G (m ³)	10.44
V_S (m ³)	4.03
V_L (m ³)	48.33
h_L (m ³ /m ³)	0.77

at least for such a low solid loading (6.5% of the total reactor volume). The same holds for the effect of liquid flow, as its flow rate is low (2% of the gas flow rate).

Mass transfer coefficients: The liquid–solid mass transfer coefficient can be evaluated by means of the correlation of Sano *et al.* (eq. (3.266)):

$$\frac{k_f d_p}{D_f} = 2 + 0.4 \left(\frac{\bar{\varepsilon} d_p^4 \rho_L^3}{\mu_L^3} \right)^{0.25} \left(\frac{\mu_L}{\rho_L D_f} \right)^{1/3} \Rightarrow k_f = 6.97 \times 10^{-4} \text{ m/s}$$

and the gas–liquid mass transfer coefficient is (eq. (3.268))

$$k_{fg} = 0.592 D_{fg}^{0.5} \left(\frac{\bar{\varepsilon}}{v_L} \right)^{0.25} = 2.41 \times 10^{-3} \text{ m/s}$$

The corresponding interfaces per unit volume of reactor are (eq. (3.219))

$$a_{c,\text{tot}} = \frac{6m_s}{d_p \rho_p} h_L = 769.64 \text{ m}^2/\text{m}^3$$

and from eq. (3.229),

$$a_{GL,\text{tot}} = \frac{6}{d_{\text{bub}}} h_G = 965.79 \text{ m}^2/\text{m}^3$$

where the bubble diameter has been evaluated to be 1.01 mm by using the Calderbank equation (3.263).

Reactor model: Since we have at hand the mass transfer per volume of reactor, we can use the model equations as presented in the previous paragraphs by expressing the involved

parameters per unit volume of reactor and using the volume of the reactor instead of the volume of the liquid. The only modification is that the parameter ζ should be divided by the liquid hold up h_L . To determine the coefficient k^o , the catalyst loading per unit volume of reactor is needed, which is

$$m_{s,\text{tot}} = m_s h_L = 76.96 \text{ kg/m}^3$$

Then, from eq. (5.155), $k^o = 1.09 \times 10^{-3} \text{ s}^{-1}$. One more input is needed for the model, which is the dimensionless Henry's constant for oxygen at 30 °C. Henry's constant is estimated by using the IAPWS correlation (see Section I.3.2 in Appendix I) and is $H = 34.03$. Then, by using model equations (5.156)–(5.160), we have $\psi = 2.66 \times 10^{-3}$ and $\xi = 0$ and thus the conversion of ethanol is found to be equal to 10.8%. The exit concentrations in both phases are shown in Table 5.8.

Table 5.8

The exit concentrations

Gas-phase concentration of oxygen ($C_{AG,o}$, mol/m ³)	1427.05
Liquid-phase concentration of oxygen ($C_{AL,o}$, mol/m ³)	41.90
Liquid-phase concentration of ethanol ($C_{BL,o}$, mol/m ³)	374.43

A few comments: Beyond water, ethanol is perhaps the most commonly used solvent in chemistry. It has also been used extensively in some countries as fuel. As a result, its presence in the environment, aquatic and atmospheric, is increased. Ethanol in great doses has been recognized as a human teratogen, well before experimental studies in animals were undertaken. However, the consumption of alcohol via drinks and beverages covers any adverse effects due to ethanol's presence in the environment.

Gas–liquid reactions and batch liquid

In this case, the solutions derived for the slurry bubble column reactor are applicable.

Gas-phase reactions and batch liquid Consider the reaction



Using the appropriate equations and following the procedure illustrated in Section 3.4.6 for first-order reaction with respect to A, we have

$$(-r_u)_A = K^o C_{AG,o} \quad (5.169)$$

where

$$\frac{1}{K^\circ} \cong H_A \left(\frac{1}{k_{fg} a_{GL}} + \frac{1}{k_f a_c} + \frac{1}{\eta_s m_s k_m} \right) \quad (5.170)$$

The equations to be solved are

$$\frac{\tau}{C_{AG,i}} = \frac{x_A}{(-r_u)_A} \quad (5.171)$$

$$\frac{\tau}{C_{B,i}} = \frac{x_B}{(r_u)_B} = \frac{ax_B}{(-r_u)_A} \quad (5.172)$$

The solution of the model for a first-order irreversible reaction is the same as that of homogeneous reactions ($\varepsilon_R = 0$) (Levenspiel, 1972):

$$\frac{K^\circ \tau}{C_{G,i}} = \frac{x_A}{C_{G,i}(1-x_A)} \quad (5.173)$$

or

$$x_A = \frac{K^\circ \tau}{1 + K^\circ \tau} \quad (5.174)$$

and

$$x_B = \frac{K^\circ \tau}{a} \frac{C_{AG,o}}{C_{BG,i}} \quad (5.175)$$

or

$$x_B = \frac{K^\circ \tau}{1 + K^\circ \tau} \frac{C_{AG,i}}{a C_{BG,i}} = x_A \frac{C_{AG,i}}{a C_{BG,i}} \quad (5.176)$$

If A or B is the limiting reactant, then by setting $x_A = 1$ or $x_B = 1$ the maximum residence time τ needed for complete conversion can be evaluated. This value can be used to determine the maximum conversion of the nonlimiting reactant. In any case, the equation of the limiting reactant is used for sizing the reactor.

If the gas-phase concentration of A is constant,

$$x_B = \frac{K^\circ \tau C_{AG,i}}{a C_{BG,i}} \quad (5.177)$$

If A is the limiting reactant and for the general case of $\varepsilon_R \neq 0$, the solution is

$$\frac{K^\circ \tau}{C_{AG,i}} = \frac{x_A(1 + \varepsilon_R x_A)}{C_{AG,i}(1 - x_A)} \quad (5.178)$$

Note that a_{GL} , a_c , m_s , and τ are based on the unit volume of bubble-free liquid V_L . The equation remains exactly the same if parameters per unit volume of reactor V_R are used instead in the above solution.

5.3.4 Fixed-bed reactor

The basic equations that describe fixed-bed reactors have been presented in Section 3.6.2. In the present Section Isothermal, Adiabatic and Non-isobaric fixed bed operations as well as the case of Monolithic catalysts are presented.

It is common for the volume of reactor V_R to be replaced by the catalyst weight W in catalytic reactors. The surface area of the catalyst could also be used, but since it is much harder to determine than its weight, it is common in industry to give catalytic reaction rates per catalyst weight. Keep in mind that

$$V_R = \frac{W}{\rho_b} \quad (5.179)$$

where ρ_b is the bulk density of the catalyst.

For constant superficial velocity (zero expansion factor) and negligible pressure drop (see the subsection Nonisobaric fixed-bed operation), the general mass and thermal energy continuity equations for the catalytic fixed-bed reactor are

$$\varepsilon \frac{\partial C}{\partial t} - D_L \frac{\partial^2 C}{\partial z^2} - D_R \left(\frac{\partial^2 C}{\partial r^2} + \frac{1}{r} \frac{\partial C}{\partial r} \right) + u_s \frac{\partial C}{\partial z} = -\rho_b (-r_m) \quad (5.180)$$

$$\rho c_p \frac{\partial T}{\partial t} - \lambda_L \frac{\partial^2 T}{\partial z^2} - \lambda_R \left(\frac{\partial^2 T}{\partial r^2} + \frac{1}{r} \frac{\partial T}{\partial r} \right) + \rho c_p u_s \frac{\partial T}{\partial z} + \frac{4h^\circ}{D} (T - T_w) = -\Delta H \rho_b (-r_m) \quad (5.181)$$

Nowadays, high computer capacities and sophisticated programs provide us with the capability to design reactors and simulate their operation managing all the complexity of the equations. However, the presentation of numerical solutions of complex equation systems is beyond the scope of this book. Various simplifications, not far from reality, will

allow us to connect the conversion with the various reactor design parameters such as catalyst weight, reactor dimensions, and flow conditions.

At steady-state operation ($\partial C/\partial t = \partial T/\partial t = 0$), the conservation equations presented above simplify to

$$-D_L \frac{\partial^2 C}{\partial z^2} - D_R \left(\frac{\partial^2 C}{\partial r^2} + \frac{1}{r} \frac{\partial C}{\partial r} \right) + u_s \frac{\partial C}{\partial z} = -\rho_b (-r_m) \quad (5.182)$$

$$-\lambda_L \frac{\partial^2 T}{\partial z^2} - \lambda_R \left(\frac{\partial^2 T}{\partial r^2} + \frac{1}{r} \frac{\partial T}{\partial r} \right) + \rho_c u_s \frac{\partial T}{\partial z} + \frac{4h^\circ}{D} (T - T_w) = -\Delta H \rho_b (-r_m) \quad (5.183)$$

In addition, if no radial dispersion takes place, these equations further simplify to

$$-D \frac{\partial^2 C}{\partial z^2} + u_s \frac{\partial C}{\partial z} = -\rho_b (-r_m) \quad (5.184)$$

$$-\lambda_L \frac{\partial^2 T}{\partial z^2} + \rho_c u_s \frac{\partial T}{\partial z} + \frac{4h^\circ}{D} (T - T_w) = -\Delta H \rho_b (-r_m) \quad (5.185)$$

Finally, for the ideal plug-flow reactor, the equations reduce to

$$u_s \frac{\partial C}{\partial z} = -\rho_b (-r_m) \quad (5.186)$$

$$\rho_c u_s \frac{\partial T}{\partial z} + \frac{4h^\circ}{D} (T - T_w) = -\Delta H \rho_b (-r_m) \quad (5.187)$$

Note that the global rate ($-r_m$) is expressed per unit mass of catalyst.

Isothermal fixed-bed operation

First-order reactions without internal mass transfer limitations A number of reactions carried out at high temperatures are potentially mass-transfer limited. The surface reaction is so fast that the global rate is limited by the transfer of the reactants from the bulk to the exterior surface of the catalyst. Moreover, the reactants do not have the chance to travel within catalyst particles due to the use of nonporous catalysts or very fast reaction on the exterior surface of catalyst pellets. Consider a first-order reaction $A \rightarrow B$ or a general reaction of the form $aA \rightarrow bB \rightarrow \text{products}$, which is of first order with respect to A. For the following analysis, a zero expansion factor and an effectiveness factor equal to 1 are considered.

We should recall that in such a case,

$$r_{ov} = (-r_m) = k_{ov} C_{Ab} \quad (5.188)$$

where C_{Ab} is the bulk fluid-phase concentration and

$$\frac{1}{k_{ov}} = \frac{1}{k_m} + \frac{1}{k_f a_s} \quad (5.189)$$

Consequently,

$$u_s \frac{dC}{dz} = -\rho_b k_{ov} C_{Ab} \quad (5.190)$$

Integrating with the condition, at $z = 0$, $C_{Ab} = C_{Ai}$,

$$\frac{C_{Ab}}{C_{Ai}} = \exp\left(-\frac{\rho_b k_{ov}}{u_s} Z\right) \quad (5.191)$$

or

$$\frac{C_{Ab}}{C_{Ai}} = \exp\left(-\frac{k^o}{u_s} Z\right) \Rightarrow \ln\left(\frac{1}{1-x_A}\right) = \frac{k^o}{u_{s,i}} Z \quad (5.192)$$

where Z is the bed height and

$$\frac{1}{k^o} = \frac{1}{\rho_b k_{ov}} = \frac{1}{\rho_b k_m} + \frac{1}{k_f \frac{\rho_b a_s}{a_u}} \quad (5.193)$$

The coefficient k^o introduces the external surface area of catalyst per unit volume of reactor α_u , which is more appropriate in fixed- and trickle-bed reactor analysis.

External mass transfer-limited reactions In the expression (5.191), k_m has to be known, but it is not necessary if the external mass transfer phenomena are very intense. Actually, if strong mass resistance exists, the knowledge of the rate law is not essential, because the rate can be written as

$$r_{ov} = r_f = k_f \alpha_s (C_{Ab} - C_{As}) \quad (5.194)$$

In most cases, the surface concentration is far less than the bulk concentration and we can consider

$$C_{Ab} - C_{As} \cong C_{Ab} \Rightarrow r_{ov} = k_f \alpha_s C_{Ab} \quad (5.195)$$

Then, eq. (5.190) can be rewritten as

$$u_s \frac{dC}{dz} = -\rho_b k_f \alpha_s C_{Ab} = -k_f \alpha_u C_{Ab} \quad (5.196)$$

and finally,

$$\frac{C_{Ab}}{C_{Ai}} = \exp\left(-\frac{k_f \alpha_u}{u_s} Z\right) \quad (5.197)$$

where $C_{A,i}$ is the inlet concentration of solute.

First-order reactions with internal mass-transfer limitations Since the following equation is valid, under the assumption made earlier, we only have to replace the right form of the global rate as expressed in eq. (5.196):

$$u_s \frac{dC}{dz} = -\rho_b (-r_m) \quad (5.198)$$

and

$$(-r_m) = \eta_{ov} k_s S_{s,in} C_{Ab} \quad (5.199)$$

where $S_{s,in}$ is the internal specific surface area of the catalyst and k_s the rate coefficient per unit surface of the catalyst. Recall eq. (5.87):

$$\eta_{ov} = \frac{\eta_s}{1 + \frac{\eta_s k_{vs} V_p}{k_f S_{ex}}} \quad (5.200)$$

From eq. (3.10):

$$k_{vs} V_p = k_s S_{in} \quad (5.201)$$

where S_{in} is the internal surface area of the catalyst. Then, eq. (5.200) becomes

$$\eta_{ov} = \frac{\eta_s}{1 + \frac{\eta_s k_s S_{in}}{k_f S_{ex}}} = \frac{\eta_s}{1 + \frac{\eta_s k_s (S_{in}/V_R)}{k_f (S_{ex}/V_R)}} \quad (5.202)$$

Here, note that (S_{ex}) and (S_{in}) refer to properties of a *single* particle. Then

$$\frac{S_{in}/V_R}{S_{ex}/V_R} = \frac{(nS_{in})/V_R}{(nS_{ex})/V_R} \quad (5.203)$$

where n is the number of catalyst particles in the bed. This manipulation is convenient because we can now express the above ratio in terms of fixed-bed properties:

$$(nS_{ex})/V_R = \alpha_u \quad (5.204)$$

Recall that

$$\rho_b = \frac{nM_p}{V_R} \Rightarrow V_R = \frac{nM_p}{\rho_b} \quad (5.205)$$

where M_p is the mass of a single particle. Then

$$(nS_{in})/V_R = \frac{nS_{in}}{\frac{nM_p}{\rho_b}} = \frac{S_{in}}{M_p} \rho_b = S_{s,in} \rho_b \quad (5.206)$$

So, eq. (5.203) becomes

$$\frac{(nS_{in})/V_R}{(nS_{ex})/V_R} = \frac{S_{s,in} \rho_b}{\alpha_u} \quad (5.207)$$

and finally η_{ov} can be obtained from

$$\eta_{ov} = \frac{\eta_s}{1 + \frac{\rho_b k_s S_{s,in} \rho_b}{k_f a_u}} \quad (5.208)$$

After integrating eq. (5.198), we obtain

$$\frac{C_{Ab}}{C_{Ai}} = \exp\left(-\frac{\rho_b k_s S_{s,in} \eta_{ov}}{u_s} z\right) \quad (5.209)$$

and the conversion achieved at the reactor's exit, $z = Z$, is

$$x = 1 - \exp\left(-\frac{\rho_b k_s S_{s,in} \eta_{ov}}{u_s} Z\right) \quad (5.210)$$

Note that if in the expression of k° we include the effectiveness factor η_s ,

$$\frac{1}{k^\circ} = \frac{1}{k_f \alpha_u} + \frac{1}{\eta_s k_m \rho_b} \quad (5.211)$$

then eq. (5.210) is equivalent to eq. (5.192) because

$$\rho_b k_s S_{s,\text{in}} \eta_{\text{ov}} = k^\circ \quad (5.212)$$

since

$$k_s S_{s,\text{in}} = k_m \quad (5.213)$$

Then, for combined resistances (internal and external), we can use the following equivalent form:

$$\frac{C_{\text{Ab}}}{C_{\text{Ai}}} = \exp\left(-\frac{k^\circ}{u_s} Z\right) \quad (5.214)$$

where k° is obtained using eq. (5.211).

Keep in mind that the analysis above is valid when the internal surface area of the catalysts constitutes the total surface area of the catalyst. This model is valid for a first-order reaction with zero expansion factor.

In case of a variable-volume system, the following form of the material balance should be used (eq. (3.293)):

$$\frac{dF_A}{dV} + (-R) = 0 \quad (5.215)$$

Taking into account the fact that

$$\frac{dF_A}{dV} = -F_{\text{Ai}} \frac{dx}{dV} = -F_{\text{Ai}} \frac{dx}{d(zA)} = -\frac{Q_i C_{\text{Ai}}}{A} \frac{dx}{dz} = u_{s,i} C_{\text{Ai}} \frac{dx}{dz} \quad (5.216)$$

and if A is the limiting reactant,

$$C_{\text{Ab}} = C_{\text{Ai}} \frac{1 - x_A}{1 + \varepsilon_R x_A} \quad (5.217)$$

the solution of the model is

$$(1 + \varepsilon_R) \ln \left(\frac{1}{1 - x_A} \right) - \varepsilon_R x_A = \frac{k^\circ Z}{u_{s,i}} \quad (5.218)$$

Example 6

Managing all complexity: Calculation of the overall reaction rate combining external mass transfer, internal mass transfer, and reaction

A waste gas stream containing 500 ppm of a VOC has to be treated in a fixed-bed reactor so that the concentration of VOC reduces to 50 ppm. A solid catalyst will be employed for the oxidation of VOC to CO_2 , at a temperature of 900 °C and a pressure of 1 atm. The reaction is first order with respect to the VOC concentration with a reaction rate coefficient $k_s = 1.5 \times 10^{-8} \text{ m}^3/\text{m}^2 \text{ s}$. Given that

volumetric feed rate = 0.0072 m ³ /s	particle density of catalyst = 1000 kg/m ³
NO diffusivity in air = 2×10^{-7} m ² /s	kinematic viscosity = 1.53×10^{-8} m ² /s
solid specific area = 200 m ² /g	pellet radius = 0.005 m
porosity = 0.3	effective diffusivity of VOC = 1.6×10^{-7} m ² /s
reactor radius = 0.05	

Calculate the weight of solids and the reactor length that are necessary for the desired conversion.

Solution

(1) Calculation of the internal effectiveness factor for spherical pellets and first order reaction: The Thiele modulus is

$$\phi = \frac{r_p}{3} \sqrt{\frac{k_m \rho_p}{D_{\text{eff}}}}$$

Recall that (eq. (3.10))

$$k_m = k_s S_s$$

Then

$$\phi = \frac{r_p}{3} \sqrt{\frac{(k_s S_s) \rho_p}{D_{\text{eff}}}} = 0.14$$

$$\eta_s = \frac{1}{\phi} \left(\frac{1}{\tanh(3\phi)} - \frac{1}{3\phi} \right) = 0.999$$

(2) Calculation of the external mass transfer coefficient:

$$A = \frac{\pi D^2}{4} = 0.00785 \text{ m}^2$$

$$u_s = \frac{Q}{A} = 0.917 \text{ m/s}$$

$$Re = \frac{u_s d_p}{\nu} = 11,989$$

$$Sc = \frac{\nu}{D_g} = 0.0765$$

Using eq. (3.352), we obtain

$$Sh = \left(\frac{Re}{\varepsilon} \right)^{1/2} Sc^{1/3} = 84.9$$

Then,

$$k_f = \left(\frac{D_g}{d_p} \right) Sh = 0.084 \text{ m/s}$$

(3) Calculation of the external area per volume of solids

$$\alpha_u = \frac{6}{d_p} (1 - \varepsilon) = 21,000 \text{ m}^2/\text{m}^3$$

(4) Calculation of the overall effectiveness factor

$$\rho_b = \rho_p (1 - \varepsilon) = 700 \text{ kg/m}^3$$

$$\eta_{ov} = \frac{\eta_s}{1 + \frac{\eta_s k_s S_{s,in} \rho_b}{k_f \alpha_u}} = 0.998$$

(5) Calculation of the weight of solids for the specific conversion

$$x = \frac{C_{A,i} - C_{A,o}}{C_{A,i}} = 0.72$$

$$W = \frac{Q}{\eta_{ov} k_s S_{s,in}} \ln\left(\frac{1}{1-x}\right) = 3080 \text{ g}$$

(6) Calculation of the reactor length

$$Z = \frac{W}{A\rho_b} = 0.56 \text{ m}$$

Reaction-limited second-order reaction For a second-order reaction of the form $2A \rightarrow$ products, or in the more general case of a reaction of the form $aA + bB \rightarrow$ products of second order with respect to A, the intrinsic reaction rate is

$$(-r_m) = \eta_s k_m C_{As}^2 \quad (5.219)$$

The overall reaction rate based on the unit volume of reactor is

$$(-R_A) = \rho_b r_m = \rho_b \eta_s k_m C_{As}^2 = (k_f a_u)(C_{Ab} - C_{As}) \quad (5.220)$$

After the elimination of the surface concentration,

$$C_{As} = \frac{-(k_f a_u) + \sqrt{(k_f a_u)^2 + 4(k_f a_u)(\rho_b \eta_s k_m)C_{Ab}}}{2\rho_b \eta_s k_m} \quad (5.221)$$

If $k_f \rightarrow \infty$ or $k_f \gg k_m$, then by the rate-controlling step concept, the resistance to the overall rate is due to the intrinsic reaction rate and thus

$$(-R_A) = \rho_b \eta_s k_m C_{Ab}^2 \quad (5.222)$$

For zero expansion factor, the model of the reactor is

$$u_s \frac{dC_{Ab}}{dz} = -\rho_b \eta_s k_m C_{Ab}^2 \quad (5.223)$$

On integrating, we obtain

$$\frac{C_{Ai} - C_{Ab}}{C_{Ab}} = \left(\frac{C_{Ai} \rho_b \eta_s k_m}{u_s} \right) Z \quad (5.224)$$

or in terms of conversion,

$$\frac{x_A}{1 - x_A} = \frac{\eta_s k_m \rho_b C_{Ai}}{u_s} Z \quad (5.225)$$

where $C_{A,i}$ is the inlet concentration of the solute.

Adiabatic fixed-bed operation

An issue that has to be taken into account while analyzing adiabatic fixed-bed reactors is the importance of the axial dispersion of heat and concentration. Generally, axial dispersion can be neglected due to the high velocities and high depths of beds found in industrial applications. However, it is an assumption that has to be verified. The ratio of Z/d_p can be used as a criterion to determine if axial dispersion has to be considered. If this ratio is higher than 150, the influence of concentration and temperature gradients on the axial direction can be considered negligible (see also Section 3.6.3). In contrast, if axial dispersion is to be taken into account, a system of differential equations comes up that can be solved only by numerical methods.

Recall the plug-flow steady-state energy balance (eq. (5.187)):

$$\rho c_p u_s \frac{\partial T}{\partial z} + \frac{4h^\circ}{D} (T - T_w) = -\Delta H \rho_b (-r_m) \quad (5.226)$$

In an adiabatic fixed bed, heat is not exchanged with the environment through the reactor wall. Note that for the derivation of eq. (5.226), it has been assumed that the flow is ideal plug flow and thus the radial dispersion term is eliminated; in an adiabatic fixed bed, the assumption of perfect radial mixing is not necessary since no radial gradients exist.

Furthermore, reactors that have large diameters or are well insulated can be considered to approach adiabatic operation, and in this case the term $4h^\circ(T - T_w)/D$ drops out. Consequently, the above equation further simplifies to

$$(\rho u_s) c_p \frac{dT}{dz} = -\Delta H \rho_b (-r_m) \quad (5.227)$$

where:

- T = the fluid temperature, (K)
- c_p = the specific heat of the fluid (J/kg K)
- ρ = the fluid density (kg/m³)

ΔH = the heat of reaction (J/mol). Heat of reaction is *negative* for an exothermic reaction and *positive* for an endothermic reaction.

ρ_b = the bulk density of the bed (kg/m^3)

u_s = the superficial velocity of fluid (m/s)

$(-r_m)$ = the rate of disappearance of reactant ($\text{m}^3/\text{kg s}$).

Note that in an adiabatic fixed bed, the temperature varies from inlet to the outlet of the bed and thus the fluid density, volumetric flow rate, and superficial velocity are not constant. However, the product ρu_s in the above equation is the mass flow rate per unit cross-sectional area of the bed ($\text{kg/m}^2 \text{ s}$), which is constant throughout the bed length.

The mass balance equation is (eq. (5.215))

$$\frac{dF}{dV} = -(-R) \Leftrightarrow \frac{F_i}{A} \frac{dx}{dz} = \rho_b (-r_m) \quad (5.228)$$

where F_i is the inlet molar feed concentration of the reactant (mol/s) and A the cross-sectional area of the bed (m^2). This form of the material balance is the appropriate one as it is applicable for variable-density systems as is the case of the adiabatic fixed beds.

Substituting $(-r_m)$ from eq. (5.228) in the energy balance equation (5.227), we get (Smith, 1981)

$$dT = -\frac{\Delta H}{c_p} \left(\frac{F_i}{A \rho u_s} \right) dx = -\frac{\Delta H}{c_p} \left(\frac{F_i}{F_m} \right) dx \quad (5.229)$$

where F_m is the total mass flow rate of the reaction mixture $A \rho u_s$ in kg/s, which is constant throughout the bed length.

Integrating this equation under the assumption of constant ΔH and c_p ,

$$T_o = T_i - \frac{\Delta H}{c_p} \frac{F_i}{F_m} x \quad (5.230)$$

Taking into account that at steady state at any point in the reactor, $F_m = A \rho u_s = A \rho_i u_{s,i}$, we have

$$\frac{F_i}{F_m} = \frac{Q_i C_i}{A \rho u_s} = \frac{Q_i C_i}{A \rho_i u_{s,i}} = \underbrace{\left(\frac{Q_i}{A} \right)}_{u_{s,i}} \frac{C_i}{\rho_i} = \frac{C_i}{\rho_i} \quad (5.231)$$

Then, we can derive the following equivalent form:

$$T_o = -\frac{\Delta H C_i}{\rho_i c_p} x + T_i \quad (5.232)$$

where:

- C_i = the concentration of the reactant at reactor feed (mol/m³)
- ρ_i = the inlet fluid density (kg/m³)
- x = the conversion (–)
- T_i = the temperature at reactor inlet (K)
- T_o = the temperature at reactor outlet (K).

Now, the global rate can be estimated at any conversion, since temperature can be calculated from eq. (5.232). Then, the conversion versus reactor depth or catalyst mass can be determined from the mass conservation equation (5.228). Only arithmetic solutions of the adiabatic model are possible.

For the special case of a first-order reaction, the mass balance equation (5.228) becomes

$$\frac{dx}{dz} = \frac{\rho_b}{u_{s,i}} k_m(T) \left(\frac{1-x}{1+\epsilon_R x} \frac{P}{P_i} \frac{T_i}{T} \right) \quad (5.233)$$

where $u_{s,i}$ is the inlet superficial velocity of the fluid (m/s) and k_m is the rate coefficient which is a function of temperature:

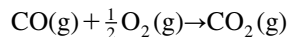
$$k_m(T) = k_o \exp\left(-\frac{E_a}{RT}\right) \quad (5.234)$$

where k_o is the preexponential factor and E_a the activation energy in the Arrhenius equation. Eq. (5.233) represents the general case of a nonisobaric, nonisothermal process with expansion factor. Note that for a liquid-phase reaction without phase change, the term in parenthesis becomes equal to $1 - x$, even if the temperature and/or the pressure in the reactor is not constant. The effect of pressure is nearly always negligible in systems involving liquid components while the effect of temperature on the reactor performance is expressed through the energy balance equation (5.232) and eq. (5.234).

Furthermore, eq. (5.233) is valid for a reaction-limited system, i.e. the controlling mechanism is the reaction step. Furthermore, the effectiveness factor is unity. The situation becomes more complex in the case where internal and external resistances exist as the effectiveness factor and the mass transfer coefficient should be taken into account (see eq. (5.211)) and they are a function of temperature.

Example 7

Zhang and Hu (2004) studied the catalytic oxidation of carbon monoxide:



The catalyst used is commercial Type 111 Cu/Cr/Ag impregnated coal-based carbon of 0.3 mm particle size and bulk density of 700 kg/m³. This study confirmed that for this particle

size, the internal diffusion is negligible and the reaction is first order in respect to CO concentration. At 50 °C, the reaction coefficient $k_m = 2 \times 10^{-6} \text{ m}^3/\text{kg s}$ and the activation energy $E_a = 107.23 \text{ kJ/mol}$.

Then, assume that the reaction takes place in a fixed bed of 1.61 m diameter and 16.1 m height, under contact time of 5 min, and the inlet temperature of gas being 50 °C, for different CO inlet concentration (several runs). Estimate the conversion of CO in an isothermal and adiabatic fixed-bed reactor and under the following assumptions: isobaric process, negligible external mass transfer resistance, and approximately constant heat capacity of air ($c_p = 1 \text{ kJ/kg K}$) and heat of reaction ($\Delta H = -67,636 \text{ cal/mol}$). The inlet temperature of the reaction mixture is 50 °C and its composition is 79% N_2 and approximately 21% O_2 , while the inlet CO concentration varies from 180–4000 ppm ($\text{mg/kg}_{\text{air}}$) (for each individual run).

Assume that the particles are spherical. The experimental conversion of CO at 50 °C and for $\tau = 5 \text{ min}$ is approximately 0.38 (isothermal operation and 180 ppm initial CO concentration). The density of air at 50 °C is 1.09 kg/m^3 .

Solution

At first it should be mentioned that due to the great excess of inerts (79%) and low concentration of CO (180–4000 ppm), the expansion factor could be taken equal to zero.

Isothermal fixed bed: Since the phenomenon is rate-limited,

$$\frac{1}{k^o} = \frac{1}{\rho_b k_m} + \frac{1}{k_f a_u} \cong \frac{1}{\rho_b k_m} \Rightarrow k^o = 1.4 \times 10^{-3} \text{ s}^{-1}$$

The volume of the bed is 32.76 m^3 and its cross-sectional area 2.04 m^2 and thus,

$$\begin{aligned} \tau &= \frac{V_R}{Q} \Rightarrow Q = \frac{V_R}{\tau} = \frac{32.76}{(5 \times 60)} = 0.11 \text{ m}^3/\text{s} \\ u_s &= \frac{Q}{A} = \frac{0.11}{2.04} = 0.054 \text{ m/s} \end{aligned}$$

Then, eq. (5.192) becomes

$$\ln\left(\frac{1}{1-x}\right) = \frac{\rho_b k_m}{u_s} Z \Rightarrow x = 0.343$$

which is close to the experimental value of 0.38. This indicates that the assumptions of unity effectiveness factor, rate-controlling mechanism, and zero expansion factor are close to reality. Note that the conversion in the isothermal fixed beds is the same for different CO inlet concentration.

Adiabatic fixed bed: Since

- the controlling mechanism is the reaction step
- the effectiveness factor is unity
- the expansion factor is zero ($\epsilon_R = 0$)
- the operation is isobaric ($P_i = P$),

the material balance equation (5.233) becomes

$$\frac{dx}{dz} = \frac{\rho_b}{u_{s,i}} \left[k_o \exp\left(-\frac{E_a}{RT}\right) \right] (1-x) \frac{T_i}{T}$$

where k_o is the preexponential factor and E_a the activation energy in the Arrhenius equation. We have

$$\frac{E_a}{RT} = \frac{107,230}{8.314(273+50)} = 39.93$$

and thus

$$k_m = k_o \exp\left(-\frac{E_a}{RT}\right) \Rightarrow k_o = 4.39 \times 10^{11} \text{ m}^3/\text{kg s}$$

At a distance z corresponding at a conversion level x from the bed inlet and for constant ΔH and c_p (eq. (5.232)),

$$T = -\frac{\Delta H C_i}{\rho_i c_p} x + T_i$$

The final equations to be solved are

$$\frac{dx}{dz} = 1.85 \times 10^{18} \left[\exp\left(-\frac{12897.5}{T}\right) \right] \frac{(1-x)}{T}$$

$$T = 323 + 259.08 C_i x$$

The solutions are only arithmetic and Polymath software has been used. Note that T is in K and that the concentration of CO is in mol/m³. The conversion of ppm into mol/m³ is done by using the molar weight of CO (28 kg/kmol) and the density of air (1.09 kg/m³).

In Figure 5.7, the final conversion and exit temperature is plotted against the inlet CO concentration.

As we see, for a specific reaction, the higher the inlet concentration, the higher the conversion and the exit temperature. This is a result of the positive effect of the temperature rise, due to the exothermic nature of the reaction, on the rate coefficient and thus on the reaction rate and conversion. Note that for higher inlet CO concentration, the conversion for the isothermal operation is the same, while for the adiabatic operation the conversion is higher for higher inlet concentrations. Furthermore, the conversion in the adiabatic fixed bed is always higher in comparison to the isothermal fixed bed. Of course, these results are such because the reaction is of first order in respect to CO.

In Figure 5.8, the conversion and temperature profile in the reactor versus the distance from the reactor length for inlet CO concentration of 4000 ppm is given.

As expected, the conversion and the temperature are higher as the reaction mixture approaches the reactor exit. This is true irrespective of the inlet concentration of CO.

Monolithic catalysts

Monolithic catalysts have found a wide range of applications in the removal of pollutants from air, especially in the automotive industry. Specifically, the demand for large surface to small volume, high conversions achieved for low retention times, and low pressure drop led to the development of monolithic supports. More information on automotive catalytic converters has been given in Chapter 1. Usually, a thin layer of alumina is deposited onto a monolith for keeping the precious metal used for air pollutants abatement dispersed. The oxidations that take place are highly exothermic and the reaction rates achieved are in turn high. Hence, the reactants diffuse only a small distance

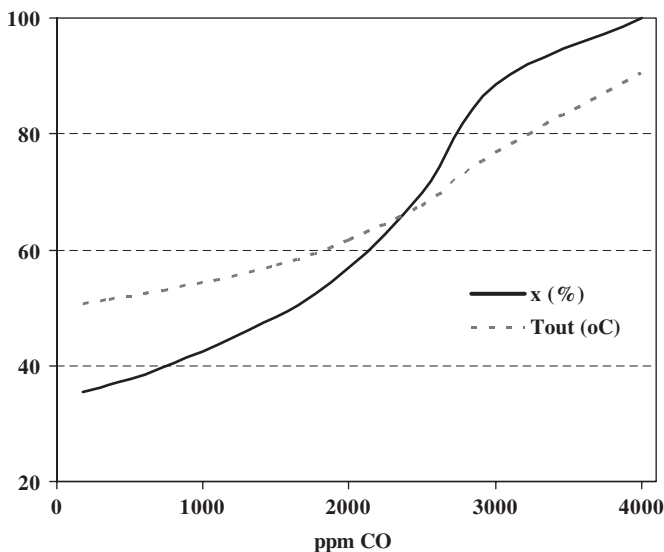


Figure 5.7 Final conversion and exit temperature versus inlet CO concentration.

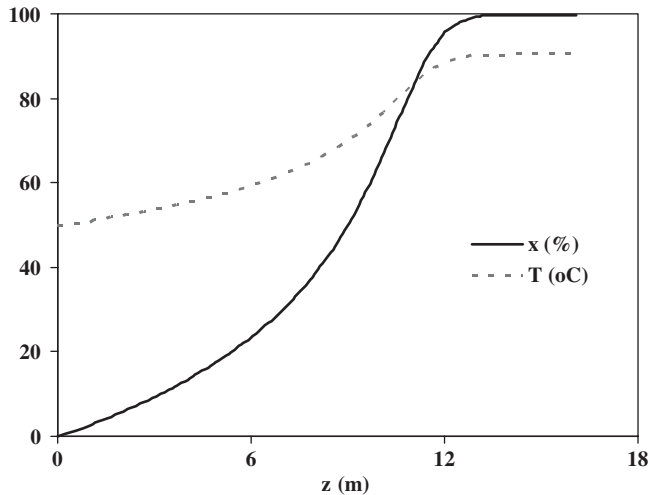


Figure 5.8 Conversion and temperature profile in the reactor.

within the catalyst. Therefore, the intraparticle concentration and temperature gradients can be safely considered negligible in monolithic catalysts. On the other hand, the external mass and heat transfer resistances are significant. Moreover, heat transfer by conduction and radiation may take place due to the continuous form of the monolith and the high temperatures found in such catalysts. So, the mathematical models describing monoliths show some variations from those in classical packed beds. We will develop a model for monoliths based on the following assumptions (Hegedus, 1975):

- heat transfer by radiation is negligible
- the catalyst is continuous in the flow direction
- the flow follows plug-flow pattern
- the oxygen is in excess
- the reaction order is first order with respect to the concentration of pollutant:

$$Q \frac{dC}{dz} + k_f \alpha_L (C - C_s) = 0 \quad (5.235)$$

where:

Q = the volumetric flow rate

k_f = the mass transfer coefficient from gas to catalyst surface

α_L = the mass or heat transfer area per unit length of catalyst

dz = the section of catalyst length.

For the solid phase, the mass concentration of the pollutant requires

$$k_f \alpha_L (C - C_s) = k_m \delta C_s \quad (5.236)$$

where:

k_m = reaction rate coefficient per unit mass of catalyst at T_s
 δ = catalyst mass per unit length of reactor.

Taking into account the axial conduction of heat in the solid phase, the energy conservation equation for the gas is

$$Q\rho c_p \frac{dT}{dz} + h\alpha_L(T - T_s) = 0 \quad (5.237)$$

and for the catalyst,

$$\Delta x\alpha_L \frac{d^2T_s}{dz^2} + h\alpha_L(T - T_s) + (-\Delta H)k_m\delta C_s = 0 \quad (5.238)$$

where Δx is the thickness of the solid support.

Neglecting the heat loss from the end of the catalyst, the boundary conditions are

$$C = C_{in}, T = T_{in}, dT_s/dz = 0 \quad \text{at} \quad z = 0$$

$$dT_s/dz = 0 \quad \text{at} \quad z = L$$

Considering that the temperature is constant, the manipulation of the above equation leads to the following equation:

$$\frac{dC}{dz} = -\frac{C}{Q\left(\frac{1}{k_m\delta} + \frac{1}{k_f\alpha_L}\right)} \quad (5.239)$$

Integrating this equation, we get

$$1 - x = \frac{C}{C_{in}} = \exp\left[-\frac{z}{Q\left(\frac{1}{k_m\delta} + \frac{1}{k_f\alpha_L}\right)}\right] \quad (5.240)$$

Now, the conversion x can be estimated at any reactor length z .

Example 8

The oxidation of gaseous ethanol (first-order reaction) was studied in a spinning basket reactor with Pt/Al₂O₃ on a ceramic monolith as catalyst. The inlet concentration of ethanol

Table 5.9

Experimental results

Experiment number	Rotation speed (rpm)	C_E ($\mu\text{mol}/\text{cm}^3$)	T ($^\circ\text{C}$)
1	80	0.0180	203
2	120	0.0167	203
3	240	0.0149	203
4	400	0.0138	203
5	450	0.0135	203
6	600	0.0135	203
7	600	0.0087	228

Note: T is the reactor temperature and C_E the concentration of ethanol at the reactor outlet.

was $0.0242 \mu\text{mol}/\text{cm}^3$ in nitrogen, whereas oxygen was in great excess. The feed flow rate was $750 \text{ cm}^3/\text{min}$ at 25°C and 1 atm. The catalyst was placed in two baskets and had a total mass of 2 g. The external area of the catalyst was 20 m^2 . The reactor operated isothermally. The results obtained are shown in Table 5.9.

Find:

- the activation energy of ethanol oxidation,
- the coefficient of mass transfer to the catalyst surface with respect to the rotation speed of the catalyst.

Solution

(a) The specific type of reactor is appropriate for kinetic analysis because it can be operated under conditions of absence of external phenomena of mass and heat transfer. By adjusting the rotation speed of the catalyst, the stagnant film around the catalyst can be practically eliminated, and thus the resistance of mass and heat transfer from the bulk of the fluid to the external area of the catalyst can be neglected. Moreover, the resistance to the diffusion of the fluid inside the pores of the catalyst and the intraparticle gradients of concentration and temperature in general can also be considered negligible since the depth of the washcoat Al_2O_3 , where the active metals are dispersed, is very small, about $50 \mu\text{m}$ (Smith, 1997).

The energy balance of ethanol in this type of reactor (CSTR type) is
flux in – flux out = disappearance by reaction

$$QC_{Eo} - QC_E = (-r_m)W$$

and thus

$$(-r_m) = \frac{Q}{W}(C_{Ei} - C_E)$$

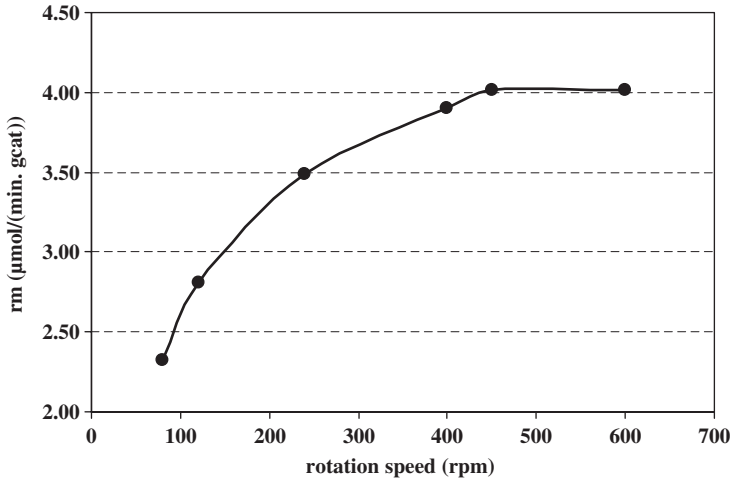


Figure 5.9 The reaction rate versus the rotation speed at 203 °C.

where:

$(-r_m)$ = the reaction rate per unit mass of catalyst, $\mu\text{mol}/(\text{min} \cdot \text{g}_{\text{cat}})$

C_{Ei} = the concentration of ethanol at the reactor inlet, $\mu\text{mol}/\text{cm}^3$

C_E = the concentration of ethanol at the reactor outlet, $\mu\text{mol}/\text{cm}^3$

Q = the feed flow rate, cm^3/min

W = the mass of catalyst, g

It is obvious that the calculation of the reaction rate is very easy in this reactor. Now, let us sketch the reaction rate versus the rotation speed using the data obtained at 203 °C. As shown in Figure 5.9, the reaction rate is stabilized at rotation speeds above 400–450 rpm. This means that the external mass transfer does not affect the global rate, and thus values of the intrinsic rate can be safely considered to be obtained at those rotation speeds.

Consequently, the activation energy will be determined by means of the data obtained at 600 rpm, where the values of the observed rate represent the actual intrinsic rate. Since the reaction is of first order with respect to ethanol,

$$(-r_m) = k_m C_E$$

and

$$k_m = k_o e^{-E_a/RT}$$

Applying the first equation for 203 and 228 °C and dividing, we obtain

$$\frac{k_{m,203} C_{E,203}}{k_{m,228} C_{E,228}} = \frac{(-r_{m,203})}{(-r_{m,228})} = \frac{\frac{Q}{W}(C_{Ei} - C_{E,203})}{\frac{Q}{W}(C_{Ei} - C_{E,228})}$$

or

$$\frac{k_{m,203}}{k_{m,228}} \frac{0.0135}{0.0087} = \frac{4.0125}{5.8125}$$

$$\frac{k_{m,203}}{k_{m,228}} = 0.4449$$

$$\frac{k_o e^{-E_a/1.987(273+203)}}{k_o e^{-E_a/1.987(273+228)}} = 0.4449$$

$$\frac{e^{-E_a/1.987(273+203)}}{e^{-E_a/1.987(273+228)}} = 0.4449$$

$$\frac{E_a}{1.987} \left(\frac{1}{273+228} - \frac{1}{273+203} \right) = \ln(0.4449)$$

Finally, we obtain the activation energy $E_a = 15,474$ cal/mol. Substituting the value of the activation energy in

$$k_{m,203} C_{E,203} = (-r_{m,203})$$

$$k_o e^{-15474/1.987(273+203)} C_{E,203} = (-r_{m,203})$$

and finally, the preexponential is also obtained: $k_o = 3.79 \times 10^9$ cm³/(g_{cat} min).

(b) Now, we can use the intrinsic reaction rate coefficient to estimate the mass transfer coefficient at the various rotation speeds of the catalyst. Recall that

$$(-r_m) = \frac{1}{\frac{1}{k_m} + \frac{1}{k_f a_s}} C_{\text{bulk}}$$

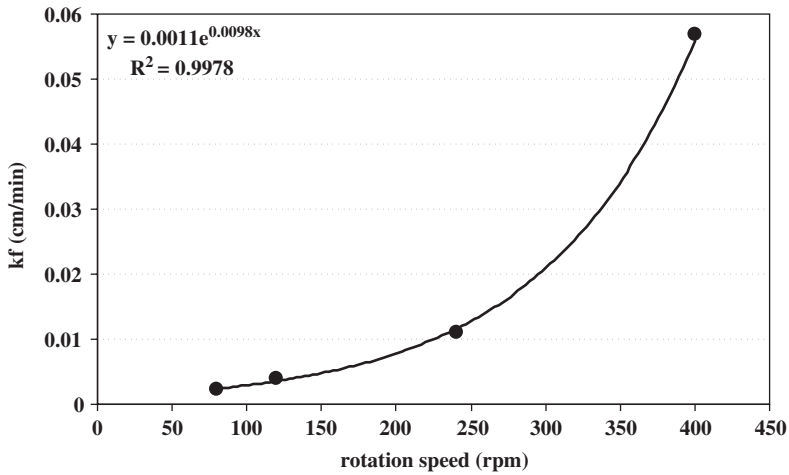
for a first-order catalytic reaction when the reaction is considered to take place at the external surface of the catalyst, which is the case for a monolith. Since the mass of the catalyst is 2 g and its external area 20 m², it can be seen that $a_s = 10$ m²/g_{cat} = 10⁵ cm²/g_{cat}. Moreover, $C_{\text{bulk}} = C_E$. After some manipulations, the following can be easily derived for the region of external mass transfer existence:

$$k_f = \frac{k_m (-r_m)}{\alpha_s [k_m C_E - (-r_m)]}$$

So, Table 5.10 can be formed.

Table 5.10The value of k_f for each catalyst rotation speed

Experiment number	Rotation speed (rpm)	k_f (cm/min)
1	80	0.002283
2	120	0.003883
3	240	0.01099
4	400	0.05681

**Figure 5.10** k_f versus catalyst rotation speed.

Now, since k_m has been estimated for each catalyst rotation speed, the relation between k_m and rpm can be easily deduced using an exponential equation, as shown in Figure 5.10. Consequently,

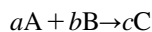
$$k_f = 0.0011e^{0.0098N}$$

where N is the rotation speed in rpm.

Non-isobaric fixed-bed operation

The following analysis focuses on catalytic processes involving a gas phase. However, the principles are applicable in the case of the adsorption of solutes from gas phase.

Reactor model with pressure drop Consider the gas phase reaction



where A is the limiting reactant. In the general case of nonisothermal, nonisobaric, and variable-density reaction (eq. (3.91)),

$$\frac{V}{V_i} = (1 + \varepsilon_R x_A) \frac{P_i}{P} \frac{T}{T_i} \quad (5.241)$$

and thus, the concentration is

$$C_A = C_{A,i} \frac{1 - x_A}{1 + \varepsilon_R x_A} \frac{P}{P_i} \frac{T_i}{T} = f(x_A, \frac{P}{P_i}, \frac{T}{T_i}) \quad (5.242)$$

To simplify the analysis, the operation is considered isothermal ($T = T_i$).

Reactor model for a first-order reaction: To illustrate the effect of pressure drop, consider an isothermal two-phase fixed-bed operation (gas–solid system). In terms of a reactant, the intrinsic reaction rate is

$$(-r_m) = k_m C_{AS} \quad (5.243)$$

The rate per unit volume of reactor is

$$(-R_A) = \rho_b (-r_m) = \rho_b k_m C_{AS} = (k_f a_u) [C_A - C_{AS}] \quad (5.244)$$

Following the well-known procedure for the elimination of surface concentration, we have

$$C_{AS} = \frac{(k_f a_u)}{(k_f a_u) + \rho_b k_m} C_A \quad (5.245)$$

Then, the rate in terms of the fluid bulk-phase concentration (overall rate per unit volume of reactor) is

$$(-R_A) = (\rho_b k_m) C_{AS} = k^\circ C_A = k^\circ f\left(x_A, \frac{P}{P_i}\right) \quad (5.246)$$

where

$$\frac{1}{k^\circ} = \frac{1}{(k_f a_u)} + \frac{1}{\rho_b k_m} \quad (5.247)$$

Here, C_A denotes the bulk -phase concentration and k° the overall kinetic coefficient. According to Fogler (1999), the differential form of the design equations should be used

whenever pressure-drop effects are accounted for. Then, the design equation per unit volume of a fixed-bed reactor is (eq. (3.293))

$$\frac{dF_A}{dV} + (-R_A) = 0 \Leftrightarrow -F_{A,i} \frac{dx_A}{dV} + (-R_A) = 0 \Leftrightarrow -F_{A,i} \frac{dx_A}{dW} + \frac{(-R_A)}{\rho_b} = 0 \quad (5.248)$$

Or

$$\frac{dx_A}{dW} = \frac{k^\circ}{\rho_b F_{A,i}} f\left(x_A, \frac{P}{P_i}\right) \quad (5.249)$$

In terms of the reactor length,

$$\frac{dx_A}{dV} = \frac{k^\circ}{F_{A,i}} f\left(x_A, \frac{P}{P_i}\right) \Leftrightarrow \frac{dx_A}{dz} = \frac{Ak^\circ}{F_{A,i}} f\left(x_A, \frac{P}{P_i}\right) \quad (5.250)$$

Model for a second-order reaction with negligible resistance in the gas film ($k_f \rightarrow \infty$): In this case, the intrinsic reaction rate is

$$(-r_m) = k_m C_{AS}^2 \quad (5.251)$$

The overall reaction rate based on unit volume of reactor is

$$(-R_A) = \rho_b r_m = \rho_b k_m C_{AS}^2 = (k_f a_u)(C_A - C_{AS}) \quad (5.252)$$

and after the elimination of the surface concentration, we have

$$C_{AS} = \frac{-(k_f a_u) + \sqrt{(k_f a_u)^2 + 4(k_f a_u)(\rho_b k_m)C_A}}{2\rho_b k_m} \quad (5.253)$$

It is obvious that this form of reaction rate becomes very complicated to work with when the surface concentration is introduced. In this case, we can use the concept of the rate-controlling step. In our case, we assume that $k_f \rightarrow \infty$ or $k_f \gg k_m$, the resistance to the overall rate is owing to the intrinsic reaction rate. Then, due to the equality of the individual rates, if $k_f \rightarrow \infty$ then $(C_A - C_{AS}) \rightarrow 0$ or $C_A \rightarrow C_{AS}$, and so the individual rates are finite and equal to the overall rate. The rate in terms of the fluid bulk-phase concentration (overall rate per unit volume of reactor) is

$$(-R_A) = \rho_b k_m C_A^2 = \rho_b k_m \left[f\left(x_A, \frac{P}{P_i}\right) \right]^2 \quad (5.254)$$

Note that here, k_m is found with the bulk concentration of fluid and not with the surface concentration as in the case of the first-order reaction. This is why in this example, the fluid-phase resistance has been eliminated.

The design equation per unit volume of reactor is (eq. (3.293))

$$\frac{dF_A}{dV} + (-R_A) = 0 \Leftrightarrow -F_{A,i} \frac{dx_A}{dV} + (-R_A) = 0 \Leftrightarrow -F_{A,i} \frac{dx_A}{dW} + \frac{(-R_A)}{\rho_b} = 0 \quad (5.255)$$

or

$$\frac{dx_A}{dW} = \frac{k_m}{F_{A,i}} \left[f \left(x_A, \frac{P}{P_i} \right) \right]^2 \quad (5.256)$$

In terms of the reactor length,

$$\frac{dx_A}{dV} = \frac{\rho_b k_m}{F_{A,i}} \left[f \left(x_A, \frac{P}{P_i} \right) \right]^2 \Leftrightarrow \frac{dx_A}{dz} = \frac{A \rho_b k_m}{F_{A,i}} \left[f \left(x_A, \frac{P}{P_i} \right) \right]^2 \quad (5.257)$$

where A is the cross-section of the reactor.

Pressure drop analysis For a fixed bed, the Ergun equation for pressure drop in a differential form is (eq. (3.302))

$$\frac{dP}{dz} = - \left[\frac{150 \mu u_s (1-\varepsilon)^2}{\Phi_s^2 d_p^2 \varepsilon^3} + \frac{1.75 \rho u_s^2 (1-\varepsilon)}{\Phi_s d_p \varepsilon^3} \right] \quad (5.258)$$

where d_p is the particle diameter for spherical particles or the nominal diameter for irregular-shaped particles, ρ the density of the fluid, g the gravity acceleration constant (9.81 m²/cm), μ the dynamic viscosity of the fluid, ε the fixed-bed voidage, u_s the superficial fluid velocity, and Φ_s the sphericity of the particle. In eq. (5.258), the pressure-dependent parameters are the superficial velocity and the gas density. In analogy to the reaction mixture volume,

$$\frac{Q}{Q_i} = \frac{\left(\frac{Q}{A} \right)}{\left(\frac{Q_i}{A} \right)} = \frac{u_s}{u_{s,i}} = (1 + \varepsilon_R x_A) \frac{P_i}{P} \quad (5.259)$$

while for gas density,

$$\rho = \frac{M_G}{V} = \left(\frac{M_G}{V_i} \right) \frac{1}{(1 + \varepsilon_R x_A)} \frac{P}{P_i} = \frac{\rho_i}{(1 + \varepsilon_R x_A)} \frac{P}{P_i} \quad (5.260)$$

or

$$\frac{\rho}{\rho_i} = \frac{1}{(1 + \varepsilon_R x_A)} \frac{P}{P_i} \quad (5.261)$$

where the subscript “i” denotes the value of the parameter at the inlet conditions. It is interesting to note here that from the last two equations,

$$\frac{Q}{Q_i} = \frac{u_s}{u_{s,i}} = \frac{\rho_i}{\rho} = (1 + \varepsilon_R x_A) \frac{P_i}{P} \quad (5.262)$$

which is the equation of continuity:

$$Q_i \rho_i = Q \rho \Leftrightarrow u_{s,i} \rho_i = u_s \rho \quad (5.263)$$

or in words, under steady state conditions, the mass flow rate (kg/s) at any point of the reactor is constant and equal to the entering mass flow rate. Substituting in eq. (5.258) we have:

$$\begin{aligned} \frac{dP}{dz} = & - \left[\frac{150 \mu u_{s,i} (1 - \varepsilon)^2}{\Phi_s^2 d_p^2 \varepsilon^3} \right] (1 + \varepsilon_R x_A) \frac{P_i}{P} - \\ & - \left[\frac{1.75 \rho_i u_{s,i}^2 (1 - \varepsilon)}{\Phi_s d_p \varepsilon^3} \right] (1 + \varepsilon_R x_A)^2 \left(\frac{P_i}{P} \right)^2 \frac{1}{(1 + \varepsilon_R x_A)} \frac{P}{P_i} \end{aligned} \quad (5.264)$$

or

$$\frac{dP}{dz} = -a(1 + \varepsilon_R x_A) \frac{P_i}{P} \quad (5.265)$$

where $a = - \left(\frac{dP}{dZ} \right)_i$, is given by eq. (5.258) with $\rho = \rho_i$. Here note that

- if ε_R is negative, the pressure drop will be less than that for zero expansion
- if ε_R is positive, the pressure drop will be greater than that for zero expansion.

The reactor length is

$$\rho_b Z = \rho_b \frac{V_B}{A} = \frac{W}{A} \Leftrightarrow Z = \frac{W}{\rho_b A} \quad (5.266)$$

where A is the cross-sectional area of the bed and V_b its volume. Then, eq. (5.265) becomes

$$\frac{dP}{dW} = -a \frac{1}{\rho_b A} g\left(x_A, \frac{P_i}{P}\right) \quad (5.267)$$

and

$$g\left(x_A, \frac{P_i}{P}\right) = (1 + \varepsilon_R x_A) \frac{P_i}{P} \quad (5.268)$$

In terms of the reactor length,

$$\frac{dP}{dz} = -ag(x_A, \frac{P_i}{P}) \quad (5.269)$$

Now, from eqs. (5.249) and (5.267), or (5.250) and (5.269), it is clear that the reactor model becomes a system of two coupled differential equations, which should be solved simultaneously.

Overall model for a first-order reaction: For the first-order reaction, we have

$$C_A = C_{A,i} \frac{1 - x_A}{1 + \varepsilon_R x_A} \frac{P}{P_i} \quad (5.270)$$

The rate becomes

$$(-R_A) = k^\circ C_A = k^\circ C_{A,i} \frac{1 - x_A}{1 + \varepsilon_R x_A} \frac{P}{P_i} \quad (5.271)$$

Then, eq. (5.250) is

$$\frac{dx_A}{dz} = \left[\frac{Ak^\circ}{F_{A,i}} C_{A,i} \right] \frac{1 - x_A}{1 + \varepsilon_R x_A} \frac{P}{P_i} = \frac{k^\circ}{u_{s,i}} \frac{1 - x_A}{1 + \varepsilon_R x_A} \frac{P}{P_i} \quad (5.272)$$

and eq. (5.249) is

$$\frac{dx_A}{dW} = \left[\frac{k^\circ}{\rho_b F_{A,i}} C_{A,i} \right] \frac{1 - x_A}{1 + \varepsilon_R x_A} \frac{P}{P_i} = \frac{k^\circ}{\rho_b Q_{A,i}} \frac{1 - x_A}{1 + \varepsilon_R x_A} \frac{P}{P_i} \quad (5.273)$$

The pressure-drop eqs. (5.267) and (5.269) are

$$\frac{dP}{dW} = -a \frac{(1 + \varepsilon_R x_A) P_i}{\rho_b A P} \quad (5.274)$$

$$\frac{dP}{dz} = -a(1 + \varepsilon_R x_A) \frac{P_i}{P} \quad (5.275)$$

Overall model for a second-order reaction: With negligible resistance in the gas film ($k_f \rightarrow \infty$): In this case, the rate becomes

$$(-R_A) = \rho_b k_m \left[C_{A,i} \frac{1 - x_A}{1 + \varepsilon_R x_A} \frac{P}{P_i} \right]^2 \quad (5.276)$$

Then, eq. (5.257) is

$$\frac{dx_A}{dz} = \frac{A \rho_b k_m}{F_{A,i}} \left[C_{A,i} \frac{1 - x_A}{1 + \varepsilon_R x_A} \frac{P}{P_i} \right]^2 \quad (5.277)$$

and eq. (5.256) is

$$\frac{dx_A}{dW} = \frac{k_m}{F_{A,i}} \left[C_{A,i} \frac{1 - x_A}{1 + \varepsilon_R x_A} \frac{P}{P_i} \right]^2 \quad (5.278)$$

The pressure-drop eqs. (5.267) and (5.269) are

$$\frac{dP}{dW} = -a \frac{(1 + \varepsilon_R x_A) P_i}{\rho_b A P} \quad (5.279)$$

$$\frac{dP}{dz} = -a(1 + \varepsilon_R x_A) \frac{P_i}{P} \quad (5.280)$$

Pressure drop for zero expansion: In the case where

- the expansion factor ε_R is zero or
- x_A is low, so that $\varepsilon_R x_A \ll 1$ or
- there is no reaction.

From eq. (5.279), we have

$$\frac{dP}{dW} = -a \frac{1}{\rho_b A} \frac{P_i}{P} \quad (5.281)$$

or, in terms of bed length (eq. (5.280)),

$$\frac{dP}{dz} = -a \frac{P_i}{P} \quad (5.282)$$

In this case, the pressure drop is independent of the conversion and the two differential equations are decoupled.

Fortunately, this is the case in many environmental applications where the gas species to be removed are in such low concentrations (large excess of inerts) that the expansion factor is practically zero. As pointed out in the introduction of this section, the basic principles of the analysis are also applicable in the case of adsorption of solutes from the gaseous phase. Again, for environmental applications, the concentration of solutes is so low that the pressure drop is only due to the flow of the gas. Here, the expansion factor has the same meaning, i.e. it measures the change of the volume of the gas phase, which is negligible in the case of low concentrations of the removed gas species.

The solution of eqns. (5.281) and (5.282) is

$$P^2 = P_i^2 - a \frac{2P_i}{\rho_b A} W \Leftrightarrow \frac{P}{P_i} = \left[1 - a \frac{2W}{P_i \rho_b A} \right]^{0.5} \quad (5.283)$$

$$P^2 = P_i^2 - 2a P_i Z \Leftrightarrow \frac{P}{P_i} = \left[1 - a \frac{2Z}{P_i} \right]^{0.5} \quad (5.284)$$

Note that when $\varepsilon_R x_A \ll 1$,

$$\frac{\rho}{\rho_i} = \frac{P}{P_i} \quad (5.285)$$

or

$$\frac{P}{P_i} = (1 - \gamma Z)^{0.5} \quad (5.286)$$

or in terms of the mass of the solid phase,

$$\frac{P}{P_i} = (1 - \beta W)^{0.5} \quad (5.287)$$

where

$$\gamma = \frac{2a}{P_i} \quad (5.288)$$

$$\beta = \frac{2a}{P_i \rho_b A} \quad (5.289)$$

Then, eqs. (5.286) and (5.287) can be inserted into eqs. (5.250) and (5.249), respectively to derive the design equation for the fixed bed.

Approximate solution for a first-order reaction with zero expansion ($\varepsilon_R=0$): For a first-order reaction, the solution of eq. (5.249) is

$$\ln\left(\frac{1}{1-x_A}\right) = \frac{k^\circ}{1.5\gamma u_{s,i}} \left[1 - (1 - \beta W)^{1.5}\right] \quad (5.290)$$

or in terms of the reactor length,

$$\ln\left(\frac{1}{1-x_A}\right) = \frac{k^\circ}{1.5\gamma u_{s,i}} \left[1 - (1 - \gamma Z)^{1.5}\right] \quad (5.291)$$

Approximate solution for the second-order reaction with negligible resistance in the gas film and zero expansion ($k_f \rightarrow \infty$ and $\varepsilon_R=0$): In this case, the solution of eq. (5.249) is (Fogler, 1999)

$$\frac{x_A}{1-x_A} = \frac{k_m C_{A,i} W}{Q_i} \left(1 - \frac{\beta W}{2}\right) \quad (5.292)$$

or in terms of the reactor length,

$$\frac{x_A}{1-x_A} = \frac{k_m \rho_b C_{A,i} Z}{u_{s,i}} \left(1 - \frac{\gamma Z}{2}\right) \quad (5.293)$$

Analysis of the models *First-order reaction:* Let us have a deeper look into the solution of the model for a first-order reaction with zero expansion (eq. (5-291)):

$$\ln\left(\frac{1}{1-x_A}\right) = \frac{k^\circ}{1.5\gamma u_{s,i}} \left[1 - (1 - \gamma Z)^{1.5}\right] \quad (5.294)$$

We can compare it with the well-known solution for fixed beds for no expansion of the gas phase (eq. (5.192):

$$\ln\left(\frac{1}{1-x_A}\right) = \frac{k^\circ Z}{u_{s,i}} \quad (5.295)$$

This solution ignores the pressure drop in the reactor. The difference of these two equations is that the first one has the following parameter instead of Z :

$$f(Z) = \frac{1 - (1 - \gamma Z)^{1.5}}{1.5\gamma} \quad (5.296)$$

The difference between these two equations can be expressed as follows:

$$DZ = \frac{Z - f(Z)}{Z} \quad (5.297)$$

Note that γZ has certain limits originating from eq. (5.286) and as well as from $f(Z)$:

$$(1 - \gamma Z) \geq 0 \Leftrightarrow \gamma Z \leq 1 \quad (5.298)$$

Since $Z \neq 0$ and $\gamma \geq 0$, the above condition means that

$$0 \leq \gamma \leq \frac{1}{Z} \quad (5.299)$$

Now, we are interested in the limits of the function $f(Z)$. It is easy to show that

$$\lim_{\gamma \rightarrow 0} f(Z) = Z \quad (5.300)$$

$$\lim_{\gamma \rightarrow 1/Z} f(Z) = \frac{Z}{1.5} \quad (5.301)$$

Second-order reaction: For a second-order reaction with $k_f \rightarrow \infty$ and zero expansion (eq. (5.293)),

$$\frac{x_A}{1 - x_A} = \frac{k_m \rho_b C_{A,i} Z}{u_{s,i}} \left(1 - \frac{\gamma Z}{2} \right) \quad (5.302)$$

We can compare it with the solution for fixed beds for zero pressure drop and no expansion of the gas phase (eq. (5.225)):

$$\frac{x_A}{1 - x_A} = \frac{k_m \rho_b C_{A,i} Z}{u_{s,i}} \quad (5.303)$$

This solution ignores the pressure drop in the reactor. The difference between these two equations is that the first one has the following parameter instead of Z :

$$g(Z) = Z \left(1 - \frac{\gamma Z}{2} \right) \quad (5.304)$$

The difference between these two equations can be expressed as follows:

$$DDZ = \frac{Z - g(Z)}{Z} \quad (5.305)$$

The limits originating from eq. (5.286) for γZ still hold and thus the limits of the function $g(Z)$ are

$$\lim_{\gamma \rightarrow 0} f(Z) = Z \quad (5.306)$$

$$\lim_{\gamma \rightarrow 1/Z} f(Z) = \frac{Z}{2} \quad (5.307)$$

which are similar to the first-order reaction rate.

To illustrate the situation we set $Z = 1$. Then the condition becomes

$$0 \leq \gamma \leq 1$$

And the limits of the function $f(Z)$ for the first-order reaction are

$$\begin{aligned} \lim_{\gamma \rightarrow 0} f(Z) &= 1 \\ \lim_{\gamma \rightarrow 1} f(Z) &= 0.67 \end{aligned}$$

The corresponding limits for DZ are 0 and 0.33, respectively. For the second-order reaction,

$$\begin{aligned} \lim_{\gamma \rightarrow 0} g(Z) &= 1 \\ \lim_{\gamma \rightarrow 1} g(Z) &= 0.5 \end{aligned}$$

The corresponding limits for DDZ are 0 and 0.5 respectively. This is shown in Figure 5.11.

The pressure drop in the case of reaction: The above analysis means that when $\gamma \rightarrow 0$ the two model solutions converge, for both cases, i.e. the solution becomes the same as the one considering negligible pressure drop. Actually what happens is

$$\left(\frac{2a}{P_i} \right) \rightarrow 0 \Rightarrow \left(\frac{a}{P_i} \right) \rightarrow 0 \quad (5.308)$$

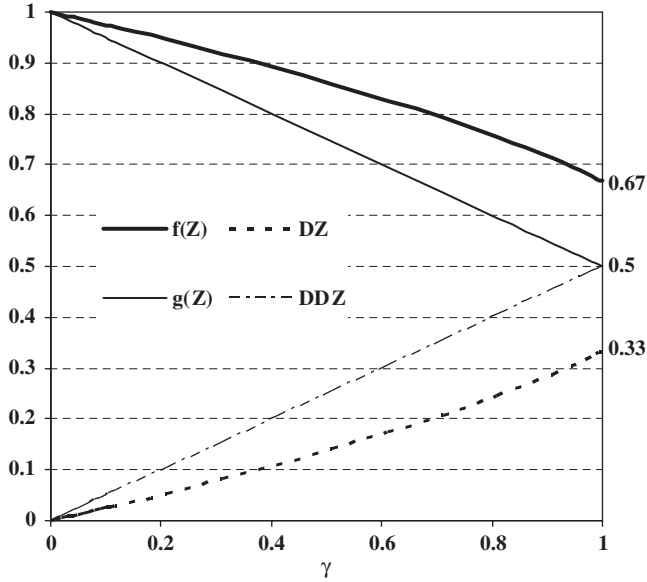


Figure 5.11 The limits of $f(Z)$, $g(Z)$, DZ , and DDZ versus γ .

which means that the inlet pressure is high and/or the pressure gradient in the reactor based on inlet density is relatively low, and from eq. (5.286) we have

$$P_i \gg a \Rightarrow \gamma Z \rightarrow 0 \Rightarrow 1 - \gamma Z \rightarrow 1 \Rightarrow \frac{P}{P_i} \rightarrow 1 \tag{5.309}$$

or in other words, the pressure drop in the reactor becomes negligible. On the other extreme, when $\gamma \rightarrow 1/Z$, the deviation between the two model solutions is significant. What happens is that

$$\left(\frac{2a}{P_i}\right) \rightarrow \frac{1}{Z} \Rightarrow \left(\frac{a}{P_i}\right) \rightarrow \frac{0.5}{Z} \tag{5.310}$$

From eq. (5.286) we have

$$(1 - \gamma Z) \rightarrow 0 \Rightarrow \frac{P}{P_i} \rightarrow 0 \tag{5.311}$$

or in other words, the pressure drop in the reactor becomes very high. This is why Smith (1981) states: “In most cases pressure drop is small with respect to the total pressure so

that ignoring this effect is justified. However, for gaseous reactions at low pressures the change in pressure may affect the global rate significantly.”

As engineers, we need some approximate values not only for design purposes but also to have a sense of the parameter’s magnitude. Thus, to go one step further in our analysis, we would like to answer the question “what is the practical limit above which the two solutions deviate considerably,” or in other words “what should be limit of the pressure drop in the reactor in order to assume that its effect is negligible.”

First-order reaction: Now, first of all we have to define what is a “considerable difference.” For a first order reaction with zero expansion this would be

$$f(Z) \geq 0.95Z \quad (5.312)$$

or

$$DZ = \frac{Z - f(Z)}{Z} \leq 0.05 \quad (5.313)$$

which means that $f(Z)$ deviates from Z by less than 5%. The condition we set is the following:

$$\frac{1 - (1 - \gamma Z)^{1.5}}{1.5\gamma} \geq 0.95Z \quad (5.314)$$

or, because γ is positive,

$$1 - (1 - \gamma Z)^{1.5} \geq 1.425\gamma Z \quad (5.315)$$

and rearranging,

$$1 - (1 - \gamma Z)^{1.5} - 1.425\gamma Z \geq 0 \quad (5.316)$$

It is easy to show that this function has two roots, i.e. $\gamma Z = 0$ and 0.193 and for $\gamma Z > 0.193$ the function becomes negative. From the definition of γ ,

$$\gamma Z = \frac{2a}{P_i} Z \leq 0.193 \quad (5.317)$$

or

$$aZ \leq 0.097P_i \quad (5.318)$$

The pressure gradient a can be easily evaluated from the Ergun equation by setting $\rho = \rho_i$. By using eq. (5.286) and for $(\gamma Z) \leq 0.193$:

$$\frac{P}{P_i} \leq 0.898 \quad (5.319)$$

and the total pressure drop in the reactor is

$$|\Delta P| = P_i - P \leq 0.102P_i \quad (5.320)$$

or

$$\frac{|\Delta P|}{P_i} \leq 0.102 \quad (5.321)$$

which means that the total pressure drop should be less than 10.2%, and in this case the pressure-drop effect on the reactor model can be neglected.

Second-order reaction: As in the previous case, the safety criterion could be

$$g(Z) \geq 0.95Z \quad (5.322)$$

or

$$DDZ = \frac{Z - g(Z)}{Z} \leq 0.05 \quad (5.323)$$

which means that $g(Z)$ deviates from Z by less than 5%. The condition we set is the following:

$$Z \left(1 - \frac{\gamma Z}{2} \right) \geq 0.95Z \quad (5.324)$$

or, because Z is positive and nonzero,

$$1 - \frac{\gamma Z}{2} \geq 0.95 \quad (5.325)$$

and rearranging,

$$\gamma Z \leq 0.1 \quad (5.326)$$

From the definition of γ ,

$$\gamma Z = \frac{2a}{P_i} Z \leq 0.1 \quad (5.327)$$

or

$$aZ \leq 0.05P_i \quad (5.328)$$

The pressure gradient a can be easily evaluated from the Ergun equation by setting $\rho = \rho_i$. By using eq. (5.286) and for $(\gamma Z) \leq 0.1$,

$$\frac{P}{P_i} \leq 0.949 \quad (5.329)$$

and the total pressure drop in the reactor is

$$|\Delta P| = P_i - P \leq 0.051P_i \quad (5.330)$$

or

$$\frac{|\Delta P|}{P_i} \leq 0.051 \quad (5.331)$$

which means that the pressure drop should be less than 5.1%, and in this case the pressure-drop effect on the reactor model can be neglected.

The pressure drop in the absence of reaction: In a fixed bed where no reaction takes place, the outlet pressure can be evaluated as follows:

$$\left(\frac{P}{P_i}\right)_A = \left(1 - \frac{2aZ}{P_i}\right)^{0.5} \quad (5.332)$$

where

$$\frac{a}{P_i} Z \leq 0.5 \quad (5.333)$$

Assuming that the density is constant, we can use the Ergun equation to evaluate the exit pressure as follows. We have

$$\frac{\Delta P}{Z} = -a \quad (5.334)$$

then

$$P - P_i = -aZ \Rightarrow \left(\frac{P}{P_i}\right)_E = 1 - \frac{aZ}{P_i} \quad (5.335)$$

we define the difference as

$$\omega = \left(\frac{P}{P_i}\right)_A - \left(\frac{P}{P_i}\right)_E = \left(1 - \frac{2aZ}{P_i}\right)^{0.5} - \left(1 - \frac{aZ}{P_i}\right) \quad (5.336)$$

From this equation, it can be proved that ω is negative and thus the outlet pressure derived from the Ergun equation is always higher than the actual one, or in other words, the pressure drop is lower than the actual one. This is shown in Figure 5.12, where

$$\% \omega = \left| \frac{\omega}{(P/P_i)_A} - 100 \right| \quad (5.337)$$

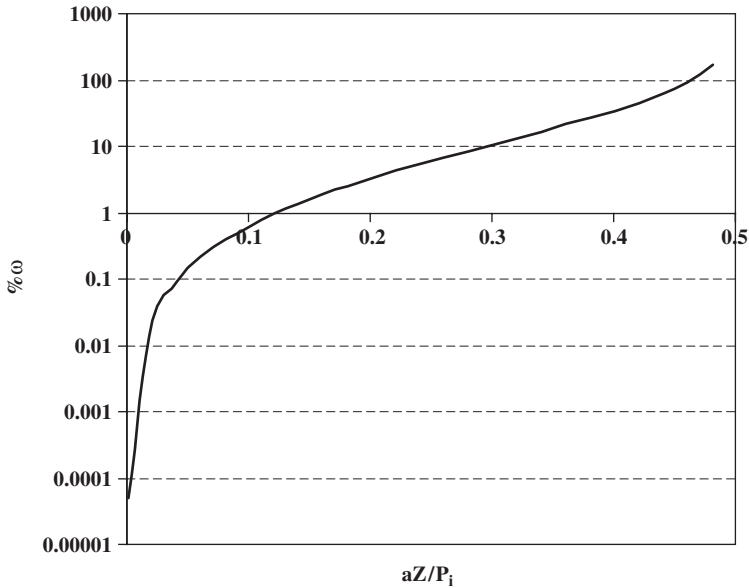


Figure 5.12 $\% \omega$ versus aZ/P_i

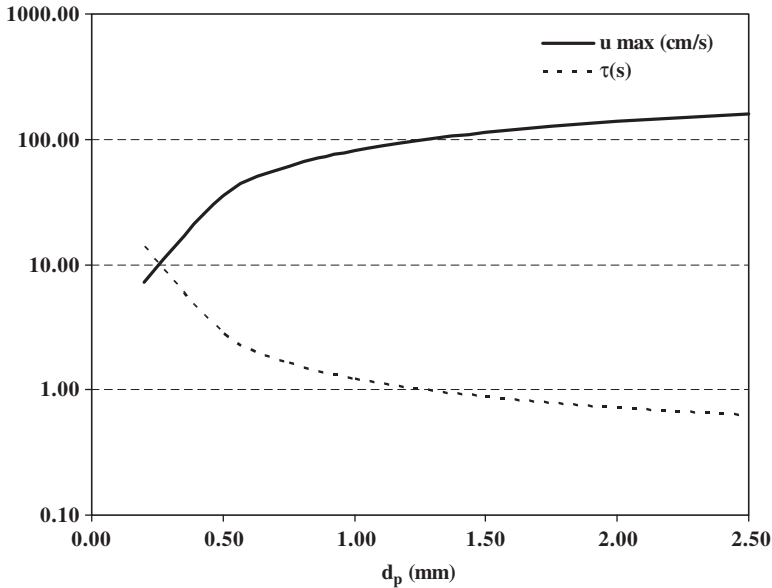


Figure 5.13 The effect of particle density on the limiting contact time in a typical fixed bed (air at 20 °C, $P_i = 1$ atm, $\varepsilon = 0.5$, $\rho_p = 2$ g/cm³, $Z = 1$ m).

As can be seen, $aZ/P_i = 0.1$ seems to be an adequate upper limit to assume the error in the pressure drop estimation introduced by assuming constant fluid density to be negligible (% ω is lower than about 0.64%). As has been analyzed previously, the limiting value of aZ/P_i is different (lower) in the case of a reacting system. This is why the analysis here is on the differences in pressure-drop estimation originating from the assumption of constant fluid density in a non-reacting system, while in reacting systems the analysis is on the effect of zero pressure drop assumption in the simplified models.

In Figure 5.13, the maximum superficial velocity and the corresponding minimum contact time for keeping aZ/P_i lower than 0.1 is shown for a typical fixed bed with no reaction.

It is clear that the limit in aZ/P_i can be easily satisfied in fixed beds with particles larger than about 1 mm, where the bed can be operated in a wide range of superficial fluid velocities up to values in the vicinity of 100 cm/s.

Example 9

Suppose we have measured the total pressure drop in a packed bed of known length. Then, one expressed the opinion that to calculate the pressure gradient, we have to only divide the pressure drop with the bed length. Do you agree?

Solution

Pressure drop is a function of bed length and in the general case,

$$\Delta P = -f(z)$$

Then, by dividing the total pressure drop by the bed length we obtain

$$\frac{\Delta P}{Z} = \frac{-f(z)}{Z}$$

Furthermore,

$$\Delta P = P - P_i \Rightarrow P = P_i - f(z)$$

Then, the pressure gradient is

$$\frac{dP}{dz} = \frac{d[P_i - f(z)]}{dz} = -f'(z)$$

Consequently,

$$\frac{dP}{dz} \neq \frac{\Delta P}{Z}$$

unless

$$f'(z) = \frac{f(z)}{Z}$$

which is true only for a linear function of the form

$$f(z) = az$$

This is the case where the total pressure drop is a linear function of bed length, or

$$\Delta P = -aZ$$

Then, by dividing the total pressure drop by the bed length we obtain:

$$\frac{\Delta P}{Z} = -a$$

Furthermore,

$$\Delta P = P - P_i \Rightarrow P = P_i - aZ$$

Then, the pressure gradient is

$$\frac{dP}{dz} = \frac{d[P_i - az]}{dz} = -a$$

Consequently,

$$\frac{dP}{dz} = \frac{\Delta P}{Z}$$

In this special case, the pressure gradient is independent of the bed length and this could be the case only if the expansion due to reaction is zero, or in absence of any reaction and the constant fluid density throughout the reactor volume. Then, it is clear that the general impression that the pressure gradient is equal to the total pressure drop divided by the bed length it is true only under certain conditions.

In the case of a reaction with no expansion or in absence of any reaction, by using eq. (5.286),

$$\Delta P = P - P_i = -P_i [1 - (1 - \gamma Z)^{0.5}]$$

Then, by dividing the total pressure drop by the bed length, we get

$$\frac{\Delta P}{Z} = \frac{-P_i [1 - (1 - \gamma Z)^{0.5}]}{Z}$$

Furthermore, by using eq. (5.286),

$$\begin{aligned} \Delta P &= P - P_i \\ \Rightarrow P &= P_i - P_i [1 - (1 - \gamma Z)^{0.5}] \\ \Rightarrow P &= P_i (1 - \gamma Z)^{0.5} \end{aligned}$$

Then, the pressure gradient is

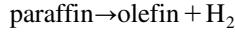
$$\frac{dP}{dz} = \frac{d[P_i (1 - \gamma Z)^{0.5}]}{dz} = -\frac{\gamma P_i}{2(1 - \gamma Z)^{0.5}}$$

And thus

$$\frac{dP}{dz} \neq \frac{\Delta P}{Z}$$

Example 10

Consider the following typical reaction in petroleum reforming process:



which can be considered a first-order reaction in respect to paraffin. The reaction constant is $2 \times 10^{-5} \text{ m}^3/\text{kg s}$ and the internal effectiveness factor 0.5. The reaction takes place in a fixed bed 20 m long and 3 m in diameter. The spherical particles used are of 1.5 mm diameter and 2.6 g/cm^3 density. The bed voidage is 0.4. Pure paraffin enters the reactor with a rate of $0.25\text{--}1.55 \text{ m}^3/\text{s}$ and pressure of 10 atm. The density of paraffin is 0.032 g/cm^3 , its viscosity $1.5 \times 10^{-5} \text{ kg/m s}$, the diffusion coefficient $0.1 \text{ cm}^2/\text{s}$, and the average molecular weight 0.1 kg/mol .

Calculate the conversion of paraffin in the following cases:

- Using the real ε_R and pressure drop (case 1)
- Assuming $\varepsilon_R = 0$ and taking into account the pressure drop (case 2)
- Assuming $\varepsilon_R = 0$ and ignoring pressure drop (case 3)
- Using the real ε_R and ignoring pressure drop (case 4)

Solution

Reactor models: At first, we write the general model for the reactor consisting of two coupled differential equations.

The mass balance for a first-order reaction, eq. (5.272):

$$\frac{dx_A}{dz} = \frac{k^\circ}{u_{s,i}} \frac{1-x_A}{1+\varepsilon_R x_A} \frac{P}{P_i}$$

The pressure drop equation (5.275):

$$\frac{dP}{dz} = -a(1+\varepsilon_R x_A) \frac{P_i}{P}$$

where for spherical particles $\Phi_s = 1$ and thus (eq. (5.258))

$$a = -\frac{dP}{dz} = \frac{150\mu u_{s,i} (1-\varepsilon)^2}{d_p^2 \varepsilon^3} + \frac{1.75\rho_i u_{s,i}^2 (1-\varepsilon)}{d_p \varepsilon^3}$$

Furthermore (eq. (5.211)),

$$\frac{1}{k^\circ} = \frac{1}{(k_f a_u)} + \frac{1}{\rho_b k_m}$$

Then, we have the following simplified models.

For zero expansion and taking into account the pressure-drop effect, the solution is (eq. (5.291))

$$\ln\left(\frac{1}{1-x_A}\right) = \frac{k^\circ}{1.5\gamma u_{s,i}} [1 - (1 - \gamma Z)^{1.5}]$$

where (eq. (5.288))

$$\gamma = \frac{2a}{P_i}$$

For zero expansion and ignoring the pressure-drop effect, the solution is (eq. (5.192))

$$\ln\left(\frac{1}{1-x_A}\right) = \frac{k^\circ}{u_{s,i}} Z$$

Taking into account the expansion and ignoring the pressure-drop effect, the solution is (eq. (5.218))

$$(1 + \varepsilon_R) \ln\left(\frac{1}{1-x_A}\right) - \varepsilon_R x_A = \frac{k^\circ}{u_{s,i}} Z$$

It is evident that for case 1 we need an arithmetic solution, and a software package like Polymath can be used. The rest of the cases have analytic solutions.

Parameters of the system: For the specified reaction $\delta = 1$ (eq. (3.87)) and since we have a pure gas in the feed, $\varepsilon_R = 1$ (eq. (3.88)). The rest of the parameters we need are shown in Table 5.11 for three different volumetric flow rates. For the mass transfer coefficient, the correlation of Petrovic and Thodos is used (eq. (3.353)).

From the values of the Table 5.11, it is clear that the mass transfer coefficient is quite high and its contribution to the overall coefficient k° is negligible, and thus the reaction on

Table 5.11

The values of the parameters

Q_i (m ³ /s)	k_f (m/s)	k° (s ⁻¹)	a (Pa/m)
0.25	0.0443	1.56×10^{-2}	637
0.5	0.069	1.56×10^{-2}	2151
1	0.107	1.56×10^{-2}	7808
1.5	0.139	1.56×10^{-2}	16971
1.55	0.156	1.56×10^{-2}	18080

the surface is the rate-controlling mechanism. By using these parameters and the data given in this example, the conversion of paraffin is shown in Table 5.12.

The total pressure drop is evaluated by the general model (case 1), i.e. is the real one. The general model, case 1 (eqs. (5.572) and (5.575)) can be solved only by numerical methods, e.g. Polymath software.

For better inspection, the results are shown graphically in Figure 5.14. From the results, the following is evident

- The models of cases 1 and 4 give approximately the same results up to a pressure drop of 27% (1 m³/s). The difference between these two models is that in case 4, the pressure-drop effect is ignored. Thus, even for relatively high pressure drop, a simplified model that takes into account the expansion but not the pressure drop is able to approximate the real conversion.

Table 5.12

The conversion for each case

Q_i (m ³ /s)	ΔP (%)	Case 1	Case 2	Case 3	Case 4
0.25	2	0.99	1	1	0.99
0.5	7	0.93	0.99	0.99	0.93
1	27	0.74	0.87	0.89	0.77
1.5	73.2	0.55	0.69	0.77	0.65
1.55	87.2	0.53	0.67	0.76	0.64

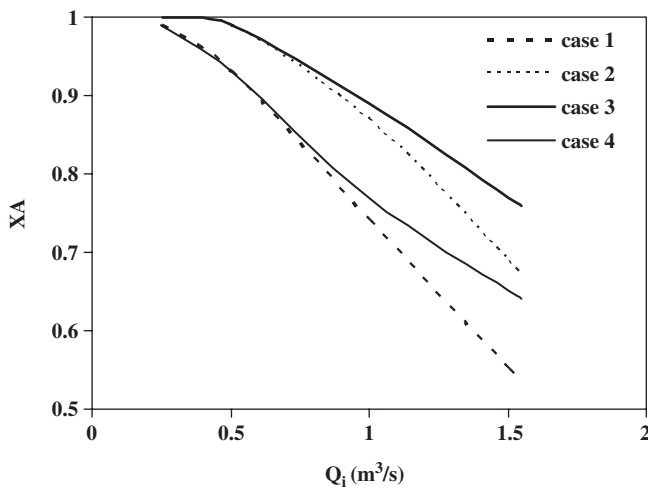


Figure 5.14 The conversion versus volumetric feed for each case.

- The models of cases 2 and 3 give approximately the same results up to a pressure drop of 27% ($1 \text{ m}^3/\text{s}$). The difference between these two models is that in case 4, the pressure-drop effect is ignored. Again, the pressure-drop effect seems to be of less importance for this level of pressure drop. Of course, the differences between these two models and not to their performance is being referred to, as we see that they deviate a lot from the general solution in the whole region of volumetric flow rates.

It is clear that ignoring the expansion, the deviation is very serious for the whole region of volumetric flow rates while ignoring the pressured-drop effect, but using the expansion factor the results could be very good up to a certain pressure-drop level, which is approximately 27% in our example.

5.3.5 Trickle-bed reactors

In the following sections, the solutions of the models as well as examples will be presented for the case of trickle-bed reactors and packed bubble bed reactors. Plug flow and first-order reaction will be assumed in order to present analytical solutions. Furthermore, the expansion factor is considered to be zero unless otherwise stated. Some solutions for other kinetics will be also given. The reactant A is gas and the B is liquid unless otherwise stated.

Conservation equations for each flowing phase—Smith's approach

Pure component in gas phase and saturated liquid phase *First-order kinetics in A:* In this case, the gas phase is a pure component A (C_{AG} is constant) and the liquid phase is considered to be saturated with A (C_{AL} is constant). Furthermore, the intrinsic rate is considered to be of first order with respect to A: $-r_m = k_m C_{AS}$, per unit mass of catalyst. Under these conditions, the material balances for the gas component A in the gas and liquid phases (eqs. (3.365) and (3.367)) are not needed: C_{AL} is constant and equal to $C_{ALeq} = C_{AG}/H_A$. The same analysis is valid for reactions of first order for both components, if $C_{BL} \gg C_{AL}$ and thus $C_{BS} \cong \text{const.}$ (pseudo-first order) (Smith, 1981). Then (eq. (3.369))

$$(k_f a_u)_A [C_{AL} - C_{AS}] = \rho_b \eta_s k_m C_{AS} \quad (5.338)$$

or

$$C_{AS} = \frac{(k_f a_u)_A}{(k_f a_u)_A + \rho_b \eta_s k_m} C_{AL} = \frac{(k_f a_u)_A}{(k_f a_u)_A + \rho_b \eta_s k_m} \left(\frac{C_{AG}}{H_A} \right) \quad (5.339)$$

And thus

$$(k_f a_u)_B [C_{BL} - C_{BS}] = \frac{\rho_b \eta_s k_m C_{AS}}{a} = \frac{1}{a} \frac{(k_f a_u)_A \rho_b \eta_s k_m}{(k_f a_u)_A + \rho_b \eta_s k_m} \left(\frac{C_{AG}}{H_A} \right) \quad (5.340)$$

where η_s is the internal effectiveness factor. The overall coefficient k° is

$$k^\circ = \frac{(k_f a_u)_A \rho_b \eta_s k_m}{(k_f a_u)_A + \rho_b \eta_s k_m} \Leftrightarrow \frac{1}{k^\circ} = \frac{1}{(k_f a_u)_A} + \frac{1}{\rho_b \eta_s k_m} \quad (5.341)$$

Then using the mass conservation in the liquid phase for the liquid reactant B (eq. (3.368)),

$$u_{sL} \frac{dC_{BL}}{dz} + (k_f a_u)_B [C_{BL} - C_{BS}] = 0 \Rightarrow u_{sL} \frac{dC_{BL}}{dz} + \frac{k^\circ}{a} \left(\frac{C_{AG}}{H_A} \right) = 0 \quad (5.342)$$

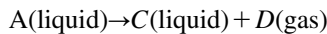
The boundary (feed) condition is $C_{BL} = C_{BL,f}$ at $z = 0$. Then, the integration of the previous equation yields

$$C_{BL} - C_{BL,f} = -\frac{k^\circ Z}{a u_{sL}} \left(\frac{C_{AG}}{H_A} \right) \quad (5.343)$$

where Z is the catalyst bed depth. In terms of the fractional removal of B:

$$x_B = \frac{C_{BL,f} - C_{BL}}{C_{BL,f}} = \frac{k^\circ Z}{a u_{sL}} \left(\frac{C_{AG}}{C_{BL,f} H_A} \right) \quad (5.344)$$

First order kinetics in B: As in the previous case, the gas phase is composed of a pure component A (C_{AG} is constant) and the liquid phase is considered to be saturated with A (C_{AL} is constant). However, in this case, the intrinsic rate is considered to be of first order with respect to B: $-r_m = k_m C_{BS}$, per unit mass of catalyst. Under these conditions, the same analysis is valid for reactions of first order for both components, if C_{BL} is very low, i.e. the reaction rate is pseudo-first order in respect to B (Smith, 1981). Furthermore, the analysis is valid for reactions of the type (Wu, 1996)



Then

$$(k_f a_u)_B [C_{BL} - C_{BS}] = \rho_b \eta_s k_m C_{BS} \quad (5.345)$$

or

$$C_{BS} = \frac{(k_f a_u)_B}{(k_f a_u)_B + \rho_b \eta_s k_m} C_{BL} \quad (5.346)$$

The overall coefficient k° is

$$k^\circ = \frac{(k_f a_u)_B \rho_b \eta_s k_m}{(k_f a_u)_B + \rho_b \eta_s k_m} \Leftrightarrow \frac{1}{k^\circ} = \frac{1}{(k_f a_u)_B} + \frac{1}{\rho_b \eta_s k_m} \quad (5.347)$$

Then using the mass conservation in the liquid phase for the liquid reactant B (eq. (3.368)),

$$u_{sL} \frac{dC_{BL}}{dz} + (k_f a_u)_B [C_{BL} - C_{BS}] = 0 \Rightarrow u_{sL} \frac{dC_{BL}}{dz} + k^\circ C_{BL} = 0 \quad (5.348)$$

The boundary (feed) condition is $C_{BL} = C_{BL,f}$ at $z = 0$. Then, the integration yields

$$\frac{C_{BL}}{C_{BL,f}} = \exp\left(-\frac{k^\circ Z}{u_{sL}}\right) \quad (5.349)$$

where Z is the catalyst bed depth. In terms of the fractional removal of B ,

$$x_B = \frac{C_{BL,f} - C_{BL}}{C_{BL,f}} = 1 - \exp\left(-\frac{k^\circ Z}{u_{sL}}\right) \quad (5.350)$$

or

$$\ln\left(\frac{1}{1 - x_B}\right) = \frac{k^\circ Z}{u_{sL}} \quad (5.351)$$

Pure component in gas phase and first-order kinetics in the gas reactant In this case, the gas phase is a pure component A (C_{AG} is constant) and the concentration of A in the feed liquid phase is considered to be zero (unsaturated liquid phase). Furthermore, A is slightly soluble in the liquid (H_A is large) so that $K_L \cong k_{fg}$, while the intrinsic rate is of first order with respect to A: $-r_m = k_m C_{AS}$, per unit mass of catalyst.

For reactant A in the liquid phase, at steady state (eq. (3.367)),

$$-u_{sL} \frac{dC_{AL}}{dz} + (K_L a_{GL})_A \left[\frac{C_{AG}}{H_A} - C_{AL} \right] - (k_f a_u)_A [C_{AL} - C_{AS}] = 0 \quad (5.352)$$

Then

$$(k_f a_u)_A [C_{AL} - C_{AS}] = \rho_b \eta_s k_m C_{AS} \quad (5.353)$$

or

$$C_{AS} = \frac{(k_f a_u)_A}{(k_f a_u)_A + \rho_b \eta_s k_m} C_{AL} \quad (5.354)$$

or

$$C_{AL} - C_{AS} = \frac{\rho_b \eta_s k_m}{(k_f a_u)_A + \rho_b \eta_s k_m} C_{AL} \quad (5.355)$$

Then, the equation for reactant A in the liquid phase becomes

$$-u_{sL} \frac{dC_{AL}}{dz} + (K_L a_{GL})_A \left[\frac{C_{AG}}{H_A} - C_{AL} \right] - k^\circ C_{AL} = 0 \quad (5.356)$$

where

$$k^\circ = \frac{(k_f a_u)_A \rho_b \eta_s k_m}{(k_f a_u)_A + \rho_b \eta_s k_m} \Leftrightarrow \frac{1}{k^\circ} = \frac{1}{(k_f a_u)_A} + \frac{1}{\rho_b \eta_s k_m} \quad (5.357)$$

This equation could be integrated to give the following equation for C_{AL} as a function of z :

$$C_{AL} = \frac{\left(\frac{C_{AG}}{H_A} \right)}{1 + \left[\frac{k^\circ}{(K_L a_{GL})_A} \right]} \left\{ 1 - \exp \left[- \left[(K_L a_{GL})_A + k^\circ \right] \frac{z}{u_{sL}} \right] \right\} \quad (5.358)$$

Then the mass conservation in the liquid phase for the liquid reactant B (eq. (3.368)) should be integrated:

$$u_{sL} \frac{dC_{BL}}{dz} + (k_f a_u)_B [C_{BL} - C_{BS}] = 0 \quad (5.359)$$

To do this, the surface concentration in the term in brackets must be eliminated. So, we use the equation

$$(k_f a_u)_A [C_{AL} - C_{AS}] = \rho_b \eta_s k_m C_{AS} \quad (5.360)$$

or

$$C_{AS} = \frac{(k_f a_u)_A}{(k_f a_u)_A + \rho_b \eta_s k_m} C_{AL} = \frac{(k_f a_u)_A}{(k_f a_u)_A + \rho_b \eta_s k_m} C_{AL} \quad (5.361)$$

Then

$$(k_f a_u)_B [C_{BL} - C_{BS}] = \frac{\rho_b \eta_s k_m C_{AS}}{a} = \frac{1}{a} \frac{(k_f a_u)_A \rho_b \eta_s k_m}{(k_f a_u)_A + \rho_b \eta_s k_m} C_{AL} = \frac{k^\circ}{a} C_{AL} \quad (5.362)$$

Then, using expression (5.358) derived above for C_{AL} ,

$$(k_f a_u)_B [C_{BL} - C_{BS}] = m [1 - \exp(-nz)] \quad (5.363)$$

where the parameters m and n are

$$m = \frac{k^\circ}{a} \frac{\left(\frac{C_{AG}}{H_A} \right)}{1 + \left[\frac{k^\circ}{(K_L a_{GL})_A} \right]} \quad (5.364)$$

$$n = \frac{(K_L a_{GL})_A + k^\circ}{u_{sL}} \quad (5.365)$$

Then, the mass conservation equation for reactant B in the liquid phase becomes

$$u_{sL} \frac{dC_{BL}}{dz} + m [1 - \exp(-nz)] = 0 \quad (5.366)$$

Integrating, with the boundary condition $C_{BL} = C_{BL,f}$ at $z = 0$,

$$C_{BL} - C_{BL,f} = -m \frac{Z}{u_{sL}} - \frac{m}{nu_{sL}} \{ [\exp(-nZ)] - 1 \} \quad (5.367)$$

where Z is the catalyst bed depth. In terms of the fractional removal of B,

$$x_B = \frac{C_{BL,f} - C_{BL}}{C_{BL,f}} = \frac{m}{C_{BL,f}} \left\{ \frac{Z}{u_{sL}} + \frac{1}{nu_{sL} C_{BL,f}} \{ [\exp(-nZ)] - 1 \} \right\} \quad (5.368)$$

Gas mixture and first-order kinetics In the previous cases, the gas-phase conservation equation was not needed because the gas was pure A. This is the case where a trickle-bed reactor is used to remove pollutants from a gas stream. In this case, the gas phase is a mixture. Consider the reaction



The reaction is catalyzed by the solid phase and the product dissolves in the liquid phase. The intrinsic rate is $-r_m = k_m C_{AS}$, per unit mass of catalyst. Then

$$(k_f a_u)_A [C_{AL} - C_{AS}] = \rho_b k_m \eta_s C_{AS} \quad (5.369)$$

or

$$C_{AS} = \frac{(k_f a_u)_A}{(k_f a_u)_A + \rho_b \eta_s k_m} C_{AL} = \lambda C_{AL} \quad (5.370)$$

where

$$\lambda = \frac{(k_f a_u)_A}{(k_f a_u)_A + \rho_b \eta_s k_m} \quad (5.371)$$

For reactant A in the liquid phase (eq. (3.367)),

$$-u_{sL} \frac{dC_{AL}}{dz} + (K_L a_{GL})_A \left[\frac{C_{AG}}{H_A} - C_{AL} \right] - (k_f a_u)_A C_{AL} (1 - \lambda) = 0 \quad (5.372)$$

For reactant A in the gas phase (eq. (3.365)),

$$u_{sG} \frac{dC_{AG}}{dz} + (K_L a_{GL})_A \left[\frac{C_{AG}}{H_A} - C_{AL} \right] = 0 \Rightarrow \frac{C_{AG}}{H_A} - C_{AL} = - \left[\frac{u_{sG}}{(K_L a_{GL})_A} \right] \frac{dC_{AG}}{dz} \quad (5.373)$$

or

$$C_{AL} = \frac{C_{AG}}{H_A} + \left[\frac{u_{sG}}{(K_L a_{GL})_A} \right] \frac{dC_{AG}}{dz} \quad (5.374)$$

Differentiation of the last equation yields

$$\frac{dC_{AL}}{dz} = \frac{1}{H_A} \frac{dC_{AG}}{dz} + \left[\frac{u_{sG}}{(K_L a_{GL})_A} \right] \frac{d^2 C_{AG}}{dz^2} \quad (5.375)$$

If eqs. (3.573)–(3.575) are substituted into eq. (3.372), a second-order differential equation is obtained with C_{AG} as the only dependent variable. The expression may be written as

$$\frac{d^2 C_{AG}}{dz^2} + \xi \frac{dC_{AG}}{dz} + \psi C_{AG} = 0 \quad (5.376)$$

where

$$\xi = \frac{u_{sG} + \left(\frac{u_{sL}}{H_A} \right) + (k_f a_u)_A (1 - \lambda) \left(\frac{u_{sG}}{(K_L a_{GL})_A} \right)}{\left(\frac{u_{sL} u_{sG}}{(K_L a_{GL})_A} \right)} \quad (5.377)$$

$$\psi = \frac{(k_f a_u)_A (K_L a_{GL})_A (1 - \lambda)}{H_A u_{sL} u_{sG}} \quad (5.378)$$

The boundary conditions are $C_{AG} = C_{AG,f}$ (feed) at $z = 0$ and $C_{AL} = (C_{AG,f}/H_A)$ (equilibrium). Using eq. (5.374), the second boundary condition becomes $dC_{AG}/dZ = 0$ at $z = 0$.

The solution of eq. (5.376) under these boundary conditions is

$$\frac{C_{AG}}{C_{AG,f}} = \frac{1}{m_2 - m_1} [m_2 \exp(m_1 Z) - m_1 \exp(m_2 Z)] \quad (5.379)$$

or

$$x_A = 1 - \frac{C_{AG}}{C_{AG,f}} \quad (5.380)$$

where

$$m_1 = -\frac{\xi}{2} + \frac{1}{2} (\xi^2 - 4\psi)^{0.5} \quad (5.381)$$

$$m_2 = -\frac{\xi}{2} - \frac{1}{2} (\xi^2 - 4\psi)^{0.5} \quad (5.382)$$

The above solution is also valid in the cases where A is a component of a gas mixture with inerts and B is liquid but its concentration does not change considerably, e.g. in the case where B is a pure liquid.

Neglecting the change in the concentration of A in the liquid between feed and effluent ($C_{AL} \cong \text{constant}$), the reaction requires that for each mole of A, b moles of B are removed from the gas stream:

$$b(C_{AG,f} - C_{AG}) = (C_{BG,f} - C_{BG}) \quad (5.383)$$

Then, the fractional removal of B is

$$x_B = \frac{C_{BG,f} - C_{BG}}{C_{BG,f}} = b \frac{C_{AG,f}}{C_{BG,f}} \left(1 - \frac{C_{AG}}{C_{AG,f}} \right) = b \frac{C_{AG,f}}{C_{BG,f}} x_A \quad (5.384)$$

This equation can be used for the calculation of the fractional removal of B from the gas only by reaction. This does not account for B that might be removed from the effluent liquid (Smith, 1981).

Material balances using an overall rate—Fogler's approach

Mass transfer of the gaseous reactant limiting For a first-order reaction in both A and B, if the first two terms in the denominator of K_A^o (eq. (3.387)) are dominant or if the liquid-phase concentration of B does not vary significantly through the bed ($C_{Bs} = \text{const.}$),

$$\ln \left(\frac{1}{1 - x_A} \right) = \frac{K_A^o Z}{u_{sG}} = \frac{K_A^o V_R}{Q_G} = \frac{K_A^o \left(\frac{M_s}{\rho_b} \right)}{Q_G} \quad (5.385)$$

In this case, the material balance of B is not needed. The same solution holds for the case of a first-order reaction rate with respect to A without the assumption of constant liquid concentration of B.

In the case of variable-volume systems ($\varepsilon_R \neq 0$) (Fogler, 1999),

$$(1 + \varepsilon_R) \ln \left(\frac{1}{1 - x_A} \right) - \varepsilon_R X_A = \frac{K_A^o V_R}{Q_{G,i}} = \frac{K_A^o \left(\frac{M_s}{\rho_b} \right)}{Q_{G,i}} \quad (5.386)$$

where $Q_{G,i}$ the inlet gas flow rate.

In trickle beds, if the gas pressure changes due to pressure drop, then this effect should be taken into account. If the pressure drop of the gas phase is a_o in atm/m, then

$$P = P_i - a_o Z \Leftrightarrow \frac{P}{P_i} = 1 - \frac{a_o Z}{P_i} \quad (5.387)$$

Since

$$M_s = \rho_b V_R = \rho_b Z A \quad (5.388)$$

or

$$Z = \frac{M_s}{\rho_b A} \quad (5.389)$$

where A is the cross-sectional area of the bed. Then, in terms of the mass of the solid phase (Fogler 1999),

$$\frac{P}{P_i} = 1 - \beta_o M_s \quad (5.390)$$

$$\beta_o = \frac{a_o}{P_i \rho_b A} \quad (5.391)$$

Then, the solution is (Fogler, 1999)

$$(1 + \varepsilon_R) \ln \left(\frac{1}{1 - x_A} \right) - \varepsilon_R X_A = \frac{K_A^o}{\rho_b Q_{g,i}} \left(M_s - \frac{\beta_o}{2} M_s^2 \right) \quad (5.392)$$

or in terms of the reactor volume,

$$(1 + \varepsilon_R) \ln \left(\frac{1}{1 - x_A} \right) - \varepsilon_R X_A = \frac{K_A^o}{u_{sG}} \left(Z - \frac{\beta_o}{2} \rho_b A Z^2 \right) \quad (5.393)$$

Mass transfer and reaction of the liquid species limiting For a first-order reaction in both A and B and provided that the liquid phase is entirely saturated with A throughout the bed, i.e. C_{AS} is constant,

$$\ln \left(\frac{1}{1 - x_B} \right) = \frac{K_B^o Z}{u_{sL}} = \frac{K_B^o V_R}{Q_L} = \frac{K_B^o \left(\frac{M_s}{\rho_b} \right)}{Q_L} \quad (5.394)$$

Note that the same solution has been found for the case of a first-order reaction rate with respect to B, when the gas-phase concentration of A is constant and the liquid is saturated with A (eq. (5.351)).

Note that Fogler's approach is convenient when

- the reaction rate is of first order in both reactants A and B
- the gas phase is a mixture of A and inerts, and B is a liquid
- in variable-volume systems ($\varepsilon_R \neq 0$)
- when the pressure drop of the gas phase is significant

A typical example of this kind is the hydrogenation of unsaturated organics as presented by Fogler (1999). The reaction is of the form



This reaction is of first order in both A and B and the gas phase is a mixture of hydrogen and inerts. Furthermore, the liquid phase is normally pure organic B, and thus it can be assumed that its concentration does not vary significantly through the bed, and thus the case where the mass transfer of the gaseous reactant is limiting is applicable.

However, it cannot cover the cases

- when both reactants are in the gas phase
- when the liquid concentration of A is changing in the reactor

Example 11

Consider the hydrogenation of an unsaturated organic carried out in a trickle-bed reactor. The reaction is



The reaction is of first order in both hydrogen and the organic. However, if the liquid is pure organic and its conversion low, we can assume that its concentration is constant and the reaction rate becomes first order in hydrogen. The gas feed is a mixture of hydrogen and inerts.

Suppose that the reaction takes place in a commercial trickle-bed reactor with $D = 1$ m and $Z = 10$ m and that the gas superficial velocity is 0.02 m/s. The feed is H_2 and 98% inerts. The liquid mass superficial velocity varies between 2 and 12 kg/m² s.

Use the approach of Smith and Fogler, compare the achieved conversions, and explain the differences.

The following data are given by Fogler (1999): $T = 400$ K, $P = 20$ atm, $k_m = 3 \times 10^{-5}$ m³/kg s, $H_A = 3.81$, $\rho_b = 900$ kg/m³, $\rho_l = 840$ kg/m³, $\mu_l = 0.0018$ kg/m s, $D_{fg} = 2.4 \times 10^{-9}$ m²/s, $\varepsilon = 0.4$ and $\eta_s = 0.28$.

Since the reaction is of first order with respect to hydrogen for 50% inerts, it is reasonable to assume that for even lower hydrogen concentration (98% inerts) the reaction order does not change.

Solution

With the specified hydrogen concentration of 2%, the expansion factor is -0.02 and thus it can be assumed to be approximately zero. To use the models, the next step is to find the pressure drop in the reactor. This is vital because if the pressure drop is significant, then its effect on the operation should be taken into account.

In order to evaluate the pressure drop in the reactor, we can use the Ergun equation for both phases and then the two-phase pressure drop can be evaluated by using the Larkins equation (eq. (3.390)). For the determination of pressure drop of the gas phase, we need the viscosity and the density of the gas stream. Assuming that the inert phase is N_2 or a similar gas, we can take $\rho_1 = 17.07 \text{ kg/m}^3$, $\mu_1 = 2.21 \times 10^{-5} \text{ kg/m s}$.

The resulting gas ($0.357 \text{ kg/m}^2 \text{ s}$) and liquid mass superficial velocities ($2\text{--}12 \text{ kg/m}^2\text{s}$) are within the operating region for commercial trickle beds (see Figure 3.47 and Satterfield, 1975).

The gas-phase pressure drop is better evaluated by using the differential form of Ergun's equation and taking into account the gas density variance. However, it is easy to show that the parameter aZ/P_i is about 0.001, and thus the Ergun equation in its classic form can be accurately used (see subsection Nonisobaric fixed-bed operation).

Then, the total pressure drop for the maximum mass superficial velocity of liquid is, for the single phases, 0.02 atm for the gas and 0.68 atm for the liquid, and for the two-phase system 1.43 atm. Thus, we can assume that the pressure-drop effect is minimal.

Under the reasonable assumptions of zero expansion and negligible pressure drop, the model of Smith for gas mixture eq. (5.379) is also applicable.

The gas–liquid mass transfer for organic solutions and the liquid–solid mass transfer are evaluated using the appropriate correlations (eqs. (3.427) and (3.435), respectively), while the Fogler's overall coefficient (K_A^o) is (eq. (3.379))

$$K_A^o = K^o = \frac{1/H}{\frac{1}{(K_L a_{GL})_A} + \frac{1}{(k_f a_u)_A} + \frac{1}{\rho_b \eta k_m}}$$

The results are shown in Table 5.13.

Using the Smith and Fogler models (eqs. (5.379) and (5.385) respectively), we obtain the results shown in Figure 5.15.

It is evident that the models result in close though slightly different hydrogen conversions. The model of Smith results in lower conversions and the difference between the

Table 5.13

The values of the various coefficients

G_L (kg/m ² s)	$k_{fg} a_{GL}$ (s ⁻¹)	$k_f a_u$ (s ⁻¹)	K_A^o (s ⁻¹)
2	1.72×10^{-3}	1.39×10^{-2}	3.34×10^{-4}
5	2.17×10^{-3}	3.98×10^{-2}	4.23×10^{-4}
8	2.44×10^{-3}	6.83×10^{-2}	4.70×10^{-4}
12	2.70×10^{-3}	10.9×10^{-2}	5.11×10^{-4}

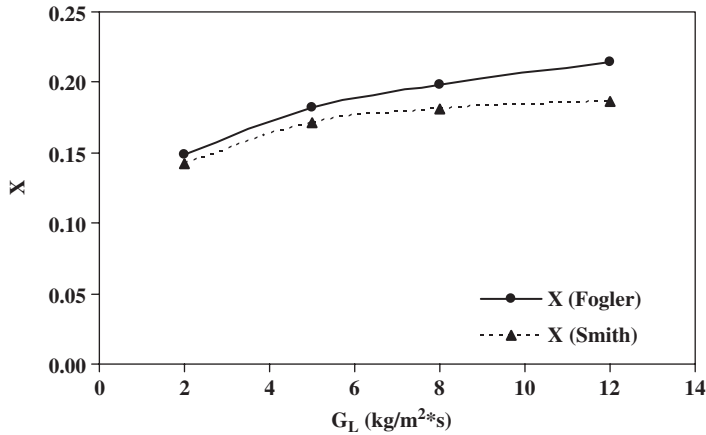


Figure 5.15 The conversion versus G_L .

models is higher for a higher mass superficial velocity, i.e. higher liquid superficial velocity, reaching the maximum value of 15%.

This result illustrates the effect of Fogler's assumption of zero liquid superficial velocity, analyzed in Section 3.7.2 and eq. (3.374). Indeed, for a low liquid superficial velocity, the models result in almost the same values. Thus, it can be stated that Smith's approach is more accurate for high liquid superficial velocities. However, Fogler's approach is more useful and accurate in the case of considerable pressure drop and gas-phase expansion.

One more important parameter is the wetting of the catalyst, which for the simplified models is assumed to be 100%. Using the Al-Dahhan *et al.* (eq. (3.414)) correlation for high pressures, the results shown in Table 5.14 are obtained.

This result indicates the need for an efficient distributor design for this trickle-bed operation at low flow rates ($G_L < 12$).

Trickle-bed models assume plug flow for both phases. Thus, it is interesting to evaluate the respective Peclet numbers. The correlations of Michell–Furzer for liquid (eq. (3.417)) and Hochman–Efron for gas (eq. (3.419)) are used and the results are shown in Table 5.15. The Reynolds number for the gas phase is 32.28.

Taking into account that the ratio Z/d_p is 5000, we can assume that the plug-flow condition is assured for both phases. Here, we can use the criterion of Mears (eq. (3.421)):

$$\frac{Z}{d_p} > \frac{20n}{Pe_L} \ln \left(\frac{C_f}{C_o} \right)$$

where C_f and C_o are the feed and outlet concentrations, respectively. This criterion gives the minimum Z/d_p ratio required to hold the reactor length within 5% of that needed for plug flow. In our case, the limit of this ratio is only 5.63–6. Thus, this criterion is satisfied as well.

Table 5.14 f_w versus G_L

G_L (kg/m ² s)	f_w
2	0.51
5	0.71
8	0.85
12	0.99

Table 5.15

Reynolds and Peclet numbers

G_L (kg/m ² s)	Re_L	Pe_L	Pe_G
2	2.62	0.54	0.15
5	5.55	0.60	0.15
8	8.89	0.65	0.14
12	13.34	0.68	0.14

Example 12

Wu *et al.* (1996) studied the liquid-phase decomposition of hydrogen peroxide in a trickle bed of 2.2 cm diameter and 30 cm height, at 22 °C and 1 atm:



The inlet concentration of H_2O_2 is 1.18% (w/w), the space-time based on liquid flow is between 60 and 300 s and the gas superficial velocity is 5.5 cm/s. The catalyst is copper chromite on alumina support with the following characteristics: $d_{p,avr} = 1.159$ mm, $\rho_p = 1.05$ g/cm³, $S_s = 120$ m²/g, and $V_p = 0.36$ cm³/g.

The reaction is first order with respect to hydrogen peroxide and the effectiveness factor η_s is found to be equal to 0.24. This effectiveness factor accounts only for internal transport effects. Due to the dilute feed of hydrogen peroxide, the operation can be considered isothermal.

In Table 5.16, some of the experimental results for the runs in the trickle-bed reactor are presented (approximate values).

- Evaluate the intrinsic reaction coefficient by using the appropriate kinetic data.
- Using the evaluated intrinsic reaction coefficient, compare the predictions made by using the simple trickle-bed reactor model for this type of reaction. Explain the differences.
- Evaluate the tortuosity of the catalyst support.
- What is the expected conversion for different particle size and space-time of 60 s?

Table 5.16

Experimental results	
τ (s)	x
60	0.44
100	0.60
200	0.80
300	0.85

Solution

First, we have to check the wetting efficiency of the bed because the simple trickle-bed model assumes complete wetting and thus it is not applicable otherwise. By using the El-Hisnawi *et al.* correlation, the wetting efficiency can be estimated (eq. (3.411)). To do that, we need the Galileo number and the Reynolds number. The liquid superficial velocity can be evaluated as follows:

$$u_{L,s} = \frac{Z}{\tau}$$

while the Galileo number is 4.83×10^4 (eq. (3.412)). The results are summarized in Table 5.17.

At this point, it is also important to check the plug-flow assumption, as the models assume plug flow for liquid. The correlation of Michell–Furzer (eq. (3.417)) for the liquid is used and the results are shown in Table 5.17. The minimum values of Z/d_p are evaluated by using the Mears criterion (eq. (3.421)).

The value of Z/d_p used in the experiments is 188.98, and thus the plug-flow assumption is valid in the whole region of working residence time. Furthermore, from the point of view of catalyst wetting, it is clear that the appropriate experimental point that we can use is the one of 60 s space-time where $x = 0.44$ and $f_w = 1$. Then, from eq. (5.351),

$$\ln\left(\frac{1}{1-x_B}\right) = \frac{k^o Z}{u_{sL}} \Rightarrow k^o = 9.67 \times 10^{-3} \text{ s}^{-1}$$

where

$$\frac{1}{k^o} = \frac{1}{(k_f a_u)_B} + \frac{1}{\rho_b \eta_s k_m}$$

Table 5.17

Hydraulic parameters and Mears criterion for plug flow

τ (s)	Re_L	f_w	Pe_L	$(Z/d_p)_{\min}$
60	8.80	1.03	0.64	18.22
100	5.28	0.96	0.59	30.12
200	2.64	0.87	0.54	59.85
300	1.76	0.82	0.51	74.67

Then, to evaluate the intrinsic reaction coefficient, we need the mass transfer coefficient in the liquid film, which can be calculated by means of the correlation of Dharwadkar and Sylvester ($f_w = 1$) (eq. (3.433)):

$$k_f a_u = 1.637 a_u u_{sL} Re_L^{-0.331} \left(\frac{\rho_L D_f}{\mu_L} \right)^{2/3}$$

Assuming that the bed porosity is 0.4, the specific area a_u is (eq. (3.447))

$$a_u = \frac{6(1-\varepsilon)}{d_p} = 2267.72 \text{ m}^2/\text{m}^3$$

The next parameter we need is the diffusion coefficient D_f of hydrogen peroxide in water. Here, we can assume the approximate value of $10^{-9} \text{ m}^2/\text{s}$. However, this coefficient will be needed further in this example for the determination of the effective solid-phase diffusion coefficient, in a calculation that is extremely sensitive to the value of the liquid-phase diffusion coefficient. For this reason, coefficient should be evaluated with as much accuracy as possible. The diffusion coefficient of solutes in dilute aqueous solutions can be evaluated using the Hayduk and Laudie equation (see eq. (I.26) in Appendix I):

$$D_w = \frac{8.621 \times 10^{-14}}{\mu_w^{1.14} V_{GB}^{0.589}}$$

For this, we need the molar volume V_{GB} of hydrogen peroxide at normal boiling point, which can be evaluated using the following correlation (see eq. (I.26) in Appendix I):

$$V_{GB} = 0.285 \times V_C^{1.048}$$

where V_C is the molar volume of hydrogen peroxide at critical conditions, which is $77.7 \text{ cm}^3/\text{mol}$ (see Table I.9 in Appendix I) and then $V_{GB} = 27.29 \text{ cm}^3/\text{mol}$. The resulting diffusion coefficient is $2.13 \times 10^{-9} \text{ m}^2/\text{s}$. Note that SI units have to be used with the Hayduk

and Laudie correlation, while CGS units have been used in the correlation for the molar volume at normal boiling point. Then, the resulting mass transfer coefficient is 0.16 s^{-1} . Furthermore, the bulk density of the bed is

$$\rho_b = (1 - \varepsilon)\rho_p = 630 \text{ kg/m}^3$$

Then

$$\frac{1}{\rho_b \eta_s k_m} = \frac{1}{k^\circ} - \frac{1}{(k_f a_u)_B} \Rightarrow k_m = 6.81 \times 10^{-5} \text{ m}^3/\text{kg s}$$

The comparison of the experimental and model conversions is shown in Figure 5.16.

It is evident that the model predictions are very close to the experimental values for a high wetting efficiency, while the model predicts higher conversions for lower wetting efficiencies. This is expected as the simple model assumes complete wetting, i.e. better performance of the reactor.

For a first-order reaction and isothermal operation, the effectiveness factor is (eq. (5.77))

$$\eta_s = \frac{1}{\phi} \left(\frac{1}{\tanh(3\phi)} - \frac{1}{3\phi} \right)$$

Applying a trial-and-error procedure, the Thiele modulus is estimated as 3.80. Assuming spherical particles, the Thiele modulus is (eq. (5.76))

$$\phi = \frac{r_p}{3} \sqrt{\frac{k_m \rho_p}{D_{\text{eff}}}}$$

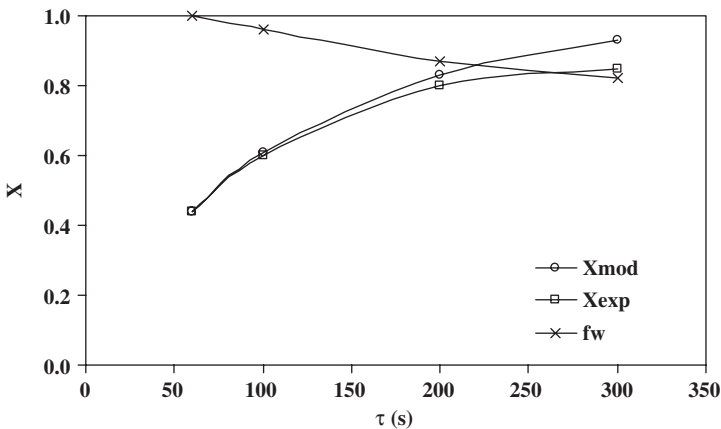


Figure 5.16 The comparison of the experimental and model conversions.

Using this expression, the effective solid-phase diffusion coefficient is found to be equal to $3.46 \times 10^{-10} \text{ m}^2/\text{s}$. This coefficient is related to the liquid-phase coefficient as follows (eq. (3.602)):

$$D_{\text{eff}} = \frac{\varepsilon_p D_f}{\tau_p}$$

In order to evaluate the tortuosity of the catalyst, we need its porosity. From the data given,

$$\varepsilon_p = V_p \rho_p = 0.38$$

So, the value of tortuosity is 2.33, within the expected limits for alumina, i.e. between 2 and 6.

By changing the particle size, the effectiveness factor, liquid mass transfer coefficient, and wetting efficiency are affected. We choose such particle sizes to have complete wetting and thus be able to use the simple model. For the specified space velocity, the particle size should be lower than about 2.5 mm. On the other hand, particles smaller than 0.5 should be avoided for preventing a high pressure drop appearance. Furthermore, the values of Z/d_p for $0.5 < d_p < 2.5 \text{ mm}$ are between 120 and 600 assuring plug-flow conditions.

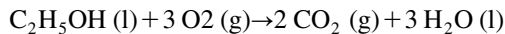
The results are shown in Figure 5.17.

The benefit from using lower particle sizes as well as the strong effect of particle size is clear. For example, by increasing the space-time from 60 to 100 s (66.67% increase), the conversion is increased by 38.64%, while by decreasing the particle size by the same percentage, i.e. from 1.59 to 0.53 mm, the conversion is increased by 72.73%, which is almost double.

A few comments: Hydrogen peroxide is an odorless and colorless liquid used as a source of hydroxyl radicals in environmental applications. There is no conclusive evidence for the carcinogenicity of hydrogen peroxide to humans. However, it leads to genetic damage *in vitro* through the formation of free radicals, whereas acute lung damage and edema has been reported as the respiratory effect of hydrogen peroxide (Cralley and Cralley, 1985).

Example 13

Consider the catalytic oxidation of ethanol:



This reaction is catalyzed by a hydrophilic spherical Pt- γ -Al₂O₃ catalyst of 3 mm particle size at 70 °C and 1 atm and is considered to be first order with respect to oxygen and 0.5 order with respect to ethanol (Horowitz *et al.*, 1999). The effective rate coefficient, i.e. the rate coefficient including the effect of the internal diffusion is $1.95 \times 10^{-4} \text{ (m}^3/\text{kg s) (m}^3/\text{kmol)}^{0.5}$.

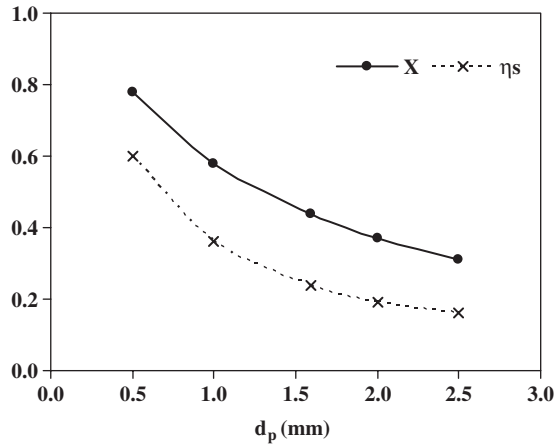


Figure 5.17 Conversion and effectiveness factor versus particle size.

The reaction takes place in a trickle bed of 4.1 cm diameter and 1 m height with liquid flow rate of 2.17 kg/s m^2 , gas flow rate of 0.017 kg/s m^2 , and inlet ethanol concentration of 0.006 kmol/m^3 . Horowitz *et al.* (1999) noted that pure oxygen was used as the gas feed, and under the experimental conditions the conversion of O_2 was less than 5%. Thus, the gas-phase concentration of O_2 can be considered constant. Furthermore, the liquid phase entered the reactor saturated with O_2 . Under these conditions, the conversion of the ethanol was about 14%.

Estimate the height of the bed to achieve the same performance of the reactor by using the appropriate simplified model, assuming that the liquid phase remains saturated with O_2 throughout the reactor length, plug-flow conditions exist, and the external wetting of the catalyst particle is complete.

Assume that the particle density of alumina is 1050 kg/m^3 and the bed porosity is 0.45.

Solution

The intrinsic reaction rate is

$$(-r_m) = k_{m,\text{eff}} C_{\text{O}_2,S} C_{\text{EtOH},S}^{0.5}$$

Then, the oxygen balance around the catalyst particles is (eq. (3.369))

$$(k_f a_u)_A [C_{\text{O}_2,L} - C_{\text{O}_2,S}] = \rho_b k_{m,\text{eff}} C_{\text{O}_2,S} C_{\text{EtOH},S}^{0.5}$$

or

$$C_{\text{O}_2,S} = \frac{(k_f a_u)_A}{(k_f a_u)_A + \rho_b k_{m,\text{eff}} C_{\text{EtOH},S}^{0.5}} \left(\frac{C_{\text{O}_2,G}}{H_A} \right)$$

then

$$(k_f a_u)_B [C_{\text{EtOH,L}} - C_{\text{EtOH,S}}] = \frac{\rho_b k_{m,\text{eff}} C_{\text{O}_2,\text{S}} C_{\text{EtOH,S}}^{0.5}}{a} = \frac{k^\circ}{a} \left(\frac{C_{\text{O}_2,\text{G}}}{H_A} \right)$$

In analogy to eq. (5.341), the coefficient k° is defined as

$$k^\circ = \frac{(k_f a_u)_A \rho_b k_{m,\text{eff}} C_{\text{EtOH,S}}^{0.5}}{(k_f a_u)_A + \rho_b k_{m,\text{eff}} C_{\text{EtOH,S}}^{0.5}} \Leftrightarrow \frac{1}{k^\circ} = \frac{1}{(k_f a_u)_A} + \frac{1}{\rho_b k_{m,\text{eff}} C_{\text{EtOH,S}}^{0.5}}$$

The second term of k° in the above equation is a function of the surface ethanol concentration, which is unknown. However, its maximum value cannot be higher than the feed ethanol concentration and under the specific operating conditions,

$$\frac{1}{(k_f a_u)_A} = 13.52 \text{ s}$$

$$\left(\frac{1}{\rho_b k_{m,\text{eff}} C_{\text{EtOH,S}}^{0.5}} \right)_{\min} = \frac{1}{\rho_b k_{m,\text{eff}} C_{\text{EtOH,f}}^{0.5}} = 114.64 \text{ s}$$

$$\frac{1}{k^\circ} = 128.16 \text{ s}$$

The mass transfer term of k° is about 10.6% of k° . Considering that the second term will be even higher due to the lower surface concentration of ethanol during the reaction evolution, the contribution of the mass transfer term to k° can be considered minimal. This approximation, though rough, greatly simplifies the problem solution. Then

$$k^\circ \cong \rho_b k_{m,\text{eff}} C_{\text{EtOH,S}}^{0.5}$$

The ethanol balance around the catalyst particles is (eq. (3.370))

$$(k_f a_u)_B [C_{\text{EtOH,L}} - C_{\text{EtOH,S}}] = \frac{\rho_b k_{m,\text{eff}} C_{\text{EtOH,S}}^{0.5}}{a} \left(\frac{C_{\text{O}_2,\text{G}}}{H_A} \right)$$

The above equation becomes

$$\beta^2 C_{\text{EtOH,S}}^2 - (\gamma^2 + 2\beta^2 C_{\text{EtOH,L}}) C_{\text{EtOH,S}} + \beta^2 C_{\text{EtOH,L}}^2 = 0$$

$$\beta = (k_f a_u)_B$$

$$\gamma = \frac{\rho_b k_{m,\text{eff}}}{a} \left(\frac{C_{\text{O}_2,\text{G}}}{H_A} \right)$$

Rearranging the trionym,

$$C_{\text{EtOH,S}}^2 - \varpi C_{\text{EtOH,S}} + C_{\text{EtOH,L}}^2 = 0$$

$$\varpi = \left(\frac{\gamma^2}{\beta^2} + 2C_{\text{EtOH,L}} \right)$$

It is easy to show that for the specified conditions ($x = 0.14$),

$$\frac{\gamma^2}{\beta^2} = 1.78 \times 10^{-7}$$

$$(2C_{\text{EtOH,L}})_{\text{min}} = 2C_{\text{EtOH,f}}(1-x) = 1.03 \times 10^{-2}$$

and thus

$$\varpi \cong 2C_{\text{EtOH,L}}$$

The trionym becomes

$$C_{\text{EtOH,S}}^2 - 2C_{\text{EtOH,L}} C_{\text{EtOH,S}} + C_{\text{EtOH,L}}^2 = 0$$

$$(C_{\text{EtOH,S}} - C_{\text{EtOH,L}})^2 = 0$$

$$C_{\text{EtOH,S}} = C_{\text{EtOH,L}}$$

This is a result of the assumption that the mass transfer coefficient is minimal. Then, using the mass conservation equation for ethanol in the liquid phase (eq. (3.368)),

$$u_{sL} \frac{dC_{\text{EtOH,L}}}{dz} + (k_f a_u)_B [C_{\text{EtOH,L}} - C_{\text{EtOH,S}}] = 0$$

$$u_{sL} \frac{dC_{\text{EtOH,L}}}{dz} + \frac{\rho_b k_{\text{eff}} C_{\text{EtOH,L}}^{0.5}}{a} \left(\frac{C_{\text{O}_2,\text{G}}}{H_A} \right) = 0$$

The boundary (feed) condition is $C_{\text{EtOH,L}} = C_{\text{EtOH,L,f}}$ at $z = 0$. Then, on integration,

$$C_{\text{EtOH,L}} = \left[C_{\text{EtOH,f}}^{0.5} - 0.5 \frac{\rho_b k_{\text{eff}} Z}{a u_{sL}} \left(\frac{C_{\text{O}_2,\text{G}}}{H_A} \right) \right]^2$$

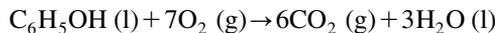
For 14% conversion, $C_{\text{EtOH,L}} = 0.00516 \text{ kmol/m}^3$ and $Z = 0.795 \text{ m}$.

The difference from the real value (1m) is mainly due to the approximation made about the mass transfer coefficient as well as the complete wetting of the catalyst, as the actual wetting efficiency is 88%. Furthermore, the problem is more complicated because under incomplete wetting, the gas reactant reaches the catalyst surface more easily than the unwetted part, as Horowitz *et al.* found out experimentally.

The aim of this example is to demonstrate the use of the simplified model for reactions other than first order with respect to the gas reactant and zero order to the liquid one, and more specifically to demonstrate the case of first order with respect to the gas reactant and half order to the liquid one, which may have, under specific operating conditions, an analytic solution. For example, if the liquid mass superficial velocity was higher, say $10 \text{ kg/m}^2 \text{ s}$, the wetting efficiency is 1 and the mass transfer contribution lower than 4.07%. At the same time, there is no contribution of the unwetted part of the catalyst. Under these conditions, the approximate model is expected to exhibit a better performance. The same result can be achieved for smaller particles.

Example 14

Consider the catalytic oxidation of phenol:



This reaction is catalysed by a Pt–Ru catalyst with activated carbon support at 35°C and it is considered to be pseudo-first order with respect to phenol under the condition of O_2 excess (Atwater *et al.*, 1997). The reaction was studied in a trickle-bed microreactor of 1.27 cm diameter and volume of 4.8 cm^3 . The bed porosity is 0.28, while the ratio of bed length-to-particle size is about 30. The reactor was operated under pressure enough to keep a single-phase flow, while the liquid feed was saturated with oxygen. Under these conditions, we can assume complete wetting of the catalyst particles.

The feed phenol concentration is 0.16 mM (15 mg/L) and the contact time based on superficial velocity is 4.3 s. The exit concentration under the specified conditions is about 0.10 mM. Assume that the bulk density of the carbon catalyst is 800 kg/m³.

- Evaluate the effective rate coefficient, i.e. the product of internal effectiveness factor and intrinsic rate coefficient for this reaction
- Evaluate the time needed to achieve the same conversion in a packed bubble bed reactor of the same dimensions under complete recycle of the liquid phase with $V_L/V_R = 2$.
- What is the volume of liquid that the trickle bed can treat if it is operated for the same time?

Solution

Trickle-bed reactor: First, we have to evaluate the bed length and the particle size used. The bed length is

$$Z = \frac{V_R}{A} = \frac{V_R}{(\pi D^2/4)} = 3.79 \text{ cm}$$

The particle size is

$$d_p = \frac{30}{Z} = 0.126 \text{ cm}$$

For the specified particle size and bed porosity, the specific area a_u is

$$a_u = \frac{6(1-\varepsilon)}{d_p} = 3418.54 \text{ m}^2/\text{m}^3$$

Furthermore, for the specified contact time, the superficial velocity is

$$u_{sL} = \frac{Z}{\tau} = 0.88 \text{ cm/s}$$

which corresponds to a Reynolds number of 12.36.

As the reactor was operated under pressure enough to keep a single-phase flow while the liquid feed was saturated with oxygen, the situation is equivalent to constant gas-phase concentration and saturated liquid phase. Thus, the model solution appropriate for a first-order reaction with respect to the liquid reactant is (eq. (5.350))

$$\ln\left(\frac{1}{1-x_B}\right) = \frac{k^\circ Z}{u_{sL}}$$

where

$$\frac{1}{k^\circ} = \frac{1}{(k_f a_u)_B} + \frac{1}{\rho_b \eta_s k_m}$$

For the specified exit concentration, $x_B = 0.375$ and thus $k^\circ = 0.109 \text{ s}^{-1}$.

In order to evaluate the effective reaction coefficient, we need the mass transfer coefficient in the liquid film, which can be calculated by using the correlation of Dharwadkar and Sylvester ($f_w = 1$) (eq. (3.433)):

$$k_f a_u = 1.637 a_u u_{sL} Re_L^{-0.331} \left(\frac{\rho_L D_f}{\mu_L} \right)^{2/3}$$

The next parameter required is the diffusion coefficient of phenol in water (D_{fg}). Here, we can assume the typical value of $10^{-9} \text{ m}^2/\text{s}$. Then, the resulting mass transfer coefficient is 0.23 s^{-1} . Subsequently,

$$\frac{1}{\rho_b \eta_s k_m} = \frac{1}{k^\circ} - \frac{1}{(k_f a_u)_B} \Rightarrow \eta_s k_m = 2.6 \times 10^{-4} \text{ m}^3/\text{kg s}$$

At this point, it is also important to check the plug-flow assumption as the simple model assumes plug flow for the liquid. For the specified Reynolds number, the Peclet number is found to be 0.59 using the Michell–Furzer correlation (eq. 3.417). The minimum value of Z/d_p , evaluated using the Mears criterion, is 15.87 (eq. (3.421)), lower than the value used in the experiments, which is about 30. Thus, the operation can be assumed as plug flow.

Packed bubble bed reactor with complete recycle: The model solution for the specific reactor and constant gas-phase concentration is (eq. (5.151))

$$t = \frac{V_L}{V_R} \frac{1}{k^\circ} \ln \left(\frac{1}{1 - x_B} \right)$$

where

$$\frac{1}{k^\circ} = \frac{1}{\rho_b \eta_s k_m} + \frac{1}{(k_f a_u)_B}$$

and $V_L/V_R = 2$. In order to evaluate the coefficient k° , the mass transfer coefficient in the liquid film is needed, which can be calculated from the Mochizuki–Matsui correlation ($f_w = 1$, $Re_L > 5$) (eq. (3.438)):

$$\frac{k_f d_{pe}}{D_{fg}} = 0.75 \left(\frac{u_{sL} \rho_L d_{pe}}{\mu_L} \right)^{0.5} \left(\frac{\mu_L}{\rho_L D_{fg}} \right)^{0.33} \quad (1 + 49)$$

Due to the absence of gas flow, the parameter θ is zero. Note that CGS units are used with this correlation. Furthermore (eq. (3.437)),

$$d_{pe} = \frac{2}{3} d_p \frac{\varepsilon}{1 - \varepsilon} = 0.033 \text{ cm}$$

The resulting mass transfer coefficient is 3.87×10^{-3} cm/s, and thus

$$k_f a_u = 0.132 \text{ s}^{-1}$$

and the coefficient k^o is equal to 0.081 s^{-1} and the time needed for achieving the conversion level of 0.375 in this reactor mode is 11.62 s.

The space velocity of the trickle-bed reactor is

$$s = \frac{1}{\tau} = 0.23 \text{ s}^{-1}$$

which means that it can treat 0.23 bed volumes per second. Then, if the trickle bed were operated for the same time as the packed bubble bed reactor, the treated volume would be 2.7 times its volume, or $V_L/V_R = 2.7$. From this point of view, the trickle-bed reactor is preferred.

At this point it, has to be noted that the use of recycle reactors is very attractive, in commercial as well as laboratory applications. Specifically, they can be operated for long periods, thus leading to high conversions, in cases where the per-pass conversion of the liquid component is small. Moreover, they present some of the benefits of continuous operations, though being batch, such as easy filling and removing of the catalyst (Ramachandran and Chaudhari, 1984). In the laboratory, recycle reactors are suitable for kinetic studies of catalytic reactions (Smith, 1981). By adjusting the recycle rate, i.e. the flow rate, the reactor operates in differential mode.

A few comments on phenol: Phenol is a monosubstituted aromatic hydrocarbon. In its pure state, it exists as a colorless or white solid. This pure compound is mixed with water and commercially sold as a liquid product. Phenol gives off a sweet, acrid smell detectable to most people at 40 ppb in air and at about 1–8 ppm in water (EPA, 2002). It evaporates more slowly than water and is moderately soluble in water. Phenol is also combustible.

Phenol is produced through both natural and anthropogenic processes. It is naturally occurring in some foods, human and animal wastes, and decomposing organic material, and is produced endogenously in the gut from the metabolism of aromatic amino acids. Phenol has been isolated from coal tar, but it is now synthetically manufactured (EPA, 2002). Currently, the largest use of phenol is as an intermediate in the production of phenolic resins, which are used in the plywood, adhesive, construction, automotive, and appliance industries. Phenol is also used in the production of synthetic fibers such as nylon and for epoxy resin precursors such as bisphenol-A.

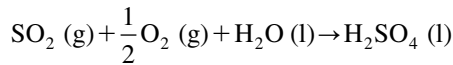
Phenol is toxic to bacteria and fungi, and it is used as a slimicide and disinfectant. Because of its anesthetic effects, phenol is used in medicines such as ointments, ear and nose drops, cold sore lotions, throat lozenges and sprays (such as those sold under the Cepastat® and Chloraseptic® labels), and antiseptic lotions (EPA, 2002).

Phenol does not appear to accumulate significantly in the body. Several epidemiological studies have evaluated the carcinogenicity of phenol, but they have not found a consistent dose-related association (EPA, 2002). Because all the subjects were also exposed to other chemicals and there was no correction for smoking, these studies are not adequate to reach conclusions on the carcinogenic potential of phenol.

A number of toxic effects secondary to decreased water consumption have been observed, including decreased body weight compared to controls, decreased pup weight, and decreased pup survival, preculling. Other effects that may not have been secondary to decreased water consumption were kidney inflammation and decreased motor activity (EPA, 2002). Gavage studies found more severe effects and reported these effects at lower doses. Observed effects included lung, liver, and kidney pathology; tremors and other nervous-system effects; and at sufficiently high doses, death.

Example 15

Medeiros *et al.* (2001) studied the catalytic oxidation of sulfur dioxide on active carbon particles in a trickle-bed reactor at 25 °C and 1.1 atm:



The size of catalyst particles is 2.5 mm, packed in a fixed bed of 5 cm diameter, 25 cm height, and porosity of 0.4. The gas is a mixture of sulfur dioxide and air with a flow rate of $1.515 \times 10^{-3} \text{ m}^3/\text{s}$ and feed concentration of SO_2 $0.0777 \text{ mol}/\text{m}^3$. For such low sulfur concentration, the inlet oxygen concentration can be considered approximately equal to its concentration in air. For the same reason, the expansion factor of the gas mixture can be taken as zero.

Under these conditions, the reaction rate is first order with respect to sulfur dioxide and the rate coefficient per unit volume of catalyst, including the effect of internal diffusion, is equal to $k_{\text{vs}} = 0.3 \text{ m}^3/\text{m}^3 \text{ s}$.

According to the experimental results of Medeiros *et al.* (2001), the wetting efficiency is 100% and plug flow is assumed for liquid flow rates in the vicinity of $14 \times 10^{-5} \text{ m}^3/\text{s}$, which is the case in this example.

Furthermore, a liquid-phase distributor is used on the top of the bed and the overall gas-phase mass transfer coefficient was experimentally measured as 0.153 s^{-1} for liquid flow rate equal to $14 \times 10^{-5} \text{ m}^3/\text{s}$. Under these conditions, the experimental value of sulfur dioxide conversion was approximately 18%.

- Evaluate the theoretical conversion of sulfur dioxide by using the model derived for gas mixture in trickle beds. Check if the assumptions of the model are met.
- Evaluate the conversion of sulfur dioxide in the trickle flow regime by proposing an appropriate gas and liquid flow rate.

Solution

Before applying any model, we should first check if the assumptions of the model are satisfied by the experimental conditions. If not, the model results are questionable.

The experiments for the specified study have been made in the pulsing flow regime. This is stated in the original article, and it is evident by calculating the liquid and gas mass superficial velocities, which are

$$G_L = u_{sL}\rho_L = 71.19 \text{ kg/m}^2 \text{ s}$$

$$G_G = u_{sG}\rho_G = 0.93 \text{ kg/m}^2 \text{ s}$$

By using the approximate Figure 3.47, it is clear that we are by far away from the trickling region and into the pulsing-flow regime. However, this does not mean that we cannot use the models derived for the trickle-bed regime as long as

- (a) we use the appropriate mass transfer coefficients, especially the gas–liquid one
- (b) it is sure that the wetting efficiency of the catalyst particles is near to 100%
- (c) it is assured that plug-flow conditions exist, especially in the liquid phase
- (d) the expansion of the gas mixture is approximately zero
- (e) it is assured that the pressure drop is relatively low in comparison to the inlet pressure of the gas.

The conditions (a), (b), (c), and (d) are met since we have the experimental value of the gas–liquid mass transfer coefficient, the wetting efficiency is given to be 100%, plug-flow condition is assumed in the original study, and the expansion factor is zero as the oxygen concentration has been taken as constant.

The only problem with the application of the simplified model is the pressure drop in the trickle bed. By using the Ergun equation (3.449), the pressure drop in the liquid phase is very high, approaching the value of 42 kPa/m, while the gas-phase pressure drop is approximately 1.9 kPa/m. Using the correlation of Larkins *et al.* (eq. (3.390)), the two-phase pressure drop is almost 103 kPa/m, which is equal to the inlet pressure drop of the gas mixture. Here, we have to note that it becomes so high because of the high pressure drop in the liquid phase. Furthermore, the Larkins *et al.* correlation holds for the trickling-flow regime, and thus the above calculations are rough. However, it seems that the pressure drop is quite high, due to the very high liquid-phase flow rate.

Basic parameters evaluation: Before proceeding to the application of models, some basic parameters are needed. The first and most important one is the rate coefficient of the reaction. The rate coefficient should be expressed in terms of the catalyst mass (eq. (3.10)):

$$k_m = \frac{k_{vs}}{\rho_p} = 3.75 \times 10^{-4} \text{ m}^3/\text{kg s}$$

Note, that this coefficient is the effective one as it includes the contribution of the intra-particle diffusion.

The second parameter is the Henry constant for sulfur dioxide, which can be found in Table I.18, Appendix I, and is 1.23 mol/L atm. The Henry constant has to be expressed in its dimensionless form, which is (see eq. (I.35) in Appendix I)

$$H = \frac{H^\circ \left(\frac{\text{atm L}}{\text{mol}} \right)}{0.082 \left(\frac{\text{atm L}}{\text{mol K}} \right) 298 \text{ K}} = \left[\frac{1.23 \left(\frac{\text{mol}}{\text{atm L}} \right)}{24.44 \left(\frac{\text{atm L}}{\text{mol}} \right)} \right]^{-1} = 0.0333$$

The inlet oxygen concentration is evaluated by using the ideal gas law:

$$C_{\text{BG},i} = \frac{P}{RT} = \frac{1.1 \text{ atm}}{82.057 \left(\frac{\text{atm m}^3}{\text{mol K}} \right) 298 \text{ K}} = 9.38 \times 10^{-6} \text{ mol/cm}^3$$

The liquid-phase diffusion coefficient of sulfur dioxide can be found from Table I.10, Appendix I, and is equal to $1.7 \times 10^{-9} \text{ m}^2/\text{s}$.

Finally, note that the material balances will be written for sulfur dioxide and thus $b = 0.5$.

Model application in the pulsing-flow regime: The mass transfer coefficient in the liquid-solid film is evaluated by means of the Dharwadkar and Sylvester correlation (eq.3.433), and is found to be 0.45 s^{-1} . Then, the several parameters of the model eq. (5.379) are shown in Table 5.18.

The model conversion is 16.3%, which is very close to the experimental value.

Model application in the trickle-flow regime: In order to assure operation in the trickle-flow regime, the gas as well as the liquid flow rate has to be considerably lowered. At the same time, the conditions (a) and (d) are met in the reactor, while the rest of the conditions have to be checked.

Operating conditions: Following Figure 3.47 in order to operate in the trickle-flow regime, the gas and especially the liquid flow rate should be lowered. We choose a liquid

Table 5.18

Model parameters

Parameter	Value
λ	0.71
ξ	9.89
ψ	10.7
m_1	-1.24
m_2	-8.66

and gas flow rate of $9.33 \times 10^{-6} \text{ m}^3/\text{s}$ and $7.58 \times 10^{-4} \text{ m}^3/\text{s}$, respectively, which leads to the following mass superficial velocities:

$$G_L = u_{sL}\rho_L = 4.75 \text{ kg/m}^2\text{s}$$

$$G_L = u_{sG}\rho_G = 0.46 \text{ kg/m}^2\text{s}$$

Wetting efficiency: The Reynolds and Galileo numbers are 13.18 and 1.88×10^5 . Using the correlation of El-Hisnawi (eq. (3.411)), the wetting efficiency is 0.99, satisfying condition (b).

Pressure drop: Using the Ergun equation, the liquid and the gas pressure drop are 0.726 and 2.12 kPa/m, respectively. Then, by using the correlation of Larkins *et al.*, the two-phase pressure drop is equal to 10.8 kPa/m, ten times lower than in the pulsing-flow regime and low enough to assure that the gas density is almost constant. Thus, the condition (e) is satisfied.

Plug-flow assumption: Using the Michell and Furzer correlation (eq. (3.417)), the liquid-phase Peclet value is 0.66 and the minimum value of Z/d_p , evaluated by using the Mears criterion (eq. (3.421)) 4.81, which is much lower than the experimental one, which is 100. Then, condition (c) is satisfied.

Results: The mass transfer coefficient in the liquid–solid film is evaluated using the Dharwadkar and Sylvester correlation (eq. (3.433)), and is found to be 0.073 s^{-1} . The mass transfer coefficient in the gas–liquid film is evaluated by means of the Goto and Smith correlation (eq. (3.426)), and is equal to $1.49 \times 10^{-2} \text{ s}^{-1}$. It is evident that the mass transfer coefficients are much lower than the coefficients in the pulsing-flow regime.

Then, the several parameters of the model eq. (5.379) are shown in Table 5.19.

The model conversion is 14.7%, which is close to the value calculated for the pulsing-flow regime. The oxygen conversion is very low, as assumed, about 0.06 %.

Although the mass transfer coefficients are much higher in the pulsing-flow regime, the contact time is much lower due to the higher liquid and gas flow rates, and thus these two effects are “balanced,” resulting in a good conversion in the trickle-flow regime.

Example 16

Consider the catalytic oxidation of ethanol:

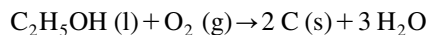


Table 5.19

Model parameters	
Parameter	Value
λ	0.29
ξ	15.20
ψ	12.66
m_1	-0.88
m_2	-14.32

This reaction is catalyzed by Pd–Al₂O₃ catalyst at 30 °C and is considered to be first order with respect to oxygen (Hopper *et al.*, 2001; Ramachandran, and Chaudhari, 1980). The rate coefficient for this reaction is $k_m = 0.0177 \text{ cm}^3/\text{g s}$.

The reaction takes place in a trickle-bed reactor of 20 cm diameter and 500 cm height and in a packed bubble bed reactor of the same dimensions. Compare these two reactors under the following conditions:

- constant gas-phase concentration and saturated liquid phase with oxygen
- constant gas-phase concentration and zero inlet liquid-phase concentration of oxygen.

The gas superficial velocity is 0.36 cm/s, the liquid superficial velocity is 1.06 cm/s, the ethanol inlet concentration is $4 \times 10^{-4} \text{ mol/cm}^3$, the oxygen pressure 35.5 atm, the catalyst particle size 2 mm, the particle density 1800 kg/m³, the bed voidage 0.42, the tortuosity of alumina 3, and its particle porosity 0.4.

Solution

Due to the high pressure, it is important to evaluate the properties of the gas phase, i.e. of oxygen. Here, we don't present the calculations but

- the density is evaluated from calculations based on the ideal gas law,
- the viscosity is evaluated using the Jossi *et al.* correlation (see eq. (I.12) in Appendix I)

The correlations as well as the parameters needed for these calculations are given in Appendix I. The resulting density is 45.72 kg/m³ and viscosity $2.48 \times 10^{-5} \text{ Pa s}$.

Hydraulic analysis:

a. Trickle-bed reactor: The pressure drop in the trickle-bed reactor is evaluated using the correlation of Larkins *et al.* (eq. (3.390)). However, at first we have to evaluate the single-phase pressure drop for the gas and the liquid. Using the Ergun equation (3.449), the pressure drop is 2380.74 and 19.10 Pa/m for the liquid and the gas phase, respectively. Then (eq. (3.391))

$$X = \left[\frac{(\Delta P_L/Z)}{(\Delta P_G/Z)} \right]^{0.5} = 11.16$$

and thus (eq. (3.390))

$$\begin{aligned} (\Delta P_{GL}/Z) &= [(\Delta P_L/Z) + (\Delta P_G/Z)] \exp \left[\frac{5.0784}{3.531 + (\ln X)^2} \right] \\ &\cong 4131 \text{ Pa/m} \end{aligned}$$

Due to the relatively high pressure, the wetting efficiency is evaluated from the correlation of Al-Dahhan *et al.* (eq. (3.414)):

$$f_w = 1.104 Re_L^{1/3} \left\{ \frac{1 + \left[\left(\frac{\Delta P}{Z} \right) / \rho_L g \right]^{1/9}}{Ga_L} \right\} = 0.92$$

where $Re_L = 23.42$ and $Ga_L = 9.65 \times 10^4$. It is evident that the wetting efficiency is high enough to assume complete wetting, and thus to use the simplified reactor models.

The next parameter of importance is the Peclet number of the liquid and the gas phase. For the specified Reynolds number, the Peclet number for the liquid phase using the Michell–Furzer correlation (eq. (3.417)) is 0.74. The minimum value of Z/d_p for ethanol conversion between 0.1 and 0.9, evaluated using the Mears criterion (eq. (3.421)), is 2.84 and 62.11 respectively, much lower than the value used in the example, which is about 2500. Thus, the operation can be assumed to follow the plug-flow model.

Packed bubble bed reactor: The pressure drop in the packed bubble bed reactor is evaluated using the Huntington correlation (eq. (3.395)). The parameters needed are the following (eqs. 3.396, 3.397, and 3.398):

$$d_{pe} = \frac{2}{3} d_p \frac{\varepsilon}{1 - \varepsilon} = 0.25 \text{ cm}$$

$$\psi = \left[\frac{\left(\frac{u_{sG} \rho_G d_{pe}}{\mu_G} \right)^{1.167}}{\left(\frac{u_{sL} \rho_L d_{pe}}{\mu_L} \right)^{0.767}} \right] \left(\frac{\mu_w}{\mu_L} \right)^{0.9} = 339.61$$

$$\zeta = \exp[8 - 1.12 \ln(\psi) - 0.0769 [\ln(\psi)]^2 + 0.0152 [\ln(\psi)]^3] = 6.49$$

and thus (eq. (3.395))

$$\frac{\Delta P_{GL}}{Z} = \frac{2u_{sG}^2 \rho_G \zeta}{d_{pe}} = 245.71 \text{ dyn/m}^3 \cong 2457 \text{ Pa/m}$$

In this correlation, CGS units are used. It can be seen that the pressure drop in this reactor is lower than that in the trickle-bed reactor, under the same operating conditions.

Concerning packed bubble bed reactors, the evaluation of the Peclet number of the liquid phase is important in order to decide if we have to use a plug- or backmixed-flow model. For the specified Reynolds number, the Peclet number for the liquid phase using the Stiegel–Shah correlation (eq. (3.422)) is 0.15, much lower than in the trickle bed, which was expected as the backmixing in the liquid phase in packed bubble bed reactors is relatively high. The liquid phase can be considered to be well mixed if (Ramachandran, and Chaudhari, 1980) (eq. (3.423))

$$Pe_L \frac{Z}{d_p} \leq 4$$

In our case the right hand parameter of this criterion is about 373, which means that we can use the plug-flow model.

Note that we are less interested in the mixing of the gas phase. This explains why the gas-phase concentration is considered to be constant, and thus its material balance is not involved in the model.

Mass transfer coefficients: In the mass transfer calculations, we need the Henry constant of oxygen in water at 30 °C, which can be evaluated using the relevant correlations presented in Section I.3.2, Appendix I, and is equal to 34.03. The next parameter we need is the diffusion coefficient of oxygen in water at 30 °C, which can be also found in Table I.10, Appendix I. The correction for the temperature has been also presented in eq. (I.28) Appendix I. The evaluated diffusion coefficient is 2.5×10^{-9} m²/s.

- a. *Trickle bed reactor:* Using the Goto and Smith correlation (eq. 3.426), the gas–liquid mass transfer is found to be 2.5×10^{-2} s⁻¹. The liquid–solid mass transfer is evaluated using the Dharwadkar–Sylvester correlation (eq. (3.433)) with $a_u = 1740$ m⁻¹ and is equal to 0.21 s⁻¹.
- b. *Packed bubble bed reactor:* Using the Reiss correlation (eq. (3.432)), the gas–liquid mass transfer is found to be 9.02×10^{-2} s⁻¹. The liquid–solid mass transfer is evaluated from the Mochizuki–Matsui correlation (eq. (3.436)) for $Re_L > 5$ and is equal to 0.24 s⁻¹. The parameter θ is equal to 0.51 (eq. (3.439)), while (eq. (3.437))

$$d_{pe} = \frac{2}{3} d_p \frac{\varepsilon}{1-\varepsilon} = 0.097 \text{ cm}$$

In the Mochizuki–Matsui correlation, CGS units should be used.

Note that the mass transfer coefficients are higher in the packed bubble bed reactor compared to those in the trickle-bed reactor under the same conditions, as expected.

The intraparticle phenomena: The next step is the evaluation of the internal effectiveness factor. The unknown parameter is the effective solid-phase diffusion coefficient, which is (eq. (3.602))

$$D_{\text{eff}} = \frac{\varepsilon_p D_f}{\tau_p} = 3.36 \times 10^{-10} \text{ m}^2/\text{s}$$

Assuming spherical particles, the Thiele modulus is (eq. (5.76))

$$\phi = \frac{r_p}{3} \sqrt{\frac{k_m \rho_p}{D_{\text{eff}}}} = 3.25$$

For a first-order reaction and isothermal operation, the effectiveness factor is (eq. (5.77))

$$\eta_s = \frac{1}{\phi} \left(\frac{1}{\tanh(3\phi)} - \frac{1}{3\phi} \right) \cong 0.28$$

The application of the models: The gas-phase concentration of oxygen, which is needed for the application of the models, is evaluated from the ideal gas law and is 1.43×10^{-3} mol/cm³.

a. *Trickle-bed reactor:* The coefficient k° is

$$\frac{1}{k^\circ} = \frac{1}{(k_f a_u)_A} + \frac{1}{\rho_b \eta_s k_m} \Rightarrow k^\circ = 4.99 \times 10^{-3} \text{ s}^{-1}$$

Then, for zero inlet liquid-phase concentration of oxygen, we use eq. (5.368), where $m = 0.175$ and $n = 2.84$ (eqs. (5.364) and (5.365)), and thus the conversion is 20.7%. For liquid saturated with oxygen, eq. (5.344) is used and the resulting conversion is 24.8%, higher as expected.

b. *Packed bubble bed reactor:* The coefficient k° is

$$\frac{1}{k^\circ} = \frac{1}{(k_f a_u)_A} + \frac{1}{\rho_b \eta_s k_m} \Rightarrow k^\circ = 5 \times 10^{-3} \text{ s}^{-1}$$

Then, for zero inlet liquid-phase concentration of oxygen, we use eq. (5.368), where $m = 0.199$ and $n = 9.02$ (eqs. (5.364) and 5.365) which results in the conversion of 23.6%. For saturated liquid with oxygen, eq. (5.344) is used and the resulting conversion is 24.9%, higher as expected.

Note that in the packed bubble bed reactor, the conversion achieved is higher by 14.02% due to the higher mass transfer coefficients compared to the trickle bed, especially the gas–liquid one, which is 3.61 times higher in the packed bubble bed reactor.

In the case of saturated liquid feed, the conversion achieved is almost identical for both reactors. This is why in the respective reactor model, the gas-phase mass transfer is theoretically infinite and the difference in the liquid–solid mass transfer between the reactors is small, only 1.21 times higher than that in the packed bubble bed reactor.

5.3.6 Fluidized beds

In this section, some analytical solutions of fluidized-bed models are presented. Specifically, model solutions will be given for the case of a gas-phase reactant and a single solid-catalyzed reaction of the form $A \rightarrow \text{products}$ and bubbling fluidized bed (Type B fluidization). The same analysis holds for a reaction of the form $A + B \rightarrow \text{products}$, if the reaction depends only on the concentration of A. Some solutions for the cases of a single reversible reaction, for two reactions in parallel, and two reactions in series will be given as well.

The solutions of the model for particulate fluidization are the same as in two-phase fixed beds by employing the fluidized bed porosity instead the fixed-bed one. An example for this case will be also given.

Two-phase models

Emulsion phase in completely mixed state *General solution—bubble phase free of solids (Orcutt model):* In the following, the simplified Orcutt–Davidson–Pigford model (Orcutt *et al.*, 1962) is presented. This model assumes in addition that the bubble phase is free of solids, and thus $\gamma_b = 0$. This means that the reaction takes place only in the emulsion (dense) phase. Then, the third term in eq. (3.516) disappears. The gas flow is in the inlet of the bed $u_s A$, the particulate phase $u_{fm} A$, and the bubble phase $u_s u_{fm} A$, where A is the cross-sectional area of the bed and (eq. 3.476)

$$\varepsilon_{\text{bub}} = \frac{u_s - u_{fm}}{u_{\text{bub}}} \Leftrightarrow u_s - u_{fm} = \varepsilon_{\text{bub}} u_{\text{bub}} \quad (5.395)$$

Integrating eq. (3.516) with the boundary condition $C_b = C_i$ at $z = 0$,

$$C_b = C_p + (C_i - C_p) \exp\left(-\frac{L_{\text{be}} z}{u_{\text{bub}}}\right) \quad (5.396)$$

Substitution of eq. (5.396) into the material balance for the particulate phase (eq. (3.518)) gives an equation for C_p , which can be solved analytically for certain reaction kinetics. Finally, the reactant concentration at the exit of the bed C_o is

$$C_o = \frac{u_{fm} C_p + (u_s - u_{fm}) C_{b,o}}{u_s} \quad (5.397)$$

where the reactant concentration in the bubble phase at the bed exit $C_{b,o}$ can be evaluated using eq. (5.396) for $z = Z_f$:

$$C_{b,o} = C_p + (C_i - C_p) \exp\left(-\frac{L_{\text{be}} Z_f}{u_{\text{bub}}}\right) \quad (5.398)$$

Using the eq. (5.397), C_p from the material balance in the particulate phase eq. (3.518) and $C_{b,o}$ from eq. (5.398), the exit concentration of the reactant can be evaluated.

Analytical solutions: For the case of a first-order irreversible reaction ($n = 1$) in the particulate phase ($A \rightarrow B$),

$$(-r_{p,vs}) = k_{vs} C_p \quad (5.399)$$

The solution of the model is

$$x = 1 - \frac{C_o}{C_i} = (1 - f_{bub} e^{-\chi}) - \frac{(1 - f_{bub} e^{-\chi})^2}{k_R + (1 - f_{bub} e^{-\chi})} \quad (5.400)$$

where

$$k_R = \frac{k_{vs} Z_{fm} (1 - \varepsilon_{fm})}{u_s} C_o^{n-1} = \frac{k_{vs} Z_{fm} (1 - \varepsilon_{fm})}{u_s} \quad (5.401)$$

$$\chi = \frac{L_{be} Z_f}{u_{bub} \varepsilon_{bub}} = \frac{L_{be} Z_f}{f_{bub} u_s} = \frac{L_{be} Z_f}{u_s - u_{fm}} \quad (5.402)$$

where L_{be} is the mass transfer coefficient between particulate and bubble phase in (m^3 gas interchange gas volume/ m^3 reactor)(1/s) and k_{vs} is the rate coefficient based on the volume of solids in m^3 liquid/ m^3 solids. The parameter χ is related to the bubble size and generally decreases as bubble size increases, and so small bubbles are preferred. Although the Orcutt–Davidson–Pigford model is simple, it does allow us to explore the effects of operating conditions, reaction rate, and interface mass transfer on the performance of the fluidized bed reactor.

In Figure 5.18, the conversion is, $\left(1 - \frac{C_o}{C_i}\right)$ while $k_R = \frac{k_{vs} Z_{fm} (1 - \varepsilon_p)}{u_s}$. The value of f_{bub} is 0.5, i.e. the operating superficial velocity is only two times the minimum fluidization velocity. The parameter k_R expresses the rate of reaction, i.e. a measure of how fast the reaction is. At the same time, χ is a measure of the mass transfer rate. It is obvious that for a slow reaction ($k_R \ll 1$), the overall conversion of the fluidized bed is insensitive to mass transfer, and thus to bed hydrodynamics χ , while for intermediate and fast reactions ($k_R > 1$) the conversion is very sensitive to mass transfer expressed by χ and the flow distribution parameter f_{bub} , and thus the conversion is determined by the bed hydrodynamics (Grace, 1984). This happens because in the absence of particles in the bubble phase, the gas reactants must reach the emulsion phase before the reaction can take place. The effect of mass transfer and flow distribution becomes more important for reactions of higher order (Grave, 1984).

Finally, as expected, a high mass transfer rate, i.e. high χ , results in higher conversions. These results are typical for a gas-phase catalytic reaction in a fluidized bed.

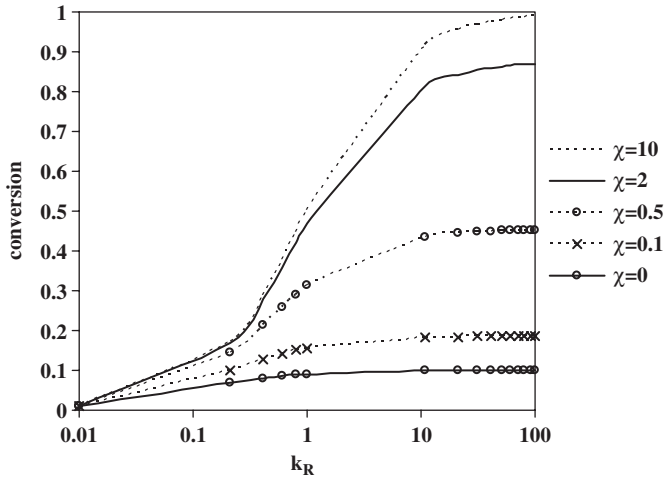


Figure 5.18 Conversion as a function of reaction rate and interface mass transfer k_R for $f_{\text{bub}} = 0.5$ for a first-order gas-phase catalytic reaction.

For the case of a zero-order irreversible reaction ($n = 0$) in the particulate phase ($A \rightarrow B$), the solution of the model is (Grace, 1984)

$$x = 1 - \frac{C_o}{C_i} = k_R \tag{5.403}$$

where

$$k_R = \frac{k_{\text{vs}} Z_{\text{fm}} (1 - \epsilon_{\text{fm}})}{u_s C_i} \tag{5.404}$$

For the case of a half-order irreversible reaction ($n = 1/2$) in the particulate phase ($A \rightarrow B$), the solution of the model is (Grace, 1984)

$$x = 1 - \frac{C_o}{C_i} = - \frac{k_R^2}{2(1 - f_{\text{bub}} e^{-x})^2} \left[1 - \left(1 + \frac{4(1 - f_{\text{bub}} e^{-x})^2}{k_R^2} \right)^{0.5} \right] \tag{5.405}$$

where

$$k_R = \frac{k_{\text{vs}} Z_{\text{fm}} (1 - \epsilon_{\text{fm}})}{u_s C_i^{0.5}} \tag{5.406}$$

For the case of a first-order reversible reaction ($n = 1$) in the particulate phase ($A \leftrightarrow B$), the solution of the model is (Grace, 1984)

$$x = 1 - \frac{C_o}{C_i} = (1 - f_{\text{bub}} e^{-\lambda}) - (1 - f_{\text{bub}} e^{-\lambda})^2 \left[(1 - f_{\text{bub}} e^{-\lambda}) + k_{R1} - \frac{k_{R1}^2}{k_{R1} + K_e (1 - f_{\text{bub}} e^{-\lambda})} \right]^{-1} \quad (5.407)$$

where $k_{\text{vs},1}$ is for the forward and $k_{\text{vs},2}$ is for the reverse reaction

$$k_{R1} = \frac{k_{\text{vs},1} Z_{\text{fm}} (1 - \varepsilon_{\text{fm}})}{u_s} \quad (5.408)$$

$$K_e = \frac{k_{\text{vs},1}}{k_{\text{vs},2}} \quad (5.409)$$

For the case of a first-order consecutive reaction ($n = 1$) in the particulate phase

($A \xrightarrow{k_{\text{vs},1}} P \xrightarrow{k_{\text{vs},2}} Q$) the solution of the model is (Grace, 1984)

$$x = 1 - \frac{C_{A,o}}{C_{A,i}} = (1 - f_{\text{bub}} e^{-\lambda}) - \frac{(1 - f_{\text{bub}} e^{-\lambda})^2}{k_R + (1 - f_{\text{bub}} e^{-\lambda})} \quad (5.410)$$

$$y_P = \frac{k_{R1}}{1 + k_{R2} - f_{\text{bub}} e^{-\lambda}} \frac{(1 - f_{\text{bub}} e^{-\lambda})^2}{1 - f_{\text{bub}} e^{-\lambda} + k_{R1}} \quad (5.411)$$

where

$$k_{R1} = \frac{k_{\text{vs},1} Z_{\text{fm}} (1 - \varepsilon_{\text{fm}})}{u_s} \quad (5.412)$$

$$k_{R2} = \frac{k_{\text{vs},2} Z_{\text{fm}} (1 - \varepsilon_{\text{fm}})}{u_s} \quad (5.413)$$

The yield of a product P is defined as the amount of product divided by the amount of A fed (initial amount):

$$y_P = \frac{C_P}{C_{A,i}} \quad (5.414)$$

For the case of a second-order irreversible reaction ($n = 2$) in the particulate phase ($A \rightarrow B$), the solution of the model is (Grace, 1984)

$$x = 1 - \frac{C_o}{C_i} = (1 - f_{\text{bub}} e^{-x}) - \frac{(1 - f_{\text{bub}} e^{-x})^2}{2k_R} \left[\left(1 + \frac{4k_R}{1 - f_{\text{bub}} e^{-x}} \right)^{0.5} - 1 \right] \quad (5.415)$$

where

$$k_R = \frac{k_{\text{vs}} Z_{\text{fm}} (1 - \varepsilon_{\text{fm}})}{u_s} C_o \quad (5.416)$$

The Orcutt model is very simple, offering analytical solutions, and thus is a useful tool for a rough estimation of the effect of various parameters on the operation of fluidized beds (Grace, 1984). However, it should be used only for qualitative comparisons, since its predictions have often been inaccurate compared to the experimental values obtained. The sources of those failures are the predicted uniform concentration of gas in the dense phase, which is not the case in experiments, and the assumption of the absence of solids in the bubble phase, which results in underestimating the conversion in the case of fast reactions.

Emulsion phase gas in plug flow *Solutions for bubble phase free of solids:* In the following, a simplified solution is presented under the following assumptions: first-order reactions, gas flow only through the bubble phase ($f_b = 1$), and absence of solids in the bubble phase ($\gamma_b = 0$). Under these conditions, the material balances (3.519) and (3.520) become the following.

For the bubble phase (gas phase),

$$-u_s \frac{dC_b}{dz} - L_{\text{be}}(C_b - C_p) = 0 \quad (5.417)$$

For the particulate phase (dense phase),

$$L_{\text{be}}(C_b - C_p) = \varepsilon_s k_{\text{vs}} C_p \quad (5.418)$$

where ε_s is the solids holdup in the reactor (solids volume per volume of reactor) (eq. 3.526):

$$\varepsilon_s = (1 - \varepsilon_{\text{bub}})(1 - \varepsilon_{\text{mf}}) \quad (5.419)$$

Note that the reaction rate is in (moles/m³ solid) (1/s), and thus by multiplying with ε_s m³ solid/m³ reactor) we obtain the material balance in (moles/m³ reactor) (1/s).

Then, solving eq. (5.418) for C_p :

$$C_p = \frac{L_{be}}{\varepsilon_s k_{vs} + L_{be}} C_b \quad (5.420)$$

Substituting in eq. (5.417) and after integrating in terms of conversion,

$$x = 1 - \frac{C_o}{C_i} = 1 - \exp\left(-\frac{Z_f \psi}{u_s}\right) \quad (5.421)$$

where

$$\psi = \frac{L_{be} \varepsilon_s k_{vs}}{\varepsilon_s k_{vs} + L_{be}} \quad (5.422)$$

Kelkar and Ng (2002) present some other cases of first-order reactions. They define the following modulus:

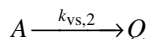
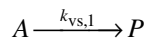
$$N_m = \frac{L_{be} Z_f}{u_s} \quad (5.423)$$

$$N_r = \frac{k_{vs} \varepsilon_s Z_f}{u_s} \quad (5.424)$$

Using this modulus, the previous solution becomes

$$x = 1 - \exp\left(-\frac{N_m N_r}{N_m + N_r}\right) \quad (5.425)$$

Parallel reactions of first order



The fractional conversion of A is

$$x = 1 - \exp\left[-\frac{N_m(N_{r1} + N_{r2})}{N_m + N_{r1} + N_{r2}}\right] \quad (5.426)$$

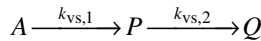
$$y_P = \left(\frac{N_{r1}}{N_{r1} + N_{r2}}\right)x \quad (5.427)$$

$$s_P = \left(\frac{N_{r1}}{N_{r1} + N_{r2}}\right) \quad (5.428)$$

where the selectivity to P is defined as the amount of product divided by the amount of A reacted:

$$s_P = \frac{C_P}{C_{A,o} - C_{A,out}} \quad (5.429)$$

Reactions of first order in series



The fractional conversion of A is

$$x = 1 - \exp\left(-\frac{N_m N_{r1}}{N_m + N_{r1}}\right) \quad (5.430)$$

$$y_P = \left(\frac{N_{r1}}{N_{r1} + N_{r2}}\right) \left[\exp\left(-\frac{N_m N_{r2}}{N_m + N_{r2}}\right) - \exp\left(-\frac{N_m N_{r1}}{N_m + N_{r1}}\right) \right] \quad (5.431)$$

$$s_P = \left(\frac{N_{r1}}{N_{r1} - N_{r2}}\right) \cdot \frac{\exp\left[\frac{N_m^2(N_{r1} - N_{r2})}{(N_m + N_{r1})(N_m + N_{r2})}\right] - 1}{\exp\left(-\frac{N_m N_{r1}}{N_m + N_{r1}}\right) - 1} \quad (5.432)$$

Solutions for solids presence in bubble phase: This model has been proposed by Chavarie and Grace as a two-phase simplification of the three-phase Kunii–Levenspiel model (Grace, 1984). Here, the solution is given under the following assumptions: first-order reaction, gas flow only through the bubble phase ($f_b = 1$) and absence of solids in

the bubble phase ($\gamma_b \neq 0$). Under these conditions, the material balances (3.519) and (3.520) become the following.

For the bubble phase (gas phase),

$$-u_s \frac{dC_b}{dz} - L_{be}(C_b - C_p) - \varepsilon_{bub} \gamma_b (-r_{b,vs}) = 0 \quad (5.433)$$

For the particulate phase (dense phase),

$$L_{be}(C_b - C_p) - (1 - \varepsilon_{bub})(1 - \varepsilon_{mf})(-r_{p,vs}) = 0 \quad (5.434)$$

For the case of a first-order irreversible reaction ($n = 1$) in the particulate phase ($A \rightarrow B$), the solution of the model is

$$x = 1 - \frac{C_o}{C_i} = 1 - \exp \left\{ \frac{-k_G [\chi_G (\gamma_b \varepsilon_{bub} + \varepsilon_s) + k_G \gamma_b \varepsilon_{bub} \varepsilon_s]}{\chi_G + k_G \varepsilon_s} \right\} \quad (5.435)$$

$$\varepsilon_s = (1 - \varepsilon_{bub})(1 - \varepsilon_{mf}) \quad (5.436)$$

where

$$k_G = \frac{k_{vs} Z_{fm}}{u_s} \quad (5.437)$$

$$\chi_G = \frac{L_{be} Z_f}{u_s} \quad (5.438)$$

This model is simpler than the Kunii–Levenspiel model and eliminates the unsubstantiated expression for cloud-to-emulsion transfer employed by Kunii and Levenspiel (Grace, 1984). Furthermore, compared to the previous models, the introduction of the parameter γ_b in the model leads to better results as the assumption that there is no solids in the bubble phase may lead to the underestimation of conversion in fast reactions. For slow reactions, the value of γ_b is of minor importance. However, for fast reactions the model may become sensitive to this parameter and the actual conversion should be bounded between the predicted ones using the upper and lower limits of γ_b , i.e. 0.01 and 0.001, respectively (Grace, 1984).

Kunii–Levenspiel three-phase model (bubbling bed model)

Here, the simple case of a first-order reaction is presented. The intrinsic reaction rate in each phase is

$$-r_{vs} = k_{vs} C_A \quad (5.439)$$

Using the material balances for the cloud and the emulsion phase, eqs. (3.537) and (3.538), it is possible to eliminate the concentrations C_c and C_e . Then, from eq. (3.536),

$$(-r_{b,u})_{\text{overall}} = \left[\gamma_b k_{vs} + \frac{1}{\xi} \right] C_b \quad (5.440)$$

The terms in the brackets represent the complex series-parallel resistances to mass transfer and reaction. The parameter ξ is

$$\xi = \frac{1}{K_{bc}} + \frac{1}{\gamma_c k_{vs} + \frac{1}{1/K_{ce} + 1/(\gamma_e k_{vs})}} \quad (5.441)$$

For very fast reaction and thus large k_{vs} ,

$$\xi \cong \frac{1}{K_{bc}} \quad (5.442)$$

Under this condition, the reactant A is unlikely to reach the emulsion phase. Integrating the material balance for the bubble phase, eq. (3.534) yields the desired performance expression in terms of conversion:

$$x = 1 - \frac{C_o}{C_i} = 1 - \frac{1}{\exp \left[\left(\gamma_b k_{vs} + \frac{1}{\xi} \right) \frac{Z_f}{u_{\text{bub}}} \right]} \quad (5.443)$$

Levenspiel proposed that approximately,

$$\frac{Z_f}{u_{\text{bub}}} \cong \left(\frac{1 - \varepsilon}{1 - \varepsilon_{\text{fm}}} \right) \frac{Z}{u_{\text{bs}}} \quad (5.444)$$

where Z and ε is the fixed bed height and porosity, respectively.

In Figure 5.19, the conversion versus $T = Z_f/u_{\text{bub}}$ is presented. The following typical values are used: $\gamma_b = 0.005$, $\gamma_c = 0.2$, $\gamma_e = 1.5$, $K_{bc} = 2 \text{ s}^{-1}$ and $K_{ce} = 1 \text{ s}^{-1}$.

It is obvious that to have high conversion, the reaction should be fast enough and the term Z_f/u_{bub} should be high. Hence, u_{bub} should be small or, in other words, d_{bub} should be small. The effect of mass transfer resistance is shown in Figures 5.20 and 5.21 for the cases of a fast ($k_{vs} = 1 \text{ s}^{-1}$) and a slow reaction ($k_{vs} = 0.01 \text{ s}^{-1}$), respectively.

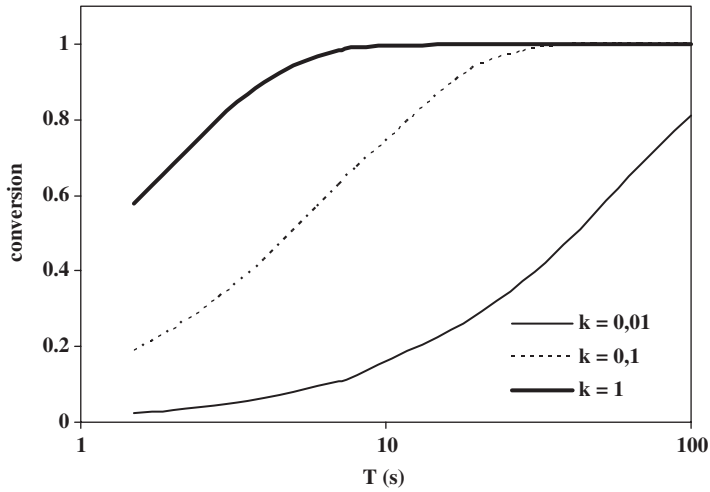


Figure 5.19 Conversion versus $T = Z_f/u_{\text{bub}}$ for $k_{\text{vs}} = 0.01, 0.1$ and 1 s^{-1} .

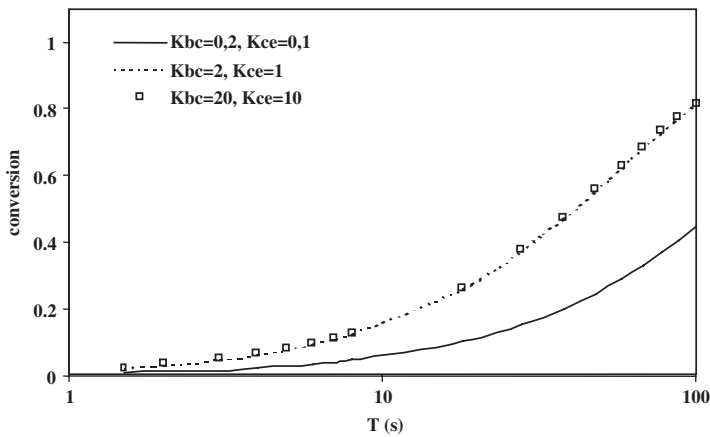


Figure 5.20 The effect of mass transfer resistance for a slow reaction ($k_{\text{vs}} = 0.01 \text{ s}^{-1}$).

As in the Orcutt model, for a slow reaction, i.e. a small k_{vs} , the overall conversion of the fluidized bed is less sensitive to mass transfer and thus to bed hydrodynamics than for a fast reaction, i.e. large k_{vs} .

Comments on the models

The basic differences between models are the following:

- the flow distribution status, expressed by f_{bub} ,
- the solids presence in the bubble phase, expressed by γ_{b} , and
- the mixing state in the emulsion phase.

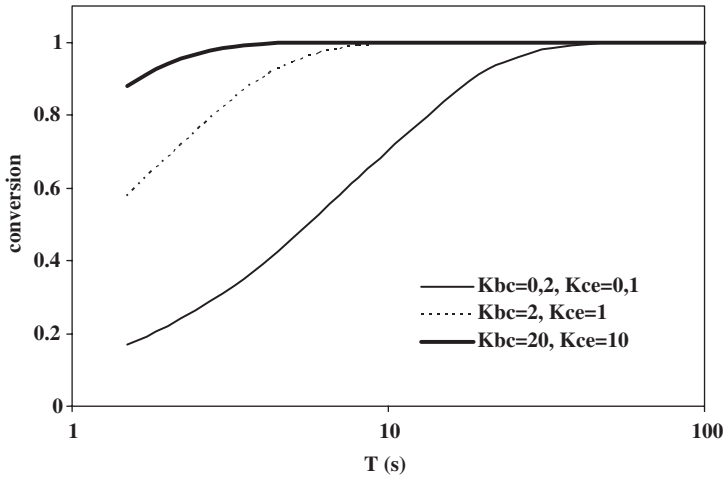


Figure 5.21 The effect of mass transfer resistance for a fast reaction ($k_{vs} = 1 \text{ s}^{-1}$).

These features are summarized in Table 5.20.

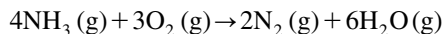
It has been stated that the effect of f_{bub} and γ_b is greatly dependent on the parameter k_R , and thus basically on the reaction coefficient. For a slow reaction, k_R is much less than unity and the effect of f_{bub} and γ_b is minimal, whereas the opposite holds for a fast reaction, where k_R is greater than unity. Furthermore, the Orcutt–Davidson–Pigford model has proved on some occasions to deviate from experimental results, probably due to the choice of the value of f_{bub} (Grace, 1984). At the same time, it is the only model that takes into account the effect of this parameter.

Taking into account all these observations, some guidelines for the use of these models are presented in Table 5.21.

Finally, in general, the models are less sensitive to the assumed gas-mixing status in the emulsion phase, i.e. complete mixing or plug flow, than to the expressions used to determine the interphase mass transfer coefficient (Grace, 1984).

Example 17

Masimilla and Johnstone studied the catalytic oxidation of ammonia:



at 1.11 atm and 250 °C, in a fluidized-bed reactor of $D = 11.4 \text{ cm}$ (Masimilla and Johnstone, 1961; Werther, 1980).

The reaction is of first order with respect to ammonia and the rate coefficient is $k_{vs} = 0.00858 \text{ (m}^3/\text{m}^3) \text{ (1/s)}$. The catalyst is spherical with a particle density of 2060 kg/m^3 and minimum fluidization velocity of 0.014 m/s. The bed height at incipient fluidization is $Z_{\text{fm}} = 58 \text{ cm}$.

Table 5.20

The main features of the models

	Orcutt–Davidson– Pigford	Kelkar–Ng	Chavarie– Grace	Kunii– Levenspiel
f_{bub}	Variable	1	1	1
γ_{b}	0	0	Variable	Variable
Mixing state	Complete mixing	Plug flow	Plug flow	Plug flow

Table 5.21

Guidelines for the use of fluidized-bed models

Flow distribution parameter	Reaction parameter	Proposed model
$f_{\text{bub}} < 1$	$k_{\text{R}} > 1$	Orcutt–Davidson–Pigford
$f_{\text{bub}} < 1$	$k_{\text{R}} \ll 1$	Orcutt–Davidson–Pigford Kelkar–Ng Chavarie–Grace
$f_{\text{bub}} = 1$	$k_{\text{R}} \ll 1$	Kelkar–Ng Chavarie–Grace Kunii–Levenspiel
$f_{\text{bub}} = 1$	$k_{\text{R}} > 1$	Chavarie–Grace Kunii–Levenspiel

The reaction gas (10% NH₃ and 90% O₂) flows through a porous stainless steel distributor under a superficial velocity in the range 0.025–0.15 m/s.

The resulted conversion under the specified conditions is shown in Table 5.22 (approximate values).

Use all the simplified models to estimate the conversion and comment on the results.

Assume that $\alpha = 0.625$, $\gamma_{\text{b}} = 0.0055$ (average values), and zero expansion factor.

Solution

For all calculations, we need the characteristic properties of the gas phase. Since the gas phase consists of 90% oxygen, we can assume that the gas properties can be represented by the properties of the oxygen alone. The gas density can be evaluated using the ideal gas law

$$\rho = MB \frac{P}{RT} = 0.828 \text{ kg/m}^3$$

The correlation of Jossi *et al.* (see eq. (I.12) in Appendix I) cannot be used for the determination of gas viscosity, as it is valid only for high pressures. Instead, Table I.2 in Appendix I can be used, where we find that the viscosity at 523 K is 3.16×10^{-5} kg/m s. The next parameter required for the gas phase is the diffusion coefficient of the species that

Table 5.22

Conversion versus u_s	
x (%)	u_s (m/s)
61	0.025
38	0.05
25	0.1
16	0.15

control the reaction rate. The Fuller–Schettler–Giddings equation (see eq. (I.29) in Appendix I) can be used for the determination of the diffusion coefficient of nonpolar gases in binary mixtures at low pressures:

$$D_{BA} = 0.01 \frac{T^{1.75} M_R^{0.5}}{P(V_A^{1/3} + V_B^{1/3})^2} = 6.16 \times 10^{-5} \text{ m}^2/\text{s}$$

where T is the temperature in K, P the pressure in Pa, and V_A and V_B the diffusion volumes of gases. The diffusion volume of ammonia is $14.9 \text{ cm}^3/\text{mol}$ and that of oxygen is $16.6 \text{ cm}^3/\text{mol}$ (see Table I.12 in Appendix I). Finally, M_R is (see eq. (I.30) in Appendix I)

$$M_R = \frac{1}{MB_A} + \frac{1}{MB_B} = 0.09$$

where MB_A and MB_B are the molecular weights of the gases.

The following calculations are based on the superficial gas velocity of 0.1 m/s and can be repeated equally for different gas velocities.

Hydrodynamics: The first and most important analysis in fluidized beds is the hydraulic one. As we see from the data given, the particle size is missing. However, the superficial velocity at incipient fluidization u_{fm} has been provided, and thus the particle size can be evaluated using the Ergun equation (3.451) by trial and error.

At first, we have to evaluate the bed porosity at incipient fluidization for the assumed particle size using the relationship of Broadhurt and Becker (eq. 3.466). Note that the resulting value cannot be lower than the fixed-bed porosity. Since we assume spherical particles, a reasonable value of bed porosity is 0.41 .

This procedure results in $\varepsilon_{fm} = 0.44$ and a particle size of 0.145 mm .

The fixed-bed length can be estimated from the given bed length at incipient fluidization (eq. 3.470):

$$Z = Z_{fm} \frac{1 - \varepsilon_{fm}}{1 - \varepsilon} = 54.69 \text{ cm}$$

The Mori–Wen correlation describes the initial bubble size for porous plates (eq. 3.502):

$$d_{\text{bub,o}} = 0.00376(u_s - u_{\text{fm}})^2 = 0.28 \text{ cm}$$

The maximum bubble size can be calculated as follows (eq. 3.504):

$$d_{\text{bub,max}} = 0.652 \left[\frac{\pi}{4} D^2 (u_s - u_{\text{fm}}) \right]^{0.4} = 9.81 \text{ cm}$$

In these equations, CGS units should be used. Then, the actual bubble diameter at height z above the bottom of the bed is (eq. 3.505)

$$\frac{d_{\text{bub,max}} - d_{\text{bub}}}{d_{\text{bub,max}} - d_{\text{bub,o}}} = \exp\left(-\frac{0.3z}{D}\right)$$

In order to calculate an average value of the bubble velocity, an average bubble diameter should be used. This diameter can be taken to be equal to the bubble diameter at $z = Z_f/2$. Thus, to calculate the bubble diameter, the fluidized bed height should be known (eq. 3.477):

$$Z_f = \frac{Z_{\text{fm}}}{1 - \varepsilon_{\text{bub}}}$$

where (eq. 3.476)

$$\varepsilon_{\text{bub}} = \frac{u_s - u_{\text{fm}}}{u_{\text{bub}}}$$

The rise velocity of bubble, cloud and wake is (eq. 3.501)

$$u_{\text{bub}} = u_s - u_{\text{fm}} + 0.711(gd_{\text{bub}})^{0.5}$$

The rise velocity of a single bubble in a fluidized bed is given by (eq. 3.500)

$$u_{\text{bs}} = 0.711(gd_{\text{bub}})^{0.5}$$

An iteration method has to be used to solve the problem (see Figure 3.60). The initial value of the fluidized bed height is the bed height at incipient fluidization. The results of the iteration process, for $u_s = 0.1 \text{ m/s}$, are shown in Table 5.23.

Table 5.23

Hydraulic parameters	
Parameter	Value
d_{bub} (cm)	5.87
u_{bs} (cm/s)	53.94
u_{bub} (cm/s)	62.54
ϵ_{bub}	0.14
ϵ_{f}	0.52
Z_{f} (cm)	67.25

For the Kunii–Levenspiel model, we need some additional hydraulic parameters. The fraction of the bed occupied by bubbles is given by (eq. 3.494)

$$\delta = \frac{u_{\text{s}} - u_{\text{fm}}}{u_{\text{bub}} - u_{\text{fm}}(1 + \alpha)} = 0.143$$

where α is the volume of wake per volume of bubbles and its average value is 0.625. Then, the fraction of the bed occupied by clouds is (eq. 3.497)

$$\beta_{\text{c}} = \frac{3\delta u_{\text{fm}}}{\epsilon_{\text{fm}} u_{\text{bs}} - u_{\text{fm}}} = 0.027$$

Then from eqs. (3.498) and (3.499), we have

$$\gamma_{\text{c}} = (1 - \epsilon_{\text{fm}}) \left(\frac{3u_{\text{fm}}}{\epsilon_{\text{fm}} u_{\text{bs}} - u_{\text{fm}}} + \alpha \right) = (1 - \epsilon_{\text{fm}}) \left(\frac{\beta_{\text{c}}}{\delta} + \alpha \right) = 0.451$$

$$\gamma_{\text{e}} = \frac{(1 - \epsilon_{\text{fm}})(1 - \delta)}{\delta} - (\gamma_{\text{c}} + \gamma_{\text{b}}) = 2.89$$

where γ_{b} is the volume of the solids dispersed in bubbles per volume of bubbles, γ_{c} is the volume of the solids within clouds and wakes per volume of bubbles, and γ_{e} is the volume of the solids in emulsion per volume of bubbles. The average value of 0.0055 is used for γ_{b} .

At this point, it is important to know if the operating gas superficial velocities, which are from 2.5–15 cm/s, are higher than the minimum bubbling velocity and lower than the minimum slugging velocity, respectively.

The minimum bubbling velocity can be calculated as (eq. 3.481)

$$u_{\text{bm}} = \frac{2.07 \rho_G^{0.06} d_p \exp(0.716 X_{45})}{\mu_G^{0.347}} = 1.08 \text{ cm/s}$$

Since, the particle size used is greater than 45 μm , the value of (X_{45}) is zero. The above equation holds for Group A particles. Using Figure 3.52, we see that for $\Delta\rho \cong 2000 \text{ kg/m}^3$, the Group A particles region is approximately between 0.03 and 0.16 mm. In our case, we have 0.145 mm and thus the particles belong to the Group A. However, this does not necessarily means that the fluidization is of Type A. This is why the reaction conditions are far from ambient. Furthermore, the resulting bubbling velocity is less than the minimum fluidization velocity (1.4 cm/s) indicating that the above equation is not adequate for our case. Here, we can use the Romero-Johnston criterion (eq. (3.488)) which is clearly indicates that the fluidization is bubbling.

The minimum slugging velocity can be evaluated as (eq. 3.491)

$$u_{\text{sm}} = u_{\text{fm}} + 0.16(1.34D^{0.175} - Z_{\text{fm}})^2 + 0.07(gD)^{0.5} = 10.61 \text{ cm/s}$$

Then, for velocities higher than 10.61 cm/s, it is expected that slugging will occur in the bed. In our case, the highest velocity is 15 cm/s, and for this velocity $d_{\text{bub}} = 7.37 \text{ cm}$. However, the maximum bubble diameter is 11.78 cm, essentially equal to the bed diameter, which is 11.4 cm. Thus, the results of these high velocities could be suspicious, as the fluidization regime is no more bubbling but slugging, or is in the transition region.

Mass transfer: For the Kunii–Levenspiel model, the mass transfer coefficient of the gas between bubble and cloud is (eq. 3.544)

$$K_{\text{bc}} = 4.5 \frac{u_{\text{fm}}}{d_{\text{bub}}} + 5.85 \frac{D_g^{1/2} g^{1/4}}{d_{\text{bub}}^{5/4}} = 3.88 \text{ s}^{-1}$$

Here, CGS units are used. The mass transfer coefficient of the gas between cloud and emulsion is (eq. 3.545)

$$K_{\text{cc}} \cong 6.78 \left(\frac{\varepsilon_{\text{fm}} D_g u_{\text{bub}}}{d_{\text{bub}}^3} \right)^{1/2} = 1.97 \text{ s}^{-1}$$

On the other hand, for the two-phase models, we need the mass transfer coefficients per unit volume of reactor (eq. (3.547)):

$$L_{\text{bc}} = k_{\text{bc}} \alpha_{\text{bub}}$$

where k_{be} is the mass transfer coefficient in m/s between bubble and emulsion (eq. (3.553)):

$$k_{be} = \frac{u_{fm}}{3} + \left(\frac{4\varepsilon_{mf} D_g u_{bub}}{\pi d_{bub}} \right)^{1/2} = 2.39 \times 10^{-2} \text{ m/s}$$

and a_{bub} is the interfacial area of the bubble phase per reactor volume ($\text{m}^2 \text{ bubbles/m}^3 \text{ reactor}$) (eq. (3.549)):

$$a_{bub} = \frac{6\varepsilon_{bub}}{d_{bub}} = 14.05 \text{ m/m}^2$$

Then, $L_{be} = 0.34 \text{ s}^{-1}$.

Models: The parameters of Orcutt model (eq. (5.400)) are the following ($u_s = 0.1 \text{ m/s}$) (eqs. 3.517, 5.401, and 5.402):

$$f_{bub} = \frac{u_s - u_{fm}}{u_s} = 0.86$$

$$k_R = \frac{k_{vs} Z_{fm} (1 - \varepsilon_{fm})}{u_s} = 0.28$$

$$\chi = \frac{L_{be} Z_f}{u_{bub} \varepsilon_{bub}} = 2.63$$

The only parameter we need for the Ng–Kelkar model (eq. (5.421)) is the following (eq. (5.422)):

$$\psi = \frac{L_{be} \varepsilon_s k_{vs}}{\varepsilon_s k_{vs} + L_{be}} = 0.037$$

where (eq. (3.526))

$$\varepsilon_s = (1 - \varepsilon_{bub})(1 - \varepsilon_{fm}) = 0.48$$

For the Chavarie–Grace model (eq. 5.435) we need two parameters (eqs. (5.437) and (5.438)):

$$k_G = \frac{k_{vs} Z_{fm}}{u_s} = 0.498$$

$$\chi_G = \frac{L_{be} Z_f}{u_s} = 2.26$$

Finally, for the Kunnii–Levenspiel model (eq. (5.443)) we need one more parameter (eq. (5.441)):

$$\xi = \frac{1}{K_{bc}} + \frac{1}{\gamma_e k_{vs} + \frac{1}{1/K_{cc} + 1/(\gamma_e k_{vs})}} = 4.12$$

In order to have an overview, the basic characteristics of the four models used as well as the conversions achieved for $u_s = 0.1$ m/s, are shown in Table 5.24.

The only model that takes into consideration the fraction of the gas that flows through the emulsion phase is the Orcutt–Davidson–Pigford one and for the specific superficial velocity of 0.1 m/s, $f_{bub} = 0.86$. The results of the models are close due to the fact that the flow

Table 5.24

Conversion for each model	
Model	x (%)
Orcutt–Davidson–Pigford	21.4
Kelkar–Ng	22.9
Chavarie–Grace	19.5
Kunii–Levenspiel	23.0

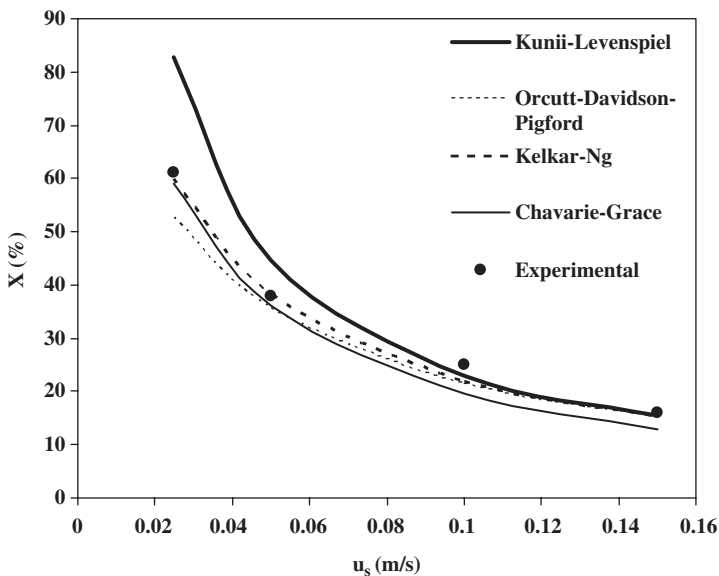


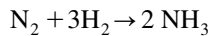
Figure 5.22 Comparison of models.

distribution parameter is of minor importance as a result of a slow reaction ($k_R = 0.28$). Furthermore, these values are close to the experimental one (approximately 25%).

All calculations can be repeated for the other superficial velocities and the results are shown in Figure 5.22.

It is evident that the Kunii–Levenspiel model deviates a lot for low values of superficial velocity and thus low f_{bub} , which shows that it cannot be used in this region. However, for a high superficial gas velocity, its predictions are slightly better than the other three models. Thus, with the exception of the Kunii–Levenspiel model at low values of f_{bub} , these models have a good behavior for the specified system.

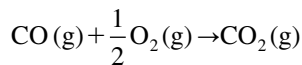
A few comments on ammonia: Ammonia (NH_3) is a gaseous compound at standard temperature and pressure with a characteristic odor, which is toxic and corrosive to some materials. It is used extensively in the production of fertilizers, explosives, and polymers. It is also produced naturally by the putrefaction of nitrogenous animal and vegetable matter. Ammonium salts are also ingredients of fertile soil and seawater. Being one of the most highly produced inorganic chemicals, ammonia is today mainly manufactured via the Haber process. Nitrogen and hydrogen react at 200 bar and 500 °C over an iron catalyst to produce ammonia:



Ammonia is not hazardous to humans and other mammals because the existence of a specific mechanism in their bodies leads to the conversion and excretion of ammonia. However, fish and amphibians lack this mechanism, and as a result ammonia is very toxic and dangerous to the aquatic environment.

Example 18

Zhang and Hu (2004) studied the catalytic oxidation of carbon monoxide:



The catalyst used is commercial Type 111 Cu/Cr/Ag impregnated, coal-based carbon of 0.6 mm particle size and bulk density of 0.7 g/cm³.

This study confirmed that for particle size lower than 0.6 mm the internal diffusion is negligible, and the reaction is first order in respect to CO concentration. The feed is air with CO concentration of 180 ppm, and thus the expansion factor is zero.

Some of the experimental results at 50 °C and for $d_p = 0.3$ mm are shown in Table 5.25 (approximate values).

Estimate the reaction coefficient k_m at 50 °C. Then, assume that we run the reaction in a fixed bed of 1.61 m diameter and 16.1 m height, under a contact time of 5 min. Estimate the conversion of CO in the fixed-bed reactor, and under the same conditions, in a fluidized-bed reactor, with the same initial (fixed bed) height.

For $P = 1$ atm and $T = 50$ °C the air properties are: $\rho = 1.09$ kg/m³ and $\mu = 2 \times 10^{-5}$ N s/m² and the diffusion coefficient of CO is 0.160 cm²/s. Assume that the fixed-bed porosity is 0.41 and that the particles are spherical.

Table 5.25

Experimental results	
τ (min)	x
5	0.38
10	0.60
15	0.75
20	0.80

Solution

Fixed bed: The performance equation in a fixed-bed reactor is (eq. (5.192))

$$\ln\left(\frac{1}{1-x_A}\right) = \frac{k^\circ}{u_{s,i}} Z$$

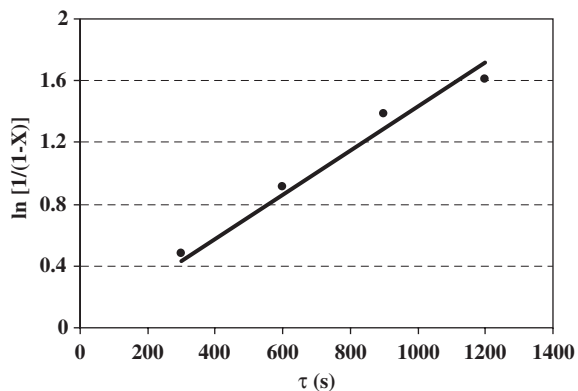
Then, the coefficient k° is the slope of the line

$$y = \ln\left(\frac{1}{1-x_A}\right) = k^\circ \tau$$

This plot is shown in Figure 5.23.

The slope of the best-fit line is 0.0014 s^{-1} while $R^2 = 0.9646$. Then (eq. 5.193)

$$\frac{1}{k^\circ} = \frac{1}{(k_f a_u)_A} + \frac{1}{\rho_b k_m}$$

**Figure 5.23** The estimation of k° .

To evaluate the rate coefficient k_m , we need the external mass transfer coefficient. Using the following correlation (eq. (3.352)):

$$Sh = \left(\frac{Re_p}{\varepsilon} \right)^{0.5} Sc^{0.33} = 1.53$$

and thus $k_f = 8.16 \times 10^{-2}$ m/s. Furthermore, $a_u = 11,800$ m²/m³ and thus $k_m = 2 \times 10^{-6}$ m³/kg s. For the fluidized-bed models, the coefficient k_{vs} is needed:

$$k_{vs} = \rho_p k_m = \frac{\rho_b}{(1-\varepsilon)} k_m = 2.37 \times 10^{-3} \text{ m}^3/\text{m}^3 \text{ s}$$

For the specified bed length and 5 min contact time, the superficial gas velocity is 5.37 cm/s.

Fluidized bed: For the specified system and particle size, the minimum fluidization velocity is 4.24 cm/s (eq. 3.451). Here, we note that the operating superficial velocity in the fixed bed is higher than the minimum fluidization velocity. This means that to retain a fixed-bed operation, we should operate in a downflow mode.

The (superficial) residence time in the fluidized bed can be defined as in a fixed-bed operation (eq. (3.98)):

$$\tau_f = \frac{V_R}{Q} = \frac{Z_f}{u_s}$$

Then, taking into account that the fluidized bed height is higher than the fixed-bed height and to have the same residence time of 5 min, the superficial velocity should be higher as well. Here, an iteration procedure is needed to evaluate the Z_f – u_s couple sufficient to give the desired contact time of 5 min. The iteration can start by choosing a low superficial velocity, near but higher than the minimum bubbling velocity. The results of the iteration procedure are shown in Table 5.26.

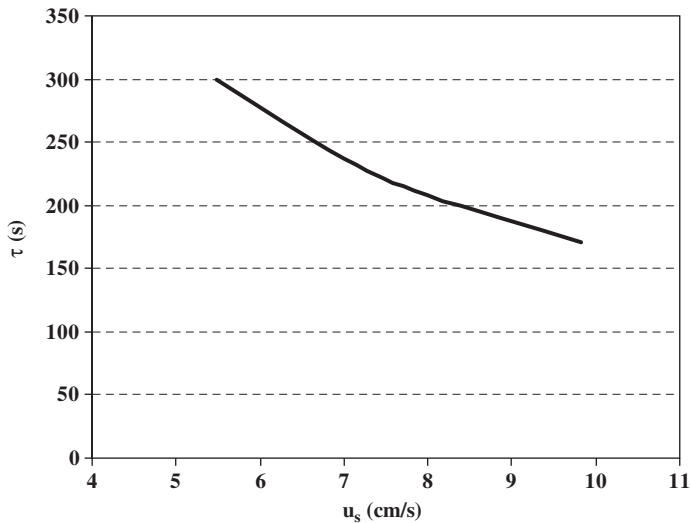
Then, we can use Orcutt–Davidson–Pigford model (eq. 5.400), where the following parameters can be evaluated from the above data: $f_{\text{bub}} = 0.23$, $k_R = 0.41$, $\chi = 5.50$, and $L_{\text{be}} = 4.15 \times 10^{-3}$ s⁻¹. Then, the conversion is equal to 29.1%, lower than the conversion evaluated by the corresponding model for fixed-bed operation, which is 34.3%.

By increasing the superficial velocity, the fluidized bed height is increased. However, it is easy to show that for a given particle size the contact time is lower for higher velocities, and that the highest contact time can be achieved by working under the lower allowable superficial velocity, which should be higher than the minimum fluidization velocity. This is shown in Figures 5.24 and 5.25.

Table 5.26

Hydraulic parameters

Parameter	Value
u_s (cm/s)	5.48
u_{in} (cm/s)	4.24
d_{bub} (cm)	29.46
u_{bs} (cm/s)	120.81
u_{bub} (cm/s)	122.05
ϵ_{bub}	0.01
ϵ_f	0.42
Z_f (m)	16.44

**Figure 5.24** Residence time versus superficial velocity.

If we use smaller particle size, the fluidised bed performance is different. For example, for $d_p = 0.15$ mm, the minimum fluidization velocity is 1.34 cm/s. If we operate the fluidized bed with this particle size, to have a contact time of 5 min, we need a superficial velocity of 5.85 cm/s, where the fluidized bed height is 17.51 m, and the resulting conversion is somewhat lower, equal to 25.8 %.

In this example, we show that for the same superficial contact time, the fluidized bed results in a different conversion, which is not the case for a fixed-bed reactor. As will be presented in Chapter 6, the complicated hydrodynamics of fluidized beds does not allow such simple “scale-up” rules to emerge.

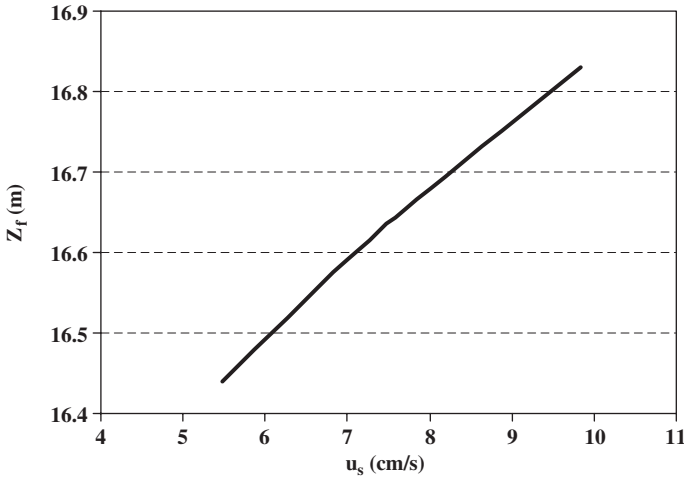


Figure 5.25 Fluidized bed height versus superficial velocity.

A few comments on carbon monoxide: Carbon monoxide is a deleterious gas that is mainly produced by the incomplete combustion of carbon-containing fuels. The exposure to carbon monoxide results in various undesirable health effects. Carbon monoxide is adsorbed through the lungs and reacts with hemoglobin to form carboxyhemoglobin, which impairs the capability of blood to carry oxygen. In addition to this mechanism, carbon monoxide combines with myoglobin, cytochromes, and metalloenzymes. However, the binding of carbon monoxide to hemoglobin appears to be the principal action mechanism underlying the toxic effects of exposure to low levels of carbon monoxide. High levels of exposure to carbon monoxide can cause death. Carbon monoxide is a pollutant frequently met in the urban environment, since it is produced via any combustion of fossil fuels, with motor vehicles being the most important source. Fortunately, the action of carbon monoxide on human health is reversible after withdrawal from exposure.

Example 19

Shen and Johnstone studied the catalytic decomposition of nitrous oxide:



at 1 atm and 371 °C in a fluidized-bed reactor of $D = 11.4$ cm (Shen and Johnstone, 1955; Werther, 1980).

The reaction is of first order in respect to nitrous oxide. The catalyst is spherical and its data are: $\rho_p = 2060$ kg/m³ and $u_{fm} = 0.005$ m/s. The bed height at incipient fluidization $Z_{fm} = 109$ cm.

The reaction gas (1% N₂O and 99% air) flows through a porous stainless steel distributor under a superficial velocity of 0.01 m/s.

The resulting conversion under the specified conditions is approximately 25%.

Evaluate the rate coefficient of the reaction using the Orcutt–Davidson–Pigford model. Assume that the internal effectiveness factor is unity and the expansion factor zero.

Solution

For all calculations, we need the characteristic properties of the gas phase. The air density can be evaluated by using the ideal gas law:

$$\rho = MB \frac{P}{RT} = 0.548 \text{ kg/m}^3$$

The air viscosity can be found in Table I.2, Appendix I, where we find that the viscosity at 644 K is about 3.1×10^{-5} kg/m s. The Fuller–Schettler–Giddings equation is proposed for the determination of the diffusion coefficient of nonpolar gases in binary mixtures at low pressure (see eq. (I.29) in Appendix I):

$$D_{BA} = 0.01 \frac{T^{1.75} M_R^{0.5}}{P(V_A^{1/3} + V_B^{1/3})^2} = 5.44 \times 10^{-5} \text{ m}^2/\text{s}$$

where T is the temperature in K, P the pressure in Pa, and V_A and V_B the diffusion volumes of gases. The diffusion volumes of nitrous oxide and air are 35.9 cm³/mol and 20.1 cm³/mol, respectively (see Table I.12 in Appendix I). Finally, M_R is (see eq. (I.30) in Appendix I)

$$M_R = \frac{1}{MB_A} + \frac{1}{MB_B} = 0.057$$

where MB_A and MB_B are the molecular weights of the gases.

Hydrodynamics: The particle size can be evaluated from the superficial velocity at incipient fluidization u_{fm} and the Ergun equation by trial and error (eq. (3.451)). For this calculation, we need the bed porosity at incipient fluidization for the assumed particle size, which can be evaluated by using the relationship of Broadhurst and Becker (eq. (3.466)). Note, that the resulting value cannot be lower than the fixed-bed porosity. Since we assume spherical particles, a reasonable value of bed porosity is 0.41. This procedure results in a particle size of 0.077 mm and $\varepsilon_{fm} = 0.47$.

The fixed-bed length can be evaluated from the given bed length at incipient fluidization (eq. (3.470)):

$$Z = Z_{fm} \frac{1 - \varepsilon_{fm}}{1 - \varepsilon} = 97.95 \text{ cm}$$

The Mori–Wen correlation is used for the initial bubble size for porous plates (eq. (3.502)):

$$d_{\text{bub},o} = 0.00376(u_s - u_{\text{fm}})^2 = 9.4 \times 10^{-4} \text{ cm}$$

The maximum bubble size is (eq. 3.504)

$$d_{\text{bub},\text{max}} = 0.652 \left[\frac{\pi}{4} D^2 (u_s - u_{\text{fm}}) \right]^{0.4} = 3.14 \text{ cm}$$

CGS units should be used in these equations. Then, the actual bubble diameter at height z above the bottom of the bed is (eq. 3.505)

$$\frac{d_{\text{bub},\text{max}} - d_{\text{bub}}}{d_{\text{bub},\text{max}} - d_{\text{bub},o}} = \exp\left(-\frac{0.3z}{D}\right)$$

To calculate an average value of the bubble velocity, an average bubble diameter should be used. This diameter can be taken to be equal to the bubble diameter at $z = Z_f/2$. Thus, to calculate the bubble diameter, the fluidized-bed height should be known (eq. (3.477)):

$$Z_f = \frac{Z_{\text{fm}}}{1 - \varepsilon_{\text{bub}}}$$

where (eq. 3.476)

$$\varepsilon_{\text{bub}} = \frac{u_s - u_{\text{fm}}}{u_{\text{bub}}}$$

The rise velocity of bubble, cloud, and wake is (eq. 3.501)

$$u_{\text{bub}} = u_s - u_{\text{fm}} + 0.711(gd_{\text{bub}})^{0.5}$$

The rise velocity of a single bubble in a fluidized bed is given by (eq. 3.500)

$$u_{\text{bs}} = 0.711(gd_{\text{bub}})^{0.5}$$

To solve the problem, an iteration method should be used (see Figure 3.60). The initial value of the fluidized-bed height is the bed height at incipient fluidization. The results of the iteration process are shown in Table 5.27.

Table 5.27

Hydraulic parameters	
Parameter	Value
d_{bub} (cm)	2.41
u_{bs} (cm/s)	34.55
u_{bub} (cm/s)	35.05
ϵ_{bub}	0.01
ϵ_{f}	0.48
Z_{f} (cm)	110.58

At this point it is important to know if the operating gas superficial velocity, which is 1 cm/s, is higher than the minimum bubbling velocity and lower than the minimum slugging velocity.

The minimum bubbling velocity can be calculated as follows (eq. 3.481):

$$u_{\text{bm}} = \frac{2.07 \rho_{\text{G}}^{0.06} d_{\text{p}} \exp(0.716 X_{45})}{\mu_{\text{G}}^{0.347}} = 0.56 \text{ cm/s}$$

Since, the particle size used is greater than 45 μm , the value of (X_{45}) is zero. The resulting minimum bubbling velocity is less than the operating velocity (1 cm/s). Thus, the operating regime is purely bubbling fluidization.

The above equation holds for Group A particles. By using Figure 3.52, we see that for $\Delta\rho \cong 2000 \text{ kg/m}^3$, the region of Group A particles is approximately between 0.03 and 0.16 mm. In our case, we have 0.077 mm and thus the particles belong to the Group A. This explains why the minimum fluidization velocity, which is 0.5 cm/s, is lower than the minimum bubbling velocity, which is 0.56 cm/s. This type of particle exhibits two types of fluidization, i.e. particulate fluidization for velocities lower than u_{bm} and bubbling fluidization for velocities higher than u_{bm} .

The minimum slugging velocity can be evaluated as follows (eq. 3.491):

$$u_{\text{sm}} = u_{\text{fm}} + 0.16(1.34D^{0.175} - Z_{\text{fm}})^2 + 0.07(gD)^{0.5} = 8.38 \text{ cm/s}$$

Then, for velocities higher than 8.38 cm/s, which is much higher than the operating velocity, it is expected that slugging will occur in the bed.

Mass transfer: For the two-phase models, we need the mass transfer coefficients per unit volume of reactor (eq. 3.547):

$$L_{\text{bc}} = k_{\text{bc}} \alpha_{\text{bub}}$$

where k_{be} is the mass transfer coefficient in m/s between bubble and emulsion (eq. 3.553):

$$k_{be} = \frac{u_{fm}}{3} + \left(\frac{4\varepsilon_{mf} D_g u_{bub}}{\pi d_{bub}} \right)^{1/2} = 2.34 \times 10^{-2} \text{ m/s}$$

and a_{bub} is the interfacial area of the bubble phase per reactor volume (m^2 bubbles/ m^3 reactor) (eq. 3.549):

$$a_{bub} = \frac{6\varepsilon_{bub}}{d_{bub}} = 3.55 \text{ m}^2/\text{m}^3$$

Then, $L_{be} = 0.083 \text{ s}^{-1}$.

Model application: The parameters of the Orcutt–Davidson–Pigford model (eq. 5.400) are the following:

$$f_{bub} = \frac{u_s - u_{fm}}{u_s} = 0.50$$

$$k_R = \frac{k_{vs} Z_{fm} (1 - \varepsilon_{fm})}{u_s} = 57.79 k_{vs}$$

$$\chi = \frac{L_{be} Z_f}{u_{bub} \varepsilon_{bub}} = 18.41$$

For a conversion level of 0.25 and by trial and error, the resulting rate coefficient is $0.0058 \text{ m}^3/\text{m}^3 \text{ s}$. Werther (1980) reported a value of $0.0051 \text{ m}^3/\text{m}^3 \text{ s}$, under the same conditions.

A few comments on nitrous oxide: Nitrous oxide (N_2O) is a gas produced mainly through natural sources. However, generally, motor vehicles and combustion processes contribute to its formation in urban areas. Unfortunately, it is involved adversely in the two global environmental problems: it contributes to the greenhouse effect and penetrates into the stratosphere, destroying the ozone layer.

Example 20

Menoud *et al.* (1998) studied the adsorption of copper from aqueous solutions by using the chelating resin Chelamine. The resin used is spherical, with an average diameter of 0.305 mm, swollen particle density of $158.4 \text{ kg}/\text{m}^3$ (dry) and hydraulic particle density (wet density) of $1064 \text{ kg}/\text{m}^3$.

The equilibrium of the copper–resin system was studied in a batch reactor at 20 °C and maximum copper concentration of 1.3 mol/m³. The isotherm follows the Langmuir model with $K = 142.86 \text{ m}^3/\text{mol}$ and $Q_M = 0.97 \text{ mol/kg}$.

The resin is packed in a bed of 5.2 cm diameter and 14.9 cm initial height while its porosity is 0.33. The fluidized bed is operated with $1.25 \times 10^{-6} \text{ m}^3/\text{s}$ flow rate and initial copper concentration of 0.308 mol/m³ at 20 °C. Calculate the time needed for the exit concentration to reach 20% of the inlet one. The experimental value is approximately 20.18 h.

Solution

Equilibrium analysis: The Langmuir isotherm equation is (eq. (4.5))

$$\frac{q_e}{Q_M} = \frac{KC_e}{1 + KC_e} \Rightarrow \frac{q_e}{0.97} = \frac{142.86C_e}{1 + 142.86C_e}$$

Then, the equilibrium parameter La is (eq. (4.8))

$$La = \frac{1}{1 + KC_o} = \frac{1}{1 + 142.86 \times 1.3} = 0.0054$$

This value indicates that the ion-exchange process is essentially irreversible, i.e. very favorable for the uptake of copper from solution.

Hydraulic analysis: The porosity of the bed at incipient fluidization is evaluated by using the Limal–Ballesteros correlation (eq. 3.467):

$$\varepsilon_{\text{fm}} = \frac{0.42}{\Phi_s^{0.376}} = 0.42$$

Then, the fluidized bed height at incipient fluidization is (eq. 3.470)

$$Z_{\text{fm}} = Z \frac{1 - \varepsilon}{1 - \varepsilon_{\text{fm}}} = 0.17 \text{ m}$$

The next step is to use the Ergun equation for the determination of the minimum fluidization velocity (eq. 3.451). For this step, we need a goal-seek procedure and the minimum fluidization velocity is found to be equal to 0.0057 cm/s, which is almost 10 times lower than the operation superficial velocity:

$$u_s = \frac{Q}{A} = \frac{1.25 \times 10^{-6}}{2.12 \times 10^{-3}} = 5.87 \times 10^{-4} \text{ m/s}$$

or 0.0587 cm/s. Note that for the determination of minimum fluidization velocity, the hydraulic density is used, i.e. the value of 1064 kg/m³. This density is used for all hydraulic calculations.

For the specified operating superficial velocity, the Reynolds number is equal to 0.2 while the Archimedes number is (eq. 3.454)

$$Ar = \frac{d_p^3 \rho_f (\rho_h - \rho_f) g}{\mu_f^2} = 22.59$$

The fluidized-bed porosity is calculated by using Pavlov's correlation (3.475):

$$\varepsilon_f = \left(\frac{18 Re_p + 0.36 Re_p^2}{Ar} \right)^{0.21} = 0.68$$

Finally, the fluidized-bed height at operation is (eq. 3.469)

$$Z_f = Z \frac{1 - \varepsilon}{1 - \varepsilon_f} = 0.31 \text{ m}$$

Mass transfer in the fluidized bed: Assuming that the diffusion coefficient of copper in the aqueous solution is approximately $10^{-9} \text{ m}^2/\text{s}$, we have (eq. 3.359)

$$Sc = \frac{v_f}{D_f} = \frac{(\mu_f/\rho_f)}{D_f} = 902$$

As long as the fluidization regime is particulate, we can use the correlation of Koloini–Sorpic–Zuner (eq. 3.543):

$$Sh = \frac{0.7}{\varepsilon_f} Re_p Sc^{1/3} = 1.98$$

Then (eq. 3.357)

$$Sh = \frac{k_f d_p}{D_f} \Rightarrow k_f = 6.48 \times 10^{-6} \text{ m/s}$$

The diffusion in the resin: The diffusion coefficient in the resin could be estimated by using the following relationship (eq. 3.607):

$$D_s = D_f \left(\frac{\varepsilon_p}{2 - \varepsilon_p} \right)^2$$

The resin internal porosity can be evaluated by using the definition of the hydraulic density (eq. 3.558):

$$\rho_h = \varepsilon_p \rho_f + \rho_p \Rightarrow \varepsilon_p = 0.91$$

Note that in this relationship, we use the swollen particle density, i.e. 158.4 kg/m³, because the resin volume changes when immersed in the solution. Then, the solid-phase diffusion coefficient is 6.9×10^{-10} m²/s.

The controlling mechanism: For the estimation of the controlling mechanism, the Miura and Hashimoto criterion is used (mechanical parameter) (eq. (4.207)):

$$\zeta = \frac{k_f a_u}{K(q_{\max}/C_o)}$$

$$K = \frac{15D_s \rho_{b,f}}{r_p^2}$$

where (eq. (4.209))

$$a_u = \frac{6(1 - \varepsilon_f)}{d_p} = 6308.5$$

In analogy to the fixed-bed bulk porosity (eq. 3.557), the fluidized-bed bulk density ($\rho_{b,f}$) is

$$\rho_{b,f} = \rho_p(1 - \varepsilon_f) = 158.4(1 - 0.91) = 50.76 \text{ kg/m}^3$$

Note that the swollen particle density, which is 158.4 kg/m³, is used for all calculations except the hydraulic ones, where the hydraulic density is used. Then, we have $K = 22.61$ and $\zeta = 0.0006$. According to the mechanical parameter criterion, if ζ is zero (practically much lower than 1), then fluid-film diffusion controls the process rate, while if ζ infinite (practically much higher than 1), then solid diffusion is controlling the process rate. It is obvious that the controlling mechanism is the fluid-film diffusion.

Analysis of the model: For the application of the model, we need the operating equilibrium loading of the resin q_{\max} , which is different (lower) than the maximum loading Q_M evaluated in batch experiments. The equilibrium loading is a function of the maximum inlet concentration of copper, which is 0.308 mol/m³. By using the equilibrium relationship (eq. (4.5)),

$$\frac{q_{\max}}{0.97} = \frac{142.86C_o}{1 + 142.86C_o} \Rightarrow q_{\max} = 0.95 \text{ mol/kg}$$

The appropriate model for the case of film-diffusion control is (eq. (4.140))

$$N_f(T-1) = \frac{\ln(X) - La \ln(1-X)}{1-La} + 1 = \frac{\ln(0.2) - 0.0054 \ln(1-0.2)}{1-0.0054} + 1 = -0.62$$

Then

$$N_f(T-1) = -0.62 \Rightarrow T = 0.97$$

Furthermore (eq. (4.135)),

$$\Lambda = \frac{\rho_{b,f} q_{\max}}{C_o} = 156.57$$

The volume of the fluidized bed is

$$V_f = Z_f A = 6.61 \times 10^{-4} \text{ m}^3$$

Then (eq. (4.137))

$$N_f = \frac{k_f a_u V_f}{Q} = 21.69$$

Finally (eq. (4.136)),

$$T = \frac{t - \left(\frac{V_f \varepsilon_f}{Q} \right)}{\left(\frac{\Lambda V_f}{Q} \right)} \Rightarrow t = 22.51 \text{ h}$$

The difference from the experimental value (20.18 h) is 11.5%. Taking into account the complexity of the system, the deviation could be considered satisfactory.

5.4 CATALYST DEACTIVATION

A major problem associated with the operation of heterogeneous catalysts is their gradual loss of activity with time. Inevitably, chemical and/or physical parameters affect the action of catalysts and progressively lead to its partial or total catalyst deactivation. Deactivation processes occur simultaneously with the main reactions.

Deactivation may proceed through chemical or physical processes, which are generally classified into

- poisoning
- fouling and coking
- thermal degradation.

In the following, the general aspects of these phenomena are presented.

5.4.1 Poisoning

Poisoning is characterized as the loss of catalyst activity due to the chemisorption of reactants, products, or contaminants in the feed onto catalyst active sites, thus occupying sites otherwise available for catalysis. In environmental catalysis, the presence of impurities hostile to the catalyst is the common case of deactivation. For example, components of lubricants may accumulate on the surface of a three-way catalyst and progressively cause its deactivation. Whether this process is irreversible or not depends on the nature of the poisoning agent. Here, we should make a distinction between poisons and inhibitors. An inhibitor is a substance weakly adsorbed, and generally its removal from the feed is sufficient for the catalyst to regain its activity, or at least a part of it. So, this type of poisoning is reversible and could be referred to as “inhibition.” On the other hand, species that interact strongly and irreversibly with the active sites are characterized as poisons and lead to chemical irreversible deactivation. The distinction is not always clear, since a poison that is very harmful at low temperatures may have an unimportant effect on catalyst activity at high temperatures.

A poison may simply block the active site, or affect the adsorptivity of other substances. Moreover, it may change the chemical nature of the active sites or form complexes with them, thereby definitely modifying their action. Moreover, the action of poisons can be nonselective or selective. In the first case, the poisoning agent affects all the active sites in the same manner. So, the activity across the catalytic surface is uniformly decreased, and the loss of activity is linearly related to the amount of the poisoning agents chemisorbed. In the second case, the poison shows a preference for specific active sites if there are different types of sites on the surface. This way, the loss in activity is not a simple linear function of the amount of poison adsorbed. Moreover, although not always the case, the selectivity of the catalyst may also be affected if the poisoned active sites have a function different from the unaffected sites in the main reactions. Whether or not the selectivity of the catalyst is affected, and to what extent, depends not only on the nature of the poisoning agents and the catalyst but also on the reactions involved. For example, in the oxidation of methanol to formaldehyde, Ag can be poisoned by Fe or Ni, whereas in the conversion of ethylene to ethylene oxide, Ag is affected by the presence of C_2H_2 .

Coulson and Richardson (1994) have used the following equation to find the ratio of activity of the poisoned catalyst to the activity of the unpoisoned catalyst:

$$F = \frac{\sqrt{1-\sigma} \tanh(\phi\sqrt{1-\sigma})}{\tanh \phi} \quad (5.445)$$

where:

F = the ratio of activity of the poisoned catalyst to the activity of the unpoisoned catalyst

σ = the fraction of active site poisoned

ϕ = Thiele modulus for a first-order reaction, which takes place in a flat plate of catalyst.

There are two limiting cases: (a) If ϕ is very small, F becomes equal to $(1 - \sigma)$ and the loss in activity is linearly connected to the amount of poison adsorbed, and (b) If ϕ is high, then F becomes $\sqrt{1 - \sigma}$ and the activity is less affected than in case (a) by the poison adsorbed because large ϕ means that the reactants have more difficulties in penetrating the interior of the particle.

5.4.2 Fouling and coking

Although coking and fouling are often used interchangeably, they are not exactly the same. Fouling is a more general term that covers all the cases where the active sites are blocked, or generally, covered physically by a deposit (masking or pore blockage). For example, Pb particulates physically block the pores inside the catalyst, if present in the feed, besides the fact that they react chemically with the active sites on catalytic converters, thereby deactivating the catalytic converter. However, the most common form of fouling is coking. Coking takes place when the surface reactions lead to the formation and deposition of carbonaceous residues, especially when hydrocarbons are involved in the catalytic reactions. It is a mechanism of a physical nature. The coke produced and deposited on the catalyst may amount to 20% of the catalyst weight. For example, extensive coking may occur during the wet oxidation of phenol aqueous solutions in the presence of a copper oxide catalyst and can lead to the deactivation of the catalyst within several hours or days, depending on the specific experimental conditions.

These deposits responsible for fouling can block out the reactants and prevent them from reaching the active sites, or even block the internal pores of the catalyst. Hydrocarbons and aromatics are usually the cause of coking. The chemical nature of the carbonaceous deposits relies on many parameters: temperature, pressure, feed composition, nature of products, and catalyst age share the responsibility of the residue formation on catalysts.

Catalysts deactivated by coking can usually be regenerated if treated properly at high temperatures so that the carbon is burned off. This way, the initial activity can be totally, or to an extent, restored.

The amount of coke deposited on the catalytic surface has been correlated to the time on stream (Voorhies, 1945):

$$C_C = At^n \quad (5.446)$$

where:

C_C = the %wt of coke on the catalyst

t = time on stream

A = fouling parameter which is a function of feedstock and reactor type

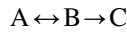
n = fouling parameter, typically close to 0.5.

This equation should be applied if the carbon deposited does not depend on the feed rate. However, this equation has been widely accepted and used, even beyond the range of its normal application.

Froment and Bischoff (1990) have developed another approach to include the effect of coking, considering the composition of the feed, catalyst temperature, and activity. They assumed that coke formation follows a reaction parallel or consecutive to the main reaction scheme:



or



where A is the reactant, B the product, and C the carbon formed.

Considering the common reaction $A \leftrightarrow B$ step first, the following expression for the rate of reaction was presented, assuming that the surface reaction is rate-controlling:

$$r = \frac{k_r C_t K_A \varphi_A \left(C_A - \frac{C_B}{K} \right)}{1 + K_A C_A + K_B C_B} \quad (5.447)$$

where r represents the reaction rate, C_t is the concentration of the active sites available to the main reaction, and φ_A the remaining activity function, defined as

$$\varphi_A = \frac{(C_t - C_{C^*})}{C_t} \quad (5.448)$$

Here, C_{C^*} is the concentration of the active sites covered by coke. The authors presented empirical relations to connect φ_A with the coke content of the catalyst C_C :

$$\varphi_A = e^{(-\alpha C_C)} \quad (5.449)$$

or

$$\varphi_A = \frac{1}{1 + \alpha C_C} \quad (5.450)$$

The constant α is a function of the operating conditions and its use should be limited within the range of conditions for which it has been estimated. For estimating the reaction rate, the relation of C_C with time has to be determined. If the formation of coke occurs in parallel with the main reaction, the following equation is applicable:

$$r_C = \frac{k_c C_t K_A \varphi_C C_A}{1 + K_A C_A + K_B C_B} \quad (5.451)$$

where

$$\varphi_C = \frac{(C_t - C_{C^*})}{C_t} \quad (5.452)$$

Following a similar approach, a rate equation in the case of the consecutive scheme can be also derived.

Various reports can be found in the literature in connection with catalyst deactivation kinetics (Wojchiechowsky, 1968), some of them also taking into account the effects of diffusion resistance (Beeckman and Froment, 1980).

5.4.3 Thermal degradation

Continuous exposure of catalysts to high temperatures may cause an alteration in its components and gradually lead to its deactivation. Thermal degradation may have an undesirable impact on both the catalyst substrate and noble metal load in various ways. Thermal degradation covers two phenomena: sintering and solid-state transformation.

“Sintering,” also termed “aging,” is the loss of catalytic action caused either by the loss of catalytic surface area due to crystal growth, or by the loss of washcoat area due to a collapse of pore structure, as a consequence of the exposure of the catalyst to high temperatures. So, sintering proceeds via crystal agglomeration and growth of the metals on the support or by closing of the pores inside the catalytic particles.

Sintering may occur in both supported and unsupported catalysts. In supported catalysts, sintering is considered to take place via agglomeration and coalescence of small metal crystallites into larger ones with lower ratios of surface to volume. In the case of unsupported catalysts, two different mechanisms have been proposed: (a) atomic migration, according to which metal atoms migrate from one crystallite to another via the surface (or in the gas phase), and thus the size of small crystallites decreases while that of the larger ones increase, and (b) crystallite migration, which involves migration of the crystallites along the surface of the support followed by collision and coalescence of two crystallites (Forzatti and Lietti, 1999).

Metal-oxide catalysts and support suffer a decrease in the surface area and porosity upon exposure to high temperatures due to the coalescence and growth of the bulk oxide crystallites.

At very high temperatures, the chemical nature of the catalytic agents may be altered so that the catalytic activity is definitely lost. This type of thermal degradation is called “solid-state transformation” and can be seen as an extreme form of sintering, which leads to the transformation one crystalline phase into a different one. Phase transformations in the bulk washcoat and incorporation of an active metal into the washcoat may take place during solid-state transformation.

Temperature is the main factor that affects sintering and solid-state transformation; experimental observations, however, have shown that the nature of the atmosphere in which the catalyst is heated may also play a part to an extent in the sintering process. For example, the presence of water vapor accelerates crystallization and structure modifications in oxide supports (Forzatti and Lietti, 1999).

Various reports can be found in the relevant literature in connection with the kinetics of sintering of supported metal catalysts. A power-law equation used is (Forzatti and Lietti, 1999)

$$\frac{d(D/D_o)}{dt} = -k(D/D_o)^n \quad (5.453)$$

where:

- D = the metal dispersion at sintering time t
- D_o = the initial metal dispersion
- k = the activated kinetic rate constant of sintering
- n = the sintering order

The metal surface area can be used in place of the metal dispersion. The variation of k with sintering time t and thus metal dispersion D has to be known for this equation to be applied.

A variation of eq. (5.453) has been proposed by Fuentes *et al.* (1991) for quantitatively determining the effect of temperature, time, and atmosphere on the sintering rate of supported metal catalysts:

$$\frac{d(D/D_o)}{dt} = -k \left(\frac{D}{D_o} - \frac{D_{eq}}{D_o} \right)^n \quad (5.454)$$

The symbols used are the same as those used in the previous relation. The term $-D_{eq}/D_o$ has been added in eq. (5.454) to account for the asymptotic approach observed in the typical dispersion versus time curves (Forzatti and Lietti, 1999).

5.4.4 Other mechanisms of deactivation

Besides the three main deactivation mechanisms described above, there are also some other ways of catalyst deactivation. At elevated temperatures, a loss of catalytic activity may be the result of volatilization. Direct metal loss through volatilization is rather

negligible. However, metals may form volatile compounds such as oxides and be lost in the effluent gas. Attrition may lead to loss of catalytic activity due to loss of catalytic material. It can be a cause of partial deactivation in moving and fluidized beds. Moreover, at high velocities and during sharp changes of temperatures, washcoat material on monolith honeycomb catalysts may be lost.

5.4.5 Regeneration of deactivated catalysts

As already discussed, if a catalyst is deactivated via coking, it could be regenerated so that its initial catalytic activity is restored. The treatment at high temperatures in an oxygen-rich atmosphere can burn off the coke deposited and the catalyst may regain its activity. Moreover, if the reduced activity is a temporary event caused by an inhibitor, the removal of the inhibiting substance of the feed can restore the catalyst to its initial potential.

However, in most cases of poisoning, fouling, sintering, solid-state transformation, volatilization and attrition, the loss of activity is irreversible and definite, and in the best scenario only a fraction of the initial activity can be restored.

Three-way catalytic converters, which constitute the widest application of catalysts in our life, are manufactured for prolonged operation under hard and constantly varying conditions. However, although at slow rates, they are progressively deactivated irreversibly through various ways: components in fuels and lubricants lead to poisoning, high temperatures lead to sintering, or loss of material results from attrition. Generally, in the case of automobile catalytic converters, deactivation can be attributed to poisoning or thermal aging of catalyst.

Poisoning: It refers to the loss in catalytic activity due to the occupation of active sites on the catalyst by substances via chemisorption. The main poisonous substances for catalytic converters are Pb, Zn, Ca, P, S, Si, and other metal compounds. The elements Pb and S come from the fuel, P, Zn, and Ca from the lubricant, whereas the metallic elements (Fe, Ni, Cu, and Cr) come from the metallic parts of the engine and the exhaust system. Although Pb has been eliminated in fuels, it can be found in unleaded gasoline at a level of 0.013 g/L, due to its presence at various stages of gasoline production. For temperatures up to 600 °C, in the presence of sulfur compounds, PbSO_4 is formed, which is physisorbed on catalytic sites (reversible poisoning). PbO_2 is formed for temperatures above 700 °C, which on being chemisorbed on catalytic sites causes irreversible poisoning. P present in oil additives may also enter exhaust emissions through unburned oils and may form compounds that can reversibly or even irreversibly poison the catalyst. Finally, S in fuel forms H_2S and oxides, which decrease the catalytic activity.

Thermal aging: Continuous exposure of the catalytic converter to the high temperatures of exhaust gases may influence the active components and/or the catalyst structure, gradually leading to its deactivation. The catalyst may be affected by thermal ageing in many ways. For operation temperatures above 600 °C, Rh_2O_3 reacts with alumina to form inactive $\text{Rh}_2\text{Al}_2\text{O}_4$ (Forzatti and Lietti, 1999), whereas above 700 °C, Pt particles condense, thus becoming larger (20 nm). This process may take place in various ways, such as crystallite migration and incorporation, via the emission of single atoms from small crystallites and their capture from larger ones, or through a combination of these mechanisms. Above 900 °C, condensation of $\gamma\text{-Al}_2\text{O}_3$ and alloying of noble metals may take place. A Pt–Rh alloy

is formed and Pt particles are covered by Rh oxides. At even higher temperatures, $\gamma\text{-Al}_2\text{O}_3$ is condensed extensively and transforms into $\delta\text{-Al}_2\text{O}_3$ or $\alpha\text{-Al}_2\text{O}_3$, and as a result its specific area decreases from 150 m²/g to 50 m²/g or even less. The formation of $\alpha\text{-Al}_2\text{O}_3$ is accompanied by mechanical tensions that lead to substrate cracking and noble metal loss. Thermal deactivation is normally irreversible, although redispersion of the sintered metal surface is possible (Angelidis and Papadakis, 1997; Pouloupoulos and Philippopoulos, 2004).

5.4.6 Deactivation of catalysts in liquid-phase applications

Although catalysts have been extensively used for the abatement of gas-phase pollutants, their application in water-phase processes for environmental purposes is a relatively novel subject with tremendous potential in the near future. However, catalyst durability and activity in such applications have to be definitely improved (Pirkanniemi and Sillanp, 2002).

Unfortunately, in liquid-phase applications, catalysts experience severe deactivation and may suffer great loss of potential at rates much higher than those in gas-phase operations. Besides poisoning, sintering, and the other deactivation mechanisms discussed above, leaching may also be another cause of deactivation. Hot and acidic media promote solubility of some metal oxides and enhance deactivation by leaching of metal or metal-oxide catalysts (Matatov-Meytal and Sheintuch, 1998). Whatever the reason for deactivation, it is dependent on the catalyst, support, and treated water. It has to be noted that in liquid applications, the pollutants concentrations faced by the catalyst are generally much higher than those found in gas treatment, let alone the presence of various poisoning agents in wastewaters. For example, noble metals are highly sensitive to poisoning if halogen-, sulfur-, or phosphorus-containing compounds are present in reaction media (Pirkanniemi and Sillanp, 2002).

For example, the most noteworthy disadvantage of catalytic wet oxidation is the severe catalyst deactivation (Larachi *et al.*, 1999). Hamoudi *et al.* (1998, 1999) systematically studied the deactivation of $\text{MnO}_2/\text{CeO}_2$ catalyst during wet catalytic oxidation of phenol and the catalyst-surface modifications. It was observed that deactivation was induced mainly by the formation of carbonaceous deposits on the catalyst surface. Ohta *et al.* (1980) reported that the size of the catalyst particles affected the stabilization of catalytic activity. For granular particles of supported copper oxide, the catalytic activity was decreased after each run, even after six successive experiments. In contrast, for larger particles the catalytic activity was stabilized after the first three runs.

Obviously, a lot of work has to be done in order to elucidate the deactivation mechanisms of catalysts in liquid-phase processes and how their span can be prolonged.

5.4.7 Kinetics of catalyst deactivation

The gradual loss of catalytic activity adds more to the existing complexity of catalytic systems. Thus, it has to be taken into account during the modeling of such systems. During the presentation of each deactivation mechanism, some kinetic models were given. Here, the

more general approach of Szepe and Levenspiel (1971) will be discussed. They developed a phenomenological treatment to cope with the problem of deactivation generally. Following this approach, the activity of a deactivating catalyst is expressed as

$$\alpha = \frac{r}{r_0} \quad (5.455)$$

where:

α = the activity of the catalyst

r = the rate of reaction after the time on stream

r_0 = the rate of the fresh catalyst

Obviously, the rate of reaction decreases with time for a deactivating catalyst, and thus the activity of the catalyst is also a function of time: α is initially equal to 1 and declines with time, approaching zero for a totally deactivated catalyst.

In general, the reaction rate depends on the reaction conditions as well as on the catalyst activity. The latter is in turn a function of the past of the catalyst. So,

$$r = f(C, T, P, \dots, \alpha) \quad (5.456)$$

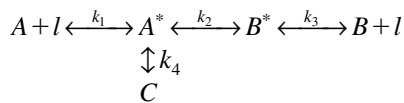
In analyzing reactions over deactivating catalysts, we can follow separable or non-separable kinetics. According to separable kinetics, Szepe and Levenspiel used two different terms: one for the reaction kinetics (independent of time) and another for activity (time dependent). Consequently,

$$r = r_0(C, T, P, \dots)\alpha(t) \quad (5.457)$$

where $0 \leq \alpha \leq 1$.

Since the decline of catalytic activity is owing to the decrease in the number of active sites, α should be correlated to the fraction N_t/N_0 , where N_t is the number of active sites after deactivating time t and N_0 is the number of active sites of the fresh catalyst. This correlation is derived from experimental observations, or an empirical form is used (Forzatti and Lietti, 1999).

Consider the dehydrogenation conversion of methyl-cyclohexane (A) to toluene (B) with coke (C) formation:



Butt and Petersen (1988) extended the Langmuir–Hinshelwood–Hougen–Watson kinetics to involve the varying activity (as a result of catalyst deactivation with time) to describe

the kinetics of the reaction scheme above. Assuming that (a) the surface reaction $A^* \leftrightarrow B^*$ controls the rate, and (b) the poisoning rate is by far smaller than the reaction rate, they derived the following expression of rate (Forzatti and Lietti, 1999):

$$r = \frac{k_2 K_A C_A C_t}{1 + K_A C_A + K_B C_B} \exp\left(-\int_0^t \frac{k_4 K_A C_A}{1 + K_A C_A + K_B C_B} dt\right) \quad (5.458)$$

If the concentrations of the reactants do not affect coke formation, eq. (5.458) can be simplified to

$$r = \frac{k_2 K_A C_A C_t}{1 + K_A C_A + K_B C_B} e^{-K't} \quad (5.459)$$

where

$$K' = \int_0^t \frac{k_4 K_A C_A}{1 + K_A C_A + K_B C_B} dt \quad (5.460)$$

It has to be noted that the separability requirement cannot always be applied. Depending on the reaction–deactivation network and the approach followed (separable or nonseparable kinetics) various expressions have been derived (Carberry, 1976).

5.4.8 Management of spent catalysts

In industry, some catalysts can be regenerated for reuse so that the operational cost associated with catalyst supply is minimized. However, in most cases as presented above, and in the case of automotive catalysts, the catalytic activity cannot be restored and the catalyst is then spent.

Specifically, catalysts are typically in the form of a ceramic support carrying small amounts of metals such as chromium, nickel, or platinum. Alumina and silica are commonly used in the construction of the ceramic support. The catalysts lose their activity progressively via various deactivation mechanisms (Pavel and Elvin, 1994). Thermal regeneration is often employed for regaining catalytic activity, if applicable, but some of the particles break during this process. Once the catalyst particles become too small to be useful, they constitute a waste disposal problem, since catalysts may contain heavy metals that are considered hazardous, or other harmful components.

In the context of sustainable development, all spent catalysts should be recycled as far as possible, or properly disposed off in an environmentally friendly manner, in case recycling is not possible (NFESC, 1996).

Catalysts contain precious metals and their recovery nowadays is recognized to be of great importance because

- precious metals that can be further used in various processes can be saved,
- energy is saved,
- the environment is protected from the accumulation of harmful materials

Nonhazardous spent catalysts can be also reused in the production of bricks. Specifically, catalysts are crushed and decreased in size to form alumina/silica sand that can replace the sand used in the manufacture of bricks. Moreover, spent fluidized-bed catalysts can be reused as cement components. Specifically, the catalyst is used to replace clinker in the final grinding (Cardenosa *et al.*, 1992). For the disposal of catalysts, the techniques presented in Section 4.3 can be largely applied.

Reactors Scale-up

The procedure during which a physical or chemical process is transferred from the laboratory or pilot scale to the commercial one is called scale-up. The term “scale-up” should not be understood only in the sense of increasing the dimensions while preserving similar systems. Often, the transposition of one system to another offers a better solution to a problem (e.g. a pilot plant operating in upflow for industrial unit operating in downflow) (Trambouze, 1990). While the rate of a given chemical reaction is independent of the size and the reactor structure, the physical processes involved in the overall rate, for example, mass and heat transfer, are usually controlled by these factors (Perry and Green, 1999). Furthermore, scale-up stands a much better chance for success if the laboratory and large-scale units are carried out in the same type of system, for example, fixed-bed, fluidized-bed, and batch reactors (Smith, 1981). From this point of view, keeping the same reactor type and thus the same reactor structure at different scales, the critical parameter is the reactor size, which incorporates its geometrical analogies and dimensions. Furthermore, in the case of adsorption and ion exchange in fixed beds, the fact that neither chemical reaction nor heat transfer occurs is crucial as these operations are essentially isothermal. Thus, scale-up mainly takes into account mass transfer phenomena, and of course the hydraulic performance of the reactor (liquid distribution, small-scale dispersion of the flow and liquid holdup).

Scale-up is limited by several factors, such as maximum working velocity in the case of adsorption/ion-exchange upflow fixed beds, and maximum allowable temperature in cases where microorganisms are involved in the process, for example, in the packed bed bioreactors (Michell *et al.*, 1999).

6.1 GENERAL ANALYSIS OF THE SCALE-UP PROBLEM

Various methods can be employed in modeling chemical or physical processes. There are three basic approaches in the scale-up procedure (Mukhyonov *et al.*, 1979): (a) mathematical modeling, (b) physical modeling, and (c) experimental scale-up.

6.1.1 Mathematical modeling

The first stage in the mathematical modeling of a process is to express mathematically the relationship between the basic process variables and the boundary conditions and set up an

algorithm. The second step consists of changing the various parameters, using the algorithm, to check whether the model corresponds to the process investigated and to select the optimal conditions. There are various advantages to the mathematical modeling method, such as deeper process understanding, more scale-up factors included, few reactor scales, and design flexibility.

In complex systems such as three-phase reactors, the methods of mathematical modeling cannot provide the required information for process design and scale-up since it is practically impossible to take into account all existing phenomena and safely predict the influence of hydrodynamics, heat and mass transfer, or kinetics on each other (Datsevich and Mukhortov, 2004). Thus, models are almost always approximate in nature. They are based on a number of assumptions that cannot be met during scale-up. So, it is not surprising that industrial unit designers do not completely trust the results obtained from mathematical modeling. Thus, several systems cannot be fully modeled mathematically and other methods for scale-up are followed.

6.1.2 Physical modeling

Physical modeling is an alternative to the mathematical one when the latter is not applicable. Two different methods can be followed in the context of physical modeling: (a) the similarity method, and (b) the dimensional analysis. However, in practice, these two methods are combined into one.

The most important method is the similarity method first proposed by Newton. In fluid dynamics, three types of similarity can be considered (Mukhlyonov *et al.*, 1979; Treybal, 1980; Holland, 1962):

- *Geometrical similarity*: Two systems exhibit geometrical similarity when the ratios of corresponding dimensions in one system are equal to those of the other system. Hence, between two pieces of equipment of different sizes, geometrical similarity exists only when they both have the same shape.
- *Kinematic similarity*: This type exists between two geometrically similar systems of different sizes when the ratios of velocities between corresponding points in each system are the same.
- *Dynamic similarity*: If two systems exhibit the same ratio of forces between corresponding points, in addition to being geometrically and kinematically similar, they also exhibit dynamic similarity.

The definition of dimensionless numbers has been given in a simple way by Noble and Terry (2004):

A group of physical quantities with each quantity raised to a power such that all the units associated with the physical quantities cancel, i.e. dimensionless.

So, the classical principle of similarity can be expressed by equations of the form

$$Q = f(R, S, \dots) \quad (6.1)$$

where the dimensionless group Q is a function of other dimensionless groups. Dimensional analysis has to be conducted for each case so that the above equation is derived. It is a way for expressing the behavior of a physical system in terms of the minimum number of independent variables.

Every dimensionless group represents a rule for scale-up. It is possible that one scale-up rule is contradictory to another one. Hence, it is a usual tactic during scale-up to deliberately suppress the effects of certain dimensionless groups in favor of a particular dimensionless group (Holland, 1962).

Physical modeling is not as accurate as mathematical modeling. This should be attributed to the fact that in dimensionless equations, the dependent number is expressed as a monomial product of the determining numbers, whereas the corresponding phenomena are described by polynomial differential equations. Moreover, errors in the experimental determination of the several constants and powers of the dimensionless equations can also lead to inaccuracies. We should also keep in mind that the dimensionless-number equations are only valid for the limits within which the determining parameters are varied in the investigations of the physical models.

The following dimensionless numbers are often employed (Mukhyonov *et al.*, 1979):

- *Geometrical dimensionless numbers:* They are expressed by ratios of several linear dimensions (height, diameter of the reactor, particle size, etc.) of the apparatus used.
- *Hydrodynamic dimensionless numbers:* Examples are the Reynolds number, Froude, Archimedes, and Euler number. These dimensionless numbers have to be functions of identical determining dimensionless numbers of the same powers and with the same value of the other constant coefficients, so that the model and the object are similar.
- *Diffusional dimensionless numbers:* The Peclet, Prandtl, Schmidt, Sherwood, and Nusselt number are the most common ones.
- *Different kinetic dimensionless numbers:* These can also be used depending on the conditions of the process. The most important is the Damköhler number.

In its simplest application, the principle of similarity attempts to represent a process by an unspecified relation between several dimensionless groups, one of which contains the unknown variable. If the groups containing the known variables are forced to have the same value on both the small and large scale, then the group containing the unknown variable will also have the same value (Edgeworth and Thring, 1957). In this form, the principle of similarity presupposes that the systems to be compared are geometrically similar. There are two methods of deriving similarity criteria: (a) empirical dimensional analysis, and (b) dimensional analysis using the differential equations (Edgeworth and Thring, 1957). When applicable, the second method is to be preferred.

Empirical dimensional analysis

To obtain the dimensionless groups for a specific process, the so-called “Buckingham Pi theorem” is frequently used. The first step in this approach is to define the variables that affect the process or assume the most important physical parameters for the specific process, if the equation that describes the process is entirely unknown. This is the weak

point of this method since it is difficult to have at hand these “significant” parameters without having a model for the process.

The theorem states that the number of dimensionless groups P_i is equal to the number of independent variables n minus the number of dimensions m . Then, each dimensionless group can be expressed as a function of other groups. In most cases, the exact functional form comes from experimental studies. The basic dimensions are length L, time T, and mass M. An independent variable is a variable that cannot be a function of the other involved variables. For example, kinematic viscosity is a function of density and dynamic viscosity. In this case, two of these three variables can be considered as independent.

Example 1

Consider the mass transfer across a flat plate. In this case, the important variables are (dimensions in parentheses): the mass transfer coefficient k (L/T), the bulk fluid velocity u (L/T), the kinematic viscosity of the fluid ν (L²/T), the solute diffusion coefficient D (L²/T), and the plate length l (L). The number of independent variables $n = 5$ and the number of the involved dimensions $m = 2$. Hence, the number of dimensionless groups $P_i = n - m = 3$.

Next, we select two of the variables that do not form a dimensionless group. These variables could be ν and l . Then, by combining these two variables with one more of the remaining three, we attempt to form three dimensionless groups by raising these two variables to the appropriate power, the aim being that all the units associated with the physical quantities are cancelled:

$$l^a \nu^b k = L^a \frac{L^{2b}}{T^b} \frac{L}{T}$$

Consequently, the following equalities should be satisfied:

$$\text{for L : } a + 2b + 1 = 0$$

$$\text{for T : } -b - 1 = 0$$

By solving this set of equations, we obtain

$$a = 1$$

$$b = -1$$

So, the first dimensionless group is

$$P_1 = \frac{kl}{\nu}$$

Repeating this procedure for D and u , the result is

$$P_2 = \frac{D}{\nu}$$

$$P_3 = \frac{ul}{\nu}$$

Finally,

$$P_1 = f(P_2, P_3) \Rightarrow \frac{kl}{v} = f\left(\frac{D}{v}, \frac{ul}{v}\right)$$

In this example, we recognize two well-known dimensionless groups, i.e. the Reynolds ($Re = ul/v$) and Schmidt ($Sc = v/D$) numbers. In contrast, the third dimensionless group in the last equation is not usually used. Instead, the Sherwood number is more useful ($Sh = kl/D$). The Sherwood number can result from multiplying both sides of the original functional form with the Sc number. The final relationship is

$$Sh = f(Re, Sc)$$

These groups have a definite, important, physical meaning. The Reynolds number is the ratio of inertial forces to viscous forces, the Sherwood number the ratio of mass transfer resistance in fluid film to mass transfer in bulk fluid, and Schmidt number the ratio of momentum diffusivity to mass diffusivity.

Edgeworth and Thring Method

Another way to derive the dimensionless groups needed for scale-up purposes has been proposed by Edgeworth and Thring (1957). The general concept is that the differential equations that describe the process could be used, since they are known for most processes that are relevant to chemical engineering. The main problem is that many of these equations cannot be easily integrated or are very difficult to be handled, in general.

Provided that these differential equations are dimensionally homogeneous, as all complete physical equations should be, they can be simplified to a generalized dimensional form by dropping the differential signs and substituting for linear coordinates a generalized linear dimension L . Dividing across by one term, one finds the relevant dimensionless groups. Following this procedure, from a complete set of differential equations, there is no doubt as to whether the correct variables have been included.

Example 2

Consider the Navier–Stokes differential equations for the isothermal flow of a Newtonian viscous fluid:

$$\rho \frac{\partial u_x}{\partial t} + \rho \left(u_x \frac{\partial u_x}{\partial x} + u_y \frac{\partial u_x}{\partial y} + u_z \frac{\partial u_x}{\partial z} \right) = \rho g \cos \alpha_x - \frac{\partial p}{\partial x} + \mu \left(\frac{\partial^2 u_x}{\partial x^2} + \frac{\partial^2 u_x}{\partial y^2} + \frac{\partial^2 u_x}{\partial z^2} \right)$$

In addition, there are two more identical equations for the y and z axes. In the equation the symbols “ u_x ,” “ u_y ” and “ u_z ” denote the velocity constituent in x , y and z axis respectively.

The corresponding generalized dimensional form of this equation is

$$\left[\frac{\rho v}{t} \right] + \left[\frac{\rho v^2}{L} \right] = [\rho g] - \left[\frac{\Delta p}{L} \right] + \left[\frac{\mu v}{L^2} \right]$$

Dividing across by $\rho v^2/L$, we obtain

$$\left[\frac{L}{vt} \right] + 1 = \left[\frac{Lg}{v^2} \right] - \left[\frac{\Delta p}{\rho v^2} \right] + \left[\frac{\mu}{\rho v L} \right]$$

For steady flow, L/vt drops out. Rearranging and omitting the plus and minus signs,

$$\frac{\Delta p}{\rho v^2} = f \left(\frac{\rho v L}{\mu}, \frac{v^2}{Lg} \right)$$

This is the well-known dimensionless equation for fluid flow. It represents the pressure coefficient as an unspecified function of the Reynolds and Froude groups. In geometrically similar flow systems, the pressure coefficients will be also equal, provided that the Reynolds and Froude numbers are both equal.

The principle of similarity requires geometrically similar systems to be compared at equal values of the appropriate dimensionless groups, called “similarity criteria.” However, in many cases, this requirement is not possible to be fulfilled, since it may be either impractical or impossible to be achieved.

To overcome this problem, the method of extrapolation has been proposed. It is found that in many cases, the unspecified function can be quite well represented by a power function. For example, for closed fluid-flow systems, the Froude group is negligible and thus

$$\frac{\Delta p}{\rho v^2} = c \left(\frac{\rho v L}{\mu} \right)^a$$

where c and a are known constants. The method of extrapolation is used to predict the performance of the large-scale apparatus at an equal value of the similarity criterion and/or extrapolate this performance to a different value of the similarity criterion assuming a power-law relation with an exponent either determined experimentally or taken from the literature.

Whether or not the fundamental differential equations governing a process are known, it is essential to discover the rate-determining factor or regime of the process, before any prediction can be made about the effects of changing of scale. The three broad types of regime that are met in chemical engineering are dynamic, thermal, and chemical. The prevailing regime must not be confused with the nature of the process itself. For example, a chemical reaction whose rate is limited only by the rate at which the reactants can be brought together by mixing, is subject to a dynamic regime.

Where no complete mathematical description of the process and no dimensionless-numbers equations are available, modeling based on individual ratios can be employed. This is the most characteristic case for a number of industrial processes, especially in the field of organic-chemicals technology. This method is referred to as “scale-up modeling” (Mukhyonov *et al.*, 1979). In such cases, individual ratios for the model and the object, which should have a constant value, are employed. For instance, there should be a constant ratio between the space velocity of the reacting mixture in the model and the industrial object. Some of the dimensionless numbers mentioned in physical modeling are also employed in this case.

6.1.3 Experimental scale-up

Experimental scale-up can be seen as part of physical and scale-up modeling. In the following, its methodology is briefly presented.

Collect and analyze data

A carefully planned test campaign is needed to collect data that adequately cover a wide range of the most important operating variables, conducting the minimum possible experiments. These laboratory-scale experiments should be held in a wide range of conditions that cover those expected in the commercial units, for five key operating variables (Dutta and Gualy, 2000): space velocity, temperature, pressure, composition, and particle size. Initially, only one variable should be changed at a time, keeping all the others constant, if possible (Dutta and Gualy, 2000). Temperature is usually expected to play the principal role in the reaction kinetics of most systems. Therefore, most of the experiments have to be connected to the effect of that variable. For reactions involving solids, catalytic or noncatalytic, both solid particle size and temperature should be varied in such a way that the data obtained represent both the absence and the presence of significant pore-diffusion phenomena.

Then, the next step is the selection of the appropriate rate expression form and, subsequently, the rate parameters should be estimated by minimizing the differences between the values predicted from the selected rate expression and the data experimentally found.

At this point it is important to consider safety. Safety issues are obviously of paramount importance and have to be dealt with adequately, especially in exothermic reactions. Specifically, laboratory and pilot reactors are usually made of small-diameter tubes and therefore effective heat removal can be achieved. On the other hand, commercial reactors have large diameters, approaching adiabatic conditions, and heat build-up may appear (Dutta and Gualy, 2000).

Define reactor type and its hydrodynamics

The reactor type is defined by the

- physical configuration of the volume occupied by the reaction system,
- flow mode of various streams in and out of the reactor,
- hydrodynamic representation of the flows within the reactor volume.

The relative importance of major phenomena that may affect reactor models are shown in Table 6.1.

Working with test reactor units

A proper laboratory or process development unit (PDU) is required if there is a lack of information on the reaction mechanism, kinetics, and the reactor hydrodynamics, especially for a new reaction system (Dutta and Gualy, 2000). In laboratory experiments, certain aspects of the process are investigated by handling small amounts of raw materials to reduce the material constraints to a minimum. In these experiments, all mechanisms that do not depend on size, such as thermodynamics and chemical kinetics, can be illuminated (Trambouze, 1990).

Table 6.1

Relative importance of major phenomena that may affect reactor models (Dutta and Gualy, 2000)

Phenomenon	Usually more important	Usually less important
Pore-diffusion resistance	Reactions involve solid particle size greater than about 1.6 mm All fast, noncatalytic gas–solid (G/S) reactions such as combustion and gasification	Reactors with particle size lower than 100 μm to 0.1 mm Catalytic bubbling fluidized beds (BFB) Slurry reactors
Film diffusion resistance	All bubbling reactors such as BFB and three-phase reactors All fast, noncatalytic G/S reactions such as combustion and gasification	Catalytic fixed-bed G/S reactors
Pressure drop	Fixed-, moving-bed, and BFB G/S reactors Liquid-phase reactors Generally all deep beds	Entrained-bed reactors
Heat-transfer resistance	Across two-phase interface in fast reactions Gas side of tube wall in liquid-cooled gas-phase or G/S reactors	Within solid particles in solid–fluid reactions
Heat loss to atmosphere	Small-diameter laboratory and pilot plant reactors	Commercial units
Axial dispersion	Low Z/D and low Reynolds number flow conditions Vessel with baffles or internals obstructing flows	High Z/D and high Reynolds flow in open pipes
Radial dispersion	Large-diameter reactors with low flow rates	(Usually ignored in preliminary models)
Temperature profile	Fixed and moving-bed G/S reactors	Dense phase of BFB reactors

First, some experiments should be conducted with the solids in the form of fine powders so that the pore-diffusion resistance is minimized and the intrinsic kinetic is revealed. Second, PDU should mimic as closely as possible the design, hydrodynamic conditions, and operation, including the solids particle size, expected in the commercial unit. Unfortunately, a close approach to the commercial system is not often possible in a lab-scale PDU. Therefore, an extensive pilot-plant study is usually undertaken. Pilot-plant experiments are realized at a scale that has wide variations, but in which all the industrial constraints are taken into account. It is during pilot-plant experiments that scale-up problems must be dealt with adequately. Representative operation implies operation that is identical or transportable by using a mathematical model (Trambouze, 1990). The pilot plant is thus a tool for the physical as well as chemical mechanisms. In particular, it is indispensable for measuring the extent of the possible interactions between the two types of mechanisms. In designing a pilot plant, the most important question is how large to make it, and unfortunately there is no a single answer to this question (Knowlton, 2000). If the pilot plant is too small, there will be problems, such as wall effects and slugging in fluidized beds. On the other hand, if it is too large, the cost could be too high.

All chemical processes regardless of type involve various mechanisms in addition to the desired chemical conversion, such as chemical reactions, thermodynamic, physical, and chemical equilibria, heat transfer, and mass transfer, which are not independent from one another, thus making it difficult to study their interactions. For example, transfer phenomena essentially depend on fluid flow. In other words, the scale or size of the equipment in which the process takes place has a different effect depending on the mechanism concerned. Extrapolation using geometric similarity can be proved extremely useful in determining the effect of size on a number of characteristic magnitudes of the system. This is shown in Table 6.2.

The aspect that is mainly affected by size is the physical behavior of the system. Therefore, by eliminating the chemically related terms from the process model, the physical aspect can be analyzed separately and adjusted appropriately by conducting specific experiments that exclude the chemical behavior of the system. This leads to the design of *mock-ups*. These PDUs are called “cold models” due to the absence of chemical reaction and may be needed to assess the hydrodynamics of a totally new reactor configuration. These cold models allow us to examine the impact of size on physical phenomena such as hydrodynamics separately (Trambouze, 1990). The mock-up simulates the physical process by adapting mild operating conditions such as ambient temperature and atmospheric pressure and by using inexpensive and harmless fluids with physical properties approaching those of the reaction fluids. The simulation, which is based on the theory of similarity, makes use of dimensionless numbers characterizing the major physical mechanisms.

6.2 PRACTICAL SCALE-UP RULES FOR CERTAIN REACTOR TYPES

6.2.1 Fixed beds

Adsorption and ion exchange

Under specified conditions, the data of the laboratory-scale unit can be used for the evaluation of the large-scale unit performance. The similarity rules can be drawn using

Table 6.2

Influence of size on a number of key mechanisms in chemical processes

Mechanism	Important variables	Influence of size
Chemical kinetics	Temperature, concentration, and pressure	None
Thermodynamics	Temperature, concentration, and pressure	None
Heat transfer	Local velocities, concentration, and pressure	Indirect
Mass transfer within a fluid phase	Temperature, concentration, and relative velocities of phases	Indirect
Transfers between phases	Temperature, concentration, and relative velocities of phases	Indirect
Forced convection	Flow rates and geometry	Important
Free convection	Temperature, concentration, pressure, and geometry	Determining

the continuity equation, the rates equations, and the hydraulic equations (for %h and Pe_d). From the continuity equation (4.129),

$$\frac{D_L}{u_s Z} \frac{\partial^2 C}{\partial(z/Z)^2} - \frac{\partial C}{\partial(z/Z)} - \rho_b \frac{Z}{u_s} \frac{\partial q}{\partial t} = \varepsilon \frac{Z}{u_s} \frac{\partial C}{\partial t} \tag{6.2}$$

it is clear that for the same ion-exchange or adsorption system and the same C_o and q_{max} , the exit concentration C at each time interval t will be the same for any bed size provided that the equation terms are the same. These terms are shown in Table 6.3.

Table 6.3

Parameters derived from the analysis of the design equations

Parameter	Equation	Parameter is a function of
ε	Continuity equation	D/d_p
Z/u_s	Continuity equation	—
Pe_L	Continuity equation	$Pe_d, Z/d_p$, or equally, $Z/d_p, Re_p$
D_s	Rate equation for solid diffusion (4.130)	—
r (or d_p)	Rate equation for solid diffusion (4.130)	—
k_f	Rate equation for liquid-film diffusion (4.131)	ε and Re_p
a_u	Rate equation for liquid-film diffusion (4.131)	d_p, ε , and particle shape
ε	Rate equation for liquid-film diffusion (4.131)	D/d_p
$h\%$	Liquid holdup correlations	u_s, d_p, ε
Isotherm— equilibrium behavior	Isotherm	Maybe influenced by contact time (Z/u_s)

Note: The parameter ρ_b is found in the continuity equation but is behavior eliminated when the rate equation is incorporated in its expression.

Table 6.4

Comments on the critical design parameters

Parameter	Comments
Z/u_s (τ)	Critical
Z/d_p	Minimal effect if higher than 150
D/d_p	Minimal effect if higher than 30
Re_p	Minimal effect if solid diffusion is the controlling mechanism and the bed is operated in near-plug-flow mode (or for Z/d_p higher than 150)
d_p	Critical
ε	Minimal effect if higher than 10 ($d_p/D < 0.1$)
u_s	Minimal effect if solid diffusion is the controlling mechanism and the unit is operated in upflow mode. The same holds for downflow mode if the liquid holdup is 100%.

Under some circumstances, the parameters in Table 6.3 may not have the same influence on the bed performance. In Table 6.4, some critical comments are summarized.

Thus, in fixed beds, the critical parameters are the contact time and particle size. Particle size should be kept the same, since it is well known that it affects the rate of adsorption and ion exchange. However, the role of particle size is more complicated because it also affects the pressure drop. For this reason, it is desirable to use a narrow particle size range during design, as the large particles control the uptake rate, whereas the small ones control the pressure drop (McKetta, 1993).

As a rule, it is not possible to keep the linear velocity constant during scale-up. The linear velocity can be similar in both units only if the pilot plant has a very high height-to-diameter ratio compared to the large unit. However, contact time is more critical than superficial velocity. Contact time is incorporated into the continuity equation, representing the physical time allowed for the contact of the phases. The physical meaning of this parameter is the time allowed for the “reaction.” However, it is known that in some systems contact time has a possible impact on the equilibrium state, leading to “partial” equilibrium behavior in the bed, at least in liquid-phase adsorption and ion-exchange processes that are reversible and of low kinetics (Inglezakis and Grigiropoulou, 2003). It is important to note that this effect is essentially another “nonideality,” which is not incorporated into the continuity equation. Thus, scale-up should be based on the same contact time and particle size.

Contact time (or space time) is determined by linear velocity as

$$\tau = \frac{\varepsilon}{Q_{\text{rel}}} = \frac{V_o \varepsilon}{Q} = \frac{Z \varepsilon}{u_s} \quad (6.3)$$

where Q_{rel} is the relative volumetric flow rate, commonly expressed in empty bed volumes per hour (BV/h). Q_{rel} is equal to the reactor space velocity:

$$Q_{\text{rel}} = \frac{Q}{V_o} = \frac{u_s}{Z} \quad (6.4)$$

and the basic scale-up rules are

$$\tau_{\text{FS}} = \tau_{\text{LS}} \Leftrightarrow \left(\frac{Z \varepsilon}{u_s} \right)_{\text{FS}} = \left(\frac{Z \varepsilon}{u_s} \right)_{\text{LS}} \quad (6.5)$$

$$(d_p)_{\text{FS}} = (d_p)_{\text{LS}} \quad (6.6)$$

where subscripts “LS” and “FS” denote lab-scale and full-scale units.

From the hydraulics perspective, if scale-up is based on the same superficial velocity, Pe_L will be higher in a large bed in downflow operation due to the higher bed height, whereas the liquid holdup will be low due to the low velocity, which is frequently used in laboratory beds. This leads to problems and special efforts are required to improve the liquid holdup, for example, a special distributor design. These problems are absent in upflow operation.

On the other hand, keeping the same contact time, the linear velocity is much higher in a large column, which is not necessarily a problem, since velocity influences the controlling

step (mass transfer in liquid film) and hydraulics (maldistribution and liquid holdup). In a large column, higher velocity leads the system to solid diffusion control, higher liquid holdup (for liquid–solid systems and downflow operation), and higher Pe_L (closer to plug flow), provided that the fluid dispersion at the inlet of the column has been well designed. In such a case, better results are expected, i.e. higher breakthrough volume will be achieved due to the fact that the liquid-film resistance can be minimized, and for downflow operation, liquid holdup (for liquid–solid systems) and Pe_L are high enough. Adsorption from the liquid phase using porous solids is frequently controlled by the solid diffusion step. From this point of view, the superficial velocity is expected to have a minimal impact on bed performance, provided that plug-flow condition is approached and the liquid holdup (for liquid–solid systems) is near to 100%. Thus, if scale-up is based on the same contact time, the results obtained from the laboratory-scale bed can be directly used in the large one and the performance of the bed can be accurately evaluated. Consequently, if we have a contact time–breakpoint volume relationship derived from the laboratory bed experiments, we can use this relationship to evaluate the breakpoint volume of the large-scale unit for the specified contact time.

In that case, when modeling is applicable to the laboratory-scale bed, a possible change in the controlling mechanism should be taken into account and a different model type is likely to be needed in the large-scale bed.

From the above analysis, some important conclusions can be drawn:

- In the case of high fluid-film resistance, keeping the same contact time at the large unit, the higher the superficial velocity, the lower the fluid film resistance, and thus higher rates can be achieved at the large bed. However, for the same contact time, the operation in downflow mode is probably the best because high superficial velocities at large beds can lead to partial fluidization and particle attrition in upflow operation. Furthermore, a different model would probably be needed for each scale.
- In the case of low resistance in fluid film or/and unfavorable equilibrium (equilibrium-limited system), a high contact time at the large bed would be beneficial for the equilibration step, whereas a high superficial velocity is not expected to lead to better results, since the fluid-film resistance is minimal. Furthermore, the same type of model can be used for different scales.

During this part of the design, we should keep in mind that the same controlling mechanism in units of different size will permit the experimental data to be directly “transferred” from the small to the large unit. In most cases, the diffusion of molecules or ions within the solid matrix is the controlling mechanism, especially in micro- and mesoporous materials such as zeolites. The fluid-film diffusion resistance is inversely proportional to the linear velocity and is not important in most cases, because the linear velocity is increased in the diffusion film at a large-scale unit. Consequently, when the solid diffusion is the controlling mechanism at the laboratory bed, the change in linear velocity (under the same contact time) has no effect on the kinetics of the system. This allows the flow rate to be varied during scale-up. However, it is safe to consider that the adsorption rate will be higher in larger columns due to the increase in the linear liquid velocity, even when the controlling mechanism incorporates fluid-film resistance in small columns. In the case of liquid–solid systems, the contact time at the two scales will be the same only

if the liquid holdup remains the same, and ideally close to 100%. Since liquid holdup is expected to be high enough in the large-scale column, provided that the liquid distributors are designed properly, especially in downflow operation, it is desirable to achieve a high liquid holdup in small columns also. However, this could be achieved only under the upflow condition.

To have near-ideal plug flow in a small-scale bed, the particle Peclet number should be high enough to cause a high bed Peclet number, whereas in a large-scale unit this particle Peclet number is of minimal importance, since it is multiplied by Z/d_p , and thus the bed Peclet number is expected to be high enough.

Example 3

In the typical case of 2 mm particle size and a small bed of 20 cm height, the multiplier Z/d_p is 100, whereas at a large bed of 200 cm height the multiplier Z/d_p is 1000. Thus, the bed Peclet number is 10 times higher at the large column, provided that the particle Peclet number is similar in both beds. It should be noted here that the particle Peclet numbers may not be similar in both scales, since they depend on the flow condition (up- and downflow) and on the Reynolds number. However, it can be shown in the case of irregular-shaped (zeolite-like) particles that the particle Peclet numbers are close enough for both flow conditions, in the range $4 < Re < 8.5$. For spheres, this is valid in a broader range of Reynolds number, e.g. $Re < 10$ (see Section 3.6.3).

To ignore the geometrical similarity between the different unit sizes, the following conditions should be satisfied (Carberry, 1976; Gunn, 1968):

$$\frac{Z}{D} \geq 5 \dots \frac{D}{d_p} \geq 30 \quad (6.7)$$

Also, the scaling factor for the bed diameter should be kept equal to or lower than 10 (Peters and Timmerhaus, 1968). Using the above relationships, the limits of volumetric flow rates can be evaluated:

$$Q = Q_{\text{rel}} V = Q_{\text{rel}} Z A \Rightarrow A = \frac{Q}{Q_{\text{rel}} Z} \Rightarrow D = \left(\frac{4Q}{Q_{\text{rel}} \pi Z} \right)^{0.5} \quad (6.8)$$

Then, the following equations hold:

$$D \leq \frac{Z}{5} \Rightarrow \left(\frac{4Q}{Q_{\text{rel}} \pi Z} \right)^{0.5} \leq \frac{Z}{5} \Rightarrow Q \leq \left(\frac{Z}{5} \right)^2 \frac{Q_{\text{rel}} \pi Z}{4} \quad (6.9)$$

$$D \geq 30d_p \Rightarrow \left(\frac{4Q}{Q_{\text{rel}} \pi Z} \right)^{0.5} \geq 30d_p \Rightarrow Q \geq (30d_p)^2 \frac{Q_{\text{rel}} \pi Z}{4} \quad (6.10)$$

$$D_{\text{FS}} \leq 10D_{\text{LS}} \Rightarrow \left(\frac{4Q_{\text{FS}}}{Q_{\text{rel}} \pi Z_{\text{FS}}} \right)^{0.5} \leq 10D_{\text{LS}} \Rightarrow Q_{\text{FS}} \leq (10D_{\text{LS}})^2 \frac{Q_{\text{rel}} \pi Z_{\text{FS}}}{4} \quad (6.11)$$

where the subscript “LS” denotes the laboratory-scale bed and “FS” the large unit. Using eqs. (6.9)–(6.11), the appropriate limits of working volumetric flow rates can be evaluated. Thus, the full-scale bed diameter can be estimated using eq. (6.8), according to the chosen working volumetric flow rate.

Maximum working velocity and maximum bed height

According to Ruthven (1984), the linear velocity should not be higher than a certain maximum value, so that extended friction between the packing material is avoided in both down- and upflow operations. This maximum velocity is 0.8 times the minimum fluidization velocity for upflow operation and 1.8 times the same velocity for downflow operation. The minimum fluidization velocity can be estimated using the equations presented in Section 3.8.2. In Figure 6.1, the maximum linear velocity versus the particle diameter is presented.

The following typical parameters are used: $\rho_h = 2.08 \text{ g/cm}^3$, $\mu = 0.9 \text{ cP}$, $\varepsilon = 1 \text{ g/cm}^3$, $\varepsilon = 0.5$, and $\Phi_s = 0.65$ (for sand-type granular materials). The bed voidage is considered to be constant, which is true for low d_p/D (see Section 3.6.3, Bed voidage considerations).

From Figure 6.1, some important conclusions can be drawn. First of all, it is well known that on increasing the particle size, the adsorption and ion-exchange rates are decreased. Thus, the use of large particles should be avoided. On the other hand, beds with small particles should be operated at low velocities, especially in the upflow mode. In laboratory beds, this is not really a problem since in this way the requirement of high residence times is satisfied. Also, in these beds, upflow operation, which is essential to avoid liquid maldistribution and low liquid holdup, can be easily employed without exceeding the maximum linear velocity. However, in a large bed, keeping the same contact time and particle size as in the laboratory bed, the linear velocity would be increased and would probably exceed the maximum allowed linear velocity. Furthermore, upflow is generally avoided because in the downflow mode, the permissible maximum linear velocity is higher, leading to a safer operation.

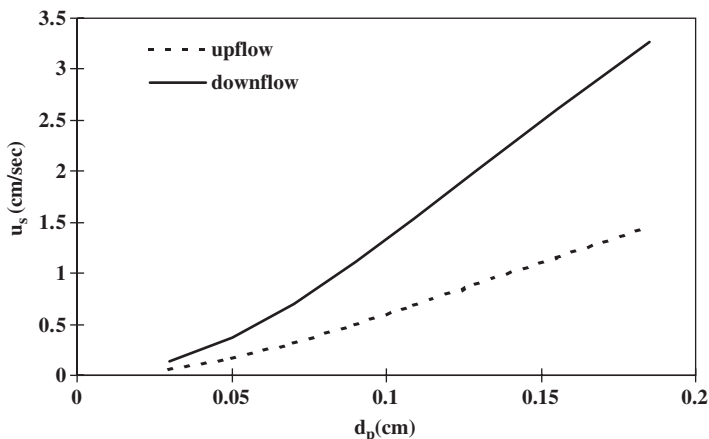


Figure 6.1 The maximum linear velocity versus particle diameter for a fixed-bed operation (water as fluid phase).

Example 4

Consider a solid of 1 mm particle size. Assume that the adsorption will operate at a high contact time, for example, 0.2 h (5 BV/h relative flow rate). The maximum linear velocity for this particle size is approximately 0.5 cm/s for upflow and 1.5 cm/s for downflow operation. For a laboratory bed of 100 cm height and for the specified contact time, the linear velocity is about 0.13 cm/s. Then, it is safe to work under upflow conditions. However, for a large fixed bed of 1000 cm height and for the same contact time, the velocity would be about 1.3 cm/s. Consequently, it is not possible to work under upflow conditions, and downflow is highly recommended. It is obvious that the particle size should be chosen taking into account the kinetics and the hydraulics of both beds (laboratory and full scale). Apart from the velocity limitations of using small particle sizes, another problem could be the increased pressure drop, which in turn could result in the flooding of the bed in the downflow operation.

Using this maximum working velocity and the contact time, the maximum bed height can be determined as follows:

$$Q_{FS} = Q_{rel} V_{FS} \Rightarrow u_{FS} = \frac{Q_{FS}}{A_{FS}} = \frac{Q_{rel} V_{FS}}{A_{FS}} \leq u_{max,FS} \Rightarrow Z_{FS} \leq \frac{u_{max,FS}}{Q_{rel}} \quad (6.12)$$

where:

$$\begin{aligned} Q_{rel} &= \text{the number of bed volumes per hour, } h^{-1} \\ u_{max} &= \text{the maximum allowable linear velocity, m/h} \\ A &= \text{the bed cross-sectional area, } m^2 \end{aligned}$$

At the bottom of the bed, the particles will be not only under the pressure of the other layers of solids but also under the hydraulic pressure of the liquid. Thus, the maximum bed height should be also be determined by using the particle strength data. The following equation could be used for the evaluation of the maximum bed height (Inglezakis, 2002):

$$Z \leq \frac{F_c d_p \rho_b}{g M_p (\rho_b + \varepsilon \rho)} \quad (6.13)$$

where:

$$\begin{aligned} Z &= \text{the bed height} \\ \rho_b &= \text{the bed bulk density} \\ M_p &= \text{the particle weight} \\ F_c &= \text{the maximum force that can be applied to a single particle} \\ &\quad \text{without breaking it (particle strength).} \end{aligned}$$

For example, for clinoptilolite (common zeolite species with particle strength of about 2 Nt) and 1.4–1.7 mm particle size, the maximum bed high is very high, near 50 m. In any case, the lower height derived from the last two equations should be used.

Catalysis

More or less, the comments above concerning the scale-up of the processes of adsorption and ion exchange in fixed beds can be also applied to catalysis. However, there are some points that should be emphasized in catalytic processes.

To begin with, the great difference between the processes mentioned above and catalysis is that high temperatures, even as high as 1200 °C, are often employed in catalysis. So, temperature is a major variable in catalysis, beyond contact time and size of catalytic particles. It dominates the chemical reactions due to its exponential effect (Arrhenius), whereas a specific minimum value of temperature is required for the activation of catalysts. For example, automotive catalysts operate at temperatures above 250 °C. Therefore, the effect of temperature over a wide range has to be thoroughly examined in the laboratory and is essential for the sound evaluation of the reaction model and the accurate estimation of the activation energies. We should also keep in mind that temperature has a dramatic impact on catalytic reactor yield, catalyst selectivity, and product quality. Small variations of temperature can lead to undesirable effects. Consequently, we should also try to determine the response of other critical factors to temperature variation. The knowledge of the temperature effect is also critical for the design and control of reactors, otherwise temperature runaways may take place.

Another issue that needs attention is that in large-scale beds, phenomena absent in the laboratory reactor may develop. For example, in commercial beds, axial gradients of temperature may appear, which are absent in bench beds due to the small diameters usually used in them. In the worst scenario, the controlling mechanism, and thus the whole behavior of the system, could change from the small to the large scale.

The approach followed for scaling-up may be also characterized by inherent weaknesses. Specifically, the application of physical modeling, either using the similarity analysis or by means of dimensionless groups, should be carried out very carefully, and even then it should be properly checked before applied. For example, a similarity analysis may lead to the conclusion that the effectiveness factor of the catalyst in the large unit should be much lower than the one in the bench scale. However, that would be really unproductive from the practical point of view, since the high effectiveness of the catalyst is generally highly desirable. Moreover, geometrical similarity may order the use of larger particles in the large unit, which could result in various problems. First of all, the use of particles as large as the similarity ratio dictates could be from unpractical to unfeasible, since we cannot use huge catalytic particles. Moreover, in laboratory reactors, very small sizes of particles are generally used and as a result the effectiveness factors are very close to 1. On the other hand, the use of larger particles in commercial units could adversely affect the catalyst effectiveness factors, let alone the appearance of intraparticle heat and mass transfer phenomena. Furthermore, we should keep in mind that by varying the size of catalytic particles, we also change what is really important in catalytic systems: the available catalytic surface (internal and external) to the reactants per reactor volume.

Haakana *et al.* (2004) used various mock-up experiments to achieve deep understanding of the different simultaneous phenomena in monolith reactors. However, they pointed out that the results obtained from mock-up experiments might not properly represent the overall reactor performance. This is an inherent limitation of mock-up experiments, where each phenomenon is studied in the absence of the others. However, during the “real” operation

of the reactors, all phenomena take place simultaneously, interacting one another. These interactions cannot be revealed in mock-up experiments. For example, in the specific case, the authors estimated gas–liquid mass transfer parameters in conditions of absence of chemical reaction. However, the overall mass transfer rate could be even higher in the presence of reaction. Moreover, the use of model fluids in mock-up experiments instead of real ones was also a source of inaccuracies. They concluded that the most feasible approach was to combine the detailed knowledge from different mock-up experiments with information from pilot tests including all the relevant phenomena.

Donati and Paludetto (1999) have presented the problems faced during the start-up of the emulsion polymerization of tetrafluoroethylene in a semibatch reactor, regarding monomer purity, initiator addition policy, type and quantity of surfactants, and the temperature and pressure to be operated. No answer could be found for one problem: the failure to reproduce in the pilot plant the productivity and emulsion concentration obtained in the laboratory. Although sophisticated mathematical models had been developed including various phenomena such as initiation, radical propagation and polymer chain termination balances, molecular weight distribution, particle growth, and population balances, the loss in productivity was neither predicted nor expected. Simple experiments illuminated the cause of that deficiency: the effect of stirrer speed on productivity and product quality had not been taken into account. The autoclaves used had no internals and the stirrer had been selected on the basis of suppliers' experience. The study was therefore focused on reactor fluid dynamics and on the selection of stirring devices.

The use of various dimensionless groups for scaling-up can also lead to contradictory results. If two different values for a parameter are estimated by means of two dimensionless groups, then the value that satisfies both phenomena related to these groups should be selected.

To sum up, special attention should be given to the effect of temperature on the process during the design and control of commercial catalytic reactors. Moreover, the same size of catalyst particles should be used at any scale so that the catalyst effectiveness factor also remains the same. The available catalytic surface per reactor volume and the space velocity (when the rate is not controlled by mass transfer phenomena) should also be left unchanged at any scale.

6.2.2 Trickle-bed reactors

The scale-up of trickle beds presents many difficulties mainly due to maldistribution of fluids, which leads to different routes for the liquid and gas, stagnant zones, and hot spots. In trickle-bed reactors, the particle diameter and residence time are the same for all scales. The consequence is that in different scales we have different Reynolds numbers and velocities.

It is highly desirable to run laboratory trickle-bed reactors at a well-defined catalyst wetting state, often complete wetting, while matching the same liquid space hour velocity (LHSV, in h^{-1}) of the large units (Dudukovic *et al.*, 1999). To achieve this, small reactors are operated under upflow conditions where complete catalyst wetting can be obtained at the expense of a much larger liquid holdup than in the large reactor (packed bubble bed reactor). This may be undesirable, if side reactions occur in the liquid phase or if gas–liquid mass transfer is impaired by larger liquid-film resistance in the small unit. To avoid these dissimilarities between the two scales, the voids in the small reactor are filled with inert fines

(Al-Dahhan and Dudukovic, 1996; Dudukovic *et al.*, 1999). This way, more solid–liquid contact points over which the liquid flows are created and the bed porosity is reduced, especially near the reactor wall. Following a proper procedure for packing a trickle bed with catalyst particles and fines decouples the apparent kinetics from hydrodynamics, which is highly desirable. The addition of fines is not the same as reducing the particle size of the catalyst, as in the latter case the particle effectiveness factor is smaller.

Failing to identify the limiting reactant can lead to failure in the scale-up of trickle-bed reactors (Dudukovic, 1999). Gas-limited reactions occur when the gaseous reactant is slightly soluble in the liquid and at moderate operating pressures. For liquid-limited reactions, concurrent upflow is preferred (packed bubble columns) as it provides for complete catalyst wetting and thus enhances the mass transfer from the liquid phase to the catalyst. On the other hand, for gas reactions, concurrent downflow operation (trickle-bed reactors), especially at partially wetted conditions, is preferred as it facilitates the mass transfer from the gas phase to the catalyst. The differences between upflow and downflow conditions disappear by the addition of fines (see Section 3.7.3, Wetting efficiency in trickle-bed reactors).

To conclude, for liquid-limited reactions scale-up can be based on constant LHSV. Thus, the large bed superficial velocity is much higher and the wetting efficiency is increased, which results in a better performance of the large-scale reactor. However, for gas-limited reactions this rule cannot be followed, because it leads to the opposite result as regards the reactor performance. The solution is to keep the same LHSV and constant reactor height, which means that scale-up is based on the same liquid superficial velocity and bed height. This may lead to undesirable “pan-cake” reactor geometry, where the problem is bad liquid distribution.

6.2.3 Fluidized beds

Processes that involve the reaction of gases and solids are extremely difficult to handle mainly due to solid flow difficulties (Knowlton, 2000). The difficulty in the scale-up of these reactors constitutes their main disadvantage. The maximum scale-up factor for fluidized beds is usually between 50 and 100, whereas for fixed beds it could reach the value of 10,000. This is due to the fact that the flow characteristics are very different in the small and the large reactor: the bubble diameter does not change upon scale-up, whereas reactor diameter does.

In addition, changes in the flow rate of the substrate stream in turn cause complex alterations in the flow pattern within these reactors, which may lead to consequent unexpected effects upon the conversion rate. The most useful tool to solve such problems in fluidized beds is the employment of cold-flow models. Thus, it is not surprising that most work in fluidized beds has been focused on the cold model behavior and thus on their hydraulic behavior.

Although the scale-up of fluidized beds has a history of over 50 years in the chemical industry, it is still more of an art than an exact science. Mathematics, history, and intuition are all involved in each new process brought to commercial practice (Matsen, 1996).

The design factors of the scale-up of fluidized beds can be generally classified in two categories:

- *Those that do not depend on the scale of the bed*, such as the bed density and the gas velocity at minimum fluidization.

- *Factors that are affected by the size of the bed*, mainly those that are connected to the bubble behavior. The size of the bubbles has an impact on various physical properties such as the bed density, whereas it also influences the gas–solids contact and reactor performance (Matsen, 1996). For example, in small equipment, the bubbles may have dimensions approaching those of the bed, whereas it is not the case in large beds and a scale-up effect will surely exist.

The operation of fluidized beds is connected to fluid mechanics within the beds (Nicastro and Glicksman, 1984). For example, heat and mass transfer are greatly influenced by the solid and fluid flow patterns, which are in turn affected by the bed geometry and internal configuration. Consequently, a thorough knowledge of fluid dynamics is a prerequisite to the successful design of a commercial unit.

Most of the research on the dynamics of fluidized beds has been conducted in laboratory-scale beds, at low velocities and temperatures, with small particles (Nicastro and Glicksman, 1984). The extrapolation of these results to commercial beds is rather unreliable, particularly when severe conditions of temperature and pressure are employed. Moreover, as already shown, it is highly unlikely that the fluidization characteristics of the large bed will be the same as those in the laboratory unit. Computer simulations are also only as accurate as their input data and empirical correlations. It seems that only pilot or larger-scale plants can provide reliable information that can be extended to commercial units. However, they present high cost of construction and difficulties in handling (Nicastro and Glicksman, 1984).

It is more efficient to conduct properly designed experiments in smaller beds operated at ambient conditions as long as there is a way to apply these results to larger-scale beds at actual operating conditions with accuracy. In many cases, commercial beds operate at elevated temperatures with fluid density and viscosity far from ambient conditions. Under these conditions, laboratory experiments are difficult to conduct and it is preferable to study such systems under ambient conditions, and then extrapolate the results to the actual operating conditions by using appropriate scaling relationships (Glicksman, 1984). This course of action is very attractive, as it exhibits many advantages (Yang *et al.*, 1995):

- easy construction and control
- material problems associated with severe operating conditions can be avoided
- plastic material that provides full visibility of the unit during operation can be used
- detailed measurements of bed behavior can be easily conducted
- less manpower
- low cost.

Scale-up methods

By converting the governing hydrodynamic equations for a particular system into nondimensional ones, Horio *et al.* (1986) and Glicksman (1988) derived the so-called “scaling laws” for fluidized beds. These laws should be seen as a guide to design small-scale, cold-flow models, which simulate the hydrodynamic behavior of the commercial units (Knowlton *et al.*, 2005).

Glicksman's approach The result of the conversion of equations into nondimensional ones is a set of dimensionless parameters (Froude number, velocity, particle size, diameter ratios, etc.) that should be matched in both small and large systems. It is not necessary for the values of the parameters to be equal in each system. Instead, the dimensionless number ratios have to remain the same. To achieve this, the particle size and/or the particle density of the solids have to be changed appropriately in the small unit. It usually results in a smaller particle size in the small unit compared to the large one.

Working with the equations of motion and conservation of mass for both fluid and particles, we have the following nondimensional parameters (Glicksman, 1984):

$$\frac{\rho_h \rho d_p^3 g}{\mu^2}, \frac{u_s^2}{g d_p}, \frac{\rho}{\rho_h}, \frac{Z}{d_p}, \frac{D}{d_p}, \Phi_s, \text{particle size distribution, bed geometry}$$

The first term is a modified Archimedes number, while the second one is the Froude number based on particle size. Alternatively, the first term can be substituted by the Reynolds number. To attain complete similar behavior between a hot bed and a model at ambient conditions, the value of each nondimensional parameter must be the same for the two beds. When all the independent nondimensional parameters are set, the dependent parameters of the bed are fixed. The dependent parameters include the fluid and particle velocities throughout the bed, pressure distribution, voidage distribution of the bed, and the bubble size and distribution (Glicksman, 1984). In the region of low Reynolds number, where viscous forces dominate over inertial forces, the ratio of gas-to-solid density does not need to be matched, except for beds operating near the slugging regime.

Example 5

Consider a fluidized bed operated at an elevated temperature, e.g. 800°C, and under atmospheric pressure with air. The scale model is to be operated with air at ambient temperature and pressure. The fluid density and viscosity will be significantly different for these two conditions, e.g. the gas density of the cold bed is 3.5 times the density of the hot bed. In order to maintain a constant ratio of particle-to-fluid density, the density of the solid particles in the cold bed must be 3.5 times that in the hot bed. As long as the solid density is set, the Archimedes number and the Froude number are used to determine the particle diameter and the superficial velocity of the model, respectively. It is important to note at this point that the rule of similarity requires the two beds to be geometrically similar in construction with identical normalized size distributions and sphericity. It is easy to prove that the length scales (Z , D) of the ambient temperature model are much lower than those in the hot bed. Thus, an ambient bed of modest size can simulate a rather large hot bed under atmospheric pressure.

However, this type of scaling should be avoided in the scale-up of new processes, where the knowledge of issues such as reaction effects and attrition is required. So, the results obtained from tests with different particle sizes and/or particle density cannot be directly applicable to the process (Knowlton *et al.*, 2005).

Interparticle forces appearing in fluidized beds cannot be taken into account using scaling laws, because it is almost impossible to characterize these forces. Moreover, it is usual

to employ small particle sizes in small units, which may result in different types of solids used at the small and the large scale. For example, Group B solids may be used in the large unit, whereas the small bed will operate with Group A solids. It is obvious that the change of the particle size, and therefore of the type of solids, will in turn alter the fluidization behavior in the reactor. To sum up, our effort to achieve dimensional similarity between the small and the large unit may lead to great alterations in particle size and thus different fluidization characteristics in each system (Knowlton *et al.*, 2005).

The same problems may also arise from scaling due to changes in the operating velocity. The latter may cause the existence of different flow regimes in the small and the large unit. So, though the dimensionless groups may be the same, the flow regime may vary significantly between the two scales, being in one bed in the bubbling region and in the other in the turbulent one.

It is clear that the flow regime and the particle Geldart Group should be the same in both sizes of beds, if a successful scale-up is to be performed.

From the above, we can now note that scaling should be applied to modifications of an existing unit rather than to a new one. Assume that a fluidized bed operates with a set of internals that need to be changed. One way to test the new set of internals would be to use the scaling laws to create a small, cold model, which would operate the same as the large, hot unit as regards the hydrodynamics. As long as the fluidizing regime does not change, due to the modification of the particle size in our effort to keep the dimensionless groups constant, this would be a fine application of the scaling laws (Knowlton, 2000; Knowlton *et al.*, 2005).

Horio's approach Horio *et al.* (1986) suggested a similarity rule, which is valid in the viscous limit. The rule states that the hydrodynamic similarity between a base model and a reactor model that is m times larger is obtained when

- (a) The geometrical and topological attributes of the bed, such as the bed diameter D , height Z_f , distributor orifice diameter P_n and orifice pitch d_n , are changed in the same proportion, that is

$$m = \frac{D_L}{D_S} = \frac{Z_{f,L}}{Z_{f,S}} = \frac{d_{\text{bub},L}}{d_{\text{bub},S}} = \frac{P_{n,L}}{P_{n,S}} = \frac{d_{n,L}}{d_{n,S}} \quad (6.14)$$

where the subscript "L" refers to the large scale unit and "S" to the small scale unit.

- (b) The minimum fluidization velocity ratio and the gas superficial velocity ratio in the two scales are equal to the square root of the scale ratio m :

$$\sqrt{m} = \frac{u_{\text{fm},L}}{u_{\text{fm},S}} = \frac{(u_s - u_{\text{fm}})_L}{(u_s - u_{\text{fm}})_S} \quad (6.15)$$

Using these rules and basic hydrodynamic relationships for Ar , u_{fm} , D , u_{bub} , Z_f , and d_{bub} that can be found in Section 3.8.2, Kelkar and Ng (2002) derived the following relationships:

$$\frac{\varepsilon_{s,L}}{\varepsilon_{s,S}} = \frac{\varepsilon_{\text{bub},L}}{\varepsilon_{\text{bub},S}} = 1 \quad (6.16)$$

$$\frac{u_{s,L}}{u_{s,S}} = \frac{u_{\text{bub,L}}}{u_{\text{bub,S}}} = \sqrt{m} \quad (6.17)$$

$$\frac{M_{s,L}}{M_{s,S}} = m^3 \quad (6.18)$$

$$\frac{Q_{g,L}}{Q_{g,S}} = m^{5/2} \quad (6.19)$$

According to Kelkar and Ng (2002), these rules for hydrodynamic similarity have been validated by several studies and thus they are quite reliable. A further step is made by considering the mass transfer coefficient L_{bc} using the following equation:

$$L_{\text{bc}} = 4.5 \frac{u_{\text{fm}}}{d_{\text{bub}}} \varepsilon_{\text{bub}} + 5.25 \frac{D_{\text{g}}^{0.5} g^{0.25}}{d_{\text{bub}}^{5/4}} \varepsilon_{\text{bub}} \quad (6.20)$$

In this equation, the first term represents the convection term and the second the gas diffusion contribution to the mass transfer. Horio *et al.* (1986) defined the ratio of the diffusion term to the convection term (eq. (6.20)):

$$\beta = \frac{D_{\text{g}}^{0.5} g^{0.25}}{u_{\text{fm}} d_{\text{bub}}^{0.25}} \quad (6.21)$$

For $\beta < 0.1$, mass transfer is dominated by convection, whereas for $\beta > 10$, diffusion dominates. Furthermore, using the above similarity rules, it is found that

$$\frac{\beta_{\text{L}}}{\beta_{\text{S}}} = m^{-1/4} \quad (6.22)$$

This proportionality means that the relative importance of diffusion in mass transfer decreases as the reactor size increases.

Finally, the particle diameter should be adjusted using u_{fm} in the large column:

$$Re_{\text{fm,L}} = \frac{(u_{\text{fm,S}} \sqrt{m}) d_{\text{p,L}} \rho}{\mu} = (1136 + 0.0408 Ar_{\text{L}})^{0.5} + 33.7 \quad (6.23)$$

$$Ar_{\text{L}} = \frac{d_{\text{p,L}}^3 \rho (\rho_{\text{h}} - \rho) g}{\mu^2} \quad (6.24)$$

It should be noted that this change in the particle diameter could lead to different diffusion characteristics and alter the effectiveness factor of the catalyst.

After the investigation of hydrodynamics and mass transfer, the next step is the examination of the reactor model. For example, let us consider here the two-phase model with plug flow of gas in both bubble and emulsion phase and first-order reaction (see Section 3.8.3). The first step at this stage is to transform its equations to dimensionless forms.

For simplifying the calculations, we consider that the gas flows only through the bubble phase ($f_b = 1$) and that there are no solids in the bubble phase ($\gamma_b = 0$). Under these conditions, the model of the reactor is (eqs. (3.519) and (3.520))

$$-u_s \frac{dC_b}{dz} - L_{be}(C_b - C_p) = 0 \quad (6.25)$$

$$L_{be}(C_b - C_p) - (1 - \varepsilon_{\text{bub}})(1 - \varepsilon_{\text{fm}})kC_p = 0 \quad (6.26)$$

The dimensionless equations become

$$-\frac{dG}{dZ} - N_m \left(G - \frac{C_{p,o}}{C_{b,o}} E \right) = 0 \quad (6.27)$$

$$N_m \left(\frac{C_{b,o}}{C_{p,o}} G - E \right) - (1 - \varepsilon_{\text{bub}})(1 - \varepsilon_{\text{fm}}) \frac{N_r}{\varepsilon_s} E = 0 \quad (6.28)$$

The dimensionless parameters are given in eqs (6.31) to (6.35). Solving eq. (6.28) for E ,

$$E = \frac{N_m G}{N_m + N_r} \frac{C_{b,o}}{C_{p,o}} \quad (6.29)$$

Substituting into eq. (6.27),

$$-\frac{dG}{dZ} + \left(\frac{-N_m N_r}{N_m + N_r} \right) G = 0 \quad (6.30)$$

where

$$Z = \frac{z}{Z_f} \quad (6.31)$$

$$G = \frac{C_b}{C_{b,i}} \quad (6.32)$$

$$E = \frac{C_p}{C_{p,i}} \quad (6.33)$$

$$N_m = \frac{L_{be} Z_f}{u_s} \quad (6.34)$$

$$N_r = \frac{k_{vs} \varepsilon_s Z_f}{u_s} \quad (6.35)$$

If all the dimensionless parameters in a reaction model are kept constant with scale change, a similarity in the reactor performance is expected, provided that the basic assumptions of the model remain unchanged in both scales, e.g. in our example the plug flow condition of gas in the bubble phase.

Scale-up methodology following hydrodynamic similarity: Following hydrodynamic similarity (eqs. (6.14)–(6.22)) and applying its equations to our system, the following additional similarity rules are derived:

$$\frac{N_{r,L}}{N_{r,S}} = \frac{m}{\sqrt{m}} = \sqrt{m} \quad (6.36)$$

For $\beta < 0.1$,

$$k_{\text{bub}} \cong 4.5 \frac{u_{\text{fm}}}{d_{\text{bub}}} \varepsilon_{\text{bub}} \quad (6.37)$$

Then

$$\frac{N_{m,L}}{N_{m,S}} = 1 \quad (6.38)$$

For $\beta > 10$,

$$k_{\text{bub}} \cong 5.25 \frac{D_g^{0.5} g^{0.25}}{d_{\text{bub}}^{5/4}} \varepsilon_{\text{bub}} \quad (6.39)$$

Then

$$\frac{N_{m,L}}{N_{m,S}} = m^{-3/4} \quad (6.40)$$

Scale-up methodology following the dimensionless reactor model: Instead of using the dimensionless numbers of the model or the hydrodynamic rules, we can use the reactor model or its performance index.

Reactor model (eq. (6.30)):

$$-\frac{dG}{dZ} + \left(\frac{-N_m N_r}{N_m + N_r} \right) G = 0 \quad (6.41)$$

Performance index (conversion—solution of eq. (6.30)):

$$x = 1 - \exp\left(-\frac{N_m N_r}{N_m + N_r} \right) \quad (6.42)$$

For achieving similarity during scaling, the following should hold:

$$\left(-\frac{N_m N_r}{N_m + N_r} \right)_L = \left(-\frac{N_m N_r}{N_m + N_r} \right)_S \quad (6.43)$$

where the subscripts L and S denote large and small unit parameters, respectively.

If we follow the similarity rule for N_r , we have to formulate a similarity rule for N_m in order to achieve the target set in eq. (6.43). After some calculations, we have

$$\omega = \frac{N_{m,L}}{N_{m,S}} = \frac{\sqrt{m}}{\sqrt{m} + (N_m/N_r)_S(\sqrt{m} - 1)} \quad (6.44)$$

This is the required variation in N_m to have the same conversion in both scales.

It is obvious that following hydrodynamic similarity eq. (6.40), the mass transfer mode is different between the two scales due to the change in the respective dimensionless parameters, and as a result the conversion will be also different:

For $\beta < 0.1$,

$$x = 1 - \exp\left(-\frac{N_{m,S} \sqrt{m} N_{r,S}}{N_{m,S} + \sqrt{m} N_{r,S}} \right) \quad (6.45)$$

For $\beta > 10$,

$$x = 1 - \exp\left(-\frac{m^{-3/4} N_{m,S} \sqrt{m} N_{r,S}}{m^{-3/4} + \sqrt{m} N_{r,S}} \right) \quad (6.46)$$

where the conversion in the small reactor will be higher:

$$x = 1 - \exp\left(-\frac{N_{m,S} N_{r,S}}{N_{m,S} + N_{r,S}} \right) \quad (6.47)$$

Thus, it is clear that hydrodynamic similarity does not lead to actual similarity between the two scales concerning the conversion. So, the large reactor should be designed following some hydraulic similarity rules, for example, the rule for N_r , and then similarity rules derived from the reactor model. In our example, N_m in the large reactor should follow rule (6.44), and therefore $N_{m,L}$ should be adjusted controlling the value of d_{bub} (Kelkar and Ng, 2002). This is possible by employing internals, baffles, or different distributor design.

6.2.4 Slurry bubble bed column reactors

It has been shown that the two-phase model for bubbling gas–solid fluidized beds can be extended to slurry bubble column reactors operating in the heterogeneous flow regime (Krishna *et al.*, 1998). Two phases are identified: the large fast-rising bubbles (dilute phase) and the slurry phase in which small bubbles are finely dispersed (dense phase). The dilute phase is equivalent to the bubble phase and the dense phase to the emulsion phase in the fluidized beds. According to this analysis, the scale effects for fluidized beds and slurry columns are analogous.

6.2.5 Agitated vessels

Scale-up involves selecting mixing variables to achieve the desired performance in both pilot and full scale. This is often a difficult task, sometimes even impossible, using geometric similarity, so that the use of nongeometric impellers in the pilot plant compared to the impellers used in the industrial plant often allows closer modeling of the mixing requirements to be achieved (Perry and Green, 1999).

For mixing operations, the scale-up criterion is customarily given as an overall equation (Montane *et al.*, 2003):

$$ND_a^n = \text{const.} \quad (6.48)$$

where N is the rotational speed and D_a the diameter of the impeller. The exponent (n) depends on the specific characteristics of the process. In agitated slurry reactors, this type of scale-up criterion is often derived from studies concerning the minimum rotational speed for the complete suspension of solids. The same type of scale-up criterion is derived by studying the solids distribution quality. Buurnam *et al.* (1986) described the quality of the solids distribution in terms of the height of the homogeneous zone above the suspension. The values of n derived from various studies on the solids distribution quality are within 0.67 (single pitched-blade turbine) and 0.93 (multiple pitched-blade turbines and multiple Rushton turbines) (Montane *et al.*, 2003).

In the design of liquid mixing systems, the following dimensionless groups are of importance (Holland, 1962):

- the Reynolds number, $\rho ND_a^2/\mu$, which represents the ratio of applied to viscous drag forces,

- the Froude number, $N^2 D_a / g$, which represents the ratio of applied to gravitational forces,
- the Weber number, $\rho N^2 D_a^2 / \sigma$, which represents the ratio of applied to surface tension forces.

Here, D_a is the impeller diameter and N the revolutions per unit time.

The Reynolds, Froude, and Weber numbers are proportional to ND_a^2 , $N^2 D_a$, and $N^2 D_a^2$, respectively. It is obvious that if one of these groups is used for scale-up, the scale-up rules represented by the other groups are automatically violated, provided that the physical properties of the fluid remain the same. The groups could, of course, be made compatible by using fluids having different physical properties on the large and small scales.

In liquid systems, we can suppress the effect of the Froude number by using baffles to eliminate vortexing and hence the gravitational effects. The Weber number is of some importance only when separate physical phases are present in the liquid mixing system.

The general equation for fluid motion in a mixing system contains no less than 13 terms. Of these terms, nine define geometric boundary conditions. If these can be fixed, and strict geometric similarity be adhered to, the equation can be simplified and written as

$$N_p = CRe^m Fr^n \quad (6.49)$$

where N_p is the power number. When the effect of the Froude number is negligible, the power number is a function of only Re and the shape factor C . The great majority of mixing operations can be handled by this equation. It should be stressed out that a power number versus Reynolds number curve for a particular system holds true irrespective of the size of the vessel. The curve depends only on the geometrical configuration. This is the reason why experiments on very small models can be used to determine the power characteristics of large-scale plant mixing systems.

Generally, the suspension of solids in large-scale vessels is maintained by lower stirrer speeds compared to small vessels, if the geometrical similarity is applied. Large differences may also appear in connection with the power requirement between the small and the large scale, because the power per unit volume P_s varies with $N^3 D_a^2$ according to Zwietering's equation (McCabe *et al.*, 1983).

If satisfactory solids suspension is obtained in a small tank, whether judged by visual observations, particle velocities, or mass transfer rates, the safe scale-up rule is to keep geometrical similarity and constant power per unit volume. The ratios $D_a/D_T = 1/3$ and $Z_a/D_T = 0.25$ are often recommended, though some prefer $D_a/D_T = 0.4$ for solids suspension. The critical speed may be reduced by decreasing the clearance, but it may be hard to start the stirrer if it is in a layer of solids very close to the bottom (McCabe *et al.*, 1983). Reynolds numbers in large tanks will be higher, typically of the order of 5 to 25 times higher than those in small tanks. For a specific power input, much attention has to be given to the ratio of the impeller diameter-to-vessel during scale-up. This ratio depends to a great extent on the nature of agitation, as its optimum value is

- 0.25 for dispersing a gas into a liquid
- 0.40 for the contact of two immiscible fluids
- 0.6 or more for some blending operations.

Keeping the power input stable in a specific operation, the impeller speed is inversely proportional to the impeller size. This means that the smaller the impeller, the higher the impeller speed. In general, operations that depend on large velocity gradients rather than on high circulation rates are best accomplished by small, high-speed impellers, whereas large, slow-moving impellers should be preferably used for operations that depend on high circulation rates (McCabe *et al.*, 1983).

Although the scale-up of agitated vessels is mainly based on geometrical similarity, there are various cases where this target is difficult to achieve. Furthermore, the application of geometrical similarity does not ensure the similarity of dynamic and kinematic phenomena. Experience and intuition have to be employed in the scale-up procedure (McCabe *et al.*, 1983).

Appendix I

Physical Properties of Water, Air and Selected Compounds

I.1 BULK-PHASE PROPERTIES OF SOLVENTS AND CARRIER GASES

I.1.1 Water

Water is the most common solvent of environmental importance and therefore its properties are presented in the following paragraphs.

The dynamic viscosity of water can be calculated using the following equation (Reid *et al.*, 1988):

$$\ln(\mu_w) = -24.71 + \frac{4209}{T} + 4.527 \times 10^{-2} T - 3.376 \times 10^{-5} T^2 \quad (\text{I.1})$$

The same equation can be safely used for dilute aqueous solutions. Another useful relationship is the following (Reid *et al.*, 1988):

$$\mu_w(T_2)^{-0.2661} = \mu_w(T_1)^{-0.2661} + \frac{T_2 - T_1}{233} \quad (\text{I.2})$$

where temperature is in K and viscosity in cP.

The density of water can be evaluated using the following equation:

$$\rho_w = 0.3471 \times 0.274 \left(1 - \frac{T}{647.3}\right)^{2/7} \quad (\text{I.3})$$

where temperature is in K and density in g/cm³. The same equation can be also used for dilute aqueous solutions.

In relation with the surface tension of water, the following correlation is available (IAPWS, 1994):

$$\sigma_w = 235.8 \tau^{1.256} (1 - 0.625\tau) \quad (I.4)$$

$$\tau = 1 - T_R \quad (I.5)$$

$$T_R = \frac{T}{T_C} \quad (I.6)$$

where σ_w is in mN/m = dyn/cm and T_C is the critical temperature of the water (647.096 K). This equation is valid between the triple point 0.01 °C and the critical temperature, T_C .

The basic thermophysical properties of water in the region of 290–355 K (17–82 °C) are given in Table I.1.

I.1.2 Gases

Air is the most common carrier gas in environmental applications, whereas nitrogen and helium are frequently used in laboratory experiments. Furthermore, oxygen in oxidations and hydrogen in hydrogenations are often used as reactants. Consequently, the most important properties of these gases among others are presented hereinafter.

Dynamic viscosity

The dynamic viscosity of the selected gases at atmospheric pressure and temperature range 298–623 K are given in Table I.2.

Generally, at low pressures, the correlation of Chung *et al.* is proposed (Reid *et al.*, 1988; Chung *et al.*, 1984):

$$\mu = 40.785 \frac{\theta(MB \times T)^{0.5}}{V_C^{2/3} \Omega} \quad (I.7)$$

Table I.1

Thermophysical properties of saturated water (Lide, 1991; IAPWS, 1994; Incropera and DeWitt, 1990)

T (K)	σ (mN/m)	μ (10^{-6} Pa s)	ρ (kg/m ³)	c_p (kJ/kg K)	λ_f (10^{-3} W/m K)
290	73.7	959	0.999	4.184	598
300	71.7	855	0.997	4.179	613
315	69.2	631	0.991	4.179	634
325	67.5	528	0.987	4.182	645
335	65.8	453	0.982	4.186	656
345	64.1	389	0.977	4.191	668
355	62.3	343	0.971	4.199	671

Table I.2

Dynamic viscosity for various gases at atmospheric pressure and temperature range 298–623 K
(10^{-5} Pa s)

Gas	298 K	373 K	473 K	523 K	573 K	623 K
Air	1.85	2.18	2.58	2.76	2.94	3.10
Nitrogen	1.77	2.1	2.49	2.67	2.85	3.02
Helium	1.99	2.32	2.73	2.93	3.13	3.31
Oxygen	2.06	2.46	2.94	3.16	3.38	3.58
Hydrogen	0.89	1.04	1.22	1.31	1.40	1.48

where the dynamic viscosity is in μP , temperature in K, critical volume in cm^3/mol and

$$\Omega = A \left(F \frac{T}{T_C} \right)^{-B} + C \exp \left[-D \left(F \frac{T}{T_C} \right) \right] + E \exp \left[-G \left(F \frac{T}{T_C} \right) \right] \quad (\text{I.8})$$

$$\theta = 1 - 0.2756\omega + 0.05935m_r^4 + \kappa \quad (\text{I.9})$$

for

$$0.3 \leq F \frac{T}{T_C} \leq 100 \quad (\text{I.10})$$

where $A = 1.16145$, $B = 0.14874$, $C = 0.52487$, $D = 0.77320$, $E = 2.16178$, $G = 2.43787$, $F = 1.2593$, ω is the acentric factor, and m_r the dimensionless dipole moment:

$$m_r = 131.3 \frac{m}{(V_C T_C)^{0.5}} \quad (\text{I.11})$$

where m is the dipole moment in debyes. For air, nitrogen, helium, oxygen, and hydrogen the dipole moment is zero. The parameter κ is a special correction factor for highly polar substances such as alcohols (0.1–0.2), acetic acid (0.09), and water (0.076). For other gases, such as sulfsulfur dioxide, it can be taken equal to zero.

For nonpolar gases at high pressures, the correlation of Jossi *et al.* is preferably used for reduced density between 0.1 and 3 (Jossi *et al.*, 1962; Reid *et al.*, 1988; Perry and Green, 1999):

$$\left[(\mu - \mu^\circ) B \times 10^7 + 1 \right]^{1/4} = 1.023 + 0.023364\rho_r + 0.58533\rho_r^2 - 0.40758\rho_r^3 + 0.093324\rho_r^4 \quad (\text{I.12})$$

where viscosity is in Pa s, μ^0 is the viscosity at low pressure, and ρ_r the reduced density of the gas:

$$\rho_r = \frac{\rho}{\rho_C} = \frac{\rho V_C}{MB} \quad (\text{I.13})$$

Here, the density ρ is evaluated under the actual conditions. The critical molar volume of some important gases is given in Table I.3.

Finally, the parameter B is given by

$$B = \frac{2173.42T_C^{1/6}}{MB^{1/2}P_C^{2/3}} \quad (\text{I.14})$$

The properties under critical conditions (P_C , T_C) for some important gases are given in Table I.4.

Density

The density of gases for temperatures above the critical temperature T_C and pressure of few atmospheres can be evaluated by the ideal gas law (Perry and Green, 1999):

$$\rho = MB \frac{P}{RT} \quad (\text{I.15})$$

Table I.3

Critical molar volume of various gases

Gas	V_C (m ³ /kmol)
Air	0.0925
Nitrogen	0.0892
Helium	0.0573
Oxygen	0.0734
Hydrogen	0.0641

Table I.4

Critical pressure and temperature for several gases

Gas	T_C (K)	P_C (10 ⁷ Pa)
Air	132.5	0.377
Nitrogen	126.2	0.340
Helium	5.2	0.023
Oxygen	154.6	0.504
Hydrogen	33.2	0.131

Practically, in environmental applications, the temperature ranges from 20 to 400 °C and pressure from 1 to 40 atm. According to available data (Perry and Green, 1999) for air, nitrogen, oxygen, and hydrogen, the compressibility factor is practically unity and only in severe conditions of pressure and temperature varies from 0.98 to 1.02. Thus, the ideal gas law can be safely used in most environmental applications.

For pressures corresponding to a reduced pressure P_r up to 0.2 and nonpolar gases, Pitzer's correlation can be used (Perry and Green, 1999):

$$\rho = MB \frac{P}{Z_f RT} \quad (\text{I.16})$$

where Z_f is the compressibility factor and can be evaluated by using the following formula (Perry and Green, 1999):

$$Z_f = 1 + \frac{P_r}{T_r} \left(A - \frac{B}{T_r} - \frac{C}{T_r^2} - \frac{D}{T_r^3} - \frac{E}{T_r^8} \right) \quad (\text{I.17})$$

where the reduced temperature and pressure are

$$T_r = \frac{T}{T_C} \quad (\text{I.18})$$

and

$$P_r = \frac{P}{P_C} \quad (\text{I.19})$$

where T_C and P_C are the critical temperature in K and critical pressure in Pa, respectively. The constants of the correlation are

$$A = 0.1445 + 0.073\omega \quad (\text{I.20})$$

$$B = 0.330 - 0.46\omega \quad (\text{I.21})$$

$$C = 0.1385 + 0.50\omega \quad (\text{I.22})$$

$$D = 0.0121 + 0.097\omega \quad (\text{I.23})$$

where ω is the acentric factor of the gas. The properties needed for the estimation of gas density are given in Table I.5.

Basic thermophysical properties of selected gases

The basic thermophysical properties of selected gases at 1 atm is shown in Table I.6.

Gas constant units

The value of the gas constant relies on the units used, as shown in Table I.7.

Table I.5

Properties of various gases for the estimation of density

Gas	MB	ω	P (atm) for $P_r = 0.2$
Air	28.95	0.00739	7.54
Nitrogen	28.01	0.0377	6.80
Helium	4	-0.39	0.46
Oxygen	32	0.0222	10.08
Hydrogen	2.02	-0.215	2.62

Table I.6

Basic thermophysical properties of selected gases at 1 atm (Incropera and DeWitt, 1990)

Temperature (K)	ρ (kg/m ³)	c_p (kJ/kg K)	λ_f (10 ⁻³ W/m K)
<i>Air</i>			
300	1.1614	1.007	26.3
350	0.9950	1.009	30.0
400	0.8711	1.014	33.8
450	0.7740	1.021	37.3
500	0.6964	1.030	40.7
550	0.6329	1.040	43.9
600	0.5804	1.051	46.9
650	0.5356	1.063	49.7
700	0.4975	1.075	52.4
750	0.4643	1.087	54.9
800	0.4354	1.099	57.3
<i>Helium</i>			
300	0.1625	5.193	152
350	—	5.193	170
400	0.1219	5.193	187
450	—	5.193	204
500	0.09754	5.193	220
550	—	5.193	—
600	—	5.193	252
650	—	5.193	264
700	0.06969	5.193	278
750	—	5.193	291
800	—	5.193	304

(Continued)

Table I.6 (Continued)

Temperature (K)	ρ (kg/m ³)	c_p (kJ/kg K)	λ_f (10 ⁻³ W/m K)
<i>Hydrogen</i>			
300	0.8078	14.31	183
350	0.06924	14.43	204
400	0.06059	14.48	226
450	0.05386	14.50	247
500	0.04848	14.52	266
550	0.04407	14.53	285
600	0.04040	14.55	305
700	0.03463	14.61	342
800	0.03030	14.70	378
<i>Nitrogen</i>			
300	1.1233	1.041	25.9
350	0.9625	1.042	29.3
400	0.8425	1.045	32.7
450	0.7485	1.050	35.8
500	0.6739	1.056	38.9
550	0.6124	1.065	41.7
600	0.5615	1.075	44.6
700	0.4812	1.098	49.9
800	0.4211	1.220	54.8
<i>Oxygen</i>			
300	1.284	0.920	26.8
350	1.100	0.929	29.6
400	0.9620	0.942	33.0
450	0.8554	0.956	36.3
500	0.7698	0.972	41.2
550	0.6998	0.988	44.1
600	0.6414	1.003	47.3
700	0.5498	1.031	52.8
800	0.4810	1.054	58.9

Table I.7

Units of gas constant	
Units	Value
$\frac{\text{L atm}}{\text{mol K}}$	0.082
$\frac{\text{m}^3 \text{ atm}}{\text{kmol K}}$	0.082
$\frac{\text{cal}}{\text{mol K}}$	1.987
$\frac{\text{J}}{\text{mol K}}$	8.314

(Continued)

Table I.7 (Continued)

Units	Value
$\frac{\text{m}^3\text{Pa}}{\text{mol K}}$	8.314
$\frac{\text{cm}^3 \text{ atm}}{\text{mol K}}$	82.057
$\frac{\text{Btu}}{\text{lbmol}^\circ\text{R}}$	1.9858
$\frac{\text{kWh}}{\text{lbmol}^\circ\text{R}}$	5.98×10^{-4}
$\frac{\text{ft-lb}_f}{\text{lbmol}^\circ\text{R}}$	1545.3

Note: °R; Degrees Rankine.

I.2 DIFFUSION COEFFICIENTS IN WATER AND GASES

I.2.1 Diffusion coefficient of salts (electrolytes) in aqueous solutions

For dilute solutions of a single salt completely dissociated, the diffusion coefficient is given by the Nernst–Haskell equation (Gambill, 1958; Reid *et al.*, 1988)

$$D_w = \frac{R_g T \left(\frac{1}{n_+} + \frac{1}{n_-} \right)}{F^2 \left(\frac{1}{\lambda_+} + \frac{1}{\lambda_-} \right)} \quad (\text{I.24})$$

where D_w is the liquid-phase diffusion coefficient at infinite dilution in cm^2/s , λ_i the limiting ionic conductances (ionic mobility) in $(\text{A}/\text{cm}^2)(\text{V}/\text{cm})(\text{greq}/\text{cm}^3)$, n_i the valence of the ion, (+) for cation and (–) for anion (absolute values), R_g the ideal gas constant (8.314 J/mol K), T the absolute temperature in K, and F the Faraday constant (96,500 Cb/greq). For ionic mobility, the following equation could be used (Reid *et al.*, 1988):

$$\lambda_i(T_2) = \lambda_i(T_1) \frac{T_2}{334\mu} \quad (\text{I.25})$$

where μ is the dynamic viscosity of the liquid in cP for temperature of T_2 (K).

Values of ionic mobility for various ions in water are shown in Table I.8. For the estimation of the diffusion coefficient of a *single ion* the second term in the right-hand part of the eq. (I.24) is replaced by λ_i/n_i .

Table I.8Ionic mobility in water at 25 °C (Gambill, 1958; Reid *et al.*, 1988)

Ion	Mobility (A/cm ²)(V/cm)(greq/cm ³)
H ⁺	349.8
Li ⁺	38.7
Na ⁺	50.1
K ⁺	73.5
Cs ⁺	73 (18 °C)
NH ₄ ⁺	73.4
½ Mg ²⁺	53.06
½ Mn ²⁺	47.2 (18 °C)
½ Ca ²⁺	59.5
½ Sr ²⁺	59.46
½ Co ²⁺	46.2 (18 °C)
½ Cu ²⁺	53.6
½ Hg ²⁺	63.6
½ Cd ²⁺	54
½ Pb ²⁺	70
½ Ni ²⁺	54
½ Fe ²⁺	48.3 (18 °C)
1/3 Fe ³⁺	65.5 (18 °C)
1/3 Cr ³⁺	48.4 (18 °C)
½ SO ₄ ²⁻	80
½ C ₂ O ₄ ²⁻	67.6 (18 °C)
½ CO ₃ ²⁻	64.5 (18 °C)
OH ⁻	199.18
NO ₃ ⁻	71.44
Br ⁻	72.7 (18 °C)
Cl ⁻	76.34

I.2.2 Diffusion coefficient of other solutes in aqueous solutions

For the determination of diffusion coefficient of solutes (except from salts and ions) in water and dilute solutions (<10%) the Hayduk and Laudie equation is used (Lyman *et al.*, 1990; Perry and Green, 1999):

$$D_w = \frac{8.621 \times 10^{-14}}{\mu_w^{1.14} V_{GB}^{0.589}} \quad (\text{I.26})$$

where D_w is the diffusion coefficient in m²/s, μ_w the viscosity of liquid in Pa s (cP, correlated for temperature), and V_{GB} the molar volume of the gas at the normal boiling point in m³/kmol. The latter can be evaluated by the Tyn and Calus equation (Perry and Green, 1984, 1999)

$$V_{GB} = 0.285 V_C^{1.048} \quad (\text{I.27})$$

where V_C is the molar volume of the gas under critical conditions (both volumes in cm^3/mol). In Table I.9, the critical molar volumes of the some gases of great environmental interest are given.

In the case that the diffusion coefficient is known at a given temperature (commonly at 20°C) the following equation can be used (Pavlov *et al.*, 1979):

$$D_w(T) = D_w(20^\circ\text{C})[1 + 0.02(T - 20)] \quad (\text{I.28})$$

Table I.9

Critical molar volume of gases (Smith, 1981)

Gas	V_C (cm^3/mol) ^a
Air	86.6
Nitrogen monoxide	57
Nitrous oxide	96.3
Carbon dioxide	94
Carbon monoxide	93.1
Sulfur dioxide	122
Hydrogen	65
Hydrogen peroxide	77.7
Nitrogen	90.1
Oxygen	74.4
Methane	99.3
C_6H_6	260
CH_3Cl	143
CHCl_3	240
CCl_4	276

^a To convert into m^3/kmol multiply values by 10^{-3} .

Table I.10

Diffusion coefficient of inorganic gases in water at 20°C (Pavlov *et al.*, 1979)

Gas	D_w ($10^{-9} \text{ m}^2/\text{s}$) ^a
Ammonia	1.8
Nitrous oxide	1.8
Carbon dioxide	1.8
Sulfur dioxide	1.7
Hydrogen sulfide	1.6
Hydrogen	5.3
Nitrogen	1.9
Oxygen	2.1

^a To convert into cm^2/s multiply values by 10^4 .

Table I.11

Diffusion coefficient of organic gases in water at 25 °C

Gas	D_w (10^{-6} cm ² /s) ^a
Benzene	9.8
Carbon tetrachloride	8.8
Chlorobenzene	8.7
2-Chlorophenol	9.46
DDD	4.76
DDE	5.87
DDT	4.95
1,2-Dichlorobenzene	7.9
1,4-Dichlorobenzene	7.9
3,3-Dichlorobenzidine	6.74
2,4-Dimethylphenol	8.69
2,4-Dinitrophenol	9.06
2,4-Dinitrotoluene	7.06
2,6-Dinitrotoluene	7.26
Ethylbenzene	7.80
Hexachlorobenzene	5.91
Hexachloroethane	6.8
2-Methylphenol	8.3
Nitrobenzene	8.6
Pentachlorophenol	6.1
Phenol	9.1
Toluene	8.6
1,2,4-Trichlorobenzene	8.23
Trichloroethylene	9.1
2,4,5-Trichlorophenol	7.03
2,4,6-Trichlorophenol	6.25
<i>m</i> -Xylene	7.8
<i>o</i> -Xylene	10
<i>p</i> -Xylene	8.44
Vinyl chloride	13.4

^a To convert into m²/s multiply values by 10⁻⁴.

where temperature is in °C. The diffusion coefficients of some inorganic and organic gases of environmental importance in water are given in Tables I.10 and I.11, respectively.

I.2.3 Diffusion coefficient of gases in binary gaseous mixtures

The Fuller–Schettler–Giddings equation is proposed for the determination of the diffusion coefficient of gases in binary mixtures at low pressure (Lyman *et al.*, 1990; Perry and Green, 1984, 1999):

$$D_{BA} = 0.01 \frac{T^{1.75} M_R^{0.5}}{P(V_A^{1/3} + V_B^{1/3})^2} \quad (\text{I.29})$$

where D_{BA} is the diffusion coefficient of a gas B in a gas A in m^2/s , T the temperature in K, P the pressure in Pa, and V_A and V_B the diffusion volumes of gases in cm^3/mol , and M_R is

$$M_R = \frac{1}{MB_A} + \frac{1}{MB_B} \quad (\text{I.30})$$

where MB_A and MB_B are the molecular weights of the gases. The diffusion volumes of molecules can be calculated by adding the volume increments of the individual atoms:

$$V_i = \sum_i u_i \quad (\text{I.31})$$

In Tables I.12 and I.13, the diffusion volumes of some molecules and the volume increments of atoms are given (Perry and Green, 1984, 1999).

Table I.12

Diffusion volumes of various molecules

Gas	V_i (cm^3/mol)
Hydrogen	7.07
Helium	2.88
Nitrogen	17.9
Oxygen	16.6
Air	20.1
Carbon monoxide	18.9
Carbon dioxide	26.9
Nitrous oxide	35.9
Ammonia	14.9
Water	12.7
Sulfur dioxide	41.1

Table I.13

Volume increments of atoms and structures

Atom or structure	u_i (cm^3/mol)
Carbon	16.5
Hydrogen	1.98
Oxygen	5.48
Nitrogen	5.69
Chloride	19.5
Sulfur	17
Aromatic ring	-20.2
Heterocyclic ring	-20.2

In the case that the diffusion coefficient is known at a given temperature (commonly at 20 °C) the following equation can be used (Pavlov *et al.*, 1979):

$$D_a(T) = D_a(25\text{ }^\circ\text{C})P^{-1}\left(\frac{T}{298}\right)^{3/2} \quad (\text{I.32})$$

where temperature is in K and the pressure in atm. The diffusion coefficients of some inorganic and organic gases of environmental importance in air under atmospheric pressure are presented in Tables I.14 and I.15, respectively.

Table I.14

Diffusion coefficients of inorganic gases in air at 20 °C
(Pavlov *et al.*, 1979)

Gas	D_a (10^{-5} m ² /s) ^a
Ammonia	1.70
Hydrogen	6.11
Sulfur trioxide	0.94
Carbon dioxide	1.38
Carbon disulfide	0.89
Sulfur dioxide	1.03
Nitrogen	1.32
Oxygen	1.78

^a To convert into cm²/s multiply by 10⁴.

Table I.15

Diffusion coefficient of organic gases in air at 25 °C

Gas	D_a (10^{-2} cm ² /s) ^a
Benzene	8.8
Carbon tetrachloride	7.8
Chlorobenzene	7.3
2-Chlorophenol	5.01
DDD	1.69
DDE	1.44
DDT	1.37
1,2-Dichlorobenzene	6.9
1,4-Dichlorobenzene	6.9
3,3-Dichlorobenzidine	1.94
2,4-Dimethylphenol	5.84
2,4-Dinitrophenol	2.73
2,4-Dinitrotoluene	20.3
2,6-Dinitrotoluene	3.27
Ethylbenzene	7.50

(Continued)

Table I.15 (Continued)

Gas	D_a (10^{-2} cm ² /s) ^a
Hexachlorobenzene	5.42
Hexachloroethane	0.25
2-Methylphenol	7.4
Nitrobenzene	7.6
Pentachlorophenol	5.6
Phenol	8.2
Toluene	8.7
1,2,4-Trichlorobenzene	3
Trichloroethylene	7.9
2,4,5-Trichlorophenol	2.91
2,4,6-Trichlorophenol	3.18
<i>m</i> -Xylene	7
<i>o</i> -Xylene	8.7
<i>p</i> -Xylene	7.69

^a To convert into m²/s multiply by 10⁻⁴.

I.3 SOLUBILITY OF GASES IN LIQUIDS—HENRY'S CONSTANT

I.3.1 General

The solubility C_L of a gas in a liquid can be calculated via Henry's constant, which is defined through the following equations:

$$C_G = HC_L \quad (\text{I.33})$$

or

$$P_{\text{partial}} = H^{\circ}C_L \quad (\text{I.34})$$

Following these equations, the units of Henry's constant are

$$H \frac{(\text{mol/cm}^3)_{\text{gas}}}{(\text{mol/cm}^3)_{\text{liquid}}} \quad \text{or} \quad H^{\circ} \left(\frac{\text{atm cm}^3}{\text{mol}} \right)$$

Frequently, H is referred to as the dimensionless Henry's constant. To convert from one unit into the other:

$$H = \frac{H^{\circ}}{RT} \quad (\text{I.35})$$

The value of R is 82.057 (atm cm³/mol K).

Another common unit used is that of H^f (MPa mol/mol) :

$$H^o = H^f 10 \left(\frac{\text{atm}}{\text{MPa}} \right) \frac{\text{MB}(\text{g/mol})}{\rho_L(\text{g/cm}^3)} \quad (\text{I.36})$$

where the liquid density should be estimated for the given temperature.

Generally, attention should be given to the units of the Henry’s constant found in literature.

I.3.2 Henry’s constant of gases in water

The following correlation for the estimation of Henry’s constant is available (IAPWS, 2004):

$$\ln \left(\frac{H^f}{p_V} \right) = \frac{A}{T_R} + \frac{B\tau^{0.355}}{T_R} + CT_R^{-0.41} \exp(\tau) \quad (\text{I.37})$$

$$\tau = 1 - T_R \quad (\text{I.38})$$

$$T_R = \frac{T}{T_C} \quad (\text{I.39})$$

where H^f is Henry’s constant in (MPa mol)/mol, T_C the critical temperature of the solvent (647.096 K for water), p_V the vapor pressure of the solvent at the temperature of interest, and A , B , and C the characteristic constants of dissolved gases (Table I.17). The vapor pressure can be calculated from the following equation (IAPWS, 2004):

$$\ln \left(\frac{p_V}{P_C} \right) = \frac{1}{T_R} \sum_{i=1}^n a_i \tau^{b_i} \quad (\text{I.40})$$

where P_C is the critical pressure of the solvent (22.064 MPa for water) and n , a_i , and b_i are characteristic constants of the solvent ($n = 6$ for water, see Table I.16).

Using the tabulation of Perry and Green (1999), the following equation can be obtained for Henry’s constant for air in the temperature range 5–90 °C and water as solvent:

$$H^f = 10^3 (-0.0008T^2 + 0.1474T + 4.0738) \quad (\text{I.41})$$

where T is the temperature in °C. Henry’s constant is slightly dependent on the partial pressure of the gas. For example, for oxygen at 23 °C, Henry’s constant is increased by 8.7% for a 10 times increase in partial pressure (800–8200 mmHg) (Perry and Green, 1999).

Table I.16

Characteristic constants for water as solvent
(IAPWS, 2004)

a_i	b_i	n
-7.86	1	1
1.84	1.5	2
-11.79	3	3
22.68	3.5	4
-15.96	4	5
1.8	7.5	6

Table I.17

Characteristic constants for gases (IAPWS, 2004)

Solute	A	B	C	Temperature range of validity (K)
H ₂	-4.73	6.09	6.06	273–636
N ₂	-9.68	4.72	11.71	278–636
O ₂	-9.45	4.44	11.42	274–616
CO	-10.53	5.13	12.01	278–588
CO ₂	-8.55	4.01	9.52	274–642
H ₂ S	-4.52	5.24	4.42	273–533
CH ₄	-10.45	4.67	12.13	275–633
C ₂ H ₆	-19.68	4.51	20.63	275–473
SF ₆	-16.56	2.15	20.35	283–505

Another correlation for estimating Henry's constant for oxygen dissolved in water in the temperature range 100–200 °C has been presented by Wu *et al.* (2003):

$$H^f(T) \times 10^{-3} = 761.1 - 108.9 \ln T - 40785.5/T \quad (\text{I.42})$$

where T is in K. Henry's constants for several atmospheric gases and organic compounds in water are shown in Tables I.18 and I.19, respectively.

I.3.3 The case of oxygen

A distinction should be made between solubility and Henry's constant. Solubility is normally expressed in mg/L and is written as C_L in the following relationship:

$$C_G = HC_L \quad (\text{I.43})$$

Table I.18

Henry's constants ($10^{-3}/H^\circ$) for atmospheric gases with water as solvent at 25 °C

Gas	Henry's constant (mol/L atm)
O ₂	1.3×10^{-3}
NO	1.9×10^{-3}
C ₂ H ₄	4.8×10^{-3}
NO ₂	1×10^{-2}
N ₂ O	2.5×10^{-2}
CO ₂	3.4×10^{-2}
H ₂ S	0.12
HCl	1.1
SO ₂	1.23
CH ₃ O ₂	6
HNO ₂	49
NH ₃	62
CH ₃ OH	220
HCOOH	3.6×10^3
CH ₃ COOH	8.8×10^3
HNO ₃	2.1×10^5
NO ₃	2.1×10^5

Note: The values given reflect only the physical solubility of the gas regardless the subsequent fate of the dissolved species, i.e. dissociation or other transformation in aqueous phase.

Table I.19

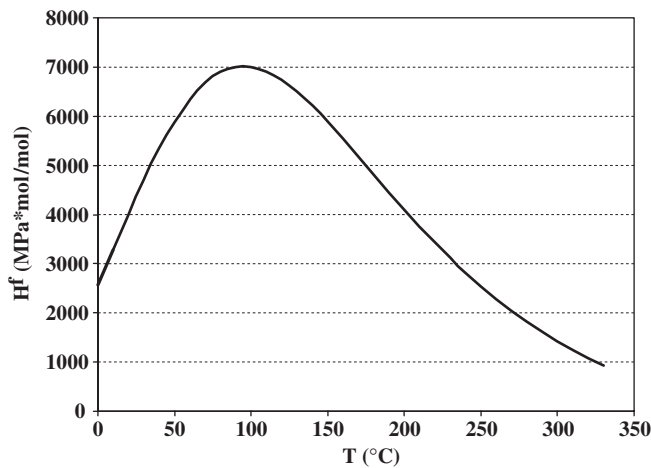
Dimensionless Henry's constants for organic compounds and water as solvent at 25 °C (partly from Howe *et al.*, 1986)

Gas	<i>H</i>
Benzene	0.216
Carbon tetrachloride	1.25
Chlorobenzene	0.147
Chloroform	0.172
2-Chlorophenol	0.016
Ethylene dibromide	0.027
DDD	1.64×10^{-4}
DDE	8.61×10^{-4}
DDT	3.32×10^{-4}
1,2-Dichlorobenzene	0.0642
1,4-Dichlorobenzene	0.130
3,3-Dichlorobenzidine	1.64×10^{-7}
2,4-Dimethylphenol	8.20×10^{-5}
2,4-Dinitrophenol	1.82×10^{-5}
2,4-Dinitrotoluene	3.8×10^{-6}
2,6-Dinitrotoluene	3.06×10^{-5}
Ethylbenzene	0.323
Hexachlorobenzene	0.0541

(Continued)

Table I.19 (Continued)

Gas	H
Hexachloroethane	0.159
2-Methylphenol	4.92×10^{-5}
Nitrobenzene	9.84×10^{-4}
Pentachlorophenol	10^{-6}
Phenol	1.63×10^{-5}
Toluene	0.262
1,2,4-Trichlorobenzene	0.0582
Trichloroethylene	0.422
2,4,5-Trichlorophenol	1.78×10^{-4}
2,4,6-Trichlorophenol	3.19×10^{-4}
<i>m</i> -Xylene	0.304
<i>p</i> -Xylene	0.304
<i>o</i> -Xylene	0.199

**Figure I.1** Henry's constant of oxygen in water.

It is evident that C_L is a function of Henry's constant and the concentration of the gas (or its partial pressure). It is clear from Figure I.1 that Henry's constant increases till the temperature of 100 °C and then decreases. As a result, under constant gas-phase concentration (or partial pressure), the solubility of oxygen decreases up to 100 °C and then increases. Consequently, the common belief of continuous decrease in the solubility of gases in water by increasing temperature is true up to a point (Debellefontaine *et al.*, 1996, 2000). There is a certain temperature, different for each gas species, above which this picture is reversed. Moreover, above a certain temperature, the volatilization of water decreases the partial pressure of the gas, and thus the solubility could be further decreased even if Henry's constant is decreased at the same time.

Note that the solubility of oxygen is frequently overestimated via Henry's constant due to the fact that solubility refers to air as gas, and thus the partial pressure of oxygen is 0.21 atm while Henry's constant is based on 1 atm gas partial pressure.

I.4 PARAMETERS FOR DUBININ–RADUSKEVISH ISOTHERM

In this section, the most important parameters for the Dubinin–Raduskevish isotherm are presented.

I.4.1 Saturated vapor pressure of selected organic compounds

Vapor pressure is the most important of the basic thermodynamic properties affecting both liquids and vapors. The vapor pressure is the pressure exerted by a pure component at equilibrium at any temperature (Perry and Green, 1999). The proposed equation is the modified Riedel (Perry and Green, 1999):

$$\ln P_s = A + \frac{B}{T} + C \ln T + DT^E \quad (\text{I.44})$$

where the vapor pressure P_s is in Pa, the temperature T in K, and A , B , C , D , and E the characteristic constants of the compound. In Table I.20, the constants of some important organic compounds for environmental applications are given.

I.4.2 Molar volumes in the liquid state of selected organic compounds

In Table I.21, the molar volumes in the liquid state of some important organic compounds found in many environmental applications are given.

Pavlov *et al.* (1979) directly gives the values of the affinity coefficient β based on the molar volumes for selected compounds (Table I.22).

Table I.20

Constants of organic compounds for the modified Riedel equation

Compound	A	B	C	D	E
Toluene	80.88	−6902	−8.7761	0.58×10^{-5}	2
Benzene	83.22	−6517.7	−9.3453	0.712×10^{-5}	2
Nitrobenzene	90.445	−9744.8	−9.5228	0.756×10^{-17}	6
Methane	38.664	−1314.7	−3.373	0.302×10^{-4}	2
Tetrachloroethylene	58.764	−6191.2	−5.3312	0.213×10^{-5}	2
Styrene	105.93	−8685.9	−12.42	0.756×10^{-5}	2
Vinyl chloride	91.43	−5141.7	−10.981	0.193×10^{-4}	2
Cyclohexane	116.51	−7103.3	−15.49	0.169×10^{-1}	1
Phenol	95.44	−10113	−10.09	0.676×10^{-17}	6

Table I.21

Molar volumes of organic compounds in the liquid state m³/kmol

Compound	V (m ³ /kmol)
Toluene	0.107
Benzene	0.089
Nitrobenzene	0.103
Methane	0.038
Tetrachloroethylene	0.103
Styrene	0.130
Vinyl chloride	0.065
Cyclohexane	0.109
Phenol	0.089

Table I.22

Affinity coefficient β based on the molar volumes for selected compounds

Compound	V (m ³ /kmol)
Methyl alcohol	0.4
Butane	0.9
Propane	0.78
Acetone	0.88
Acetic acid	0.97
Benzene	1
Cyclohexane	1.03
Diethylethere	1.09
Toluene	1.25
Hexane	1.35
Heptane	1.59

I.5 CONSTANTS OF LANGMUIR AND FREUNDLICH ISOTHERMS

The Langmuir and Freundlich constants for several systems are presented in Table I.23 and Table I.24, respectively.

Table I.23

Langmuir adsorption isotherm constants for several compounds on several adsorbents/water systems at ambient temperature

Compound	Adsorbent ^a	Q_M (mg/g)	K (L/mg)	Reference
Polyethylene glycol (PEG)	AC (F-400)	2022 (pH = 6.5)	0.014 (pH = 6.5)	Chang <i>et al.</i> (2004)
		558 (pH = 0.25)	0.056 (pH = 0.25)	

(Continued)

Table I.23 (Continued)

Compound	Adsorbent ^a	Q_M (mg/g)	K (L/mg)	Reference
Cinacron Rot F-B (C.I. 184—dye)	PAC	455	0.115	Voudrias <i>et al.</i> (2002)
Reactive blue 21 (C.I. 21—dye)	PAC	357	0.275	Voudrias <i>et al.</i> (2002)
2-Naphthol	AC	345	0.643	Dobbs and Cohen (1980); Noble and Terry (2004)
2-Chlorophenol	AC	272	0.405	Dobbs and Cohen (1980); Noble and Terry (2004)
Salicylaldehyde	AC	240	0.417	Dobbs and Cohen (1980) Noble and Terry (2004)
<i>o</i> -Cresol	AC	240	0.417	Dobbs and Cohen (1980); Noble and Terry (2004)
Benzaldehyde	AC	210	0.170	Dobbs and Cohen (1980) Noble and Terry (2004)
Benzyl alcohol	AC	158	0.176	Dobbs and Cohen (1980); Noble and Terry (2004)
Pb ²⁺	Clinoptilolite (natural zeolite)	109–144 (pH= 3–6)	(pH= 3–6) 0.05–0.09	Bektas and Kara (2004)
Aniline	AC	108	0.177	Dobbs and Cohen (1980); Noble and Terry (2004)
Reactive blue 21 (C.I. 21—dye)	Fly ash	94.3	0.465	Voudrias <i>et al.</i> (2002)
Aniline	Plain and acid-treated carbons	87–114	0.114–0.287	–
Phenol	Plain and acid-treated carbons	70–179	0.014–0.044	–
Pyridine	AC	55	0.154	Dobbs and Cohen (1980); Noble and Terry (2004)
NH ₄ ⁺	Clinoptilolite (natural zeolite)	25.77	0.018	Sarioglu (2005)
Acid orange 51 (acid dye)	Activated bleaching earth (clay)	8.45	0.0552	Tsai <i>et al.</i> (2004)
Cu ²⁺	Mesoporous aluminas (protonated and aminated)	7.09–8.55	0.25–0.31	Rengaraj <i>et al.</i> (2004)
Cu ²⁺	GAC (Filtrisorb 200)	3.34–7.04	2.05–2.55	Chen and Wang, (2004)
Nitrobenzene	AC	0.310	0.230	Dobbs and Cohen (1980); Noble and Terry (2004)

^a GAC, granular activated carbon; PAC, powdered activated carbon; AC, activated carbon (Filtrisorb 300).

Table I.24

Freundlich adsorption isotherm constants for several compounds on several adsorbents/water systems at ambient temperature

Compound	Adsorbent ^a	K_F (mg/g)(L/mg) ^{Fr}	Fr	Reference
PCB	AC	14100	1.03	Dobbs and Cohen (1980)
Endrin	AC	666	0.80	Dobbs and Cohen (1980)
Aldrin	AC	651	0.92	Dobbs and Cohen (1980)
Dieldrin	AC	606	0.51	Dobbs and Cohen (1980)
Alachlor	AC	479	0.26	Dobbs and Cohen (1980)
Hexachlorobenzene	AC	450	0.60	Dobbs and Cohen (1980)
Pentachlorophenol	AC	436	0.34	Dobbs and Cohen (1980)
4-Nitrobiphenyl	AC	370	0.27	Dobbs and Cohen (1980)
Styrene	AC	327	0.48	Dobbs and Cohen (1980)
DDT	AC	322	0.50	Dobbs and Cohen (1980)
1,2-Dichlorobenzene	AC	263	0.38	Dobbs and Cohen (1980)
<i>m</i> -Xylene	AC	230	0.75	Dobbs and Cohen (1980)
DBS	AC	178	0.147	Hashimoto <i>et al.</i> (1977)
Ethylbenzene	AC	175	0.53	Dobbs and Cohen (1980)
Cinacron Blau F-R (C.I. 182—dye)	PAC	174	0.513	Voudrias <i>et al.</i> (2002)
<i>p</i> -nitrophenol	AC	172	0.113	Hashimoto <i>et al.</i> (1977)
2,4-Dichlorophenol	AC	157	0.15	Dobbs and Cohen (1980)
2,4,6-Trichlorophenol	AC	155	0.40	Dobbs and Cohen (1980)
2,4-Dinitrotoluene	AC	146	0.31	Dobbs and Cohen (1980)
2,4-Dinitrotoluene	AC	145	0.32	Dobbs and Cohen (1980)
Naphthalene	AC	132	0.42	Dobbs and Cohen (1980)
Maxilon Scharz FBL-01 300% (basic dye)	GAC	124.4	0.219	Meshko <i>et al.</i> (2001)
1,4-Dichlorobenzene	AC	121	0.47	Dobbs and Cohen (1980)
Chlorobenzene	AC	100	0.35	Dobbs and Cohen (1980)
Toluene	AC	100	0.45	Dobbs and Cohen (1980)
2-Nitrophenol	AC	99	0.34	Dobbs and Cohen (1980)
Hexachloroethane	AC	97	0.38	Dobbs and Cohen (1980)
2,4-Dimethylphenol	AC	78	0.44	Dobbs and Cohen (1980)
Maxilon Goldberg GL EC 400% (basic dye)	GAC	77.82	0.123	Meshko <i>et al.</i> (2001)
4-Nitrophenol	AC	76	0.25	Dobbs and Cohen (1980)
Nitrobenzene	AC	68	0.43	Dobbs and Cohen (1980)
2-Chlorophenol	AC	51	0.41	Dobbs and Cohen (1980)
Tetrachloroethylene	AC	51	0.56	Dobbs and Cohen (1980)
Cinacron Blau F-R (C.I. 182—dye)	Fly ash	41	0.274	Voudrias <i>et al.</i> (2002)
2,4-Dinitrophenol	AC	33	0.61	Dobbs and Cohen (1980)
Trichloroethylene	AC	28	0.62	Dobbs and Cohen (1980)
1,2-Dibromoethene	AC	22	0.46	Dobbs and Cohen (1980)
Phenol	AC	21	0.54	Dobbs and Cohen (1980)
1,2-Dichloropropane	AC	19	0.59	Dobbs and Cohen (1980)

(Continued)

Table I.24 (Continued)

Compound	Adsorbent ^a	K_F (mg/g)(L/mg) ^{Fr}	Fr	Reference
Cinacron Rot F-B (C.I. 184—dye)	Fly ash	18.7	0.237	Voudrias <i>et al.</i> (2002)
Cinacron Blau F-R (C.I. 182—dye)	Bentonite	15.4	0.390	Voudrias <i>et al.</i> (2002)
Carbon tetrachloride	AC	11	0.83	Dobbs and Cohen (1980)
1,2-Trichloropropene	AC	8.2	0.46	Dobbs and Cohen (1980)
Maxilon Scharz FBL-01 300% (basic dye)	Clinoptilolite (natural zeolite)	7.5	0.389	Meshko <i>et al.</i> (2001)
1,1,2-Trichloroethane	AC	5.8	0.60	Dobbs and Cohen (1980)
1,1-Trichloroethylene	AC	4.9	0.54	Dobbs and Cohen (1980)
1,2-Trichloroethane	AC	3.6	0.83	Dobbs and Cohen (1980)
Chloroform	AC	2.6	0.73	Dobbs and Cohen (1980)
Maxilon Goldberg GL EC 400% (basic dye)	Clinoptilolite (natural zeolite)	2.58	0.284	Meshko <i>et al.</i> (2001)
1,1,1-Trichloroethane	AC	2.5	0.34	Dobbs and Cohen (1980)
1,1-Dichloroethane	AC	1.8	0.53	Dobbs and Cohen (1980)
Benzene	AC	1.0	1.6	Dobbs and Cohen (1980)
Benzoic acid	AC	0.76	1.8	Dobbs and Cohen (1980)
Chloroethane	AC	0.59	0.95	Dobbs and Cohen (1980)
Cinacron Rot F-B (C.I. 184—dye)	Bentonite	0.87	0.845	Voudrias <i>et al.</i> (2002)

^a GAC, granular activated carbon; PAC, powdered activated carbon; AC, activated carbon (Filtrisorb 300).

The values in Table I.24 should be seen only as a first guide or rough approximation since the parameters could be widely different with different carbons. For instance, in Table I.25, the Freundlich parameters are presented for benzene adsorption on several types of activated carbons.

Table I.25

Freundlich constants for several carbons and benzene (USACE, 2001)

Carbon	K_f (mg/g)(L/mg) ^{Fr}	Fr
Filtrisorb 300	1	1.6
Filtrisorb 400	16.6	0.4
Norit	49.3	0.6
Nuchar WV-G	29.5	0.4
Hydrodarco 1030	14.2	0.4

Appendix II

Conversion of Units

In Tables II.1 – II.20, several basic units and the basic conversion factors (CF) are presented.

Table II.1

Decimal multiples and submultiples

Multiple			Submultiple		
Prefix	Symbol	Operator	Prefix	Symbol	Operator
deca	da	$\times 10$	deci	d	$\times 10^{-1}$
hecto	h	$\times 10^2$	centi	c	$\times 10^{-2}$
kilo	k	$\times 10^3$	milli	m	$\times 10^{-3}$
mega	M	$\times 10^6$	micro	μ	$\times 10^{-6}$
giga	G	$\times 10^9$	nano	n	$\times 10^{-9}$
tera	T	$\times 10^{12}$	pico	p	$\times 10^{-12}$

Note: For example, MJ = 10^6 J, kg = 10^3 g, dm = 10^{-1} m, pF = 10^{-12} F.

Table II.2

Basic physical constants

Name	Symbol	Value	Units
Boltzmann constant	k	1.380658×10^{-23}	J/K
Avogadro number	N_A	6.02252×10^{23}	1/mol
Planck constant	h	6.626075×10^{-34}	J s
Faraday constant	F	9.648530×10^4	Cb/mol
Gravity acceleration	g_0	9.80665	m/s ²

Table II.3

Definitions of basic units

Unit	SI	Equivalent
Force	N	kg m/s ²
Energy	J	m ² kg/s ²
Surface tension	N/m	kg/s ²
Dynamic viscosity	Pa s	kg/m s
Power	W	m ² kg/s ³
Pressure	Pa	kg/m s ²

Table II.4

Temperature units

$$K = ^\circ C + 273.15$$

$$K = \frac{5}{9} \times R$$

$$^\circ C = \frac{5}{9} (F - 32)$$

$$F = R - 459.67$$

$$F = \frac{9}{5} ^\circ C + 32$$

Table II.5

Length units

$\Downarrow \times CF = \Updownarrow$	m	in	ft	Mile
m	1	3.937×10	3.281	6.214×10^{-4}
in	2.540×10^{-2}	1	8.333×10^{-2}	1.578×10^{-5}
ft	3.048×10^{-1}	1.200×10	1	1.894×10^{-4}
Mile	1.609×10^3	6.336×10^4	5.280×10^3	1

Note: $\text{\AA} = 10^{-10}$ m.

Table II.6

Mass units

$\Downarrow \times CF = \Updownarrow$	kg	lb _m	slug	oz	Metric ton
kg	1	2.205	6.852×10^{-2}	3.527×10^1	1.000×10^{-3}
lb_m	4.536×10^{-1}	1	3.108×10^{-2}	1.600×10^1	4.536×10^{-4}
slug	1.459×10^1	3.217×10	1	5.148×10^2	1.459×10^{-2}
oz	2.835×10^{-2}	6.250×10^{-2}	1.943×10^{-3}	1	2.835×10^{-5}
Metric ton	1.000×10^{-3}	2.205×10^3	6.852×10^1	3.527×10^4	1

Table II.7

Density units

$\Downarrow \times CF = \Updownarrow$	g/cm ³	kg/m ³	g/m ³	lb _m /ft ³	lb _m /US gal
g/cm³	1	1.000×10^3	1.000×10^6	6.243×10	8.345
kg/m³	1.000×10^{-3}	1	1.000×10^3	6.243×10^{-2}	8.345×10^{-3}
g/m³	1.000×10^{-6}	1.000×10^{-3}	1	6.243×10^{-5}	8.345×10^{-6}
lb_m/ft³	1.602×10^{-2}	1.602×10	1.602×10^4	1	1.337×10^{-1}
lb_m/US gal	1.198×10^{-1}	1.198×10^2	1.198×10^5	7.480	1

Table II.8

Volumetric feed units

$\Downarrow \times CF = \Updownarrow$	cm^3/s	m^3/h	L/min	ft^3/s	ft^3/min	gal/min
cm^3/s	1	3.600×10^{-3}	6.000×10^{-2}	3.531×10^{-5}	2.119×10^{-3}	1.585×10^{-2}
m^3/h	2.778×10^2	1	1.667×10	9.810×10^{-3}	5.886×10^{-1}	4.403
L/min^a	1.667×10	6.000×10^{-2}	1	5.886×10^{-4}	3.531×10^{-2}	2.642×10^{-1}
ft^3/s	2.832×10^4	1.019×10^2	1.699×10^3	1	6.000×10	4.488×10^2
ft^3/min	4.719×10^{-2}	1.699	2.832×10	1.667×10^{-2}	1	7.480
gal/min	6.309×10	2.271×10^{-1}	3.785	2.228×10^{-3}	1.337×10^{-1}	1

^aL = dm³.

Table II.9

Surface tension units

$\Downarrow \times CF = \Updownarrow$	dyn/cm	N/m	kp/m	pdl/ft	lb_f/ft
dyn/cm	1	1.000×10^{-3}	1.020×10^{-4}	2.205×10^{-3}	6.852×10^{-5}
N/m	1.000×10^3	1	1.020×10^{-1}	2.205	6.852×10^{-2}
kp/m	9.807×10^3	9.807	1	2.162×10	6.720×10^{-1}
pdl/ft	4.536×10^2	4.536×10^{-1}	4.625×10^{-2}	1	3.108×10^{-2}
lb_f/ft	1.459×10^4	1.459×10	1.488	3.217×10	1

Table II.10

Diffusion coefficient units

$\Downarrow \times CF = \Updownarrow$	cm^2/s	m^2/s	ft^2/s
cm^2/s	1	1.000×10^{-4}	1.076×10^{-3}
m^2/s	1.000×10^4	1	1.076×10
ft^2/s	9.290×10^2	9.290×10^{-2}	1

Table II.11

Dynamic viscosity units

$\Downarrow \times CF = \Updownarrow$	Poise	$\text{Pa} \times \text{s}$	$\text{kp} \times \text{s}/\text{m}^2$	$\text{lb}_m/(\text{ft} \times \text{s})$	$\text{lb}_f \times \text{s}/\text{ft}^2$
Poise	1	1.000×10^{-1}	1.020×10^{-2}	6.720×10^{-2}	2.088×10^{-3}
$\text{Pa} \times \text{s}$	1.000×10	1	1.020×10^{-1}	6.720×10^{-1}	2.088×10^{-2}
$\text{kp} \times \text{s}/\text{m}^2$	9.807×10	9.807	1	6.590	2.048×10^{-1}
$\text{lb}_m/(\text{ft} \times \text{s})$	1.488×10	1.488	1.517×10^{-1}	1	3.108×10^{-2}
$\text{lb}_f \times \text{s}/\text{ft}^2$	4.788×10^2	4.788×10	4.882	3.217×10	1

Table II.12

Kinematic viscosity units

$\Downarrow \times CF = \Uparrow$	Stokes (cm ² /s)	m ² /s	ft ² /s
Stokes	1	1.000×10^{-4}	1.076×10^{-3}
m²/s	1.000×10^4	1	1.076×10
ft²/s	9.290×10^2	9.290×10^{-2}	1

Table II.13

Heat transfer coefficient units

$\Downarrow \times CF = \Uparrow$	erg/(cm ² ×s×°C)	W/(m ² × K)	kcal/(m ² ×h×°C)	ft×pdl/(ft ² ×s×F)	Btu/(ft ² ×h×F)
erg/(cm²×s×°C)	1	1.000×10^{-3}	8.598×10^{-4}	1.225×10^{-3}	1.761×10^{-4}
W/(m² × K)	1.000×10^3	1	8.598×10^{-1}	1.225	1.761×10^{-1}
kcal/(m²×h×°C)	1.163×10^3	1.163	1	1.424	2.048×10^{-1}
ft×pdl/(ft²×s×F)	8.165×10^2	8.165×10^{-1}	7.020×10^{-1}	1	1.438×10^{-1}
Btu/(ft²×h×F)	5.678×10^3	5.678	4.882	6.955	1

Table II.14

Force units

$\Downarrow \times CF = \Uparrow$	dyn	N	kp	pdl	lbf
dyn	1	10^{-5}	1.020×10^{-6}	7.233×10^{-5}	2.248×10^{-6}
N	10^5	1	1.020×10^{-1}	7.233	2.248×10^{-1}
kP	9.807×10^5	9.807	1	7.093×10	2.205
pdl	1.382×10^4	1.382×10^{-1}	1.410×10^{-2}	1	3.108×10^{-2}
lb_f	4.448×10^5	4.448	4.536×10^{-1}	3.217×10	1

Table II.15

Power units

$\Downarrow \times CF = \Uparrow$	W	erg/s	ft × lb _f /s	Btu/h	hp
W	1	1.000×10^7	7.376×10^{-1}	3.412	1.341×10^{-3}
erg/s	1.000×10^{-7}	1	7.376×10^{-8}	3.412×10^{-7}	1.341×10^{-10}
ft × lb_f/s	1.356	1.356×10^7	1	4.626	1.818×10^{-3}
Btu/h	2.931×10^{-1}	2.931×10^6	2.162×10^{-1}	1	3.930×10^{-4}
hp	7.457×10^2	7.457×10^9	5.5000×10^2	2.544×10^3	1

Table II.16

Energy units

$\Downarrow \times CF = \Uparrow$	erg	Joule	ft \times lb _f	kcal	kW \times h	Btu	hp \times h
erg	1	10^{-7}	7.376×10^{-8}	2.388×10^{-11}	2.778×10^{-14}	9.478×10^{-11}	3.725×10^{-14}
Joule	10^7	1	7.376×10^{-1}	2.388×10^{-4}	2.778×10^{-7}	9.478×10^{-4}	3.725×10^{-7}
ft \times lb_f	1.356×10^7	1.356	1	3.238×10^{-4}	3.766×10^{-7}	1.285×10^{-3}	5.050×10^{-7}
kcal	4.187×10^{10}	4.187×10^3	3.088×10^3	1	1.163×10^{-3}	3.968	1.560×10^{-3}
kW \times h	3.600×10^{13}	3.600×10^6	2.655×10^6	8.598×10^2	1	3.412×10^3	1.341
Btu	1.055×10^{10}	1.055×10^3	7.782×10^2	2.520×10^{-1}	2.931×10^{-4}	1	3.929×10^{-4}
hp \times h	2.684×10^{13}	2.684×10^6	1.980×10^6	6.412×10^2	7.457×10^{-1}	2.545×10^3	1

Table II.17

Pressure units

$\Downarrow \times CF = \Uparrow$	Pa	atm	lb/ft ²	torr (mmHg)	mm H ₂ O	psi (lb/in ²)	in Hg (0 °C)	in H ₂ O (4 °C)
Pa	1	9.869×10^{-6}	2.088×10^{-2}	7.501×10^{-3}	1.020×10^{-1}	1.450×10^{-4}	2.953×10^{-4}	4.015×10^{-3}
atm	1.013×10^5	1	2.116×10^3	7.600×10^2	1.033×10^4	1.469×10	2.992×10	4.068×10^2
lb/ft²	4.788×10	4.725×10^{-4}	1	3.591×10^{-1}	4.882	6.944×10^{-3}	1.414×10^{-2}	1.922×10^{-1}
torr (mmHg)	1.333×10^2	1.315×10^{-3}	2.784	1	1.359×10	1.930×10^{-2}	3.937×10^{-2}	5.350×10^{-1}
mm H₂O	9.807	9.678×10^{-5}	2.048×10^{-1}	7.358×10^{-2}	1	1.422×10^{-3}	2.896×10^{-3}	3.937×10^{-2}
psi (lb/in²)	6.895×10^3	6.805×10^{-2}	1.440×10^2	5.171×10	7.031×10^2	1	2.036	2.768×10
in Hg (0 °C)	3.386×10^3	3.342×10^{-2}	7.073×10	2.540×10	3.453×10^2	4.912×10^{-1}	1	1.359×10
in H₂O (4 °C)	2.491×10^2	2.458×10^{-3}	5.203	1.867	2.540×10	3.613×10^{-2}	7.358×10^{-2}	1

Table II.18

Surface units

$\Downarrow \times CF = \Uparrow$	m ²	ha	km ²	yd ²	acre
m²	1	1.000×10^{-4}	1.000×10^{-6}	1.196	2.471×10^{-4}
ha	1.000×10^4	1	1.000×10^{-2}	1.196×10^4	2.471
km²	1.000×10^6	1.000×10^2	1	1.196×10^6	2.471×10^2
yd²	8.361×10^{-1}	8.361×10^{-5}	8.361×10^{-7}	1	2.066×10^{-4}
acre	4.047×10^3	4.047×10^{-1}	4.047×10^{-3}	4.840×10^3	1

Table II.19

Volume units

$\Downarrow \times CF = \Uparrow$	m ³	L	ft ³	US gal	Barrel (oil)
m³	1	1.000×10^3	3.5315×10^1	2.642×10^2	6.290
L	1.000×10^{-3}	1	3.532×10^{-2}	2.642×10^{-1}	6.290×10^{-3}
ft³	2.832×10^{-2}	2.832×10^1	1	7.481	1.781×10^{-1}
US gal	3.785×10^{-3}	3.783	1.337×10^{-1}	1	2.381×10^{-2}
Barrel (oil)	1.590×10^{-1}	1.59×10^2	5.615	4.200×10^1	1

Table II.20

Solution concentration

System name	Abbreviation	Definition	Common Units
Molarity	M	Mole of solute per liter of solution	mol/L
Molality	m	Mole of solute per kilogram of solvent	mol/kg
Normality	N	Gram-equivalent of solute per liter of solution	greq/L
Weight per volume	w/v	Grams of solute per volume of solvent	g/cm ³
Volume per volume	v/v	Volume of solute per volume of solution	cm ³ /cm ³
Weight per weight	w/w	Weight of solute per weight of solution	g/g
Parts per million	ppm	Milligrams of solute per kilogram of solution	mg/kg

Note: The use of the ppm unit should not be made incautiously. It has to be clarified on first use whether ppm refers to mass per mass or to volume per volume. Concerning gases, mass-ppm (mg/kg) is different from volume-ppm (cm³/m³). The estimation of density is required for connecting these units with each other. A simple choice is to express volume-ppm as ppmv. Furthermore, in aqueous solutions, ppm (mg/kg) is equivalent to mg/L due to the density of water (1 kg/L).

REFERENCES

- Abrahamsen, A.R., Geldart, D., *Powder Technology*, **26**, 35 (1980)
- Afandizadeh, S., Foumeny, E.A., *Applied Thermal Engineering*, **21**, 669 (2001)
- Al-Dahhan, M.H., Dudukovic, M.P., *Chemical Engineering Science*, **50**, 2377 (1995)
- Akita, K., Yoshida, F., *Industrial & Engineering Chemistry Process Design and Development*, **12**, 76 (1973)
- Al-Dahhan, M.H., Larachi, F., Dudukovic, M.P., Laurent A., *Industrial & Engineering Chemistry Research*, **36**, 3292 (1997)
- Al-Dahhan, Dudukovic M.P., *American Institute of Chemical Engineers Journal*, **42**, 2594 (1996)
- Andrigo, P., Bagatin R., Pagani, G., *Catalysis Today*, **52**, 197 (1999)
- Angelidis, T.N., Papadakis, V.G., *Applied Catalysis B: Environmental*, **12**, 193 (1997)
- Anthony, R.G., Philp, C.V., Dosch, R.G., *Waste Management*, **13**, 503 (1993)
- ApSimon H.M., Warren R.F., *Energy Policy*, **24**, 631 (1996)
- Armbruster, T., *Studies in Surface Science and Catalysis*, **135**, 13 (2001)
- Armenante P.M., Nagamine E.U., *Chemical Engineering Science*, **53**, 1757 (1998)
- ATSDR (Agency for Toxic Substances and Disease Registry), Toxicological Profile for Toluene, US Department of Health and Human Services, Public Health Service, USA (1989)
- ATSDR (Agency for Toxic Substances and Disease Registry), Toxicological profile for polycyclic aromatic hydrocarbons, US Department of Health and Human Services, Public Health Service, USA (1995)
- ATSDR (Agency for Toxic Substances and Disease registry), Toxicological profile for chromium, US Department of Health and Human Services, Public Health Service, USA (2000)
- Atwater, J.E., Akse, J.R., McKinnis, J.A., Thompson, J.O., *Chemosphere*, **34**, 203 (1997)
- Australian Academy of Technological Sciences and Engineering, *Urban Air Pollution in Australia*, (1997)
- Babel, S., Kurniawan, T.A., *Journal of Hazardous Materials*, **B97**, 219 (2003)
- Baycal, B.B., Oldenburg, M., Sekoulov, I., *Environmental Technology*, **17**, 717 (1996)
- Beaven, G.W., Cross, J.E., Hooper, E.W., *Study of the Behaviour of Inorganic Ion Exchangers in the Treatment of Medium Active Effluents. Part V. The Encapsulation of Inorganic Ion Exchangers in Cement*, Rep. AERE-G-4421, United Kingdom Atomic Energy Authority, Harwell (1988)
- Beeckman, J.W., Froment, G.F., *Chemical Engineering Science*, **35**, 805 (1980)
- Behkish, A., *Hydrodynamic and Mass transfer parameters in large-scale slurry bubble column reactors*, PhD Thesis, University of Pittsburgh (2004)
- Bektas, N., Kara, S., *Separation and Purification Technology*, **39**, 189 (2004)
- Bellman, R., Pennington, R.H., *Quarterly Journal of Applied Mathematics*, **12**, 151 (1953)
- Bennett, A., Goodridge, F., *Transactions of the Institution of Chemical Engineers and the Chemical Engineer*, **48**, T232 (1970)
- Berzelius, J.J., *Ann. Chim. Phys.*, **61**, 146 (1836)
- Beyens, J., Geldart, D., *Chemical Engineering Science*, **29**, 255 (1974)
- Birch, D.J., Ahmed, N., *Solids suspension in aerated agitated vessels: Role of sparger design*, 9th European Conference on Mixing: Mixing 97, **Vol. 11**, 177 (1997)
- Blanchard, G., Maunaye, M., Martin, G., *Water Research*, **18**, 1501 (1984)
- Bouaifi, M., Hebrard, G., Bastoul, D., Roustan, M., *Chemical Engineering and Processing*, **40**, 97 (2001)

- Boudart, M., *Chemical Reviews*, **95**, 661 (1995)
- Boudart, M., *Journal of Molecular Catalysis*, **30**, 27 (1985)
- Brand, R., Pulles, T., Gijiswijk, R., Fribourg-Blanc, B., Courbet, C., EPER Review Report, European Commission (2004)
- Breedlove, B.K., Ferrence, G.M., Washington, J., Kubiak, C.P., *Materials and Design*, **22**, 577 (2001)
- British Standard BS 2955, *Glossary of Terms Relating to Particle Technology*, British Standard Institution, London (1991)
- Broadhurst, T.E., Becker, H.A., *American Institute of Chemical Engineers Journal*, **21**, 238 (1975)
- Burghardt, A., Bartelmus, G., Jaroszynski, M., Kolodziej, A., *The Chemical Engineering Journal*, **58**, 83 (1995)
- Butt, J.B., Petersen, E.E., *Activation, Deactivation and Poisoning of Catalysts*, Academic Press, London, (1988)
- Buurman, C., Resoort, G., Plaschkes, A., *Chemical Engineering Science*, **41**, 2865 (1986)
- Calderbank, P.H., *Transactions of the Institute of Chemical Engineers and the Chemical Engineer*, **36**, 443 (1958)
- Carberry, J.J., *Chemical and Catalytic Reaction Engineering*, McGraw-Hill, New York (1976)
- Cardenosa, M., Grosso, J., Ramirez, N., Ramirez, C., Cement Industry Solutions to Waste Management, *Proceedings of the First International Conference*, Calgary, Alberta, Canada (1992)
- CATC Technical Bulletin, *Choosing an Adsorption System for VOC: Carbon, Zeolite, or Polymers?* EPA 456/F-99-004, Clean Air Technology Center (CATC), Information Transfer and Program Integration Division, Office of Air Quality Planning and Standards, US Environmental Protection Agency (1999)
- Chang, C.F., Chang, C.Y., Holl, W., Ulmer, M., Chen, Y.H., Grob, H.J., *Water Research*, **38**, 2559 (2004)
- Chaudhari, R.V., Ramachandran, P.A., *American Institute of Chemical Engineers Journal*, **26**, 177 (1980)
- Chen, J.P., Wang, L., *Chemosphere*, **54**, 397 (2004)
- Chen, J.W., Buege, J.A., Cunningham, F.L., Northam, J.I., *Industrial & Engineering Chemistry Process and Design Development*, **7**, 26 (1968)
- Cheng, T., Jiang, Y., Zhang, Y., Liu, S., *Carbon*, **42**, 3081 (2004)
- Chern, J.M., Chien, Y.W., *Water Research*, **36**, 647 (2002)
- Chernjatskaja, N.B., *Radiochemistry*, **27**, 618 (1988)
- Chiang, B.C., Wey, M.Y., Yeh, C.L., *Journal of Hazardous Materials*, **B101**, 259 (2003)
- Chiarle, S., Rato, M., Rovatti, M., *Water Research*, **34**, 2971 (2000)
- Chitnis, S.R., Sharma, M.M., *Reactive and Functional Polymers*, **32**, 93 (1997)
- Choy, K.K., McKay, G., *Environment International*, **31**, 845 (2005)
- Chung, S.F., Wen, C.Y., *American Institute of Chemical Engineers Journal*, **14**, 857 (1968)
- Chung, T.H., Lee, L.L., Starling, K.E., *Industrial & Engineering Chemistry Fundamentals*, **23**, 8 (1984)
- Cicero, C.M., Herman, C.A., Workman, P., Poole, K., Erich, D., Harden, J., *Commercial Ion Exchange Resin Vitrification in Borosilicate Glass*, Rep. WSRC-MS- 98-00392, Westinghouse Savannah River Co., Aiken, SC (1998)
- Cincotti, A., Lai, N., Orru, R., Cao, G., *Chemical Engineering Journal*, **84**, 275 (2001)
- Cliff, R., Grace, J.R., Webber, M.E., *Bubbles, Drops and Particles*, Academic Press, New York (1978)
- Colombo, A.J., Baldi, G., *Chemical Engineering Science*, **31**, 1101 (1976)
- Commission Decision 2000/479/EC on the implementation of an European Pollutant Emission Register (EPER), Official Journal of the European Communities, L 192/36, July (2000)

- Commission for environmental cooperation of North America, North American Power Plant Air Emissions, Canada (2004)
- Compilation of ASTM Standard Definitions*, 8th Edition, American Society for Testing Materials, Philadelphia (1994)
- Cooley, C.R., Lerch, R.E., *Waste Volume Reduction by Acid Digestion*, Rep. HEDL-SA-703, Hanford Engineering Development Lab., Richland, WA (1974)
- Cooney, D., *American Institute of Chemical Engineers Journal*, **39**, 355 (1993)
- Cooney, D.O., *Chemical Engineering Communications*, **91**, 1 (1990)
- Cooney, E.L., Booker, N.A., Shallcross, D.C., Stevens, G.W., *Separation Science and Technology*, **34**, 2741 (1999)
- Coulson, J.M., Richardson, J.F., *Chemical Engineering Vol. 3*, Pergamon, UK (1994)
- Cralley L.J., Cralley L.V. (eds) *Patty's Industrial Hygiene and Toxicology. Volume III: Theory and Rationale of Industrial Hygiene Practice. 2nd ed., 3A: The Work Environment*. Wiley, New York (1985)
- Crittenden, J., Hand, D. W., Arora, H., Lykins Jr., B.W., *Journal AWWA*, 74 (January 1987)
- Crittenden, J.C., Weber, W.J., *Journal of the Environmental Engineering Division*, **EE3**, 433 (1978)
- Dabrowski, A., *Advances in Colloid and Interface Science*, **93**, 135 (2001)
- Dabrowski, A., Podkoscielny P., Hubicki, Z., Barczak, M., *Chemosphere*, **58**, 1049 (2005)
- Darton, R.C., La Nauze, R.D., Davidson, J.F., Harrison, D., *Institute of Chemical Engineers*, **55**, 274 (1977)
- Datsevich, L., Muhkortov, D.A., *Applied Catalysis A: General*, **261**, 143 (2004)
- Davidson, J.F., Harrison, D., *Fluidized Particles*, Cambridge University Press, New York (1963)
- Deckwer, W.D., Burchhart, R., Zool, G., *Chemical Engineering Science*, **29**, 2177 (1974)
- Dixon, A.G., *Canadian Journal of Chemical Engineering*, **66**, 705 (1988)
- Dobbs, R.A., Cohen, J.M., *Carbon Adsorption Isotherms for Toxic Organics*, US Environmental Protection Agency, EPA-600/8-80-023 (1980)
- DOE, *Slurry Reactor Hydrodynamics Studies: Final Report*, US Department of Commerce, National Technical Information Service, USA (DOE, 1985)
- DOE, United States Department of Energy, *Summary of DOE Incineration Capabilities*, Rep. DOE/ID-10651, US DOE, Washington, DC (1998)
- Dohi, N., Matsuda, Y., Shimizu, K., Minekawa, K., Kawase, Y., *Chemical Engineering and Processing*, **41**, 267 (2002)
- Donati, G., Paludetto, R., *Catalysis Today*, **34**, 483 (1997)
- Donati, G., Paludetto, R., *Catalysis Today*, **52**, 183 (1999)
- Doraiswamy, L.K., Mashelkar, R.A., *Frontiers in Chemical Engineering*, **Vol. 1/2**, Wiley Eastern Limited, India (1984)
- Dosch, R.G., Brown, N.E., Stephens, H.P., Anthony, R.G., *Treatment of liquid nuclear wastes with advanced forms of titanate ion exchangers*, *Waste Management '93*, **Vol. 2** (Proceedings of the International Symposium, Tucson, 1993), Arizona Board of Regents, Phoenix, AZ, 1751 (1993)
- Dubinini, M.M., *Chemistry and Physics of Carbon* (ed. P.L. Walker Jr.), **Vol. 2**, New York, Marcel Dekker (1966)
- Dudukovic, M.P., *Catalysis Today*, **48**, 5 (1999)
- Dudukovic, M.P., Larachi, F., Mills, P.L., *Chemical Engineering Science*, **54**, 1975 (1999)
- Dudukovic, M.P., Larachi, F., Mills, P.L., Multiphase catalytic reactors, *Catalysis Review – Science and Engineering*, **44**, 123 (2002)
- Dutta, S., Gualy, R., *CEP*, **10**, 37 (2000)
- Ebach, E.A., White, R.R., *American Institute of Chemical Engineers Journal*, **4**, 161 (1958)
- EEA Signals 2004, A European Environmental Agency update on selected issues, European Environmental Agency, Copenhagen (2004)

- EEA, *Air pollution in Europe 1990–2000*, Topic Report 4/2003, Copenhagen (2004)
- Edgeworth, R., Thring, M.W., *Joint Symposium: The Scaling-Up of Chemical Plant and Processes*, London (1957)
- EI-Hisnawi, A.A., Dudukovic, M.P., Mills, P.L., *ACS Symposium Series*, **196**, 421 (1981)
- Ellis, N., Bi, H.T., Lim, C.J., Grace, J.R., *Powder Technology*, **141**, 124 (2004)
- EPA (US Environmental Protection Agency), *Health Assessment Document for Toluene*, Office of Health and Environmental Assessment, Environmental Criteria and Assessment Office, Research Triangle Park, NC. EPA/540/1-86-033 (1984)
- EPA Technical Bulletin, *Choosing and Adsorption System for VOC: Carbon, Zeolites or Polymers?* United States Office of Air Quality, EPA 456/F-99-004, Environmental Protection Planning and Standards, (May 1999)
- EPA, *Technology Screening Guide for Radioactively Contaminated Sites*, United States Office of Air and Radiation EPA 402-R-96-017, Washington, DC 20460, (November 1996)
- EPA, *Toxicological Review of Phenol*, US Environmental Protection Agency, Washington DC (2002)
- EPA, *Wastewater Technology Fact Sheet*, United States Environmental Protection Agency (EPA), EPA 832-F-00-017 (September 2000)
- European Commission, *Integrated Pollution Prevention and Control*, Reference Document on Best Available Techniques in Common Waste Water and Waste Gas Treatment/Management Systems in the Chemical Sector (February 2003)
- European Commission, *Guidance Document on EPER Implementation*, Directorate General for Environment, Luxembourg (2000)
- European Commission, *Choices for a greener future*, The European Union and the Environment, “Europe on the move” series, Luxembourg (2002)
- European Commission, *Integrated Pollution Prevention and Control*, Reference Document on Best Available Techniques in Common Waste Water and Waste Gas Treatment/Management Systems in the Chemical Sector (February 2003)
- European Commission, *EPER Review Report*, (June 2004)
- European Environment Agency, *Air pollution in Europe 1990–2000*, Topic Report 4 (2003)
- Farman, J.C., Gardiner, B.G., Shanklin, J.D., *Nature*, **315**, 207 (1985)
- Faust, R.A., *Toxicity Summary for Copper*, Oak Ridge Reservation Environmental Restoration Program, USA (1992)
- Faust, S.D., Aly, O.M., *Adsorption Processes for Water Treatment*, Butterworth Publishers, Boston, Massachusetts (1987)
- Feintuch, H.M., *Hydrocarbon Processing*, **10**, 150 (1977)
- Feng, X., Jing, S., Wu, Q., Chen, J., Song, C., *Powder Technology*, **134**, 235 (2003)
- Fernandez, M.A., Carta, G., *Journal of Chromatography A*, **746**, 169 (1996)
- Fernandez, M.A., Laughinghouse, W.S., Carta, G., *Journal of Chromatography A*, **746**, 185 (1996)
- Fishwick, R.P., Winterbottom, J.M., Stitt, E.H., *Chemical Engineering Science*, **58**, 1087 (2003)
- Fleck, R.D., Kirwan, D.J., Hall, K.R., *Industrial and Engineering Chemistry Fundamentals*, **12**, 95 (1973)
- Fogler, H.S., *Elements of Chemical Reaction Engineering*, 3rd Edition, Prentice Hall, New York (1999)
- Forgacs, E., Cserhatia, T., Orosb, G., *Environment International*, **30**, 953 (2004)
- Forzatti, P., Lietti, L., *Catalysis Today*, **52**, 165 (1999)
- Foscolo, P.U., Gibilaro, L.G., *Chemical Engineering Science*, **39**, 1667 (1984)
- Fox, J.M., Degen, B.D., *Slurry Reactor Design Studies*, Topical Report, Reactor Selection Criteria, US Department of Commerce, National Technical Information Service, USA (1990)

- Freeman, H.M., *Standard Handbook of Hazardous Waste Treatment and Disposal*, 2nd Edition, McGraw-Hill, New York (1998)
- Froment, G.F., Bischoff, K.B., *Chemical Reactor Analysis and Design*, 2nd Edition, Wiley, New York (1990)
- Fu, M.S., Tan, C.S., *Chemical Engineering Science*, **51**, 5357 (1996)
- Fukuma, M., Muroyama, K., Yasunishi, A., *Journal of Chemical Engineering of Japan*, **20**, 28 (1987)
- Fumeny, E. A., Kulkarni, A., Roshani, S., Vatani, A., *Applied Thermal Engineering*, **16**, 192 (1996)
- Gambill, W.R., *Chemical Engineering*, 113 (June 1958)
- Gates, B.C., *Catalytic Chemistry*, Wiley, New York (1992)
- Geldart, D., *Powder Technology*, **7**, 285 (1973)
- Ghutta, N.K., *Treatment of Spent Ion Exchange Resins by Incorporation into Epoxy Resins*, Middle Eastern Regional Radio Isotope Centre for Arab Countries, Cairo (1997)
- Gianetto, A., Baldi, G., Specchia, V., Sicardi, S., *American Institute of Chemical Engineers Journal*, **24**, 1087 (1978)
- Glicksman, L.R., *Chemical Engineering Science*, **39**, 1373 (1984)
- Glicksman, L.R., *Chemical Engineering Science*, **43**, 419 (1988)
- Gogoi, N.C., Dutta, N.N., *Fuel Processing Technology*, **48**, 145 (1996)
- Goodwin, J., Mareckova, K., *Emissions of Atmospheric Pollutants in Europe, 1990–99*, Topic report 5/2002, EEA, Copenhagen (2002)
- Green, N., Bjerkeng, B., Hylland, K., Ruus, A., Rygg B., Künitzer A., *Hazardous substances in the European Marine Environment: Trends in Metals and Persistent Organic Pollutants*, Topic Report 2/2003, EEA, Copenhagen (2003)
- Gregg S.J., W.Sing K.S., *Adsorption, Surface Area and Porosity*, Academic Press, London and New York (1967)
- Griffith. C.M., Moris, J., Robichaud, M., Allen, M.J., McCormick, A.V., Flickinger, M.C., *Journal of Chromatography A*, **776**, 179 (1997)
- Grover, M.R., Hilstad, M.O., Elias, L.M., Carpenter, K.G., Schneider, M.A., Hoffman, C.S., Adan-Plaza, S., Bruckner, A.P., *Extraction of Atmospheric Water on Mars, Mars Society Founding Convention*, Boulder, CO, August (1998)
- Gulfaz, M., Yagiz, M., *Separation and Purification Technology*, **37**, 93 (2004)
- Gunn, D.J., *The Chemical Engineer*, **6**, 153 (1968)
- Gupta, A., Gaur, V., Verma, N., *Chemical Engineering and Processing*, **43**, 9 (2004)
- Gupta, V.K., Shrivastava, S.K., Sharma, D.M., *Waste Management*, **17**, 517 (1997)
- Gupta, V.K., Shrivastava, S.K., Tyagi, R., *Water Research*, **34**, 1543 (2000)
- Guy, C., Carrouau, P.J., Paris, J., *Canadian Journal of Chemical Engineering*, **64**, 23 (1986)
- Guzzo, P.R., *Ion Exchange Procedures*, Technical Reports, Vol. 1, No 5, Albany Molecular Research, Inc. (1997)
- Haakana, T., Kolehmainen, E., Turunen, I., Mikkola, J.P., Salmi, T., *Chemical Engineering Science*, **59**, 5629 (2004)
- Haider, Levenspiel, O., *Powder Technology*, **58**, 63 (1989)
- Hall, K., Eagleton, L.C., Acrivos, A., Vermeulen, T., *Industrial & Engineering Chemistry Fundamentals*, **5**, 212 (1966)
- Hamoudi, S., Larachi, F., Cerella, G., Cassanello, M., *Industrial Engineering Chemistry Research*, **37**, 3561 (1998)
- Hamoudi, S., Larachi, F., Adnot, A., Sayari, A., *Journal of Catalysis*, **185**, 33 (1999)
- Hand, D.W., Crittenden, J.C., Asce, M., Tracker, W.E., *Journal of Environmental Engineering*, **110**, 440 (1984)
- Hanika, J., *Chemical Engineering Science*, **54**, 4653 (1999)
- Hanson, A., *Industrial Minerals*, 40 (December 1995)

- Harjula, R., Letho, J., Tusa, E.H., Paavola, A., *Nuclear Technology*, **107**, 272 (1994)
- Harriot P., *American Institute of Chemical Engineers Journal*, **8**, 93 (1962)
- Hashimoto, K., Miura, K., Tsukano, M., *Journal of Chemical Engineering of Japan*, **10**, 27 (1977)
- Hausmann, R., Hoffmann, C., Franzreb, M.G., Holl, W.H., *Chemical Engineering Science*, **55**, 1477 (2000)
- Hawkings, N., Horton, K.D., Snelling, K.W., *The Dissolution of Organic Ion Exchange Resins Using Iron-Catalysed H₂O₂*, Rep. AEEW-R-1390, United Kingdom Atomic Energy Authority, Winfrith (1980)
- Heijnen, J.J., Van't Riet, K., *Chemical Engineering Journal*, **28**, B21 (1984)
- Heinonen, O.J., Lehto, J., Miettinen, J.K., *Radiochimica Acta*, **28**, 93 (1981)
- Helfferich, F., *Ion Exchange*, Dover Publications, New York (1962)
- Helfferich, F.G., Hwang, Y.L., Ion Exchangers as Catalysts, in *Ion Exchange for Industry* (ed. M. Sreat), S.C.I./Ellis Horwood, Chichester (1988)
- Hikita, H., Asai, S., Tanigawa, K., Segawa, K., Kitao, M., *The Chemical Engineering Journal*, **22**, 61 (1981)
- Hilal, N., *Journal of Chemical Engineering of Japan*, **33**, 901 (2000)
- Hinshelwood, C.N., *The Kinetics of Chemical Change*, Clarendon, Oxford (1940)
- Hlavay, J., Vigh, G., Olasi, V., Inczedy, J., *Water Research*, **16**, 417 (1992)
- Holland, F.A., *Chemical Engineering*, **9**, 179 (1962)
- Holloway, T., Fiore, A., Hastings, M.G., *Environmental Science & Technology*, **37**, 4535 (2003)
- Hopper, J.R., Salsh, J.M., Pike, R., *Clean Production Processes*, **3**, 92 (2001)
- Horio, M., Ishii, H., Sawa, Y., Muchi I., *American Institute of Chemical Engineers Journal*, **32**, 1466 (1986)
- Horowitz, G.I., Martinez, O., Cukierman, A.L., Cassanello, M.C., *Chemical Engineering Science*, **54**, 4811 (1999)
- Hougen, O.A., Watson, K.M., *Chemical Process Principles*, Wiley, New York (1943)
- Howe, G.B., Mullins, M.E., Rogers, T.N., USAFESC Report No. ESL-86-66, US Air Force Engineering and Services Center, Tyndall AFB, FL, 86 (1986)
- Hughmark, G.A., *Industrial & Engineering Chemistry Process Design and Development*, **6**, 218 (1967)
- Hung, L.C., *Immobilization of Ion Exchange in Polymers*, Nuclear Energy Commission, Rio de Janeiro (1994)
- IAEA, *Application of Ion Exchange Processes for the Treatment of Radioactive Waste and Management of Spent Ion Exchangers*, Technical Reports Series No. 408, International Atomic Energy Agency (IAEA), Vienna (2002)
- IAEA, International Atomic Energy Agency, *Immobilization of Low and Intermediate Level Radioactive Wastes with Polymers*, Technical Reports Series No. 289, Vienna (1988)
- IAPWS, *Guideline on the Henry's Constant and Vapor-Liquid Distribution Constant for Gases in H₂O and D₂O at High Temperatures*, The International Association for the Properties of Water and Steam, Kyoto, Japan (2004)
- IAPWS, *Release on Surface Tension of Ordinary Water Substance*, The International Association for the Properties of Water and Steam (1994)
- Inamori, Y., Kimochi, Y., Inamori, R., Gui, P., Kong, H.N., Mizuochi, M., *Journal of Chemical Engineering of Japan*, **36**, 449 (2003)
- Incropera, F.P., DeWitt, D.P., *Fundamentals of Heat and Mass Transfer*, 3rd Edition, John Wiley & Sons International Edition (1990)
- Inglezakis, V.J., *Design of Ion Exchange Column Using Natural Minerals as Packing Materials*, PhD Thesis, National Technical University of Athens, Athens, Greece (2002)
- Inglezakis, V.J., *Journal of Colloid and Interface Science*, **281**, 68 (2005)

- Inglezakis, V.J., Grigoropoulou, H.P., *Journal of Colloid and Interface Science*, **224**, 434 (2001)
- Inglezakis, V.J., Grigoropoulou, H.P., *Microporous and Mesoporous Materials*, **61**, 273 (2003)
- Inglezakis, V.J., Hadjiandreou, K.J., Loizidou, M.D., Grigoropoulou, H.P., *Water Research*, **35**, 2161 (2001)
- Inglezakis, V.J., Lemonidou, M., Grigoropoulou, H.P., *Chemical Engineering Science*, **56**, 5049 (2001)
- Inglezakis, V.J., Papadeas, C.D., Loizidou, M.D., Grigoropoulou, H.P., *Environmental Technology*, **22**, 75 (2001)
- Inglezakis, V.J., Loizidou, M.D., Grigoropoulou, H.P., *Water Research*, **36**, 2784 (2002)
- Inglezakis, V.J., Loizidou, M.D., Grigoropoulou, H.P., Pb²⁺ Removal from Liquid Phase Using Chelating Resin Lewatit TP 207: The Effect of Operating Variables and Application of Shrinking Core Model, *Eighth International Conference on Environmental Science and Technology*, Lemnos, pp. 341–348 (2003)
- Inglezakis, V.J., Loizidou, M.D., Grigoropoulou, H.P., *Journal of Colloid and Interface Science*, **275**, 570 (2004)
- Inglezakis, V.J., Zorpas, A.A., Grigoropoulou, H.P., Arapoglou, D., Liquid holdup measurements using tracing techniques in zeolite packed beds, *5th International Scientific and Technical Conference "Water Supply and Water Quality,"* Poznan, Poland, 430–440 (2002)
- International Air Quality Advisory Board, *Summary of Critical Air Quality Issues in the Transboundary Region*, January (2004)
- IPCS, International Programme on Chemical Safety: Environmental Health Criteria 188, Nitrogen Oxides (Second Edition), World Health Organisation, Geneva (1997)
- IRIS, *Integrated Risk Information System (IRIS)*, USEPA, USA (1998)
- Ismagilov, Z.R., Kerzhentsev, M.A., *Catalysis Today*, **47**, 339 (1999)
- Jaffe, D., Anderson, T., Covert, D., Kotchenruther, R., Trost, B., Danielson, J., Simpson, W., Bernsten, T., Karlsdotir, S., Blake, D., Harris, J., Carmichael, G., Uno, I., *Geophysical Research Letters*, **26**, 711 (1999)
- Jamialahmadi, M., Branch, C., Müller-Steinhagen, H., *Transactions of the Institute of Chemical Engineers and the Chemical Engineer*, **72**, 119 (1994)
- Jantzen, C.M., Peeler, D.K., Cicero, C.A., *Vitrification of Ion-exchange (IEX) Resins: Advantages and Technical Challenges*, Rep. WSRC-MS-95-0518, Westinghouse Savannah River Co., Aiken, SC (1995)
- Johnson, C.P., Li, X., Logan, B.E., *Environmental Science and Technology*, **30**, 1911 (1996)
- Jonas, L.A., Rehrmann, J.A., *Carbon*, **12**, 95 (1974)
- Jossi, J.A., Stiel, L.I., Thodos, G., *American Institute of Chemical Engineers Journal*, **8**, 59 (1962)
- Juang, R.S., Lin, S. H., Wang, T.Y., *Chemosphere*, **53**, 1221 (2003)
- Rahman, K., Streat, M., *Chemical Engineering Science*, **36**, 293 (1981)
- Kantarci, N., Borak, F., Ulgen, K.O., *Process Biochemistry*, **40**, 2263 (2005)
- Kapoor, A., Viraraghavan, T., *Water Reserach*, **32**, 1968 (1998)
- Kato, Y., Hiraoka, S., Tada, Y., Suzuki, J., Hirose, K., Lee, Y.S., Koh, S.T., *Journal of Chemical Engineering of Japan*, **34**, 1532 (2001)
- Kato, Y., Hiraoka, S., Tada, Y., Watanabe, S., Buchs, J., *Journal of Chemical Engineering of Japan*, **36**, 1410 (2003)
- Kelkar, V.V., Ng, K.M., *American Institute of Chemical Engineers Journal*, **48**, 1498 (2002)
- Kim, K.H., Solidification of Spent Ion Exchange Resins in Polymers, *Proceedings of the International Conference on Waste Management*, Seoul (1991)
- Klemas, L., Bonilla, J.A., *Chemical Engineering Progress*, **91**, 27 (1995)
- Knaebel, K.S., *Chemical Engineering*, **102**, 92 (1995)
- Knowlton, T.M., Karri, S.B.R., Issangya, A., *Powder Technology*, **150**, 72 (2005)

- Knowlton, T.M., *Oil and Gas Science and Technology – Rev. IFP*, **55**, 209 (2000)
- Ko, D.C.K., Lee, V.K.C., Porter, J.F., McKay, G., *Journal of Chemical Technology and Biotechnology*, **77**, 1289 (2002)
- Ko, D.C.K., Porter, J.F., McKay, G., *Chemical Engineering Science*, **55**, 5819 (2000)
- Ko, D.C.K., Porter, J.F., McKay, G., *Transactions of the Institute of Chemical Engineers and the Chemical Engineer, Part B*, **81**, 73 (2003)
- Koide, K., *Journal of Chemical Engineering of Japan*, **29**, 745 (1996)
- Koide, K., Takazawa, A., Komura, M., Matsunaga, H., *Journal of Chemical Engineering of Japan*, **17**, 459 (1984)
- Koloini, T., Sopcic, M., Zumer, M., *Chemical Engineering Science*, **32**, 637 (1977)
- Komiyama, H., Smith, J.M., *American Institute of Chemical Engineers Journal*, **21**, 664 (1975)
- Kraemer, R.A., Choudhury, K., Kampa, E., Protecting water resources: pollution prevention, Thematic Background Paper, *International Conference on Freshwater*, Bonn, (December 2001)
- Kressman, T.R.E., *Industrial Chemistry*, 1 (February 1960)
- Krishna, R., *Oil and Gas Science and Technology – Rev. IFP*, **55**, 359 (2000)
- Krishna, R., van Baten, J.M., Ellenberger, J., *Powder Technology*, **100**, 137 (1998)
- Krishna, R., van Baten, J.M., Urseanu, M.I., Ellenberger, J., *Catalysis Today*, **66**, 199 (2001)
- Krishna, R., Urseanu, M.I., de Swart, J.W.A., Ellenberger, J., *The Canadian Journal of Chemical Engineering*, **78**, 442 (2000)
- Kubo, K., Aratani, T., Mishima, A., *International Chemical Engineering*, **23**, 85 (1983)
- Kunii, D., Levenspiel, O., *Fluidization Engineering*, Wiley, New York (1968)
- Kunii, D., Levenspiel, O., *Chemical Engineering Science*, **55**, 4563 (2000)
- Kwauk, M., Li, J., Liu, D., *Powder Technology*, **111**, 3 (2000)
- Laakkonen, M., Honkanen, M., Saarenrinne, P., Aittamaa, J., *Chemical Engineering Journal*, **109**, 37 (2005)
- Larachi, F., Iliuta, I., Belkacemi, K., *Catalysis Today*, **64**, 309 (2001)
- Larkins, R.P., White, R.R., Jeffrey, D.W., *American Institute of Chemical Engineers Journal*, **7**, 231 (1961)
- Lee, D., Epstein, N., Grace, J.R., *Journal of Chemical Engineering of Japan*, **36**, 1111 (2003)
- Lee, D., Epstein, N., Grace, J.R., *Journal of Chemical Engineering of Japan*, **34**, 95 (2001)
- Lehmann, M., Zouboulis, A.I., Matis, K.A., *Environmental Pollution*, **113**, 121 (2001)
- Leung, P.C., Recasens, F., Smith J.M., *American Institute of Chemical Engineers Journal*, **33**, 996 (1987)
- Levenspiel, O., *Chemical Reaction Engineering*, 2nd Edition, Wiley Eastern Limited, India (1972)
- Li, H., Lu, X., Kwauk, M., *Powder technology*, **137**, 54 (2003)
- Li, X., Yuan, Y., *Water Research*, **36**, 3110 (2002)
- Liakopoulos, C., Pouloupoulos, S., Philippopoulos, C., *Industrial Engineering Chemistry Research*, **40**, 1476 (2001)
- Lide, D.R., *Handbook of Chemistry and Physics*, 72nd Edition, CRC Press, Boca Raton, FL (1991)
- Lieu, D., Kwauk, M., Li, H., *Chemical Engineering Science*, **51**, 4045 (1996)
- Lieu, K.T., Weber, W.J., *Journal WPCF*, **53**, 1541 (1981)
- Lodewyckx, P., Vansant, E.F., *American Industrial Hygiene Association Journal*, **61**, 501 (2000)
- Low, K.S., Lee, C.K., Ng, A.Y., *Bioresource Technology*, **68**, 205 (1999)
- Lucy, C.A., *Journal of Chromatography A*, **1000**, 711 (2003)
- Lyman, W.J., Reehl, W.F., Rosenblatt, D.H., *Handbook of Chemical Property Estimation Methods*, 1st Edition, American Chemical Society, Washington DC (1990)
- Magaud, F., Souhar, M., Wild, G., Boisson, N., *Chemical Engineering Science*, **56**, 4597 (2001)
- Markovska L., Meshko, V., Noveski, V., Marinkovski, M., *Journal of the Serbian Chemical Society*, **66**, 463 (2001)

- Massimilla, L., Johnstone, R.F., *Chemical Engineering Science*, **16**, 105 (1961)
- Matatov-Meytal, Y., Sheintuch, M., *Industrial Engineering Chemistry Research*, **37**, 309 (1998)
- Matsen, J.M., *Powder Technology*, **88**, 237 (1996)
- McCabe, W., Smith, J.C., Harriott, P., *Unit Operations of Chemical Engineering*, 5th Edition, McGraw-Hill, New York (1993)
- McKay, G., Bino, M.J., *Chemical Engineering Research and Design*, **63**, 168 (1985)
- McKetta, J.J., *Unit Operations Handbook*, Volume 1. Mass Transfer, Marcel Dekker, USA (1993)
- McLaren, J., Farquhar, G.J., *Journal of the Environmental Engineering Division-ASCE*, **EE4**, 429 (1973)
- McManus, R.K., Funk, G.A., Harold, M.P., Ng, K.M., *Industrial & Engineering Chemistry Research*, **32**, 570 (1993)
- McNaught, A.D., Wilkinson, A., *The Gold Book, IUPAC Compendium of Chemical Technology*, 2nd Edition, Blackwell Science, UK (1997)
- Medeiros, E.B., Petrissans, M., Wehrer, A., Zoulalian, A., *Chemical Engineering and Processing*, **40**, 153 (2001)
- Mendelson, H.D., *American Institute of Chemical Engineers Journal*, **13**, 250 (1967)
- Menoud, P., Cavin, L., Renken, A., *Chemical Engineering and Processing*, **37**, 89 (1998)
- Meshko, V., Markovska, L., Mincheva, M., Rodrigues, A.E., *Water Research*, **35**, 3357 (2001)
- Michaels, A.S., *Industrial & Engineering Chemistry – Analytical Edition*, **44**, 1922 (1952)
- Michell, D.A., Pandey, A., Sangsurasak, P., Krieger, N., *Process Biochemistry*, **35**, 167 (1999)
- Midoux, N., Favier, M., Charpentier, J.C., *Journal of Chemical Engineering of Japan*, **9**, 350 (1976)
- Mikhlyonov, I., Averbuch, A., Tumarkina, E., Furmer, I., *Chemical Technology*, Part I, 3rd Edition, MIR Publishers, Moscow (1979)
- Miller, G.T., *Living in the Environment: Principles, Connections and Solutions*, Wadsworth Publishing Company, USA (1996)
- Miura, K., Hashimoto, K., *Journal of Chemical Engineering of Japan*, **10**, 490 (1977)
- Moller, L.B., Halken, C., Hansen, J.A., Bartholdy, J., *Industrial & Engineering Chemistry Research*, **35**, 926 (1996)
- Montante, G., Pinelli, D., Magelli, F., *Chemical Engineering Science*, **58**, 5363 (2003)
- Mori, S., Wen, C.Y., *American Institute of Chemical Engineers Journal*, **21**, 109 (1975)
- Mumpton, F.A., *Proceedings of the National Academy of Science USA*, **96**, 3463 (1999)
- Murillo, R., Garcia, T., Aylon, E., Callen, M.S., Navarro, M.V., Lopez, J.M., Mastral, A.M., *Carbon*, **42**, 2009 (2004)
- Neilson Jr., R., Colombo, P., *Solidification of Ion Exchange Resin Wastes*, Rep. BNL-51615, Brookhaven National Laboratory, Upton, NY (1982)
- Nesbitt, A.B., Petersen, F.W., *Powder Technology*, **98**, 258 (1998)
- Netpradit, S., Thiravetyan, P., Towprayoon, S., *Water Research*, **38**, 71 (2004)
- Neubauer, J., Incineration of Ion Exchange Resins: Operational Experience, Incineration and Thermal Treatment Technologies, *Proceedings of the International Conference*, University of California, Irvine, CA (1996) Nezi, C., Pouloupoulos, S., Philippopoulos, C., *Industrial Engineering Chemistry Research*, **40**, 3325 (2001)
- Nicastro, M.T., Glicksman, L.R., *Chemical Engineering Science*, **39**, 1381 (1984)
- Nixon, S.C., Hunt, D.T.E., Lallana, C., Boschet, A.F., Sustainable use of Europe's water?, *State, Prospects and Issues, Environmental Assessment Series*, No 7, European Environmental Agency, Copenhagen (2004)
- Nixon, S., Trent, Z., Marcuello, C., Lallana, C., Europe's water: An indicator-based assessment, EEA, Copenhagen (2003)
- Noble, R.D., Terry, P.A., *Principles of Chemical Separations with Environmental Applications*, Cambridge University Press, UK (2004)

- Nouri, J.M., Hockey, R.M., *Journal of Chemical Engineering of Japan*, **31**, 848 (1998)
- NTIS, *Hydrodynamic Study of a Fischer–Tropsch Bubble-Column Slurry Reactor*, US Department of Commerce, National Technical Information Service, USA (1983)
- NTIS, *Slurry Reactor Hydrodynamics Studies*, US Department of Commerce, National Technical Information Service, USA (1985)
- NTP (National Toxicology Program), Toxicology and Carcinogenesis Studies of Toluene (CAS No. 108-88-3) in F344/N Rats and B6C3F1 Mice (Inhalation Studies). Technical Report Series No. 371. US Department of Health and Human Services, Public Health Service, National Institutes of Health, Research Triangle Park, NC (1990)
- Office for Official Publications of the European Communities, State and pressures of the marine and coastal Mediterranean environment, Environmental issues series No 5, Luxembourg (1999)
- Ohta, H., Goto, S., Teshima, H., *Industrial Engineering Chemistry Research*, **19**, 180 (1980)
- Orcutt, J.C., Davidson J.F., Pigford R.L., *Chemical Engineering Progress Symposium Series*, **77**, 38 (1962)
- Panja, N.C., Phanewara Rao, D., *The Chemical Engineering Journal*, **52**, 121 (1993)
- Parliamentary Office of Science and Technology, Postnote No 188, (November 2002)
- Pavel, S.K., Elvin, F.J., *Extraction and Processing for the Treatment and Minimization of Wastes, Minerals, Metals, and Materials Society*, Warrendale, PA (1994)
- Pavlov, K.F., Romankov, P.G., Noskov, A.A., *Examples and Problems to the Course of Unit Operations of Chemical Engineering*, MIR Publishers, Moscow (1979)
- Perry, D., Nutter, D.E., Hale, A., *Chemical Engineering Progress*, **86**, 30 (1990)
- Perry, R.H., Green D., *Perry's Chemical Engineer's Handbook*, 7th Edition, McGraw-Hill, International Editions (1984)
- Perry, R.H., Green, D., *Perry's Chemical Engineer's Handbook*, 7th Edition, McGraw-Hill, International Editions (1999)
- Peters, M.S., Timmerhaus, K.D., *Plant Design and Economics for Chemical Engineers*, 2nd Edition, McGraw-Hill, International Editions (1962)
- Pirkanniemi, K., Sillanpaa, M., *Chemosphere*, **48**, 1047 (2002)
- Pironti, F., Mizrahi, D., Acosta, A., Gonzalez-Mendizabal, D., *Chemical Engineering Science*, **54**, 3793 (1999)
- Place, B.G., *Treatment Technology for Transuranic Waste Streams: Cementation, Vitrification, and Incineration Testing for the Treatment of Spent Ion Exchange Media*, Rep. WHC-EP-0462, Westinghouse Hanford Company, Richland, WA (1992)
- Poulopoulos, S.G., Grigoropoulou, H.P., Philippopoulos, C.J., *Catalysis Letters*, **78**, 291 (2002)
- Poulopoulos, S.G., Philippopoulos, C.J., *Atmospheric Environment*, **38**, 4495 (2004)
- Prasher, B.D., Wills, G.B., *Industrial & Engineering Chemistry Design and Development*, **12**, 351 (1973)
- Purolite, *Ion Exchange Resins*, Technical Data Brochure, The Purolite Company, www.purolite USA.com (US)
- Qi, G., Yang, R.T., *Journal of Catalysis*, **217**, 434 (2003)
- Ramachandran, P.A., Chaudhari, R.V., Analysis and design of three phase catalytic reactors, in *Recent advances in the engineering analysis of chemically reacting systems* (ed. L.K. Doraiswamy), Wiley Eastern Limited, India (1984)
- Ramachandran, P.A., Chaudhari, R.V., *The Chemical Engineer*, 74 (December 1980)
- Rao, J.R., Viraraghavan, T., *Bioresource Technology*, **85**, 165 (2002)
- Rao, S.V., Kothandaraman, H., Sudhakar, M., Lal, K.B., Amalraj, R.V., *Journal of Applied Polymer Science*, **52**, 1263 (1994)
- Reid, R.C., Prausnitz, J.M., Poling, B.E., *The Properties of Gases and Liquids*, 4th Edition, McGraw-Hill, International Editions (1988)

- Reilly, I.G., Scott, D.S., de Bruijn, T.J.W., Jain, A., Piskorz, J., *The Canadian Journal of Chemical Engineering*, **64**, 705 (1986)
- Rengaraj, S., Kim, Y., Kyun Joo, C., Yi, J., *Journal of Colloid and Interface Science*, **273**, 14 (2004)
- Rewatkar, V.B., Raghava Rao, K.S., Joshi, J.B., *Industrial & Engineering Chemistry Research*, **30**, 1770 (1991)
- Rhodes, M.J., *Introduction to Particle Technology*, Wiley, Chichester, England (1998)
- Richardson, J.F., Zaki, W.N., *Transactions of the Institute of Chemical Engineers and the Chemical Engineer*, **32**, 35 (1954)
- Rivero, M.J., Primo, O., Ortiz, M.I., *Journal of Chemical Technology and Biotechnology*, **79**, 822 (2004)
- Rodriguez-Reinoso, F., Linares-Solano, A., *Chemistry and Physics of Carbon: a Series of Advances* (ed. P. A. Thrower.), Marcel Dekker, Inc., New York (1989)
- Rosner, D., Markowitz, G., *American Journal of Public Health*, **75**, 344 (1985)
- Rowe, P.N., Patridge, B.A., *Particle Movement Caused by Bubbles in a Fluidized Bed*, Third Congress of European Federation of Chemical Engineering, London (1962)
- Ruthven, D.M., *Principles of Adsorption and Adsorption Processes*, Wiley, New York (1984)
- Saez, A.E., Yopez, M.M., Cabrera, C., Soria, M., *American Institute of Chemical Engineers Journal*, **37**, 1733 (1991)
- Sag, Y., Actay, Y., *Process Biochemistry*, **36**, 1187 (2001)
- Samanta, S.K., Ramaswamy, M., Misra, B.M., *Separation Science and Technology*, **27**, 255 (1992)
- Sano Y., Yamaguchi N., Adachi T., *Journal of Chemical Engineering of Japan*, **7**, 255 (1974)
- Sarioglu M., *Separation and Purification Technology*, **41**, 1 (2005)
- Saroha, A.K., Nigam, K.D.P., Trickle bed reactors. *Reviews in Chemical Engineering*, **3/4**, 207 (1996)
- Sarraf, A., Jamialahmadi, M., Müller-Steinhagen, H., Smith, J.M., *The Canadian Journal of Chemical Engineering*, **77**, 11 (1999)
- Satterfield, C.N., *American Institute of Chemical Engineers Journal*, **21**, 209 (1975)
- Saxena, S.C., *Heat Transfer Investigations in a Slurry Bubble Column: Final Report*, US Department of Energy, USA (1991)
- Schmidt, L.D., *The Engineering of Chemical Reactions*, 2nd edition, Oxford University Press, Oxford (2005)
- Semmens, M.J., Booth, A.C., Tauxe, G.W., *Journal of the Environmental Engineering Division*, **EE2**, 231 (1978)
- Sen, T.K., Mahajan, S. P., Khilar, K.C., *Colloids and Surfaces A: Physicochemical Engineering Aspects*, **211**, 91 (2002)
- SEPA, *Guidance for the large volume organic chemical sector*, IPPC, Sector Guidance Note, IPPC S4.01, Scottish Environment Protection Agency (SEPA) (2001)
- Shah, Y.T., Kelkar, B.G., Godbole, S.P., Deckwer, W.D., *American Institute of Chemical Engineers Journal*, **28**, 353 (1982)
- Sharp, D.W.A., *Dictionary of Chemistry*, Penguin Books, England (1990)
- Shelef, M., McCabe, R.W., *Catalysis Today*, **62**, 35 (2000)
- Shen, C.Y., Johnstone, H.F., *American Institute of Chemical Engineers Journal*, **1**, 349 (1955)
- Sherman, J.D., *American Institute of Chemical Engineers Symposium Series*, **74**, 98 (1978)
- Singh, A., Pant, K.K., Nigam, K.D.P., *Chemical Engineering Journal*, **103**, 51 (2004)
- Sinha, P.K., Amalraj, R.V., Krishnasamy, V., *Radiochimica Acta*, **65**, 125 (1994)
- Skoulikides, T.N., *Physical Chemistry I 1.2*, Symetria Editions, Athens, Greece (1989)
- Smith, J.M., *Chemical Engineering Kinetics*, 3rd Edition, McGraw-Hill, International Editions (1981)

- Smith, J.S., Burns, L.F., Valsaraj, K.T., Thibodeaux, L.J., *Industrial and Engineering Chemistry Research*, **35**, 1700 (1996)
- Specchia, V., Baldi, G., *Chemical Engineering Science*, **32**, 515 (1977)
- Stanek, V., *Fixed Bed Operations*, Ellis Horwood Ltd., New York (1994)
- Stitt, E.H., *Chemical Engineering Journal*, **90**, 47 (2002)
- Streat, M., Patrick, J.W., Camporro Perez, M.J., *Water Research*, **29**, 467 (1995)
- Sussman, S., *Journal of Industrial & Engineering Chemistry*, **38**, 1228 (1946)
- Szepe, S., Levenspiel, O., *Proceedings of the Fourth European Symposium on Chemical Reaction Engineering*, Pergamon Press, Brussels (1971)
- Tager, A., *Physical Chemistry of Polymers*, 2nd Edition, MIR Publishers, Moscow (1978)
- Tosun, G., *Industrial and Engineering Chemistry, Process Design and Development*, **23**, 35 (1984)
- Trambouze, P., *Chemical Engineering Progress*, **86**, 23 (1990)
- Treybal, R.P., *Mass Transfer Operations*, 3rd Edition, McGraw-Hill, International Editions (1980)
- Tsai, W.T., Chang, C.Y., Ing, C.H., Chang, C.F., *Journal of Colloid and Interface Science*, **275**, 72 (2004)
- Tsai, W.T., *Journal of Loss Prevention in the Process Industries*, **15**, 147 (2002)
- Tsitsishvili, G.V., Andronikashvili, T.G., Kirov, G.M., Filizova, L.D., *Natural Zeolites*, Ellis Horwood Ltd., New York (1992)
- UNEP, *The World Environment 1972-1992*, Chapman & Hall, London (1992)
- USACE, Engineering and Design, *Adsorption Design Guide*, Design Guide No. 1110-1-2, Department of the Army DG 1110-1-2, US Army Corps of Engineers (2001)
- US Department of Health and Human Services, Hazardous Substances Data Bank (HSDB, online database), National Toxicology Information Program, National Library of Medicine, Bethesda, MD (1993)
- Valerius, G., Zhu, X., Hofmann, H., *Chemical Engineering and Processing*, **35**, 1 (1996)
- Valkiainen, M., Nykyri, M., *Nuclear Technology*, **58**, 248 (1982)
- Van Swaaij, W.P.M., Charpentier, J.C., Villermaux, J., *Chemical Engineering Science*, **24**, 1083 (1969)
- Vandu, C.O., Krishna, R., *Chemical Engineering and Processing*, **43**, 987 (2004)
- Vermeulen, T., Quilici, R.E., *Industrial & Engineering Chemistry Fundamentals*, **9**, 179 (1970)
- Vial, Ch., Laine, R., Poncin, S., Midoux, N., Wild, G., *Chemical Engineering Science*, **56**, 1085 (2001)
- Voorhies, A., *Industrial Engineering Chemistry Research*, **37**, 318 (1945)
- Voudrias, E., Fytianos, K., Bozani, E., *Global Nest: The International Journal*, **4**, 75 (2002)
- Walker, G.M., Weatherley, L.R., *Water Research*, **31**, 2093 (1997)
- Wallis, G.B., *One Dimensional Two Phase Flow*, McGraw-Hill, New York (1969)
- Weber Jr., W.J., Pirbazari, M., *Journal AWWA*, **4**, 203 (1982)
- Weber Jr., W.J., Smith, E.H., *Environmental Science and Technology*, **21**, 1040 (1987)
- Weber, W.J., Wang, C.K., *Environmental Science and Technology*, **21**, 1096 (1987)
- Weisz, P.B., Prater, C.D., *Advances in Catalysis*, **6**, 143 (1954)
- Weitkamp, J., *Solid State Ionics*, **131**, 175 (2000)
- Wen, C.Y., Fan, L. T., *Models for flow systems and chemical reactors*, Marcel Dekker, New York (1975)
- Wen, C.Y., Flow regimes and flow models for fluidised bed reactors, in *Recent advances in the engineering analysis of chemically reacting systems* (ed. L. K. Doraiswamy), Wiley Eastern Limited, India, 256–287 (1984)
- Wen, C.Y., Yu, Y.H., *American Institute of Chemical Engineers Journal*, **12**, 610 (1966)
- Werther, J., Hydrodynamics and mass transfer between the bubble and emulsion phases in fluidised beds of sand and cracking catalyst, in *Fluidization* (eds. D. Kunii and R. Toei), Engineering Foundation, New York, 93 (1983)

- Wevers, C.J.H., *Chemical Engineering Science*, **10**, 171 (1959)
- Wheeler, A., *Advances in Catalysis*, Academic Press, New York (1950)
- WHO (World Health Organization), *Environmental Health Criteria 52, Toluene*, World Health Organization, Geneva (1985)
- WHO, *Health Aspects of Air Pollution*, Denmark (2004)
- Wilke, C.R., Chang, P., *American Institute of Chemical Engineers Journal*, **1**, 264 (1955)
- Wilks, J.P., Holman, J.D., Holt, N.S., *Organic waste treatment by wet oxidation*, Chemspec Europe '91 (*Proceedings of the British Association for Chemical Specialities Symposium Amsterdam*, 1991), British Association for Chemical Specialities, Sutton (1991)
- Wojchiechowsky, B.W., *Canadian Journal of Chemical Engineering*, **46**, 48 (1968)
- Wolff, J.J., *Catalysis by means of Ion Exchange Resins*, Purolite Technology Seminar, Breda, Holland, 12 (May 1987)
- Wood, G.O., *Carbon*, **39**, 343 (2001)
- Wood, G.O., Stampfer, J. F., *Carbon*, **31**, 195 (1993)
- Wu, Y., Al-Dahhan, M.H., Khadilkar, M.R., Dudukovic, M.P., *Chemical Engineering Science*, **51**, 2721 (1996)
- Xiu, G.H., Li, P., *Carbon*, **38**, 975 (2000)
- Yahata, T., Abe, J., *The Effect of Controlled Oxygen on the Incineration of Radio Contaminated Organic Compounds*, Rep. JAERI-M-9974, Japan Atomic Energy Research Institute, Tokyo (1982)
- Yamada I., Chibata Y., Tsurui R., *Pharmaceutical Bulletin of Japan*, **2**, 59 (1954)
- Yamasaki, N., Kanahara, S., Yanagisawa, K., *Nippon Kagaku Kaishi*, **12**, 2015 (1984)
- Yang, W.C., Newby, R.A., Keairns, D.L., *Powder Technology*, **82**, 331 (1995)
- Yasunishi, A., Fukuma, M., Muriyama, K., *Kagaku Kogaku Ronbunshu*, **12**, 420 (1986)
- Yasyerli, S., Ar, I., Dogu, G., Dogu, T., *Chemical Engineering and Processing*, **41**, 785 (2002)
- Yates, J.T., *Vacuum*, **31**, 715 (1981)
- Ye, M., van der Hoef, M.A., Kuipers, J.A., *Chemical Engineering Science*, **60**, 4567 (2005)
- Yoshida, H., Kataoka, T., Ruthven, D.M., *Chemical Engineering Science*, **39**, 1489 (1984)
- Yuang, R.S., *Proceedings of the National Science Council ROC(A)*, **23**, 353 (1999)
- Zamaraev, K.I., *Catalysis Today*, **35**, 3 (1997)
- Zanitsch, R.H., Lynch, R.T., *Selecting a Thermal Regeneration System for Activated Carbon, Carbon Adsorption Handbook*, Calgon Carbon Corporation, USA (1997)
- Zhang, H., Hu, X., *Separation and Purification Technology*, **34**, 105 (2004)
- Zulfadhly, Z., Mashitah, M.D., Bhatia, S., *Environmental Pollution*, **112**, 463 (2001)
- Zweitering, T.N., *Chemical Engineering Science*, **8**, 244 (1958)

Index

A

- absorption 32, 38, 109
- acentric factor 553, 555
- Achwal–Stepanek correlation 179
- acidification
 - acid rain 2, 4, 11, 15, 21, 22, 25
 - dry deposition 4
- activated carbon
 - bituminous GAC 243, 244
 - granular 47, 163, 189, 243, 571, 573
 - lignite GAC 244
 - powdered 243, 347, 571, 573
- active sites concentration 59, 60
- adsorbent 31, 32, 43, 44, 46–48, 140, 231, 243–245, 247, 248, 250–252, 266, 267, 269, 289, 301, 327, 347, 348, 570–573
- adsorption
 - advantages 48
 - definition 31–33
 - disadvantages 48
 - environmental applications 28, 46–49
 - historical aspects 37–38
 - special application 49
- affinity coefficient 269, 270, 569, 570
- agitated
 - slurry reactor (general) 78, 102, 114, 138, 548
 - slurry reactor modeling 107, 114, 131, 398
 - tank reactor 74, 167
- ammonia 5, 6, 24, 37, 307, 315, 499
- air emissions
 - diffuse 21
 - ducted 21
 - fugitive 21
 - main source 6, 8, 23, 24
 - mobile sources 21
 - stationary sources 21
- air pollutants
 - 1,3-butadiene 2
 - benzene 2, 3, 23–25
 - carbon dioxide 5, 9, 21, 24
 - carbon monoxide 2, 3, 5, 22, 24, 51, 503
 - incomplete combustion compounds 22
 - lead 2, 3, 26, 303
 - nitrogen dioxide 2, 3, 8, 11
 - nitrogen oxides and other nitrogen compounds 22, 24
 - ozone 1–6, 22, 23
 - particulate matter 2, 3, 5, 15, 23, 24, 27
 - photochemical oxidants 2
 - primary 2–4
 - secondary 2–4
 - sulfur dioxide 2, 3, 5, 6, 8, 11, 12, 14, 21, 394, 560, 562–563
 - sulfur oxides and other sulfur compounds 9, 21, 24
 - volatile organic compounds and organosilicon compounds 3, 22–24
- air pollution
 - Africa 11, 13, 15
 - Asia 11, 13, 14
 - Australia 11, 14, 15
 - European Union 5
 - global 2, 3, 5
 - Latin America 14
 - local 2, 3
 - North America 5, 12
 - regional 2–4
 - transboundary 3, 4
 - urban 2, 3
- Akita–Yoshida correlation 119, 123, 129, 391
- alumina 44, 47, 48, 243, 247, 251, 252, 356–357, 374, 421, 517, 520
- Archimedes number 195, 200, 235, 237, 509, 542
- axial mixing 149

B

- baffled tanks 82, 95, 100, 101
- Bayens equation 196, 201
- bed voidage 93, 143, 147, 155, 157, 158, 180, 197, 199, 200

- bed-depth-service-time (BDST) model
195–197, 327, 329
- benzene 2, 3, 23–25, 45, 104, 244, 246, 249,
270, 561, 563, 567, 569, 570, 573
- best available techniques (BATs) 21, 28
- bioaccumulation 18
- biological oxygen demand 18, 26
- Biot number 279, 290, 291, 301, 303, 305, 343
- breakpoint concentration 308, 329–331, 346
- breakthrough curve 308, 312, 316, 320, 339
- bubble column
hydraulic regimes 115
reactors 74, 78, 102, 104, 403
modeling 104, 386
- bubble diameter
agitated vessels 137
bubble column 123, 124, 126
fluidized bed 210, 212, 213, 540
- bubbling bed model *see fluidized bed models, Kunii–Levenspiel model*
- bubbling fluidization 191, 193, 200, 203, 206,
207, 212, 213, 215, 226
- Buckingham pi theorem 525
- buoyancy force 234, 239
- butadiene 2
- C**
- cadmium 20, 21, 26, 245, 260
- Calderbank correlation 101, 129, 136–137,
139, 301
- carbon dioxide 5, 9, 21, 24, 35, 49, 54, 348,
380, 560, 562, 563
- carbon disulfide 21, 563
- carbon monoxide 2, 3, 5, 22, 24, 50, 52–54,
250, 418, 499, 503, 560, 562
- catalysis
advantages 52
definition 34–37
disadvantages 52
environmental applications 28, 50–54
heterogeneous 35, 37, 41–44, 50
historical aspects 39–43
homogeneous 35, 36, 44, 45
special application 53
three-way 50, 52, 512
- catalyst
active sites 37, 57–59, 61, 65, 359–360
bulk density 63, 407
catalytic agents 231, 356
definition 34–37
molecular sieve 40, 48, 49, 248
monolithic 355, 407, 421, 422
porous 44, 60, 63, 64, 358, 373, 374, 382
promoters 356
specific area 59, 65
support 58, 355, 356, 461, 518
supported 65, 355, 515
surface arrangement 59, 65
three-way 50, 52, 512, 517
unsupported 356, 515
washcoat 355, 424, 515–517
- catalyst deactivation
attrition 517
catalyst inhibitor 512, 517
catalyst poison 512–513
Coulson and Richardson equation 512–513
fouling and coking 512–515
Froment and Bischoff approach 514
irreversible poisoning 517
kinetics of catalyst deactivation 518–520
leaching 518
management of spent catalysts 520–521
regeneration of deactivated catalysts 517–518
reversible poisoning 517
sintering 515–517
solid-state transformation 515–517
thermal aging 517–518
thermal degradation 512, 515–516
volatilization 516, 517
- catalytic converter 6, 15, 43, 50, 52, 53, 421,
513, 517
- catalytic oxidation 27, 28, 51, 367, 368, 401,
418, 465, 469, 473, 476, 491, 499, 518
- catalytic reaction steps
adsorption 43
desorption 44
dissociative adsorption 43
rate-limiting step 43
surface reaction 43
- channeling 140, 158, 184, 192
- chlorofluorocarbons 5, 6, 47
- Chu–Kail–Wetterath correlation 224
- Churchill correlation 161
- Chung equation 150
- Chung–Wen correlation 216
- clays 37, 38, 45, 46, 248, 252, 253, 255
- cold models 531

compressibility factor 88, 555
 constant pattern condition 311–312, 315, 316,
 327, 332, 338
 constriction factor 241
 contact time 308, 309, 312, 316, 338, 339,
 533–534, 536, 538
 crush strength 231

D

Damköhler number 371, 525
 density
 aggregate 233, 234
 apparent 232, 234
 bulk 63, 232, 233, 407
 effective 232
 envelope 232
 hydraulic 99, 121, 233–235, 240
 particle 63, 121, 232, 233
 skeletal 232, 233
 solid 121, 233
 true 232, 233
 destructive methods for spent materials
 acid digestion 350
 barix process 351
 incineration 350
 pyrolysis 349–350
 vitrification 350
 wet oxidation 350–351
 diffusion
 coefficient
 solid phase 66, 86, 240–242, 265, 274,
 280, 282, 285
 liquid phase 101, 129, 165, 275, 291,
 558–561
 gas phase 226, 561–563
 Knudsen diffusion 241, 374
 molecular diffusion 241, 374
 surface diffusion 304, 374
 diffusion volumes 493, 504, 562
 dimensional analysis 524, 525
 dimensionless groups 525–528, 538, 539,
 543, 548
 dimensionless numbers 525
 dioxins 18, 25, 347
 dipole moment 553
 dispersion
 axial 141–143, 149–151, 154, 169, 183,
 184, 215, 416, 530

 coefficient 126, 127, 143, 149, 150, 153,
 183, 392
 gas phase 126–127, 135, 137, 183
 liquid phase 126–127
 radial 149, 151, 154, 158, 408, 416, 530
 distribution coefficient 271
 distributor quality 158
 drag force 127, 210, 235, 236, 239, 240
 Dwivedi and Upadhyay equation 165

E

Edgeworth and Thring method 527
 Edwards–Richardson correlation 151,
 327, 330
 effective diffusivity 240, 374
 effectiveness factor
 for plate 374–377
 for spherical pellet 377–378
 internal 413, 446, 450, 470, 479, 504
 overall 382–384
 external 371–372
 El-Hisnawi et al. correlation 180, 426
 emulsion phase 191, 207–209, 214, 217, 219,
 224, 481, 485, 489, 498
 encapsulation 349, 351
 endothermic reactions 146, 368,
 369, 417
 energy of dissipation 135, 136, 402, 403
 Eotvos number 125, 156
 equilibrium isotherm
 Dubinin–Raduskevich 269–270
 favorable 268–269, 316
 Freundlich 267–269, 316–320
 irreversible 269
 ion exchange 270–272
 Langmuir 266–267, 316–320
 linear 268–269
 sigmoidal 268–269
 unfavorable 268–269, 335
 Ergun equation 146, 194, 195, 199, 430,
 440–442, 459, 474, 476, 477
 European Pollutant Emission Register (EPER)
 9, 10
 eutrophication 18–20, 24
 exothermic reactions 102, 146, 367, 368,
 417, 529
 expansion factor 87–92, 108–110, 147, 173,
 309, 407, 418, 420, 433, 449

F

- Fanning friction factor 161, 162
- Faraday constant 558, 575
- Fick's law 264–265
- Field and Davidson equation 127, 392
- fixed bed
 - adiabatic operation modeling 407, 416
 - isothermal operation modeling 407, 408
 - modeling (general) 141–148
 - monolithic catalysts 407, 421
 - nonisobaric operation 407, 427
 - reactors (general) 74, 77
 - voidage 63, 93, 143, 147, 155, 157, 312, 430
 - wetting efficiency 148
- fluidization
 - regimes 190–193
 - type A 193, 200–205, 213, 496
 - type B 193, 200–205, 213, 217, 481
- fluidized bed models
 - Chavarie–Grace model 487, 492, 497, 498
 - Kelkar–Ng model 486, 492, 498
 - Kunii–Levenspiel model 174, 207–211, 220, 226, 487–488, 492, 495, 496, 498, 499
 - Orcutt–Davidson–Pigford model 472, 481, 482, 491, 492, 498
 - two-phase model 200, 207, 217, 227, 481, 496, 506, 545
- fluidized bed voidage 199, 216, 223
- Foscolo–Gibilaro equation 203, 240
- Froude number 126, 206, 528, 542, 549
- Fuller–Schettler–Giddings equation 493, 561

G

- Galileo number 186, 462, 476
- Garner–Suckling correlation 163
- gas distribution 116–117, 162, 184–185, 216–217
- Geldart's classification of powders 191–193
- Goto and Smith equation 186
- greenhouse effect 1, 2, 5, 22

H

- Hayduk and Laudie equation 463, 559
- heat transfer
 - coefficient 146, 165, 189, 224, 367, 369, 373, 578
 - external 367–373

- internal 373–384
 - rate 102, 140, 371, 373
- heavy metals 18, 23–25, 28, 223, 250, 251, 260, 303, 307, 315, 324, 327, 347, 521
- Helfferrich–Glueckauf model 332, 333, 344
- hemoglobin 22, 503
- Henry's constant 70, 112, 405, 564–569
- Hinshelwood approach 359
- Hochman–Effron correlation 183
- holding time 92
- hold up
 - gas 116, 118–122, 128, 136, 137, 179, 403
 - liquid 63, 121, 128, 147, 155–157, 178, 308, 343, 395, 398, 402, 532, 535
 - solid 121, 128, 209, 485
- Hougen and Watson approach 359
- hydraulic diameter of the particles 155
- hydrocarbons 5, 22, 24, 26, 28, 50–53, 166, 243, 45, 251, 326, 352, 513
- hydrogen peroxide 351, 461, 463, 465, 560

I

- immobilization 349–352
- impeller
 - critical speed 135
 - discharge coefficient 94, 95
 - discharge rate 94, 95
 - power number 94, 95, 97, 98, 549
 - Reynolds number 81, 94, 98, 549
- impellers
 - axial-flow 79–80
 - disc-type turbines 81
 - flat-blade radial-flow 80
 - open-type turbines 80–81
 - pitched blade turbine 80
 - propeller 79–80
 - radial-flow 80–82
 - Rushton 81–82
- inorganic salts and acids 25
- interfacial area 128–130, 180, 185, 186, 188, 293, 393
- interstitial velocity 118, 392
- ion exchange
 - advantages 50
 - definition 33–34
 - disadvantages 50
 - environmental applications 28, 49–50
 - historical aspects 38–39

ion exchange materials
 composite 261–262
 natural inorganic 253–255
 natural organic 255
 synthetic inorganic 255–256
 synthetic organic 256–257

ionic conductances 558

ionic mobility 558, 559

isobaric operation 88, 89, 309

isothermal operation 89, 146, 147, 169, 217,
 309, 419, 421, 464, 480

isotopic exchange 264, 274–276, 279,
 282, 283

K

Kataoka correlation 163

Koloini–Sospic–Zumer correlation 225

L

Lagergren's rate equation 288

lambda sensor 53

Larkins equation 176, 177, 459

Levins and Glastonbuty correlation 101, 138,
 301

Limal–Ballesteros correlation 198, 508

limiting reactant 85–88, 104, 105, 108, 109,
 134, 173, 182, 387–389, 406, 412, 428, 540

linear driving force 309, 312, 313, 334

linear velocity 311, 338, 339, 342, 533, 534,
 536, 537

liquid distribution 158, 159, 184, 185, 523, 540

M

Mackie and Meares equation 242

maldistribution 154, 158, 160, 182, 184, 308,
 309, 534, 536, 539

mass transfer

coefficient 100, 101, 127–130, 138–139,
 162, 185, 187, 293, 303, 367, 373, 393,
 404, 479

external 100–101, 127–131, 138–139,
 185–189, 223–227, 409, 413

internal 167, 358, 373, 374, 408, 410, 413

maximum bed height 536, 537

maximum exchange level 268, 301

maximum working velocity 523, 536, 537

mercury 5, 12, 20, 23–26, 46, 245, 261

methyl tert butyl ether (MTBE) 19, 246

mean bubble rise velocity 126, 392

Mears criterion 183, 462, 463, 471,
 476, 478

mechanical parameter 290, 324, 326,
 338, 510

mechanical strength 46, 227, 231

minimum bubbling velocity 191, 193, 201,
 202, 207, 495, 496, 501, 506

minimum fluidization velocity 191, 193,
 195–197, 210, 222, 482, 536, 543

minimum voidage at incipient fluidization
 197–198

Miura and Hashimoto

criterion 510

model 316–320

Mochizuki–Matsui correlation 187, 471, 479

mock-ups 531, 538, 539

molar volume 270, 463, 464, 554, 559, 560,
 569–570

monolith 52, 74, 351, 355, 407, 421, 422,
 517, 538

Mori–Wen correlation 211, 494, 505

N

Nernst–Haskell equation 306, 558

Nernst–Haskell model 280, 282

Newton's law 237

NH_4^+ , NO_3^- , NO_2^- , PO_4^{3-} ions 24

nitrogen compounds 22

nitrogen dioxide 2, 3, 8, 11, 22

nitrogen oxide 3, 22, 36

nitrogen oxides 3, 5, 9, 14, 22, 24,
 28, 51–53

nitrous oxide 22, 24, 503, 504, 507,
 560, 562

nonisobaric operation 88, 197, 309,
 407, 418, 427

nonisothermal operation 88, 309,
 418, 428

nonmethane volatile organic compounds 5,
 6, 9

O

operating capacity 312, 334

organically modified clays 248

organic compounds 25, 244, 247, 269, 566,
 567, 569, 570

ozone

- depletion 2, 5, 6, 22
- destruction mechanism 5, 36
- stratospheric 1, 5
- tropospheric 4, 5, 22

P

packed bubble bed

- reactor 77, 168, 539
- modeling 174, 176, 394, 398, 449, 471
- particle diameter 150, 229, 536, 539, 542, 544
- particulate fluidization 191, 193, 199, 202, 205, 206, 215, 223, 224, 481
- particulate matter 2, 3, 5, 23, 24, 27
- partition ratio 273
- pathogenic microorganisms 26
- Patterson's equation 277, 282
- Pavlov's equation 200
- Peclet number 150, 151, 153, 183, 184, 215, 216, 311, 535
- perforated pipe distributors 360–362
- phenol 46, 258, 315, 328, 331, 352, 469–473, 513, 518, 561, 564, 568–572
- plug flow assumption/condition 105, 112, 115, 144, 148–151, 169, 175, 183, 208, 214, 219–223, 311, 312, 334
- polychlorinated biphenyls 5, 18, 25
- polymeric resin adsorbents 248
- pore-size distribution 230
- porosity
 - aggregate 233
 - bed 63, 197, 540
 - fluidized bed 193, 198, 481
 - internal 251, 253, 232, 241
 - macropores 32, 33, 230
 - mesopores 32, 33, 230
 - micropores 32, 33, 230
 - microporosity 33
 - particle 32, 99, 230, 374
 - supermicropores 33
 - ultramicropores 33
- pressure drop 146–147, 157, 160–162, 176, 177, 185, 194, 196, 216, 239–240, 309, 355, 407, 421, 427–449, 456, 458–458, 476–478, 530, 533, 537
- process development unit (PDU) 529

R

- radial mixing 140, 149, 151, 215, 216, 416
- rate coefficient 59–62, 64, 108, 367, 465, 470, 474
- rate-controlling step 68–69, 273, 289–293, 415
- rates
 - catalytic reaction rate 57, 62, 359
 - catalytic reaction rate law derivation 362–363
 - global rate 66, 102, 104, 371, 372, 408, 410, 418, 425
 - intrinsic reaction rate 60, 68, 415, 426, 428, 429, 488
 - observed reaction rate 373, 380
 - overall reaction rate 66, 67, 113, 174, 359, 413, 415, 429
 - per unit mass of catalyst 133, 171, 360–362, 369, 373, 408, 423, 425
 - per unit mass of the solid phase 57, 86, 144
 - per unit surface of the solid 58
 - per unit volume of reactor 57, 62, 145, 171, 220, 428, 429
 - per unit volume of the fluid phase 62, 85, 86
 - per unit volume of the solid phase 58
- phenomenological rates 62
- rate of attachment 359, 360
- rate of detachment 360
- Rayleigh–Taylor instability 124
- reactivation 347
- reactors
 - agitated slurry 78, 102, 131, 398, 548
 - batch agitated 74, 79, 84, 85, 87
 - batch stirred tank 73
 - Carberry 74, 75
 - continuous stirred tank 73
 - entrained flow 76
 - fixed bed 74, 75, 77, 139, 407, 531
 - fluidized bed 76, 101, 189, 481, 540
 - gas-liquid bubble column 74
 - gas-liquid continuous stirred tank 73–74
 - monolith 74, 421, 538
 - moving bed 75
 - packed bubble bed 77, 106, 168, 176
 - plug flow tubular 73
 - semibatch 74, 78, 104–106
 - slurry bubble column 78, 104, 386, 548
 - three-phase fluidized bed 77
 - trickle bed 77, 166, 449, 539

real exchange capacity 268
 recycle reactors 472
 regeneration
 activated carbon 347
 adsorbents 252, 347
 ion exchange regeneration 257, 260, 348–349
 pressure swing adsorption 347, 348
 thermal swing regeneration 348
 vacuum regeneration 348
 Reiss correlation 187, 479
 relative volumetric flow rate 93, 342, 343, 533
 residence time 92, 93, 118, 148, 167, 169, 225, 309, 311, 316, 340, 406, 501, 536, 539
 Richardson–Zaki equation 203

S

scale-up
 agitated vessels 548–550
 definition 523
 experimental scale-up 529–531
 fixed beds 531–539
 fluidized beds 540–548
 mathematical modeling 523–524
 physical modeling 524–528
 slurry bubble bed column reactors 548
 trickle bed reactors 539–540
 scale-up methods
 Gliksman's approach 542
 Horio's approach 543
 scaling laws 541–543
 Schmidt number 165, 323, 325, 527
 selectivity
 catalysis 35, 36, 51, 356, 512, 538
 ion exchange 46, 260, 261, 292, 295, 307
 reaction 487
 selectivity coefficient 272
 separation factor 269–271, 291, 332
 shape factor
 impeller 99, 549
 particle 128, 138
 Sherwood number 164, 165, 527
 shrinking core model 266, 283, 293
 silica gel 47, 231, 241, 243, 247, 248, 251, 252, 356, 357
 similarity
 criteria 525, 528

 dynamic 308, 524
 geometrical 308, 524, 531
 hydrodynamic 543, 544, 546, 548
 kinematic 308, 524
 single bubble rising velocity 125, 392
 slugging fluidization 191, 206–207
 smog
 photochemical 2, 3, 10, 15, 22, 23, 51
 summer-type 3
 winter-type 3, 22, 23
 solubility 105, 109, 166, 174, 245, 246, 518, 564–569
 sorption
 chemical 31
 electrostatic 31
 physical 31
 space time 92, 93
 space velocity 92, 93
 specific heat capacity 165, 224
 sphericity of the particle 146, 195, 228, 229, 290, 430, 542
 Stiegel–Shah correlation 184, 479
 stoichiometric point 337, 338
 Stoke's law 233, 234, 237
 superficial velocity
 fixed beds 146, 328, 338, 407, 430, 443, 533–534
 fluidized beds 189, 205, 482, 542–543
 slurry reactors 114, 118
 trickle beds 181–182, 540
 surface aeration 82, 139, 301
 surface tension 32, 118, 124, 139, 549, 575, 577
 swelling 34, 46, 230, 235, 256, 258, 284, 351, 352

T

terminal settling velocity 128
 terminal velocity 100, 203, 227, 234–237
 thermal conductivity 146, 165, 224
 Thiele modulus 376, 377, 378, 380, 381, 413, 464, 480
 Thomas model 327, 328, 336
 tortuosity 241, 242, 461, 465
 tortuosity factor 153, 240, 241, 374
 Toxic Release Inventory (TRI) 8, 9
 transitional fluidization 206
 treatment methods 27–28

trickle bed reactors

- Fogler's approach 174–176, 456–458
- hydraulic regimes 166–168
- modeling 169–176
- Smith's approach 169–174, 449–456
- reactor (general) 77, 166
- turbulence intensity 127
- turnover frequency 58, 59, 61, 65–66
- Tyn and Calus equation 559

U

- unbaffled tanks 82–84, 95, 100
- utilization (column/fixed bed) 335, 344–346

V

- vapor pressure 231, 269, 329, 348, 565, 569
- variable-volume systems 87, 144, 385, 386, 412, 456, 458
- Vermeulen's approximation 275, 282
- viscosity
 - dynamic 146, 178, 180, 181, 430, 526
 - kinematic 98, 101, 138, 165, 526
- volatile organic compounds (VOCs) 3, 22–24
- volume-surface mean diameter of bubbles 124

W

Wakao equation 164

water

- distribution 16–17
- drinking 16, 17
- fresh 16, 17
- quality deterioration 18
- salty 16
- use 16

water pollutants

- heavy metals 18, 23–25
- inorganic salts and acids 25
- NH_4^+ , NO_3^- , NO_2^- , PO_4^{3-} ions 24
- oil compounds 25
- organic compounds 25–26
- pathogenic microorganisms 26
- water pollution
 - Asia 20–21
 - Australia and New Zealand 20
 - biological 17–18
 - by inorganic pollutants 18–19
 - by persistent organic chemicals 18
 - Europe 19
 - eutrophication 18
 - Japan 20
 - Latin America 20
 - North America 19
 - thermal 17
- water releases
 - main source 24
 - nonpoint sources 23
 - point sources 23
- Weisz and Prater criterion 379
- wetting efficiency 179–182
- Wheeler–Jonas model 328
- Williamson correlation 163
- Wilson–Geankoplis correlation 163

Z

- zeolite molecular sieves 248–250
- zeolites 38, 40, 44–47, 150, 156, 157, 248, 249, 251–253, 255, 257, 307, 311, 356, 534
- Zwietering equation 98